Etude de la bioaccumulation, de la biotransformation de nanomatériaux minéraux et de la persistance de leurs effets biologiques au moyen de systèmes cellulaires in vitro

Anaëlle Torres

THÈSE

Pour obtenir le grade de

DOCTEUR DE L'UNIVERSITÉ GRENOBLE ALPES

École doctorale : CSV- Chimie et Sciences du Vivant
Spécialité : Virologie - Microbiologie - Immunologie
Unité de recherche : Laboratoire de Chimie et Biologie des Métaux

Etude de la bioaccumulation, de la biotransformation de nanomatériaux minéraux et de la persistance de leurs effets biologiques au moyen de systèmes cellulaires in vitro

Study of the bioaccumulation, biotransformation and of the persistence of the biological effects of mineral biomaterials, using in vitro cellular systems.

Présentée par :

Anaëlle TORRES

Direction de thèse :

Thierry RABILLOUD	Directeur de thèse
Jacques-Aurélien SERGENT SOLVAY	Co-encadrant de thèse

Rapporteurs :

Armelle BAEZA-SQUIBAN
PROFESSEUR DES UNIVERSITES, Université de Paris Cité
Catherine LADAVIERE
DIRECTRICE DE RECHERCHE, CNRS délégation Rhône Auvergne

Thèse soutenue publiquement le **28 juin 2022**, devant le jury composé de :

Thierry RABILLOUD DIRECTEUR DE RECHERCHE, CNRS délégation Alpes	Directeur de thèse
Armelle BAEZA-SQUIBAN PROFESSEUR DES UNIVERSITES, Université de Paris Cité	Rapporteure
Véronique ROSSI MAITRE DE CONFERENCE HDR, Université Grenoble Alpes	Examinatrice
Pierre LESCUYER DOCTEUR EN SCIENCES, Hôpitaux Universitaires de Genève	Examinateur
Xavier COUMOUL PROFESSEUR DES UNIVERSITES, Université de Paris Cité	Président
Catherine LADAVIERE DIRECTRICE DE RECHERCHE, CNRS délégation Rhône Auvergne	Rapporteure

Invités :

Jacques-Aurélien SERGENT
DOCTEUR EN SCIENCES, Solvay/Toxicological environment and risk assessment unit

"Don't only practice your art, but force your way into its secrets, for it and knowledge can raise men to the Divine" *Ludwig van Beethoven*

"Being a graduate student is like becoming all of the Seven Dwarves. In the beginning you're Dopey and Bashful. In the middle, you are usually sick (Sneezy), tired (Sleepy), and irritable (Grumpy). But at the end, they call you Doc and then you're Happy."
Azuma 1997

Remerciements

Je voudrais tout d'abord remercier l'entreprise Solvay pour m'avoir donné la possibilité de faire une thèse CIFRE au sein du laboratoire de Chimie et Biologie des Métaux au CEA Grenoble. Cette collaboration a fortement participé à la réalisation de cette belle thèse, et m'a permis de rencontrer un certain nombre de personnes formidables autant sur le plan professionnel qu'humain.

Je voudrais également remercier le CEA, le CNRS, l'Université Grenoble Alpes et l'Ecole doctorale Chimie et Sciences du Vivant, pour avoir permis cette collaboration.

J'aimerais remercier les membres de mon jury, Armelle BAEZA-SQUIBAN, Catherine LADAVIERE, Véronique ROSSI, Xavier COUMOUL et Pierre LESCUYER, pour avoir accepté d'être rapporteurs de ce manuscrit et d'être présents lors de ma soutenance de thèse, et ainsi d'offrir une discussion qui promet d'être riche.

J'adresse un remerciement particulier aux membres de mon CSI, Armelle BIOLA-VIDAMMENT, Marie CARRIERE et Florence COURTOIS. Lors de ces 3 discussions, elles ont apporté leur soutien, leurs précieuses recommandations, autant sur l'aspect scientifique que sur mon avenir professionnel, leurs regards extérieurs, elles n'ont pas hésité à donner leur avis, sources inépuisables de pistes d'amélioration !

Je remercie également le Pr Dominique LISON pour m'avoir permis de présenter mes travaux lors d'un séminaire d'équipe, et pour ses précieux conseils.

J'aimerais également remercier mes référents chez Solvay, d'abord Philippe COCHET puis Fahima MESSALI pour leur accueil, leur soutien et leurs lumières sur le « langage Solvay ». Je souhaite également remercier la GBU Silica, l'équipe TERA et toutes les personnes avec lesquelles j'ai pu interagir dans différents domaines (RH, IAM, microscopie à NOH, envoi d'échantillons…), cela a été un plaisir de travailler et d'échanger avec vous.

J'ai appris beaucoup de techniques durant ma thèse, et cela grâce à Véro COLLIN-FAURE en cytométrie en flux, Laëtitia KURZAWA en microscopie confocale, et Julien PERARD en ICP-AES. Je souhaite également remercier Daphna FENEL pour les heures passées en microscopie électronique pour la caractérisation des silices.

Je tiens à remercier tout particulièrement mon directeur de thèse, Thierry RABILLOUD, pour m'avoir offert cette opportunité, pour m'avoir permis d'exprimer ma créativité avec ce sujet intéressant et inépuisable, pour avoir laissé sa porte grande ouverte à toute question et tout type de discussion et pour m'avoir accordé sa confiance. Je te remercie également d'avoir cru en moi, et ce dès mon stage de Master 1, lorsque je me suis présentée en tant que jeune étudiante sans expérience mais pleine de motivation.

Je remercie également très chaleureusement mon co-encadrant de thèse Jacques-Aurélien SERGENT d'avoir fait confiance à Thierry pour se lancer dans cette thèse CIFRE. Je te remercie d'avoir montré autant d'enthousiasme lors de nos discussions et échanges sur les expériences en cours. Merci pour ton accueil lors de mon séjour à Bruxelles, pour ta disponibilité et pour ta confiance.

Je souhaite également remercier les deux personnes qui m'ont fait découvrir le monde de la recherche. Tout d'abord, Cécile LELONG qui m'a permis de me révéler en L2, pour m'avoir recommandée lors de mon stage de M1 mais aussi pour m'avoir embarquée dans l'enseignement, des heures en PEB où j'ai adoré voir « l'envers du décor » ! J'ai une pensée particulière pour Catherine AUDE-GARCIA, qui par sa bienveillance et sa passion pour la recherche, m'a fait découvrir les merveilleux aspects de ce milieu, j'aurais aimé que notre collaboration dure plus longtemps. Tout a commencé grâce à vous !

Je remercie évidemment toute l'équipe ProMIT : la regrettée Catherine AUDE-GARCIA, Serge CANDEIAS, Elisabeth CHARTIER-GARCIA, Véronique COLLIN-FAURE, Bastien DALZON, Cécile LELONG, Marie LORVELLEC, Sylvie LUCHE, Clément ROUICHI, Thierry RABILLOUD, Isabelle TESTARD, les anciens membres de l'équipe Elise EYMARD-VERNAIN et Julie DEVCIC et plus récemment l'équipe administrative Joëlle PAPARELLA et Claude SENEBIER. Ces presque 5 ans ont été une opportunité professionnelle extraordinaire, très riche d'un point de vue scientifique, mais surtout une merveilleuse expérience humaine. J'ai trouvé des personnes généreuses, absolument serviables et prêtes à m'enseigner leurs connaissances et à partager avec moi leur expérience et leurs compétences. Je les remercie pour l'accueil et l'ambiance toujours chaleureuse, je n'oublierai pas les « Tea time », les discussions lors des repas et les fous rires sur des sujets toujours plus variés : le poplité, les planches à voile, les tiroirs à décoincer, les hamacs et sièges massants… pour n'en citer que quelques-uns. Je sais que je me suis épanouie grâce à vous. Je ne pourrais jamais vous remercier assez pour cela.

Bon courage et bonne continuation aux doctorants actuels Marie et Clément, je vous souhaite d'aimer cette période autant que moi et de profiter de la super ambiance. Ce sera votre tour d'être sur le mur d'honneur des thésards de la pièce de convivialité !

Je remercie également tous mes amis qui ont suivi de près ou de loin cette thèse, et m'ont permis de décompresser quand cela était nécessaire, dans des cadres très variés (percussions, taiko, tambours français…). Merci à Mylène VERNEY pour avoir partagé avec moi les bons moments (et les moins bons même s'ils ont été peu nombreux), qui aurait cru lors de notre rencontre en L2 qu'on en serait là aujourd'hui !

Et enfin, un ENORME merci à mes parents, ma sœur et Anthony pour avoir vécu avec moi ces trois années riches en émotions et rebondissements. Merci pour votre patience et vos conseils, pour votre écoute attentive et pour les moments de partage et de détente. Je vous aime !

Résumé

L'utilisation de nanomatériaux est de plus en plus fréquente dans l'industrie pour améliorer la qualité des produits grâce à leurs propriétés particulières. Par exemple, les silices amorphes de synthèse sont utilisées dans les pneumatiques et polymères, dans la cosmétique et dans l'alimentation humaine et animale pour leurs propriétés de renforcement, de nettoyage, d'épaississement et d'antimottant. Ces utilisations très diverses exposent les travailleurs et la population à des risques potentiels à plus ou moins long terme, qui doivent être évalués, dans un contexte plus global de multiexpositions, tel que rencontré dans les populations humaines. La multiplicité des scenarii à explorer rend l'utilisation des modèles animaux problématique, pour des raisons éthiques et économiques. C'est pourquoi notre travail utilise des systèmes *in vitro* de macrophages (lignées RAW264.7 et J774A.1, macrophages primaires murins), ce type cellulaire étant une cible clé en toxicologie des particules. Les effets de différents scénarii d'exposition ont été étudiés : l'exposition aiguë pendant 24h, l'exposition chronique pendant plusieurs jours consécutifs, puis la récupération qui correspond à l'un ou l'autre des scénarii suivis de quelques jours sans nanomatériaux, qui est un paramètre fondamental en toxicologie des nanomatériaux. Les expériences réalisées sont basées sur des tests de viabilité et des tests fonctionnels (phagocytose, dosages de NO et d'espèces oxydantes, de production de cytokines pro et anti-inflammatoires) grâce à la cytométrie en flux, la spectrophotométrie, et la microscopie.

Mots-clés : nanomatériau, silice amorphe, exposition chronique, bioaccumulation

Study of the bioaccumulation, the biotransformation of mineral nanomaterials and of the perseverance of the biological effects with *in vitro* cellular systems.

Abstract

Nanomaterials are used in the industry to improve the quality of many different products (color, texture or efficiency). For example, synthetic amorphous silica are used in various applications such as rubber reinforcement, cosmetics or food. These broad uses increase human exposure and thus the potential risk related to their short- and long-term toxicity. These potential risks have to be investigated, in a global context of multi-exposure, as encountered in human populations. The scenario multiplicity makes the use of animal models difficult, because of ethical and economical reasons. This is why the experiments will be conducted on *in vitro* macrophage models (RAW264.7 and J774A.1 and mouse primary macrophages), as this cell type is an important cell target in toxicology of particles. Herein, the effect of different exposure scenarii of macrophages to silica nanomaterials will be investigated: the acute exposure for 24h, the chronic exposure for some days and the recovery scenario which consists in an exposure followed by a time period without nanomaterials, which is a fundamental parameter in toxicology of nanomaterial. The bioaccumulation of nanomaterials and the persistence of their effect will be studied. The experiments which will be carried out include the viability assay and functional tests (phagocytosis, NO and reactive oxygen species dosages, production of pro and anti-inflammatory cytokines) using flow cytometry, microscopy and spectrophotometry.

Key words: bioaccumulation, nanomaterial, amorphous silica, chronic exposure

Sommaire

Table des figures

Abréviations

APC : cellule présentatrice d'antigène (antigen-presenting cell)
Ag : Argent
ANSES : Agence national de sécurité sanitaire de l'alimentation, de l'environnement et du travail
BALF : Fluide broncho-alvéolaire
BCR : récepteur des cellules B (B cell receptor)
BSF-2 : facteur de différenciation des cellules B (B-cell stimulatory factor)
CCL2 : Chemokine (C-C motif) ligand 2
CLR : c-type lectin receptor
CMH : Complexe majeur d'histocompatibilité
CRP : C-reactive protein
DLS : dynamic light scattering
EFSA : European Safety Food Agency
ECHA : European CHemical Agency
IFN-γ : Interféron-γ
IL-1β : interleukine-1β
IL-6 : Interleukine-6
IL-10 : Interleukine-10
INRS : Institut national de recherche et de sécurité
LPS : lipopolysaccharide
LTA : acide lipotéichoïque
MBP : Mannan binding protein
MET : microscopie électronique à transmission (TEM)
NLR : nucleotide-binding oligomerization domain-like receptor
NMx : Nanomatériaux
NO : oxyde nitrique
NP : Nanoparticule
NPs : Nanoparticules
OMS : Organisation Mondiale de la Santé (WHO)
PAMP : Pathogen Associated Molecular Pattern
PRRs : Pattern Recognition Receptors
POP : poluant organique persistant
REACH : Regulation, registration, Evaluation, Authorization and Restriction of Chemical
RLR : retinoic acid-inducible gene 1 (RIG-I)-like helicase receptor
ROS : espèces réactives de l'oxygène
SAS : silice amorphe de synthèse
SiO_2 : dioxyde de silice
TLR : toll-like receptor
TNF-α : Facteur de nécrose tumorale α (tumor necrosis factor)
TNF-β : Facteur de nécrose tumorale-β
VEGF : vascular endothelial growth factor

Introduction

Première partie : L'immunologie, une branche de la Biologie

Généralités

Le terme biologie vient du grec « connaissance du vivant », qui recouvre les sciences de la nature et l'histoire des êtres vivants. Ce domaine d'étude fut définit au XVIIIème siècle par l'Allemand Théodore Georg August Roose en 1797 et par le Français Jean-Baptiste de Lamarck en 1802. La vie se présente à de nombreuses échelles : du niveau moléculaire à la population ou l'écosystème. Dans le cadre de ma thèse, la biologie a été étudiée au niveau cellulaire.

La cellule a été observée au microscope pour la première fois en 1665 par Rober Hooke qui a fait le parallèle avec les pièces ou les cellules dans lesquelles les moines habitaient. Depuis cette découverte, les connaissances se sont enrichies, et la cellule est un constituant de tout être vivant, elle est structurée et organisée, comme illustrée sur la figure 1. La cellule contient l'information génétique qu'elle transmet par division cellulaire, et des réactions biochimiques ainsi qu'une activité métabolique ont lieu dans toutes les cellules (Mazzarello 1999).

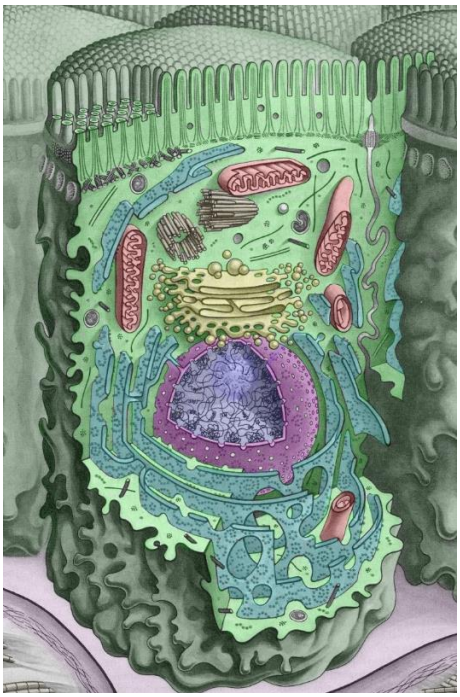

Figure 1 : Une simple cellule colonnaire s'est ouverte pour montrer l'organisation tridimensionnelle de ses principaux composants, d'après Histology guide.

Membrane plasmique (vert foncé) : La surface apicale est couverte de microvillosités. Les surfaces latérales forment des invaginations avec les cellules adjacentes. La surface basale repose sur la lame basale.
Noyau (bleu) : Nucléole (bleu clair), Enveloppe nucléaire (violet) - contient de nombreux pores nucléaires.
Appareil de Golgi (jaune)
Mitochondries (rouge)
Réticulum endoplasmique rugueux (cyan) - contient des ribosomes.
Lysosomes (en niveaux de gris)
Centrioles (beige)
Cytoplasme (vert)

Les cellules peuvent également interagir entre elles, l'immunologie est l'un des domaines étudiant cette interaction.

Pour aborder cette spécialité, il est important de définir ce qu'est l'immunologie et comment ce domaine a évolué au cours du temps. L'immunologie est une spécialité de la biologie et du secteur médical qui étudie l'ensemble des mécanismes de défense de l'organisme contre les antigènes (agents pathogènes extérieurs), d'après le dictionnaire Larousse 2022.

Nous sommes exposés en permanence aux microorganismes, dont un grand nombre est pathogène mais au final très peu entraînent des maladies. L'organisme développe des mécanismes de défenses qui sont étudiés par les immunologistes. Chez les vertébrés, le système immunitaire résulte d'une coopération entre la réponse innée et la réponse adaptative/acquise. Aujourd'hui les connaissances sont nombreuses sur ce système complexe, les cellules actrices de cette réponse immunitaire ainsi que leurs principales caractéristiques sont présentées ci-dessous.

Tableau 1 : Types cellulaires du système immunitaire, activation et signalisation.

Type cellulaire	Morphologie	Rôle	Activation	Signaux
Macrophage	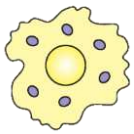	Phagocytose et activation des mécanismes antibactériens, présentation d'antigène CD86+ CD80+ CD11b+ CD14+	IL-1 IL-33 (polarisation M1-M2)	IL-6 TNF-a CXCL8 CCL2
Cellule dendritique		Antigène intégration au niveau des sites périphériques, présentation d'antigène CD80+ CD86+ CCR7+		IL-6 IL-12 TNF-a
Neutrophile		Phagocytose et activation de mécanismes antibactériens	IL-1 CXCL8 CXCL1 CXCL2	IL-1
Eosinophile		Elimination des parasites reconnus par les anticorps		IL-1
Basophile		Promotion de réponse allergique et augmentation de l'immunité anti-parasitique		IL-1
Mastocyte	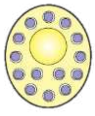	Libération de granules contenant des		TNF-a

		histamines et des agents actifs CD117+, CD34+, CD13+		
Lymphocyte B	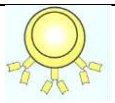	*Réponse immunitaire adaptative* Médiation humorale		
Lymphocyte T		*Réponse immunitaire adaptative* Médiation cellulaire		CXCL10 CCL5
Lymphocyte Natural Killer			IL-12 IL-33 IL-18	IFN-γ

Je vous propose de remonter un peu dans le temps et de découvrir l'histoire de l'immunologie.

Histoire

L'immunité est l'ensemble des mécanismes de défense d'un organisme contre les éléments étrangers à l'organisme. La première notion d'immunité fut évoquée par Thucydide (-465 – -395 avant Jésus-Christ), qui constate qu'une première exposition à une maladie confère l'immunité ultérieure contre cette maladie. Il relate cette observation sur la peste d'Athènes qui dura 4 ans et fit entre 75 000 et 100 000 morts (Littman 2009). Thucydide remarque que les personnes guéries de la peste, ne retombent malades une seconde fois que très rarement et de façon bénigne ('The History of the Peloponnesian War, by Thucydides 431 BC' n.d.). La seconde étape importante de l'immunologie arrive des siècles après, avec les observations faites par Rhazes (Abu Bakr Muhammad ibn Zakariyya al-Razi, 865 – 925). Il distingue la variole de la rougeole en expliquant les symptômes et les traitements ('Rhazes de Variolis et Morbillis : Arabice et Latine ; Cum Aliis Nonnullis Eiusdem Argumenti / Cura et Impensis Iohannis Channing, Natu et Civitate Londinensis. - Yale University Library' n.d.). Il est le premier à évoquer qu'il existe un équilibre dans le corps pour être en bonne santé (théorie humorale), cette théorie sera ensuite discréditée mais cette évocation de l'existence d'un équilibre reste exacte.

C'est à partir du XVIIIème siècle que de nouvelles théories scientifiques se développent, avec notamment Edward Jenner (1749 – 1823) puis Louis Pasteur (1822 - 1895). Au XVIIIème siècle, la variole est un sujet majeur de recherche car elle cause environ 400 000 morts par an en Europe et un tiers des malades guéris devenaient aveugles (Barquet 1997). Cette épidémie incite les chercheurs a étudié cette maladie, et certaines pistes de soins se développent.

La première inoculation en Europe se déroula en 1718, en Angleterre (Riedel 2005). Lady Montague (1689 – 1762) suite à la déclaration de la variole en 1715, se rendit à Istanbul où elle découvrit le principe de l'inoculation, pratiquée traditionnellement depuis des décennies dans l'Empire Ottoman. Elle communiqua la méthode lors de son retour en Angleterre, et elle fut appliquée par Charles Maitland (1668 – 1748). Après plusieurs essais sur des prisonniers et des orphelins, puis l'inoculation des princesses de Galles, le principe se répandit en Angleterre.

Dans Gloucester, en 1757, un garçon orphelin de 8 ans fut inoculé par la variole, il développa une forme bénigne et fut immunisé contre cette maladie. Ce garçon était Edward Jenner (1749 – 1823).

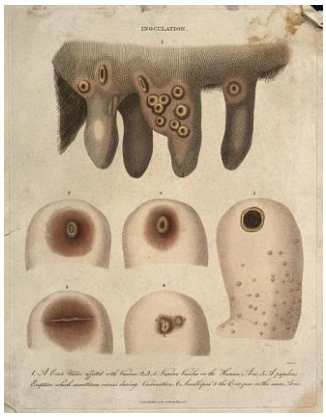

Figure 2: Lésion de la vaccine sur les pis d'une vache (Wellcome Library, Londres)

Edward Jenner étudia la biologie, la médecine, la physique, l'ornithologie, le violon et la poésie, mais il est principalement connu pour ses travaux sur l'inoculation de la vaccine (variole des vaches). Il commença ses essais en 1796, en prélevant le contenu des lésions sur les mains d'une jeune vachère, Sarah Nelms, et en inoculant un jeune garçon de 8 ans, James Phipps. Le garçon développa des symptômes sans gravité (fièvre et perte d'appétit) pendant quelques jours. Lorsque Jenner inocula le garçon deux mois plus tard avec la variole (humaine), il ne développa aucune maladie. Après plusieurs essais, Jenner en déduisit que la protection par inoculation fonctionnait. Il appela cette méthode la vaccination à partir de la vaccine (en latin, vache se dit *vacca*). Ses communications et la transmission de sa méthode à travers toute l'Angleterre participèrent à la popularisation de cette pratique. La vaccination se répandit largement à la fin du XVIIIème siècle, et elle remplaça la variolation qui fut prohibée en 1840 en Angleterre. Jenner fut le premier scientifique capable de contrôler une maladie infectieuse en utilisant la vaccination. En Europe, à la fin du XVIIIème siècle, la variole avait causé la mort de 60 millions de personnes.

C'est à la fin du XIXème siècle qu'on réalisa qu'une simple vaccination ne conférait pas une immunité à vie, et qu'il était nécessaire de revacciner. À partir de 1902, la vaccination infantile avec rappels devient obligatoire en France, même si elle est déjà systématique dans l'armée qui a vu le bénéfice chez les Prussiens lors de la guerre de 1870-1871. Lors de cette guerre, l'armée Prussienne (constituée de 800 000 hommes vaccinés tous les 7 ans) recense 8463 cas de variole, avec un taux de mortalité de 5,4% lorsque l'armée française déclare 125 000 cas et une mortalité de 18,7% (Fenner et al. 1988). Suite à cette prise de conscience, la vaccination fut plus régulière. C'est ainsi que la variole fut éradiquée en 1980 par l'Organisation mondiale de la santé.

Les travaux de Jenner sont l'initiation des études sur le système immunitaire et les mécanismes de défense de l'organisme. Il fut suivi par Louis Pasteur (1822-1895), connu pour l'idée de l'existence de la structure de composés chimiques (stéréochimie 1849), le principe de la pasteurisation (1862) et principalement pour ses travaux sur les vaccins. Son premier vaccin concernait le choléra des poules en 1879, les poules exposées à une forme atténuée du virus devinrent résistantes au virus virulent. Suite à son entrée à l'Académie française en 1882,

Pasteur se concentra sur le développement d'un vaccin contre la rage qu'il mit au point en 1885, ce qui le rendit célèbre internationalement (Institut Pasteur, biographie). A Paris, l'institut Pasteur fut inauguré deux ans plus tard.

Au même moment, un débat était en cours entre les scientifiques français et allemands sur les mécanismes de défense de l'organisme face aux agressions extérieures. Certains pensent que des cellules spécialisées interviennent, d'autres assurent qu'il s'agit de substances solubles présentes dans le sang. Ce sera le chercheur russe Elie Metchnikoff (1845-1916) qui mettra en évidence les cellules phagocytaires (cellules dévoreuses) lors d'une expérience avec une étoile de mer qu'il griffa avec une épine de rosier, en 1883. Il intégrera l'institut Pasteur suite à cette découverte. En 1890, Paul Ehrlich (1854-1915), un chercheur allemand, montre qu'une substance soluble, les anticorps, sont impliqués dans la protection contre le tétanos, il découvre également les mastocytes (des cellules de l'immunité). En 1908, ces deux chercheurs reçurent un prix Nobel, l'un pour la découverte de la phagocytose et la mise en évidence de cellules spécialisées de l'immunité, l'autre pour la découverte de l'immunité humorale.

Les découvertes de cette fin de XIXème et début de XXème siècle marquent un tournant dans le domaine de l'immunologie. Grace à une meilleure compréhension du système immunitaire et des maladies courantes, de nombreux vaccins furent mis au point, comme l'illustre la figure 3.

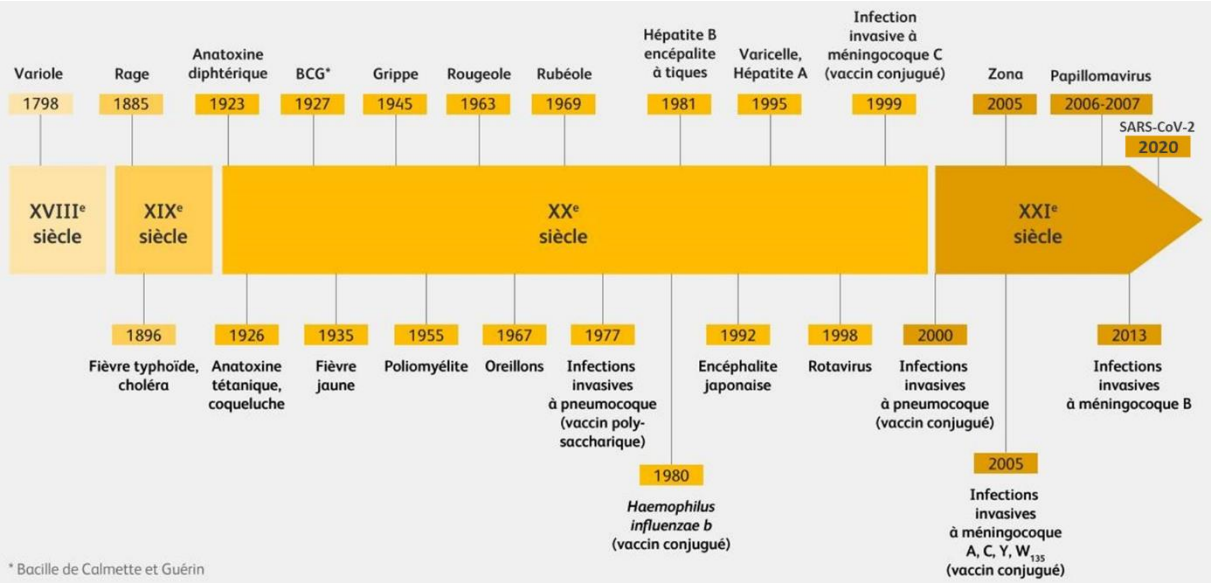

Figure 3 : Fresque chronologique du développement de la vaccination. Adapté de Guide de vaccination (2021) INPES et History of vaccination (2008) Plotkins.

Réponse immunitaire

Lors d'une infection (parasite, bactéries, virus, ou non soi) le système immunitaire est activé. Les cellules sentinelles reconnaissent les agents infectieux ce qui entraînent la sécrétion de molécules de signalisation. Le mécanisme est présenté sur la figure 4, il est détaillé dans les paragraphes ci-dessous. Un pathogène qualifie ce qui provoque une maladie, en particulier un germe capable de déterminer une infection. L'immunité est l'ensemble des mécanismes de

défense d'un organisme contre les éléments étrangers à l'organisme, en particulier les agents infectieux.

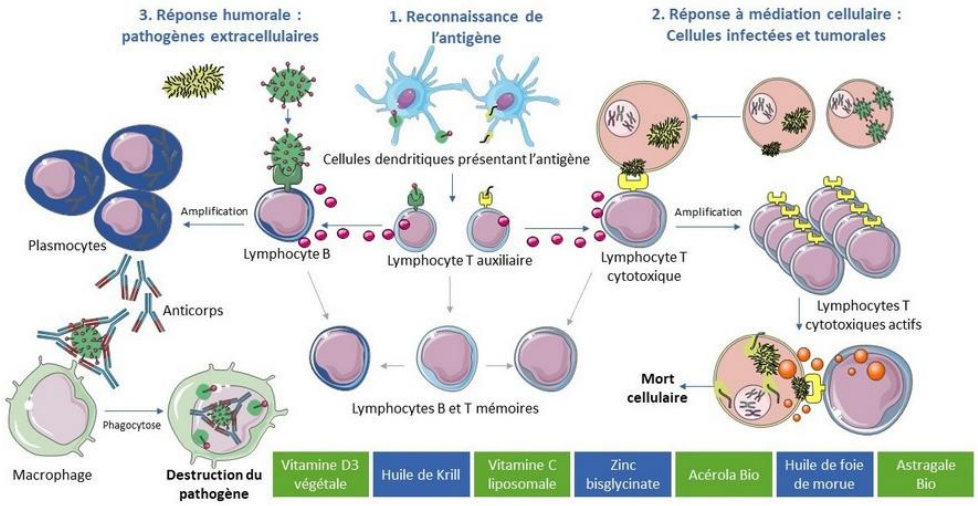

Figure 4 : Le système immunitaire, réponse innée et adaptative, d'après Dynveo.

Réponse innée

L'immunité innée est la première ligne de défense contre les pathogènes de notre environnement. C'est une réponse rapide et fonctionnelle qui se prolonge plusieurs jours. Ensuite, l'immunité adaptative entre en jeu. C'est Charles Janeway (1943 - 2003) qui remplacera le terme « résistance non spécifique aux infections » par « la réponse immunitaire innée ».

La réponse innée est constituée de plusieurs niveaux, les modules constitutifs et les modules induits. Les modules constitutifs (la peau et les muqueuses) forment les premières barrières contre l'entrée des virus et parasites. La peau, constituée de plusieurs couches de cellules (kératinocytes), remplit des fonctions barrières de différents niveaux (Coates, Blanchard, and MacLeod 2018). Tout d'abord un rôle mécanique en empêchant l'adhésion et la persistance des bactéries ou parasites à la surface de la peau (desquamation et faible perméabilité). Ensuite, les protéines et les peptides antimicrobiens remplissent le rôle de barrières chimiques en brisant et déstructurant les membranes bactériennes. Enfin, la troisième barrière est biologique, constituée de flore commensale et de cellules présentant des récepteurs de reconnaissance (pattern recognition receptors PRRs) aux motifs moléculaires associé aux pathogènes (pathogen associated molecular patterns PAMP). Les PRR se divisent en quatre groupes : les toll-like receptors (TLR), les nucleotide-binding oligomerization domain-like receptors (NOD), retinoic acid-inducible gene 1 (RIG-I)-like helicase receptors (RLR) et c-type lectin receptors (CLR). La réponse immunitaire innée est moins spécifique que la réponse adaptative, cependant certains PRRs ont évolué et reconnaissent des PAMPs spécifiques. Par exemple, les TLR1, TLR2, TLR6 et NOD2 reconnaissent des composants de la membrane de la bactérie Gram positif *Staphylococcus aureus*, et enclenchent la production de peptides antimicrobiens (Krishna and Miller 2012). La bactérie Gram négatif *Escherichia coli* est reconnue par NOD1,

TLR1, TLR2 (acide lipotéichoïque (LTA)), TLR4 (lipopolysaccharide LPS) et TLR 6 (Porcherie et al. 2012).

Les muqueuses quant à elles sont un épithélium non kératinisé mais produisant du mucus. Celui-ci contient des sucres et piège les bactéries grâce à sa viscosité. Les organes contenant ce milieu sont exposés à l'environnement extérieur (systèmes ouverts), comme par exemple les poumons ou l'intestin. C'est pourquoi le mucus fait partie des cibles étudiées dans la recherche de certaines thérapies, comme par exemple dans le cas des maladies inflammatoires chroniques, de l'intestin (MICI) et du poumon (Cornick, Tawiah, and Chadee 2015).

La deuxième phase de la réponse immunitaire innée suit la reconnaissance des PAMPs par les PRRs. Les modules induits sont des réactions déclenchées par les cellules elles-mêmes comme la phagocytose et la réponse inflammatoire par l'intermédiaire des cellules phagocytaires et des cytokines sécrétées.

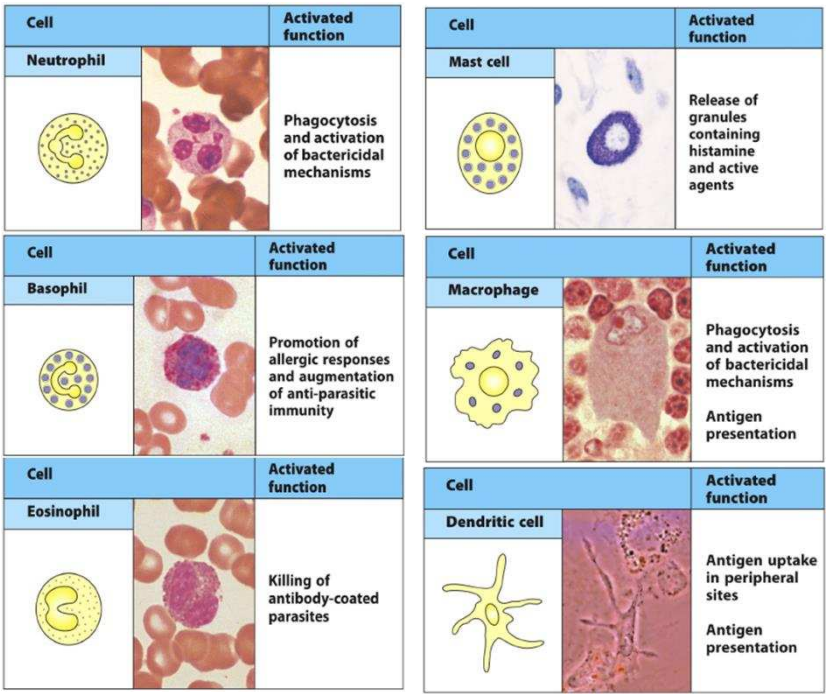

Figure 5 : Les cellules de l'immunité innée, d'après Janeway 8ème édition (2012).

Les cellules impliquées dans cette phase sont majoritairement les cellules myéloïdes : macrophages, cellules dendritiques, mastocytes et granulocytes (neutrophile, éosinophile, basophile) (figure 5).

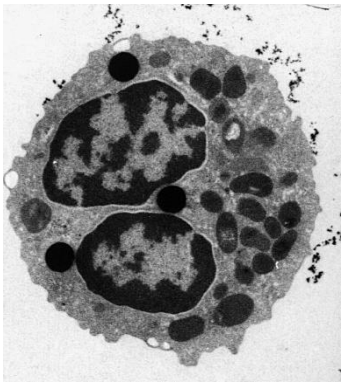

Figure 6 : Un granulocyte, observé en microscopie électronique (ens Lyon).

Les cellules dites **granulocytes** (figure 6) sont des cellules circulantes, principalement impliquées dans les réactions allergiques. Elles produisent des médiateurs inflammatoires pour combattre les bactéries (neutrophile), les parasites (éosinophile), et les allergènes (éosinophile et basophile). Les neutrophiles représentent environ 60% des globules blancs, les éosinophiles 1-3% et les basophiles environ 1% (les cellules dendritiques 1%, les macrophages 10%, les lymphocytes -B, T, NK- 25%). Leur augmentation dans la circulation sanguine est souvent le signe d'une infection, leur diminution peut refléter une anémie, une leucémie ou un effet secondaire d'un traitement anticancéreux (d'après Cleveland clinic).

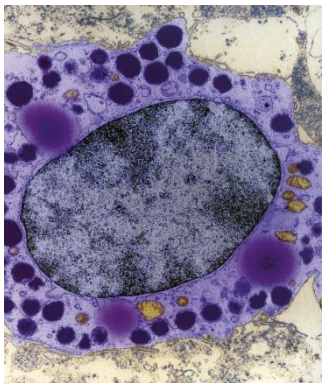

Figure 7 : Un mastocyte, observé en microscopie électronique à transmission (Chorlton et al (2004) Voyage au centre du corps humain).

Les **mastocytes** (figure 7) sont des cellules résidentes, localisées dans les tissus vascularisés à l'interface avec l'environnement comme par exemple les tissus pulmonaires et intestinaux, et l'épiderme. Chaque population de mastocytes est différente selon sa localisation : les cellules se différencient en réponse au microenvironnement qu'elles rencontrent et deviennent matures une fois dans le tissu (Milliat and François 2018). En cas de lésion, les mastocytes libèrent l'héparine (anticoagulant) et l'histamine (vasodilatateur) stockées dans leurs granules.

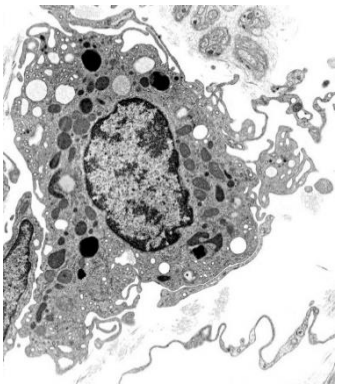

Figure 8 : Un macrophage observé en microscopie électronique à transmission (Histology guide).

Les **macrophages** (figure 8) proviennent de la différenciation des monocytes dans le cas des macrophages circulants et du foie fœtal pour les macrophages résidents, et représentent 10% des globules blancs. Ces cellules ubiquitaires sont la première barrière contre les substances étrangères qu'elles phagocytent. Les macrophages résidents au niveau des organes exposés portent des noms spécifiques en fonction des tissus dans lesquels ils sont localisés : les cellules de Kupffer (foie), les cellules microgliales (tissus nerveux), les macrophages alvéolaires (poumons). Leur principale fonction est la phagocytose – mécanisme qui permet d'internaliser du matériel de grande taille (de l'ordre du micromètre ou plus) notamment les agents pathogènes ou les bactéries, mais également les débris cellulaires. Cette fonction particulière est à l'origine de leur nom : en grec μακρός *macrós* grand et φάγομαι *phágomai* manger, grand mangeur (Académie nationale de pharmacie, université de Strasbourg). Cette activité phagocytaire participe à l'homéostasie de l'organisme, au renouvellement cellulaire et à la réponse immunitaire innée. Les macrophages expriment à leur surface les récepteurs membranaires suivants : CD11b, CD14, B7 et CCR5 (marqueurs de surface, de reconnaissances et de communication inter-cellulaires), et de nombreux PRR membranaires, ainsi que les molécules de classe 1 et 2 du complexe majeur d'histocompatibilité (CMH, permettant la

reconnaissance par les cellules de l'immunité adaptative, grâce à la présentation d'antigène). Ces molécules permettent la reconnaissance de leur environnement, des cellules voisines et également la communication entre les cellules, la signalisation, qui est la deuxième fonction importante des macrophages. En effet, en réponse aux signaux perçus grâce aux molécules présentes à leur surface, les macrophages sécrètent des médiateurs de l'inflammation : les cytokines. Les principales cytokines produites par les macrophages sont l'interleukine 6 (IL-6), l'interleukine 10, l'interleukine 12, et le facteur de nécrose tumorale α (TNFα). Selon le stress

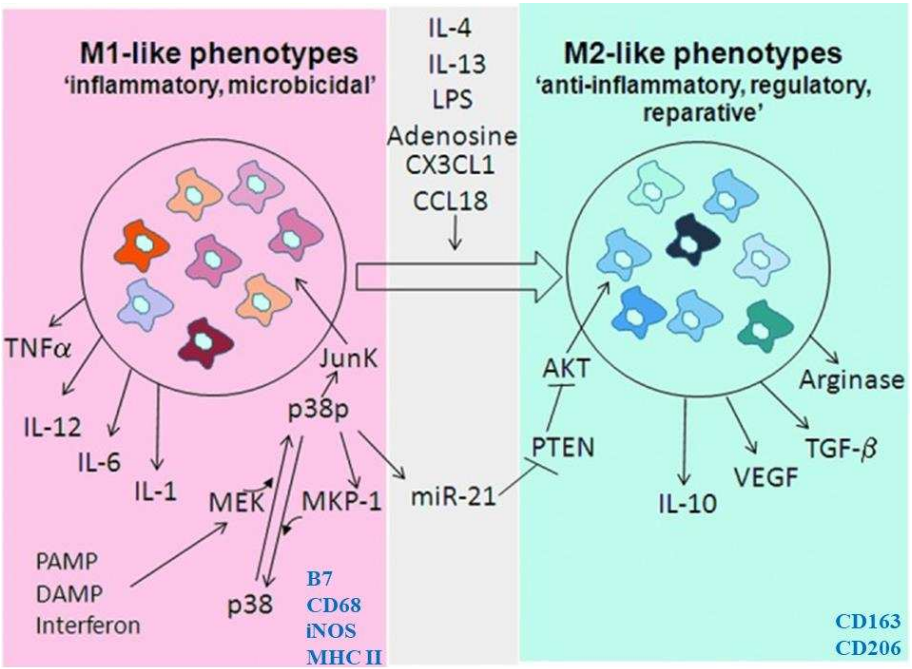

Figure 9 : Différenciation des macrophages M1 à M2, adapté de MacLeod (2016). Les marqueurs spécifiques sont renseignés en bleu. La différenciation des macrophages permet de spécialiser leur réponse en fonction de la situation (anti-) inflammatoire.

ou le signal reconnu par la cellule, les molécules sécrétées seront différentes et adaptées afin d'initier une réponse de l'organisme. Dans le cas d'une action réparatrice, le macrophage va se différencier en M2, c'est-à-dire qu'il va envoyer des signaux permettant d'activer la réparation du tissu lésé, et également modifier ses molécules de surface. En cas de reconnaissance d'un danger nécessitant une réponse inflammatoire, le macrophage se différencie en M1 et sécrète de l'IL-6, du TNFα et de l'oxyde nitrique (NO). Un macrophage M1 peut se différencier en M2, par exemple si le lipopolysaccharide des bactéries Gram négatives, l'IL-13 et l'IL-4 sont détectés (Figure 9). Ces différents signaux permettent le recrutement de cellules spécialisées au niveau du site de l'inflammation (MacLeod and Mansbridge 2016). Enfin, la dernière fonction du macrophage est la présentation d'antigène aux lymphocytes T. Cette présentation nécessite la rencontre du macrophage avec un pathogène ou une molécule reconnue comme du Non-Soi (c'est-à-dire, à éliminer), l'internalisation de cet objet, sa digestion puis la présentation d'un fragment de cet objet – l'antigène – sur les molécules du CMH de classe II, qui sera reconnu par les lymphocytes T. Cette présentation d'antigène est à l'interface entre immunité innée et immunité adaptative. Enfin, la dernière particularité de ce type cellulaire est sa durée de vie. Les macrophages résidents vivent de plusieurs jours à plusieurs mois dans les tissus (Parihar, Eubank, and Doseff 2010).

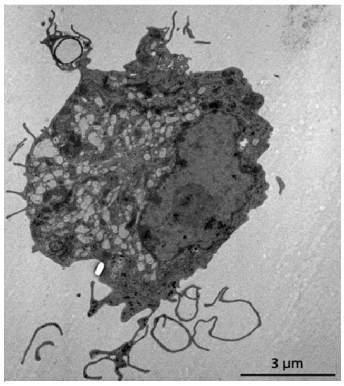

Figure 10 : Une cellule dendritique, observée en microscopie électronique à transmission (De Koker Chemical Society Review (2010).

Les **cellules dendritiques** (figure 10) sont le dernier type cellulaire impliqué dans la réponse immunitaire innée, et comme les macrophages, ces cellules permettent d'activer la réponse immunitaire adaptative. Leur principale fonction est la présentation d'antigène aux cellules T, et leur maturation permettra de recruter différents lymphocytes T ('Dendritic Cells | British Society for Immunology' n.d.). Les cellules dendritiques représentent 1% des globules blancs. Elles expriment à leur surface les molécules CD80 et CD86 mais également le récepteur à chimiokine CCR7, elles sécrètent du TNFα et IL-12.

Les différents acteurs impliqués dans la réponse innée ayant été présentés, passons à l'étape suivante de la réponse immunitaire innée. Suite aux barrières de l'organisme (muqueuses, chimiques et biologiques) la reconnaissance des PAMPs par les cellules entraîne une réponse spécifique.

La première étape de cette deuxième phase implique la phagocytose et éventuellement l'opsonisation du pathogène (nécessité d'une molécule intermédiaire pour l'interaction PAMPs/PRRs). Les opsonines peuvent être des anticorps, des composants du complément, des

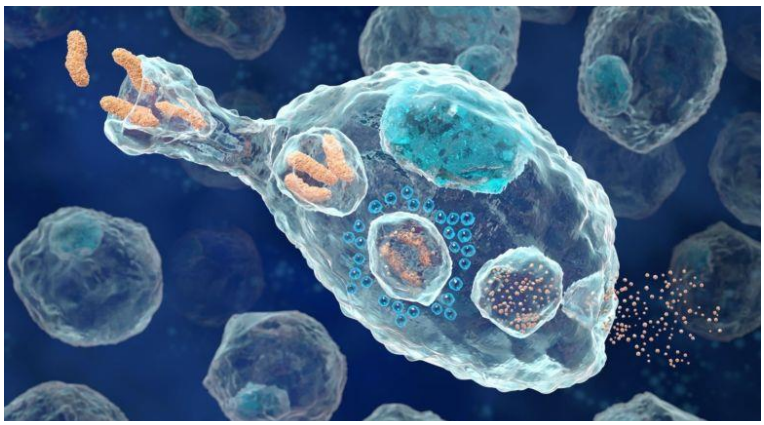
Figure 11 : Macrophage et les différentes étapes de la phagocytose de la bactérie Streptococcus pneumoniae (Medicator, 2017).

protéines MBP (Mannan binding protein) ou la protéine C réactive (CRP). La phagocytose est constituée de plusieurs étapes : l'opsonisation (facultative), le chimiotactisme, l'adhésion, le phagosome et la digestion (figure 11). L'opsonisation est le phénomène selon lequel la molécule de l'opsonine recouvre la membrane d'une cellule cible ou antigène. Le chimiotactisme est la capacité de certaines cellules à être attiré ou repoussé par des substances. L'adhésion est l'étape au cours de laquelle la membrane de la cellule phagocytaire adhère à la particule qu'elle va ingérer. Le phagosome est une vacuole ou vésicule qui contient la particule internalisée. La digestion a lieu dans les vésicules, par des enzymes et permet l'évacuation des déchets, dans le cas de particule persistante, cette digestion est impossible et le phagocyte stocke les vésicules pleines. Les cellules capables de remplir cette fonction sont les macrophages, les cellules dendritiques et les polynucléaires.

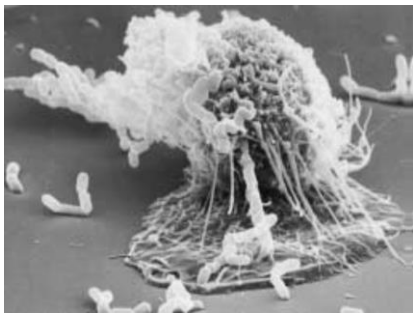

Figure 12 : Macrophage en train "d'hameçonner" des bactéries pour les phagocyter, en microscopie électronique à balayage (1800x). (Biology, Raven et Jonhson 6ème édition, p1149).

Le chimiotactisme permet de recruter les macrophages vers la bactérie (opsonisée ou non) par l'intermédiaire des chimiokines (CCL2). Ensuite, il y a adhésion de la bactérie à la surface du macrophage grâce aux récepteurs de la membrane plasmique, ce qui déclenche la phagocytose (figure 12). Le phagosome se forme suite à la reconnaissance de la bactérie et à l'élongation du cytoplasme, qui forme les pseudopodes et entourent la bactérie formant la vacuole. Ce phagosome fusionne ensuite avec les lysosomes (phago-lysosome) entrainant ainsi la digestion de la bactérie par différents mécanismes (acidification, hydrolyse par les lysozymes et protéases, production de dérivés toxiques de l'oxygène (ions superoxydes et espèces réactives de l'oxygène (ROS)) ou encore production de dérivés nitrés comme l'oxyde nitrique (NO)). La deuxième phase induite correspond à la réaction inflammatoire qui suit le signal des interactions PRR-PAMP. Les cytokines pro-inflammatoires comme l'interleukine-1β (IL-1β), le facteur de nécrose tumorale-α (TNF- α), et l'interféron-γ (IFN-γ) sont sécrétées, pour initier la cascade inflammatoire ce qui va entraîner l'expression des molécules d'adhésion (MacLeod and Mansbridge 2016). Les cytokines anti-inflammatoires comme l'interleukine-10 (IL-10) et le facteur de nécrose tumorale-β (TNF-β) sont également sécrétées afin de réguler cette réaction inflammatoire et d'éviter qu'elle ne devienne délétère. La sécrétion des cytokines pro-inflammatoires va entraîner plusieurs conséquences :

- La *vasodilatation* qui permet d'augmenter la perméabilité vasculaire, est induite par le monoxyde d'azote.
- L'*expression des molécules d'adhésion* comme les sélectines (E et P) et les immunoglobulines, à la surface des cellules endothéliales, est induite par le TNF-α et facilite la diapédèse (migration des leucocytes).
- La *coagulation* permettant de diminuer la propagation du pathogène, est induite par le TNF-α.
- L'*activation de la réponse aiguë* de l'inflammation permettant via les cytokines pro-inflammatoires la synthèse de protéines de l'inflammation au niveau de différents organes.
    - Les prostaglandines (origine de la fièvre) seront synthétisées par l'hypothalamus, via l'IL-1
    - Les facteurs de croissance seront synthétisés au niveau de la moelle osseuse
    - Les protéines du foie seront induites après activation par l'IL-6, l'IL-1 et le TNF-α
        - La protéine C réactive (CRP PRR soluble) une opsonine des microorganismes et marqueur sanguin de l'inflammation aiguë.
        - La mannose binding protein (MBP) une opsonine se fixant sur les résidus mannose à la surface des bactéries et activant le complément.
- La *synthèse de fibrinogène* et des *facteurs du complément*, modulant l'activation des

lymphocytes T, via l'IL-12 et l'IL-18

- Le *recrutement des cellules phagocytaires* (macrophages et cellules dendritiques) via les chimiokines (CXCL4), qui permettront l'activation de la réponse immunitaire adaptative.

Les étapes de la réponse immunitaire innée ont été présentées ci-dessus, dans les cas où cette réponse ne permettrait pas d'éliminer le pathogène, la réponse immunitaire adaptative est initiée par les cellules sentinelles (macrophages et cellules dendritiques).

Réponse adaptative

La deuxième phase de la réponse immunitaire est la réponse adaptative, elle intervient seulement si les cellules de l'immunité innée n'ont pas réussi à canaliser et réparer l'infection ou le dommage tissulaire. Cette deuxième phase fait intervenir les lymphocytes B et T principalement, en réponse à la stimulation par les cellules dendritiques et les macrophages, présentant des antigènes.

Figure 13 : Un lymphocyte B, observé en microscopie électronique à balayage (Chorlton et al (2004) Voyage au centre du corps humain).

Les **lymphocytes B**, aussi appelés cellules B (figure 13), sont des cellules présentatrices d'antigène, comme les cellules dendritiques et dans une moindre mesure, les macrophages. Elles représentent environ 20% des lymphocytes circulants (Alberts et al. 2002). Ces cellules expriment à leur surface les molécules du CMH II, des anticorps membranaires (appelés BCR, B cell receptor) et sécrètent des cytokines, notamment l'IL-6. La reconnaissance d'un antigène par les cellules B via les BCR et la liaison au lymphocyte T *via* les molécules de co-stimulation CD40/CD40L permettent d'initier leur différenciation/maturation en plasmocytes – cellules B matures sécrétrices d'anticorps (figure 14). Les anticorps sont des complexes de protéines solubles et circulants. Ils sont composés de deux chaînes polypeptidiques lourdes identiques et de deux chaînes polypeptidiques légères identiques. Chacune des chaînes est constituée d'une partie constante (partie terminale fixée à la surface des cellules) et d'une partie variable (site de fixation de l'antigène).

Chaque anticorps est spécifique d'un antigène, lors de la reconnaissance et de la fixation, un complexe immun insoluble va se former, ce qui permet la neutralisation des antigènes ou leur opsonisation conduisant à leur neutralisation par les phagocytes. Les anticorps membranaires sont présents à la surface des lymphocytes B.

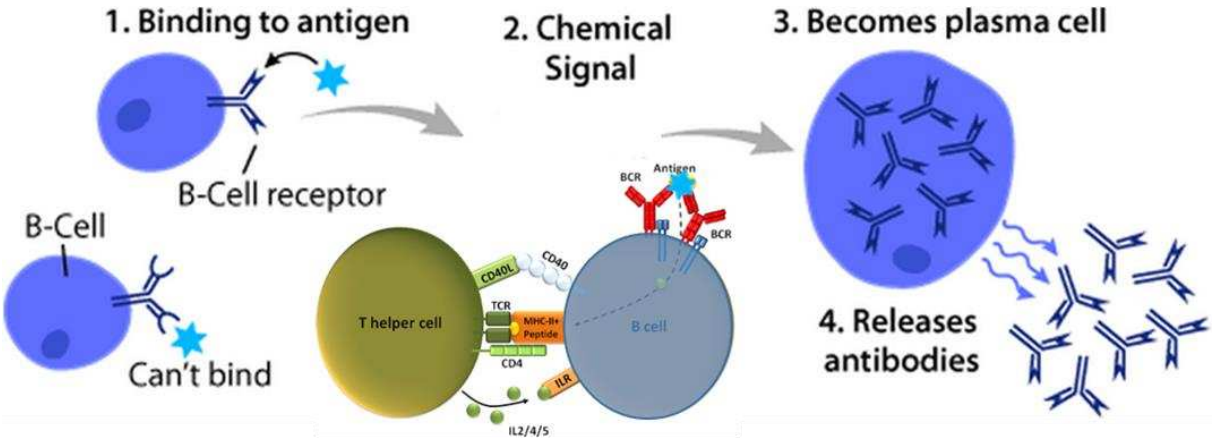

Figure 14 : Activation des lymphocytes B par les lymphocytes T, d'après "B cell function" By Arizona Science Center – (CC BY-SA 3.0) via Commons Wikimedia, Altaileopard, Allemagne (2002) et Janeway Immunology 5ème édition

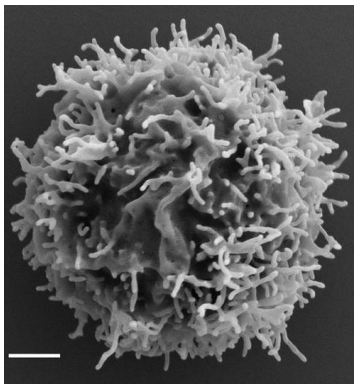

Figure 15 : Un lymphocyte T effecteur, observé en microscopie électronique à transmission, d'après Jung et al. (2016).

Les **lymphocytes T**, sont produits dans le thymus et reconnaissent les antigènes présents à la surface des cellules présentatrices d'antigène, *via* leurs T cell receptors (TCR) (figure 15). Les lymphocytes T représentent 80% des lymphocytes circulants, et il existe deux grands types de lymphocytes T : les auxiliaires et les cytotoxiques.

Les lymphocytes T auxiliaires expriment la molécule CD4 à leur surface et reconnaissent les antigènes présentés par les molécules CMH II, ce qui permet d'activer les autres cellules immunitaires (amplification du signal, maturation…). Les lymphocytes T cytotoxiques (CTL) expriment le marqueur CD8, reconnaissent les antigènes présentés *via* les CMH I, et permettent d'éliminer les cellules infectées ou tumorales (figure 16) (Janeway et al. 2001).

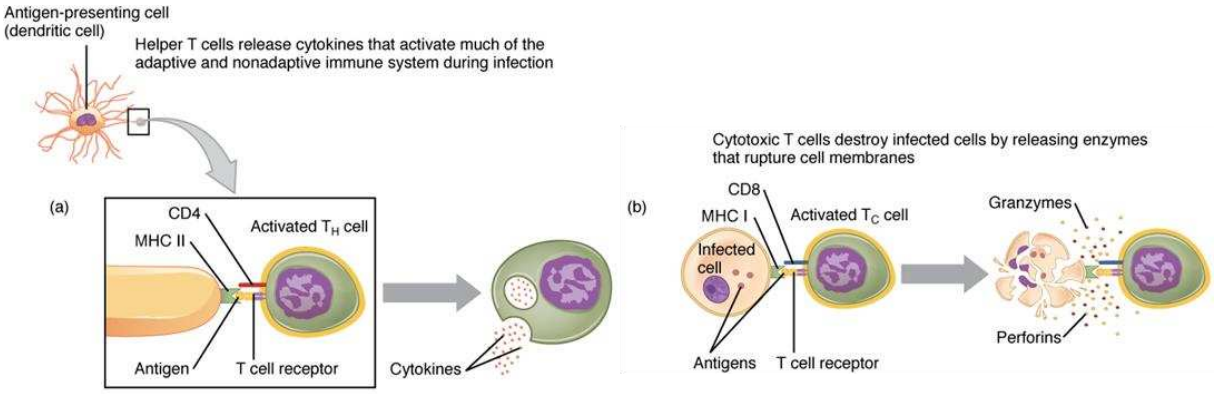

Figure 16 : Activation des lymphocytes T (helper et cytotoxique), d'après "2219 Pathogen Presentation" By OpenStax College – Anatomy & Physiology, Connexions Web site, Jun 19, 2013. (CC BY 3.0) via Commons Wikimedia

Phases of the immune response			
Response		Typical time after infection to start of response	Duration of response
Innate immune response	Inflammation, complement activation, phagocytosis, and destruction of pathogen	Minutes	Days
Adaptive immune response	Interaction between antigen-presenting dendritic cells and antigen-specific T cells: recognition of antigen, adhesion, co-stimulation, T-cell proliferation and differentiation	Hours	Days
	Activation of antigen-specific B cells	Hours	Days
	Formation of effector and memory T cells	Days	Weeks
	Interaction of T cells with B cells, formation of germinal centers. Formation of effector B cells (plasma cells) and memory B cells. Production of antibody	Days	Weeks
	Emigration of effector lymphocytes from peripheral lymphoid organs	A few days	Weeks
	Elimination of pathogen by effector cells and antibody	A few days	Weeks
Immunological memory	Maintenance of memory B cells and T cells and high serum or mucosal antibody levels. Protection against reinfection	Days to weeks	Can be lifelong

Figure 17 : Les phases de la réponse immunitaire, de Immunology Janeway, 9ème édition, p28

Afin de résumer cette partie sur la réponse immunitaire, les principales étapes sont présentées dans le tableau (figure 17) ainsi que les durées des différentes phases. La signalisation est un point important de la réponse immunitaire pour orchestrer toutes ces étapes, les cellules impliquées et les médiateurs.

La signalisation

Les médiateurs de l'inflammation sont nombreux, et permettent le recrutement de cellules circulantes, l'élimination du pathogène et la réparation de la lésion.

Les cytokines sont des protéines sécrétées par les cellules en réponse à un stimulus, et permettent la communication entre les cellules immunes et ainsi que l'orientation de la réponse immunitaire. Les cytokines pro-inflammatoires représentent un signal de danger suite à la reconnaissance des PAMPs par les PRRs. Le TNF-α est sécrété par les macrophages, les cellules dendritiques et les mastocytes résidents, et remplit trois rôles importants. Cette cytokine stimule l'expression des molécules d'adhérence (ELAM-1, VCAM-1, et ICAM-1) et la production de chimiokines (IL-8, CCL3, CCL2, CCL4) par les cellules endothéliales, ce qui permet le recrutement des leucocytes sanguins (neutrophiles, éosinophiles, monocytes ou NK) vers le site de l'inflammation. Le TNF-α active les systèmes microbicides des cellules phagocytaires et la division cellulaire des lymphocytes T et B, en prévision de la réponse immunitaire adaptative. Enfin, le dernier rôle du TNF-α est d'activer la production de facteurs de croissance (vascular endothelial growth factor VEGF) qui seront nécessaires à la réparation tissulaire du site de l'inflammation. La deuxième cytokine pro-inflammatoire importante est l'interleukine-1 est sécrétée par les leucocytes, les cellules endothéliales, les fibroblastes, après la reconnaissance de PAMPs (Garlanda, Dinarello, and Mantovani 2013). Cette cytokine stimule elle-aussi l'expression des molécules d'adhésion de l'endothélium vasculaire pour

favoriser la migration des leucocytes circulants vers le site de l'inflammation. Le principal symptôme induit par l'IL-1 est la fièvre, qui permet une division cellulaire des lymphocytes, la mobilisation plus rapide du système immunitaire adaptatif et parfois un ralentissement de la division du pathogène. La troisième cytokine ayant un rôle important dans l'inflammation est l'interleukine-6. Elle est sécrétée par les phagocytes (macrophages et cellules dendritiques) et par les cellules endothéliales, et permet d'induire localement l'activation des cellules phagocytaires et la modification de l'endothélium, et également de recruter des monocytes sanguins vers le site de l'inflammation. Elle se fixe au récepteur IL-6R (soluble ou membranaire) qui interagit avec le récepteur membranaire gp-130 (Scheller et al. 2011). L'IL-6 est également à l'interface de l'immunité innée et l'immunité adaptative, notamment en stimulant les lymphocytes, principaux acteurs de l'immunité spécifique. L'IL-6 a historiquement été identifiée comme étant un facteur de différenciation des cellules B (BSF-2) (Kishimoto et al. 1995).

Les chimiokines sont impliquées dans le recrutement des leucocytes et la résistance innée face à une infection (Combadière, Combadière, and Deterre 2007). Elles servent de guide aux cellules du système immunitaire, en circulant dans le sang, afin de positionner les cellules dans des sites stratégiques (sentinelle) ou de faire interagir ces cellules avec d'autres pour éliminer un pathogène.

L'histamine est une amine qui augmente la perméabilité et la contraction des muscles lisses localement chez les carnivores et les primates (Dale and Richards 1918). Cette vasodilatation permet l'afflux des cellules immunitaires circulantes au niveau du site de l'inflammation et également l'augmentation du métabolisme s'il s'agit d'un organe. Cette amine est libérée par les mastocytes activés par la reconnaissance des PAMPs.

La figure 18 illustre la complexité des signaux de l'inflammation (cytokines) qui permettent une communication efficace entre tous les acteurs de la réponse immunitaire, en impliquant les types cellulaires vus précédemment. Les cytokines sont les médiateurs de l'inflammation, elles pilotent la réponse immunitaire et la balance entre réponse innée et réponse adaptative.

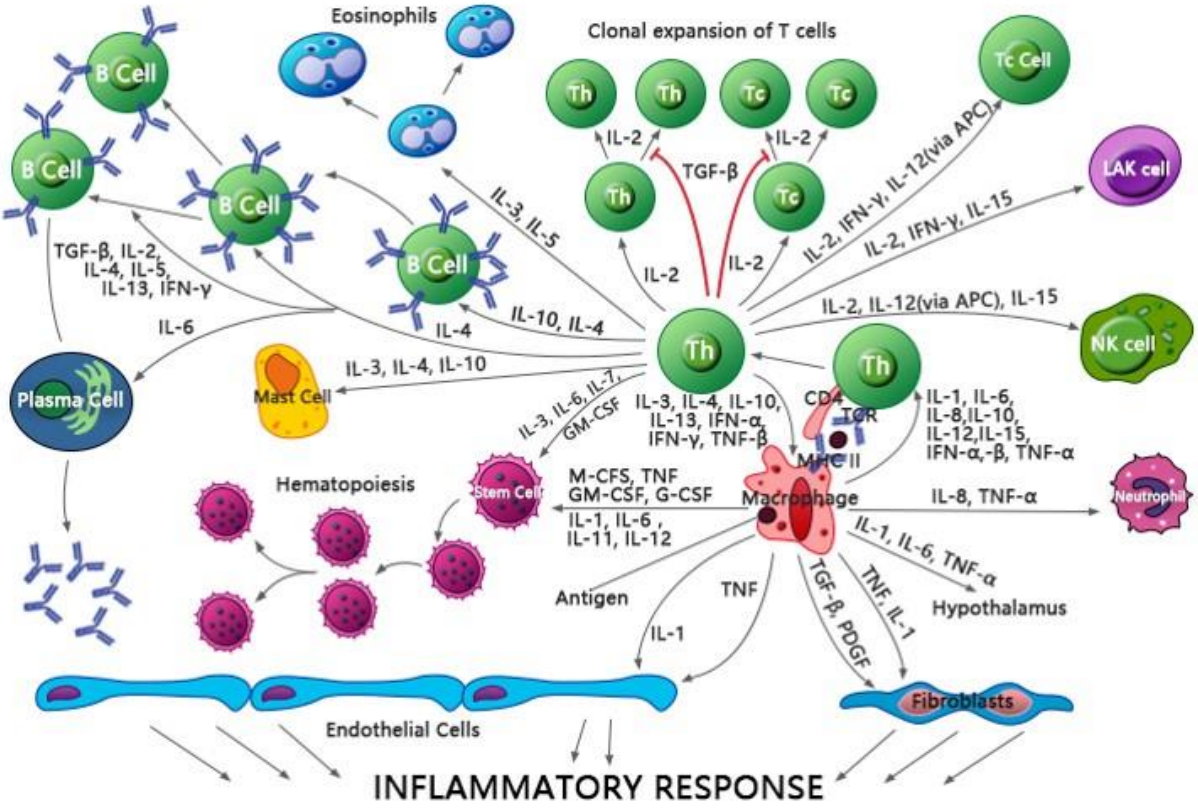

Figure 18 : cytokines, leurs cibles et réponse inflammatoire de Origene.

Cette première partie de l'introduction a permis de présenter le domaine de l'immunologie, les types cellulaires impliqués dans la première phase, la réponse immunitaire innée et ceux impliqués dans la seconde phase, la réponse adaptative, plus spécifique. Les principaux médiateurs, les cytokines, les chimiokines et autres PRR ont été présentés, ainsi que les mécanismes la réponse immunitaire. Cette grande diversité d'acteurs nous oblige à se concentrer sur un type cellulaire, dans notre cas, le macrophage. Maintenant que le modèle expérimental est présenté, la deuxième partie de l'introduction détaille le type de matériaux principalement étudié durant cette thèse.

Deuxième partie : Les nanomatériaux

Généralités

Définition nanomatériau

Il existe plusieurs définitions pour les termes « nano » selon les pays, le domaine d'utilisation, le public exposé… La Commission Européenne a adopté la recommandation de la définition suivante comme référence en 2011 :

« 'Nanomatériau' correspond à un matériau naturel, accidentel ou manufacturé qui contient des particules, dans un état libre, agrégé ou aggloméré et dans lequel au moins 50% des particules ont une ou plus de leurs trois dimensions externes comprise entre 1 et 100nm. »

La Commission Européenne s'est basée sur le rapport du comité scientifique sur les risques émergents et nouvellement identifiés pour la santé (SCENIHR), Scientific basis for definition

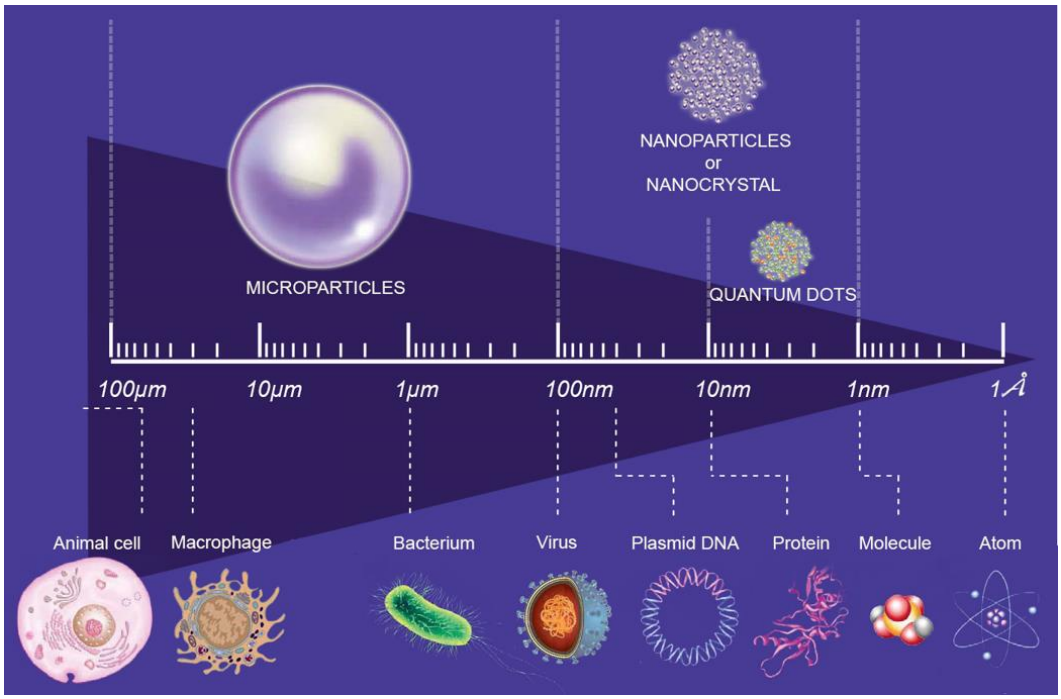

Figure 19 : Echelle de différents objets de référence. (adapté de Hamed Laroui, gastrointestinal and Liver Physiology, 2011)

of the term "nanomaterial" de 2010. Sur la figure 19, sont représentés des objets courants dans le domaine de la biologie, les nanomatériaux sont du même ordre de grandeur que les protéines, l'ADN et les virus.

En 2011, la Commission Européenne vote l'article 18 de la réglementation 2011/1869 pour imposer la mention « nano » dans la liste des ingrédients de tout produit alimentaire en contenant. Cette loi sera appliquée à partir de décembre 2014. La régulation pour les produits cosmétiques (n°1233/2009, appliquée depuis juillet 2013) définie le nanomatériau comme insoluble ou biopersistant et intentionnellement produit dont au moins une dimension externe ou structure interne est comprise entre 1 et 100nm. REACh est l'actuelle agence règlementaire qui valide la mise sur le marché d'un nanomatériau.

Il faut distinguer la nanoscience, qui est l'étude des structures et molécules de taille comprise entre 1 et 100nm, de la nanotechnologie qui utilise ces objets dans des applications pratiques (Bayda et al. 2019).

Dans la nature

Avant de découvrir les utilisations actuelles des nanomatériaux, allons voir dans la nature ce qui a inspiré leur utilisation, et découvrir comment cette dernière peut dater de plusieurs siècles. Les nano-objets sont présents dans la nature sous forme organique et inorganique (figure 20). Dans le premier cas, ils confèrent certaines propriétés à leurs propriétaires. Par exemple, les ventouses des pattes de gecko sont d'une taille proche de 200nm

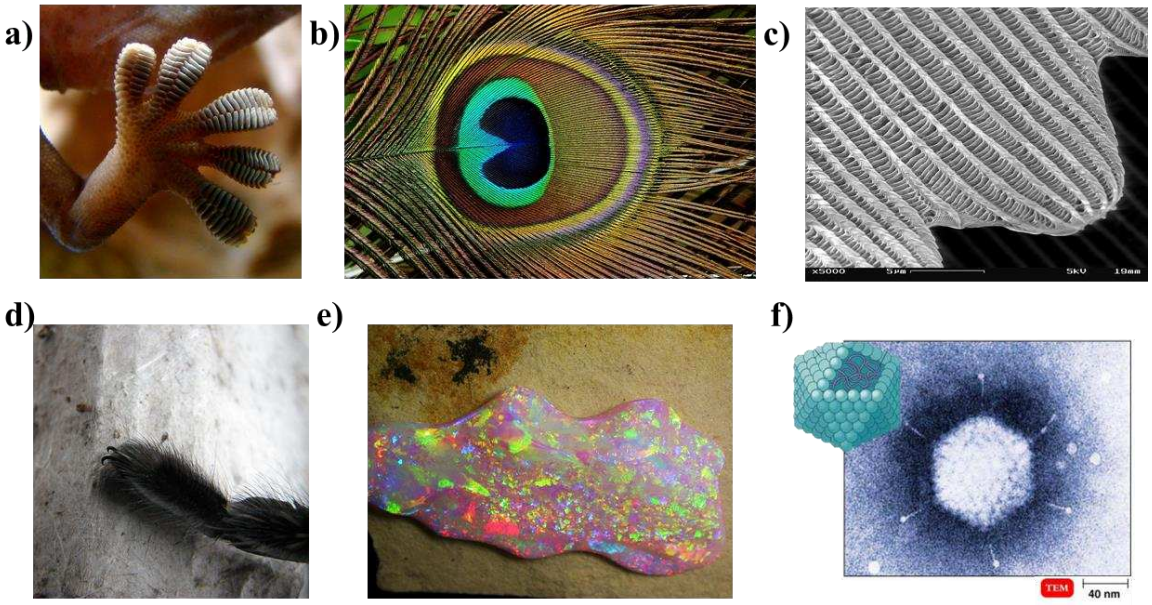

Figure 20 : Présence naturelle d'objets de taille nanométrique.

a) Ventouse de patte de gecko par Bjørn Christian Tørrissen © CC BY-SA 3.0 (doigt : 200x10-15nm)
b) Plume de paon par Schnobby © CC BY-SA 3.0
c) Aile de papillon (SEM x5000) par SecretDisc © CC BY-SA 3.0
d) Patte de tarentule (450 ± 20 nm)
e) Cristal d'opale brésilien par Daniel Mekis © CC BY-SA 3.0. Diffraction de la lumière entre les sphères de silices de différentes tailles (150-300nm).
f) Capside virale (MET mastadenovirus) de Pearson education

et grâce aux interactions de Van der Waals, lui permettent une certaine adhérence sur les surfaces lisses. Un autre exemple est la couleur irisée des plumes de paon qui intriguèrent Robert Hooke (1635-1703) dès le XVIIème siècle (Ball 2015). Les plumes mouillées perdaient leurs couleurs, il décida de les observer sous un microscope et la structure « en strie » des plumes apparurent. C'est quelques dizaines d'années plus tard, que la nanostructure des plumes fut décrite. Les bactéries, comme *Pseudomonas aeruginosa,* peuvent aussi produire des nanoparticules, par réduction ou oxydation de certains sels (de sélénium, d'argent, d'or..) afin de former les particules de taille nano (Griffin et al. 2018). Les extraits de plantes sont également capables de réactions biochimiques qui permettent de purifier par réduction les métaux (cuivre, platine, or, zinc) sous forme de nanoparticules (Kuppusamy et al. 2016). Les scientifiques utilisent ces propriétés naturelles afin de catalyser ces réactions chimiques en laboratoire.

Les formes inorganiques peuvent provenir du résultat de l'érosion, d'évènement météorologiques ou d'autres évènements naturels (Sharma et al. 2015). La cendre produite par les incendies ou les éruptions volcaniques est également un résidu de taille nanométrique, formant des particules de 100 à 200nm de diamètre sous la chaleur qui se retrouvent dans l'air

(‘What Nanomaterials Exist in Nature?’ 2018). Les déserts sont également une source de nanoparticules, et représentent 50% des nanoparticules présentes dans la troposphère (zone la plus basse de l’atmosphère, d’une épaisseur de 8 à 15km et précède la stratosphère, Larousse encyclopédie 2022). Ces particules proviennent de tempêtes de sable et sont composées principalement de silice, mais également d’aluminium, de calcium et de fer.

Les nanoparticules existent donc depuis des millions d’années dans la nature. Elles ont ensuite été utilisées par l’Homme pour des raisons esthétiques, sans vraiment identifier les matériaux ni comprendre la source de ces propriétés particulières.

Histoire

Les nanomatériaux existent depuis des centaines d’années, quelques exemples sont présentés sur la fresque chronologique (figure 24).

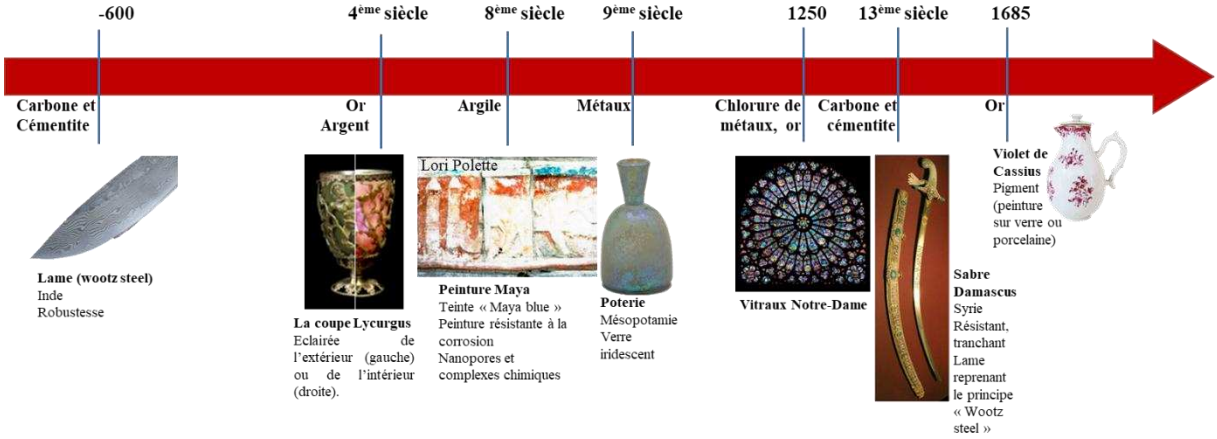

Figure 21 : Histoire et découverte de l'utilisation des nanoparticules, adapté de Nano.gov.

La première découverte d’un objet contenant des matériaux en forme nano, une lame en acier qui était constituée de nanotubes de carbone et de nanofibres de cémentite (carbure de fer) et avait été fabriqué dans le Sud de l’Inde au 6ème siècle avant Jésus-Christ (Sanderson 2006). Cette lame possède une surface qui reproduit les nervures d’une pièce en bois, grâce au mélange de nanotubes et de nanofibres. Ce sabre était reconnu pour sa robustesse. Le procédé de fabrication n’est pas totalement connu mais l’utilisation de formes nano est volontaire. De fait, il faut retenir que les nanomatériaux existent depuis longtemps et sont recherchés pour les propriétés qu’ils confèrent. C’est pour cette raison que le procédé de fabrication de cet acier résultant de ce mélange a traversé les siècles et que cet objet a inspiré les artisans pour créer l’acier du sabre de Damas à partir de la fin du 12ème siècle, plus connu de nos jours. Un deuxième objet très connu et ancien (4ème siècle) est la coupe de Lycurgue qui est constituée d’argent et de verre dichroïque, c’est-à-dire que la couleur du verre est différente selon l’exposition à la lumière. Ce verre particulier contient des nanoparticules d’or et d’argent, qui sont des particules métalliques qui lui confèrent ses propriétés colorées (Lafait et al. 2009). D’autres œuvres utilisent des nanoparticules, et l’une d’entre elles fait la fierté de la capitale française : les vitraux de la cathédrale Notre-Dame de Paris

Figure 22 : Vitraux de la rosace sud de la cathédrale Notre-Dame à Paris. Construite en 1250

(figure 22). Ceux-ci datent du XIII^{ème} siècle et sont constitués de nanoparticules d'or et d'autres métaux. Ces propriétés particulières ont été remarquées, et à partir du XIX^{ème} siècle, des scientifiques ont commencé à étudier les caractéristiques des nanoparticules. C'est ainsi qu'en 1857, Michael Faraday (1791 – 1867) démontra que la forme des nanoparticules d'or était responsable de la couleur des solutions dans lesquelles elles se trouvaient en utilisant des nanoparticules colloïdales d'or, il obtint une solution « rubis ». En 1959, Richard Feynman (1918 - 1988), développe l'idée qu'il est possible de manipuler les molécules et les atomes séparément, c'est le début de la recherche à l'échelle nano. C'est seulement en 1974, que Norio Taniguchi (1912 – 1999) utilise le terme de *nanotechnologie* : « nanotechnology mainly consists of the processing of separation, consolidation, and deformation of materials by one atom or one molecule » (TANIGUCHI 1974). Les avancées technologiques et l'amélioration des connaissances scientifiques ont permis de faire émerger ce domaine, notamment en découvrant que les caractéristiques physico-chimiques des nanoparticules permettent d'obtenir des propriétés particulières si elles sont utilisées de façon optimale. L'évolution de la technologie a permis d'apprivoiser le monde nano et c'est ainsi que la nanotechnologie émerge au XXème siècle. Une certaine maîtrise de ce domaine scientifique permet aux scientifiques de manipuler les particules, ce qui peut aboutir à la création d'œuvres originales (figure 23).

Nano-Explosions
Nanofils cobalt Fer Bore
Micrographie électronique à balayage d'un réseau de nanofils magnétiques déposés par électrolyse
(Image: Fanny Beron, École Polytechnique de Montréal, Canada)

Changement climatique
Nanotubes de carbone sur une surface de silicium
(Mr Miguel Ângel Fernández Vindel, Universidad Autonoma de Madrid/Spain)

Nano PacMan
Oxyde de cuivre
Image SEM, Diamètre 3,5 µm
Évaporation et condensation sur un substrat d'alumine
(Image: Elisabetta Comini, University of Brescia, Italy)

Ours Teddy nano
Oxyde de zinc sur une couche recouverte d'oxyde d'indium
Image SEM
(Image: Helia Jalili, University of Waterloo)

Spaghetti et boulette de viande nano
Nanofils d'Or de 100 nm de diamètre (spaghetti) et nanoparticules de silice de 1,5µm avec nanocristaux d'or sur la surface
Image SEM
(Image: Blythe G. Clark and Dan Gianola, par Thomas Cornelius – GSI Darmstadt et Gunther Richter – MPI Stuttgart)

Nanofleur
Nitrure d'indium cristallin
Synthétisée par molecular beam epitaxy
Indium et acide
(Image: PaiChun Wei, Center for Condensed Matter Science, National Taiwan University, Taipei, Taiwan)

Monde nano
Nanotube de nitrure de Bore sur un substrat de silicium
Image SEM
Diamètre environ 50nm
(Image: Chee Huei Lee, Michigan Technological University, USA)

***Escherichia coli* (*E. coli*) avec Pili et Flagelle**
AFM en condition sèche
taille de la cellule 1,9µm sur 1µm
pili de 20 nm et flagelle de 30nm
(Mr Ang Li, National University of Singapore)

Figure 23 : Exemples de création avec des nanomatériaux Nano.gov

Utilisations (manufacturées)

De nos jours, les nano-objets, objets dont au moins une dimension est à l'échelle nano selon la recommandation de l'ISO/TS 80004-1 :2015(en), sont très utilisés et existent sous diverses formes (fibres, tubes, sphères, 2D ou 3D...), divers éléments (or, argent, silice, fer, carbone…), diverses tailles (1 à 500nm) et sont produites par plusieurs méthodes (précipitation, pyrolyse, bottom-up, top-down…). Tous ces paramètres permettent d'exploiter au maximum les propriétés spécifiques de chaque type de nano-objet : antimicrobien, anti-mottant, anti-UV, texture, couleur enrichie, résistance…

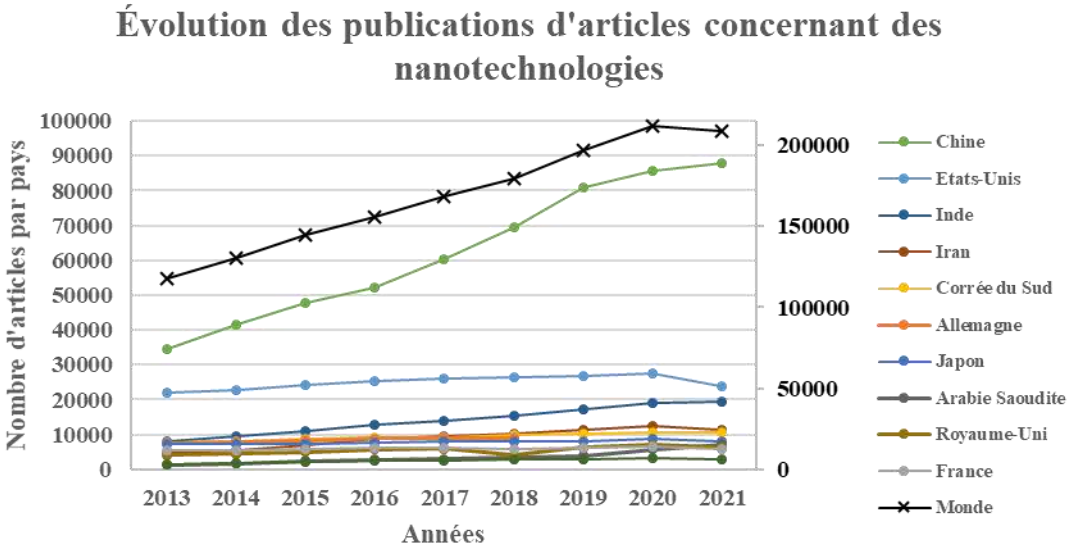

Figure 24 : Publications sur les nanotechnologies, d'après StatNano, et basé sur Web of Science. Nombre de publications par pays (axe des ordonnées principal) et nombre total de publications (axe secondaire).

En 2000, le président Clinton aux Etats-Unis lança le National Nanotechnology Initiative afin de regrouper les inventions américaines et dynamiser ce domaine émergent. Ce qui permit la création de deux grands centres de recherches sur la toxicologie humaine et l'écotoxicologie, à Los Angeles et à Duke University. Un inventaire (Consumer inventory product) a été mis en place à partir de 2005 pour recenser et enregistrer les produits contenant des nanomatériaux (Vance et al. 2015). Face à cette émergence, certains chercheurs ont essayé d'estimer l'évolution de l'utilisation des nanomatériaux, et également des domaines d'applications (Inshakova and Inshakov 2017). C'est ainsi que de nombreux paramètres sont mesurés afin de suivre cette évolution. Par exemple, le nombre de publications mondiales dans le domaine de la nanotechnologie a presque doublé en 8 ans, en passant de 118 000 à 208 000 entre 2013 et 2021, d'après StatNano (figure 24). Cette augmentation est principalement due aux articles de chercheurs chinois, mais cela se confirme également lorsqu'on regarde un autre paramètre, comme, par exemple, le nombre de brevet déposé chaque année. Au niveau mondial, le nombre de brevet enregistré est passé de 1255 à 2888 entre 2013 et 2021 (figure 25). La France est en 3ème position avec 247 brevets enregistrés en 2021. Cette importante augmentation de brevets s'explique par les propriétés particulières que confèrent les nanomatériaux, et les industries les utilisent de plus en plus.

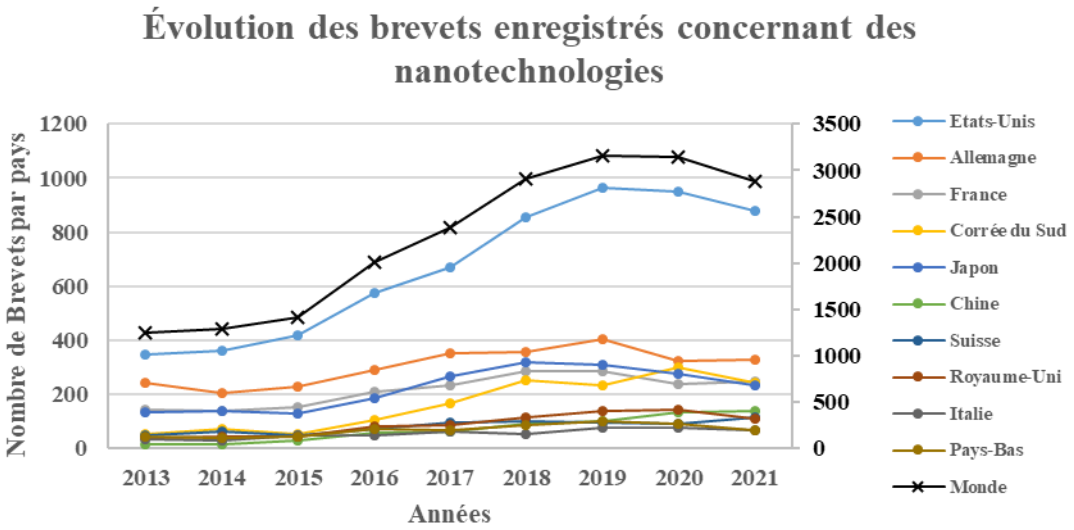

Figure 25 : Nombre de brevets (European Patent Office) déposés chaque année, d'après StatNano. Nombre de brevets par pays (axe des ordonnées principal) et nombre total de brevets (axe secondaire).

L'utilisation des nanomatériaux dans les produits du quotidien est très variée. En effet, comme illustré sur la figure 26, les domaines d'application des nanomatériaux sont divers comme l'environnement, la santé, le textile, l'électronique… Ces utilisations très différentes sont dues aux propriétés particulières des nanomatériaux. Les caractéristiques avantageuses apportées par les nano-objets permettent d'être utilisé dans plusieurs domaines, par exemple l'activité antimicrobienne peut servir pour les textiles, la santé ou les peintures. Leur utilisation s'est développée rapidement à la fin de XXème siècle en parallèle des avancées faites en nanotechnologie. Leur utilisation est devenue très courante et de plus en plus spécifique comme le montre la frise chronologique de la figure 27. L'une des premières utilisations référencée est celle de la silice dans le caoutchouc des pneus de voiture, il y a environ 800g de silice par pneu, cela permet de diminuer la résistance de roulement du pneu sur la route entraînant ainsi une économie de carburant et une diminution de la production de CO_2 comme indiqué par Solvay et Evonik. Une autre utilisation est celle de l'or ou de nanocéramiques dans certaines peintures, cela permet un auto-nettoyage du bâtiment ou de la voiture en éliminant les poussières en cas de pluie ou de rinçage, cette technique est utilisée par l'institut de soudure (TWI) (Iwakoshi, Nanke, and Kobayashi 2005). Les nanomatériaux sont également utilisés en cosmétiques, dans les textiles, l'informatique, la médecine, ou encore l'électroménager…

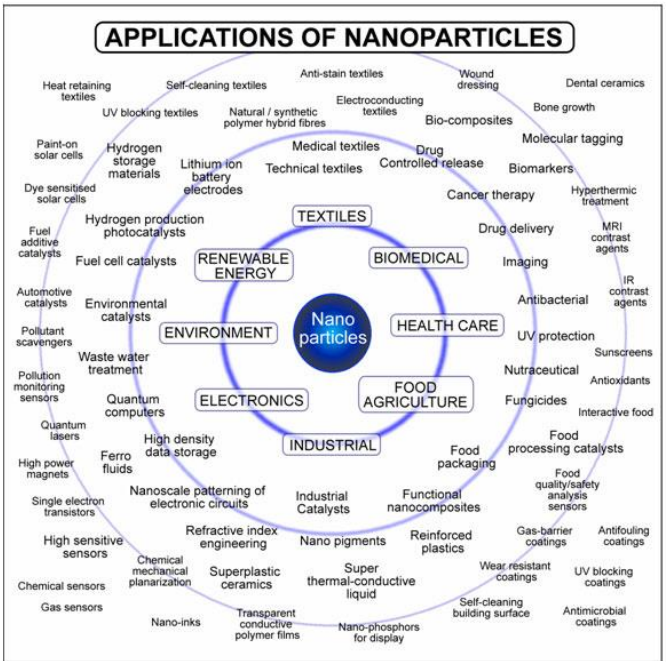

Figure 26 : Utilisations et domaines d'application des nanoparticules (Tsuzuki 2009).

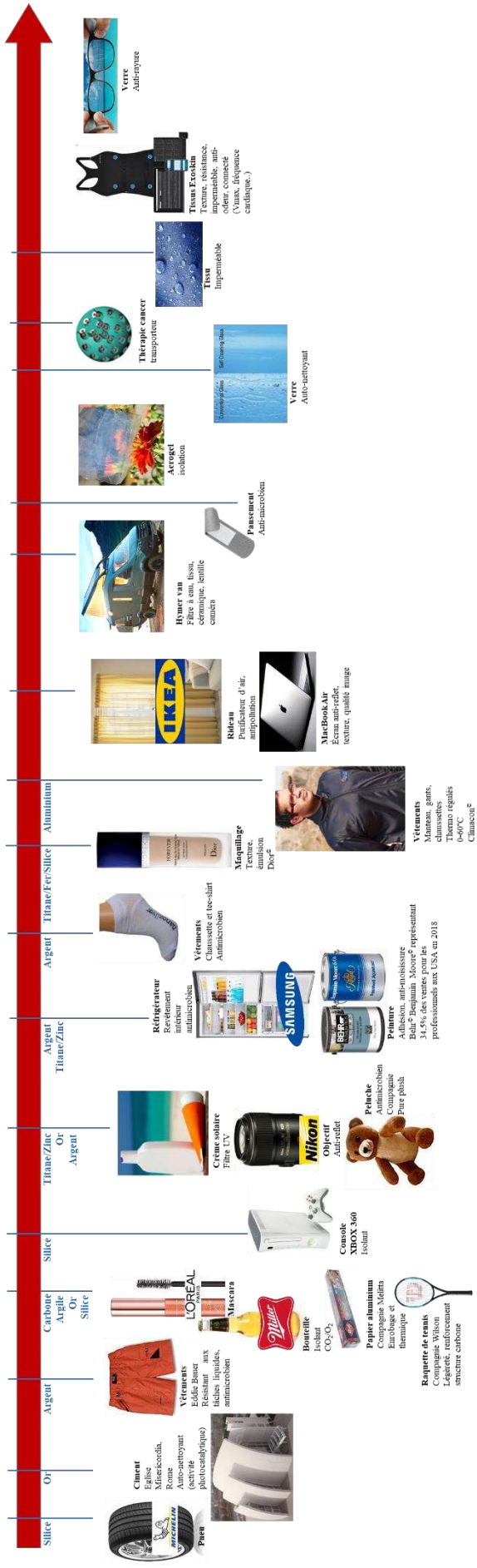

Figure 27 : Utilisation des nanomatériaux dans les objets de la vie courante.

La diversité des nanomatériaux utilisés est grande, mais certains sont plus répandus comme par exemple l'argent, le dioxyde de titane (TiO_2), le dioxyde de silicium (SiO_2), le disulfure de tungstène (WS_2) ou le graphène (figure 28). L'argent est principalement utilisé en cosmétique, dans les textiles, en médecine ou pour des applications domestiques. Le dioxyde de titane est majoritairement utilisé dans les cosmétiques, la construction ou les énergies renouvelables. Enfin, le dioxyde de silicium est utilisé dans les textiles, la construction et le secteur automobile.

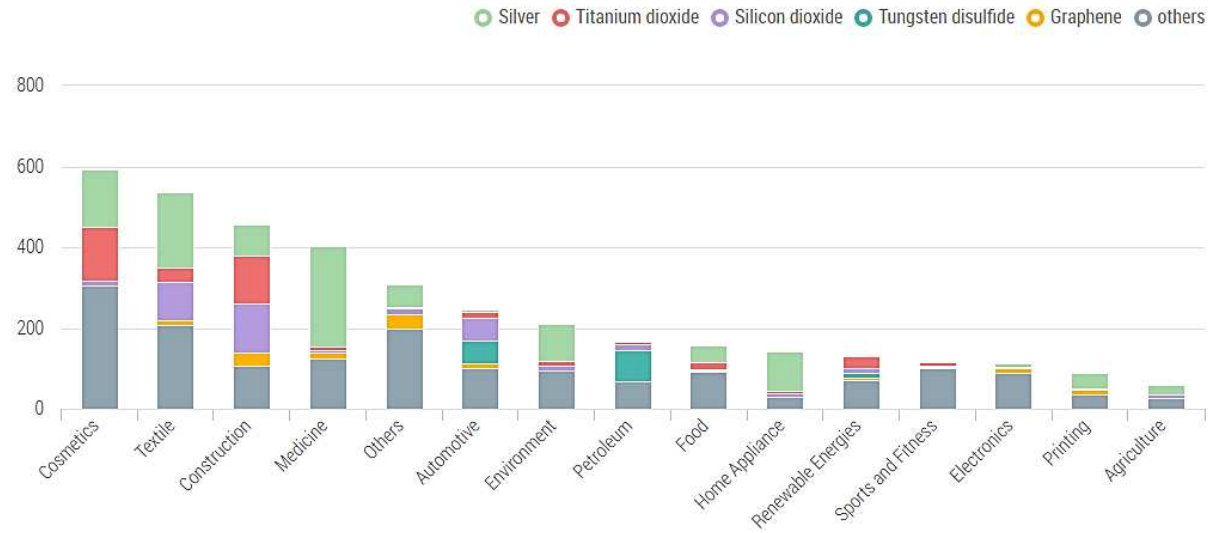

Figure 28 : Type de nanomatériaux utilisés dans différents secteurs de l'industrie, d'après StatNano.

A la nature des nanomatériaux, s'ajoutent des caractéristiques physiques telles que la forme, le mode de fabrication, ou la structure. Quelques exemples sont illustrés sur la figure 29,

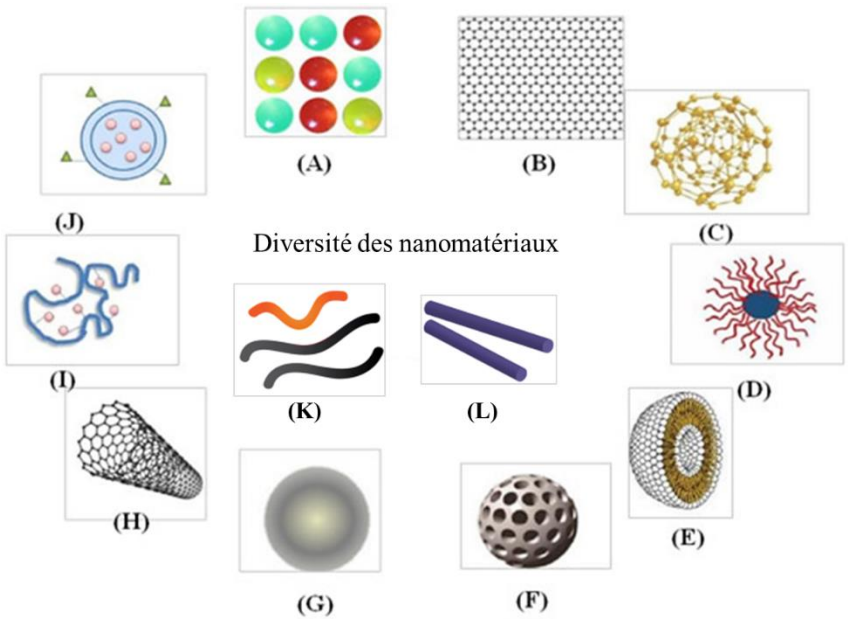

Figure 29 : exemple de formes de nanomatériaux adapté de Rai et al. (2021) et Poh et al. (2018).

(**A**) quantum dots (**B**) graphène (**C**) nanoparticules d'or (**D**) micelles de polymère (**E**) liposomes (**F**) nanoparticules de silice (**G**) nanoparticules magnétiques (**H**) nanotubes de carbone (**I**) conjugué polymère-médicament (**J**) nanoparticules de polymères (**K**) nanofils d'or, nanofibres de polymères, structure auto-assemblée et (**L**) bâtonnets métalliques, cristaux de céramique.

il s'agit ici des nano-objets utilisés dans la thérapie anticancéreuse, mais chacune des formes de nanomatériaux peut être utilisée pour une autre application. Certaines formes servent de transporteurs pour des molécules, d'autres permettent d'emprisonner une substance afin de la délivrer dans un site particulier (organe ou localisation précise) (Rai et al. 2021). Il existe aussi des formes isolées de particules, agrégées ou agglomérées (figure 30). Ces particules sont souvent caractérisées par microscopie électronique à transmission (MET) ou à balayage (MEB) afin de connaître la taille et l'état des particules.

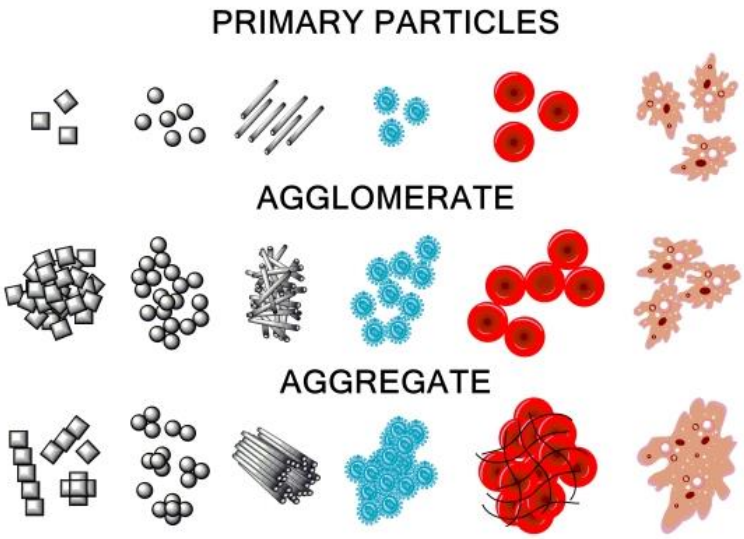

Figure 30 : Différence d'état de cluster de nanoparticules, de Roman Valuilin (2016)

Les particules primaires peuvent s'agglomérer de façon désordonnée, par des liaisons faibles en énergie (van der Waals), le retour à la particule isolée est relativement facile. Les particules agrégées forment des particules plus grosses et sont denses, elles sont reliées par des liaisons plus fortes. Il est important de connaître l'état dans lequel se trouvent les nanomatériaux, car les propriétés physico-chimiques ne sont pas les mêmes : 100 particules isolées n'ont pas les mêmes propriétés que ces mêmes particules liées. En effet la taille des matériaux, la surface spécifique (surface des matériaux en contact avec l'environnement), les propriétés optiques et

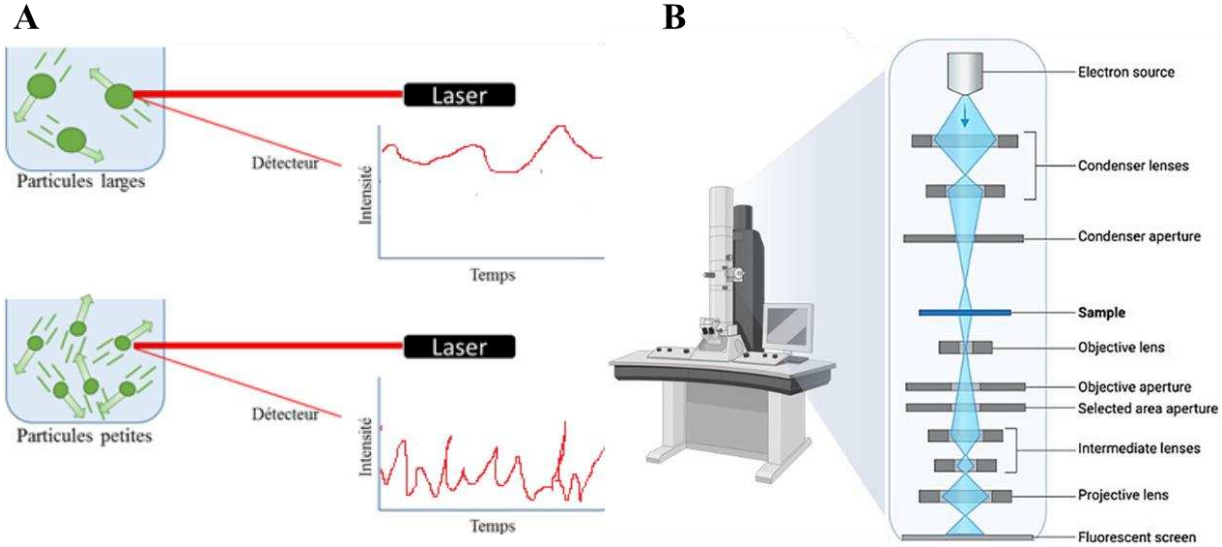

*Figure 31 : Méthodes de caractérisation des nanomatériaux. **A**) Diffusion dynamique de la lumière, par Kévin Plourde **B**) microscope électronique à transmission, créé par BioRender de Researchtweet.*

leurs capacités d'interaction changent. Il est possible de réduire la taille de ces agrégats par sonication, microfluidisation ou broyage, mais il n'y a aucune garantie que les particules résultantes soient équivalentes à la particule isolée initiale. Afin de caractériser les nanomatériaux, il existe plusieurs techniques : microscopie électronique à transmission (MET), diffusion dynamique de la lumière (DLS, dynamic light scattering.) ou une centrifugation permettant de déterminer la taille des matériaux (CPS). Le DLS permet de mesurer la taille moyenne et la distribution hydrodynamique des particules en solution, pour des tailles comprises entre 0,1nm et 1µm (figure 31A). Les principales limites sont dues à la vitesse de sédimentation et à l'impossibilité de mesurer des tailles supérieures à 10µm (says 2013). La MET permet d'obtenir des images des objets, avec différents grossissements, et de déterminer les tailles et les structures, cependant il s'agit d'une méthode qualitative, il est fastidieux de caractériser plusieurs objets afin d'obtenir une population représentative, l'échantillon doit également être transparent aux électrons (figure 31B) ('Transmission Electron Microscope (TEM) - Uses, Advantages and Disadvantages' n.d.). Une dernière méthode de caractérisation est le DLS par centrifugation, les échantillons sont centrifugés et la taille des objets réfléchissant le laser est analysée.

Les caractéristiques d'agglomération ou d'agrégation des nanomatériaux peuvent en partie être expliquées par la méthode de fabrication (figure 32). Il existe deux méthodes principales de fabrication : ascendante (bottom-up) et descendante (top-down). La technique « top-down » consiste à réduire un objet à la taille nano, en le fractionnant. Pour cela, il existe plusieurs méthodes, l'une d'elle consiste à broyer l'objet afin d'obtenir des fragments, la deuxième technique consiste à projeter un laser par pulsation pour réduire l'objet (nanotilographie) (Charitidis et al. 2014). La fabrication "bottom-up" contrôlée consiste à assembler des atomes ou molécules, jusqu'à obtenir la taille de nanomatériau désirée. Ce procédé a lieu en phase liquide, en phase gazeuse, il existe également un procédé utilisant des techniques de laser pulsé ou encore un faisceau à épitaxie moléculaire. La fabrication "bottom-

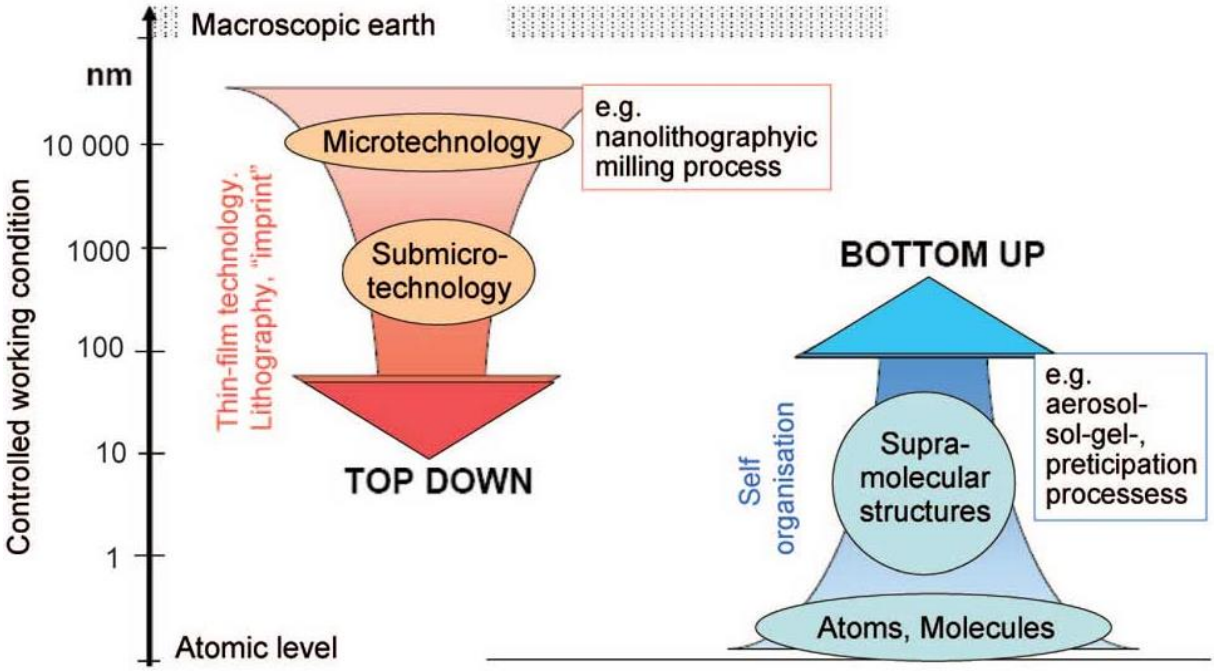

Figure 32 : Méthodes de production de nanomatériaux : top-down et bottom-up. (Image: Laboratory for Micro and Nanotechnology, Paul Scherrer Institut)

up" chaotique consiste à amener les atomes ou molécules dans un état instable et à changer rapidement d'état, les produits résultants sont retravaillés et controlés à la fin du procédé. Les techniques basées sur ce principe sont la combustion, la pyrolyse (flamme), la précipitation, l'ablation laser ou le fil explosif ('Manufacturing at the Nanoscale | National Nanotechnology Initiative' n.d.).

La diversité des nanomatériaux est grande, comme expliqué ci-dessus, de par la nature, le procédé de fabrication, l'utilisation finale, les interactions possibles, la taille ou les caractéristiques physico-chimiques. Dans les paragraphes suivants, 4 matériaux vont être détaillés : l'argent, le fer, le cuivre et la silice.

Argent

L'utilisation de l'argent sous forme de matériau date de l'époque pré-chrétienne, et a été mise en évidence par le philosophe grec Hérodote (-480 - -425). Les propriétés de l'argent sous forme nanométrique sont nombreuses, ce qui explique la diversité des domaines d'applications qui peuvent être le médical, l'alimentation ou l'industrie (X.-F. Zhang et al. 2016). L'argent sous forme de nano-objets confère des propriétés optiques, électriques, thermiques, de conductivité ou biologiques (Calderón-Jiménez et al. 2017). Sa principale utilisation est antimicrobienne (Chernousova and Epple 2013). En effet, la corrosion de l'argent est lente, ce qui permet un relargage d'ion continu et durable dans le temps. Par exemple, des cartouches de filtration contiennent des particules d'argent afin de filtrer l'eau sans développement de bactéries ou d'algues, procédé largement utilisé en Suisse. De nombreux pansements ou bandages contenant du nano-argent sont également commercialisés, qui permettent de limiter le risque d'infection. Cette application est très utilisée dans le secteur de la santé, et d'autant plus depuis ces dernières années avec l'émergence de bactéries résistantes aux antibiotiques. Les différentes propriétés de l'argent dépendent de la taille des particules utilisées, et donc de la surface disponible. Cette même propriété anti-microbienne est exploitée dans le domaine des jouets pour enfants, c'est dans ce contexte que des chercheurs de la commission indépendante des Etats-Unis, Consumer Product Safety Commission, ont mené une étude sur l'exposition des enfants aux nanomatériaux d'argent (Quadros et al. 2013). En mesurant la quantité d'ion et nanoparticules d'argent dans l'eau, l'air, l'alimentation (lait, jus de fruit) et l'urine, ils ont établi une classification des produits les plus susceptibles de libérer de l'argent. Les jouets libèrent des ions, la transpiration et l'urine des enfants contiennent également une grande quantité d'ion argent, alors que l'eau du robinet n'en contient que très peu. Ce type d'étude incite à se demander ce que deviennent les nanomatériaux utilisés et quels sont leur durée de vie et leur devenir dans l'environnement. Il a été montré que l'argent n'est pas seulement toxique pour les bactéries, mais aussi pour certaines algues, champignons et virus (Marambio-Jones and Hoek 2010) et quelques autres organismes plus complexes, la drosophile (Ahamed et al. 2010) ou le poisson zèbre (Yeo and Yoon 2009) par exemple. Chez la mouche, un stress oxydant, des dommages à l'ADN et de l'apoptose ont été observés, chez le poisson zèbre, les ions pénètrent la peau et les vaisseaux sanguins de la forme larvaire.

Les études chez l'Homme sont relativement limitées sur les formes de NMx stables, sans dissolution sous forme ionique, et si jusqu'en 2010 la présence d'argent dans l'organisme était

considérée comme non toxique (systèmes immunitaire, cardiovasculaire, nerveux ou reproducteur) avec l'argyrisme comme seule pathologie définie, cette opinion évolue (Lansdown 2010) (figure 33). La toxicité d'un nanomatériau provient principalement de la voie d'exposition, et du passage des barrières biologiques (la peau, le tractus intestinal et les poumons), et éventuellement de sa localisation dans la circulation sanguine qui a pour conséquence sa distribution dans l'organisme (système nerveux central, rein, cœur…). Une étude sur des rongeurs a montré une accumulation des nanoparticules d'argent dans le foie et les poumons, mais également les muscles, dans le cas d'une exposition cutanée (Mitra, Mehdi, and Giti 2013; Korani, Rezayat, and Arbabi Bidgoli 2013). Les études *in vitro* et *in vivo* restent cependant assez limitées.

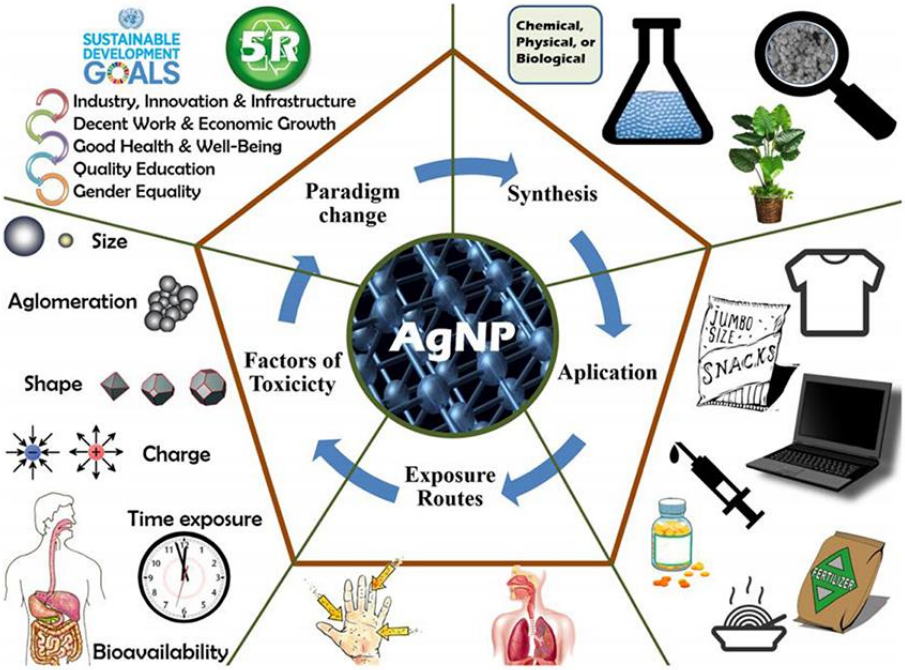

Figure 33 : Synthèse, application, mode d'exposition, et paramètres de toxicité à étudier, liés à la fabrication et à l'utilisation des nanomatériaux d'argent de Leon-Silva et al (2016, Water, air and soil pollution)

Quelques études ont montré une persistance des nanoparticules d'argent dans les poumons de rat, après une exposition sous forme d'aérosols (Anderson et al. 2015). Les poumons des rats exposés durant 6h à deux tailles de nanoparticules (20 et 110nm) sont analysés 1 jour après l'exposition, et 33% de la quantité mesurée 24h après l'exposition est toujours mesurable 7, 21 et 56 jours après l'exposition aux petites nanoparticules. Celles-ci sont principalement présentes au niveau de la jonction des bronches et des alvéoles, c'est-à-dire au niveau inférieur des poumons. A ce niveau du site pulmonaire, les macrophages représentent 98% des cellules obtenues après un lavage broncho-alvéolaire. Il s'agit donc de cellules clés pour étudier les effets de l'exposition pulmonaire à une substance.

Fer

Le fer constitue un autre type de nanomatériau largement utilisé en nanotechnologie (magnétisme, méthode de séparation, ratio surface-volume pour transport de molécules…) mais

il s'agit également d'un sous-produit de taille nano métrique résultant par exemple d'une soudure ou de la transformation de matériaux en fer. Le fer est également un composé de l'écorce terrestre, et représente environ 5% des éléments la constituant. L'Homme a donc toujours été exposé à cet élément. Cependant, ces dernières décennies, cette exposition a considérablement augmenté, et elle a également changé de voie d'exposition à cause des applications et objets pour lesquels sont utilisés les oxydes de fer. Une première exposition est celle aux sous-produits, lors de soudure ou du freinage par exemple. Les oxydes de fer sont très courants, peu coûteux et largement utilisés comme pigment ou dans la médecine, car ils sont naturellement présents dans notre organisme sous forme d'ions complexés (A. Ali et al. 2016). Les oxydes de fer utilisés pour cibler une thérapie ou pour le transport de substances se répartissent dans l'organisme en fonction de leurs caractéristiques physico-chimiques. L'accumulation principale a lieu au niveau de la rate et du foie. Les reins et le foie sont impliqués dans l'élimination des nanoparticules de fer. Une étude a également mis en évidence une persistance des nanoparticules de fer dans le système pulmonaire de rat 3 mois après l'exposition, et sans cytotoxicité apparente, mais avec une sécrétion pro-inflammatoire d'Il-1 et IL-6 (Chaves et al. 2005). La ferritine et la transferrine sont responsables de l'homéostasie en oxyde de fer de l'organisme en formant un complexe ion-protéine. Tout l'enjeu de l'utilisation des nanoparticules de fer en médecine résulte de la balance entre biocompatibilité (non toxique) et biodégradabilité, qui dépendent de la surface, de la taille des nanoparticules et de l'interaction avec les autres molécules.

Cuivre

Le cuivre est un des autres éléments régulièrement utilisés dans les nouvelles technologies. Son abondance dans l'écorce terrestre (0,006%) étant assez faible, l'exposition au cuivre est assez récente. Cet élément a été le premier métal à être travaillé par l'Homme, si à l'origine il a été

Figure 34 : Mine de Chuquicamata, Chili, par Diego Delso CC BY-SA 4.0 Wikimedia.

utilisé comme outil ou pour faire des pièces de monnaies, le cuivre est maintenant utilisé pour ses propriétés conductrices, mécaniques et de résistance à la corrosion en électricité ou en plomberie (Tableau périodique de la Royal society of Chemistry). Le sulfate de cuivre est utilisé comme pesticide en agriculture, et comme algicide pour le traitement de l'eau. Le cuivre est principalement extrait au Chili et au Pérou. La plus grande mine à ciel ouvert du monde se situe au Chili, la mine Chiquicamata à Calamata, ouverte en 1915, et qui contient 13% des réserves mondiales en cuivre. Elle s'étend sur 8km² et atteint jusqu'à 850m de profondeur, il s'agit de la 2ème mine la plus profonde (figure 34). Sa production était de 1,2Mt en 2007 et 1,73Mt en 2021 ce qui représente plus de 10% de la production mondiale en minerai (Codelco Février 2022). Cependant, l'extraction du cuivre entraîne une production importante de déchets qui touche toute la région de Calamata. Des études ont montré des taux supérieurs à la normale d'arsenic et de cuivre dans les cheveux des travailleurs mais également des enfants de 6 ans, vivant dans un périmètre de 1500m autour de la mine (Jamett et al. 1991). Chez les mineurs, les taux étaient supérieurs aux données bibliographiques (4 fois pour l'arsenic, et 3 fois pour le cuivre), la valeur d'exposition professionnelle pour l'arsenic était fixée à 5ppm dans les années 90, le taux mesuré chez les mineurs était de 15,14ppm. Chez les enfants le taux mesuré d'arsenic était de 19,25ppm (contre 3,03ppm dans la littérature) et 30,8ppm contre 15,4ppm pour le cuivre. Les mineurs sont régulièrement en grève pour demander une amélioration des conditions de travail mais aussi une prolongation de la couverture santé après leur retraite (actuellement de 5 ans), les données sur l'état de santé ou les maladies professionnelles des mineurs ne sont pas répertoriées. Si le cuivre est un élément essentiel pour le corps humain, étant donné qu'un adulte nécessite 1,2mg de cuivre par jour pour un bon métabolisme énergétique, de fortes doses de cuivre peuvent s'avérer toxiques. Ces expositions anormalement élevées impliquent des conséquences potentiellement graves pour la population, et cela nécessite d'être étudié. Cette toxicité s'observe dans le cas de maladies génétiques (maladies de Wilson et de Menkes) dans lesquelles les mécanismes d'excrétion du cuivre sont déficients (Bull and Cox 1994). Elle s'observe aussi pour des populations exposées à de fortes concentrations de cuivre, comme dans les régions viticoles (Dixon 2004) avec des pathologies parfois sévères (Pimentel and Menezes 1975; Šantić et al. 2005).

Silice

Le silicium est le deuxième composé le plus abondant dans la nature (après l'oxygène), il représente 28% des éléments de la lithosphère ('Abundances of the Elements in Earth's Crust, - Biosphere - BNID 110362' n.d.). Le silicium est présent sous forme de silicate dans les roches (granite, basalte, argiles…), le sable (dioxyde de silice) ou les fossiles (terre de diatomée), il est utilisé pour le ciment et le verre mais également pour des produits plus techniques.

Ces dernières décennies, la silice est aussi produite de manière industrielle, et utilisée en grande quantité. En 2020, la France a produit ou importé plus de 97 000 tonnes de silice malgré la crise sanitaire, et 180 000 tonnes en 2019, contre 155 000 tonnes en 2014. Son utilisation est très variée grâce à ses propriétés particulières et diverses. Par exemple, la silice est connue pour son rôle abrasif dans les dentifrices, et comme renfort dans les pneumatiques et les polymères ou encore pour ses propriétés anti-agglomérantes dans l'alimentation déshydratée ou en poudre. Pour ces usages, la silice est présente sous forme nanostructurée et

amorphe. Une silice amorphe de synthèse est fabriquée par l'Homme et constituée d'atomes de silicium et d'oxygène désorganisés en opposition à la silice cristalline qui est composée de silicium entouré de façon répétée d'oxygène et organisée en motifs cristallin.

Formes

- La silice cristalline : forme naturelle

La silice cristalline peut se présenter sous différentes formes : quartz, cristobalite, tridymite, coésite, moganite, stishovite, calcédoine… pour ne citer que quelques exemples. Elle se trouve donc dans de nombreux rochers et le sable. Les travailleurs peuvent être exposés aux poussières de silice cristalline (« respirable particles ») notamment lorsqu'ils coupent, ou travaillent la roche et le sable. Les domaines d'exposition sont les activités minières, la céramique, la porcelaine, la joaillerie, la fonderie, ou l'utilisation du sable pour l'abrasion dans le domaine maritime ('OSHA's Respirable Crystalline Silica Standard for General Industry and Maritime', n.d.). Ces particules fines peuvent être inhalées et se déposer dans les poumons, et causer la silicose ou des cancers pulmonaires. Dans la majorité des cas, ces pathologies surviennent après des années d'expositions aux silices cristallines. Dans ce rapport de l'agence gouvernementale Occupational safety and Health Administration, certaines requêtes ont été soulevées :

- déterminer la quantité à laquelle sont exposés les travailleurs,
- protéger les travailleurs de la limite d'exposition professionnelle (50µg/m3 sur 8heures),
- limiter l'accès aux zones dans lesquelles cette dose serait atteinte ou dans le cas contraire fournir des appareils respiratoires,
- contrôler la qualité de l'air, offrir un suivi médical régulier comprenant des examens radiographique des tests des fonctions pulmonaires,
- informer les travailleurs des risques auxquels ils sont exposés
- répertorier ces données afin de les analyser.

Les effets d'une exposition à la silice cristalline sont largement référencés dans la littérature, comme (Rees and Murray 2007) mais aussi (Pollard 2016; Thakur et al. 2009; Parks, Conrad, and Cooper 1999). Ces effets ont par exemple été analysés dans cette revue de (Castranova and Vallyathan 2000). Les effets de l'exposition à la silice cristalline sur différents modèles sont présentés ; *in vitro*, *in vivo* et santé humaine. Les pathologies résultantes sont la pneumoconiose et l'inflammation aiguë ou chronique de silicose. Les mécanismes sous-jacents sont la cytotoxicité de la poussière de silice provoquant des dommages cellulaires et la production de protéases. Le deuxième mécanisme est l'activation de la réponse antioxydante des cellules phagocytaires, suivi du recrutement de lymphocytes par les macrophages, induisant la production de cytokines proinflammatoires et d'espèces réactives de l'oxygène. Le dernier mécanisme est la sécrétion de facteurs de croissance par les macrophages et l'épithélium alvéolaire induisant la prolifération des fibroblastes. Dans un rapport de 1994, le National Institute for Occupational Safety and Health (NIOSH) estimait que 2,3 million de travailleurs avaient été exposés à des poussières de silices cristallines en 1983, et dans les années 2000, 1500 cas de silicose étaient recensés chaque année. Entre 1968 et 1990, 13 744 décès furent

attribués à la silicose, leurs nombre diminuant fortement de 1157 en 1968 à 301 en 1988. Un rapport du gouvernement du Royaume-Uni estime que 216 cas de silicose entre 1996 et 2017 ont été enregistrés par le programme anglais SWORD (Surveillance of Work-related and Occupational Respiratory Disease). Les pathologies liées à l'exposition à la silice peuvent survenir des années après cette exposition, et sont souvent létales. Si cette prévalence a fortement diminué depuis le milieu du XXème siècle, c'est notamment grâce aux mesures de prévention mises en place (équipements de sécurité, diminution de l'exposition, détermination des valeurs limites d'exposition…).

- La silice amorphe de synthèse : forme manufacturée

Dans ce contexte, les études sur les caractéristiques et les effets des silices amorphes de synthèse sont justifiées. Il existe de nombreux polymorphes de silice répertoriés, comme illustré sur la figure 35. Le chapitre sur la silice de (Flörke et al. 2008) présente la majorité des formes existantes.

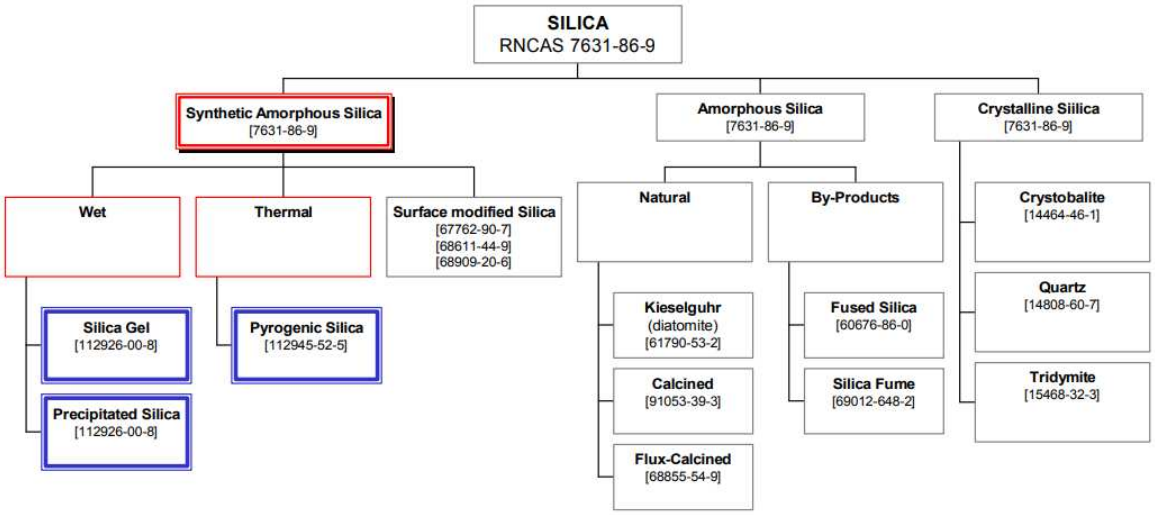

Figure 35 : Polymorphes de silices, de CEFIC-ASASP, 2002

Il existe cinq formes de silices amorphes de synthèse (SAS) : précipitée, gel, fondue, colloïdale et pyrogénée.

Tout d'abord, la silice amorphe de synthèse précipitée, produite par voie humide dans un solvant, est utilisée comme un agent de renforcement dans les caoutchoucs et également comme un agent nettoyant et polissant dans les dentifrices (Murphy et al. 2012). La silice précipitée est aussi utilisée comme un anti-mottant dans la nourriture ou encore comme additif pharmaceutique (Flörke et al. 2000). Et pour finir, l'additif alimentaire E551 est commercialisé sous la forme de silice amorphe de synthèse et possède une taille de particules primaires de 10-20 nm. Cet additif se compose d'agrégats d'agglomérats d'une taille micrométrique, proche de la fumée de silice mais ne contenant pas de partie cristalline (Dekkers et al. 2011). Dans le contexte occidental actuel, la dose ingérée est estimée à 35 mg/jour (Powell et al. 2010) chez l'adulte.

Les principaux producteurs en Europe sont Evonik corporation, W.R. Grace & Co, PPG industries et Solvay. La répartition de la production de silice entre ces différentes formes est présentée ci-après, sur la figure 36. Les différentes formes de silices sont détaillées ci-dessous.

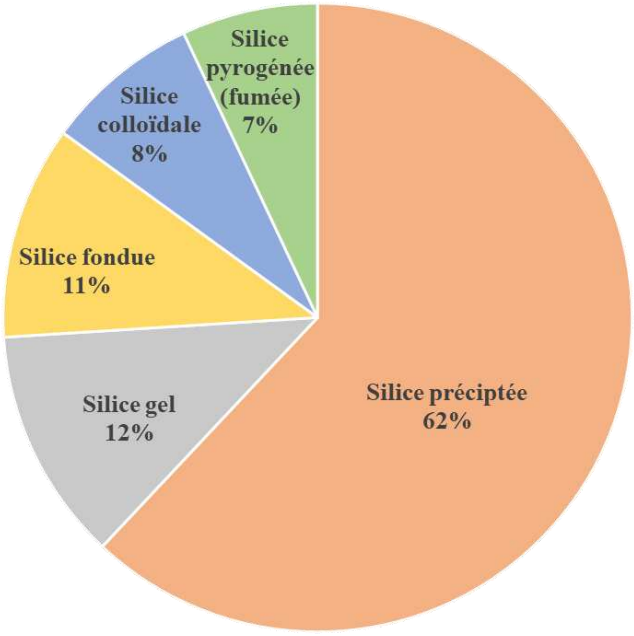

Figure 36 : Consommation mondiale des différents types de silices amorphes de synthèse, adapté de IHS Markit, décembre 2021.

La **silice pyrogénée** ou fumée est principalement utilisée pour la production d'élastomère de silicone ou bien dans le ciment, pour améliorer la résistance et la durabilité. Elle se présente sous forme de poudre de grains très fins, elle est obtenue soit comme un sous-produit de la production du silicium par réduction du quartz dans les fours à arcs-électriques (1700°C), soit par combustion de tetrachlorosilane ($SiCl_4$) dans une flamme d'hydrogène et d'oxygène. Elle est composée de petites particules primaires qui ont souvent une grande surface spécifique, ces particules sont souvent présentes sous forme d'agrégats.

La **silice colloïdale** est une dispersion de particules de SiO_2, produites en polymérisant des noyaux de silice à partir de solutions de silicate dans des conditions alcalines pour former des sols de silice de taille nanométrique avec une surface élevée. Le pH alcalin induit une charge négative à la surface des nanoparticules de silice, ce qui permet aux particules de silice de se repousser mutuellement et de former une dispersion stable, ou colloïde. Ces particules sont de tailles inférieures, par rapport aux autres SAS, et grâce à la charge présente à leur surface, elles ont moins tendance à s'agglomérer. Cette forme de silice est principalement utilisée en industrie électronique ou semi-conducteurs comme agent de polissage, pour la planarisation chimico-mécanique des semi-conducteurs (tranche de silicium). Les SAS colloïdales sont également utilisées dans les usines de papeterie, dans les systèmes de rétention et drainage avec un polymère. Les caractéristiques de cette forme de silice sont nombreuses : les tailles peuvent varier de 5 à 40nm avec une distribution plus ou moins homogène, leur stabilité peut varier selon les éléments de surface et leur charge, mais elle se situe généralement autour d'un pH 8-10,5. Ce procédé de fabrication n'a été maîtrisé que dans les années 40 où la quantité de silice a pu être optimisée, LUDOX® et DuPont utilisent cette SAS colloïdale comme antidérapant dans les produits d'entretien du sol.

La **silice fondue** ou **verre de silice** est une forme très pure de silice obtenue par fusion de quartz ou de sable contenant une grande quantité de silice. Les propriétés de ce verre d'une grande qualité sont la pureté, la résistance (thermique, radiation et mécanique), et la transparence (des ultraviolets aux infrarouges). Cette forme de silice est utilisée pour ses propriétés optiques, notamment dans la fibre optique, le verre de quartz pouvant conduire la lumière sur plusieurs kilomètres. Il est aussi utilisé en verrerie de laboratoire, dans l'industrie des semi-conducteurs, dans les systèmes optiques (prismes, miroirs des instruments somme par exemple les rétroréflecteurs lunaires ou satellites géodésiques, comme LAGEOS ('LAGEOS: LAser GEOdynamic Satellite' n.d.)). Cette silice est produite sous une flamme d'oxygène et hydrogène.

Le **gel de silice** est utilisé comme adsorbant et solution déshydratante comme par exemple dans les cosmétiques ou la litière pour les chats. Il s'agit d'un hydroxyde de silicium ($SiO_2 \cdot x\ H_2O$), qui se présente sous forme solide et se distingue par sa microporosité et sa surface hydroxylée. La structure du gel de silice est un réseau aléatoire interconnecté de particules de silicate polymérisées, appelées micelles, qui sont sphéroïdales et ont un diamètre de 2 à 10 nm (ce qui donne des surfaces spécifiques élevées d'environ 300 à 1000 m^2/g de SiO_2). C'est cette structure en micelles qui lui confère ses propriétés absorbantes. Une équipe de chercheur a développé un système peu conventionnel de production de gel de silice, à partir de cendres de noix de coco qui permet de conserver ses propriétés déshydratantes (Pattanayak,DK et al. 2021).

La **silice précipitée** représente la majorité des silices amorphes de synthèse (62%). C'est sur cette forme de silice que reposent mes travaux de thèse.

Production de la silice précipitée

C'est le chimiste suédois Jöns Jacob Berzelius en 1824 qui a obtenu du silicium en chauffant du fluorosilicate de potassium avec du potassium, puis après une phase de purification

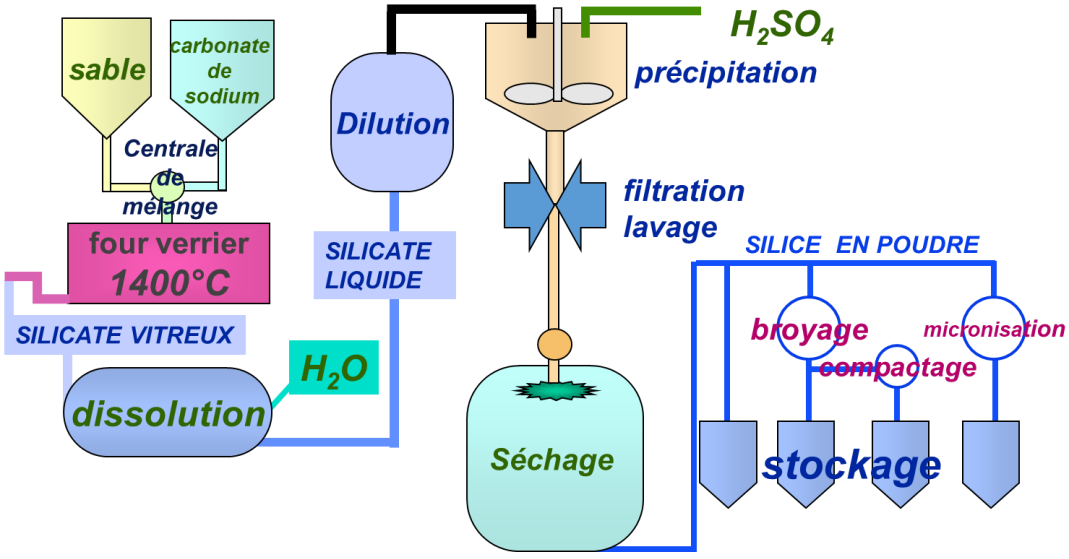

Figure 37: Production de silice précipitée (Solvay GBU Silica)

en eau, et il a ainsi obtenu une poudre de silicium relativement pure (Periodic Table, Royal society of chemistry). Le silicium peut être associé à l'oxygène pour former des dioxydes de

silice ou à de l'oxygène et d'autres éléments pour former des silicates. Le procédé de fabrication des silices amorphes de synthèse précipitée est illustré sur la figure 37. Le sable (source de silice) et le carbonate de sodium sont mélangés puis chauffés dans un four à 1400°C, le silicate vitreux (ainsi formé) est ensuite récupéré puis dissout dans de l'eau. Le silicate liquide va ensuite précipiter avec l'ajout de sulfate d'hydrogène (acide sulfurique), puis après une étape

Figure 38: Forme de silice après compactage, broyage et micronisation (Solvay GBU Silica). Les granules ont une taille de 1 à 3mm, les microperles d'environ 200µm et les poudres de 15 à 30µm.

de filtration puis lavage, le « gâteau » (silice + eau) est séché pour obtenir la poudre de dioxyde de silicium. Différents traitements peuvent ensuite être réalisés afin d'obtenir des caractéristiques particulières : micronisation, broyage suivi ou non d'un compactage (figure 40). Les silices en poudre produites possèdent des surfaces spécifiques comprises entre 60 et 300m²/g, ce qui leur permet d'avoir des applications différentes.

Solvay produit plus de 400 000 tonnes de silice chaque année, dont environ 100 000 tonnes à Collonges-au-Mont d'or (69 660, France). Pour rappel, l'ANSES estime que 180 000 tonnes ont été produites ou importées en France, en 2019, contre 155 000 tonnes en 2014 (Rapport ANSES, 2015). A titre de comparaison, en 2020, la production de l'Union européenne est estimée à environ 866 000 tonnes.

Utilisation de la silice précipitée

La silice amorphe de synthèse précipitée, produite par voie humide, est utilisée comme un agent de renforcement dans les caoutchoucs et également comme un agent nettoyant et polissant dans les dentifrices (Murphy et al. 2012). La silice précipitée est aussi utilisée comme un anti-mottant dans la nourriture ou encore comme additif pharmaceutique (Flörke et al. 2000). Et pour finir, l'additif alimentaire E551 est commercialisé sous la forme de silice amorphe de synthèse et possède une taille de particules primaire de 10-20 nm. Cet additif se compose d'agrégats d'agglomérats d'une taille micrométrique, proche de la fumée de silice mais ne contenant pas de partie cristalline (Dekkers et al. 2011). La dose ingérée est estimée à 35 mg/jour (Powell et al. 2010) chez l'adulte, dans un régime de type occidental moderne. Ces utilisations sont présentées sur la figure 39.

Figure 39: Applications de la silice amorphe de synthèse précipitée produite par Solvay

Dans ce contexte d'utilisation croissante et d'exposition quotidienne, il est important de connaître la dose à laquelle les travailleurs et les consommateurs sont exposés mais également d'examiner les effets de la silice amorphe industrielle.

Exposition

De nombreuses études sur les nanomatériaux de silices amorphe de synthèse (SAS) ont déjà été réalisées et publiées dans la littérature scientifique mais en utilisant un scénario d'exposition à une haute dose unique de silice (Johnston et al. 2000; Joshi, Gilberti, and Knecht 2017). Dans le cas de ces nanoparticules, il faut prendre en compte les faibles doses et les différentes voies d'exposition auxquelles sont exposés les industriels qui produisent cette silice mais également les consommateurs qui, quotidiennement, mangent, absorbent ce composé minéral.

Il existe différents types d'exposition professionnelle aux nanomatériaux, d'après un rapport de 2012 de l'Institut National de recherche et de la sécurité (INRS) : premièrement celle liée au procédé de fabrication qui génère des NMx mais dont ce n'est pas la finalité. Dans ce premier cas, il peut s'agir de procédés thermiques, mécaniques ou de combustion tels que le coupage, le soudage, ou le polissage des métaux, le fumage de denrées alimentaires, les émissions de moteurs (diesel, essence ou gaz), l'application de résines ou cires… Le deuxième type d'exposition professionnelle est celle liée à la fabrication et à l'utilisation des NMx. Elle concerne donc la production, le conditionnement, l'expédition, la réception, l'entreposage et enfin l'utilisation des NMx, mais également le nettoyage et l'entretien des locaux et

équipements et l'élimination des déchets. Dans ces deux cas, les sources d'exposition sont nombreuses, et nécessitent de prendre certaines précautions.

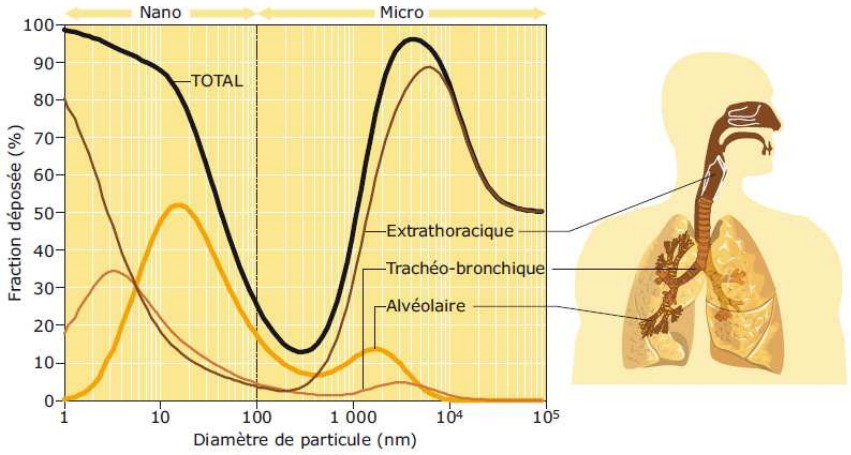

Figure 40 : Dépôt théorique total et régional des particules dans le système respiratoire chez l'homme, en fonction du diamètres des particules inhalées, de l'INRS (2012), modèle de la commission internationale de protection radiobiologique.

Les voies d'expositions sont elles aussi diverses : l'inhalation, l'ingestion ou le contact cutané. Cela est dû aux procédés de fabrication et d'utilisation pour les travailleurs mais également à la diversité des produits contenant des NMx, pour les consommateurs. La principale voie d'exposition est l'inhalation, notamment pour les travailleurs, une fois les particules dans le système respiratoire, elles peuvent être exhalées ou bien se déposer à différents niveaux du système respiratoire. Le site de dépôt dépend de la taille, de l'agglomération ou agrégation et du comportement dans l'air de ces nano-objets (figure 40). Il a été montré que les objets compris entre 10 et 100nm se déposent majoritairement au niveau des alvéoles, les objets inférieurs à 10nm ou micrométriques se retrouvent dans les voies supérieures, la trachée ou les bronches. La deuxième voie d'exposition est la voie gastro-intestinale, celle-ci concerne les travailleurs et les consommateurs. Tout d'abord, les particules inhalées peuvent, après déglutition, se retrouver ingérées. Ensuite, les nano-objets sont également présents dans l'alimentation (emballage ou additif alimentaire)(Störmer et al. 2017).

La dernière voie d'exposition, cutanée, concerne elle-aussi les travailleurs et les consommateurs. Les travailleurs sont exposés en cas de dépôt des poussières produites lors des manipulations des matériaux, les consommateurs sont exposés via les cosmétiques, ou les textiles par exemple. Cette pénétration peut être favorisée en cas de lésion, de peau fragilisée, de sueur, de flexion de la peau…elle dépend également de la taille, des propriétés de surface et de l'élasticité des nano-objets. Il a été montré que les nanoparticules de dioxyde de zinc et titane présentes dans les crèmes solaires restent dans les couches superficielles de la peau (intacte), et cela grâce notamment à leur taille (TiO_2 : quelques µm, ZnO : 30-200nm) (Baroli 2010). Cependant, une dégradation des NMx pourrait induire un passage de la barrière cutanée, de même qu'une peau altérée pourrait faciliter le passage des nanoparticules dans les couches inférieures.

Le devenir des NMx entrés dans l'organisme dépend de la voie d'exposition et de l'élimination par l'organisme (clairance). Il existe un procédé chimique qui implique la dissolution des NMx solubles dans les fluides biologiques (surfactants pulmonaires, salive, sucs gastriques, mucus intestinal...). Dans le cas d'une élimination chimique insuffisante, ou pour

des NMx peu solubles, l'élimination physique entre en jeu. Les NMx inhalés peuvent être éliminés par transport muco-ciliaire jusqu'à la bouche ou le nez, puis évacuer par déglutition ou éternuement/mouchage. Les NMx présents dans les alvéoles pulmonaires ou les autres sites d'entrées, sont majoritairement phagocytés par les macrophages environnants. Cependant, certains nano-objets sous forme particulaire peuvent ne pas être phagocytés efficacement par les macrophages, ce qui résulte en une accumulation dans les alvéoles pulmonaires et peut causer une inflammation. Ces nano-objets peuvent aussi franchir les barrières biologiques et migrer vers les organes comme le foie, le cœur ou les ganglions, et dans certains cas jusqu'au système nerveux central (Guglielmotti et al. 2015).

L'utilisation croissante des nanomatériaux ainsi que ces problématiques d'exposition et d'effets potentiels sur l'organisme ont mené les autorités à s'interroger sur les dangers liés aux nanomatériaux. Des études se sont développées et la règlementation s'est précisée en parallèle. C'est ainsi que des limites d'exposition professionnelle ont été établies ainsi que des consignes sur les équipements de protection à mettre en place, par exemple.

La caractérisation de l'exposition professionnelle a débuté il y a une cinquantaine d'année, en France. Elle est caractérisée quantitativement par la concentration massique moyenne des particules dans l'air (mg/m^3 ou $\mu g/m^3$ d'air) pour une période donnée. La valeur limite d'exposition professionnelle en France est fixée aujourd'hui à 0,1mg/m3, d'après le rapport de l'Institut national de recherche et sécurité (INRS). Le rapport de l'INRS de décembre 2019 rassemble les données d'exposition humaine et de tests toxicologiques, une conclusion sur les effets de l'exposition professionnelle n'est pas possible à ce stade. Une enquête est en cours sur l'étude des biomarqueurs d'effets précoces de l'exposition aux SAS, menée de 2019 à 2023, sur des travailleurs exposés. Cette enquête permettra de renforcer les connaissances actuelles sur l'exposition aux SAS et éventuellement d'adapter les mesures de prévention pour diminuer ou supprimer le risque.

Réglementation

OMS

Il existe plusieurs règlementations des nanomatériaux, et à différentes échelles. Elles évoluent en fonction des nouvelles découvertes concernant les nanomatériaux mais aussi selon leurs utilités et leurs propriétés.

Au niveau international, l'Organisation mondiale de la santé (OMS – world health organization WHO) s'intéresse aux nanomatériaux et a élaboré des lignes directrices contenant des recommandations pour protéger les travailleurs contre les risques potentiels liés aux nanomatériaux manufacturés (NMx) ('Principles and Methods to Assess the Risk of Immunotoxicity Associated with Exposure to Nanomaterials' n.d.). Ce document est également disponible en français, traduction de l'Institut de recherche Robert-Sauvé en santé et en sécurité du travail (IRSST) ('Lignes directrices de l'OMS pour la protection des travailleurs contre les risques potentiels des nanomatériaux manufacturés', n.d.). Leur politique est le principe de précaution, c'est-à-dire qu'en cas d'incertitude sur les effets (indésirables) sur la santé, l'exposition doit être réduite. Les mesures prises afin de réduire l'exposition doivent en priorité

être proche de la racine du problème, et seulement en dernier recours, le port d'un équipement de protection individuel sera envisagé (afin d'entraver au minimum les travailleurs). Afin de rédiger ces lignes directrices, l'OMS se base sur 3 axes principaux. Tout d'abord, les tests de toxicité ne pouvant être réalisés sur l'ensemble des NMx existants, elle recommande de regrouper les NMx en catégorie (toxicité spécifique, forme de fibres, forme de particules granulaires biopersistantes…). Ensuite, le deuxième axe s'oriente autour de l'éducation et la formation des travailleurs aux dangers potentiels d'une exposition, en expliquant les problèmes de santé et de sécurité spécifiques aux NMx. Enfin, l'implication des travailleurs dans les différentes phases d'évaluation et du contrôle des risques permet une meilleure compréhension de ces derniers. Dans le but de couvrir ces trois axes, les recommandations sont réparties en sous parties : Evaluer les risques sanitaires des NMx, Evaluer l'exposition aux NMx, Contrôler l'exposition aux NMx, Veille sanitaire et Formation et implication des travailleurs. Les données d'expositions et de toxicité n'étant pas connues pour tous les NMx, l'OMS suggère de prendre comme référence un NMx similaire et référencé.

OCDE

L'Organisation de coopération et de développement économique (OCDE) est un organisme international, regroupant 34 pays, très actif dans le domaine de la sécurité des nanomatériaux. En 2006, un groupe de travail des nanomatériaux manufacturés (GTNM) a été mis en place, il vise à « promouvoir la coopération internationale en matière de sécurité des NMx manufacturés dans le secteur de la santé humaine et de l'environnement afin d'aider à ce que leur développement se fasse en toute sécurité » (‘Sécurité Des Nanomatériaux Manufacturés - OCDE’ n.d.). Ce groupe est lui-même divisé en quatre groupes de pilotage : Test et évaluation des NMx manufacturés, Évaluation des risques et du programme de réglementation, Mesure de l'exposition et de son atténuation et De l'utilisation durable des NMx manufacturés. Le premier groupe effectue des tests sur un panel de NMx sélectionnés et représentatifs dans le but de, premièrement, comprendre les propriétés intrinsèques qui peuvent s'avérer pertinente pour évaluer l'exposition et les risques, deuxièmement, valider les méthodes de tests actuelles ou éventuellement de développer d'autres méthodes, et enfin concevoir des tests standardisés. Le choix des NMx constituant le panel est basé sur les propriétés physico-chimiques, l'évolution dans l'environnement, la toxicologie environnementale, la toxicologie chez les mammifères et la sécurité du matériau. Le deuxième sous-groupe de travail fait principalement le lien entre les résultats des tests et la règlementation en vigueur, et essaie également de regrouper les NMx par famille en fonction des résultats aux tests. Le troisième sous-groupe de travail évalue l'exposition aux NMx en se basant sur des prélèvements dans le milieu professionnel principalement, et en adaptant les méthodes de mesure et d'évaluation de l'exposition. Ces études permettent de mettre en place des techniques afin de diminuer cette exposition, et également d'améliore la gestion des déchets. Le dernier sous-groupe de travail cherche les avantages à long terme de l'utilisation des NMx manufacturés, il étudie également leur cycle de vie afin de diminuer l'impact environnemental et d'atténuer les incertitudes liées à la nanotechnologie.

Depuis la mise en place de ce groupe de travail, l'OCDE a publié 103 rapports sur la sécurité des NMx manufacturés. Les tests effectués pour rédiger ces rapports se basent sur les

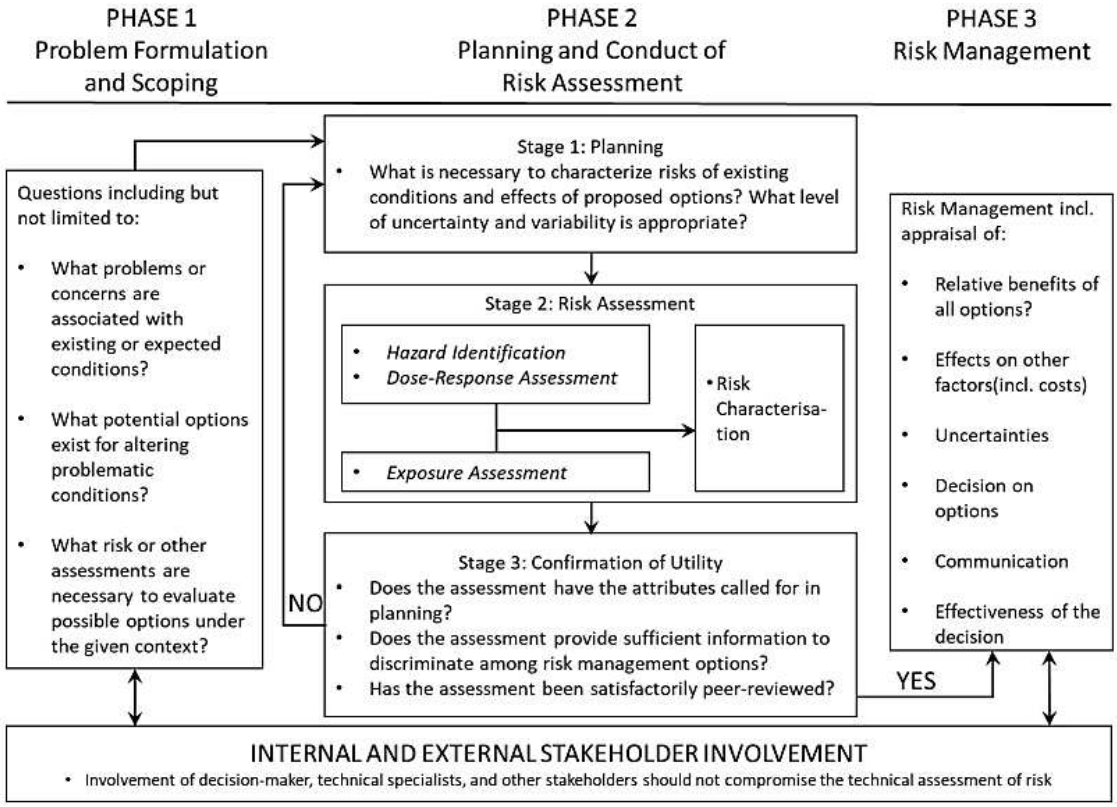

Figure 41 : Un arbre de décision des risques potentiels afin de maximiser l'utilité de l'évaluation du risque, rapport n°103 de l'OCDE du 3 février 2022, d'après Nuclear Regulatory Commission (2009).

lignes directrices suivantes : les propriétés physico-chimiques, les effets sur le système biologique, la dégradation et l'accumulation, les effets sur la santé et d'autres plus spécifiques à chaque NM. Ces 16 années d'étude et de recherches ont permis de mieux appréhender le monde de la nanotechnologie en établissant des classifications des NMx manufacturés en utilisant notamment l'arbre de décision présenté sur la figure 41.

ISO

L'Organisation internationale pour la standardisation (International Standardization Organization ISO) a également mis en place, en 2005, un groupe de travail dans le domaine des nanotechnologies, le Comité technique 229 (CT229). Celui-ci réunit 39 pays, il est constitué de 5 groupes, le troisième groupe notamment est chargé de l'élaboration des normes relatives à la sécurité des NMx et des nanotechnologies. Ces normes portent sur les enjeux de santé et de sécurité, et comportent des consignes précises sur la manipulation des NMx sur les sites professionnels que doivent faire appliquer les responsables hygiène et sécurité. En date du 21 février 2022, 98 standards ISO/TC229 ont été publiés et 29 sont en cours d'élaboration. Par exemple, l'ISO/TS 80004-1 (2015) définissait un nanomatériau comme un matériau ayant toute dimension externe à l'échelle nanométrique ou ayant une structure interne ou une structure de surface à l'échelle nanométrique (longueur comprise entre 1 et 100nm). Cette définition a été mise à jour en 2021 *via* la norme ISO/DIS 80004-1 afin de devenir un standard international.

UNION EUROPEENNE

ECHA (REACH)

Au niveau de l'Union européenne, l'agence européenne de la Chimie (European chemical agency ECHA) est responsable de la mise sur le marché de nouvelles substances et de leur utilisation convenable en appliquant : la règlementation REACH (**R**egistration, **E**valuation, **A**utorisation and restriction of **Ch**emicals). Ce règlement est entré en vigueur le 1er juin 2007, avec pour objectif de protéger la santé humaine et l'environnement contre les risques liés aux substances chimiques. La règlementation REACH concerne les fabricants, les importateurs, les distributeurs, les utilisateurs (aval, final industriel ou professionnel), et les consommateurs. REACH donne des obligations règlementaires ayant pour but de collecter et d'évaluer les informations sur les propriétés et les dangers de substances. Ces obligations varient en fonction du volume des substances (à partir de 1 tonne par an) (figure 42). Les entreprises doivent enregistrer leurs substances et collaborer avec d'autres entreprises enregistrant les mêmes substances. Ces enregistrements sont ensuite analysés par l'ECHA d'un point de vue administratif, les Etats membres de l'UE interviennent ensuite pour déterminer les risques des substances (évaluation du risque, toxicologie, écotoxicologie, rapport sur la sécurité) et si les

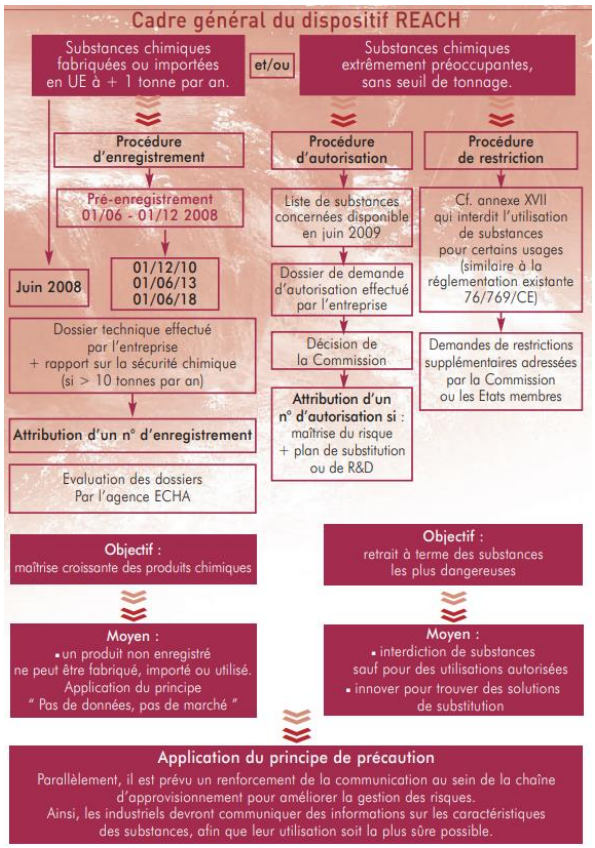

Figure 42 : INERIS, Guide : 30 questions pour être conforme à la réglementation européenne, 3ème version, juin 2008

mesures de précaution prises sont suffisantes. Une limitation du domaine d'utilisation peut également être imposée en raison du danger. Chaque substance mise sur le marché est accompagnée d'une fiche de données de sécurité (FDS) comportant les caractéristiques physico-chimiques, les précautions d'utilisation, les consignes de stockage et les données de toxicité connues.

Lors de l'émergence des nanomatériaux, seule la réglementation pour les produits chimiques était applicable. Grâce aux collaborations avec l'OMS, l'OCDE, les états membres et des associations professionnelles une législation européenne relative aux produits contenants des nanomatériaux a été mise en œuvre.

Au niveau de l'Union Européenne, une loi du 22 novembre 2006 précisant la définition d'un nanomatériau, stipule de mentionner leur présence dans tout produit alimentaire (Règlement (UE) no 1169/2011 du Parlement européen et du Conseil du 25 octobre 2011). Lorsqu'un nanomatériau entre dans la composition d'un cosmétique, celui-ci doit être mentionné sur l'étiquette depuis juillet 2013. Enfin, les biocides contenant des NMx nécessitent une autorisation spécifique et d'un étiquetage informatif sur les risques liés aux NMx utilisés depuis septembre 2013. Le 11 décembre 2015 une nouvelle règlementation a été votée, créant ainsi une nouvelle catégorie constituée d'aliments contenant des nanomatériaux (*Règlement (UE) 2015/2283 du Parlement européen et du Conseil du 25 novembre 2015 relatif aux nouveaux aliments*)

Depuis le 1er janvier 2020, des obligations légales s'appliquent aux entreprises (fabricants ou importateurs) manipulant des nanoformes. Lors de leur déclaration, les entreprises doivent renseigner la caractérisation des nanoformes concernés par l'enregistrement, évaluer la sécurité chimique, remplir les exigences en matière d'information pour l'enregistrement et informer l'utilisateur en aval des obligations qui lui incombent. Les attentes de REACH selon la quantité de NMx produite sont plus ou moins importantes, comme illustré sur la figure 43.

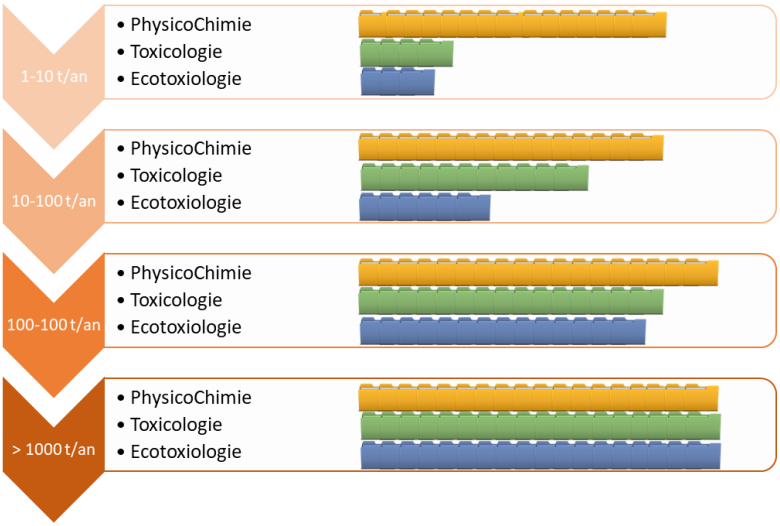

Figure 43 : Représentation des études nécessaires pour la mise sur le marché d'un substance, en fonction du volume. (D'après Jacques-Aurélien Sergent (2016) KUL)

EFSA

Depuis 2006, l'Agence Européenne de la sécurité alimentaire (European food safety agency EFSA) suit le développement des nanotechnologies en se basant sur des rapports de scientifiques indépendants sur des nouveaux résultats ou des mises à jour, dans le domaine de l'alimentation et de l'agroalimentaire. L'EFSA se base sur l'approche intégrée, sûre et responsable de l'Union Européenne, pour publier des rapports sur les NMx dans le circuit agroalimentaire, c'est ainsi que 8 rapports sont parus sur les micro et nanoplastiques, les tests et modèles d'étude de toxicité, et la présence de petites particules dans la chaîne de l'agroalimentaire. L'EFSA donne des consignes aux travailleurs/fournisseurs dans le secteur agroalimentaire sur les applications et l'utilisation des NMx comme additif alimentaire, enzymes, arôme… Les consignes concernent principalement les risques pour la santé et les animaux, mais devrait à terme s'intéresser également à l'impact environnemental des nanomatériaux. Le dernier rapport publié par l'EFSA date d'août 2021, il s'agit d'une révision du rapport de 2018 (Committee et al. 2021).

Les deux agences nationales responsables de la gestion des risques d'exposition à différentes substances sont l'Agence nationale de la sécurité environnement et santé (ANSES) et l'Institut national de la recherche et de sécurité (INRS).

ANSES

L'ANSES s'intéresse principalement aux nanomatériaux présents dans l'alimentation, ce qui concerne les additifs alimentaires tels que E551 (dioxyde de silice amorphe), E171 (dioxyde de titane) ou les NMx présents dans les emballages (nano-argent comme actif anti-microbien par exemple). Au niveau national, la loi n°2010-188 de juillet 2010 (loi Grenelle II) prévoit la mise en place d'un dispositif de déclaration annuelle des « substances à l'état nanoparticulaire » en l'état ou contenues dans des mélanges, sans y être liées, ou des matériaux destinés à les rejeter dans des conditions normales ou raisonnablement prévisibles d'utilisation. Cette loi concerne les fabricants, les importateurs et les distributeurs en France. Les entreprises concernées doivent déclarer l'identité, les quantités, les usages de ces substances et les fournisseurs (origine) de ces substances, *via* le registre R-Nano. A cette loi, s'ajoute un décret depuis le 17 février 2012, qui demande aux entreprises et aux laboratoires de recherche (privés ou publics) de déclarer toute substance produite, distribuée ou importée, à l'état nanoparticulaire, lorsqu'elle est supérieure à une quantité de 100g (*Décret N° 2012-232 Du 17 Février 2012 Relatif à La Déclaration Annuelle Des Substances à l'état Nanoparticulaire Pris En Application de l'article L. 523-4 Du Code de l'environnement* 2012). Ces déclarations annuelles sont réceptionnées par le Ministère de l'environnement puis gérées par l'Agence nationale de sécurité sanitaire de l'alimentation, de l'environnement et du travail (ANSES). Le rapport d'expertise collective de mai 2020 sur les nanomatériaux dans les produits destinés à l'alimentation souligne le manque de données concernant l'exposition des travailleurs aux nanomatériaux, et qu'il existe certains

transferts de nanomatériaux (de l'emballage vers l'aliment par exemple). Il est nécessaire de développer des systèmes d'analyses et de toxicologies adaptées à l'évaluation du risque sanitaire, de limiter l'exposition des travailleurs, des consommateurs et de l'environnement, de renforcer la traçabilité des produits contenant des NMx, et finaliser la caractérisation du danger de l'additif E171. Les déclarations sur le registre et les enquêtes en cours permettront une traçabilité des substances contenant des nanomatériaux ou susceptibles d'en produire, de mieux connaître le marché, les volumes en circulation et également de collecter des informations sur leurs propriétés (éco)toxicologiques.

L'institut national de recherche et de sécurité (INRS) pour la prévention des accidents du travail et des maladies professionnelles a été créé en 1947. Il est à l'origine d'un rapport de 2012 sur les risques auxquels sont exposés les professionnels en entreprise ou industries ('Les Nanomatériaux. Définitions, Risques Toxicologiques, Caractérisation de l'exposition Professionnelle et Mesures de Prévention - Brochure - INRS' n.d.) . L'INRS a également publié un rapport résumant les données connues sur les effets de l'exposition aux silices amorphes de synthèse, en décembre 2019, il rapporte le manque de connaissances sur ces effets, et la nécessité de poursuivre et approfondir les recherches, d'une part les mesures d'exposition aux SAS et le suivi médical des travailleurs mais également les recherches de biomarqueurs précoces au moyen de systèmes *in vitro* ou *in vivo*.

Les agences règlementaires s'accordent sur le manque d'informations concernant les dangers liés aux NMx. Le principe de précaution s'applique en limitant l'exposition des travailleurs, des consommateurs mais également de l'environnement. Des enquêtes sont en cours pour compléter les connaissances sur la toxicité éventuelle et les mesures de sécurité à mettre en place.

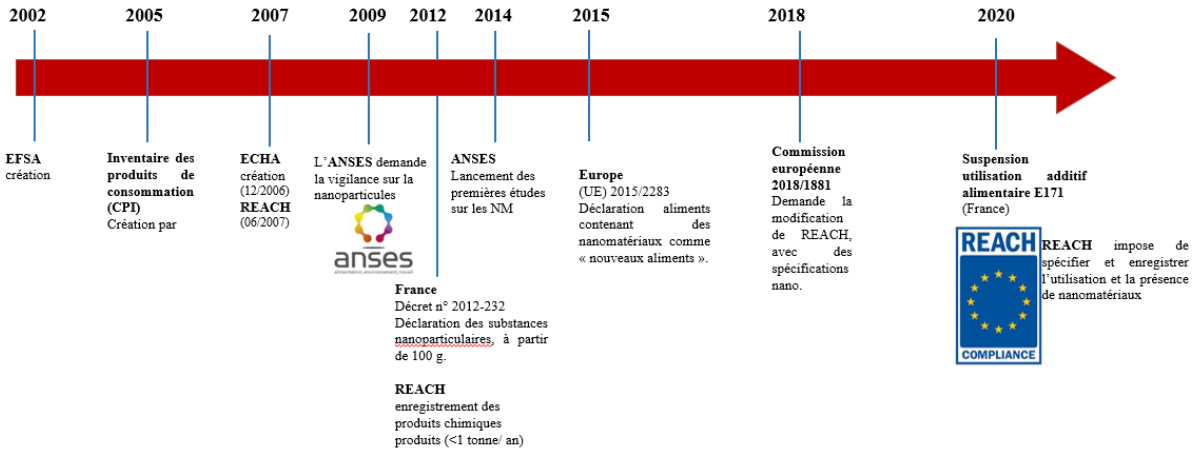

Figure 44 : Chronologie de la règlementation sur les nanomatériaux.

Ces différentes règlementations sont résumées sur la figure 44, cependant les demandes d'enregistrements et de tests de toxicité évoluent en permanence, en fonction des dernières données disponibles et des enquêtes réalisées.

Ces agences de règlementation des nanomatériaux existent depuis quelques années, et on constate que les études scientifiques sur les nanomatériaux se sont développées en parallèle de l'émergence de ces agences.

Troisième partie : les études toxicologiques sur les nanomatériaux

Avec l'émergence des nanomatériaux, les études de toxicologie se sont développées. Et s'il n'existe pas de tests réglementaires spécifiques aux nanomatériaux dans les années 2010, ceux-ci sont apparus en se basant sur les tests de toxicité des substances chimiques. Les domaines d'utilisation des NMx sont variés, et l'organisme est donc exposé par plusieurs voies. Les premiers systèmes de défense d'un organisme exposé à une substance sont les barrières biologiques (cutanée, mécanique, chimique...) puis le système immunitaire. Celui-ci se compose tout d'abord de la réponse immunitaire innée au cours de laquelle le nanomatériau (NM) va être reconnu comme une particule étrangère (Non-soi) qui peut activer les molécules de reconnaissance (PRR). Cette reconnaissance peut avoir différentes conséquences : modification d'expression des gènes, réponse inflammatoire (cytokines, production d'oxyde nitrique), mortalité cellulaire, diminution des fonctions de la cellule exposée… Dans le cas de NMx biodégradables (en médecine les systèmes de délivrance de médicaments ou gènes d'intérêts) ces effets sont transitoires et la réponse inflammatoire reste localisée et limitée dans le temps (Anagnostou et al. 2020). Cependant, certains NMx minéraux sont difficilement ou pas du tout (si inorganiques) biodégradables de même que certains plastiques qui peuvent notamment persister dans l'environnement et les eaux : l'Organisation Mondiale de la Santé alerte sur les potentiels dangers de l'absorption de nanoparticules de plastiques. Un rapport de l'OCDE souligne également l'importance d'évaluer la biodégradabilité des nanomatériaux manufacturés afin de limiter les dangers pour la santé humaine (rapport de 2018 « Assessment of Biodurability of Nanomaterials and their Surface ligands Series on the Safety of Manufactured Nanomaterials »). Malgré ces recommandations, certains nanomatériaux sont biopersistants par nature ce qui implique que les effets dus à leur exposition peuvent également l'être. Une manifestation importante associée à la biopersistance est la réponse inflammatoire qui peut être soutenue dans le temps. Par exemple, les polluants organiques persistants (POP), sont connus pour être accumulés dans les tissus adipeux (Joffin et al. 2018). Cette étude d'une greffe d'un tissu de souris exposée durant 48h à un POP (tétrachlorodibenzo-p-doxine TCDD) sur une souris non exposée a montré un relargage du TCDD pouvant aller jusqu'à 10 semaines. Les effets observés sont un changement de l'expression de certains gènes dans le foie et les tissus adipeux de la souris hôte (greffée) montrant des signes d'une inflammation, et de fibrose (IL6, TNF, MCP1, alpha SMA, COL1A1). Ces mêmes résultats avaient été constatés sur une étude *in vivo* sur des souris directement exposées au TCDD (Duval et al. 2017). Un autre exemple est celui de l'amiante, fibre minérale naturelle contenant du silicate, du fer et du magnésium, utilisée dans le monde entier pour ses propriétés isolantes jusqu'à la fin du XXème siècle et interdite en France depuis le 1er janvier 1997. L'amiante est connue pour être à l'origine de deux types de maladies : des cancers et des maladies non malignes (Frank and Joshi 2014). Les fibres d'amiante peuvent provoquer des verrues, un épanchement pleural asbestosique bénin ou l'asbestose et également des cancers pulmonaires, et parfois ovariens, du larynx, intestinaux, du pharynx et du rein. Les fibres d'amiante restent principalement au niveau des ganglions lymphatiques et de la cavité pleurale et induisent une inflammation chronique par l'intermédiaire de la production d'espèces réactives de l'oxygène entrainant notamment une réduction de l'immunité tumorale (Matsuzaki et al. 2012).

Outre ce problème de persistance du nanomatériau, il y a également une problématique d'accumulation en cas d'exposition répétée. En effet, pour certaines substances l'exposition peut être quotidienne. Si nous reprenons l'exemple de l'amiante, certes majoritairement micrométriques mais contenant une fraction nanométrique, les producteurs et les couvreurs ont

été exposés 5 jours par semaine durant une quarantaine d'années. Il est connu que les nanomatériaux sont utilisés dans l'alimentation ou les cosmétiques ce qui expose la population, certes à une dose faible, mais de façon répétée. Il a été déjà été observé dans l'environnement une accumulation de certaines substances telles que les polychlorobiphényles (PCB) ce qui a conduit au développement de tests d'écotoxicologie tenant compte de l'accumulation, de l'internalisation et de la dégradation de la substance (Franke et al. 1994).

Il est donc nécessaire d'étudier d'une part, la persistance des effets et d'autre part les effets d'une exposition répétée (avec ou sans bioaccumulation). Pour cela, il existe des expériences réglementaires *in vivo*, et quelques systèmes d'études *in vitro*.

Etudes *in vivo* : expérimentation animale

L'utilisation d'animaux pour réaliser des tests *in vivo* remonte au 4ème siècle avant Jésus Christ, notamment par Aristote (-384 - -322) et Erasistratus (-304 - -258) puis Galien (129 - 201) qui souhaitaient mieux comprendre l'anatomie (Hajar 2011). Le physicien Ibn Zuhr Avenzoar (1074 – 1162) fut le premier à utiliser les animaux pour tester des chirurgies avant d'opérer les patients humains. Le physicien Ivan Pavlov (1849 – 1936) utilisa le chien pour décrire le réflexe conditionnel. Les débats éthiques sur l'utilisation de l'expérimentation animale commencèrent au XVIIème siècle, les arguments principaux étaient que le bénéfice pour l'Homme ne justifiait pas de blesser les animaux mais également que l'animal étant inférieur à l'Homme, les résultats obtenus n'étaient pas transposables. Le physiologiste Claude Bernard (1813 – 1878) établit l'expérimentation animale comme méthode scientifique standard en justifiant son utilisation par la cohérence des résultats entre l'Homme et l'animal pour la toxicologie et l'hygiène humaine, avec une différence d'intensité de réponse mais avec les

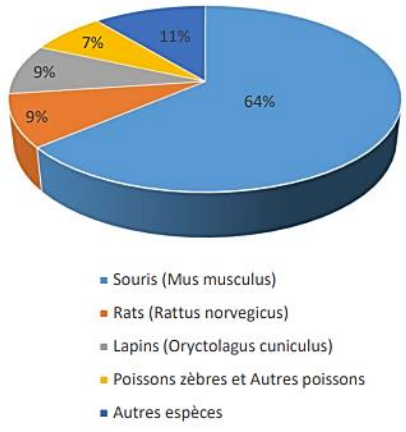

Figure 45 : Espèces d'animaux utilisés à des fins scientifiques en France en 2020, d'après un rapport de la direction générale de la recherche et de l'innovation (Ministère de l'enseignement supérieur, de la recherche et de l'innovation).

Espèces	Total	%
Souris (Mus musculus)	1 048 864	63,8
Rats (Rattus norvegicus)	149 068	9,1
Lapins (Oryctolagus cuniculus)	144 190	8,8
Autres poissons	84 936	5,2
Poules, coqs et poulets (Gallus gallus domesticus)	75 108	4,6
Cochons d'Inde (Cavia porcellus)	42 841	2,6
Poissons zèbres (Danio rerio)	35 175	2,1
Autres oiseaux	21 272	1,3
Porcs (Sus scrofa domesticus)	11 843	0,7
Hamsters dorés (Mesocricetus auratus)	8 467	0,5
Chiens (Canis familiaris)	4 079	0,2
Macaque cynomolgus monkey (Macaca fascicularis)	3 570	0,2
Xénopes (Xenopus laevis and Xenopus tropicalis)	3 049	0,2
Moutons (Ovis aries)	2 827	0,2
Bovins (Bos primigenius)	1 817	0,1
Reptiles	1 680	0,1
Autres rongeurs	1 037	0,1
Chats (Felis catus)	970	0,1
Chèvres (Capra aegagrus hircus)	534	0,0
Chevaux, ânes et croisements (Equidae)	483	0,0
Autres amphibiens	432	0,0
Gerbilles de Mongolie(Meriones unguiculatus)	342	0,0
Céphalopodes	299	0,0
Autres mammifères	181	0,0
Furets (Mustela putorius furo)	169	0,0
Ouistitis, Marmoset et tamarins	159	0,0
Hamsters de Chine (Cricetulus griseus)	110	0,0
Babouins (Papio spp.)	84	0,0
Macaque Rhesus (Macaca mulatta)	77	0,0
Prosimiens	51	0,0
Singes vervets (pygerythrus or sabaeus)	37	0,0
Autres carnivores (other Carnivora)	18	0,0
Autres espèces desinges de l'ancien monde	18	0,0
Total général	**1 643 787**	

tendances conservées. Suite à quelques évènements tragiques de substances commercialisées sans tests préalables sur les animaux, l'expérimentation animale devint réglementaire.

La directive européenne 2010/63/UE applicable depuis le 1er janvier 2013, impose aux établissements français utilisant des animaux (vertébrés et céphalopodes) à des fins scientifiques de le déclarer au Ministère de l'enseignement supérieur, de la recherche et de l'innovation. Le département des pratiques de recherches réglementées publie un rapport annuel sur ces enregistrements. C'est ainsi qu'en 2020, 1 643 787 animaux ont été utilisés dans les établissements français. Cela représente une baisse par rapport à 2019 (1 865 403 enregistrements) et 2018 (1 910 519 enregistrements). Pour la cinquième année consécutive, le nombre d'animaux utilisés à des fins scientifiques diminue. Cependant la forte diminution observée en 2020 s'explique par l'épidémie de COVID-19 qui a contraint de nombreux établissements à suspendre leurs activités. La souris est l'animal le plus utilisé puisqu'elle représente 64% des espèces d'animaux enregistrés, suivie par le rat (9%) les lapins (9%) puis les poissons (7%) (figure 45). Les autres espèces représentent 11% des animaux.

Le rapport de 2020 renseigne également les domaines d'utilisation des animaux, et sans surprise, la recherche fondamentale représente 37% des utilisations, suivie par les études toxicologiques et règlementaires (31%) puis les recherches appliquées (27%) (figure 46).

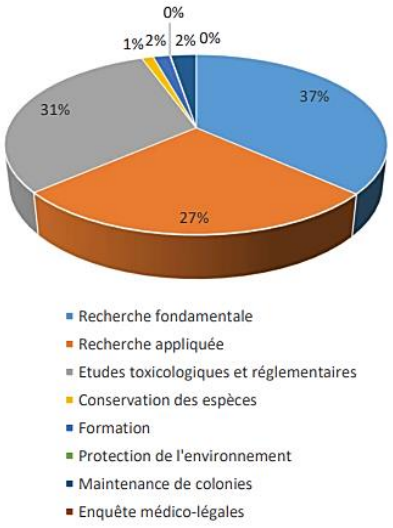

Figure 46 : Domaines d'utilisation des animaux en France en 2020, d'après un rapport de la direction générale de la recherche et de l'innovation (Ministère de l'enseignement supérieur, de la recherche et de l'innovation).

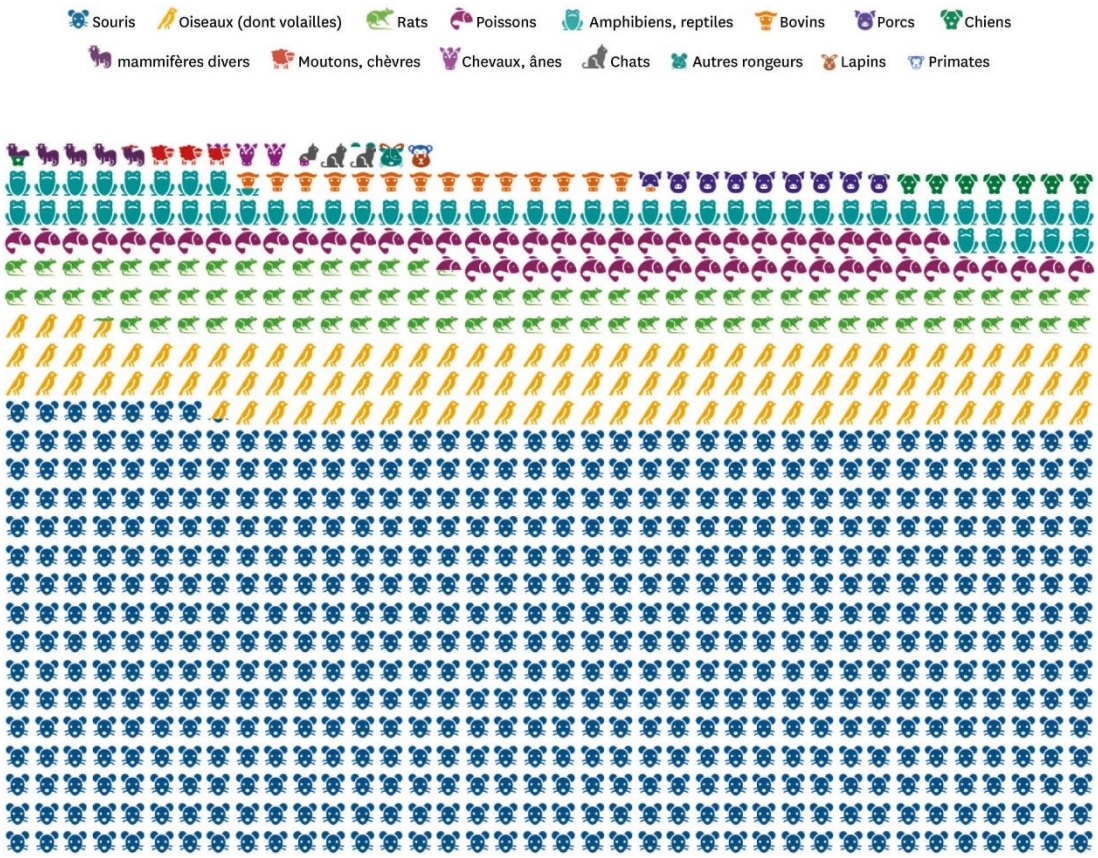

Figure 47 : Espèces utilisées pour l'expérimentation animale en Suisse, en 2020. Sciences & Climat, le 4 février 2022 par Yvan Pandelé Une silhouette représente 600 animaux

Lorsque l'on compare avec les pays voisins européens, la Belgique enregistre 437 275 animaux utilisés en 2020 (58% sont des souris), et 39% des animaux sont utilisés en recherche fondamentale, 29% pour des études toxicologiques et réglementaires et 28% en recherche appliquée d'après les données du rapport statistique de Belgique (2020) (environnement.brussels). La Suisse quant à elle a déclaré l'utilisation de 556 107 animaux en 2020, dont 62% sont des souris (figure 47).

L'utilisation d'animaux dans les laboratoires est très règlementée, elle nécessite une installation particulière, du personnel formé, de respecter le bien-être de l'animal et le dépôt d'une demande d'autorisation de projet qui, en France,sera accordée par le Ministère l'éducation nationale, de l'enseignement supérieur et de la recherche (‘Risques biologiques en animalerie de recherche - Article de revue - INRS’ n.d.). Avec le renforcement de cette règlementation, les animaleries sont de plus en plus mutualisées entre les laboratoires de recherches pour permettre la bonne conduite des expériences et la réalisation des tests sur les animaux, qui sont utilisés dans de nombreux domaines, dont la toxicologie.

Le premier exemple que nous citons ici de l'utilisation de l'expérimentation animale en toxicologie est cette étude sur la fumée de silice et la présence de silanols en surface (Sun et al. 2015). Comme expliqué précédemment, la fumée de silice contient un anneau de groupements hydroxyles à sa surface, celui-ci est plus dense que pour les silices précipitées par exemple. Cette bague extérieure pourrait expliquer la forme d'agrégation en « collier de perles » de cette SAS par rapport aux autres, causant des trous dans les membranes cellulaires ce qui rendrait cette silice plus toxique. En se basant sur cette hypothèse, les chercheurs ont calciné ou

réhydraté la fumée de silice afin de modifier sa structure de surface et la densité de silanols. Ils observent une diminution des effets proinflammatoires *in vitro* (MCP1, IL-6, MIP-1α : cascade d'inflammation NLRP3) pour la fumée calcinée. Cette chimie de surface contenant moins de silanols peut être stabilisée par l'addition d'atomes de titane ou d'aluminium et lors des tests sur les souris C57BL/6, par inhalation, les mêmes tendances sont observées avec une diminution de cytokines IL-1β et MIP-1α dans les tissues analysés après euthanasie. L'hypothèse initiale sur la présence de silanols pouvant expliquer la toxicité de la fumée de silice semble donc se confirmer.

Une autre exemple pouvant être cité est cette expérience menée *in vivo* a permis d'étudier les effets d'une exposition répétée aux polluants organiques persistants (POP) (Duval et al. 2017). Les 60 souris du test sont soumises à un régime pauvre ou riche en acide gras durant 8 semaines avant puis durant l'exposition. Le schéma d'exposition est celui d'une exposition répétée à une faible dose (5µg/kg) du polluant 2,3,7,8-tetrachlorodibenzo-*p*-dioxine (TCDD), 1 injection par semaine durant 6 semaines. L'analyse histologique du foie a révélé une stéatose accompagnée d'une modification de l'expression des gènes du métabolisme hépatique des lipides et l'augmentation du collagène et des transaminases traduisent une fibrose chez les souris au régime riche en lipides et exposée au TCDD. Le TCDD, chez les deux groupes de souris, augmente également l'expression de certains marqueurs de l'inflammation (IL-1β, CD68) et de fibrose (COL1A1, ACTA2). Cette étude a montré la synergie entre l'exposition à un POP et un régime riche en lipides, favorisant le développement d'une fibrose du foie.

Enfin, une dernière expérience *in vivo* permet la comparaison entre les deux protocoles d'exposition au TCDD : l'exposition aiguë (24 heures) et l'exposition chronique (5 jours/semaine durant 13 semaines) (Slezak et al. 2000). Les souris ont été réparties en 15 groupes de 10 souris et exposées par voie orale (gavage) selon le protocole et la dose choisie : 6 doses différentes durant 24h, et euthanasie 7 jours plus tard, ou 6 doses différentes 5 jours par semaine, durant 13 semaines avant euthanasie. La présence de TCDD est mesurée dans les tissus (poumon, rein, rate et foie), et il s'avère que ce polluant est majoritairement accumulé dans le foie, et de façon dose-dépendante selon l'exposition. Cependant le stress oxydant n'est pas directement prédictible à partir de la concentration en TCDD dans les tissus, le niveau de glutathion hépatique est multiplié par deux après une exposition aiguë. L'exposition chronique à 0,15ng/kg/jour, quant à elle, induit une diminution du glutathion (foie, poumon et rein) par rapport aux souris non traitées, l'augmentation du glutathion est à nouveau observée, dans le foie seulement, à partir de 0,45ng/kg/jour. Cette étude montre d'une part qu'une exposition à une faible dose de TCDD pourrait rendre plus vulnérable un individu s'il est exposé à une forte dose ensuite, par rapport à un individu naïf au TCDD. D'autre part, les deux types d'exposition n'induisent pas les mêmes réponses tissulaires : la tendance est opposée selon la dose d'exposition mais également selon le tissu observé.

Ce dernier exemple montre l'importance du protocole d'exposition utilisé dans une étude de toxicologie, selon le contexte et le matériau étudié. Il est également important de souligner le nombre d'animaux utilisés pour ces études, une trentaine et soixantaine de souris C57BL/6 (Duval et al. 2017; Sun et al. 2015) et 150 souris B6C3F1(Slezak et al. 2000). Les études sont également fort longues, les souris sont généralement achetées âgées de 8 semaines, maintenues en quarantaine puis en période d'adaptation à l'animalerie locale et enfin l'expérience commence pour une durée pouvant aller jusqu'à 13 semaines dans le cas de

l'exposition chronique mentionnée ci-dessus. Un dernier aspect important est le coût de telles études, une souris C57BL/6 âgée de 8 semaines est estimée à 26€ (Jackson laboratory, catalogue 2022), auxquels s'ajoutent le transport, l'élevage, la nourriture, les cages, le personnel d'animalerie…

Les études règlementaires sont basées sur l'expérimentation animale, notamment pour les produits chimiques, les industriels sont réglementés au niveau européen par la directive REACH (« Registration, Evaluation and Authorisation of Chemicals »), qui impose de réaliser des tests de toxicité avant toute mise sur le marché. Cependant un mouvement international tend vers une nouvelle utilisation des animaux et encourage le développement des systèmes *in vitro*.

Etudes *in vitro* : systèmes biologiques

Les études requises par REACH utilisent des systèmes *in vitro*, mais également des modèles animaux, notamment la souris, il existe un mouvement européen d'éthique expérimentale, la stratégie 3R (Refine, Reduce, Replace) qui encourage l'utilisation de moyens alternatifs à l'expérimentation animale.

Le débat sur l'utilisation des animaux pour des tests d'expérimentation a toujours existé, cependant il a été exacerbépar la publication « La Libération animale » paure en 1975 par le philosophe Peter Singer. Ce dernier assimile la notion de spécisme comme analogue au racisme ou au sexisme, en avançant que les générations futures auraient le même sentiment sur l'expérimentation animale que celui que nous avons à propos des arènes et des combats de gladiateurs de l'époque romaine. Le débat s'est poursuivi en 1981 avec les photos prises dans un laboratoire Silver Spring du Maryland par un militant de People for the Ethical Treatment of Animals (PETA), sur lesquelles des singes mutilés ou attachés sont visibles. Enfin, c'est un rapport publié en 2007 par le Conseil national de la recherche de l'Académie nationale des sciences qui encourage à la réduction de l'expérimentation animale en recommandant l'utilisation de systèmes *in vitro* utilisant des cellules humaines (Council 2007). Dans ce rapport, il est toutefois reconnu que les connaissances actuelles des systèmes *in vitro* ne permettent pas d'abolir totalement l'expérimentation animale mais que ces systèmes peuvent les compléter. C'est en mars 2009 que l'Union européenne interdit l'importation et la vente de produits cosmétiques utilisant des ingrédients testés sur des animaux et en 2013 pour la toxicité répétée et aiguë sur les ingrédients et les produits. Cependant certains chercheurs ont expliqué à cette occasion qu'il n'existait pas de tests *in vitro* équivalents aux tests *in vivo* pour toutes les expériences règlementaires. La pandémie mondiale COVID-19 a relancé le débat sur l'expérimentation animale, notamment face à la pénurie notamment de souris génétiquement modifiées (communiqué The Jackson Laboratory, march 2020, *expediting covid-19 research)* pour tester les vaccins contre le coronavirus mais également de singes sur lesquels sont habituellement testés les vaccins en développement (afin de garantir leur efficacité et leur sécurité). Face à cette pénurie, certaines entreprises ont développé de nouvelles techniques afin de s'affranchir de l'utilisation d'animaux, comme par exemple Moderna Therapeutics qui a utilisé une copie synthétique de l'ADN du virus et non la forme atténuée (« Moderna's work on a potential vaccin against covid-19 » march 2020). La FDA (Food and Drug Administration)

a approuvée cette technique le 4 mars 2020, pour permettre ainsi de passer aux essais cliniques directement.

Ci-dessous sont présentées quelques études utilisant des systèmes *in vitro* pour évaluer la toxicité des matériaux ou substances et également les risques liés à l'exposition des travailleurs (dans le cas des isolants thermiques (Boyles et al. 2018)) ou de la population globale (dans les cas des bisphénols, utilisés dans les plastiques (Verbanck et al. 2017))

Un premier exemple de l'utilisation de systèmes *in vitro* pour étudier l'effet d'une exposition aux bisphénols est celui de (Verbanck et al. 2017) utilisant des adipocytes primaires humains. Si le bisphénol A (BPA) est probablement associé à l'obésité et des maladies liées au métabolisme, peu de données toxicologiques sont connues sur ses analogues les bisphénols F (BPF) et S (BPS). Cette étude a pour objectif de définir les gènes cibles des bisphénols afin d'estimer les effets possibles d'une exposition, notamment chronique (10nM dose faible, similaire à celle de la vie quotidienne et 10µM dose forte, pendant 10 jours). Les adipocytes de trois femmes non diabétiques ont été prélevés et différenciés en laboratoire. L'expression de gènes impliqués dans les voies du cancer ou lésion et anomalies de l'organisme est modifiée par l'exposition aux trois types de bisphénols. Les voies altérées sont par exemple la matrice extracellulaire, les régulateurs de la transcription, le cytosquelette ou encore les hormones. Ce qui souligne les effets de dérégulation hormonale, connus pour le BPA, mais probablement communs à ses substituts. Ces résultats sont cohérents avec ceux de la littérature : *in vitro* sur les tubules séminifères de rat (S. Ali et al. 2014) et *in vivo* sur le poisson (Villeneuve et al. 2012). Ce système de pré-adipocytes humains a mis en évidence l'impact d'une exposition répétée à de faibles doses de BPA mais également à ses substituts BPF et BPS, qui mériteraient une étude de toxicologie à part entière.

Un deuxième exemple est celui de (Boyles et al. 2018) qui compare deux systèmes de cultures *in vitro* (macrophages murins J774A.1 et cellules humaines d'épithélium alvéolaires A549) pour évaluer l'activité de la silice cristalline dans des isolants thermiques industriels à base de silicate. Après 24h d'exposition, les fibres de l'isolant et le dioxyde de titane (contrôle négatif) n'induisent pas de cytotoxicité, mais une augmentation de la sécrétion de certaines protéines est mesurée : pour les A549, la sécrétion de GRO-α est significativement augmentée en réponse aux fibres de silicate de magnésium et calcium (chauffées ou non), de silicate de magnésium chauffées. Pour les J774A.1, le TNF-α est davantage sécrété en réponse aux fibres chauffées de silicate de magnésium et calcium et au silicate de calcium, de même que CCL5 (RANTES) en réponse aux fibres chauffées de sulfate de magnésium et calcium et aux fibres de sulfate de calcium (chauffées ou non), ces niveaux restant toutefois inférieurs à ceux induits par la DQ12 (87% de silice cristalline, contrôle positif). L'exposition des A549 et J774A.1 aux fibres d'isolants utilisés dans l'industrie induit des effets modérés sur les cellules, la présence de cristobalite (formée après chauffage de l'isolant) n'explique pas toujours ces effets, les paramètres physico-chimiques (dimensions, chimie des fibres et solubilité du matériau) sont à prendre en compte, même si les réponses cellulaires observées restent inférieures au matériau de référence DQ12. La réponse inflammatoire de la lignée murine semble plus sensible à la cristobalite, en donnant des réponses plus proches de la DQ12.

Ces deux études ont permis d'évaluer un grand nombre de paramètres (cytotoxicité, production de ROS, réponse inflammatoire, modification de l'expression des gènes,) pour un grand nombre de conditions : dans la première étude trois substances avec 2 concentrations, dans la seconde étude, 6 substances sur 2 lignées. Au-delà du grand nombre de paramètres possibles à tester, il existe d'autres avantages des systèmes *in vitro*.

Premièrement, il existe un aspect éthique et sociétal favorisant l'utilisation de méthodes alternatives à l'expérimentation animale. En effet, pour l'opinion publique le traitement des animaux de laboratoire n'a pas évolué depuis la photo du singe des laboratoires Silver Spring, datant d'une quarantaine d'années. De plus, l'animal n'est plus seulement considéré comme un outil de travail (agriculture, locomotion…), notamment à cause de l'industrialisation mais aussi comme un animal de compagnie. En 2020, 52% des Français déclaraient posséder un animal de compagnie d'après les statistiques du Ministère de l'Agriculture. La perception de l'animal a également évolué avec la création en 1977 de la Déclaration universelle des droits de l'animal qui, si elle n'a aucune valeur juridique, concrétise la vision philosophique de l'animal et formalise les rapports qui doivent exister entre l'espèce humaine et l'espèce animale. La citation de Gandhi illustre cette évolution : « La grandeur d'une nation et son progrès moral peuvent être jugés à la manière dont les **animaux** sont traités ». En janvier 2018, cette Déclaration est suivie par l'article 515-14 du code civil, adopté par l'Assemblée nationale qui reconnaît les animaux comme des êtres sensibles. C'est dans cet esprit que la stratégie des 3R au niveau européen se développe (figure 48). Les 3R signifient Remplacer, Réduire et Raffiner (*Replacement, Reduction, Reffinement* en anglais), ils ont été formulés en 1959 par William Russel (1925 - 2006) et Rex Burch (1926 – 1996) dans leur livre « *The Principles of humane experimental technique* ». C'est dans ce livre qu'ils fournissent des idées pour combiner bien-être animal et recherche de bonne qualité. C'est sur ce principe que s'est basée la législation européenne en 1986, lors de la première loi sur la protection animale, suivie ensuite par la directive 2010/63/EU (plus spécifique aux animaux de laboratoire). Le Remplacement encourage l'utilisation de méthodes alternatives comme des systèmes *in vitro* de cellules ou tissus, les

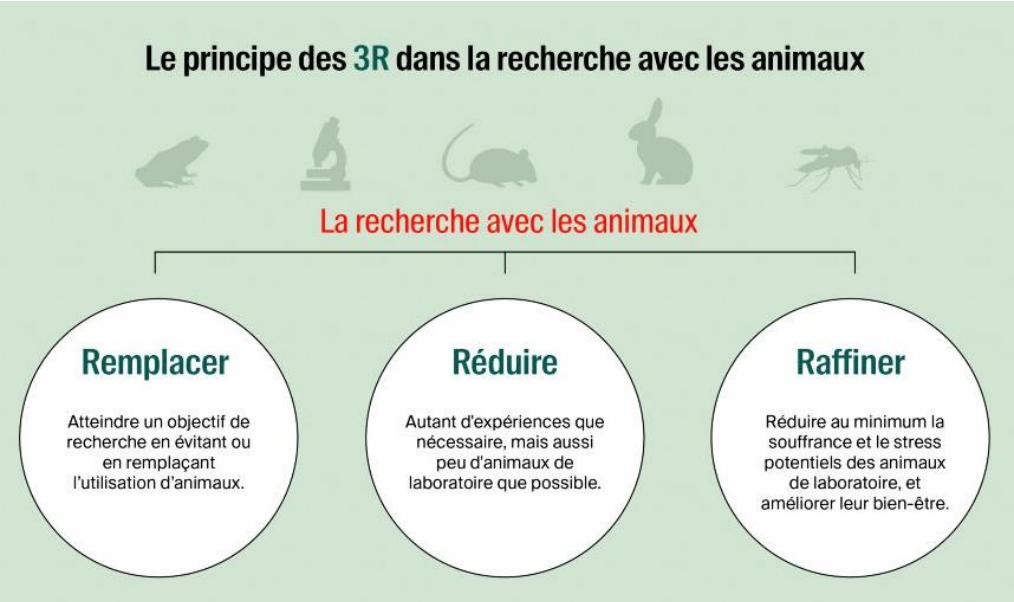

Figure 48 : Principe de la stratégie des 3R, d'après l'EPFL.

approches biochimiques utilisant des molécules synthétiques, de la bioinformatique (prédiction de modèle ou approche Adverse Outcome Pathways (AOP), les méthodes « omiques »…La Réduction se rapporte à toutes les techniques qui permettent d'utiliser moins d'animaux, notamment en optimisant leur utilisation et en calculant leur nombre au plus juste. Enfin, le Raffinement se rapporte au bien-être afin de diminuer les risques de souffrance, mais cela peut également être la substitution par un animal considéré comme moins sensible (par exemple les daphnies plutôt que le poisson).

Le deuxième point important est l'aspect financier. En effet, comme mentionné plus haut, l'expérimentation animale est coûteuse. Les recherches règlementaires validées par l'OCDE demandent principalement l'utilisation de souris. L'exemple des souris C57BL/6 à 26€/souris de 8 semaines peut sembler anodin, cependant il faut tenir compte du nombre de souris par étude, dans un nombre suffisant pour être statistiquement exploitable, soit en moyenne 10 souris par condition. Le prix de l'hébergement dans un centre de recherche spécialisé, par exemple au CHU de Québec Université de Laval, est de 3€/jour pour les personnes externes et 0,40€/jour pour les internes. Si on estime une expérience sur 3 semaines, en testant 3 conditions (non-traitées, exposées à la concentration 1, et exposées à la concentration 2) cela revient à un coût de 2 670€, en comptant seulement l'hébergement et l'achat des souris. A cela s'ajoute le salaire des zootechniciens, les chirurgies ou manipulations éventuelles, et les formations (initiale et de recyclage).

Enfin, le dernier aspect est le temps. Un système cellulaire est rapide à cultiver, les lignées sont généralement bien connues et génétiquement stables, de plus elles se divisent, le stock est donc entretenu si la culture est bien faite. Dans les cas de cellules plus spécifiques, provenant de prélèvements (de tissus, de patients…) s'ils sont non invasifs, la quantité de matériel peut elle-aussi être importante. La variabilité est plus faible, quasiment inexistante dans le cas de lignées et mieux contrôlée dans le cas de prélèvement et de cellules différenciées en laboratoire. Il est ainsi possible d'obtenir une meilleure reproductibilité mais également d'appliquer des approches expérimentales plus fines et plus sensibles, et ainsi de détecter plus rapidement des effets ou des phénomènes qui seraient visibles plus tardivement chez l'animal. Il est également plus simple et rapide de mener des études mécanistiques qui permettront ensuite d'étudier des toxicités croisées.

Afin de replacer mon travail de thèse dans le contexte général de la toxicologie *in vitro* des silices amorphes (voir (Murugadoss et al. 2017; Fruijtier-Polloth 2012) , quelques exemples des travaux réalisés *in vitro* sur des SAS sont mentionnés plus en détail ici. Une étude de (Nattrass et al. 2015) qui étudie les effets d'une exposition à la terre de diatomée qui contient entre 1 et 3% de silice cristalline.

Un premier exemple est l'utilisation de cellules épithéliales humaines Caco-2 afin de comparer différentes silices amorphes de synthèse (précipitées et fumées, avec différentes surfaces spécifiques) utilisées en alimentation et produites par Evonik GmbH (Hempt et al. 2020). L'objectif de cette étude est de caractériser 10 SAS clairement identifiées afin de combler les informations manquantes sur leurs effets spécifiques, en réponse à la demande de l'EFSA. Les SAS caractérisées dans cette étude ont des particules primaires de tailles variées (3 à 30nm de diamètre), des tailles d'agrégats diverses (45 à 276nm) et des surfaces spécifiques

différentes (45 à 460 m²/g), elles sont solubilisées en eau et dispersées, obtenant ainsi des SAS similaires à celles retrouvées dans les matrices alimentaires (Younes et al. 2018). Les cellules sont exposées durant 24h à une dose de SAS jusqu'à 50µg/ml, pour mesurer la viabilité cellulaire et la production d'espèces réactives à l'oxygène (ROS, après 2h ou 24h d'exposition). Il n'y a pas de mortalité cellulaire ou de production de ROS pour les cellules exposées aux SAS, et l'intégrité de la barrière épithéliale est maintenue (mesure de la résistance électrique et observation en microscopie). La vitesse de sédimentation des SAS est différente selon la taille des agrégats, en 3h 80% de la précipitée composée des plus gros agglomérats (750nm) est déposée, en 48h seuls 5,8% de la fumée 380F est déposée (agglomérat de 318nm), pour une même concentration ajoutée de 50µg/ml. Cette étude ne montre aucun effet des dix SAS testées sur les cellules d'épithélium intestinal, la fumée de SAS étant connue pour induire plus d'effets que la précipitée dans la littérature, leur hypothèse principale étant que l'effet d'une SAS est spécifique de la cellule exposée, ce qui expliquerait les effets observés sur les macrophages (Rubio et al. 2019) ou les cellules dendritiques (Winkler et al. 2017) et non sur leur modèle. Cependant, les tests d'intégrité ont été réalisés avec des contrôles positifs (par exemple le sodium au sulfate de dextrane) ayant une action chimique, il aurait pu être intéressant d'utiliser une silice cristalline (structure plus tranchante) afin d'observe un effet mécanique et potentiellement la réponse associée.

Afin d'obtenir un système physiologiquement plus proche de la réalité, un système de co-culture de cellules humaines (Caco-2/HT-29 sécrétant du mucus /Raji) pour simuler la barrière intestinale a été utilisé pour étudier les effets de SAS sur un modèle intestinal (Hempt et al. 2021). Certaines des SAS de l'étude précédente ont été testées sur ce modèle cellulaire plus complexe (4 SAS précipitées et 2 SAS pyrogénées). L'exposition aiguë aux SAS n'induit pas de cytotoxicité, l'intégrité de la barrière épithéliale est maintenue, la production de mucus est homogène et régulière, le bon fonctionnement des microvillosités n'a pas pu être mesuré, l'absorption de lipides est maintenue et enfin il n'y a pas de réponse inflammatoire (IL-8 et CCL2). Ce système de co-culture de cellules intestinales confirment les résultats de l'étude précédente, les SAS alimentaires aux doses choisies n'induisent pas d'effets toxiques. Une réserve peut être émise sur ces études par le manque de contrôle positif permettant de valider le système.

Les études mentionnées ci-dessus, qui montrent peu d'effets des SAS sur les systèmes épithéliaux, posent la double question de la spécificité de la toxicité de la silice sur certains types cellulaires, et du mécanisme chimique conduisant à cette toxicité. En effet, contrairement aux NMx métalliques ou d'oxydes métalliques comme l'argent, le cuivre ou les oxydes de zinc ou de fer, il n'est pas possible de proposer pour la silice un mécanisme toxique basé sur la libération d'un ion toxique comme un ion métallique lourd (Ag) ou de transition (Fe, Cu, Zn). De plus il a été démontré (Rabolli et al. 2010) sur des silices colloïdales que la silice était sélectivement toxique pour les cellules fortement phagocytaires comme les macrophages, et que la toxicité augmentait quand la taille primaire des particules diminuait, ce qui faisait penser à un effet de chimie de surface. En conséquence, un certain nombre d'étude a utilisé des systèmes *in vitro* de macrophages pour étudier les bases chimiques de la toxicité de la silice.

Pour ce faire, les études ont cherché à modifier la chimie de surface de la silice puis à observer les effets de ces silices modifiées sur les macrophages. Il a été ainsi possible de montrer que la

cristallinité de la silice n'était pas en tant que telle un déterminant de la toxicité. Par exemple, la calcination de silice cristalline à haute température (>1300°C) n'induit aucun changement de cristallinité mais diminue considérablement la toxicité vis-à-vis de la lignée de macrophages J774 (Fubini et al. 1999). De même, des monocristaux de silice cristalline se sont avérés non toxiques sur la lignée de macrophages RAW264.7 (Turci et al. 2016), alors que de la silice cristalline micronisée par broyage l'est. En parallèle, la silice vitreuse, ou verre de quartz, qui est parfaitement amorphe, s'avère aussi toxique que la silice cristalline après broyage (Ghiazza et al. 2010).

Dans le domaine des SAS, des différences de toxicité entre diverses formes de SAS ont été observées et reliées au degré d'hydratation des silanols de surface (SiOH vs Si-O-Si), la toxicité diminuant quand l'hydratation augmente (Gazzano et al. 2012). Si ce paramètre d'hydratation semblait pouvoir expliquer la différence de toxicité entre silices amorphes et silice cristalline, dont l'hydratation est très faible, les travaux sur la silice calcinée et les monocristaux de silice mentionnés ci-dessus permettent d'infirmer cette hypothèse.

De fait, des travaux récents (Pavan et al. 2020) ont permis de montrer qu'une catégorie particulière de silanols, les silanols vicinaux en interaction (SiOH---OHSi, --- représentant une liaison hydrogène) étaient l'entité chimique à la base de la toxicité de la silice. Ces structures sont peu présentes naturellement à la surface de la silice mais sont produites en nombre lors de la fracture mécanique de la silice, ce qui explique la toxicité des poussières respirables de silice cristalline, qui sont issues de la fracturation de cristaux plus gros. Ce mécanisme pourrait aussi expliquer la toxicité observée de fragments de SAS produits par sonication à haute énergie (Murugadoss et al. 2020).

Ces exemples montrent la puissance des systèmes *in vitro* pour étudier rapidement les mécanismes chimiques de toxicité. Cependant, l'immense majorité des études *in vitro* (et qui serait bien trop nombreuses pour les citer) se concentre sur la détermination de doses toxiques et la lecture de quelques paramètre perçus comme importants voire critiques, comme illustré dans la publication de Boyles (Boyles et al. 2018) en réponse à des expositions courtes aux substances d'intérêt. Si ce choix est parfaitement pertinent pour la majorité des substances solubles, qui sont dégradées rapidement dans le milieu et/ou dans les cellules, il pose question pour les substances biopersistantes comme nombre de NMx minéraux ou les polluants organiques persistants. Cependant, il est possible d'adapter les systèmes *in vitro* pour étudier les phénomènes de persistance et leurs effets induits, comme illustré précédemment sur les bisphénols par l'étude de Verbanck (Verbanck et al. 2017). Dans ce cadre conceptuel, quelques études ont adapté des systèmes *in vitro* pour étudier les effets persistants de NMX minéraux, elles seront mentionnées et discutées plus loin dans ce manuscrit.

Enfin, un aspect très important pour lesquels les systèmes *in vitro* s'avèrent très prometteurs est celui de l'étude des effets cocktails ou de toxicité croisée, qui représentent un vrai défi pour la toxicologie moderne.

En effet, il existe un très grand nombre de possibilités pour des expositions de toxicité croisées. Notre vie quotidienne est un environnement complexe composé d'un grand nombre de substances et de stimuli : l'alimentation, la qualité de l'air (polluants, pollen, poussières de sol…), les cosmétiques, les produits ménagers ou encore les pathogènes. Cet environnement varié multiplie le nombre de combinaison de substances à étudier. De plus, cet environnement évolue, non seulement au cours d'une vie (déménagements, habitudes de vie, régime…) mais

également à l'échelle mondiale. Par exemple, certains paramètres évoluent en moins d'une décennie : l'avancée des nouvelles technologies, le changement de consommation, le réchauffement climatique…. Les voitures électriques sont en plein essor : en 2010, 17 000 voitures électriques étaient recensées au niveau mondial, en 2019, c'est plus de 7,2 millions d'après un rapport de l'Agence internationale de l'énergie (2020). Cette tendance va se poursuivre ce qui implique une diminution voire une disparition des particules diesel dans l'air.

Le deuxième paramètre d'exposition à tester, après la nature de la substance, est la concentration, ce qui multiplie encore le nombre de combinaisons à tester. En effet, il faut parvenir à déterminer les concentrations auxquelles sont exposées la population ou des sous-populations afin d'être pertinent lors de l'étude toxicologique. Cette donnée est parfois difficile à calculer, de plus elle peut varier selon la (sous)-population étudiée (particule diesel : ville/campagne, tabac : adulte/enfant…). Tout cela constitue ce que l'on appelle l'exposome. Celui-ci a rapidement désigné les facteurs non-génétiques qui influencent la santé d'un individu au cours de sa vie (Price et al. 2022). Il a également laissé place à plusieurs interprétations sur le lien entre les effets observés (réponses biologiques) et les causes (exposition environnementale). Et si les deux communautés (recherche environnementale et recherche biologique) ont pu travailler séparément, l'exposome défini par l'ANSES a réuni toute la communauté « omiques » des petites molécules. La définition de l'ANSES est la suivante : *Le concept d'exposome est né de la nécessité de mieux comprendre l'influence sur la santé de* ***toutes les expositions auxquelles est soumis un individu pendant sa vie entière****, en prenant en compte les expositions environnementales aux agents chimiques, physiques, biologiques et les facteurs socio-économiques.*

Des chercheurs de l'ANSES ont justement mené cet exercice complexe d'analyse de l'exposome sur la population française (Traoré et al. 2016) mais également sur la sous-population des femmes françaises enceintes (Traoré et al. 2018). Afin de réaliser l'étude globale sur la population française, les chercheurs ont réuni un grand nombre de données (régime alimentaire, sexe, âge, salaire, indice de masse corporelle…) sur chaque personne de l'étude (2607 adultes triés d'échantillons précédents) et ils se sont basés sur l'enquête Individual and National Food Consumption Survey (INCA2), menée de 2005 à 2007. Cette analyse leur a permis de mettre en évidence 440 substances et plus particulièrement 6 groupes de substances (pesticide, bisphénol…) dont l'origine peut être déterminée (pollution, fruit et légumes…), ensuite ses informations sont croisées avec les données des adultes participants à l'étude. Ces études croisées, ont montré que certaines substances étaient plus présentes dans certaines populations (sexe, classe d'âge, classe socio-économique…), un classement des substances peut être fait pour hiérarchiser les études de toxicologies à réaliser.

Un problème majeur est l'évolution de l'exposome au cours du temps, celui-ci évoluant rapidement et une étude à un temps donné est rapidement dépassée même si cette étude reste intéressante et informative. Les polluants, les doses changent avec les temps et ce qui nécessite que l'analyse de l'exposome soit régulière et renouvelée.

Pour tenter de résoudre cette difficulté des toxicités croisées et de leur explosion combinatoire, un deuxième concept se base sur les études mécanistiques. En effet, si les mécanismes d'action sur le vivant sont connus pour plusieurs composés, il devient possible de prédire des interactions entre eux et donc les combinaisons les plus pertinentes à tester.

Dans ce cadre conceptuel, la première approche consiste à déterminer des voies critiques d'effets négatifs (Adverse Outcome Pathways), à déterminer l'effet de composés d'intérêt sur ces voies et à en déduire des interactions négatives (synergies toxiques) qui peuvent ensuite être testées. Cette approche, en plein essor actuellement (voir le rapport sur les tests et l'évaluation de l'OCDE n°344 ENV/CBC/MONO(2021)22) représente un progrès certain par rapport à des tests de paramètres uniques. Cependant, elle reste focalisée sur quelques voies bien connues et présente donc des limitations pour prédire des interactions peu prévisibles selon ce système de voies. Cette approche « AOP » est illustrée sur la figure 49.

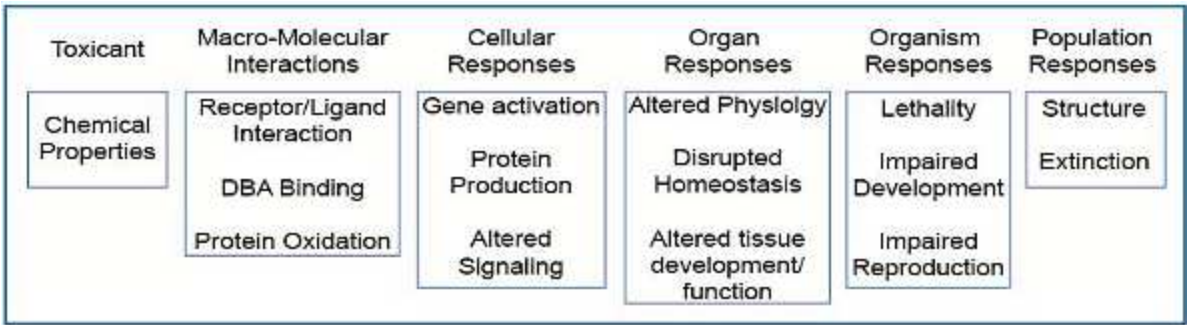

Figure 50 : Représentation schématique de l'AOP illustrée en référence à un certain nombre de voies, d'après l'OCDE. Un modèle qui identifie la séquence des événements moléculaires et cellulaires nécessaires pour produire un effet toxique lorsqu'un organisme est exposé à une substance.

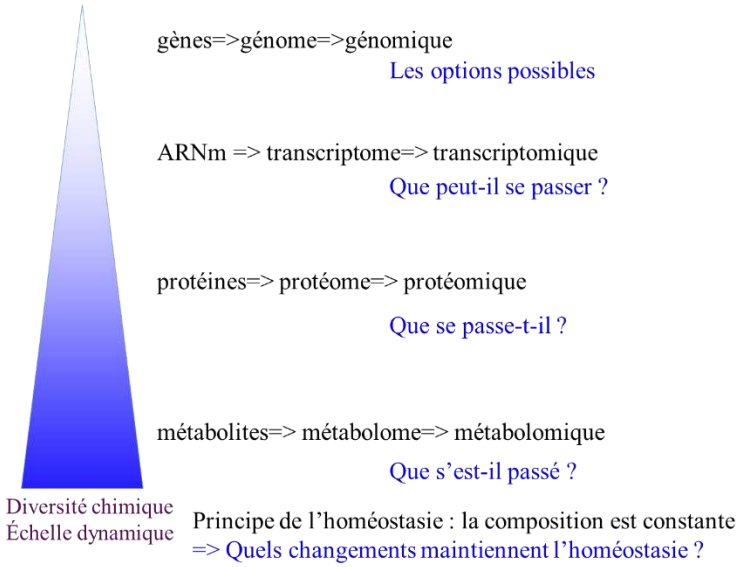

Figure 49 : Technique de screening : la protéomique

La deuxième approche basée sur les données mécanistiques s'appuie sur les techniques à grande échelle, dites techniques « omiques ». Conceptuellement, l'idée est de caractériser de la façon la plus large possible et avec le minimum d'a priori conceptuels la réponse d'un modèle biologique à une perturbation donnée, par exemple une substance chimique d'intérêt. Une fois cette réponse caractérisée, il devient possible de prédire quels composés ou paramètres risquent d'entraîner une interaction avec le composé d'intérêt, en utilisant les connaissances (omiques ou non) accumulées sur différents composés. Cette interaction peut ensuite être testée. De plus, en étudiant simultanément un grand nombre de macromolécules biologiques, ces analyses omiques enrichissent la détermination des AOPs pour les différents composés étudiés.

Il existe différentes techniques d'analyses « omiques » : la génomique, la transcriptomique, la protéomique et la métabolomique (figure 50). Ces techniques analysent le contenu des cellules ou organismes à différents niveaux d'expression : les gènes (options possibles), l'ARNm (options probables), les protéines (état actuel) et métabolites (état passé). Par exemple, une étude sur l'exposition répétée, mais non quotidienne, aux nanoparticules d'argent sur des cellules humaines de l'épithélium pulmonaire est basée sur la transcriptomique (Gliga et al. 2018). L'étude transcriptomique et les tests de validation ont montré un effet pro-fibrotique et une modification des cellules d'épithélium à mésenchyme (perte d'adhésion et de polarité) ce qui favorise l'apparition de cellules cancéreuses.

La protéomique est une méthode permettant d'identifier et quantifier un grand nombre de protéines présentes dans les cellules, un tissu ou un organisme. Cette technique est utilisée pour trouver des cibles thérapeutiques, poser un diagnostic, produire des vaccins et comprendre les mécanismes cellulaires (pathogénicité, toxicité, maladie…) (Aslam et al. 2017). En effet, la présence d'une protéine ou d'un ensemble de protéines est un témoin de l'état de la cellule et de son activité, à un moment donné. Le terme « protéomique » a été utilisé pour la première fois en 1994-1995, par Marc Wilkins pour désigner le complément PROTéine du génOME (Wasinger et al. 1995). Le protéome des cellules eucaryotes exprime non seulement l'information génétique mais également une certaine dynamique. Cependant son analyse est complexe étant donné sa grande diversité (nature des protéines, quantité, taille moléculaire, structure, modification post-traductionnelle…). Il existe différentes techniques d'analyse du protéome (figure 51), les tests ELISA, les western blots sont utilisés pour des analyses à échelle réduite. Dans le cas d'échantillons d'analyses à plus grande échelle (grand nombre de paramètres), le SDS-PAGE (Sodium dodecyl sulfate-polyacrylamide gel electrophoresis), 2-DE (two-dimensional gel electrophoresis) et le 2D-DIGE (two-dimensional differential gel electrophoresis) sont utilisés pour séparer les protéines (Marcus and Rabilloud 2020). De nouvelles techniques plus rapides comme la spectrométrie de masse (MS) se sont développées, elles sont plus sensibles que les gels d'électrophorèse, et basées sur les peptides. Après ces techniques d'analyses, un traitement des données est réalisé en utilisant des outils de biostatistiques tels que R, PAST ou python. En effet, plusieurs milliers de protéines peuvent être identifiées dans chaque échantillon, selon le nombre de conditions et réplicats, la quantité de données à traiter devient rapidement très importante. En se basant sur le principe d'homéostasie, qui veut que les organismes vivants cherchent à maintenir un fonctionnement constant, les analyses statistiques pointent dans les données d'abondance les protéines dont l'expression change et qui sont donc liées à

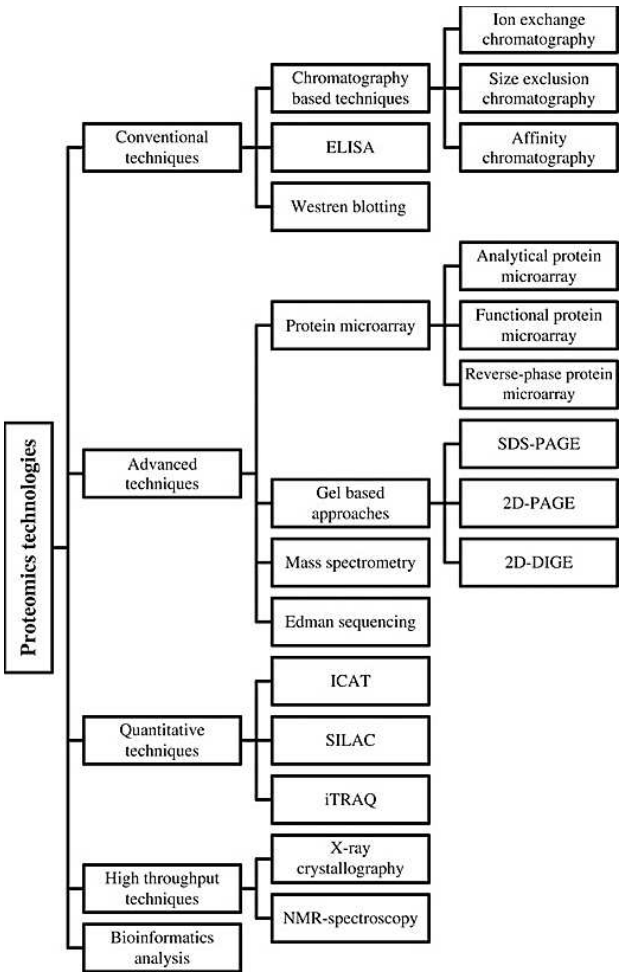

Figure 51 : Techniques de protéomiques, d'après Aslam et al. 2017.

la réponse biologique au phénomène d'intérêt (dans notre cas, l'exposition à un nanomatériau). Dans un deuxième temps, l'analyse de voies au moyen de logiciels spécialisés comme DAVID ou Panther permet de regrouper les protéines par familles (pathways), et ainsi de hiérarchiser les voies métaboliques ou les fonctions des cellules exposées qui sont modifiées par rapport à la condition contrôle. Cette analyse permet ensuite d'orienter les tests de validation, et ainsi d'obtenir une réponse complète sur le profil des cellules et le phénomène biologique qui en résulte.

L'analyse protéomique a déjà été utilisée pour étudier la toxicologie de nombreuses substances : médicaments, produits naturels, produits chimiques ou nanoparticules. Cette technique peut également être utilisée à plusieurs niveaux, pour déterminer les cibles d'actions d'un médicament ou bien pour comprendre l'effet moléculaire d'un polluant au niveau d'une cellule ou d'un tissu. Les possibilités offertes par l'analyse protéomique sont présentées dans cette revue (Rabilloud and Lescuyer 2015). La protéomique a souvent été utilisée en complément d'autres techniques « omiques » ou bien pour étudier les effets des hydrocarbures aromatiques polycycliques (HAP), mais d'autres substances ont également été analysées afin d'anticiper les effets secondaires possibles ou les réactions complexes qu'un médicament pourraient provoquer. Certaines études ont combiné les médicaments pour examiner les effets de traitements croisés (médicaments avec la même cible ou même classe thérapeutique). Certaines familles de protéines, dont l'expression est modifiée, sont communes à de nombreuses substances (médicaments, produit naturel, produits industriels, métaux) comme les protéines mitochondriales, les chaperonnes, l'énolase, le stress du réticulum endoplasmique ou les sous-unités du protéasome. Pour certaines substances, les effets sont observables longtemps après l'exposition, comme par exemple pour les hydrocarbures, la protéomique pourrait être un moyen de détection précoce au niveau moléculaire. Cependant, certaines études s'appuient seulement sur les résultats de protéomique, sans réaliser de tests de validation, ce qui peut entraîner des conclusions prématurées sur les effets réels induits par la substance. En effet, certaines modifications du protéome permettent de maintenir l'homéostasie de l'organisme, du tissu ou de la cellule étudié(e) ce qui résulte en une réponse détectable au niveau des analyses omiques mais un fonctionnement normal (observé grâce aux tests de validation).

Actuellement, les deux principales techniques utilisées en « omiques » sont la transcriptomique et la protéomique. La première est une étude exhaustive des 20 000 gènes codants ou non chez l'Homme mais qui ne tient pas compte des régulations cellulaires qui peuvent avoir lieu (Marcus and Rabilloud 2020). La protéomique analyse un grand nombre des protéines présentes dans la cellule ou le tissu, cependant elle ne tient pas compte de certaines modifications post-traductionnelles. Les deux techniques sont assez proches, la protéomique reste cependant plus proche de la réalité ou de l'état de la cellule au moment de l'analyse car elle permet une certaine caractérisation des protéines et pas seulement leur identification, qui est ensuite validée à l'aide de tests complémentaires et ciblés.

En effet, la combinaison études protéomiques-études de validation permet de mettre en évidence des voies conduisant à des mécanismes toxiques et à des synergies toxicologiques très difficiles à prédire. Par exemple l'analyse protéomique réalisée dans une étude sur les réponses aux nanoparticules d'oxyde de cuivre (CuO) (S. Triboulet et al. 2015) a permis de montrer dans un premier temps la spécificité des effets observés. En effet, les effets sont différents de ceux induits par une exposition à une autre nanoparticule (TiO2) ou de ceux induits par l'ion cuivre. En approfondissant les voies suggérées par les protéines modifiées en réponse au nano CuO, des voies originales ont été mises en évidence. Par exemple, une diminution de la quantité de la protéine sépiaptérine réductase a été observée en réponse au nano CuO. Cette protéine

catalyse la synthèse de la tetrahydrobiopterine, impliquée dans l'hydroxylation de certains acides aminés (Phe, Tyr et Trp) Un test d'interaction entre l'hydroxylation des acides aminés et la sensibilité au cuivre a été réalisé en utilisant les produits de cette hydroxylation (tyrosine, DOPA ou 6-hydroxytryptophane). Seule la DOPA (hydroxylation de la tyrosine par la tetrahydrobiopterine) augmente la toxicité du cuivre sur les macrophages J774 ce qui se traduit avec une cytotoxicité très importante du CuO d'autant plus marqué pour les ions que pour les nanoparticules. Cette toxicité croisée avait seulement été observée pour les neurones catecholaminergiques. C'est l'analyse protéomique qui a mis en évidence cette voie métabolique d'oxydation des acides aminés et a permis de tester cette observation grâce à un test de viabilité après une co-exposition (inhibiteur 6h puis cuivre 18h).

Toujours dans la même étude, une forte induction de l'hème oxygénase est observée. Cette protéine étant supposée jouer un rôle protecteur contre le stress oxydant, l'étude de son rôle protecteur éventuel contre la toxicité du nano CuO a été menée (S. Triboulet et al. 2015). Pour ce faire, la production de la protéine a été induite par traitement des cellules avec la lovastatine (un médicament contre le cholestérol). Cette induction préalable à l'exposition au nano CuO a produit un effet protecteur comme prédit.

Dans une autre étue portant sur les réponses des macrophages aux nanoparticules d'oxyde de zinc (Aude-Garcia, Dalzon, et al. 2016), les auteurs ont mis en évidence, *via* l'analyse protéomique, une augmentation d'abondance de protéines impliquées dans la réparation de l'ADN, de protéines impliquées dans la détoxification des aldéhydes, et de certaines enzymes métaboliques comme la GAPDH. Par des études ciblées, les auteurs ont ensuite mis en évidence un mécanisme toxique des nanoparticules d'oxyde de zinc passant par l'inhibition de la GAPDH par les ions zinc libérés par la dissolution intracellulaire des nanoparticules, cette inhibition conduisant à l'augmentation de la production intracellulaire de méthylglyoxal, aldéhyde toxique dont on retrouve ensuite un adduit sur la déoxyguanosine de l'ADN.

Ces exemples montrent que l'analyse protéomique permet de mettre en évidence des réponses cellulaires variées. Appliquée aux systèmes *in vitro*, elle permet une étude assez rapide et large des réponses cellulaires, permettant ainsi dans certains cas de prédire des phénomènes de toxicité croisée qui peuvent être ensuite étudiés de façon ciblée.

Nous avons donc utilisé la protéomique pour certains des articles présentés ci-après, l'étude du protéome a donné des pistes à explorer pour comprendre les mécanismes biologiques et les éventuels effets toxicologiques suite à l'exposition des cellules aux nanomatériaux notamment. Cette technique a été combinée aux études *in vitro* pour étudier la toxicologie des nanomatériaux, notamment en utilisant une exposition répétée afin d'évaluer le débit de dose mais également d'étudier la persistance des nanomatériaux et de leurs effets. Ces deux problématiques ont été l'objet de mon travail de thèse sur la silice amorphe de synthèse principalement. La première partie concerne le protocole de persistance suivi par celui des expositions répétées.

Etudes en cours au laboratoire et démarche expérimentale

Le contexte global de la toxicologie et plus spécifiquement celle des nanomatériaux a été présentée dans les parties précédentes. L'activité de l'équipe ProMIT (Protéomique pour la Microbiologie, l'immunologie et la toxicologie, anciennement Protéomique Métaux et Différenciation) était l'étude des effets d'une exposition aux métaux sous différentes formes, notamment le cuivre, l'argent, ou le zinc (Aude-Garcia, Dalzon, et al. 2016; Toybou et al. 2019; S. Triboulet et al. 2014; 2015; Dalzon et al. 2016; Aude-Garcia, Villiers, et al. 2016; Dalzon et al. 2017; Chevallet et al. 2011; Veronesi et al. 2015; Armand et al. 2016; Sarah Triboulet et al. 2013).

Les premières études publiées par le laboratoire (2013-2015) s'étaient focalisées sur l'apport de l'analyse protéomique pour réaliser des études à visées mécanistiques, et ainsi mieux comprendre les effets des nanoparticules métalliques sur les macrophages, ce qui permettait en retour de prédire de possibles synergies toxiques, ou au contraire des mécanismes protecteurs. Dans ce contexte général, des mécanismes originaux de toxicité du zinc ont été mis en évidence (Aude-Garcia, Dalzon, et al. 2016), et des phénomènes de synergies toxiques ou de protection ont été mis en évidence pour le cuivre (Sarah Triboulet et al. 2013; S. Triboulet et al. 2015) . Cependant, ces études utilisaient des systèmes classiques d'exposition à court terme (24h) avec une lecture des effets immédiatement après l'exposition.

A partir de 2015-2016, l'équipe s'est progressivement intéressée à la question de la persistance des effets et à celle des effets d'expositions répétées. Ce sujet s'est développé sur les nanoparticules d'argent (Aude-Garcia, Villiers, et al. 2016). A partir de cette publication initiale, qui montrait à la fois la réversibilité des effets des nanoparticules d'argent et des effets différents entre une exposition unique à forte dose et une exposition à la même dose cumulative mais fractionnée dans le temps, l'équipe a enclenché une série d'études utilisant à la fois ces scénarii d'exposition (exposition répétée, exposition unique suivie d'une période de récupération) et l'analyse protéomique pour mieux comprendre les phénomènes moléculaires présidant aux réponses cellulaires dans ces scénarii d'exposition. A mon arrivée au laboratoire, différentes études étaient en cours sur les nanoparticules et les nanofils d'argent, et j'ai pu participer à l'une d'entre elles sur la persistance des effets des nanoparticules d'argent sur les macrophages (Dalzon et al. 2019). Cette étude montrait un retour à la normale partiel après exposition à des nanoparticules d'argent puis récupération, avec une adaptation moléculaire complexe. Une autre étude (Dalzon, Torres, et al. 2020), montrait que contrairement à ce qui était attendu, des macrophages exposés de façon répétée à des doses modérées d'argent montraient des perturbations moléculaires plus importantes que ceux exposés à la même dose cumulée, mais en une exposition unique. Enfin, les travaux sur les nanofils d'argent (Toybou et al. 2019) avait montré des effets inflammatoires différents selon la longueur des nanofils et surtout une persistance différente de ces effets, toujours selon la longueur, les nanofils longs (>10µm) induisant des effets inflammatoires persistants. De façon très encourageante, ces résultats obtenus *in vitro* en quelques jours reproduisaient les effets observés *in vivo* sur les nanofils d'argent (Schinwald, Chernova, and Donaldson 2012; Chung et al. 2017) et ce à la fois en termes de persistance et d'effets différentiels des nanofils de différentes longueurs.

Ces résultats suggéraient que le système de macrophages en culture prolongée pouvait être intéressant dans le cadre d'une approche 3R dans un contexte d'utilisation raisonnée et minimale du modèle animal. Cependant, seule l'étude sur les nanofils d'argent avait une correspondance avec des expériences *in vivo*. De plus, tous les résultats avaient été obtenus avec des nanomatériaux à base d'argent, et il ne pouvait donc pas être exclu que la

correspondance *in vivo-in vitro* observée sur les nanofils soit due à un effet particulier de la chimie d'argent et donc soit de l'ordre de la coïncidence.

Il est donc souhaitable de valider ces approches *in vitro* faisant appel aux scénarii développés au laboratoire sur un nanomatériau complètement de chimie totalement différente, si possible un matériau bien connu et pour lequel des études de toxicité *in vivo* seraient disponibles, mais qui soit aussi un matériau sur lequel des développements sont toujours en cours, ce qui validerait l'intérêt pratique de nos systèmes *in vitro* dans le cadre d'une approche « safe by design », qui nécessite des tests de toxicologie rapide et pas trop onéreux. La silice amorphe de synthèse s'est rapidement imposée comme un matériau de choix. En effet, la silice amorphe de synthèse est utilisée depuis longtemps dans de nombreuses applications et donc avec de forts tonnages (Flörke et al. 2008). De plus, et du fait des effets persistants bien connus de la silice cristalline (American Thoracic Society Committee of the Scientific Assembly on Environmental and Occupational Health 1997), la question de la persistance des effets reste centrale dans la toxicologie de toutes les formes de silice. Enfin, la silice amorphe de synthèse est un nanomatériau dont le développement industriel continue, afin de proposer des performances techniques toujours accrues. Par exemple, la chimie des silanes permet de modifier à façon les propriétés de surface des silices amorphes de synthèse et de proposer des silices hydrophobes ou de charge de surface modifiée. D'autres possibilités techniques de modification des silices amorphes de synthèse sont aussi développées chez les industriels du secteur. Du fait de ces modifications, qui peuvent conduire à des altérations substantielles des réponses biologiques à ces matériaux, les résultats obtenus *in vivo* sur des silices amorphes de synthèse classiques (Arts et al. 2007; Sayes, Reed, and Warheit 2007) ne seront pas transposables à de nouveaux types de silice amorphe de synthèse. Dans ce cadre, et même si les tests règlementaires de toxicologie requis par la directive REACH devront être conduits, des tests rapides de toxicologie *in vitro* pourraient s'avérer d'un grand intérêt dans le cadre d'une approche safe by design. Cependant, il est crucial dans cette approche que les tests *in vitro* soient aussi pertinents que possible, et soient donc concordants avec les tests *in vivo* quand des paramètres similaires sont étudiés.

Mon travail de thèse sur les effets de la silice amorphe de synthèse sur les macrophages s'est donc engagé puis déployé selon deux axes :

Le premier axe portait sur la validation du système *in vitro* de macrophages pour étudier les phénomènes de persistance et de débit de dose. En particulier, il fallait vérifier si le système *in vitro* pouvait reproduire les effets pro-inflammatoires induits *in vivo* par différentes formes de silice, à savoir des effets transitoires pour la silice amorphe et persistants pour la silice cristalline (Arts et al. 2007). Cette condition devait absolument être remplie pour s'assurer de la pertinence du système *in vitro*, et pouvait nous conduire à devoir adapter le système *in vitro* pour s'assurer de ce point.

Le deuxième axe portait sur l'exploitation de ce système *in vitro*, dans les scénarii d'exposition développés au laboratoire, pour documenter au mieux les effets des silices amorphes de synthèse sur les macrophages. Au vu des résultats obtenus au laboratoire sur les nanoparticules d'argent, il était *a priori* intéressant de documenter trois types d'effets au niveau moléculaire :

1) Les effets d'une exposition aiguë à une dose subtoxique
2) La réversibilité de ces effets après une période de récupération post-exposition
3) Les effets d'une exposition répétée à une faible dose

L'étude de la réversibilité était particulièrement intéressante, vu qu'elle pouvait éventuellement donner des pistes moléculaires à un effet observé *in vivo*. Lors d'expériences de toxicologie par inhalation, la disparition des effets inflammatoires s'accompagne d'une diminution du taux de silice dans les poumons, mesurée par analyse élémentaire (Arts et al. 2007). Cependant, cette diminution peut être liée à des mécanismes complètement différents. Il peut s'agir en effet soit d'une dissolution de la silice dans l'environnement biologique, comme observé pour des nanoparticules d'oxyde de fer (Beck-Speier et al. 2009) ou d'argent (Kreyling et al. 2020), soit d'une élimination avec les macrophages ayant internalisé la silice, par l'ascenseur muco-ciliaire, comme observé pour des particules d'iridium (Semmler et al. 2004) ou d'or (Kreyling et al. 2018). Le fait de disposer d'un système *in vitro* permettant d'étudier les phénomènes de persistance ou de réversibilité devrait pouvoir permettre d'aborder cette question, qui reste difficile à aborder *in vivo* du fait du silicium présent dans l'eau de boisson et dans la nourriture des animaux de laboratoire, ce qui complique considérablement l'étude du transfert vers le tube digestif *via* l'ascenseur muco-ciliaire.

Au-delà de cette question spécifique, mon travail de thèse devait s'atteler à une documentation large des effets moléculaires des silices amorphes de synthèse sur les macrophages, en utilisant l'analyse protéomique. En effet, des travaux préalables menés sur une silice colloïdale (un type de silice amorphe de synthèse) au moyen de l'analyse protéomique avaient permis de suggérer des effets de toxicité croisée entre cette silice colloïdale et des agents génotoxiques (Dalzon et al. 2017), ce qui démontrait encore une fois la puissance de l'analyse protéomique. Cependant, ce travail même montrait l'importance des expériences de validation pour vérifier les hypothèses issues de l'analyse protéomique et en particulier pour interpréter correctement les données de protéomique en termes de physiologie cellulaire.

Dans un premier temps, la protéomique permet de voir des modifications dans l'abondance des protéines entre les différentes conditions étudiées, et ce sans faire d'hypothèse préalable. L'objectif des cellules étant de maintenir une certaine homéostasie, chaque changement est important et pertinent pour comprendre les effets de l'exposition à une substance. Ce changement d'abondance peut être le résultat de deux réponses différentes : une réponse essentielle ou une réponse « fitness ». Dans le premier cas, le changement observé est indispensable à la survie cellulaire, alors que dans le deuxième cas, il s'agit d'une ré-optimisation de l'homéostasie cellulaire. Dans les deux situations, le système est altéré sur le plan protéomique, mais rien ne permet de déterminer *a priori* si les changements observés lors de l'analyse protéomique sont essentiels ou de fitness. L'analyse de ces changements d'abondance permet de regrouper les protéines par famille (ou pathways) et ensuite de réaliser des tests de validation qui permettent de comprendre les phénomènes en cours. Ces expériences renseignent sur le fonctionnement des cellules et permettent d'interpréter correctement les changements d'abondance observés en protéomiques.

Ce point souvent négligé est pourtant d'une importance cruciale, comme le montrent les travaux du groupe de Martins-de-Souza sur la schizophrénie. Dans cette maladie, l'analyse protéomique du thalamus montre une surexpression des enzymes de la glycolyse (Martins-de-Souza et al. 2010). Or cette surexpression peut être interprétée de deux façons très différentes, pour ne pas dire opposée. Dans la première interprétation, la glycolyse est considérée comme exacerbée par rapport à la situation normale, et ce sur-métabolisme peut conduire à une production accrue d'espèces oxygénées réactives, conduisant à des anomalies cellulaires qui seraient la cause de la maladie mentale. Dans la deuxième hypothèse, la surexpression des enzymes de la glycolyse serait au contraire un phénomène compensatoire visant à rétablir un métabolisme déficient car trop faible. De fait, seules des expériences de validation menées sur les métabolites permettent de trancher entre ces deux hypothèses, et ces tests de validation ont

validé l'hypothèse d'un métabolisme faiblement efficace dans le cerveau des patients schizophrènes (Martins-de-Souza et al. 2010). La reconnaissance de cette dimension métabolique de la schizophrénie a permis de faire évoluer les traitements pour une meilleure prise en charge des patients. La co-administration de l'antipsychotique clozapine et de l'antidiabétique metformine ont amélioré le contrôle métabolique chez les patients, en réduisant le poids corporel, les taux d'insuline et de triglycérides, sans altération de l'état mental (Carrizo et al. 2009). De même, le co-traitement par l'olanzapine et la metformine permet de réguler le poids corporel et contrôle le métabolisme des glucides, sans compromettre l'efficacité de l'antipsychotique (Baptista et al. 2007). Les hypothèses et pistes soulevées par ces analyses du protéome des patients souffrants de schizophrénie ont été explorées en détail, ce qui a permis d'apporter des réponses, une meilleure compréhension de cette maladie et une meilleure prise en charge des patients.

Nous avons donc utilisé ce même principe exploratoire dans nos études sur les silices amorphes de synthèse, en utilisant des tests de validation en routine (phagocytose, production d'oxyde nitrique et de cytokines) et des tests ciblés résultant de l'analyse protéomique (potentiel mitochondrial, métabolisme spécifique, marqueurs de surface, observation du cytosquelette…). Nous avons également utilisé différents grades de silices amorphes de synthèse et différents modes d'expositions selon le contexte de l'étude. Pour la partie protéomique *stricto sensu*, la partie d'analyse en spectrométrie de masse a été réalisée par nos collaborateurs de l'Institut Pluridisciplinaire Hubert Curien, mais j'ai appris au cours de ma thèse à réaliser la partie en amont (dessin et planification expérimentale, préparation des échantillons) et la partie en aval de la spectrométrie de masse, à savoir l'analyse et l'interprétation des données, ainsi que les tests de validation mentionnés ci-dessus.

Les deux dimensions de validation et d'exploitation du système de macrophages *in vitro* n'ont pas été abordées séquentiellement (validation puis exploitation). Pour des raisons d'efficacité temporelle, les expériences d'analyse protéomique ont souvent été planifiées et réalisées dès lors que les expériences préliminaires avaient donné des indications que le système se comportait correctement, en particulier pour les phénomènes de persistance, d'où des publications intégrant souvent les deux dimensions (validation et exploitation) en même temps. En conséquence, les dates de publication des articles composant cette thèse ne reflètent pas un ordre logique, mais plutôt les difficultés rencontrées pour achever certains travaux et les difficultés inhérentes au processus de publication en lui-même.

Quatrième partie : Méthodes expérimentales et résultats

I Système d'études de la persistance

Lors d'études de la persistance des effets biologiques via des systèmes *in vitro*, il est nécessaire de maintenir les cellules en culture pendant des périodes prolongées. Il a donc été nécessaire de commencer par vérifier la cohérence de certains choix techniques par rapport à ceux utilisés dans les études à court terme.

I a) Vérification du système

A proteomic-informed view of the changes induced by loss of cellular adherence: The example of mouse macrophages

Présentation du projet

Au vu des protocoles d'exposition envisagés afin de tester la persistance des effets suite à une exposition à des nanomatériaux, les supports de culture ont dû être adaptés. En effet, lors d'une exposition courte de 24 heures des plaques de cultures non adhérentes sont utilisées. En effet, les macrophages sont des cellules très fortement adhérentes, et qui sont donc endommagées quand on essaye de les décoller des supports de culture adhérents. Il est donc plus efficace et moins dommageable pour les cellules de les cultiver sur des supports non-adhérents. Cependant, afin d'étudier la persistance, il est nécessaire de cultiver les cellules durant une semaine, et donc d'effectuer des changements de milieux. Cela nécessite de cultiver les cellules sur un support adhérent et traité. De plus, lors d'observation en microscopie, les cellules doivent être cultivées sur lamelle en verre, et il s'agit également d'un support adhérent. Dans la littérature, l'adhésion est référencée comme étant une élément important permettant de contrôler la division cellulaire, la migration et la survie des cellules (Huang and Ingber 1999). Il est également connu que les changements d'adhésion cellulaire sont à l'origine de nombreuses pathologies, comme par exemple la migration des cellules cancéreuses. Dans ce projet, nous avons donc voulu vérifier les éventuelles modifications dans les réponses aux expériences, entre les cellules en suspension et les cellules adhérentes. Pour cela, nous avons réalisé une étude protéomique afin d'obtenir un panel de protéines dont l'expression pourrait être modifiée selon l'état d'adhésion des cellules. Des expériences ciblées ont ensuite été réalisées sur le cytosquelette, le métabolisme cellulaire, l'activité phagocytaire et la réponse inflammatoire.

PLOS ONE

RESEARCH ARTICLE

A proteomic-informed view of the changes induced by loss of cellular adherence: The example of mouse macrophages

Sacnite Ramirez Rios[1☯], Anaelle Torres[2☯], Hélène Diemer[3,4], Véronique Collin-Faure[2], Sarah Cianférani[3,4], Laurence Lafanechère[1], Thierry Rabilloud[2]*

1 Institute for Advanced Biosciences, Univ. Grenoble Alpes, CNRS UMR 5309, INSERM U1209, Grenoble, France, **2** Chemistry and Biology of Metals, Univ. Grenoble Alpes, CNRS UMR5249, CEA, IRIG-DIESE-CBM-ProMD, Grenoble, France, **3** Laboratoire de Spectrométrie de Masse BioOrganique (LSMBO), Université de Strasbourg, CNRS, IPHC UMR 7178, Strasbourg, France, **4** Infrastructure Nationale de Protéomique, FR2048 ProFI, Strasbourg, France

☯ These authors contributed equally to this work.
* thierry.rabilloud@cnrs.fr

Citation: Ramirez Rios S, Torres A, Diemer H, Collin-Faure V, Cianférani S, Lafanechère L, et al. (2021) A proteomic-informed view of the changes induced by loss of cellular adherence: The example of mouse macrophages. PLoS ONE 16(5): e0252450. https://doi.org/10.1371/journal.pone.0252450

Editor: Jon M. Jacobs, Pacific Northwest National Laboratory, UNITED STATES

Received: November 12, 2020

Accepted: May 14, 2021

Published: May 28, 2021

Peer Review History: PLOS recognizes the benefits of transparency in the peer review process; therefore, we enable the publication of all of the content of peer review and author responses alongside final, published articles. The editorial history of this article is available here: https://doi.org/10.1371/journal.pone.0252450

Data Availability Statement: All relevant data are within the manuscript and its supporting information.

Abstract

Except cells circulating in the bloodstream, most cells in vertebrates are adherent. Studying the repercussions of adherence *per se* in cell physiology is thus very difficult to carry out, although it plays an important role in cancer biology, e.g. in the metastasis process. In order to study how adherence impacts major cell functions, we used a murine macrophage cell line. Opposite to the monocyte/macrophage system, where adherence is associated with the acquisition of differentiated functions, these cells can be grown in both adherent or suspension conditions without altering their differentiated functions (phagocytosis and inflammation signaling). We used a proteomic approach to cover a large panel of proteins potentially modified by the adherence status. Targeted experiments were carried out to validate the proteomic results, e.g. on metabolic enzymes, mitochondrial and cytoskeletal proteins. The mitochondrial activity was increased in non-adherent cells compared with adherent cells, without differences in glucose consumption. Concerning the cytoskeleton, a rearrangement of the actin organization (filopodia *vs* sub-cortical network) and of the microtubule network were observed between adherent and non-adherent cells. Taken together, these data show the mechanisms at play for the modification of the cytoskeleton and also modifications of the metabolic activity between adherent and non-adherent cells.

Introduction

In vertebrates, all cells except circulating blood cells must adhere to support their normal growth and functions. The adherence to extracellular matrix and/or other cells is critical and adherent cells placed in non-adherent conditions either die or form multicellular spheroids. Placing cells in non-adherent conditions has been used to induce differentiation in teratocarcinoma cells [1–3] and more recently to form organoids (e.g. in [4, 5]). Because of such

Funding: This work was supported by Agence Nationale pour la Recherche, France in the form of a grant awarded to SC (ANR-10-INBS-08-03), as well as University Grenoble Alpes and French National Centre for Scientific Research (CNRS) in the form of recurring basic funding for the labs and research teams. The funders had no role in study design, data collection and analysis, decision to publish, or preparation of the manuscript.

Competing interests: The authors have decalred no competing interests.

important consequences induced by cell adhesion on cell growth and function, the transition between adherent and non-adherent states is rather rare. There are however physiological situations, such as blood cells diapedesis, during which cells that circulate into the blood stream must adhere to the endothelial cells and cross the endothelial barrier to reach target tissues.

Another example of transition, from an adherent to a non-adherent state, is observed in the metastatic process, where cells detach from the tumor mass and circulate in the blood and lymphatic vasculature prior to reattaching and extravasating to colonize distant organs [6].

The comparative analysis of the only effects of adherence on cellular functions is complicated by the fact that in many studies models the acquisition or loss of adherence induces major alterations in cell physiology that would obscure the effects of the adherence itself. For example, P19 teratocarcinoma cells differentiate in suspension spheroids while they do not in adhering conditions [7]. In this context, the comparison between spheroids and adherent cells would not be a comparison between adherent and non-adherent cells, but between differentiated cells adhering between them and undifferentiated cells adhering on plastic.

Mouse macrophage cell lines represent one of the rare experimental models that may be suitable to compare the adherent and non-adherent states. Indeed, they grow equally well under adherent and non-adherent conditions and keep their differentiated functions under both conditions. We therefore decided to use this model to analyze the changes between the adherent and the non-adherent state using a broad approach, based on proteomics.

Materials and methods

Unless specified otherwise, the chemicals used in this work were purchased from Sigma-Millipore and were at least 99% pure.

Cell culture

The mouse monocyte/macrophage cell line RAW264.7 was purchased from the European Cell Culture Collection (Salisbury, UK). The cells were cultured in RPMI 1640 medium supplemented with 10% fetal bovine serum. Because the cells are strongly adherent to classical culture plastics, they are easily damaged when passaged, either with trypsin digestion, chemical detachment with EDTA or with scraping. They were thus routinely cultured on non-treated plastics for non-adherent cells, from which they were easily removed for passaging. Cells were seeded every two days at 200,000 cells/mL and harvested at 1,000,000 cells per ml. For the adherent vs. suspension cultures, cells were seeded at 500,000 cells/ml on either adherent T75 flasks or 6-well plates (Corning) or on non-adherent T75 flasks or 6-well plates (suspension culture flasks from Greiner) and let to grow for 24 hours. For harvesting the adherent cells in the adherent flasks, the culture medium (containing a few non-adherent cells) was removed, and the adherent cell layer was rinsed 3 times with serum-free RPMI 1640 medium. The cells were then scraped in Hepes buffered saline (Hepes-NaOH pH 7.5 10mM, NaCl 150mM, MgCl2 2mM) and collected by centrifugation (400g, 5 minutes). For harvesting the non-adherent cells in the non-adherent flasks, the flasks were shaken and the cell medium containing the non-adherent cells was collected, allowing the few adherent cells to stay within the culture flask. The suspension was centrifuged (400g, 5 minutes) and the cell pellet was rinsed 3 times with serum-free RPMI 1640 medium and once with Hepes buffered saline. The cell pellets were then processed for further use.

For harvesting cells from adherent plates, the culture medium was removed, and the adherent cell layer was rinsed once with serum-free RPMI 1640 medium. The cells were then detached by incubation in PBS containing 1mM EDTA for 5 minutes, following by flushing repeatedly the cell layer. The cell suspension was then diluted with an equal volume of serum-

free RPMI 1640 medium, and the cells were collected by centrifugation. For harvesting the non-adherent cells in the non-adherent plates, repeated flushing was used. The suspension was centrifuged (400g, 5 minutes) and the cell pellet was rinsed 3 times with serum-free RPMI 1640 medium.

Adherence tests and cell cycle analysis

For the adherence test, cells were seeded at 500,000 cells/ml on either adherent T25 flasks (Corning) or on non-adherent T25 flasks (suspension culture flasks from Greiner) and let to grow for 24 hours. The culture medium was then recovered and the number of non-adherent cells was determined by cell counting.

For the cell cycle analysis, the cells were cultured on adherent or non-adherent plates, as described above. To avoid any bias that may be due to selective damage of adherent cells in any phase of the cell cycle, the analysis was carried out on isolated nuclei rather than on detached cells. To this purpose, a protocol based on the citric acid method described by Miller [8] was used. Cells were seeded at 500,000 cells/ml on 6-well plates (Corning) or on non-adherent 6-well plates (suspension culture flasks from Greiner) and let to grow for 24 hours. For adherent cells, the culture medium was removed, and the cell layer rinsed twice with PBS. The cell layer was the lysed by addition of 0.5 ml of ice-cold fractionation buffer (25 mM Hepes pH 7.5, 25 mM NaCl, 10 mM MgCl2, 0.5% Triton X100). After 1 minute of lysis, 25 μl of 20% (w/v) citric acid were added, and the plate was swirled for another 2 minutes. The suspension was then recovered and centrifuged (800g, 2 minutes, 4˚C). the nuclei pellet was then resuspended in 500μl PBS containing 5 μl RNAse A (1mg/ml) and 5μl propidium iodide (1mg/ml).

For non-adherent cells, the cells were first collected by centrifugation (400g, 5 minutes), then washed twice with PBS. The cell pellet was then resuspended in 0.5 ml of ice-cold fractionation buffer and lysed for 1 minute. After that time, 25 μl of 20% (w/v) citric acid were added and mixed by pipetting, and the lysis was allowed to proceed for another 2 minutes. The nuclei were recovered and treated as described above for adherent cells.

Cell cycle analysis was carried out on the labelled nuclei by flow cytometry. A FacsCalibur cytometer (Beckton Dickinson) was used with the CellQuest Pro software. The data were obtained using the following parameters: linear acquisition of the events, doublets eliminated by gating on singlet events and the mean fluorescent intensity of the propidium iodide was represented on a linear mode to identify the different cell cycle stages.

Proteomics

The 2D gel based proteomic experiments were essentially carried out as previously described [9], on independent biological quadruplicates.

Briefly, the spots selected for identification were excised from silver-stained gels and destained with ferricyanide/thiosulfate on the same day as silver staining in order to improve the efficiency of the identification process [10, 11]. In gel digestion was performed with an automated protein digestion system, MassPrep Station (Waters, Milford, USA). The gel plugs were washed twice with 50 μL of 25 mM ammonium hydrogen carbonate (NH_4HCO_3) and 50 μL of acetonitrile. The cysteine residues were reduced by 50 μL of 10 mM dithiothreitol at 57˚C and alkylated by 50 μL of 55 mM iodoacetamide. After dehydration with acetonitrile, the proteins were cleaved in gel with 10 μL of 12.5 ng/μL of modified porcine trypsin (Promega, Madison, WI, USA) in 25 mM NH_4HCO_3. The digestion was performed overnight at room temperature. The generated peptides were extracted with 30 μL of 60% acetonitrile in 0.1% formic acid. Acetonitrile was evaporated under vacuum before nanoLC-MS/MS analysis.

NanoLC-MS/MS analysis was performed using a nanoACQUITY Ultra-Performance-LC (Waters Corporation, Milford, USA) coupled to a TripleTOF 5600 (Sciex, Ontario, Canada) mass spectrometer. Mass calibration of the analyser was achieved using peptides from digested BSA. The complete system was fully controlled by AnalystTF 1.7 (Sciex). Raw data collected were processed and converted with MSDataConverter in.mgf peak list format.

For protein identification, the MS/MS data were interpreted using a local Mascot server with MASCOT 2.6.2. algorithm (Matrix Science, London, UK) against UniProtKB/Swiss-sProt (version 2020–04, 563,082 sequences). The protein identification search was carried out in all species. Spectra were searched with a mass tolerance of 15 ppm for MS and 0.05 Da for MS/MS data, allowing a maximum of one trypsin missed cleavage. Carbamidomethylation of cysteine residues, oxidation of methionine residues, acetylation of protein N-terminus, phosphorylation of serine, threonine and tyrosine residues were specified as variable modifications. Protein identifications were validated with at least two peptides with Mascot ion score above 30.

Mass spectrometry data are available via ProteomeXchange with identifier PXD021593.

Enzyme assays

The enzymes activities were assayed according to published procedures (see below).

The cell extracts for enzyme assays were prepared by lysing the cells for 20 minutes at 0˚C in 20 mM Hepes pH 7.5, 2 mM $MgCl_2$, 50 mM KCl, 1 mM EGTA, 0.15% (w/v) tetradecyldimethylammonio propane sulfonate (SB 3–14), followed by centrifugation at 15,000 g for 15 minutes to clear the extract. The protein concentration was determined by a dye-binding assay [12]. The dehydrogenases or dehydrogenases-coupled activities were assayed at 500nm using the phenazime methosulfate/iodonitrotetrazolium coupled assay [13, 14]. The enzyme assay buffer contained 25mM Hepes NaOH pH 7.5, 5mM magnesium acetate, 100mM potassium chloride and 1%(w/v) Triton X-100. It also contained 30μM phenazine methosulfate, 200μM iodonitrotetrazolium chloride, 250μM of the adequate cofactor (NAD or NADP) and 1-5mM of the organic substrate, which was used to start the reaction. Triose phosphate isomerase was assayed with dihydroxyacetone phosphate and a glyceraldehyde dehydrogenase-coupled assay [15]. Hexokinase was assayed by a glucose 6-phosphate dehydrogenase (G6PDH)-coupled assay [16]. Enolase was assayed at 340nm by a pyruvate kinase-lactate dehydrogenase-coupled assay [17]. Phosphoglycerate mutase was assayed by measuring the decrease of NADH at 340 nm in a pyruvate kinase-lactate dehydrogenase-coupled assay [18]. Pyruvate kinase was assayed by measuring the decrease of NADH at 340 nm in a lactate dehydrogenase-coupled assay [19].

Mitochondrial transmembrane potential measurement

The mitochondrial transmembrane potential was assessed by Rhodamine 123 uptake. Cells were incubated with Rhodamine 123 (80 nM) for 30 minutes at 37˚C [20], 5% CO2 then rinsed twice in cold Glucose (1 mg/mL)—PBS (PBSG) and harvested in cold PBSG supplemented with Propidium Iodide (1 μg/mL). The mitochondrial potential of cells was analyzed by flow cytometry on a FacsCalibur instrument (Beckton Dickinson). The dead cells (propidium positive) were excluded of the analysis. The low rhodamine concentration was used to avoid intra-mitochondrial fluorescence quenching that would result in a poor estimation of the mitochondrial potential [21].

The glucose concentration in conditioned media was determined using a clinical glucometer and measuring the residual glucose concentration at the end of the culture period and in the starting culture medium.

Phagocytosis and nitric oxide production assay

The phagocytic capacity of the cells was measured using fluorescent latex beads and flow cytometry [22, 23]. Both the proportion of phagocytic cells and the mean fluorescence, giving an index of the number of phagocytosed beads, were determined. Nitric oxide production induced by lipopolysaccharide (LPS) stimulation was determined using the Griess reagent, as previously described [23], and corrected by the number of cells in the wells. For cytokine production, a commercial kit (BD Cytometric Bead Array, catalog number 552364 from BD Biosciences) was used.

Microscopic analysis of the cytoskeleton

Antibodies. For microtubule cytoskeleton analysis the primary antibody used was the anti α-tubulin (clone α3A1) produced by L. Lafanechère [24]. Actin microfilaments were visualized using phalloidin-rhodamine (Sigma, P1951). DNA was stained with 20 μM Hoechst 33342 (Sigma, #23491-52-3).

Immunofluorescence. For immunofluorescence analysis cells were seeded at 300 000 cells/ml on 12-well plates in adherent or suspension conditions (see above). After 24 hours cells were fixed with 3.7% PFA (Sigma) for 20 min, permeabilized with 0.1% Triton in PBS (Sigma), then washed with PBS, and blocked with a blocking solution (3% BSA/10% goat serum/PBS) for 1 hr. Samples were incubated for 2hours at room temperature with the primary antibody and phalloidin diluted in blocking solution, followed by three washes with PBS containing 0.2% Tween20. The cells were then incubated with secondary antibody at room temperature for 1 hr followed by three washes with PBS containing 0.2% Tween20. In the case of non-adherent/suspension cells, samples were centrifuged at 1200 rpm for 4 minutes between each step. Samples were finally mounted using mounting Mowiol medium. Images were captured with a Zeiss AxioimagerM2 microscope equipped with the acquisition software AxioVision. Contrast of the colored images was adjusted using the ImageJ software.

Results

Adherence and cell cycle

As cells were routinely cultured on non-adherent flasks, we first determined which percentage of cells were adherent or non-adherent when transferred to the corresponding culture substrates. When cells were seeded at 500,000 cells/ml and harvested 24 hours later, 855,555 ±156,741 cells/ml (range 688,888–1,000,000) were recovered as non-adherent from non-adherent flasks (indicating cell growth) whereas 29,629±27962 cells/ml (range 0–55,555) were recovered as non-adherent from adherent flasks. Even if assuming no cell growth, this means that more that 94% of the cells adhered on classical culture plastics.

In order to investigate if cell proliferation could be different under both conditions, the cell cycle was analyzed and the results are presented in Table 1.

These data showed that the proportion of cells engaged in cycling (S and G2/M) was not significantly different between adherent and non-adherent cells.

Table 1. Cell cycle of non-adherent and adherent cells.

	Cell cycle stages			
	% Sub G1	% G1	% S	% G2/M
Non adherent	1.4 ± 0.1	59.9 ± 0.5	15.8 ± 0.1	20.6 ± 0.8
Adherent	3.2 ± 0.2	55.3 ± 0.5	16.8 ± 0.6	21.7 ± 0.8

https://doi.org/10.1371/journal.pone.0252450.t001

Proteomics

Adherent and non-adherent cells extracts were prepared and their protein content was separated using two-dimensional gel electrophoresis. The raw images used for the analysis are shown in S1 and S2 Figs. Proteins were then identified using quantitative proteomics.

Spots of interest were selected on the two-dimensional gel images on the basis of statistical tests, using the numerical data provided by the 2D gel analysis software (S1 Table). Selected spots showed either a U value of 0 in the Mann-Whitney test (corresponding to a p value ≤ 0.028) or a U value of 1 (corresponding to a p value ≤ 0.058 and a p value 0.05 in the Welch test). Of the 198 spots that met that criteria, 111 were identified by mass spectrometry, and the spot statistical and identification parameters are shown in S2 Table. Annotated gel images showing these proteins are shown in Fig 1 and S3 Fig. The spot list was then processed using the David software tool [25, 26] to highlight modulated pathways, and the results are displayed in S3 Table.

As expected, "cell adhesion" appeared in the top clusters, but other pathways were also highlighted, which prompted us to validate them. A selection of such proteins is presented in Table 2.

Furthermore, 2D gel-based proteomics allows the visualization of unmodified- and post-translationally modified protein forms. Our data indeed often showed proteins appearing as

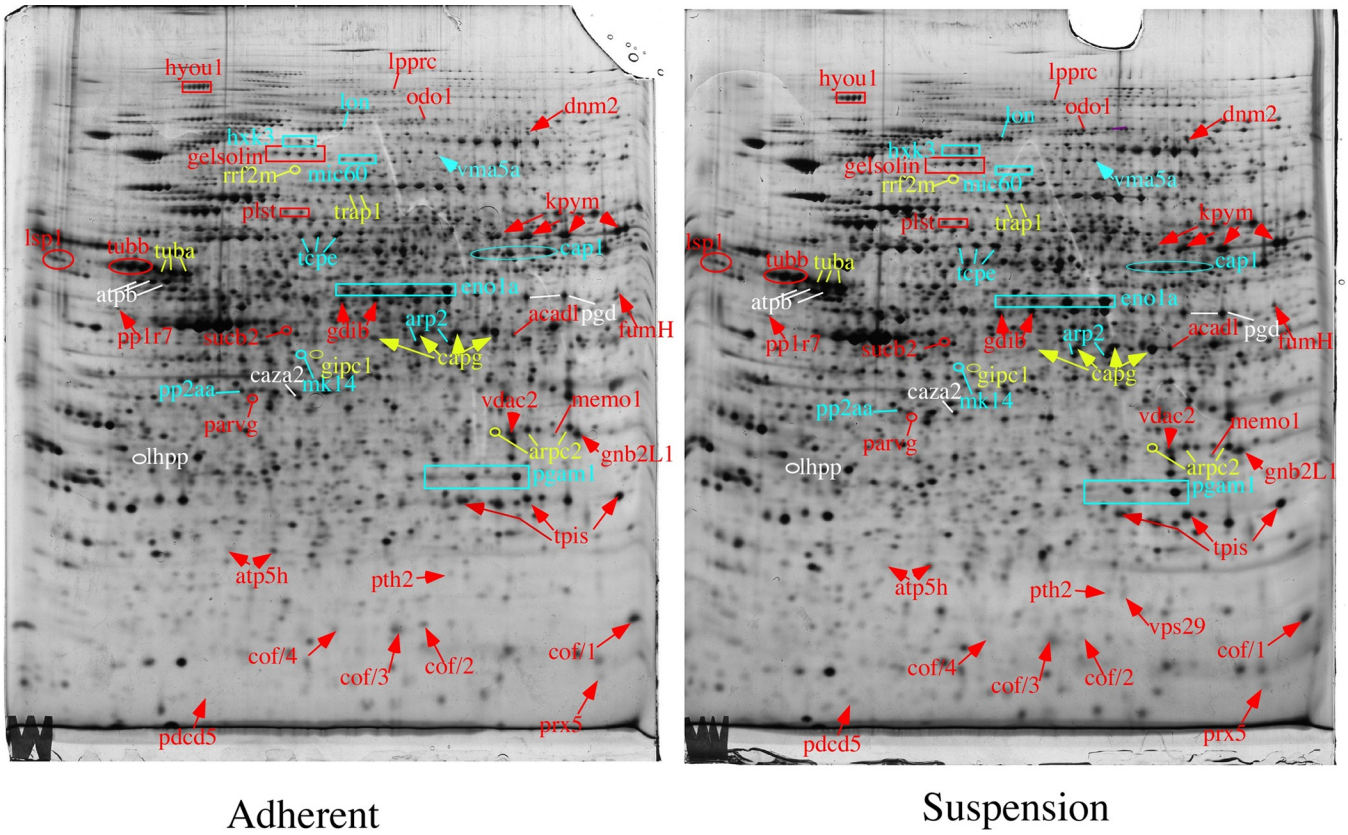

Fig 1. Proteomic analysis of total cell extracts by 2D electrophoresis. Total cell extracts of RAW264.7 cells were separated by two-dimensional gel electrophoresis. The first dimension covered a 4–8 pH range and the second dimension a 15–200 kDa range. Total cellular proteins (150 μg) were loaded on the first-dimension gel. The proteins highlighted on the figure show changes between the adherent and suspension conditions, for at least one spot in case of proteins showing multiple spots. Only the proteins belonging to the categories: "associated with cytoskeleton", "associated with signal transduction", "associated with tumors", "central metabolism" and "mitochondrial" are shown on this figure. The other proteins are shown in S3 Fig.

https://doi.org/10.1371/journal.pone.0252450.g001

Table 2. Selection of proteins changing in abundance between adherent and non-adherent cells.

Short name (spot code)	Uniprot accession number	Protein name	Condition of highest abundance
Cytoskeleton-associated proteins			
arp2/2	P61161	Actin-related protein 2	A
arpc2/3	Q9CVB6	Actin-related protein 2/3 complex subunit 2	A
capg/2	P24452	Macrophage-capping protein	A
capg/3	P24452	Macrophage-capping protein	A
caza2	P47754	F-actin-capping protein subunit alpha-2	A
cof1/2	P18760	Cofilin-1	A
cof1/4	P18760	Cofilin-1	A
dnm2	P39054	Dynamin-2	NA
gdib/1	Q61598	Rab GDP dissociation inhibitor beta	A
gelsolin/1	P13020	Gelsolin	NA
gipc1	Q9Z0G0	PDZ domain-containing protein GIPC1	NA
lsp1/1	P19973	Lymphocyte-specific protein 1	A
lsp1/2	P19973	Lymphocyte-specific protein 1	A
memo1	Q91VH6	Protein MEMO1	A
parvg	Q9ERD8	Parvin gamma	A
plst/1	Q61233	Plastin-2	NA
plst/2	Q61233	Plastin-2	NA
tcpe/2	P80316	T-complex protein 1 subunit epsilon	A
tubb/2	P99024	Tubulin beta	A
tubb/3	P99024	Tubulin beta	A
Central metabolism enzymes			
eno1/3	P17182	Alpha-enolase	A
kpym/2	P52480	pyruvate kinase	A
hxk3/2	Q3TRM8	Hexokinase-3	NA
pgam/2	Q9DBJ1	Phosphoglycerate mutase 1	A
pgam/3	Q9DBJ1	Phosphoglycerate mutase 1	A
pgd/2	Q9DCD0	6-phosphogluconate dehydrogenase, decarboxylating	A
tpis/3	P17751	Triosephosphate isomerase	A
Detoxification proteins			
aldr/2	P45376	Aldose reductase	A
prx1 ox	P3570	Peroxiredoxin-1	A
prx3*	P20108	Peroxiredoxin-3	NA
prx5*	P99029	Peroxiredoxin-5	NA
Annexins			
anxa1/3	P10107	Annexin A1	A
anxa3/3	O35639	Annexin A3	A
anxa4/2	P97429	Annexin A4	A
Mitochondrial proteins			
atp5h/2	Q9DCX2	ATP synthase subunit d, mitochondrial	A
atpb/2	P56480	ATP synthase subunit beta, mitochondrial	A
atpb/3	P56480	ATP synthase subunit beta, mitochondrial	A
acadl	P51174	Long-chain specific acyl-CoA dehydrogenase	NA
fumh	P97807	Fumarate hydratase, mitochondrial	A
lon	Q8CGK3	Lon protease homolog, mitochondrial	NA

(*Continued*)

Table 2. (Continued)

Short name (spot code)	Uniprot accession number	Protein name	Condition of highest abundance
lpprc	Q6PB66	Leucine-rich PPR motif-containing protein, mitochondrial	NA
mic60/3	Q8CAQ8	MICOS complex subunit Mic60	NA
odo1	Q60597	2-oxoglutarate dehydrogenase, mitochondrial	NA
pth2	Q8R2Y8	Peptidyl-tRNA hydrolase 2, mitochondrial	NA
rrf2m	Q8R2Q4	Ribosome-releasing factor 2, mitochondrial	NA
sucb2	Q9Z2I8	Succinyl-CoA ligase [GDP-forming] subunit beta, mitochondrial	NA
trap1/1	Q9CQN1	Heat shock protein 75 kDa, mitochondrial	
vdac2	Q60930	Voltage-dependent anion-selective channel protein 2	NA
Associated with tumors			
gipc1	Q9Z0G0	PDZ domain-containing protein GIPC1	NA
hyou1/1	Q9JKR6	Hypoxia up-regulated protein 1	NA
pdcd5	P56812	Programmed cell death protein 5	NA
vma5a	Q99KC8	von Willebrand factor A domain-containing protein 5A	NA
Proteasome/ubiquitin			
atg3	Q9CPX6	Ubiquitin-like-conjugating enzyme ATG3	NA
brcc3	P46737	Lys-63-specific deubiquitinase BRCC36	NA
mindy3	Q9CV28	Protein FAM188A	NA
psb4/2	P99026	Proteasome subunit beta type-4	A
psd13	Q9WVJ2	26S proteasome non-ATPase regulatory subunit 13	NA
Associated with signal transduction			
gnb2L1	P68040	Guanine nucleotide-binding protein subunit beta-2-like 1	A
lhpp	Q9D7I5	Phospholysine phosphohistidine inorganic pyrophosphate phosphatase	NA
mk14	P47811	Mitogen-activated protein kinase 14	NA
pp1R7	Q3UM45	Protein phosphatase 1 regulatory subunit 7	A
pp2aa	P63330	Serine/threonine-protein phosphatase 2A catalytic subunit alpha isoform	A

A: adherent cells; NA: non-adherent cells

*: prx 3 and prx5 are also mitochondrial proteins.

https://doi.org/10.1371/journal.pone.0252450.t002

spots. We noticed differences between the changes of abundance of some spots in such series, when comparing between the two conditions tested, as exemplified in Fig 1. We therefore decided to reanalyze the MS/MS spectra to detect modified peptides, and especially phosphorylations and acetylations. Phosphorylations were detected on modified forms of capg (T3), annexin 1 (T101; T114; T169; S244) and annexin 3 (T106/108; S139). To our knowledge, none of these phosphorylations has been described yet. Regarding cofilin, for which the phosphorylation landscape is easier to investigate [27], we could compare by spectral counts the degree of phosphorylation on different sites. The results, displayed in S4 Table, showed a higher phosphorylation level for adherent cells, not only on the well-known S3 site [28], but also on less well known sites such as S23/24 [29], T 63 and Y82 [27].

Enzyme activities

The comparison of adherent cells with non-adherent cells using this proteomic approach highlighted abundance changes in protein forms for several metabolic enzymes, such as acyl-CoA dehydrogenase (acadl P51174), hexokinase (hxk3 Q3TRM8), phosphoglycerate mutase

Table 3. Enzyme activities.

	adherent	non adherent	ratio	T-test	U-test
long chain acylCoA DH	5.78±1.54	9.28±0.96	1.61	0.011	0
enolase	218.2±16.6	201.2±17.11	0.92	0.2	3
hexokinase	8.11±0.57	10.11±0.79	1.25	0.0078	0
phosphoglycerate mutase	1004±117	808±60	0.80	0.036	0
pyruvate kinase	1737±43	1635±157	0.94	0.29	4
triose phosphate isomerase	91.6±7.9	112±6.2	1.22	0.0074	0

All the activities are expressed in nmole substrate converted/min/mg total protein.

https://doi.org/10.1371/journal.pone.0252450.t003

(PGAM Q9DBJ1), pyruvate kinase (KPYM P52480) or triose phosphate isomerase (TPIS P17751). Indeed, the pathway "carbon metabolism" appeared in the pathway analyses. We thus tested the activity of some of these enzymes to validate the proteomic findings. The results, displayed on Table 3, showed a good agreement between the proteomic data and the activity data, with a concomitant increase in hexokinase and acyl-CoA dehydrogenase when comparing the adherent state to the non-adherent one, and a concomitant decrease for phosphoglycerate mutase. Regarding the enolase and pyruvate kinase activities, the general trends were similar between the proteomic and activity data, although the changes in activity were not statistically significant. For triose phosphate isomerase, the only spot changing in abundance was decreased while the activity increased. These discrepancies indicate that the relationship between activity and modification profiles can be complex. For example, phosphorylation can increase activity (e.g. biliverdin reductase [30]) but also decrease it (e.g. pyruvate dehydrogenase [31]). The same unpredictable trend also holds true for acetylation [32].

Mitochondrial transmembrane potential

Several mitochondrial proteins were highlighted in the proteomic screen, such as trap1 (Q9CQN1), odo1 (Q60597), mic60 (Q8CAQ8), lon (Q8CGK3), lpprc (Q6PB66), peroxiredoxins 3 (P20108) and 5 (P99029), succinylCoA ligase (sucb2 Q9Z2I8), and the "mitochondrion" cluster appeared in the pathway analysis. Furthermore, most of the mitochondrial proteins detected as changing showed an increase in their relative abundance in the non-adherent state compared to the adherent one, leading to the hypothesis that the mitochondrial function may be increased in non-adherent cells. To test this hypothesis, we measured the mitochondrial transmembrane potential. The results showed that the proportion of rhodamine-positive cells (i.e. viable, metabolically active cells) was high and similar under both conditions (99.8±0.06% for adherent cells vs. 99.7±0.35 for non-adherent cells). However, the rhodamine fluorescence intensity, which is a surrogate marker of the mitochondrial transmembrane potential [21], was significantly increased in the non-adherent condition (3844±335 fluorescence units) compared to the adherent one (2571±103 fluorescence units) suggesting an increased mitochondrial activity in the non-adherent cells. In addition, GIPC1, which is one the proteins highlighted in the proteomic screen, interacts with the glucose transporter GLUT1 [33]. Consequently, there could be a different glucose usage between adherent and non-adherent cells.

We thus measured the glucose consumption of the cells after 24 hours in culture. At an equal seeding density of 500,000 cells/ml, adherent cells consumed 0.29±0.017 g/l glucose while non-adherent cells consumed 0.293±0.015 g/l glucose, i.e. equivalent amounts. Thus, the increased mitochondrial activity was not just due to an overall greater energy consumption, but represented a modification induced by adherence loss.

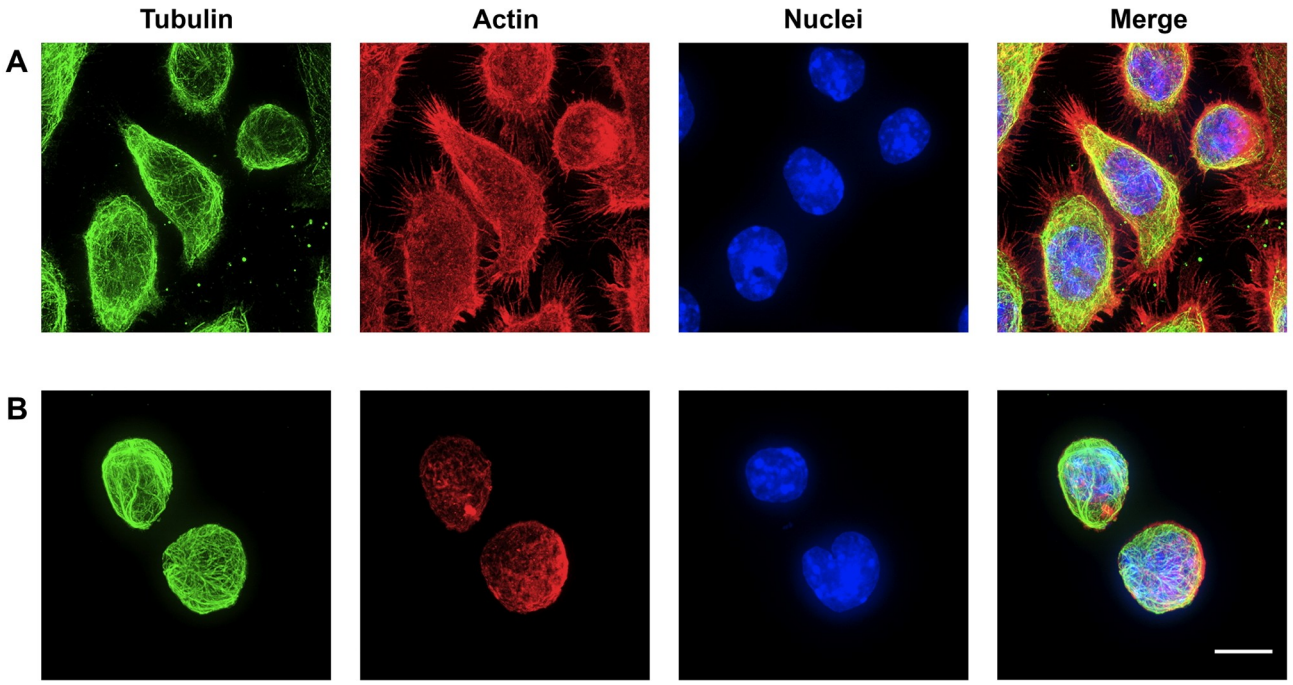

Fig 2. Analysis of the effect of adhesion on the morphology of the actin and tubulin networks. The actin and tubulin networks are visualized by confocal microscopy as described in the material and methods section, on adherent RAW264.7 cells (row A) and non-adherent RAW 264.7cells (row B). The contrast between the basket-like shape for the microtubule network in non-adherent cells and the more spider web-like shape in adherent cells is noteworthy, as well as the reorganization of the actin network. Scale bar: 20μm.

https://doi.org/10.1371/journal.pone.0252450.g002

Effects on the cytoskeleton

As expected, many proteins involved in the control of the cytoskeleton were highlighted in the proteomic screen, which was further illustrated by the "cell-cell adhesion" and "actin binding" clusters found in the pathway analysis. Such proteins for which a change in abundance was detected in at least one protein form included arp2 (P61161), arpc2 (Q9CVB6), capg (P24452), caza2 (P47754) cofilin 1 (P18760), dynamin 2 (P39054), GDIB (Q61598), gelsolin (P13020), GIPC1 (Q9Z0G0), lsp1 (P19973), memo1 (Q91VH6), gamma parvin (Q9ERD8), plastin-2 (Q61233) and beta tubulin itself (P99024).

To validate these findings further, we performed a microscopic analysis of the tubulin and actin cytoskeleton. As shown in Fig 2, the network of microtubules, which extends like a spider's web when the cells are adherent (Fig 2A), reorganizes into a basket net-like network that extends into the thin cytoplasmic space surrounding the nucleus. In this latter state, many microtubules appear to form bundles (Fig 2B).

The actin cytoskeleton of adherent cells shows rare/no stress fibers, but abundant filopodia and branched actin. The actin network is completely reorganized in non-adherent cells, with the disappearance of filopodia and the presence of a sub-cortical network.

Phagocytosis and nitric oxide production

Phagocytosis, i.e. one of the important functions of macrophages, depends on the cytoskeleton, as shown by its well-known inhibition by cytochalasin, which blocks actin polymerisation [34]. In addition, GIPC1, which is one the proteins highlighted in the proteomic screen, is known to modulate phagocytosis [35]. Furthermore, the stiffness of the substrate to which the cells adhere has been described to modulate the differentiated functions of the macrophages

Table 4. Assay of macrophages functions.

Condition	Adherent	Non-adherent
%phagocytic cells	65.1±4.3	70.9±1.3
Phagocytosis MFI *	2536±203	2698±76
LPS-induced NO production	4.79±0.17 μM	4.52±0.13 μM
LPS-induced IL-6 production	8516±262 pg/ml	8799±198 pg/ml
LPS-induced TNF production	4311±461 pg/ml	4241±143 pg/ml

*: the mean fluorescence index (MFI), expressed in arbitrary fluorescence units, is an indicator of the number of fluorescent beads internalized by the cells, and thus of the capacity of phagocytic cells to internalize several beads.

https://doi.org/10.1371/journal.pone.0252450.t004

[36]. Consequently, there could be a difference in these specialized functions between adherent and non-adherent cells. We thus measured the phagocytic capacity and the LPS-induced nitric oxide (NO), interleukin 6 (IL-6) and tumor necrosis factor alpha (TNF) production for cells in the adherent and non-adherent state. The results, displayed in Table 4, did not indicate significant differences in functionalities between adherent and non-adherent cells.

Discussion

Adherence to a substrate is a requisite for most cells types, and cells are able to adopt various shapes to adapt to the adhesive characteristics of their substrate [37]. Nevertheless, there are a few situations, such as the metastatic process or blood cell diapedesis, where cells alternate between adherent and non-adherent behaviors. In order to test the changes that occur between these two states, a system is needed where cell physiology is not too altered between the adherent and non-adherent states, so as not to confuse changes in cell physiology with changes in adhesion status. Macrophage cell lines are among the models that allow such studies. Although they are known to respond to the characteristics of their substrate when they adhere [36, 38], their differentiated functions such as phagocytosis and inflammatory response to LPS are equivalent between an adherent state on plastic and a non-adherent state.

We thus used this model to study the changes linked to the adherence status, using a proteomic screen to get a wider appraisal of the phenomena at play. To this purpose, we chose to perform 2D gel-based proteomics, as this proteomic setup is able to detect changes in post-translationally modified protein forms [39] and thus get closer to the cell physiology [40]. In the same trend, we chose to validate the proteomic results by functional assays rather than assays based on protein amounts [41]. Furthermore, in the case of 2D gel-based proteomics, a significant change in a modified form of a protein, which can be biologically significant because of the importance of post-translational modifications, can be revealed while the bulk of the protein remains constant, which would mask the change of interest in a protein amount-based validation.

The first (and expected) class of proteins that were found modulated corresponded to proteins playing a role in the cytoskeleton architecture. Several proteins implicated in the actin cytoskeleton regulation were modulated. Among them, several changes were detected at the post translational level as indicated by changes observed for acidic, modified forms of the proteins while the bulk of the proteins, as measured by the sum of the various protein spots for the same protein, did no change (e.g. arpc2 (Q9CVB6), capg (P24452), cofilin (P18760), GDIB (Q61598)). Furthermore, a change in the amount of gamma parvin (Q9ERD8) was detected. This protein belongs to the actinin superfamily [42] and plays a role in leukocyte adhesion [43]. Consistent with its role, gamma parvin was found in higher amounts in adherent cells.

Indirect regulators of the microtubule cytoskeleton were also found modulated, such as Memo-1 [44], pdcd 5 [45] or gpic, which is known to interact with integrins alpha-5 and 6 [46], integrins being known in turn to play a role in the architecture of the microtubules network [47]. Furthermore, a change in one beta tubulin spot was also detected. In view of what is known of the complexity of post-translational modifications for tubulin [48], and of the sequence similarities in the tubulin multigene family, a single spot assigned to one tubulin gene can be expected to be a mixture of several tubulin variants if not also products of different tubulin genes. It is therefore highly likely that the detected changes reflect a modification in the post-translational landscape of tubulin and not an overall change in the tubulin amount.

In line with all these changes, the architecture of the actin filaments and microtubules were found to be different between the adherent and non-adherent state, as expected. Regarding the actin network, the increase in the expression of gelsolin, a globular actin binding protein with severing activity, the actin-binding protein plastin-2, observed in cells in suspension (S1 Table), as well as the increase in the amount of S3-phosphorylated cofilin in the adherent cells, leading to a decrease of the actin severing activity in this condition, are most likely related to the rearrangement of the actin network that was observed.

Although gaining details in the mechanisms by which the cytoskeleton is modulated between the adherent and non-adherent states is of interest, an important added value of the proteomic screen lies in the less expectable pathways found modulated between the adherent and non-adherent states. A good example, still linked in some aspects to cell shape, is represented by the annexins. As in the case of cytoskeleton-associated proteins, the observed changes occurred in only one of the gel spots, generally an acidic, and thus modified variant. This may affect the fate or function of the protein, as described for annexin A1, where phosphorylation is associated with protein secretion [49], implicated itself in immune modulation [50]. Annexins are generally associated with cell membrane stability [51]. This can be on endosomal membranes, For instance annexin A1 regulates endosomal membranes stability [52], while annexin A4 is involved in plasma membrane curvature [53].

Another good example of rather unexpected results provided by the proteomic analysis is represented by the higher mitochondrial activity in the non-adherent state. This result is in sharp contrast with the loss of respiration observed upon cell detachment [54]. However, in this example, the respiration loss occurs in cells that are subject to massive death if left detached. Thus, this increase in mitochondrial activity may represent a survival mechanism to resist detachment. As metastatic cells are also an example of cells surviving to detachment, targeting the increase in mitochondrial activity may represent a putative therapeutic opportunity to fight metastatic cells. This change in the mitochondrial status is further supported by the increased abundance of the two mitochondrial antioxidant proteins prx3 and prx5 in the non-adherent state.

Beside mitochondrial activity, our proteomic and enzyme activity data pointed to changes in the central metabolism. Once again most of these changes occur on only a protein spot among several spots representing the same protein (e.g. pyruvate kinase, triose phosphate isomerase, enolase or phosphoglycerate mutase).

Changes in the central metabolism have also been observed in the epithelial-mesenchymal transition (EMT) [55]. In our case there was not a uniform trend for the enzyme activities changes. However, it may be worth noting that the two significant increases concern enzymes that catalyze the first step toward substrate utilization, namely hexokinase for glucose and acadl for lipids. Early enzymes in pathways are often controlling steps, as shown for hexokinase [56] and acadl [57], so that our findings may also correspond to a higher metabolic rate, as observed in EMT.

Finally, it is intriguing to find proteins associated with tumor progression in this proteomic screen, and with a mixed trend. Both proteins whose high level is associated with tumorigenesis and metastasis such as gipc1 [58, 59] or hyou1 [60] and proteins associated with tumor suppression such as vma5a [61] or pdcd5 [62] are found higher in abundance in non-adherent cells. Annexin A3, which has also been correlated with tumorigenesis [63], is found at a higher abundance in adherent cells. Although it must be kept in mind that the cells used in this study are cell lines, and thus cancer cells, they keep highly differentiated properties whether adherent or not. The mixed trend observed may represent a balance by which the cells keep their properties. In this respect, the situation investigated in the present study is radically different from EMT, where the cells change fate. Interestingly, when comparing the results obtained in the present study with those obtained by a proteomic investigation of EMT [55], the results were similar for the cytoskeleton associated proteins (e.g. arp2, arpc2, capg) and for other proteins such as vigilin or wdr1. However, the modulations of the mitochondrial proteins and of the tumor–associated proteins found in the present study were not found in the study on EMT, except for annexin A3 found higher in the epithelial state in [55] and higher in the adherent state in the present study. This argues in favor of a balance-keeping mechanism at play in the present case and not in EMT.

Supporting information

S1 Fig. Raw 2D gel images, adherent cells.
(JPG)

S2 Fig. Raw 2D gel images, non-adherent cells.
(JPG)

S3 Fig. Complementary annotated 2D gel images.
(JPG)

S1 Table. Raw results from the quantitative analysis of the 2D gels.
(PDF)

S2 Table. Proteins showing a significant change in abundance between adherent and non-adherent cells.
(PDF)

S3 Table. Modulated pathways highlighted by the DAVID annotation tool.
(PDF)

S4 Table. Semi-quantitative peptide analysis by spectral counting in the mono-phosphorylated form of cofilin.
(PDF)

S1 File. Cover supplementary material.
(PDF)

Acknowledgments

On a scientific level, the authors would like to thank the curators of the Swissprot database for the quality of their functional annotations, which made the exploitation of the proteomic data much more fruitful and straightforward.

Author Contributions

Conceptualization: Laurence Lafanechère, Thierry Rabilloud.

Formal analysis: Sacnite Ramirez Rios, Anaelle Torres, Hélène Diemer, Sarah Cianférani, Laurence Lafanechère, Thierry Rabilloud.

Funding acquisition: Sarah Cianférani, Thierry Rabilloud.

Investigation: Sacnite Ramirez Rios, Anaelle Torres, Hélène Diemer, Véronique Collin-Faure, Thierry Rabilloud.

Methodology: Sacnite Ramirez Rios, Anaelle Torres, Hélène Diemer, Véronique Collin-Faure.

Project administration: Laurence Lafanechère.

Supervision: Laurence Lafanechère, Thierry Rabilloud.

Visualization: Anaelle Torres, Hélène Diemer.

Writing – original draft: Laurence Lafanechère, Thierry Rabilloud.

Writing – review & editing: Sacnite Ramirez Rios, Anaelle Torres, Hélène Diemer, Véronique Collin-Faure, Sarah Cianférani, Laurence Lafanechère, Thierry Rabilloud.

References

1. Martin GR, Evans MJ. Differentiation of clonal lines of teratocarcinoma cells: formation of embryoid bodies in vitro. Proc Natl Acad Sci U S A. 1975; 72: 1441–1445. https://doi.org/10.1073/pnas.72.4.1441 PMID: 1055416
2. Jones-Villeneuve EM, McBurney MW, Rogers KA, Kalnins VI. Retinoic acid induces embryonal carcinoma cells to differentiate into neurons and glial cells. J Cell Biol. 1982; 94: 253–262. https://doi.org/10.1083/jcb.94.2.253 PMID: 7107698
3. Kawata M, Sekiya S, Kera K, Kimura H, Takamizawa H. Neural rosette formation within in vitro spheroids of a clonal human teratocarcinoma cell line, PA-1/NR: role of extracellular matrix components in the morphogenesis. Cancer Res. 1991; 51: 2655–2669. PMID: 2021944
4. Eder T, Eder IE. 3D Hanging Drop Culture to Establish Prostate Cancer Organoids. Methods Mol Biol Clifton NJ. 2017; 1612: 167–175. https://doi.org/10.1007/978-1-4939-7021-6_12 PMID: 28634942
5. Panek M, Grabacka M, Pierzchalska M. The formation of intestinal organoids in a hanging drop culture. Cytotechnology. 2018; 70: 1085–1095. https://doi.org/10.1007/s10616-018-0194-8 PMID: 29372467
6. Follain G, Herrmann D, Harlepp S, Hyenne V, Osmani N, Warren SC, et al. Fluids and their mechanics in tumour transit: shaping metastasis. Nat Rev Cancer. 2020; 20: 107–124. https://doi.org/10.1038/s41568-019-0221-x PMID: 31780785
7. McBurney MW. P19 embryonal carcinoma cells. Int J Dev Biol. 1993; 37: 135–140. PMID: 8507558
8. Miller L. A detergent-citric acid technique for isolating nuclear and cytoplasmic fractions containing undegraded RNA from cells of Xenopus laevis. Anal Biochem. 1979; 100: 166–173. https://doi.org/10.1016/0003-2697(79)90127-1 PMID: 94513
9. Dalzon B, Torres A, Diemer H, Ravanel S, Collin-Faure V, Pernet-Gallay K, et al. How reversible are the effects of silver nanoparticles on macrophages? A proteomic-instructed view. Environ Sci Nano. 2019; 6: 3133–3157.
10. Gharahdaghi F, Weinberg CR, Meagher DA, Imai BS, Mische SM. Mass spectrometric identification of proteins from silver-stained polyacrylamide gel: A method for the removal of silver ions to enhance sensitivity. Electrophoresis. 1999; 20: 601–605. https://doi.org/10.1002/(SICI)1522-2683(19990301)20:3<601::AID-ELPS601>3.0.CO;2-6 PMID: 10217175
11. Richert S, Luche S, Chevallet M, Van Dorsselaer A, Leize-Wagner E, Rabilloud T. About the mechanism of interference of silver staining with peptide mass spectrometry. Proteomics. 2004; 4: 909–916. https://doi.org/10.1002/pmic.200300642 PMID: 15048973
12. Rabilloud T. Optimization of the cydex blue assay: A one-step colorimetric protein assay using cyclodextrins and compatible with detergents and reducers. PLoS One. 2018; 13: e0195755. https://doi.org/10.1371/journal.pone.0195755 PMID: 29641569

13. Mayer KM, Arnold FH. A colorimetric assay to quantify dehydrogenase activity in crude cell lysates. J Biomol Screen. 2002; 7: 135–40. https://doi.org/10.1177/108705710200700206 PMID: 12006112

14. Dommes V, Kunau WH. A convenient assay for acyl-CoA-dehydrogenases. Anal Biochem. 1976; 71: 571–578. https://doi.org/10.1016/s0003-2697(76)80026-7 PMID: 1275256

15. Plaut B, Knowles JR. pH-dependence of the triose phosphate isomerase reaction. Biochem J. 1972; 129: 311–20. https://doi.org/10.1042/bj1290311 PMID: 4643319

16. Ritov VB, Kelley DE. Hexokinase isozyme distribution in human skeletal muscle. Diabetes. 2001; 50: 1253–1262. https://doi.org/10.2337/diabetes.50.6.1253 PMID: 11375324

17. Anderson VE, Weiss PM, Cleland WW. Reaction intermediate analogues for enolase. Biochemistry. 1984; 23: 2779–2786. https://doi.org/10.1021/bi00307a038 PMID: 6380574

18. Sutherland EW, Posternak T, Cori CF. Mechanism of the phosphoglyceric mutase reaction. J Biol Chem. 1949; 181: 153–159. PMID: 15390402

19. Malcovati M, Valentini G. AMP- and fructose 1,6-bisphosphate-activated pyruvate kinases from Escherichia coli. Methods Enzymol. 1982; 90 Pt E: 170–179. https://doi.org/10.1016/s0076-6879(82)90123-9 PMID: 6759852

20. Dalzon B, Aude-Garcia C, Collin-Faure V, Diemer H, Beal D, Dussert F, et al. Differential proteomics highlights macrophage-specific responses to amorphous silica nanoparticles. Nanoscale. 2017; 9: 9641–9658. https://doi.org/10.1039/c7nr02140b PMID: 28671223

21. Perry SW, Norman JP, Barbieri J, Brown EB, Gelbard HA. Mitochondrial membrane potential probes and the proton gradient: a practical usage guide. Biotechniques. 2011; 50: 98–115. https://doi.org/10.2144/000113610 PMID: 21486251

22. Abel G, Szollosi J, Fachet J. Phagocytosis of fluorescent latex microbeads by peritoneal macrophages in different strains of mice: a flow cytometric study. Eur J Immunogenet. 1991; 18: 239–45. https://doi.org/10.1111/j.1744-313x.1991.tb00024.x PMID: 1764431

23. Torres A, Dalzon B, Collin-Faure V, Rabilloud T. Repeated vs. Acute Exposure of RAW264.7 Mouse Macrophages to Silica Nanoparticles: A Bioaccumulation and Functional Change Study. Nanomaterials. 2020; 10: 215. https://doi.org/10.3390/nano10020215 PMID: 32012675

24. Peris L, Thery M, Fauré J, Saoudi Y, Lafanechère L, Chilton JK, et al. Tubulin tyrosination is a major factor affecting the recruitment of CAP-Gly proteins at microtubule plus ends. J Cell Biol. 2006; 174: 839–849. https://doi.org/10.1083/jcb.200512058 PMID: 16954346

25. Huang DW, Sherman BT, Lempicki RA. Bioinformatics enrichment tools: paths toward the comprehensive functional analysis of large gene lists. Nucleic Acids Res. 2009; 37: 1–13. https://doi.org/10.1093/nar/gkn923 PMID: 19033363

26. Huang DW, Sherman BT, Lempicki RA. Systematic and integrative analysis of large gene lists using DAVID bioinformatics resources. Nat Protoc. 2009; 4: 44–57. https://doi.org/10.1038/nprot.2008.211 PMID: 19131956

27. Prudent R, Demoncheaux N, Diemer H, Collin-Faure V, Kapur R, Paublant F, et al. A quantitative proteomic analysis of cofilin phosphorylation in myeloid cells and its modulation using the LIM kinase inhibitor Pyr1. PLoS One. 2018; 13: e0208979. https://doi.org/10.1371/journal.pone.0208979 PMID: 30550596

28. Yang N, Higuchi O, Ohashi K, Nagata K, Wada A, Kangawa K, et al. Cofilin phosphorylation by LIM-kinase 1 and its role in Rac-mediated actin reorganization. Nature. 1998; 393: 809–812. https://doi.org/10.1038/31735 PMID: 9655398

29. Sakuma M, Shirai Y, Yoshino K, Kuramasu M, Nakamura T, Yanagita T, et al. Novel PKCalpha-mediated phosphorylation site(s) on cofilin and their potential role in terminating histamine release. Mol Biol Cell. 2012; 23: 3707–21. https://doi.org/10.1091/mbc.E12-01-0053 PMID: 22855535

30. Salim M, Brown-Kipphut BA, Maines MD. Human Biliverdin Reductase Is Autophosphorylated, and Phosphorylation Is Required for Bilirubin Formation. J Biol Chem. 2001; 276: 10929–10934. https://doi.org/10.1074/jbc.M010753200 PMID: 11278740

31. Linn TC, Pettit FH, Reed LJ. Alpha-keto acid dehydrogenase complexes. X. Regulation of the activity of the pyruvate dehydrogenase complex from beef kidney mitochondria by phosphorylation and dephosphorylation. Proc Natl Acad Sci U S A. 1969; 62: 234–241. https://doi.org/10.1073/pnas.62.1.234 PMID: 4306045

32. Xiong Y, Guan K-L. Mechanistic insights into the regulation of metabolic enzymes by acetylation. J Cell Biol. 2012; 198: 155–164. https://doi.org/10.1083/jcb.201202056 PMID: 22826120

33. Bunn RC, Jensen MA, Reed BC. Protein Interactions with the Glucose Transporter Binding Protein GLUT1CBP That Provide a Link between GLUT1 and the Cytoskeleton. Guidotti G, editor. Mol Biol Cell. 1999; 10: 819–832. https://doi.org/10.1091/mbc.10.4.819 PMID: 10198040

34. Malawista SE, Gee JB, Bensch KG. Cytochalasin B reversibly inhibits phagocytosis: functional, metabolic, and ultrastructural effects in human blood leukocytes and rabbit alveolar macrophages. Yale J Biol Med. 1971; 44: 286–300. PMID: 5132788

35. Bohlson SS, Zhang M, Ortiz CE, Tenner AJ. CD93 interacts with the PDZ domain-containing adaptor protein GIPC: implications in the modulation of phagocytosis. J Leukoc Biol. 2005; 77: 80–89. https://doi.org/10.1189/jlb.0504305 PMID: 15459234

36. Sridharan R, Cavanagh B, Cameron AR, Kelly DJ, O'Brien FJ. Material stiffness influences the polarization state, function and migration mode of macrophages. Acta Biomater. 2019; 89: 47–59. https://doi.org/10.1016/j.actbio.2019.02.048 PMID: 30826478

37. Théry M, Pépin A, Dressaire E, Chen Y, Bornens M. Cell distribution of stress fibres in response to the geometry of the adhesive environment. Cell Motil Cytoskeleton. 2006; 63: 341–355. https://doi.org/10.1002/cm.20126 PMID: 16550544

38. Van Goethem E, Poincloux R, Gauffre F, Maridonneau-Parini I, Le Cabec V. Matrix Architecture Dictates Three-Dimensional Migration Modes of Human Macrophages: Differential Involvement of Proteases and Podosome-Like Structures. J Immunol. 2010; 184: 1049–1061. https://doi.org/10.4049/jimmunol.0902223 PMID: 20018633

39. Marcus K, Lelong C, Rabilloud T. What Room for Two-Dimensional Gel-Based Proteomics in a Shotgun Proteomics World? Proteomes. 2020; 8: 17. https://doi.org/10.3390/proteomes8030017 PMID: 32781532

40. Marcus K, Rabilloud T. How Do the Different Proteomic Strategies Cope with the Complexity of Biological Regulations in a Multi-Omic World? Critical Appraisal and Suggestions for Improvements. Proteomes. 2020; 8: 23. https://doi.org/10.3390/proteomes8030023 PMID: 32899323

41. Rabilloud T, Lescuyer P. The proteomic to biology inference, a frequently overlooked concern in the interpretation of proteomic data: a plea for functional validation. Proteomics. 2014; 14: 157–161. https://doi.org/10.1002/pmic.201300413 PMID: 24273051

42. Olski TM, Noegel AA, Korenbaum E. Parvin, a 42 kDa focal adhesion protein, related to the alpha-actinin superfamily. J Cell Sci. 2001; 114: 525–538. PMID: 11171322

43. Yoshimi R, Yamaji S, Suzuki A, Mishima W, Okamura M, Obana T, et al. The gamma-parvin-integrin-linked kinase complex is critically involved in leukocyte-substrate interaction. J Immunol Baltim Md 1950. 2006; 176: 3611–3624. https://doi.org/10.4049/jimmunol.176.6.3611 PMID: 16517730

44. Zaoui K, Honoré S, Isnardon D, Braguer D, Badache A. Memo-RhoA-mDia1 signaling controls microtubules, the actin network, and adhesion site formation in migrating cells. J Cell Biol. 2008; 183: 401–408. https://doi.org/10.1083/jcb.200805107 PMID: 18955552

45. Tracy CM, Gray AJ, Cuéllar J, Shaw TS, Howlett AC, Taylor RM, et al. Programmed Cell Death Protein 5 Interacts with the Cytosolic Chaperonin Containing Tailless Complex Polypeptide 1 (CCT) to Regulate β-Tubulin Folding. J Biol Chem. 2014; 289: 4490–4502. https://doi.org/10.1074/jbc.M113.542159 PMID: 24375412

46. El Mourabit H, Poinat P, Koster J, Sondermann H, Wixler V, Wegener E, et al. The PDZ domain of TIP-2/GIPC interacts with the C-terminus of the integrin alpha5 and alpha6 subunits. Matrix Biol J Int Soc Matrix Biol. 2002; 21: 207–214. https://doi.org/10.1016/s0945-053x(01)00198-6 PMID: 11852236

47. LaFlamme SE, Mathew-Steiner S, Singh N, Colello-Borges D, Nieves B. Integrin and microtubule crosstalk in the regulation of cellular processes. Cell Mol Life Sci. 2018; 75: 4177–4185. https://doi.org/10.1007/s00018-018-2913-x PMID: 30206641

48. Eddé B, Rossier J, Le Caer JP, Berwald-Netter Y, Koulakoff A, Gros F, et al. A combination of posttranslational modifications is responsible for the production of neuronal alpha-tubulin heterogeneity. J Cell Biochem. 1991; 46: 134–142. https://doi.org/10.1002/jcb.240460207 PMID: 1680872

49. Solito E, Christian HC, Festa M, Mulla A, Tierney T, Flower RJ, et al. Post-translational modification plays an essential role in the translocation of annexin A1 from the cytoplasm to the cell surface. FASEB J. 2006; 20: 1498–1500. https://doi.org/10.1096/fj.05-5319fje PMID: 16720734

50. D'Acquisto F, Perretti M, Flower RJ. Annexin-A1: a pivotal regulator of the innate and adaptive immune systems: Anx-A1: a pivotal regulator of the innate and adaptive immune systems. Br J Pharmacol. 2009; 155: 152–169. https://doi.org/10.1038/bjp.2008.252 PMID: 18641677

51. Gerke V, Creutz CE, Moss SE. Annexins: linking Ca2+ signalling to membrane dynamics. Nat Rev Mol Cell Biol. 2005; 6: 449–461. https://doi.org/10.1038/nrm1661 PMID: 15928709

52. Seemann J, Weber K, Osborn M, Parton RG, Gerke V. The association of annexin I with early endosomes is regulated by Ca2+ and requires an intact N-terminal domain. Mol Biol Cell. 1996; 7: 1359–1374. https://doi.org/10.1091/mbc.7.9.1359 PMID: 8885232

53. Boye TL, Maeda K, Pezeshkian W, Sønder SL, Haeger SC, Gerke V, et al. Annexin A4 and A6 induce membrane curvature and constriction during cell membrane repair. Nat Commun. 2017;8. https://doi.org/10.1038/s41467-017-00021-9 PMID: 28364116

54. Danhier P, Copetti T, De Preter G, Leveque P, Feron O, Jordan BF, et al. Influence of Cell Detachment on the Respiration Rate of Tumor and Endothelial Cells. Moschetta A, editor. PLoS ONE. 2013; 8: e53324. https://doi.org/10.1371/journal.pone.0053324 PMID: 23382841

55. Biarc J, Gonzalo P, Mikaelian I, Fattet L, Deygas M, Gillet G, et al. Combination of a discovery LC–MS/MS analysis and a label-free quantification for the characterization of an epithelial–mesenchymal transition signature. J Proteomics. 2014; 110: 183–194. https://doi.org/10.1016/j.jprot.2014.05.026 PMID: 25242195

56. Marín-Hernández A, Rodríguez-Enríquez S, Vital-González PA, Flores-Rodríguez FL, Macías-Silva M, Sosa-Garrocho M, et al. Determining and understanding the control of glycolysis in fast-growth tumor cells: Flux control by an over-expressed but strongly product-inhibited hexokinase. FEBS J. 2006; 273: 1975–1988. https://doi.org/10.1111/j.1742-4658.2006.05214.x PMID: 16640561

57. Bharathi SS, Zhang Y, Mohsen A-W, Uppala R, Balasubramani M, Schreiber E, et al. Sirtuin 3 (SIRT3) Protein Regulates Long-chain Acyl-CoA Dehydrogenase by Deacetylating Conserved Lysines Near the Active Site. J Biol Chem. 2013; 288: 33837–33847. https://doi.org/10.1074/jbc.M113.510354 PMID: 24121500

58. Westbrook JA, Cairns DA, Peng J, Speirs V, Hanby AM, Holen I, et al. CAPG and GIPC1: Breast Cancer Biomarkers for Bone Metastasis Development and Treatment. JNCI J Natl Cancer Inst. 2016; 108. https://doi.org/10.1093/jnci/djv360 PMID: 26757732

59. Wu D, Haruta A, Wei Q. GIPC1 interacts with MyoGEF and promotes MDA-MB-231 breast cancer cell invasion. J Biol Chem. 2010; 285: 28643–28650. https://doi.org/10.1074/jbc.M110.107649 PMID: 20634288

60. Stojadinovic A, Hooke JA, Shriver CD, Nissan A, Kovatich AJ, Kao T-C, et al. HYOU1/Orp150 expression in breast cancer. Med Sci Monit Int Med J Exp Clin Res. 2007; 13: BR231–239. PMID: 17968289

61. Anghel SI, Correa-Rochal R, Budinska E, Boliganl KF, Abraham S, Colombetti S, et al. Breast cancer suppressor candidate-1 (BCSC-1) is a melanoma tumor suppressor that down regulates MITF: BCSC-1—a melanoma tumor suppressor that represses MITF. Pigment Cell Melanoma Res. 2012; 25: 482–487. https://doi.org/10.1111/j.1755-148X.2012.01018.x PMID: 22594792

62. Li G, Ma D, Chen Y. Cellular functions of programmed cell death 5. Biochim Biophys Acta BBA—Mol Cell Res. 2016; 1863: 572–580. https://doi.org/10.1016/j.bbamcr.2015.12.021 PMID: 26775586

63. Wang J, Jia X, Meng X, Li Y, Wu W, Zhang X, et al. Annexin A3 may play an important role in ochratoxin-induced malignant transformation of human gastric epithelium cells. Toxicol Lett. 2019; 313: 150–158. https://doi.org/10.1016/j.toxlet.2019.07.002 PMID: 31276768

Conclusion et discussion

Il avait été montré que le support de culture et l'affinité d'une macrophages humains primaires pour celui-ci peut modifier l'activité phagocytaire des cellules (Lee et al. 2021) et donc l'internalisation d'objets. De même, la culture de macrophages THP-1 sur gel polyacrylamide-collagène peut favoriser la polarisation des macrophages selon la rigidité du gel vers un profil M1 (pro-inflammatoire et faiblement phagocytaire) ou M2 (anti-inflammatoire et fortement phagocytaire) (Sridharan et al. 2019).

Dans cette première étude, l'analyse protéomique a d'abord mis en évidence que les protéines impliquées dans l'adhésion cellulaire n'étaient pas la seule famille de protéines dont l'expression était modifiée par le mode de culture. Les enzymes du métabolisme, les protéines mitochondriales, le protéasome et les protéines de signalisation sont également modifiées entre les cellules en suspension et les cellules adhérentes. Il a également été mis en évidence que les modifications post-traductionnelles ne sont pas les mêmes entre les deux types de culture, les protéines des cellules adhérentes sont plus phosphorylées que les cellules en suspension.
Les expériences de validation ont permis de montrer que l'activité mitochondriale est augmentée chez les cellules en suspension, sans augmentation de la consommation de glucose. Cependant, l'état d'adhésion n'impacte pas le cycle cellulaire, l'activité phagocytaire, ni la réponse inflammatoire en réponse à un stimulus au LPS (Interleukin-6, TNF, NO). En conclusion, il semble que le type de culture des macrophages RAW264.7 ne modifie pas leurs réponses fonctionnelles. Nous pouvons donc nous affranchir de ce paramètre pour nos protocoles d'exposition.

La discordance entre nos données et celles de la littérature peut s'expliquer par des supports différents. Dans la publication du groupe de Sridharan (Sridharan et al. 2019), les macrophages sont cultivés sur des gels de polyacrylamide de duretés différentes et tapissés de protéines d'adhésion. Dans la publication de Lee (Lee et al. 2021), les macrophages sont cultivés sur un support basal recouvert de particules de dureté différentes. Dans notre cas, le support est dans les deux cas lisse et rigide (polystyrène), et c'est uniquement la chimie de surface qui cause l'adhésion ou la non-adhésion des cellules. Ces différences importantes peuvent expliquer les différences observées entre nos résultats et ceux de la littérature.

Une fois cette vérification effectuée, nous avons pu réaliser nos études sur la persistance des effets et sur les effets d'expositions répétées. Si de telles études sont rares dans la littérature, et tout particulièrement sur les systèmes *in vitro*, elles ne sont pas inexistantes, et nous allons aborder maintenant le contexte scientifique prévalant pour ces études sur les effets à moyen-long terme des NMx, ou aux effets croisés entre NMx et d'autres perturbations

I b) Contexte scientifique

Etudes existantes : *in vivo* et *in vitro*

Des études *in vivo* sur la silice amorphe de synthèse existent, comme par exemple celle de (Delaval et al. 2015) qui exposent des souris aux nanoparticules (NPs) de silice colloïdale pour étudier la capacité des macrophages alvéolaires à ensuite éliminer une infection pulmonaire à la bactérie *Pseudomonas aeruginosa*. Les souris C57Bl/6j sont exposées par voie intra-nasale à 5mg/kg aux nanoparticules de silice (diamètre 50nm environ) et 5h après cette exposition, les souris sont exposées à la bactérie *P. aeruginosa*. Ce temps court de pré-exposition à la silice permet d'infecter les souris avant que la réponse inflammatoire due à la silice se mette en place. En effet, après 24h d'exposition à la silice, il y a une augmentation de la sécrétion d'IL6 (environ 2 fois supérieure au contrôle) et de la chimiokine CXCL1 (neutrophile) (environ 4 fois supérieure au contrôle). De plus, la quantité d'immunoglobuline M (IgM) est doublée ce qui est lié avec une augmentation de la perméabilité de la barrière alvéolo-capillaire. Après 18h d'infection bactérienne, les réponses inflammatoires sont analysées : il semble que la pré-exposition (5h) aux NPs de silice augmente la susceptibilité des souris à déclencher une pneumonie létale mais cela est dû à l'altération de la barrière alvéolo-capillaire (qui devient perméable) plutôt qu'à une diminution de la réponse inflammatoire des macrophages. Une autre étude *in vivo* sur la persistance des effets suite à une exposition à la silice cristalline ou à la silice amorphe de synthèse a été réalisée (Arts et al. 2007). Dans cette étude, trois types de SAS sont utilisées : précipitée, gel et fumée. Les rats Wistar sont exposés par inhalation durant 5 jours, 6h par jour, à 1, 5 ou 25mg/m^3 à une des trois SAS. Un autre groupe de rats (contrôle positif) est exposé de la même manière à 25mg/m^3 de silice cristalline, le dernier groupe (contrôle négatif) est exposé à de l'air ne contenant pas de silice. Les rats sont ensuite autopsiés après les 5 jours d'exposition, ou 1 ou 3 mois plus tard. Pour les SAS, les effets observés le lendemain des 5 jours d'exposition sont transitoires et communs aux trois types SAS : à 25mg/m^3 le silicium est détecté dans les poumons, des modifications histopathologiques sont observables et les marqueurs de cytotoxicité sont détectés. A 5mg/m^3, seule une modification du fluide broncho-alvéolaire (TNF, lymphocyte) et un changement histopathologique sont constatés. A 1mg/m^3, aucun effet n'est observable. Pour les trois SAS, les effets constatés sont modérés et temporaires, ils ne sont plus observables 3 mois après l'exposition. Au contraire, les effets de la silice cristalline à 25mg/m3 sont persistants, et plus sévères : le silicium est quantifié dans les poumons et il est présent en quantité équivalente le lendemain de l'exposition, 1 et 3 mois plus tard. Le jour suivant l'exposition et 1 mois après,

Cost and Time Savings

	Method	
	Conventional (*in vivo*)	Motility Assay
Preparation Time	months to days (2 to 3 days)	10 min
Analyst Performance Time*	22.5 min	0.5 min
Materials	2.50	0.05
Supplies	8.00	8.00
Culture		
Labor**	9.45	0.21
	19.95	8.26

*Based on performance times of similar tasks as cited in Working Time Units Catalog, DOL, 1992.
**Assume analyst salary, benefits, and overhead of $25 (W.S.)/hour.

Figure 52 : Comparaison des coûts entre les tests in vivo et in vitro pour le temps de travail uniquement dans l'évaluation de l'irritabilité chimique

les marqueurs de toxicité du fluide broncho-alvéolaire sont détectés, et ils augmentent 3 mois après l'exposition. Cet effet est cohérent avec la faible élimination pulmonaire de la silice cristalline qui est à l'origine de la silicose.

Ces deux études *in vivo* abordent deux protocoles d'exposition importants en toxicologie, la dose accidentelle et la persistance des effets. Le premier, exposition aiguë, permet de connaître les effets d'une exposition accidentelle, souvent professionnelle, à une forte dose d'une substance particulière. Le deuxième scénario d'exposition permet d'étudier la persistance des effets suite à une exposition aiguë, et évaluer la capacité des cellules ou de l'organisme exposé(e)s à récupérer. Ces études sont longues et coûteuses, *in vivo*, il faut posséder l'installation respectant le bien-être animal, disposer d'une animalerie et de personnels formés à l'expérimentation animale. Il pourrait donc être intéressant d'utiliser des études *in vitro*, plus simples et moins coûteuses, mais leur pertinence doit être démontrée. Par exemple, une étude (Noever et al. 1994) compare une méthode d'analyse du comportement de nage (motilité) des ciliés *Tetrahymena pyriformis* par rapport au test *in vivo* règlementaire (irritation oculaire sur des lapins) pour tester un grand nombre de substances chimiques. Elle estime le temps et le coût de chacune des techniques (figure 52) : le gain financier est de l'ordre de 60% (rapidité de la technique, temps d'analyse par le manipulateur (salaire), prix du matériel utilisé), concernant le gain de temps, 10min de préparation sont nécessaire pour le test de motilité et moins d'une minute pour l'analyse par le manipulateur, contre plusieurs jours voire mois de préparation pour le test *in vivo* et une vingtaine de minute d'analyse par le manipulateur. Un rapport de 2018 de l'Agence de protection environnementale des Etats-Unis estime le coût d'un test réglementaire de toxicité cutanée de 28 jours à 114000$ (référence 870.3200 équivalente à la TG 407 de l'OCDE) (OECD 2008), et 145000$ pour 90 jours (référence 870.3250). Une étude de toxicité par inhalation de 90 jours sur le rat (référence 870.3465) est estimée à 576000$, enfin une étude combinée de toxicité chronique et carcinogénicité par inhalation (référence 870.3355) est estimée à 4 millions de dollars. Dans le but de réduire l'utilisation de l'expérimentation animale, d'obtenir des réponses plus rapides, de multiplier les études de toxicité croisée et de réduire les coûts des études toxicologiques, des systèmes *in vitro* se développent ces dernières années.

Un premier système utilisant une lignée cellulaire murine a été développé au sein de notre laboratoire pour étudier les effets d'une exposition à l'oxyde de zinc et aux nanoparticules d'oxyde de zirconium (Aude-Garcia, Dalzon, et al. 2016). Les macrophages ont été exposés durant 24h puis analysés à l'aide d'une étude protéomique et de tests de validation. *In vivo*, l'oxyde de zinc est connu pour être à l'origine de la pathologie appelée « fièvre des métaux » pour une dose d'exposition autour de 50mg/m^3 d'air, soit environ 5µg/ml dans ce système d'exposition, proche de la dose létale 20 (DL20) utilisée dans cette étude (8µg/ml). Les effets observés en protéomique sont principalement observés sur le cytosquelette, la signalisation, les mitochondries et sur quelques protéines impliquées dans la réponse au stress oxydant. Les tests de validation ont confirmé les modifications de cytosquelette, du potentiel mitochondrial et de l'activité phagocytaire. Les effets observés sont plus prononcés pour l'oxyde de zinc que pour les nanoparticules de dioxyde de zirconium. Ces observations *in vitro* sont cohérentes avec celles observées chez les personnes souffrant de la fièvre des métaux (Greenberg and Vearrier 2015). Une deuxième étude d'exposition aiguë aux nanofils d'argent (AgNWs) a été menée sur la lignée de macrophages murins J774A.1 (Toybou et al. 2019). Il a été montré que la toxicité des AgNWs est faible et dépendantes de leurs longueurs, cette toxicité diminue avec la longueur. Cependant il existe un effet pro-inflammatoire des nanofils longs (20µm) qui persiste pour le TNF, de même que pour la silice cristalline (BCR66, utilisée comme contrôle positif) après 72 heures sans nanomatériaux, c'est la première observation *in vitro* d'une persistance

des effets. Ces résultats sont cohérents avec ceux observés *in vivo* (Chung et al. 2017; Schinwald, Chernova, and Donaldson 2012).

I c) Persistance des effets (nanoparticules d'argent)

Présentation du projet

L'étude initiale sur les nanoparticules d'argent (Aude-Garcia, Villiers, et al. 2016) a été approfondie et le système a été développé dans l'équipe afin d'étudier la récupération des cellules suite à une exposition aiguë aux nanomatériaux. Les macrophages ont donc été exposés 24h aux nanoparticules d'argent puis après un changement de milieu, les cellules ont récupéré durant 72h (figure 53). Dans ce projet également, l'analyse protéomique a été combinée avec des tests de validation, afin de confirmer les résultats pro-inflammatoires précédemment observés et de comprendre les mécanismes en jeu dans la persistance des effets.

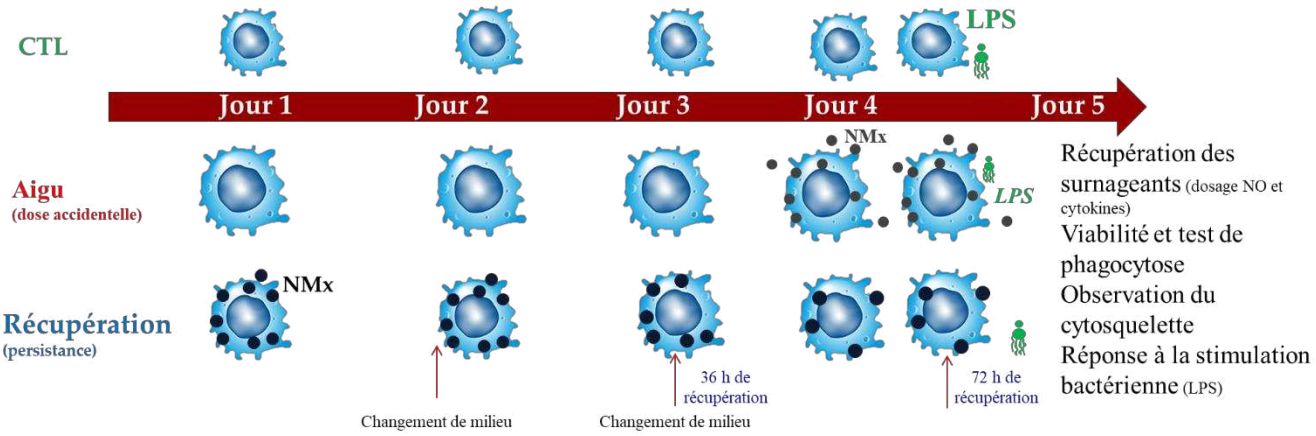

Figure 53 : Protocole d'exposition permettant d'étudier la persistance des effets suite à une exposition aigue. NMx : nanomatériaux, LPS : lipopolysaccharides, CTL : contrôle, NO : oxyde nitrique.

How reversible are the effects of silver nanoparticles on macrophages? A proteomic-instructed view

Bastien Dalzon, Anaelle Torres, Hélène Diemer, Stephane Ravanel, Véronique Collin-Faure, Karin Pernet-Gallay, Pierre-Henri Jouneau, Jacques Bourguignon, Sarah Cianférani, Marie Carrière, et al.

Environmental Science Nano

PAPER

View Article Online
View Journal | View Issue

Check for updates

Cite this: *Environ. Sci.: Nano*, 2019, 6, 3133

How reversible are the effects of silver nanoparticles on macrophages? A proteomic-instructed view†

Bastien Dalzon,‡[a] Anaelle Torres,‡[a] Hélène Diemer,[b] Stéphane Ravanel,[c] Véronique Collin-Faure,[a] Karin Pernet-Gallay,[d] Pierre-Henri Jouneau,[e] Jacques Bourguignon,[c] Sarah Cianférani,[b] Marie Carrière,[f] Catherine Aude-Garcia§[a] and Thierry Rabilloud *[a]

Silver nanoparticles are known to strongly affect biological systems, and numerous toxicological studies have investigated their effects. Most of these studies examine the effects immediately following acute exposure. In this work, we have conducted further investigation by studying not only the acute, post-exposure response, but also the cellular response after a 72 hour-recovery-phase post exposure. As a biological model we have used macrophages, which are very important cells with respect to their role in the immune response to particulate materials. To investigate the response of macrophages to nanoparticles and their recovery post exposure, we have used a combination of proteomics and targeted experiments. These experiments provided evidence that the cellular reaction to nanoparticles, including the reaction during the recovery phase, is a very active process involving massive energy consumption. Pathways such as the oxidative stress response, central and lipid metabolism, protein production and quality control are strongly modulated during the cellular response to nanoparticles, and restoration of basic cellular homeostasis occurs during the recovery period. However, some specialized macrophage functions, such as lipopolysaccharide-induced cytokine and nitric oxide production, did not return to their basal levels even 72 hours post exposure, showing that some effects of silver nanoparticles persist even after exposure has ceased.

Received 8th April 2019,
Accepted 21st July 2019

DOI: 10.1039/c9en00408d

rsc.li/es-nano

Environmental significance

Silver nanoparticles are known to have profound effects on living cells. Because of their widespread use, contamination is almost unavoidable. In this context, it is important not only to assess the immediate effects of silver nanoparticles on cells, but also how they recover after exposure. Using macrophages as the target cell type and a combination of proteomic and targeted experiments, we show here that the recovery phase is not just a "return to normal" condition. For example, some of the specialized macrophage functions are still not restored after this time, showing that subtle but sustained effects can occur after a single exposure. Although cell survival is not affected, such effects may impact the health status of living beings.

1. Introduction

Silver nanoparticles (AgNPs) are used as a biocide in a variety of consumer and medical products, because of the toxic effects that they have on microorganisms. However, as an unwanted side effect, AgNPs also show toxicity to mammalian cells. Thus, numerous toxicological studies have been conducted both *in vitro* in bacterial and eukaryotic model cell systems and *in vivo* in animal models, including at the microbiome level.[1–3] Although some studies, especially those using

[a] *Chemistry and Biology of Metals, Univ. Grenoble Alpes, CNRS UMR5249, CEA, IRIG, CBM-ProMD, 17 Rue des Martyrs, F-38054 Grenoble Cedex 9, France. E-mail: thierry.rabilloud@cnrs.fr; Tel: +33 438 783 212*
[b] *Laboratoire de Spectrométrie de Masse BioOrganique (LSMBO), Université de Strasbourg, CNRS, IPHC UMR 7178, 67000 Strasbourg, France*
[c] *Univ. Grenoble Alpes, INRA, CNRS UMR5168, CEA, IRIG, Laboratory of Plant Cellular Physiology, Grenoble, F-38000 France*
[d] *Univ. Grenoble Alpes, Inserm U1216 Grenoble Institut des Neurosciences, 38000 Grenoble, France*
[e] *Univ. Grenoble Alpes, Modelization and Exploration of Materials, CEA-DRF-IRIG-DEPHY-MEM-LEMMA, F-38000 Grenoble, France*
[f] *Univ. Grenoble-Alpes, CEA, CNRS UMR 5819, IRIG, SyMMES, Chimie Interface Biologie pour l'Environnement, la Santé et la Toxicologie (CIBEST), F-38054 Grenoble, France*

† Electronic supplementary information (ESI) available. See DOI: 10.1039/c9en00408d

‡ These authors contributed equally to this work.

§ Deceased: Nov. 21st, 2018. This paper is dedicated to her memory.

animal models, have examined the effects of NPs after repeated, low-dose exposures,[4–8] most of the cellular, toxicological studies have been conducted in an acute exposure mode, meaning that high doses have been used and exposure times have been short, spanning less than or equal to 24 hours. In these types of studies, toxicological endpoints are investigated at the end of the exposure period.[9–16] In terms of exposure, the acute schemes relate most closely to accidental, acute exposures, while chronic schemes correspond highly to occupational exposures. It is of interest to study how biological systems recover after a single, high, non-lethal exposure. This is not a trivial question, as some mineral toxicants such as beryllium or crystalline silica show very prolonged effects, even after the exposure has ceased.[17,18] This poor recovery has also been observed for silver nanomaterials such as silver nanowires[19] and silver nanoparticles.[20]

Many toxicological studies have reported pro-inflammatory responses[5,11,12,21] and/or immunological effects[15,22] pointing to macrophages as a cell type of major interest in toxicological studies of AgNPs. This is in accordance with the important scavenging function of macrophages in many different tissues.

This work investigates the recovery of macrophages after a unique, acute, but subtoxic dose of AgNPs. Targeted experiments carried out primarily on macrophages showed that several functional effects (*e.g.* LPS-induced cytokine and NO production, mitochondrial transmembrane potential and phagocytosis) were altered immediately after exposure to AgNPs. However, these functions tended to return to normal after a 72 h recovery period.[23] We therefore decided to get a broader view of cellular recovery using a proteomic approach.

Proteomic approaches have been used to study cellular responses to AgNPs in several models such as intestinal cells[9,24,25] or liver cells.[10] This allowed several important pathways modulated in response to acute exposures to AgNPs to be highlighted. These included mitochondrial proteins, pointing at potential mitochondrial dysfunction,[9,10,24] and proteins involved in intermediate metabolism[9,10,24] or in inflammatory responses.[10] The latter findings reinforced the interest in studying macrophages, which are major players in inflammation. We therefore decided to use proteomics to study the cellular responses using a macrophage J774 cell line, directly after acute exposure and after a recovery period had lapsed. This model cell line was selected because, unlike human monocyte cell lines,[26,27] mouse macrophage cell lines such as RAW264.7 and J774 do not need to be chemically differentiated into macrophages, a process that deeply alters cell physiology and causes some cell death. Furthermore, as opposed to primary macrophages derived from human blood, these mouse cell lines do not show extensive variability from one experiment to another. This explains why these cell lines are extensively used as models for testing of a wide variety of nanomaterials,[28–31] including large scale projects.[32–34]

2. Experimental

Most experiments have been performed essentially as described in previous publications.[35–37] Details are given here for the sake of the consistency of the paper. All biological experiments were carried out at least on three independent biological replicates.

2.1 Nanoparticles

PVP-coated silver nanoparticles were purchased from Sigma, directly as a concentrated suspension (catalog number #758329). Their characteristics have been published previously.[23,38] These experiments confirmed the manufacturer's data and showed that the nanoparticles are spherical, with a diameter in the 50–110 nm range, and did not aggregate upon dilution in water or culture medium.

2.2 Cell culture

The mouse macrophage cell line J774 was obtained from the European Cell Culture Collection (Salisbury, UK). The cells were cultured in DMEM + 10% fetal bovine serum (FBS). For routine culture, cells were seeded in non-adherent flasks (*e.g.* suspension culture flasks from Greiner) at 200 000 cells per ml and harvested 48 hours later, at 1 000 000 cells per ml. Cell viability was measured by a dye exclusion assay, either with eosin (1 mg ml^{-1})[39] under a microscope or with propidium iodide (1 μg ml^{-1})[40] in a flow cytometry mode.

For determination of the useful dose, cells were seeded at 500 000 cells per ml. They were treated with nanoparticles on the following day and harvested after a further 24 hours in culture.

For treatment with nanoparticles, cells were seeded in classical cell culture flasks and left for 24 hours at 37 °C for cell adhesion and confluence. For the recovery condition, cells were treated with nanoparticles on the following day. After 24 hours of exposure, the cell culture medium was removed and replaced by fresh medium. For consistency reasons, this operation was also carried out on cells used for control and for acute exposure. Another medium culture change was carried out 36 hours after the initial medium change, *i.e.* mid-term of the 72 hour recovery period. Finally, acute exposure was carried out for the final 24 hours and the cells were used immediately afterwards.

2.3 Phagocytosis and particle internalization assay

The phagocytic activity was measured using fluorescent latex beads (1 μm diameter, green labelled, catalog number L4655 from Sigma). The beads were pre-incubated at a final concentration of 55 μg mL^{-1} for 30 minutes at 37 °C in PBS/FBS (v/v). Then, they were incubated with cells (5 μg mL^{-1}) for 2 h 30 at 37 °C. Cells were harvested and washed with PBS. Cells were resuspended by vortexing with addition of 3/4 water volume and then 1/4 NaCl (35 mg mL^{-1}) volume was added under vortexing in order to clean the cell surface of adsorbed particles. Cells were harvested in PBS with propidium iodide

($1\ \mu g\ mL^{-1}$). Viability and phagocytic activity were measured simultaneously by flow cytometry on a FacsCalibur instrument (Beckton Dickinson). The dead cells (propidium positive) were excluded from the analysis.

2.4 Mitochondrial transmembrane potential measurement

The mitochondrial transmembrane potential was assessed by rhodamine 123 uptake. Cells were incubated with rhodamine 123 (80 nM) for 30 minutes at 37 °C, 5% CO_2 then rinsed twice in cold glucose ($1\ mg\ mL^{-1}$)–PBS (PBSG) and harvested in cold PBSG supplemented with propidium iodide ($1\ \mu g\ mL^{-1}$). The mitochondrial potential of the cells was analysed by flow cytometry on a FacsCalibur instrument (Beckton Dickinson). The dead cells (propidium positive) were excluded from the analysis. The low rhodamine concentration was used to avoid intramitochondrial fluorescence quenching that would result in a poor estimation of the mitochondrial potential.[41]

2.5 Enzyme assays

The enzymes were assayed according to published procedures (see below).

The cell extracts for enzyme assays were prepared by lysing the cells for 20 minutes at 0 °C in Hepes (20 mM, pH 7.5), $MgCl_2$ (2 mM), KCl (50 mM), EGTA (1 mM), and tetradecyldimethylammonio propane sulfonate (SB 3-14) (0.15% (w/v)), followed by centrifugation at 15 000*g* for 15 minutes to clear the extract. The protein concentration was determined by a dye-binding assay.[42] The dehydrogenase or dehydrogenase-coupled activities were assayed at 500 nm using the phenazine methosulfate/iodonitrotetrazolium coupled assay.[43] The enzyme assay buffer contained 25 mM Hepes, NaOH (pH 7.5), 5 mM magnesium acetate, 100 mM potassium nitrate and 1% Triton X-100. It also contained 30 μM phenazine methosulfate, 200 μM iodonitrotetrazolium chloride, 250 μM of the adequate cofactor (NAD or NADP) and 1–5 mM of the organic substrate, which was used to start the reaction. For phosphate-dependent enzymes such as glyceraldehyde dehydrogenase (GAPDH) and purine phosphorylase (PNPH), 50 mM potassium phosphate (pH 7.5) was added to the enzyme assay buffer. Triose phosphate isomerase was assayed with dihydroxyacetone phosphate and a glyceraldehyde dehydrogenase-coupled assay.[44] Purine phosphorylase (PNPH) was assayed by a xanthine oxidase-coupled assay.[45] Hexokinase was assayed by a glucose phosphate dehydrogenase (G6PDH)-coupled assay.[46] Biliverdine reductase was assayed at 450 nm as described.[47] Pyridoxal kinase was assayed directly at 388 nm.[48] Enolase was assayed at 340 nm by a pyruvate kinase–lactate dehydrogenase-coupled assay.[49]

2.6 NADP/NADPH and glucose assays

The glucose concentration in conditioned media was determined by a hexokinase–G6PDH assay.[50] Briefly, culture media collected at the end of the exposure period were centrifuged for 15 min at 15 000*g* to pelletize the particulate material. The supernatant was collected, and diluted 100-fold in the dehydrogenase assay buffer described above, containing also 1 mM EGTA, 30 μM phenazine methosulfate, 200 μM iodonitrotetrazolium chloride, 10 IU ml^{-1} G6PDH and 7.5 IU ml^{-1} hexokinase. The reaction was started by the addition of ATP (1 mM final concentration) and the increase in absorbance at 500 nm read for 1 minute. The linear part of the absorbance curve was used to determine the reaction speed, which was proportional to the glucose concentration. Fresh culture media supplemented with 10% fetal calf serum, *i.e.* high glucose DMEM ($4.5\ g\ L^{-1}$ glucose), RPMI1640 ($2\ g\ L^{-1}$ glucose) and 199 medium ($1\ g\ L^{-1}$ glucose) were used as standards.

The NADP–NADPH concentration was determined using an adapted alkaline extraction buffer.[51] Briefly, at the end of the exposure period, cells were collected by scraping, rinsed twice in PBS and pelleted. The packed cell pellet (PCP) volume was estimated, and the cells were lysed in 10 PCP volumes of 10 mM CAPS, 1 mM EGTA and 2 mM $MgCl_2$ for 10 minutes on ice with occasional vortexing. The suspension was centrifuged (10 000*g*, 5 minutes, 4 °C), the viscous cell pellet discarded and the supernatant collected and split into two aliquots. The first aliquot was neutralized on ice by adding 0.1 volume of 1 M tricine. This aliquot contained both the oxidized and reduced forms of the pyridine nucleotides, and was also used to determine the protein concentration by a dye-binding assay.[42]

The other aliquot was heated at 60 °C for 30 minutes in a thermostated water bath to destroy the oxidized forms of the pyridine nucleotides.[51] It was then cooled on ice, neutralized by adding 0.1 volume of 1 M tricine, and centrifuged for 10 minutes at 10 000*g* at 4 °C to eliminate any particulate material.

The NADP–NADPH concentration was then determined by using an enzyme cycling assay and standard NADP solutions.[52]

2.7 NO production and cytokine production

The cells were grown to confluence in a 6-well plate and pretreated with nanoparticles as described above. For the final 18 hours of culture, half of the wells were treated with 100 ng ml^{-1} LPS (from salmonella, purchased from Sigma), and arginine monohydrochloride was added to all the wells (5 mM final concentration) to give a high concentration of the substrate for nitric oxide synthase. After 18 hours of incubation, the cell culture medium was recovered and centrifuged at 10 000*g* for 10 minutes to remove cells and debris, and the nitrite concentration in the supernatants was read at 540 nm after addition of an equal volume of Griess reagent and incubation at room temperature for 30 minutes.

For cytokine production, a commercial kit (BD Cytometric Bead Array, catalog number 552364 from BD Biosciences) was used.

2.8 F-actin staining

The experiments were performed essentially as previously described.[53] The cells were recovered at the mid-term medium

change (see above) and cultured on coverslips placed in 6-well plates. For the acute exposure condition, the cells were exposed to silver nanoparticles for 24 h at 37 °C. At the end of the exposure time, the cells were washed twice for 5 min at 4 °C in PBS and fixed in 4% paraformaldehyde for 30 min at room temperature. After two washes (5 min/4 °C in PBS), they were permeabilized in 0.1% Triton X100 for 5 min at room temperature. After two more washes in PBS, 500 nM Phalloidin-Atto 550 (Sigma) was added to the cells and left for 20 min at room temperature in the dark. Coverslip-attached cells were washed, placed on microscope slides (Thermo Scientific) using a Vectashield mounting medium containing DAPI (Eurobio) and imaged using a Zeiss LSM 800 confocal microscope. The images were processed using ImageJ software.

2.9 Silver assay by ICP-MS

For measuring the Ag-NP uptake and release in cells, 2 mL cell cultures in 6-well plates were used, with the exposure scheme described above in section 2.2. At the end of the exposure period, the culture medium was removed and saved and the cell layer was gently rinsed twice with culture medium without serum.

The cells were then lysed by scraping in 2 ml of lysis buffer (50 mM Hepes (pH 7.5), 4 mM magnesium acetate, 200 mM sorbitol, and 0.1% (w/v) tetradecyldimethylammonio propane sulfonate (SB 3-14)). The lysate was pipetted into a microtube and incubated for 20 minutes on ice to complete cell lysis. For determination of soluble silver, aliquots of the culture media and of the cell lysates were centrifuged for 45 minutes at 16 000*g*, and the upper half of the supernatant was collected.

The samples were mineralized by the addition of one volume of suprapure 65% HNO_3 and incubation on a rotating wheel at room temperature for 18 h.

Mineralized samples were diluted in 0.5% (v/v) HNO_3 and analysed using an iCAP RQ quadrupole mass instrument (Thermo Fisher Scientific GmbH, Germany) equipped with an ASX-560 auto-sampler (Teledyne CETAC Technologies, Omaha, USA). The instrument was used with a MicroMist U-Series glass concentric nebulizer, a quartz spray chamber cooled at 3 °C, a Qnova quartz torch, a nickel sample cone, and a nickel skimmer cone equipped with a high-sensitivity insert. ^{24}Mg, ^{25}Mg, ^{107}Ag and ^{109}Ag concentrations were determined using standard curves and corrected using an internal standard solution of 103Rh added online. Data integration was done using the Qtegra software (version 2.8.2944.115). The results were normalized using the Mg concentration (4 mM in the cellular extracts and 0.82 mM in culture medium). To take into account the cellular concentration effects, the protein concentration of the extracts was determined by a dye-binding assay.[42]

2.10 Proteomics

The 2D gel-based proteomic experiments were essentially carried out as previously described,[35] at least on independent biological triplicates. However, detailed materials and methods are provided for the sake of paper consistency.

2.10.1 Sample preparation. The cells were collected by scraping and then washed three times in PBS. The cells were then washed once in TSE buffer (10 mM Tris-HCl (pH 7.5), 0.25 M sucrose, and 1 mM EDTA), and the volume of the cell pellet was estimated. The pellet was resuspended in its own volume of TSE buffer. Then 4 volumes (respective to the cell suspension just prepared) of concentrated lysis buffer (8.75 M urea, 2.5 M thiourea, 5% w/v CHAPS, 6.25 mM TCEP-HCl, 20 mM spermine base, and 20 mM spermine tetrahydrochloride) were added and the solution was left to extract at room temperature for 1 hour. The nucleic acids were then pelleted by centrifugation (270 000*g* at room temperature for 1 h), and the protein concentration in the supernatant was determined by a dye-binding assay.[42] Carrier ampholytes (Pharmalytes, pH 3–10) were added to a final concentration of 0.4% (w/v), and the samples were kept frozen at −20 °C until use.

2.10.2 Isoelectric focusing. Home-made 160 mm long 4–8 linear pH gradient gels[54] were cast according to published procedures.[55] Four mm-wide strips were cut and rehydrated overnight with the sample, diluted to a final volume of 0.6 ml of the rehydration solution (7 M urea, 2 M thiourea, 4% CHAPS, 0.4% carrier ampholytes (Pharmalytes 3–10) and 100 mM dithiodiethanol).[56]

The strips were then placed in a Multiphor plate (GE Healthcare), and IEF was carried out with the following electrical parameters: 100 V for 1 hour, then 300 V for 3 hours, then 1000 V for 1 hour, then 3400 V up to 60–70 kVh. After IEF, the gels were equilibrated for 20 minutes in 125 mM Tris, 100 mM HCl, 2.5% SDS, 30% glycerol and 6 M urea.[57] They were then transferred on top of the SDS gels and sealed in place with 1% agarose dissolved in 125 mM Tris, 100 mM HCl, 0.4% SDS and 0.005% (w/v) bromophenol blue.

2.10.3 SDS electrophoresis and protein detection. Ten percent gels (160 × 200 × 1.5 mm) were used for protein separation. The Tris taurine buffer system[58] was used and operated at an ionic strength of 0.1 and a pH of 7.9. The final gel composition is thus 180 mM Tris, 100 mM HCl, 10% (w/v) acrylamide, and 0.27% bisacrylamide. The upper electrode buffer is 50 mM Tris, 200 mM taurine, and 0.1% SDS. The lower electrode buffer is 50 mM Tris, 200 mM glycine, and 0.1% SDS. The gels were run at 25 V for 1 hour, then 12.5 W was applied per gel until the dye front reached the bottom of the gel. Detection was carried out by tetrathionate silver staining[59] .

2.10.4 Image analysis and global analysis of the spot abundance data. The gels were scanned after silver staining on a flatbed scanner (Epson perfection V750), using 16 bit grayscale image acquisition. The gel images were then analyzed using the Delta 2D software (v 3.6). The spots that were never expressed above 100 ppm of the total spots were first filtered out. Then, significantly-varying spots were selected on the basis of their Student's *T*-test *p*-value between the treated and the control groups. Spots showing a *p*-value lower than 0.05

were selected. This strategy is used to avoid the use of arbitrary thresholds, which can result in discarding statistically-valid relevant changes and including non-valid changes.[60] The false positive concern was taken into account using several approaches such as the Benjamini Hochberg approach,[61] the sequential goodness of fit approach[62] and the sequential Fisher test approach.[63] Furthermore, we checked that all the spots that we found through the *T*-test also had a $p < 0.05$ in a non-parametric Mann–Whitney *U*-test.

For the global analysis of the spot abundance data, we used directly the spot abundance data as provided by the gel analysis software. The software directly normalizes each spot abundance by the sum of all spot abundances detected on the gel. These relative abundance data were used directly for global analysis using the PAST software suite[64] without any transformation. No limitation in the number of principal components was implemented in the principal component analysis.

2.10.5 Mass spectrometry. The spots selected for identification were excised from silver-stained gels and destained with ferricyanide/thiosulfate on the same day as silver staining in order to improve the efficiency of the identification process.[65,66] In-gel digestion was performed with an automated protein digestion system, MassPrep Station (Waters, Milford, USA). The gel plugs were washed twice with 50 μL of 25 mM ammonium hydrogen carbonate (NH_4HCO_3) and 50 μL of acetonitrile. The cysteine residues were reduced by 50 μL of 10 mM dithiothreitol at 57 °C and alkylated by 50 μL of 55 mM iodoacetamide. After dehydration with acetonitrile, the proteins were cleaved in the gel with 10 μL of 12.5 ng μL^{-1} modified porcine trypsin (Promega, Madison, WI, USA) in 25 mM NH_4HCO_3. The digestion was performed overnight at room temperature. The generated peptides were extracted with 30 μL of 60% acetonitrile in 0.1% formic acid. Acetonitrile was evaporated under vacuum before nanoLC-MS/MS analysis.

NanoLC-MS/MS analysis was performed using a nanoACQUITY Ultra-Performance-LC (Waters Corporation, Milford, USA) coupled to a Synapt™ High Definition Mass Spectrometer™ (Waters Corporation, Milford, USA), or to a TripleTOF 5600 (Sciex, Ontario, Canada).

The nanoLC system was composed of an ACQUITY UPLC® CSH130 C18 column (250 mm × 75 μm with a 1.7 μm particle size, Waters Corporation, Milford, USA) and a symmetry C18 precolumn (20 mm × 180 μm with a 5 μm particle size, Waters Corporation, Milford, USA). The solvent system consisted of 0.1% formic acid in water (solvent A) and 0.1% formic acid in acetonitrile (solvent B). 4 μL of the sample were loaded into the enrichment column over 3 min at 5 μL min^{-1} with 99% of solvent A and 1% of solvent B. Elution of the peptides was performed at a flow rate of 300 nL min^{-1} with a 8–35% linear gradient of solvent B in 9 minutes.

The Synapt™ High Definition Mass Spectrometer™ (Waters Corporation, Milford, USA) was equipped with a Z-spray ion source and a lock mass system. The system was fully controlled by MassLynx 4.1 SCN639 (Waters Corporation, Milford, USA). The capillary voltage was set at 2.8 kV and the cone voltage at 35 V. Mass calibration of the TOF was achieved using fragment ions from Glu-fibrino-peptide B in the [50;2000] *m*/*z* range. Online correction of this calibration was performed with Glu-fibrino-peptide B as the lock-mass. The ion $(M + 2H)^{2+}$ at *m*/*z* 785.8426 was used to calibrate MS data and the fragment ion $(M + H)^{+}$ at *m*/*z* 684.3469 was used to calibrate MS/MS data during the analysis.

For tandem MS experiments, the system was operated with automatic switching between the MS (0.5 s per scan in the *m*/*z* range [150;1700]) and MS/MS mode (0.5 s per scan in the *m*/*z* range [50;2000]). The two most abundant peptides (intensity threshold 20 counts per s), preferably doubly and triply charged ions, were selected in each MS spectrum for further isolation and CID fragmentation using a collision energy profile. Fragmentation was performed using argon as the collision gas.

Mass data collected during analysis were processed and converted into .pkl files using ProteinLynx Global Server 2.3 (Waters Corporation, Milford, USA). Normal background subtraction was used for both MS and MS/MS with a 5% threshold and polynomial correction of order 5. Smoothing was performed on MS/MS spectra (Savitzky–Golay, 2 iterations, window of 3 channels). Deisotoping was applied for MS (medium deisotoping) and for MS/MS (fast deisotoping).

The TripleTOF 5600 (Sciex, Ontario, Canada) was operated in positive mode, with the following settings: ion spray voltage floating (ISVF) 2300 V, curtain gas (CUR) 10, interface heater temperature (IHT) 150, ion source gas 1 (GS1) 2, declustering potential (DP) 80 V. The information-dependent acquisition (IDA) mode was used with Top 10 MS/MS scans. The MS scan had an accumulation time of 250 ms in the *m*/*z* [400;1250] range and the MS/MS scans 100 ms in the *m*/*z* [150;1800] range in high sensitivity mode. Switching criteria were set to ions with a charge state of 2–4 and an abundance threshold of more than 500 counts; the exclusion time was set at 4 s. The IDA rolling collision energy script was used for automatically adapting the CE. Mass calibration of the analyser was achieved using peptides from digested BSA. The complete system was fully controlled by AnalystTF 1.7 (Sciex). Raw data collected were processed and converted with MSDataConverter in the .mgf peak list format.

For protein identification, the MS/MS data were interpreted using a local Mascot server with the MASCOT 2.4.1 algorithm (Matrix Science, London, UK) against UniProtKB/SwissProt (version 2016_01, 550 299 sequences). The research was carried out in all species. Spectra were searched with a mass tolerance of 15 ppm for MS and 0.05 Da for MS/MS data, allowing a maximum of one trypsin missed cleavage. Carbamidomethylation of cysteine residues and oxidation of methionine residues were specified as variable modifications. Protein identifications were validated with at least two peptides with a Mascot ion score above 30.

2.11 Electron microscopy

J774 macrophage cells were grown on coverslips and treated with AgNPs as described above. Cells were allowed to recover for 72 hours before being fixed with 2.5% glutaraldehyde in 0.1 M cacodylate buffer (pH 7.4) for 2 hours at room temperature. Cells were then washed with buffer, post fixed with 1% osmium tetroxide in the same buffer for 1 hour at 4°, and washed with water. Cells were then dehydrated through a series of graded alcohol (30–60–90–100–100–100%) and infiltrated with a mix of 1/1 epon/alcohol (100%) for 1 hour before several baths of fresh epon (Fluka) for 3 hours. Finally, a capsule full of epon was placed on the surface of the cells and the resin was allowed to polymerise for 72 h at 60 °C. The polymerised bloc was then detached from the coverslip with HF (48%) over 1 hour. Ultrathin sections of the cell monolayer were cut with an ultramicrotome (Leica). For transmission electron microscopy (TEM) observation, the sections were post-stained with 5% uranyl acetate and 0.4% lead citrate and observed with a transmission electron microscope at 80 kV (JEOL 1200EX). Images were acquired with a digital camera at magnification ranging from 15k to 50k (Veleta, Olympus). For scanning transmission electron microscopy observation (STEM) and energy dispersive spectroscopic analysis (EDS), the sections were not post-stained. They were coated with a thin layer of carbon and observed and analyzed with an OSIRIS microscope (TECNAI) operating at 200 kV.

3. Results

3.1 Silver accumulation upon treatment with silver nanoparticles and after recovery

First, the effect of silver nanoparticles and soluble silver on cell viability was assayed, and the results are shown in Fig. 1. For all the subsequent experiments, a dose of 20 μg ml^{-1} was selected, corresponding to the lethal dose 20% (LD20). This dose ensures strong effects on cells while keeping cellular mortality at an acceptable level for subsequent experiments. We also checked the presence of nanoparticles in cells by electron microscopy. Control cells did not show any electron-dense materials (Fig. 2A and B), while cells exposed to Ag nanoparticles acutely showed some electron-dense particles located in large membrane compartments called macropinosomes (Fig. 2C and D). After the recovery period, these electron dense particles were still observed in the macropinosomes (Fig. 2E and F). Energy dispersive spectroscopic analysis of these electron-dense features confirmed that they contained Ag (Fig. 2G–I).

Silver accumulation in cells was measured by ICP-MS. The results are summarized in Table 1. They showed a strong accumulation of silver in cells at the end of the 24 hour exposure followed by a moderate loss of total silver. The cells were able to cycle once during the 72 h recovery period, as shown by the increase in the protein amount in the extracts, which resulted in a further reduction of the cellular silver content. A moderate but detectable silver excretion was also evidenced. It should be also noted that the protein concentration is used in toxicology as an indicator for cell number,[67,68]

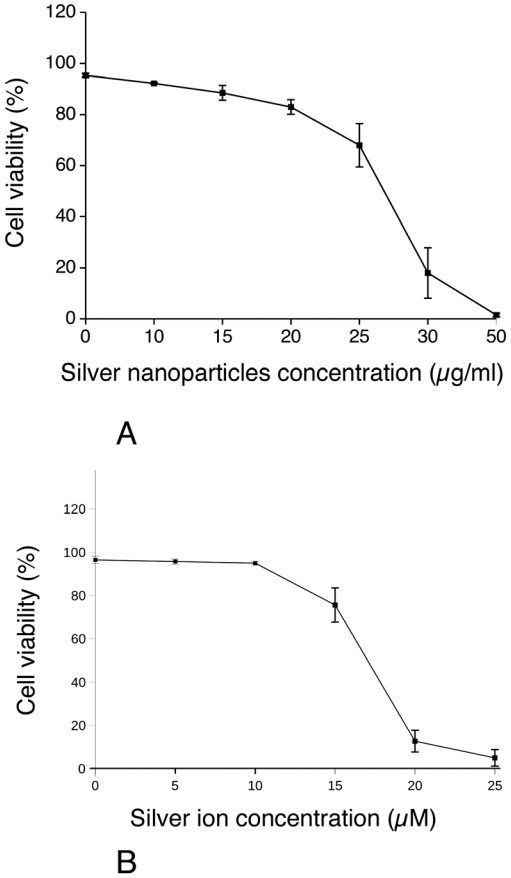

Fig. 1 Dose response curve to silver nanoparticles and ionic silver. Cell viability was measured by dye exclusion. The cells were exposed to silver nanoparticles (panel A) or silver lactate (panel B) for 24 hours before measurement of cell viability (n = 3).

3.2 Global analysis of the proteomic results

From the total protein expression data obtained from the gel analysis software, a subset of variable proteins ($p < 0.25$ in either the acute *vs.* control or the recovery *vs.* control comparisons) was extracted. This allowed the noise brought by proteins that do not show a consistent variation in the biological phenomena under investigation to be decreased. This subset was then tested using the PAST statistical suite.[64] As a first test, a hierarchical clustering was performed, and the results are shown in Fig. 3A. Clustering clearly separates the control group from the two silver-treated ones, but gives no information regarding which silver treatment condition is closer to the control. Principal component analysis gave a more valuable indication, as shown in Fig. 3B. The recovery group appeared to be in an intermediate position between the control and acute groups along component one, which carries most of the variance. This is an expected position in a "return to normal" model during the recovery phase. However, the recovery group separated from both the control and the acute groups in component 2. This suggested that the three conditions were fairly different from each other. This was further confirmed by analysis of similarities (ANOSIM), which gave the following results for the p-values of the pairwise comparisons:

$p = 0.031$ for the acute *vs.* control comparison

$p = 0.032$ for the recovery *vs.* control comparison

$p = 0.027$ for the acute *vs.* recovery comparison

These figures suggest that the recovery phase was a very active state, which did not represent just an intermediate state between the control and the acute stage, *i.e.* immediately after exposure to silver nanoparticles. To further investigate this aspect, we extracted the intensity values for the spots that were significantly altered ($p < 0.05$) between the control group and at least one of the silver-treated groups. In order

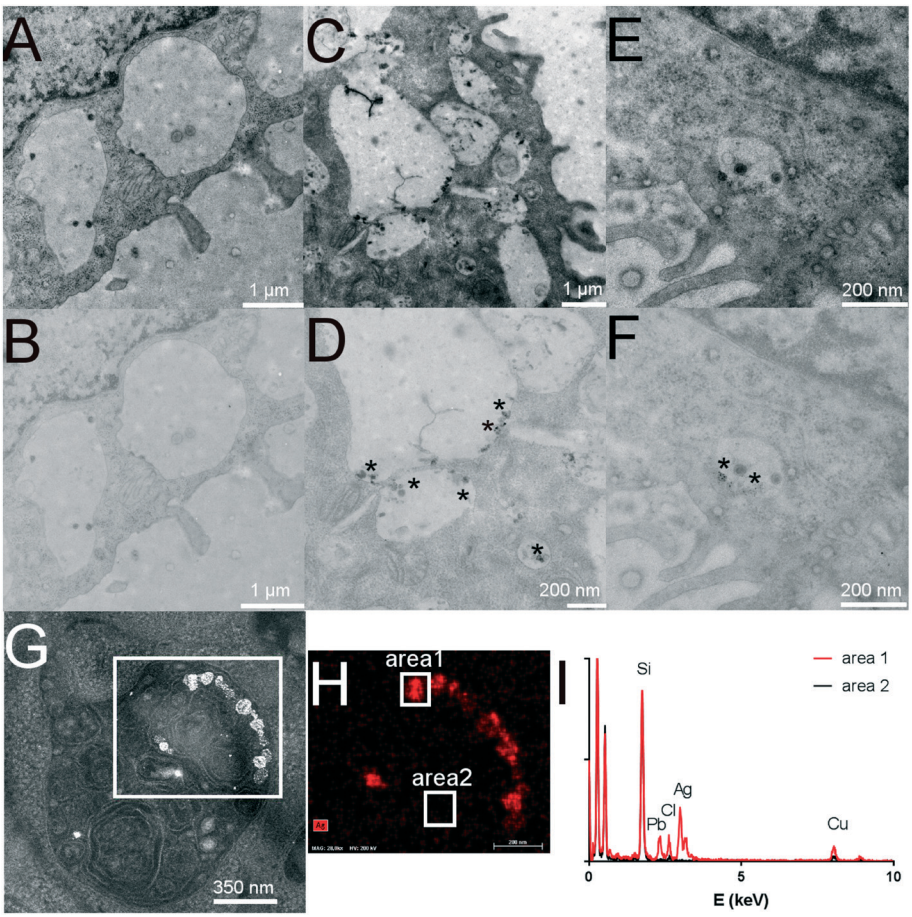

Fig. 2 Ag distribution in macrophages. Control cells (A and B) or cells exposed to Ag nanoparticles (C–G) were imaged by transmission electron microscopy (A–F) or scanning transmission electron microscopy (G). Panels A and B: control cells; panels C and D: cells acutely exposed to Ag nanoparticles; panels E and F: recovering cells. A, C and E: High contrast images; B, D and F: low contrast images highlighting the presence of electron-dense materials, which are probably Ag nanoparticles or debris of Ag nanoparticles (*). Panel G is a HAADF image of a multilamellar body containing electron-dense materials. H and I: Chemical element distribution of the area of G delimited by the white square, analyzed by energy dispersive spectroscopy. Panel H shows the Ag distribution and panel I shows the EDS spectra of area1 (an intracellular region containing some Ag) and area2 (an intracellular region that does not contain any Ag) of H.

Table 1 Measurements of silver concentrations

	Unexposed	Exposed to 20 µg ml^{-1} AgNPs	72 h recovery after exposure to AgNPs
Protein concentration in the cell extract (mg ml^{-1})	0.352 ± 0.02	0.322 ± 0.02	0.657 ± 0.04
Total silver concentration in the cell extract (µg l^{-1})	0	9794 ± 1159	8258 ± 1536
Soluble silver concentration in the cell extract (µg l^{-1})	0	39.86 ± 11.83	47.57 ± 3.11
Soluble silver concentration in culture medium (µg l^{-1})		457 ± 64[a]	142 ± 4
Normalized silver content (ng Ag mg^{-1} protein)	0	30 608 ± 5055	12 530 ± 1984
Soluble silver fraction in cells	0	0.0041 ± 0.0014	0.0059 ± 0.001
Fraction of silver excreted[b]	0	ND	0.017 ± 0.003

[a] This value contains both the soluble silver that is actively excreted by cells during the exposure and the soluble silver that arises from nanoparticle dissolution directly in the culture medium. [b] Defined as soluble silver in medium/total silver (*i.e.* silver in medium + silver in cells).

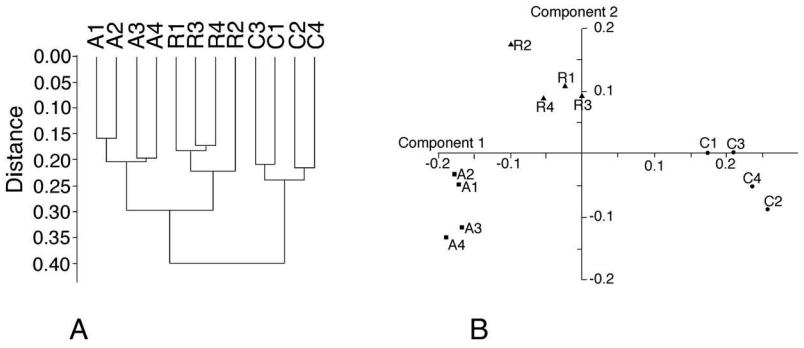

Fig. 3 Global analysis of proteomic data. Global data analysis was performed on the proteomic data to derive the relationships between the various samples used. Panel A: Hierarchical clustering. The Euclidean distance similarity index and Ward's algorithm were used for this analysis. C1–C4: Control (non-exposed) cells. A1–A4: Acutely exposed cells (24 hours). R1–R4: Recovering cells (72 hours post-exposure). Panel B: Principal component analysis. A representation displaying the first two principal components is shown. The PCA yielded 11 components, of which the first two, represented in the figure, explained 70% of the total variance (axis 1 – 54%, axis 2 – 16%). Component 3 explained 7.5% of the variance, component 4 explained 6%, and the remaining components explained less than 4% of the variance each. Samples labelled as in panel A.

to cope with the multiple testing issue, we used several approaches such as the Benjamini Hochberg approach,[61] the sequential goodness of fit approach[62] and the sequential Fisher test approach.[63] All the selected spots showed a very low *q*-value for the condition for which they were variable compared to the control (Table S1†).

We then divided this dataset of 239 spots into lists (Table S2†). The first list, labelled as "returning spots", contained the spots for which the amplitude of the change in abundance between the recovery and control stages is lower than the amplitude of the change in abundance between the acute exposure and control stages. 135 spots belonged to this list. It was then divided into subsets. The first subset contained "fast returning spots". It was defined as spots for which the quantitative change in the acute *vs.* control comparison shows an amplitude at least twice that in the recover *vs.* control comparison (*i.e.* more than 50% convergence). 44 spots belonged to this subset. The other subset of this list contained the 91 "slow returning spots", for which the return-to-normal trend was lower than 50% in the 72 hour recovery period.

The other list, labelled as "diverging spots", contained the 104 spots for which the amplitude of the change in abundance between the recovery and control stages is higher than the amplitude of the change in abundance between the acute exposure and control stages. This list was also divided into subsets. The "fast diverging spots" subset was defined as the spots for which the quantitative change in the recover *vs.* control comparison was at least 1.5 higher than the quantitative change in the acute *vs.* control comparison (*i.e.* more than 50% divergence). 53 spots belonged to this subset. The other subset of this list contained the 51 "slow diverging spots", for which the diverging trend was lower than 50% in the 72 hour recovery period.

3.3 Detailed analysis of the proteomic results

In order to gain more precise insights, we investigated which proteins were significantly altered ($p < 0.05$) between the control group and at least one of the silver-treated groups. The list of modulated proteins is given in Table 2 and the corresponding 2D gel images are shown in Fig. 4. As 2D gels separate protein forms, a variation in a spot does not necessarily mean that the whole amount of the protein is modulated. In fact, a single protein can be represented by various 2D gel spots, which do not necessarily all change upon the treatment with nanoparticles. To alleviate this problem, we systematically identified by mass spectrometry not only the modulated spots, but also the neighboring spots to check for such isoform issues. The quantitative results have been integrated in Table 2 and the mass spectrometry identification parameters are detailed in Table S3.† The results for some classes (apoptosis, cell fate and energy metabolism) are also shown in gel images in Fig. 4, and the results for the other classes are shown in Fig. S1–S5.† For global analysis of the modulated proteins, we used the DAVID annotation tool,[69,70] available at https://david.ncifcrf.gov/, and the results are shown in Tables S4 and S5.† The results showed that some functional classes such as energy metabolism, cytoskeleton especially actin cytoskeleton, protein folding and quality control (especially the ubiquitin/proteasome pathway), nucleotide and nucleic acid metabolism, cell signaling, oxidative stress response and detoxification proteins are strongly represented among the modulated proteins. This prompted us to carry out validation experiments on some of these proteins or pathways.

3.4 Enzymatic activities

For some of the modulated proteins, we first checked whether their enzyme activities (Table 3), *i.e.* the relevant parameter in terms of cell physiology, followed or not the trends observed *via* proteomics. There is no obvious inference between the two parameters, as the activity may be modulated by PTM and thus correlate with one or several spots, or with the sum of the spots representing the same protein. One good example is represented by malate dehydrogenase,

Table 2 Differentially-expressed proteins identified in the proteomic screen

Spot number	Protein name	Accession number	Ratio acute/ctrl	*T* test acute *vs.* ctrl	Ratio recov/ctrl	*T* test recov *vs.* ctrl
A1	Casp3	P70677	0.59	0.04	1.00	0.99
A2	Efhd2	Q9D8Y	1.24	0.02	1.18	0.23
C1	Actin	P60710	1.51	<0.01	1.67	0.01
C2a	Actn4/1	P57780	1.45	0.04	1.18	0.16
C2b	Actn4/2	P57780	1.43	0.04	1.38	0.01
C2c	Actn4/3	P57780	1.25	0.33	1.17	0.03
C2d	Actn4/4	P57780	1.44	0.20	1.28	0.05
C2S	∑ Actn4	P57780	1.36	0.16	1.23	0.02
C3a	Arp2/1	P61161	0.90	0.06	0.76	<0.01
C3b	Arp2/2	P61161	1.10	0.41	0.94	0.63
C3c	Arp2/3	P61161	1.19	0.04	1.32	<0.01
C3S	∑ Arp2	P61161	1.15	0.07	1.14	0.06
C4a	Arpc2/1	Q9CVB6	0.57	0.03	0.52	0.02
C4b	Arpc2/2	Q9CVB6	0.76	0.04	0.78	0.06
C4c	Arpc2/3	Q9CVB6	0.91	0.51	1.12	0.41
C4S	∑Arpc2	Q9CVB6	0.80	0.11	0.90	0.39
C5a	Arpc5/1	Q9CPW4	0.59	0.03	0.25	0.01
C5b	Arpc5/2	Q9CPW4	1.06	0.51	0.99	0.90
C5S	∑ Arpc5	Q9CPW4	0.88	0.30	0.71	0.04
C6a	Capg/1	P24452	0.81	0.01	1.00	0.97
C6b	Capg/2	P24452	1.16	0.15	1.04	0.58
C6S	∑ capg	P24452	0.35	0.39	0.35	0.39
C7	Capza2	P47754	1.30	0.01	1.28	0.01
C8a	Capzb/1	P47757	1.07	0.37	1.20	0.06
C8b	Capzb/2	P47757	0.80	0.02	1.01	0.95
C8S	∑ capzb	P47757	0.98	0.60	1.13	0.14
C9a	Cof/1	P18760	0.67	0.05	0.60	0.03
C9b	Cof/2	P18760	1.49	0.01	1.26	0.10
C9c	Cof/3	P18760	0.74	<0.01	0.73	<0.01
C9S	∑ Cof	P18760	0.86	0.02	0.79	<0.01
C10a	Dyncli2/1	O88487	1.21	0.49	2.20	<0.01
C10b	Dyncli2/2	O88487	1.43	0.26	1.69	0.04
C10S	∑ dyncli2	O88487	1.36	0.30	1.84	0.01
C11a	Gelsolin/1	P13020	1.16	0.44	0.94	0.71
C11b	Gelsolin/2	P13020	1.16	0.36	1.00	0.97
C11c	Gelsolin/3	P13020	1.39	0.16	1.27	0.26
C11d	Gelsolin/4	P13020	1.57	0.05	1.32	0.13
C11S	∑ gelsolin	P13020	1.33	0.15	1.15	0.39
C12	Gmfg	Q9ERL7	0.54	<0.01	0.66	<0.01
C13	Lasp1	Q61792	0.41	<0.01	0.38	<0.01
C14	Ml12b	Q3THE2	0.92	0.51	0.81	0.01
C15a	Moesin/1	P26041	0.94	0.75	0.86	0.41
C15b	Moesin/2	P26041	0.90	0.53	0.78	0.08
C15c	Moesin/3	P26041	1.22	0.17	0.89	0.13
C15d	Moesin/4	P26041	1.18	0.07	1.09	0.10
C15e	Moesin/5	P26041	1.52	0.03	1.24	0.04
C15S	∑ Moesin	P26041	1.20	0.08	1.01	0.91
C16	Mtap	Q9CQ65	1.04	0.83	1.30	0.02
C17	RhoA	Q9QUI0	0.59	<0.01	0.76	0.02
C18a	Rhogdi1/1	Q99PT1	0.71	<0.01	0.67	<0.01
C18b	Rhogdi1/2	Q99PT1	1.16	0.13	1.11	0.08
C18S	∑ RhoGdi1	Q99PT1	0.99	0.85	0.95	0.28
C19a	Rhogdi2/1	Q61599	0.64	<0.01	0.54	<0.01
C19b	Rhogdi2/2	Q61599	1.00	0.99	0.95	0.17
C19S	∑ rhogdi2	Q61599	0.87	0.02	0.80	<0.01
C20a	Stmn/1	P54227	0.84	0.19	0.70	0.01
C20b	Stmn/2	P54227	0.60	0.02	0.53	0.01
C20c	Stmn/3	P54227	0.88	0.14	0.76	0.01
C20S	∑ Stmn	P54227	0.83	0.05	0.71	0.01
C21a	Sw70/1	Q6A028	1.63	0.02	1.50	0.20
C21b	Sw70/2	Q6A028	2.02	0.02	1.76	0.08
C21S	∑ Sw70	Q6A028	1.77	0.01	1.60	0.14
C22	Tbcb	Q9D1E6	1.31	0.03	1.11	0.45
C23a	Tctp/1	P63028	0.60	<0.01	0.54	<0.01
C23b	Tctp/2	P63028	0.84	0.03	0.85	0.05
C23S	∑ Tctp	P63028	0.84	0.03	0.72	<0.01
C24a	Twf1/1	Q91YR1	0.58	<0.01	0.93	0.39

Table 2 *(continued)*

Spot number	Protein name	Accession number	Ratio acute/ctrl	*T* test acute *vs.* ctrl	Ratio recov/ctrl	*T* test recov *vs.* ctrl
C24b	Twf1/2	Q91YR1	0.25	0.01	0.86	0.52
C24S	∑ Twf1	Q91YR1	0.40	<0.01	0.89	0.47
C25	Twf2	Q9Z0P5	0.70	0.01	0.60	0.01
C26	Vime	P20152	1.54	0.05	1.35	0.04
C27a	Vinculin/1	Q64727	1.28	0.25	1.24	0.11
C27b	Vinculin/2	Q64727	1.32	0.07	1.16	0.24
C27c	Vinculin/3	Q64727	1.63	0.01	1.12	0.28
C27S	∑ Vinculin	Q64727	1.39	0.07	1.18	0.16
D1	Cbx1	P83917	0.91	0.27	0.72	<0.01
D2a	Ddb1/1	Q3U1J4	1.74	0.04	1.40	0.16
D2b	Ddb1/2	Q3U1J4	0.93	0.65	0.78	0.21
D2S	∑ Ddb1	Q3U1J4	1.31	0.14	1.07	0.73
D3	Nt5c	Q9JM14	1.18	0.08	1.39	0.03
D4a	Pcna/1	P17918	0.57	<0.01	0.57	<0.01
D4b	Pcna/2	P17918	0.82	0.02	0.80	0.03
D4c	Pcna/3	P17918	1.00	0.92	0.98	0.73
D4S	∑ Pcna	P17918	0.84	<0.01	0.82	0.02
D5	Ruvb2	Q9WTM5	1.46	0.06	1.42	0.04
E1a	6pgd/1	Q9DCD0	0.88	0.05	0.95	0.42
E1b	6pgd/2	Q9DCD0	1.05	0.32	1.01	0.90
E1S	∑ **6pgd**	**Q9DCD0**	0.98	0.45	0.99	0.82
E2a	Aacs/1	Q9D2R0	1.79	0.11	1.39	0.52
E2b	Aacs/2	Q9D2R0	3.12	0.01	2.56	<0.01
E2S	∑ **Aacs**	**Q9D2R0**	2.17	0.01	1.73	0.16
E3	Acadl	P51174	1.13	0.14	1.27	0.01
E4a	Eno1a/1	P17182	0.99	0.96	0.89	0.28
E4b	Eno1a/2	P17182	1.10	0.50	0.89	0.42
E4c	Eno1a/3	P17182	1.18	0.10	1.21	0.10
E4d	Eno1a/4	P17182	1.50	<0.01	1.42	<0.01
E4S	∑ **Eno1A**	**P17182**	1.26	0.02	1.19	0.06
E5	GalK	Q9R0N0	1.45	<0.01	1.50	0.03
E6	Gapdh	P16858	0.56	<0.01	0.60	<0.01
E7	Gpd1L	Q3ULJ0	2.27	<0.01	1.42	0.14
E8a	Hxk3/1	Q3TRM8	1.91	0.02	1.80	0.03
E8b	Hxk3/2	Q3TRM8	1.23	0.04	1.22	0.09
E8c	Hxk3/3	Q3TRM8	1.52	0.02	1.52	0.02
E8S	∑ **Hxk3**	**Q3TRM8**	1.51	0.01	1.49	0.01
E9	Idhc	O88844	1.24	0.02	1.19	<0.01
E10a	Ldha/1	P06151	0.79	0.02	0.86	0.06
E10b	Ldha/2	P06151	0.97	0.81	0.89	0.40
E10S	∑ **Ldha**	**P06151**	0.89	0.26	0.88	0.21
E11a	Mdhc/1	P14152	0.47	0.02	0.72	0.11
E11b	Mdhc/2	P14152	0.83	0.01	0.84	0.01
E11c	Mdhc/3	P14152	1.38	0.02	1.40	<0.01
E11S	∑ **Mdhc**	**P14152**	1.01	0.91	1.05	0.20
E12	Pckgm	Q8BH04	1.30	0.20	0.61	0.01
E13	Pfkap	Q9WUA3	0.84	0.01	0.86	0.01
E14	Pfkl	P12382	1.83	0.01	1.62	0.03
E15a	Pgls/1	Q9CQ60	0.78	0.02	0.97	0.75
E15b	Pgls/2	Q9CQ60	1.11	0.16	1.22	0.01
E16	Pgp	Q8CHP8	1.37	0.02	1.60	0.05
E17a	Taldo1	Q93092	0.80	0.02	0.66	<0.01
E17b	Taldo/2	Q93092	1.17	0.12	1.18	0.08
E17c	Taldo/3	Q93092	1.24	0.02	1.23	<0.01
E17d	Taldo/4	Q93092	0.81	0.06	0.79	0.02
E17e	Taldo/5	Q93092	1.22	0.06	1.36	0.02
E17S	∑ **Taldo**	**Q93092**	1.08	0.16	1.09	0.06
E18a	Tpis/1	P17751	0.74	0.01	0.82	0.04
E18b	Tpis/2	P17751	1.04	0.61	1.20	0.09
E18c	Tpis/3	P17751	1.45	0.04	1.43	0.05
E18S	∑ **Tpis**	**P17751**	1.09	0.29	1.16	0.17
F1	Cdk4	P30285	0.69	<0.01	0.71	<0.01
F2	Cdk6	Q64261	0.71	0.04	0.77	0.02
F3a	Ndrg1/1	Q62433	1.32	0.09	1.52	0.04
F3b	Ndrg1/2	Q62433	1.38	0.01	1.33	0.02
F3S	∑ ndrg1	Q62433	1.34	0.02	1.44	0.03
F4	Pa2 g4	P50580	1.50	<0.01	1.31	0.01

Table 2 *(continued)*

Spot number	Protein name	Accession number	Ratio acute/ctrl	*T* test acute *vs.* ctrl	Ratio recov/ctrl	*T* test recov *vs.* ctrl
F5a	Vma5a/1	Q99KC8	1.60	0.06	0.99	0.97
F5b	Vma5a/2	Q99KC8	1.31	0.11	1.19	0.10
F5c	Vma5a/3	Q99KC8	1.84	<0.01	1.59	0.02
F5S	∑ Vma5a	Q99KC8	1.54	0.02	1.25	0.12
G1	GalE	Q8R059	0.50	0.03	1.09	0.50
G2	Gnpda1	O88958	0.47	<0.01	0.63	0.01
G3	Gt25c	Q8K297	1.53	0.01	1.48	0.01
G4	Mlec	Q6ZQI3	1.49	0.02	1.79	<0.01
G5a	Naga/1	Q8JZV7	1.19	0.07	1.19	0.06
G5b	Naga/2	Q8JZV7	1.05	0.56	1.18	0.08
G5S	∑ Naga	Q8JZV7	1.12	0.16	1.19	0.06
H1	Adh5	P28474	0.72	0.09	0.74	0.11
H2a	Aldr/1	P45376	0.57	0.01	0.66	0.01
H2b	Aldr/2	P45376	0.84	0.09	0.73	0.04
H2c	Aldr/3	P45376	1.18	0.04	1.25	0.01
H2S	∑ Aldr	P45376	0.85	0.02	0.89	0.10
H3	Aldr2	P47738	1.16	0.08	1.23	<0.01
H4a	Bvra/1	Q9CY64	0.54	0.02	0.62	0.03
H4b	Bvra/2	Q9CY64	1.23	0.08	1.30	0.06
H4S	∑ **Bvra**	**Q9CY64**	0.98	0.81	1.06	0.54
H5	Bvrb	Q923D2	1.45	0.01	0.96	0.77
H6	Ca13	Q9D6N1	0.62	0.01	0.83	0.11
H7a	Esd/1	Q9R0P3	0.56	<0.01	0.64	0.01
H7b	Esd/2	Q9R0P3	0.78	<0.01	0.92	0.15
H7S	∑ Esd	Q9R0P3	0.73	<0.01	0.86	0.02
H8	Frih	P09528	0.61	0.01	0.67	0.02
H9	Gclm	O09172	1.32	0.01	0.98	0.86
H10	Hmox2	O70252	1.53	<0.01	1.03	0.69
H11a	Lgul/1	Q9CPU0	0.80	0.04	0.77	0.05
H11b	Lgul/2	Q9CPU0	1.10	0.24	1.10	0.16
H11S	∑ **Lgul**	**Q9CPU0**	1.00	0.99	1.00	0.96
L1	Anxa1	P10107	0.78	0.02	1.11	0.06
L2a	Anxa2/1	P07356	0.79	0.01	0.60	<0.01
L2b	Anxa2/2	P07356	0.44	<0.01	0.56	<0.01
L2S	∑ Anxa2	P07356	0.67	<0.01	0.59	<0.01
L3	Anxa3	O35639	1.34	0.01	1.30	0.02
L4	Anxa4	P97429	1.30	0.01	1.33	<0.01
L5a	Anxa5/1	P48036	0.88	0.02	0.81	<0.01
L5b	Anxa5/2	P48036	1.09	0.34	1.07	0.37
L5S	∑ Anxa5	P48036	0.95	0.35	0.90	0.08
L6	Anxa6	P14824	1.54	0.02	1.80	<0.01
L7	Anxa7	Q07076	1.14	0.44	1.57	0.02
L8	Idi1	P58044	1.40	0.02	1.34	0.01
L9	Lypla2	Q9WTL7	1.07	0.28	1.22	0.02
L10	Mbd3	Q9Z2D8	1.52	0.02	1.77	<0.01
L11	Pipna	P53810	1.22	0.11	1.32	0.01
L12	Ppt1	O88531	1.24	0.14	1.34	0.03
M1a	Clic4/1	Q9QYB1	0.90	0.12	0.95	0.58
M1b	Clic4/2	Q9QYB1	1.27	0.02	1.27	0.04
M1S	∑ Clic4	Q9QYB1	1.12	0.04	1.14	0.01
M2	Clybl	Q8R4N0	1.80	0.03	1.41	0.19
M3	Gatm	Q9D964	0.68	0.01	0.54	0.01
M4	Hmgcl	P38060	0.61	<0.01	0.76	0.07
M5	Nduv2	Q9D6J6	1.24	0.01	1.49	0.05
M6	Oat	P29758	1.30	0.05	1.50	0.01
M7	Odba	P50136	1.54	0.02	1.28	0.12
M8	Phb	P67778	1.12	0.16	1.18	0.05
M9	Tmem11	Q8BK08	1.78	0.04	1.46	0.41
M10	Vdac2	Q60930	0.63	0.02	0.72	0.05
M11a	Atpb ac	P56480	1.23	0.16	1.41	0.03
M11b	Atpb bas	P56480	1.60	0.04	1.58	<0.01
M11S	∑Atpb	P56480	1.41	0.06	1.49	<0.01
M12	Clpp	O88696	1.28	0.33	1.84	0.02
M13a	Trap1/1	Q9CQN1	1.74	0.02	1.32	0.13
M13b	Trap1/2	Q9CQN1	1.21	0.25	0.92	0.64
M13S	∑Trap1	Q9CQN1	1.47	0.03	1.11	0.51
N1a	Aprt/1	P08030	0.52	<0.01	0.72	<0.01

Table 2 *(continued)*

Spot number	Protein name	Accession number	Ratio acute/ctrl	*T* test acute *vs.* ctrl	Ratio recov/ctrl	*T* test recov *vs.* ctrl
N1b	Aprt/2	P08030	1.06	0.43	1.08	0.39
N1S	∑ Aprt	P08030	0.92	0.19	0.99	0.85
N2	Bpnt1	Q9Z0S1	1.77	0.02	1.87	0.01
N3	Guaa	Q3THK7	1.42	0.02	1.12	0.25
N4	Hint1	P70349	1.46	0.30	0.64	0.02
N5	Ndka	P15532	0.42	0.03	0.75	0.22
N6	Paps1	Q60967	5.54	0.04	2.44	0.01
N7a	Pnph/1	P23492	0.83	0.12	0.72	0.05
N7b	Pnph/2	P23492	1.25	0.02	1.22	0.08
N7S	∑ **Pnph**	**P23492**	1.08	0.17	1.02	0.76
N8a	Prps1/1	Q9D7G0	0.69	0.01	0.92	0.48
N8b	Prps1/2	Q9D7G0	0.57	<0.01	0.77	0.16
N8c	Prps1/3	Q9D7G0	0.52	0.01	0.83	0.21
N8S	∑ Prps1	Q9D7G0	0.60	<0.01	0.83	0.14
N9a	Pur4/1	Q5SUR0	1.71	0.14	1.27	0.07
N9b	Pur4/2	Q5SUR0	2.53	0.01	2.01	0.01
N9c	Pur4/3	Q5SUR0	1.15	0.53	1.25	0.22
N9S	∑ Pur4	Q5SUR0	1.65	0.07	1.43	0.01
N10	Pur9	Q9CWJ9	1.16	0.27	1.23	0.01
N11	Nt5c3b	Q3UFY7	1.55	<0.01	1.64	0.01
O1	Prx1ox	P35700	0.58	0.02	0.70	0.04
O2a	Prx3/1	P20108	0.93	0.69	1.13	0.08
O2b	Prx3/2	P20108	1.23	0.06	1.32	0.01
O2S	∑ Prx3	P20108	1.16	0.22	1.27	0.01
O3	Prx4	O08807	0.75	0.06	0.56	0.01
O4a	Prx6/1	O08709	0.56	0.02	0.45	0.01
O4b	Prx6/2	O08709	1.05	0.64	0.97	0.76
O4S	∑ Prx6	O08709	0.96	0.63	0.87	0.23
P1	Aars	Q8BGQ7	1.65	0.01	1.18	0.20
P2a	Eef2/1	P58252	0.77	0.02	0.63	<0.01
P2b	Eef2/2	P58252	1.06	0.41	0.96	0.39
P2c	Eef2/3	P58252	0.84	0.07	0.90	0.20
P2d	Eef2/4	P58252	0.99	0.88	0.98	0.61
P2e	Eef2/5	P58252	1.39	0.01	1.29	0.01
P2S	∑ Eef2	P58252	1.02	0.72	0.97	0.43
P3	If3g	Q9Z1D1	0.77	0.31	0.56	0.03
P4a	If5a/1	P63242	0.54	<0.01	0.62	<0.01
P4d	If5a/2	P63242	1.07	0.26	1.03	0.58
P4S	∑ If5a	P63242	0.86	0.04	0.87	0.04
P5	If4a1	P60843	1.55	0.01	1.51	0.01
P6	If4a3	Q91VC3	1.27	0.05	1.09	0.28
P7	Rla0	P14869	1.28	0.07	1.33	0.04
P8	Rs4y1	P62702	0.50	0.04	0.62	0.07
P9a	Sars/1	P26638	1.42	0.03	1.05	0.59
P9b	Sars/2	P26638	1.52	0.04	1.10	0.42
P9S	∑ Sars	P26638	1.48	0.02	1.08	0.46
Q1a	Dpp3/1	Q99KK7	1.28	0.22	1.75	<0.01
Q1b	Dpp3/2	Q99KK7	1.55	0.04	1.84	<0.01
Q1S	∑ Dpp3	Q99KK7	1.40	0.09	1.79	<0.01
Q2a	Hsp74/1	Q61316	0.77	0.22	0.77	0.23
Q2b	Hsp74/2	Q61316	1.33	0.08	1.18	0.23
Q2c	Hsp74/3	Q61316	1.31	0.09	1.14	0.29
Q2d	Hsp74/4	Q61316	1.26	0.15	1.31	<0.01
Q2S	∑ Hsp74	Q61316	1.07	0.58	1.03	0.80
Q3a	Hyou1/1	Q9JKR6	1.18	0.25	0.83	0.20
Q3b	Hyou1/2	Q9JKR6	1.38	0.01	1.18	0.03
Q3c	Hyou1/3	Q9JKR6	1.35	0.01	1.21	0.05
Q3d	Hyou1/4	Q9JKR6	0.80	0.23	0.79	0.11
Q3S	∑ Hyou1	Q9JKR6	1.04	0.67	0.93	0.27
Q4	Lxn	P70202	0.98	0.80	1.26	<0.01
Q5	Pfd2	O70591	0.72	0.01	0.70	0.01
Q6a	Ppce/1	Q9QUR6	1.40	0.15	1.78	0.01
Q6b	Ppce/2	Q9QUR6	1.58	0.04	1.66	0.01
Q6S	∑ Ppce	Q9QUR6	1.50	0.07	1.71	0.01
Q7a	Ppia/1	P17742	0.68	0.11	0.57	0.05
Q7b	Ppia/2	P17742	0.80	0.21	0.79	0.21
Q7c	Ppia/3	P17742	0.81	0.09	0.99	0.97

Table 2 *(continued)*

Spot number	Protein name	Accession number	Ratio acute/ctrl	*T* test acute *vs.* ctrl	Ratio recov/ctrl	*T* test recov *vs.* ctrl
Q7S	∑ Ppia	P17742	0.78	0.09	0.83	0.21
Q8a	Spb6/1	Q60854	1.66	0.02	1.49	0.01
Q8b	Spb6/2	Q60854	1.43	0.01	1.42	0.01
Q8S	∑ Spb6	Q60854	1.57	0.01	1.46	<0.01
Q9	Stip1	Q60864	1.72	<0.01	0.94	0.67
Q10	Tcpa	P11983	1.55	0.02	1.09	0.55
R1a	Btf3/1	Q64152	0.56	0.01	0.50	0.01
R1b	Btf3/2	Q64152	0.76	0.05	0.76	0.05
R1S	∑ Btf3	Q64152	0.66	0.02	0.64	0.01
R2	Dcps	Q9DAR7	1.30	<0.01	1.20	0.02
R3	Ddx39a	Q8VDW0	1.64	0.03	1.31	0.02
R4	Ddx39b	Q9Z1N5	1.59	0.03	1.35	0.11
R5	Mgn	P61327	0.96	0.60	0.56	0.01
R6a	Sf3b2/1	Q3UJB0	1.03	0.91	0.87	0.49
R6b	Sf3b2/2	Q3UJB0	1.16	0.44	1.32	<0.01
R6c	Sf3b2/3	Q3UJB0	1.26	0.38	1.80	<0.01
R6S	∑ Sf3b2	Q3UJB0	1.13	0.54	1.27	0.03
R7	ExoS4	Q921I9	0.88	0.42	0.51	0.02
R8	ExoS6	Q8BTW3	1.50	0.02	1.53	0.01
S1a	14-3-3 gam/1	P61982	0.85	0.28	0.67	0.02
S1b	14-3-3 gam/2	P61982	0.83	0.06	0.91	0.24
S1S	∑ 14-3-3 gam	P61982	0.84	0.10	0.82	0.07
S2	14-3-3 th	P68254	1.31	0.01	1.19	0.04
S3	Cab39	Q06138	0.70	0.03	0.62	<0.01
S4	Fam49b	Q921M7	1.47	0.02	1.59	0.05
S5	Gbb1	P62874	1.17	0.03	1.18	0.03
S6a	Gnai2/1	P08752	1.33	0.06	1.42	0.05
S6b	Gnai2/2	P08752	1.51	<0.01	1.67	0.01
S6S	∑ Gnai2	P08752	1.45	0.01	1.59	0.02
S7	Gnb2L1	P68040	0.89	0.02	0.81	<0.01
S8	Grb2	Q60631	1.06	0.83	1.46	0.02
S9	Igbp1	Q61249	1.36	0.06	1.36	0.04
S10	In35	Q9D8C4	1.25	0.04	1.21	0.14
S11	Inpp	P49442	2.46	0.01	1.76	0.17
S12	Ppp1ca	P62137	1.17	0.07	1.27	0.02
S13a	Ppp1r7/1	Q3UM45	0.30	0.02	0.38	0.04
S13b	Ppp1r7/2	Q3UM45	0.67	0.02	0.73	0.08
S13c	Ppp1r7/3	Q3UM45	0.90	0.51	0.94	0.72
S13S	∑ Ppp1r7	Q3UM45	0.61	0.03	0.68	0.06
S14	Ppp6	O00743	1.48	0.03	1.04	0.82
S15a	Snd1/1	Q78PY7	0.65	0.03	0.66	0.04
S15b	Snd1/2	Q78PY7	0.59	0.02	0.50	0.01
S15c	Snd1/3	Q78PY7	0.89	0.34	0.78	0.18
S15d	Snd1/4	Q78PY7	1.11	0.34	0.91	0.47
S15S	∑ Snd1	Q78PY7	0.79	<0.01	0.70	0.01
U1	Chip	Q9WUD1	0.59	<0.01	0.73	0.11
U2	Csn4	O88544	1.34	0.03	1.37	0.03
U3a	Prs8/1	P62196	0.60	<0.01	0.65	<0.01
U3b	Prs8/2	P62196	0.85	0.04	0.85	0.22
U3S	∑ Prs8	P62196	0.31	0.33	0.32	0.34
U4a	Psa2/1	P49722	0.58	<0.01	0.58	<0.01
U4b	Psa2/2	P49722	1.15	0.12	1.28	0.07
U4S	∑ Psa2	P49722	0.86	0.04	0.92	0.36
U5a	Psa5/1	Q9Z2U1	0.80	0.01	0.84	0.11
U5b	Psa5/2	Q9Z2U1	0.92	0.33	0.99	0.83
U5S	∑ Psa5	Q9Z2U1	0.86	0.07	0.92	0.22
U6	Psb10	O35955	0.73	0.12	0.43	0.02
U7a	Psb2/1	Q9R1P3	0.67	0.02	0.76	0.14
U7b	Psb2/2	Q9R1P3	0.90	0.36	1.01	0.91
U7S	∑ Psb2	Q9R1P3	0.82	0.09	0.92	0.50
U8	Psb3 mod	Q9R1P1	0.47	0.01	0.65	<0.01
U9a	Psb4/1	P99026	0.74	0.05	0.69	0.03
U9b	Psb4/2	P99026	0.98	0.71	0.94	0.25
U9S	∑ Psb4	P99026	0.90	0.05	0.86	0.01
U10	Psmd14	O35593	1.03	0.61	1.32	<0.01
U11a	Psmd2/1	Q8VDM4	0.82	0.22	1.12	0.24
U11b	Psmd2/2	Q8VDM4	1.10	0.11	1.09	0.02

Table 2 *(continued)*

Spot number	Protein name	Accession number	Ratio acute/ctrl	*T* test acute *vs.* ctrl	Ratio recov/ctrl	*T* test recov *vs.* ctrl
U11c	Psmd2/3	Q8VDM4	1.39	0.02	1.13	0.17
U11S	∑ Psmd2	Q8VDM4	1.03	0.70	1.12	0.12
U12	Psmd7	P26516	0.68	0.03	0.68	0.02
U13	Psme1	P97371	1.40	<0.01	1.40	<0.01
U14a	Psme2/1	P97372	1.00	0.98	0.71	<0.01
U14b	Psme2/2	P97372	1.22	<0.01	1.07	0.34
U14S	∑ Psme2	P97372	1.15	<0.01	0.96	0.50
U15	Ubl7	Q91W67	0.41	0.02	0.88	0.55
V1	Asna1	O54984	1.29	0.09	1.46	<0.01
V2	Chm2a	Q9DB34	0.83	<0.01	0.92	0.09
V3	CopE	O89079	1.35	0.01	1.41	0.07
V4	Emc2	Q9CRD2	0.56	0.01	0.84	0.07
V5	Erp29	P57759	0.78	0.12	0.68	0.05
V6	Mss4	Q91X96	0.52	0.04	0.64	0.10
V7	Nsf1c	Q9CZ44	1.55	0.01	1.51	0.01
V8	Pef1	Q8BFY6	0.64	0.05	0.50	0.02
V9	Snaa	Q9DB05	1.53	<0.01	1.99	0.05
V10	Snap23	O09044	0.53	0.02	0.34	0.01
V11	Stxb2	Q64324	2.07	<0.01	1.30	0.09
V12a	Tera/1	Q01853	1.31	0.13	1.18	0.16
V12b	Tera/2	Q01853	1.49	0.02	1.06	0.38
V12c	Tera/3	Q01853	1.39	0.02	1.29	0.04
V12d	Tera/4	Q01853	1.48	0.10	1.35	<0.01
V12S	∑ Tera	Q01853	1.43	0.02	1.25	0.01
V13	Tpd52	Q62393	1.42	0.04	1.31	0.10
V14	Vat1	Q62465	1.48	0.01	1.22	0.15
V15	Vps29	Q9QZ88	1.30	0.05	1.29	0.08
V16a	Vps35/1	Q9EQH3	2.44	0.16	2.33	<0.01
V16b	Vps35/2	Q9EQH3	1.80	0.17	2.03	0.01
V16c	Vps35/3	Q9EQH3	1.53	0.33	2.25	<0.01
V16S	∑ Vps35	Q9EQH3	1.79	0.18	2.20	<0.01
V17	Vta1	Q9CR26	2.84	0.01	2.97	0.02
X1	Pdxk	Q8K183	1.29	<0.01	1.45	0.02
X2	Spee	Q64674	1.55	0.02	1.43	0.07
X3	Sps1	Q8BH69	1.49	0.02	1.95	0.01
X4a	Ran/1	P62827|	0.83	0.04	0.87	0.12
X4b	Ran/2	P62827|	1.18	0.08	1.11	0.17
X4S	∑ Ran	P62827|	1.03	0.62	1.00	0.98
Y1	CatD	P18242	1.38	0.01	1.48	<0.01
Y2	CatZ	Q9WUU7	1.79	0.04	1.08	0.85
Y3	Ncf4	P97369	1.15	0.02	1.19	0.01

∑: sum of the different spots identified for the same protein.

which is known to be up-regulated by acetylation.[71] In our case, the activity correlated with the amount of the acidic, modified spots and not with the total amount of the protein. For other activities, *e.g.* lactate dehydrogenase, triose phosphate isomerase and purine phosphorylase, the activity correlated with the total protein amount and not with a single spot. For several other enzymes such as enolase, hexokinase, pyridoxal kinase and isocitrate dehydrogenase, we detected an increase of the protein amount by proteomics and a stable or decreased enzyme activity.

3.5 Mitochondrial potential and glucose consumption

Several mitochondrial proteins appeared modulated upon exposure of macrophages to silver nanoparticles, among which are a few subunits of the respiratory complexes (NDUV2 and ATPB), some components of the mitochondrial protein quality control (TRAP1 and CLPP) and an antioxidant protein (PRX3). As this may suggest perturbations in the mitochondrial functions, we investigated the mitochondrial transmembrane potential. The results, shown in Fig. 5, indicated that all viable cells accumulated rhodamine 123 and thus had a strong mitochondrial transmembrane potential. However, the amount of accumulated rhodamine 123 and thus the level of the mitochondrial transmembrane potential were lower for the acute condition and went back to normal after 72 hours of recovery. As a lower transmembrane potential is indicative of a less efficient oxidative phosphorylation chain, we investigated the global metabolism under the three experimental conditions.

We thus measured the glucose consumption during the last 36 hours of the experiments by measuring the remaining glucose in the culture medium at the end of the experiment. The initial medium contained 4.1 g of glucose per liter due

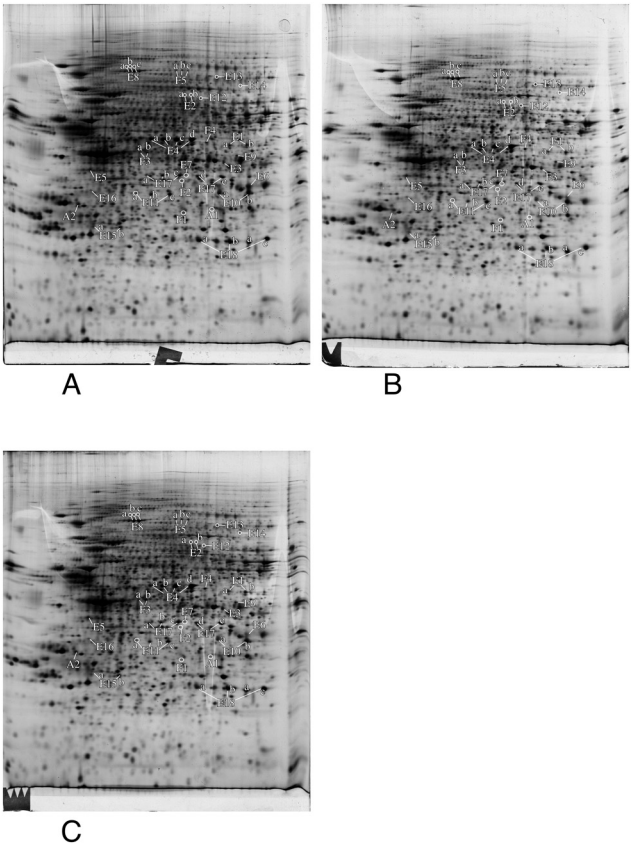

Fig. 4 Proteomic analysis of total cell extracts by 2D electrophoresis. Total cell extracts of RAW274.7 cells were separated by two-dimensional gel electrophoresis. The first dimension covered a 4–8 pH range and the second dimension a 15–200 kDa range. Total cellular proteins (150 μg) were loaded on the first dimension gel. A: Gel obtained from control cells. B: Gel obtained from cells treated for 24 hours with 20 μg ml^{-1} silver nanoparticles. C: Gel obtained from cells treated for 24 hours with 20 μg ml^{-1} silver nanoparticles and left to recover for 72 hours. Only the proteins involved in apoptosis (A), energy metabolism (E) and control of cell fate and proliferation (F) are shown in this figure.

to the dilution brought by the addition of fetal serum to obtain the complete medium. In the untreated, control cells, 1.8 ± 0.2 g of glucose per liter remained in the culture medium after 36 hours of culture. In contrast, 1 ± 0.05 g of glucose and 0.9 ± 0.04 g of glucose remained in the medium for the acute and recovery conditions, respectively. These differences were statistically significant (Mann Whitney U test, $p < 0.05$).

The increased glucose consumption in the acute exposure condition could be correlated with the less efficient mitochondria *via* a Warburg effect. However, this correlation did not hold for the recovery condition, in which the mitochondria appear as efficient as those of the control cells. This may suggest that the silver expulsion process that takes place during the recovery period consumes a lot of energy.

3.6 Glutathione levels

One of the proteins that is induced after acute exposure to silver nanoparticles is GCLM, *i.e.* the regulatory subunit of the enzyme involved in the first step of glutathione biosynthesis, which is the limiting step of the pathway.[72] We thus investigated the levels of free glutathione, as studies on primary macrophages had shown that treatment with silver nanoparticles decreased the levels of free glutathione.[23] This result may be due to the formation of silver–glutathione complexes.[73] We thus measured by flow cytometry the proportion of cells with high levels of reduced glutathione, and the level of glutathione in this population. The results, shown in Fig. 6, indicated that the glutathione level is only 70% of the normal one just after the exposure to silver nanoparticles, and is 85% of the normal after 3 days of recovery. Thus, here again, the increase in GCLM amount can be interpreted as a cellular mechanism to compensate for the decrease of free glutathione caused by silver.

3.7 Actin cytoskeleton and phagocytosis

Cytoskeletal proteins, especially proteins implicated in the actin cytoskeleton dynamics, were among the most important classes emerging from the proteomic screen. Of note, many of these proteins have activities that are modulated by phosphorylation, such as cofilin[74,75] or Rho-GDIs.[76,77] As the regulation patterns

Table 3 Enzyme activities

Enzyme	Control	Acute	Recov	Ctrl + silver ion
LDH	74.4 ± 2.75	68.9 ± 1.14*	73.8 ± 4.13	ND
MDH	37.4 ± 0.95	31.3 ± 2.85*	31.7 ± 2.36*	ND
TPIS	70.7 ± 8.75	76.6 ± 5.58	76.3 ± 7.80	ND
BVR	0.67 ± 0.04	0.53 ± 0.1*	0.79 ± 0.06*	ND
PDXK	7.4 ± 0.95	5.9 ± 0.6*	7.5 ± 0.68*	ND
GAPDH	157.12 ± 14.5	144.25 ± 9.77	157.44 ± 5.91	ND
6PGDH	30.69 ± 3.17	39.37 ± 4.92*	38.75 ± 1.24*	ND
PNPH	8.97 ± 1.17	9.12 ± 1.6	9.06 ± 0.77	ND
HXK	23.4 ± 3.04	16.3 ± 4*	23.3 ± 2.45	(1 μM) 14.2 ± 2.93
ENO	214.5 ± 13.6	166.4 ± 28.1*	184 ± 41	(10 μM) 167 ± 12.4
IDHC	16.37 ± 1.48	17.62 ± 2.79	23.75 ± 2.97**	(5 μM) 8.06 ± 1.09

All the activities are expressed in nmol substrate converted per min per mg total protein. Statistical significance of the results in the Student T test: *$p < 0.05$. ND: not determined. Abbreviations: LDH: lactate dehydrogenase; MDH: malate dehydrogenase; TPIS: triose phosphate isomerase; BVR: biliverdine reductase; PDXK: pyridoxal kinase; GAPDH: glyceraldehyde phosphate dehydrogenase; 6PGDH: 6-phosphogluconate dehydrogenase; PNPH: purine nucleoside phosphorylase; HXK: hexokinase; ENO: enolase; IDHC: NADPH-dependent isocitrate dehydrogenase.

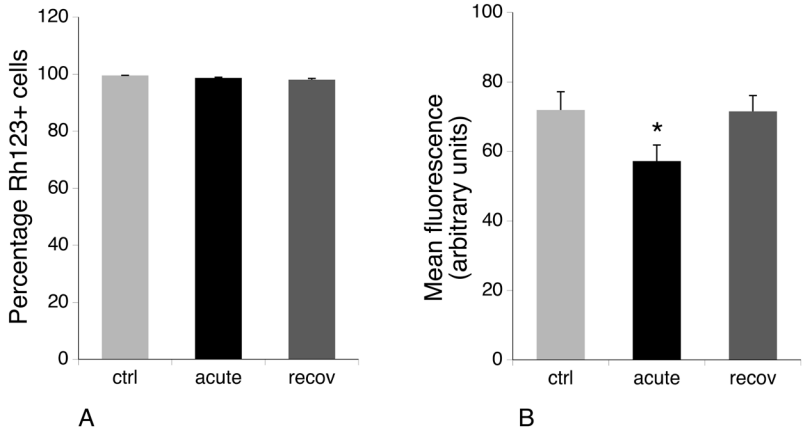

Fig. 5 Mitochondrial transmembrane potential analysis. The rhodamine 123 accumulation method was used. Panel A: Proportion of rhodamine123-positive cells in the viable cell population. Panel B: Mean rhodamine 123 fluorescence (in the viable cell population only). Symbols indicate the statistical significance (Student's *T*-test): *: $p < 0.05$. ctrl: Non exposed cells. acute: Cells exposed for 24 hours to silver nanoparticles (20 μg ml^{-1}). recov: Recovering cells (72 hours post exposure to silver nanoparticles). Symbols indicate the statistical significance (Student's *T*-test): *: $p < 0.05$.

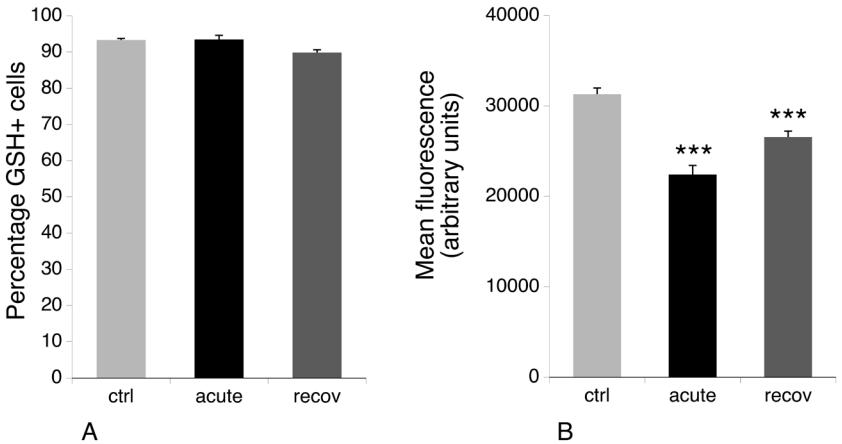

Fig. 6 Free glutathione levels. The chlorobimane (mCB) conjugation method was used. Panel A: Proportion of GSH-positive cells in the viable cell population. Panel B: Mean GSH-mCB conjugate fluorescence (in the viable cell population only). Symbols indicate the statistical significance (Student's *T*-test): ***: $p < 0.001$. ctrl: Non exposed cells. acute: Cells exposed for 24 hours to silver nanoparticles (20 μg ml^{-1}). recov: Recovering cells (72 hours post exposure to silver nanoparticles).

that emerged from the proteomic screen for these proteins were very complex, with some spots modulated while others were constant, we directly examined the consequences on the actin cytoskeleton. The results, shown in Fig. 7, indicated a strong vesicularization of the cells during the recovery period.

Phagocytosis is one of the specialized functions of the macrophages that is highly dependent on the actin cytoskeleton. We thus tested the phagocytic activity of the cells. The results, shown in Fig. 8, indicated that the proportion of phagocytic cells does not change upon treatment with silver nanoparticles. However, the number of internalized particles per cell, as described by the mean fluorescence, slightly decreased immediately after exposure to nanoparticles and went back to quasi-normal values after 72 hours of recovery.

3.8 NO and cytokine production, redox balance

Production of nitric oxide and pro-inflammatory cytokines such as IL-6 and TNF upon stimulation is another specialized function of macrophages. We thus investigated their production after treatment of macrophages with silver nanoparticles under two schemes: either after treatment with nanoparticles only, or after treatment with nanoparticles and lipopolysaccharide (LPS) for the last 24 hours of culture. The first scheme investigated the intrinsic pro-inflammatory action of the nanoparticles, while the second one investigated the interference of nanoparticles with a standard pro-inflammatory response induced by a bacterial stimulus. The results, shown in Fig. 9, indicated that silver nanoparticles have a weak but significant intrinsic pro-inflammatory effect, as detected from NO and TNF production, which returned to normal values after the recovery period. The situation was however very different for the combined nanoparticle–LPS treatment. In this case, the acute exposure condition did not differ significantly from the control cells (exposed to LPS only), while the cytokine and NO production were significantly lower after the recovery period. As the NO production

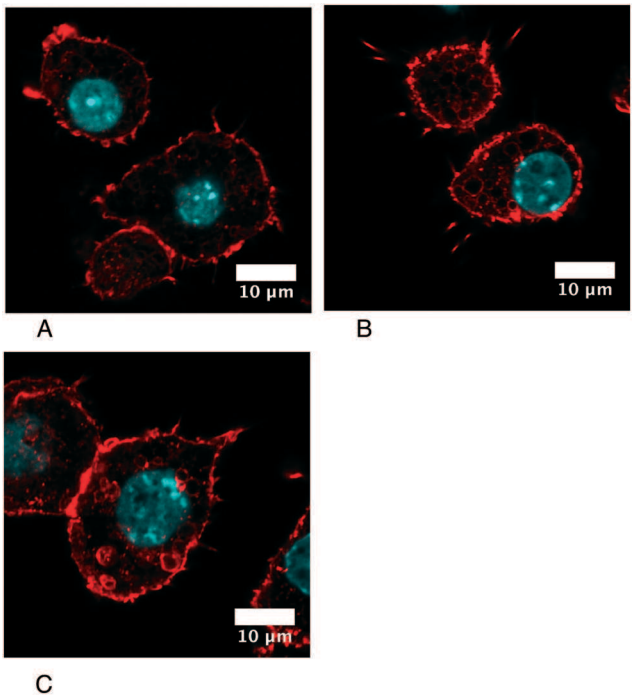

Fig. 7 Confocal imaging of the F-actin cytoskeleton. Only one confocal plane inside the cells is shown (going through the cell nucleus). A: Unexposed cells. B: Acutely-exposed cells. C: Recovering cells. Silver-treated cells show an important vesicularization, compatible with the presence of nanoparticles within the cell phagosomes.

is NADPH-dependent, we investigated the NADP–NADPH levels after treatment with nanoparticles. The results, shown in Table 4, indicated that both the total NADP + NADPH and NADPH levels were similar for the three conditions tested.

4. Discussion

Silver nanoparticles are usually produced through a wet route and need to be stabilized as soon as prepared to avoid irreversible aggregation. Stabilization of AGNPs is usually achieved through interaction with complex ions such as citrate, or by polymers such as polyethylene glycol or polyvinylpyrrolidone (PVP). As such, PVP-coated silver nanoparticles are industrial products used in several applications including as antibacterial compounds,[78] conductive inks,[79–81] and sensors,[82] and in electromechanics.[83] In the course of their use, nanoparticles can be aerosolized. In this case they can contaminate living organisms without being modified. In the specific case of inhalation contamination, the nanoparticles reach the alveolae where there will be internalized by the lung macrophages, which is the reason why we made the choice to use this cell type in this study. Regarding other environmental dispersion routes, PVP-coated silver nanoparticles have been shown to be the most resistant in freshwater environments,[84] and thus recommended for ecotoxicological testing.[84] The PVP-coated silver nanoparticles, therefore, appear to be relevant for assessing the toxicity of silver nanoparticles.

Most of the toxicological studies on nanoparticles use an acute exposure scheme; they expose cells to a high, but non-lethal dose. Such a scheme does not represent chronic daily exposure under, for example, occupational conditions, but may represent the dose following an accidental exposure. To fully evaluate the toxicity of AgNPs, it is therefore important to know not only the acute effects post exposure, but also how cells recover from such exposures to high dosages of AgNPs. To accomplish this, a ternary comparison must be made between cells before and immediately after treatment and also between cells at the end of a recovery period. In this experimental frame, the acute exposure point is not the primary focus of attention. We therefore decided not to investigate in detail the role of silver ions in the acute response, based on the fact that the rather large silver nanoparticles used in this study dissolve to a very low extent,[23] producing free silver ion concentrations that are far below the LD20 observed for silver ions. Furthermore, this aspect has been investigated in numerous studies (*e.g.* in ref. 8, 15, 59 and 85) and the general outcome of these studies is that the mechanisms observed for silver nanoparticles cannot be explained by silver ions, at least for large nanoparticles.[15]

In this frame, the proteomic approach is of interest because it can be used to explore not only a few parameters, as

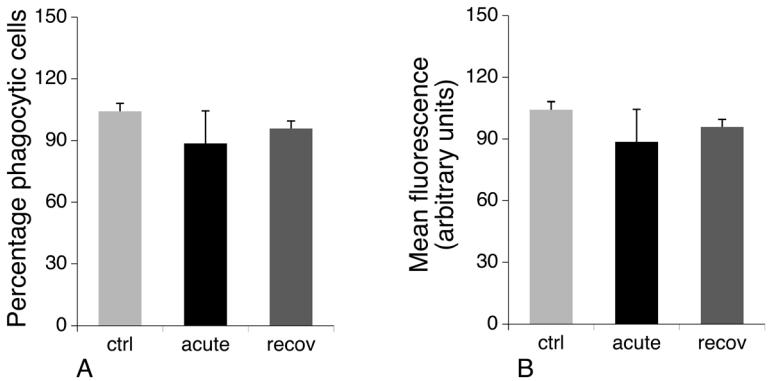

Fig. 8 Phagocytosis. The phagocytic capacity was assessed by fluorescent latex bead internalization. Panel A: Proportion of positive cells in the viable cell population. Panel B: Mean cellular fluorescence (in the viable cell population only). ctrl: Non exposed cells. acute: Cells exposed for 24 hours to silver nanoparticles (20 µg ml^{-1}). recov: Recovering cells (72 hours post exposure to silver nanoparticles).

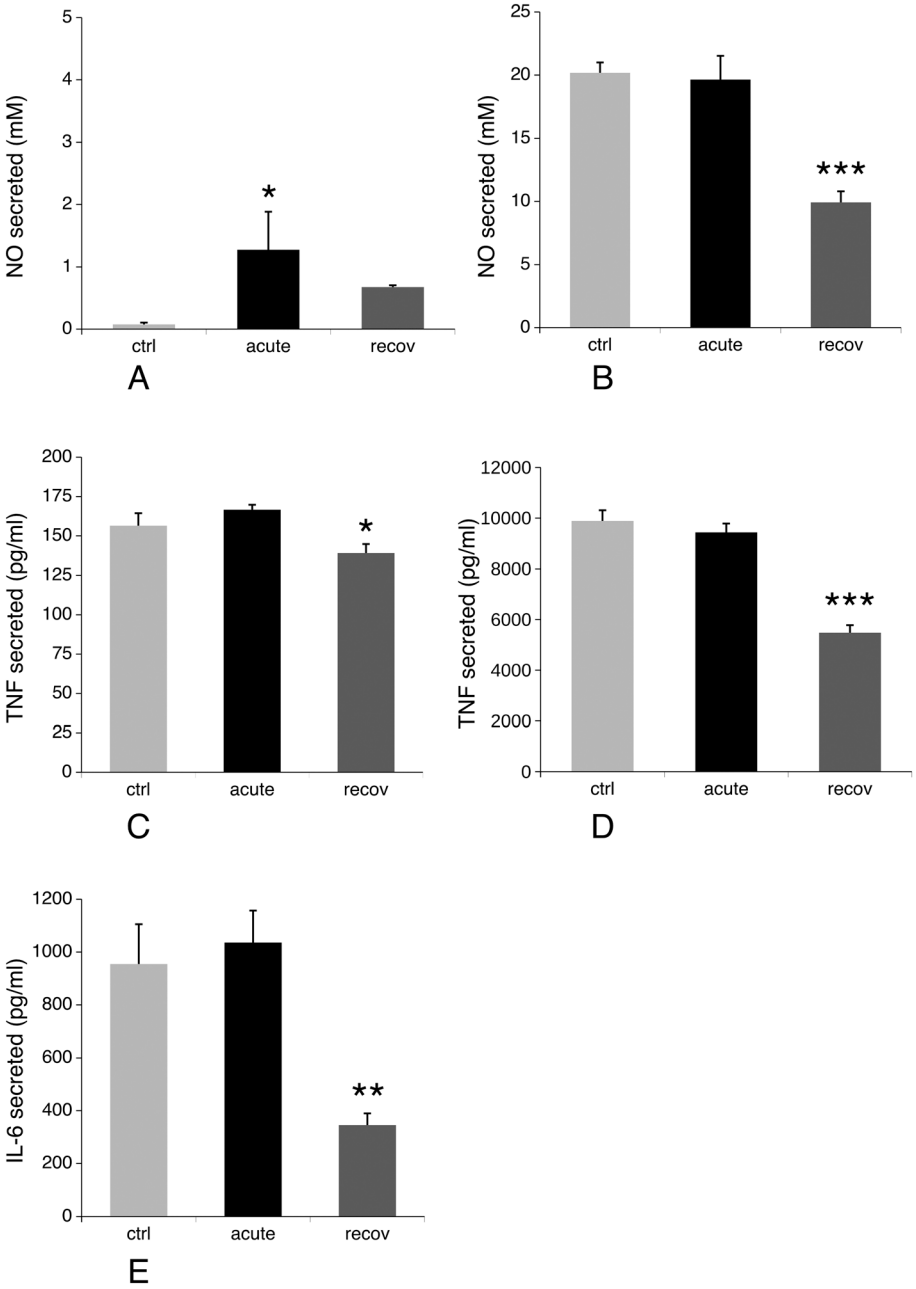

Fig. 9 NO and cytokine production. NO, TNF-alpha and IL-6 production were measured under the different cell culture conditions, with and without further exposure to LPS. ctrl: Non exposed cells. acute: cells exposed for 24 hours to silver nanoparticles (20 μg ml^{-1}). recov: Recovering cells (72 hours post exposure to silver nanoparticles). Symbols indicate the statistical significance (Student's *T*-test): *: $p < 0.05$; **: $p < 0.01$; ***: $p < 0.001$. A and B: NO production, without (panel A) and with (panel B) exposure to LPS. C and D: TNF-alpha production, without (panel C) and with (panel D) exposure to LPS. E: IL-6 production with exposure to LPS. IL-6 is undetectable under the three culture conditions tested when the cells are not exposed to LPS.

targeted approaches do, but also can be used to investigate a few hundred parameters at the same time, *i.e.* the abundances of the various proteins analyzed in a proteomic screen. In this respect, the use of a 2D gel-based proteomic approach may appear as a medium scale approach, compared to deep shotgun proteomic approaches. However, compared to shotgun proteomics, 2D gels have the unique ability to separate protein forms, without the requirement that they appear as a single product. With growing recognition of the importance of post-translational modifications, the ability to do this is biologically relevant. Indeed, we have shown both in this study and in previous ones[53,86] that some enzyme activities correlate with a single protein form and not with the sum of all the protein forms, showing the relevance of this parameter.

First, we performed a global analysis of the proteomic results. Both the principal component analysis and the analysis of similarity (ANOSIM) indicated that the recovery state was

Table 4 NADP(H) concentrations in cells

	Ctrl	Acute	Recov
NADPH	1.87 ± 0.12	1.88 ± 0.03	1.85 ± 0.01
NADP + NADPH	2.5 ± 0.09	2.33 ± 0.04	2.62 ± 0.06
NADPH/(NADP + NADPH)	0.75 ± 0.07	0.81 ± 0.02	0.71 ± 0.02

All the concentrations are expressed in nmol nucleotide per mg total protein.

not just an intermediate state between the unexposed cells and the acutely-exposed cells. If this were the case, the recovery state should not have been separated from the other two states as it is in the principal component analysis. This is further confirmed by ANOSIM. The fact that all the *p*-values in the binary comparison are low and rather similar shows that the three states are significantly different from each other. If the recovery stage was just between the other two stages, at least one of the *p*-values between the recovery stage and one of the other two stages should be much higher than the *p*-value between the control and the acute stage. As this is not the case, we can reject the hypothesis that the recovery phase is only an intermediate between the control and acutely-treated stages.

We then performed a more detailed analysis of the proteomic results. The first important challenge was to determine to what extent the changes observed through proteomics are specific to silver nanoparticles and which are due to the simple presence of a PVP-coated nanoparticle. We have addressed this question in previously published studies.[35,53] In these studies, we showed that PVP-coated zirconium oxide nanoparticles induced minimal changes at the proteomic level. This ruled out the possibility that the changes that we observe in the present study could be due either to the internalization process *per se* or are due to the effect of the addition of PVP.

As a further step, we compared our results obtained immediately after exposure to those published in the literature.[9,10,24] It should be noted that this comparison is challenging because these other studies did not use the same cell type as was used here (although two of them use human intestinal cell lines, however different ones[9,24]) or the same silver nanoparticles. Citrate-coated silver nanoparticles were used in one study,[24] while the other two used surfactant-coated nanoparticles,[9,10] and in this study PVP-coated nanoparticles were used. These differences are very likely to explain the wide differences observed between the studies in which proteins were differentially modulated by treatment, with a minimal overlap between the results. Despite this general trend, several convergences could be observed between our study and those previously published. For example, increases in the abundances of Ran, Moesin, RuvB2, EfhD2, Pfkl, Anxa3, Tcpa and Tbcb were observed both in our study and the one published by Verano-Braga *et al.*[24]

However, proteomics is prone to multiple testing issues, so that the results obtained by proteomics must be verified by independent, targeted experiments. To accomplish this, we analyzed enzyme activities. Our enzyme activity results were consistent with observations made about changes at the proteomic level. However, a few discrepancies occurred, which were always of the same type: increases in the protein level by proteomics, corresponding to stable or decreased activities. We could, however, show that these enzyme activities are very sensitive to the silver ion, which was released within cells during their exposure to silver nanoparticles. Thus, the increase in protein levels can be seen in such cases as a cellular mechanism to compensate for the decrease of activity brought by silver.

We then carried out indirect validation studies, for example on the free glutathione levels, which were decreased immediately after exposure, a phenomenon that was previously observed for copper nanopartlcles.[35] We also tested phagocytosis, which is an important function of macrophages and is important for clearing bacteria. For this assay we used micron-sized fluorescent beads, which functioned as bacterial mimics. This allowed us to investigate whether nanoparticle-treated cells were still able to clear bacteria. The proteomic screen suggested that phagocytosis might be altered after treatment with silver nanoparticles, which was confirmed in our assay testing the ability of the cell to clear bacteria. These results were previously observed for primary macrophages.[23]

The key question asked in this study, however, does not revolve around the acute response to silver nanoparticles, but instead asks to what extent and by which means do cells recover after such an exposure. In a simple model for recovery, protein changes should exhibit trends that return to normal, *i.e.* the amplitude of the change in abundance between the recovery and control stages should be lower than the amplitude of the change in abundance between the acute exposure and control stages. Out of the 239 spots that are highlighted in the proteomic screen, 135 (56%) show such a trend. This means that 104 (44%) show a stronger response at the recovery phase than immediately after exposure. With such a split trend, it is interesting to evaluate the results of targeted experiments during the recovery phase.

Interestingly, this split trend was also apparent in the results of targeted experiments. General metabolic processes seem to return to normal (mitochondrial potential, glutathione levels, and most enzymatic activities), as well as phagocytosis and basal NO production (without LPS stimulation). Oppositely, the LPS-induced activities (*e.g.* NO, IL-6 and TNF production) worsen during the recovery phase, as well as the isocitrate dehydrogenase activity, and the glucose consumption, which stays much higher at both the recovery and acute exposure phases than in unexposed cells.

It was the necessary to check in detail how proteomic changes correlate with observed functional changes. For example, for mitochondrial proteins, the proteomic screen detects an increase in the beta subunit of ATP synthase (ATPB) and an increase in one subunit of respiratory complex I (NDUV2) upon cell exposure to silver nanoparticles. At the same time the mitochondrial transmembrane potential

decreases slightly, showing that this increase in mitochondrial proteins could be an attempt to restore normal energy production in cells. Upon recovery, one of the ATPB spots slightly decreases compared to the value immediately after exposure, while the other spot further increases. The NDUV2 spot is also enhanced. However, even the ATPB spot that decreased is still significantly more abundant at this stage of recovery than in control cells. This shows that the cellular situation is still not back to normal, as can be expected from the still high intracellular silver content, and that restoring the metabolic activity of a cell is an active process requiring an upregulation of several proteins.

Opposite to the delayed return to control values, GCLM, for example, shows an increase just after exposure. When the glutathione demand is high and the free glutathione levels are low, there is a return to control values at the end of the recovery period, at which point free glutathione levels are close to normal again.

In contrast to this simple case, the regulation of the actin cytoskeleton is much more complex. Many of the proteins interacting with actin and regulating its dynamics are regulated by phosphorylation. This holds true for cofilin,[74] actinin 4,[87] vinculin,[88] swap70,[89] arpc5,[90] gelsolin[91] and Arp2.[92] While this further demonstrates the interest of taking into account modified protein forms, there are no obvious rules to predict which modified spot(s) is (are) effector(s) on the actin cytoskeleton. For example, the effector spot for cofilin is the median spot.[93] Consistent with what has been described in the literature, we observe mostly modulations on acidic, modified forms of the above-cited proteins.

In line with the sustained changes in the actin cytoskeleton observed even at the recovery stage, we observe sustained changes in these modified spots, as exemplified by spots 2 of actinin 4 and cofilin, and spots 1 for Arp2 and Arpc5. It must be recalled, however, that such changes are not induced by the particle internalization process *per se*, as they were not observed for cells treated with the non-toxic zirconium oxide nanoparticles.[53] They are also not induced by every toxic nanoparticle, as they were observed neither with zinc oxide[53] nor with copper oxide, except for arpc5 which also decreased in response to treatment with copper oxide.[37]

Overall, the proteomic results suggest that the recovery process is a slow process. To evaluate this aspect, we determined the number of spots that showed a fast recovery. This category was defined as spots for which the quantitative change in the acute *vs.* control comparison showed an amplitude at least twice that in the recovery *vs.* control comparison. Only 44 spots were identified that fell in this category (including GCLM).

A striking result of our study was the observation that some changes in protein levels that were not immediately significant after exposure became significant at the end of the 72 h recovery phase. Such changes were observed both in targeted experiments (*e.g.* for the LPS-dependent responses) and in the proteomic screen. 51 spots showed such an expression profile, *i.e.* 21% of the total variable spots.

Functionally speaking, the results obtained when evaluating LPS-induced activities contrast with those previously described on primary macrophages,[23] in which the cytokine and TNF productions also tended to return to normal values during the recovery phase. This discrepancy may have several origins. One such cause for the discrepancy could be differences in the persistence of silver between differing experimental conditions. In the experiments on primary macrophages, measurements of silver by PIXE showed a strong decrease (50%) in cellular silver content upon recovery, without any cellular multiplication (primary macrophages are post-mitotic *in vitro*). In the current experiments using the J774 cell line, the total silver content decreased by only 15%, and the decrease in cellular silver content is due mostly to cell division. The simple fact that the cells are able to divide shows that the silver concentration present in the cells is not toxic and explains also why, generally, the cellular parameter tends to return to normal levels. The remaining silver concentration may, however, may be high enough to inhibit specialized macrophage functions that depend on cell signaling, such as LPS-dependent activities.

In this context, it is tempting to dismiss the results obtained on the cell lines and favor those obtained using primary cells. The situation may, however, not be so simple. First, primary macrophages *in vitro* survive for only a few days once differentiated, while resident macrophages, such as those used in experiments using cell lines, have a very long lifespan,[94,95] Furthermore, the condition in which the results between cell lines and primary macrophages diverge corresponds to an acute exposure to silver nanoparticles followed by a massive exposure to bacteria (mimicked by exposure to LPS), *i.e.* conditions that have not been tested *in vivo*. Therefore, we are currently unable to determine which system best represents the *in vivo* situation.

5. Conclusions

Overall, our results obtained both by targeted measurements and by proteomic experiments involving hundreds of proteins show that recovery after an acute exposure to silver nanoparticles is a very active process that involves a massive energy consumption, 50% higher than normal. This process leads to the quasi restoration of cellular homeostasis within 72 hours post exposure, as confirmed by targeted experiments testing the activity of enzymes, on mitochondrial function and on phagocytosis. Proteomic experiments also show, however, that this restoration of cellular homeostasis involves changes in the levels of many proteins, of which many are sustained, or even amplified, at the end of the 72 hour recovery period studied. The persistence of proteomic changes might be linked with the persistence of intracellular silver during the recovery period, which may require a long-lasting cellular adaptation process. Some other specialized macrophage functions, such as LPS-induced cytokine or nitric oxide production, did not return to normal within the 72 hour recovery period.

Author contributions

AT performed the phagocytosis, rhodamine uptake and glutathione assay experiments. BD performed the cytokine assays and confocal microscopy experiments. HD, SC, VSF and TR performed the proteomic experiments. TR performed in addition the enzymatic, NADP(H) and glucose assays. SR and JB performed the ICP-MS experiments. MC, KPG and PHJ performed the electron microscopy experiments.

Funding

This work was funded by ANSES (Agence Nationale de Sécurité Alimentaire, Environementale et du Travail) (PNREST 2011/25, Innimmunotox project) and by the CEA toxicology program (Nanostress grant). It is a contribution to the Labex Serenade (no. ANR-11-LABX-0064) funded by the "Investissements d'Avenir" French Government program of the French National Research Agency (ANR) through the A*MIDEX project (no. ANR-11-IDEX-0001-02). STEM-EDS analyses were conducted with the TEM OSIRIS, Nano-Safety Platform, CEA-Grenoble, operated by P. H. Jouneau. This project was managed by Agence National de la Recherche (ANR), program 'Investissements d'Avenir', reference ANR-10-EQPX-39.

Conflicts of interest

There are no conflicts of interest to declare.

Acknowledgements

We thank Anne Bertrand and the electron microscopy facility of the Grenoble Institute of Neurosciences for the preparation of the samples and her kind help during the acquisition of the electron microscopy images.

References

1 S. Chernousova and M. Epple, Silver as antibacterial agent: ion, nanoparticle, and metal, *Angew. Chem., Int. Ed.*, 2013, **52**, 1636–1653.
2 C. A. Dos Santos, M. M. Seckler, A. P. Ingle, I. Gupta, S. Galdiero, M. Galdiero, A. Gade and M. Rai, Silver nanoparticles: therapeutical uses, toxicity, and safety issues, *J. Pharm. Sci.*, 2014, **103**, 1931–1944.
3 S. van den Brule, J. Ambroise, H. Lecloux, C. Levard, R. Soulas, P. J. De Temmerman, M. Palmai-Pallag, E. Marbaix and D. Lison, Dietary silver nanoparticles can disturb the gut microbiota in mice, *Part. Fibre Toxicol.*, 2016, **13**, 38.
4 J. H. Sung, J. H. Ji, J. D. Park, J. U. Yoon, D. S. Kim, K. S. Jeon, M. Y. Song, J. Jeong, B. S. Han, J. H. Han, Y. H. Chung, H. K. Chang, J. H. Lee, M. H. Cho, B. J. Kelman and I. J. Yu, Subchronic inhalation toxicity of silver nanoparticles, *Toxicol. Sci.*, 2009, **108**, 452–461.
5 R. Ebabe Elle, S. Gaillet, J. Vide, C. Romain, C. Lauret, N. Rugani, J. P. Cristol and J. M. Rouanet, Dietary exposure to silver nanoparticles in Sprague-Dawley rats: effects on oxidative stress and inflammation, *Food Chem. Toxicol.*, 2013, **60**, 297–301.
6 R. Pecoraro, F. Marino, A. Salvaggio, F. Capparucci, G. Di Caro, C. Iaria, A. Salvo, A. Rotondo, D. Tibullo, G. Guerriero, E. M. Scalisi, M. Zimbone, G. Impellizzeri and M. V. Brundo, Evaluation of Chronic Nanosilver Toxicity to Adult Zebrafish, *Front. Physiol.*, 2017, **8**, 1011.
7 S. Juling, L. Bohmert, D. Lichtenstein, A. Oberemm, O. Creutzenberg, A. F. Thunemann, A. Braeuning and A. Lampen, Comparative proteomic analysis of hepatic effects induced by nanosilver, silver ions and nanoparticle coating in rats, *Food Chem. Toxicol.*, 2018, **113**, 255–266.
8 W. H. De Jong, L. T. Van Der Ven, A. Sleijffers, M. V. Park, E. H. Jansen, H. Van Loveren and R. J. Vandebriel, Systemic and immunotoxicity of silver nanoparticles in an intravenous 28 days repeated dose toxicity study in rats, *Biomaterials*, 2013, **34**, 8333–8343.
9 A. Oberemm, U. Hansen, L. Bohmert, C. Meckert, A. Braeuning, A. F. Thunemann and A. Lampen, Proteomic responses of human intestinal Caco-2 cells exposed to silver nanoparticles and ionic silver, *J. Appl. Toxicol.*, 2016, **36**, 404–413.
10 A. Braeuning, A. Oberemm, J. Gorte, L. Bohmert, S. Juling and A. Lampen, Comparative proteomic analysis of silver nanoparticle effects in human liver and intestinal cells, *J. Appl. Toxicol.*, 2018, **38**(5), 638–648.
11 F. Martinez-Gutierrez, E. P. Thi, J. M. Silverman, C. C. de Oliveira, S. L. Svensson, A. Vanden Hoek, E. M. Sanchez, N. E. Reiner, E. C. Gaynor, E. L. Pryzdial, E. M. Conway, E. Orrantia, F. Ruiz, Y. Av-Gay and H. Bach, Antibacterial activity, inflammatory response, coagulation and cytotoxicity effects of silver nanoparticles, *Nanomedicine*, 2012, **8**, 328–336.
12 R. P. Nishanth, R. G. Jyotsna, J. J. Schlager, S. M. Hussain and P. Reddanna, Inflammatory responses of RAW 264.7 macrophages upon exposure to nanoparticles: role of ROS-NFkappaB signaling pathway, *Nanotoxicology*, 2011, **5**, 502–516.
13 E.-J. Park, J. Yi, Y. Kim, K. Choi and K. Park, Silver nanoparticles induce cytotoxicity by a Trojan-horse type mechanism, *Toxicol. In Vitro*, 2010, **24**, 872–878.
14 M. J. Piao, K. A. Kang, I. K. Lee, H. S. Kim, S. Kim, J. Y. Choi, J. Choi and J. W. Hyun, Silver nanoparticles induce oxidative cell damage in human liver cells through inhibition of reduced glutathione and induction of mitochondria-involved apoptosis, *Toxicol. Lett.*, 2011, **201**, 92–100.
15 A. Pratsinis, P. Hervella, J. C. Leroux, S. E. Pratsinis and G. A. Sotiriou, Toxicity of silver nanoparticles in macrophages, *Small*, 2013, **9**, 2576–2584.
16 S. Arora, J. Jain, J. M. Rajwade and K. M. Paknikar, Cellular responses induced by silver nanoparticles: In vitro studies, *Toxicol. Lett.*, 2008, **179**, 93–100.
17 D. B. Warheit, T. A. McHugh and M. A. Hartsky, Differential pulmonary responses in rats inhaling crystalline, colloidal or

amorphous silica dusts, *Scand. J. Work, Environ. Health*, 1995, **21**(Suppl 2), 19–21.

18 B. M. Levy and G. M. Higgins, Experimental berylliosis. I. Effects of a single intradermal injection of beryllium nitrate into guinea pigs, *J. Invest. Dermatol.*, 1961, **37**, 175–182.

19 D. Toybou, C. Celle, C. Aude-Garcia, T. Rabilloud and J.-P. Simonato, A toxicology-informed, safer by design approach for the fabrication of transparent electrodes based on silver nanowires, *Environ. Sci.: Nano*, 2019, **6**, 684–694.

20 K. S. Song, J. H. Sung, J. H. Ji, J. H. Lee, J. S. Lee, H. R. Ryu, J. K. Lee, Y. H. Chung, H. M. Park, B. S. Shin, H. K. Chang, B. Kelman and I. J. Yu, Recovery from silver-nanoparticle-exposure-induced lung inflammation and lung function changes in Sprague Dawley rats, *Nanotoxicology*, 2013, **7**, 169–180.

21 A. Murphy, A. Casey, G. Byrne, G. Chambers and O. Howe, Silver nanoparticles induce pro-inflammatory gene expression and inflammasome activation in human monocytes, *J. Appl. Toxicol.*, 2016, **36**, 1311–1320.

22 Y. Xu, H. Tang, J. H. Liu, H. Wang and Y. Liu, Evaluation of the adjuvant effect of silver nanoparticles both in vitro and in vivo, *Toxicol. Lett.*, 2013, **219**, 42–48.

23 C. Aude-Garcia, F. Villiers, V. Collin-Faure, K. Pernet-Gallay, P. H. Jouneau, S. Sorieul, G. Mure, A. Gerdil, N. Herlin-Boime, M. Carriere and T. Rabilloud, Different in vitro exposure regimens of murine primary macrophages to silver nanoparticles induce different fates of nanoparticles and different toxicological and functional consequences, *Nanotoxicology*, 2016, **10**, 586–596.

24 T. Verano-Braga, R. Miethling-Graff, K. Wojdyla, A. Rogowska-Wrzesinska, J. R. Brewer, H. Erdmann and F. Kjeldsen, Insights into the cellular response triggered by silver nanoparticles using quantitative proteomics, *ACS Nano*, 2014, **8**, 2161–2175.

25 R. Miethling-Graff, R. Rumpker, M. Richter, T. Verano-Braga, F. Kjeldsen, J. Brewer, J. Hoyland, H. G. Rubahn and H. Erdmann, Exposure to silver nanoparticles induces size- and dose-dependent oxidative stress and cytotoxicity in human colon carcinoma cells, *Toxicol. In Vitro*, 2014, **28**, 1280–1289.

26 H. G. Drexler, K. Otsuka, G. Gaedicke and J. Minowada, Changes in isoenzyme profiles during induction of differentiation in human myelomonocytic leukemia cell lines, *Cancer Res.*, 1986, **46**, 6078–6082.

27 H. G. Welgus, N. L. Connolly and R. M. Senior, 12-o-Tetradecanoyl-phorbol-13-acetate-differentiated U937 cells express a macrophage-like profile of neutral proteinases. High levels of secreted collagenase and collagenase inhibitor accompany low levels of intracellular elastase and cathepsin G, *J. Clin. Invest.*, 1986, **77**, 1675–1681.

28 P. Kumarathasan, D. Breznan, D. Das, M. A. Salam, Y. Siddiqui, C. MacKinnon-Roy, J. Guan, N. de Silva, B. Simard and R. Vincent, Cytotoxicity of carbon nanotube variants: a comparative in vitro exposure study with A549 epithelial and J774 macrophage cells, *Nanotoxicology*, 2015, **9**, 148–161.

29 P. Oberbek, T. Bolek, A. Chlanda, S. Hirano, S. Kusnieruk, J. Rogowska-Tylman, G. Nechyporenko, V. Zinchenko, W. Swieszkowski and T. Puzyn, Characterization and influence of hydroxyapatite nanopowders on living cells, *Beilstein J. Nanotechnol.*, 2018, **9**, 3079–3094.

30 M. Shoeb, V. Kodali, B. Farris, L. M. Bishop, T. Meighan, R. Salmen, T. Eye, J. R. Roberts, P. Zeidler-Erdely, A. Erdely and J. M. Antonini, Evaluation of the molecular mechanisms associated with cytotoxicity and inflammation after pulmonary exposure to different metal-rich welding particles, *Nanotoxicology*, 2017, **11**, 725–736.

31 M. Chen, Y. Li, J. Zhou, Z. Yang, Z. Wang, Y. Yang, H. Zhang, Z. Li and X. Mei, In vitro toxicity assessment of nanocrystals in tissue-type cells and macrophage cells, *J. Appl. Toxicol.*, 2018, **38**, 656–664.

32 A. Kroll, C. Dierker, C. Rommel, D. Hahn, W. Wohlleben, C. Schulze-Isfort, C. Gobbert, M. Voetz, F. Hardinghaus and J. Schnekenburger, Cytotoxicity screening of 23 engineered nanomaterials using a test matrix of ten cell lines and three different assays, *Part. Fibre Toxicol.*, 2011, **8**, 9.

33 L. Farcal, F. Torres Andon, L. Di Cristo, B. M. Rotoli, O. Bussolati, E. Bergamaschi, A. Mech, N. B. Hartmann, K. Rasmussen, J. Riego-Sintes, J. Ponti, A. Kinsner-Ovaskainen, F. Rossi, A. Oomen, P. Bos, R. Chen, R. Bai, C. Chen, L. Rocks, N. Fulton, B. Ross, G. Hutchison, L. Tran, S. Mues, R. Ossig, J. Schnekenburger, L. Campagnolo, L. Vecchione, A. Pietroiusti and B. Fadeel, Comprehensive In Vitro Toxicity Testing of a Panel of Representative Oxide Nanomaterials: First Steps towards an Intelligent Testing Strategy, *PLoS One*, 2015, **10**, e0127174.

34 D. Breznan, D. D. Das, J. S. O'Brien, C. MacKinnon-Roy, S. Nimesh, N. Q. Vuong, S. Bernatchez, N. DeSilva, M. Hill, P. Kumarathasan and R. Vincent, Differential cytotoxic and inflammatory potency of amorphous silicon dioxide nanoparticles of similar size in multiple cell lines, *Nanotoxicology*, 2017, **11**, 223–235.

35 S. Triboulet, C. Aude-Garcia, M. Carriere, H. Diemer, F. Proamer, A. Habert, M. Chevallet, V. Collin-Faure, J. M. Strub, D. Hanau, A. Van Dorsselaer, N. Herlin-Boime and T. Rabilloud, Molecular responses of mouse macrophages to copper and copper oxide nanoparticles inferred from proteomic analyses, *Mol. Cell. Proteomics*, 2013, **12**, 3108–3122.

36 S. Triboulet, C. Aude-Garcia, L. Armand, A. Gerdil, H. Diemer, F. Proamer, V. Collin-Faure, A. Habert, J. M. Strub, D. Hanau, N. Herlin, M. Carriere, A. Van Dorsselaer and T. Rabilloud, Analysis of cellular responses of macrophages to zinc ions and zinc oxide nanoparticles: a combined targeted and proteomic approach, *Nanoscale*, 2014, **6**, 6102–6114.

37 S. Triboulet, C. Aude-Garcia, L. Armand, V. Collin-Faure, M. Chevallet, H. Diemer, A. Gerdil, F. Proamer, J. M. Strub, A. Habert, N. Herlin, A. Van Dorsselaer, M. Carriere and T. Rabilloud, Comparative proteomic analysis of the molecular responses of mouse macrophages to titanium dioxide and copper oxide nanoparticles unravels some toxic mechanisms for copper oxide nanoparticles in macrophages, *PLoS One*, 2015, **10**, e0124496.

38 E. Eymard-Vernain, C. Lelong, A. E. Pradas Del Real, R. Soulas, S. Bureau, V. Tardillo Suarez, B. Gallet, O. Proux, H. Castillo-Michel and G. Sarret, Impact of a Model Soil Microorganism and of Its Secretome on the Fate of Silver Nanoparticles, *Environ. Sci. Technol.*, 2018, **52**, 71–78.

39 W. E. Hathaway, L. A. Newby and J. H. Githens, The Acridine Orange Viability Test Applied to Bone Marrow Cells. I. Correlation with Trypan Blue and Eosin Dye Exclusion and Tissue Culture Transformation, *Blood*, 1964, **23**, 517–525.

40 A. Moore, C. J. Donahue, K. D. Bauer and J. P. Mather, Simultaneous measurement of cell cycle and apoptotic cell death, *Methods Cell Biol.*, 1998, **57**, 265–278.

41 S. W. Perry, J. P. Norman, J. Barbieri, E. B. Brown and H. A. Gelbard, Mitochondrial membrane potential probes and the proton gradient: a practical usage guide, *BioTechniques*, 2011, **50**, 98–115.

42 T. Rabilloud, Optimization of the cydex blue assay: A one-step colorimetric protein assay using cyclodextrins and compatible with detergents and reducers, *PLoS One*, 2018, **13**, e0195755.

43 K. M. Mayer and F. H. Arnold, A colorimetric assay to quantify dehydrogenase activity in crude cell lysates, *J. Biomol. Screening*, 2002, **7**, 135–140.

44 B. Plaut and J. R. Knowles, pH-dependence of the triose phosphate isomerase reaction, *Biochem. J.*, 1972, **129**, 311–320.

45 P. Fossati, Phosphate determination by enzymatic colorimetric assay, *Anal. Biochem.*, 1985, **149**, 62–65.

46 V. B. Ritov and D. E. Kelley, Hexokinase isozyme distribution in human skeletal muscle, *Diabetes*, 2001, **50**, 1253–1262.

47 D. E. Baranano, M. Rao, C. D. Ferris and S. H. Snyder, Biliverdin reductase: a major physiologic cytoprotectant, *Proc. Natl. Acad. Sci. U. S. A.*, 2002, **99**, 16093–16098.

48 J. A. Kerry, M. Rohde and F. Kwok, Brain pyridoxal kinase. Purification and characterization, *Eur. J. Biochem.*, 1986, **158**, 581–585.

49 V. E. Anderson, P. M. Weiss and W. W. Cleland, Reaction intermediate analogues for enolase, *Biochemistry*, 1984, **23**, 2779–2786.

50 W. R. Wright, J. C. Rainwater and L. D. Tolle, Glucose assay systems: evaluation of a colorimetric hexokinase procedure, *Clin. Chem.*, 1971, **17**, 1010–1015.

51 T. C. Wagner and M. D. Scott, Single extraction method for the spectrophotometric quantification of oxidized and reduced pyridine nucleotides in erythrocytes, *Anal. Biochem.*, 1994, **222**, 417–426.

52 K. Wosikowski, K. Mattern, I. Schemainda, M. Hasmann, B. Rattel and R. Loser, WK175, a novel antitumor agent, decreases the intracellular nicotinamide adenine dinucleotide concentration and induces the apoptotic cascade in human leukemia cells, *Cancer Res.*, 2002, **62**, 1057–1062.

53 C. Aude-Garcia, B. Dalzon, J. L. Ravanat, V. Collin-Faure, H. Diemer, J. M. Strub, S. Cianferani, A. Van Dorsselaer, M. Carriere and T. Rabilloud, A combined proteomic and targeted analysis unravels new toxic mechanisms for zinc oxide nanoparticles in macrophages, *J. Proteomics*, 2016, **134**, 174–185.

54 E. Gianazza, F. Celentano, S. Magenes, C. Ettori and P. G. Righetti, Formulations for immobilized pH gradients including pH extremes, *Electrophoresis*, 1989, **10**, 806–808.

55 T. Rabilloud, C. Valette and J. J. Lawrence, Sample application by in-gel rehydration improves the resolution of two-dimensional electrophoresis with immobilized pH gradients in the first dimension, *Electrophoresis*, 1994, **15**, 1552–1558.

56 S. Luche, H. Diemer, C. Tastet, M. Chevallet, A. Van Dorsselaer, E. Leize-Wagner and T. Rabilloud, About thiol derivatization and resolution of basic proteins in two-dimensional electrophoresis, *Proteomics*, 2004, **4**, 551–561.

57 A. Gorg, W. Postel, J. Weser, S. Gunther, J. R. Strahler, S. M. Hanash and L. Somerlot, Elimination of Point Streaking on Silver Stained Two-Dimensional Gels by Addition of Iodoacetamide to the Equilibration Buffer, *Electrophoresis*, 1987, **8**, 122–124.

58 C. Tastet, P. Lescuyer, H. Diemer, S. Luche, A. van Dorsselaer and T. Rabilloud, A versatile electrophoresis system for the analysis of high- and low-molecular-weight proteins, *Electrophoresis*, 2003, **24**, 1787–1794.

59 P. Sinha, J. Poland, M. Schnolzer and T. Rabilloud, A new silver staining apparatus and procedure for matrix-assisted laser desorption/ionization-time of flight analysis of proteins after two-dimensional electrophoresis, *Proteomics*, 2001, **1**, 835–840.

60 A. G. Herrmann, J. L. Searcy, T. Le Bihan, J. McCulloch and R. F. Deighton, Total variance should drive data handling strategies in third generation proteomic studies, *Proteomics*, 2013, **13**, 3251–3255.

61 D. Yekutieli and Y. Benjamini, Resampling-based false discovery rate controlling multiple test procedures for correlated test statistics, *J. Stat. Plan. Inference*, 1999, **82**, 171–196.

62 A. Carvajal-Rodriguez and J. de Una-Alvarez, Assessing significance in high-throughput experiments by sequential goodness of fit and q-value estimation, *PLoS One*, 2011, **6**, e24700.

63 A. P. Diz, A. Carvajal-Rodriguez and D. O. Skibinski, Multiple hypothesis testing in proteomics: a strategy for experimental work, *Mol. Cell. Proteomics*, 2011, **10**, M110 004374.

64 Ø. Hammer, D. A. T. Harper and P. D. Ryan, Paleontological statistics software package for education and data analysis, *Palaeontol. Electronica*, 2001, **4**, XIX–XX.

65 F. Gharahdaghi, C. R. Weinberg, D. A. Meagher, B. S. Imai and S. M. Mische, Mass spectrometric identification of proteins from silver-stained polyacrylamide gel: A method for the removal of silver ions to enhance sensitivity, *Electrophoresis*, 1999, **20**, 601–605.

66 S. Richert, S. Luche, M. Chevallet, A. Van Dorsselaer, E. Leize-Wagner and T. Rabilloud, About the mechanism of interference of silver staining with peptide mass spectrometry, *Proteomics*, 2004, **4**, 909–916.

67 P. Skehan, R. Storeng, D. Scudiero, A. Monks, J. McMahon, D. Vistica, J. T. Warren, H. Bokesch, S. Kenney and M. R. Boyd, New colorimetric cytotoxicity assay for anticancer-drug screening, *J. Natl. Cancer Inst.*, 1990, **82**, 1107–1112.

68 V. Vichai and K. Kirtikara, Sulforhodamine B colorimetric assay for cytotoxicity screening, *Nat. Protoc.*, 2006, **1**, 1112–1116.

69 D. W. Huang, B. T. Sherman and R. A. Lempicki, Bioinformatics enrichment tools: paths toward the comprehensive functional analysis of large gene lists, *Nucleic Acids Res.*, 2009, **37**, 1–13.

70 D. W. Huang, B. T. Sherman and R. A. Lempicki, Systematic and integrative analysis of large gene lists using DAVID bioinformatics resources, *Nat. Protoc.*, 2009, **4**, 44–57.

71 S. M. Zhao, W. Xu, W. Q. Jiang, W. Yu, Y. Lin, T. F. Zhang, J. Yao, L. Zhou, Y. X. Zeng, H. Li, Y. X. Li, J. Shi, W. L. An, S. M. Hancock, F. C. He, L. X. Qin, J. Chin, P. Y. Yang, X. Chen, Q. Y. Lei, Y. Xiong and K. L. Guan, Regulation of Cellular Metabolism by Protein Lysine Acetylation, *Science*, 2010, **327**, 1000–1004.

72 Y. Chen, H. G. Shertzer, S. N. Schneider, D. W. Nebert and T. P. Dalton, Glutamate cysteine ligase catalysis: dependence on ATP and modifier subunit for regulation of tissue glutathione levels, *J. Biol. Chem.*, 2005, **280**, 33766–33774.

73 G. Veronesi, C. Aude-Garcia, I. Kieffer, T. Gallon, P. Delangle, N. Herlin-Boime, T. Rabilloud and M. Carriere, Exposure-dependent Ag+ release from silver nanoparticles and its complexation in AgS_2 sites in primary murine macrophages, *Nanoscale*, 2015, **7**, 7323–7330.

74 N. Yang, O. Higuchi, K. Ohashi, K. Nagata, A. Wada, K. Kangawa, E. Nishida and K. Mizuno, Cofilin phosphorylation by LIM-kinase 1 and its role in Rac-mediated actin reorganization, *Nature*, 1998, **393**, 809–812.

75 K. Mizuno, Signaling mechanisms and functional roles of cofilin phosphorylation and dephosphorylation, *Cell. Signalling*, 2013, **25**, 457–469.

76 C. DerMardirossian, A. Schnelzer and G. M. Bokoch, Phosphorylation of RhoGDI by Pak1 mediates dissociation of Rac GTPase, *Mol. Cell*, 2004, **15**, 117–127.

77 C. DerMardirossian, G. Rocklin, J. Y. Seo and G. M. Bokoch, Phosphorylation of RhoGDI by Src regulates Rho GTPase binding and cytosol-membrane cycling, *Mol. Biol. Cell*, 2006, **17**, 4760–4768.

78 L. Kvitek, A. Panacek, J. Soukupova, M. Kolar, R. Vecerova, R. Prucek, M. Holecova and R. Zboril, Effect of surfactants and polymers on stability and antibacterial activity of silver nanoparticles (NPs), *J. Phys. Chem. C*, 2008, **112**, 5825–5834.

79 M. A. H. Khondoker, S. C. Mun and J. Kim, Synthesis and characterization of conductive silver ink for electrode printing on cellulose film, *Appl. Phys. A: Mater. Sci. Process.*, 2013, **112**, 411–418.

80 M. Ismail and R. Jabra, Investigation the parameters affecting on the synthesis of silver nanoparticles by chemical reduction method and printing a conductive pattern, *J. Mater. Environ. Sci.*, 2017, **8**, 4152–4159.

81 D. Mau Chien, D. T. M. Dung and E. Fribourg-Blanc, Silver nanoparticles ink synthesis for conductive patterns fabrication using inkjet printing technology, *Adv. Nat. Sci.: Nanosci. Nanotechnol.*, 2015, **6**, DOI: 10.1088/2043-6262/6/1/015003.

82 D. R. Raj, S. Prasanth, T. V. Vineeshkumar and C. Sudarsanakumar, Ammonia sensing properties of tapered plastic optical fiber coated with silver nanoparticles/PVP/PVA hybrid, *Opt. Commun.*, 2015, **340**, 86–92.

83 Q. Liu, L. Seveyrat, F. Belhora and D. Guyomar, Investigation of polymer-coated nano silver/polyurethane nanocomposites for electromechanical applications, *J. Polym. Res.*, 2013, **20**, DOI: 10.1007/s10965-013-0309-z.

84 M. Tejamaya, I. Romer, R. C. Merrifield and J. R. Lead, Stability of citrate, PVP, and PEG coated silver nanoparticles in ecotoxicology media, *Environ. Sci. Technol.*, 2012, **46**, 7011–7017.

85 A. R. Gliga, S. Skoglund, I. O. Wallinder, B. Fadeel and H. L. Karlsson, Size-dependent cytotoxicity of silver nanoparticles in human lung cells: the role of cellular uptake, agglomeration and Ag release, *Part. Fibre Toxicol.*, 2014, **11**, 11.

86 B. Dalzon, C. Aude-Garcia, V. Collin-Faure, H. Diemer, D. Beal, F. Dussert, D. Fenel, G. Schoehn, S. Cianferani, M. Carriere and T. Rabilloud, Differential proteomics highlights macrophage-specific responses to amorphous silica nanoparticles, *Nanoscale*, 2017, **9**, 9641–9658.

87 H. Shao, C. Wu and A. Wells, Phosphorylation of alpha-actinin 4 upon epidermal growth factor exposure regulates its interaction with actin, *J. Biol. Chem.*, 2010, **285**, 2591–2600.

88 Z. Zhang, G. Izaguirre, S. Y. Lin, H. Y. Lee, E. Schaefer and B. Haimovich, The phosphorylation of vinculin on tyrosine residues 100 and 1065, mediated by SRC kinases, affects cell spreading, *Mol. Biol. Cell*, 2004, **15**, 4234–4247.

89 G. Pearce, T. Audzevich and R. Jessberger, SYK regulates B-cell migration by phosphorylation of the F-actin interacting protein SWAP-70, *Blood*, 2011, **117**, 1574–1584.

90 R. Silverman-Gavrila, L. Silverman-Gavrila, G. Hou, M. Zhang, M. Charlton and M. P. Bendeck, Rear polarization of the microtubule-organizing center in neointimal smooth muscle cells depends on PKCalpha, ARPC5, and RHAMM, *Am. J. Pathol.*, 2011, **178**, 895–910.

91 P. Singaravelu, W. L. Lee, S. Wee, U. Ghoshdastider, K. Ding, J. Gunaratne, J. M. Grimes, K. Swaminathan and R. C. Robinson, Yersinia effector protein (YopO)-mediated phosphorylation of host gelsolin causes calcium-independent activation leading to disruption of actin dynamics, *J. Biol. Chem.*, 2017, **292**, 8092–8100.

92 L. L. LeClaire, M. Baumgartner, J. H. Iwasa, R. D. Mullins and D. L. Barber, Phosphorylation of the Arp2/3 complex is necessary to nucleate actin filaments, *J. Cell Biol.*, 2008, **182**, 647.

93 R. Prudent, N. Demoncheaux, H. Diemer, V. Collin-Faure, R. Kapur, F. Paublant, L. Lafanechere, S. Cianferani and T. Rabilloud, A quantitative proteomic analysis of cofilin phosphorylation in myeloid cells and its modulation

using the LIM kinase inhibitor Pyr1, *PLoS One*, 2018, **13**, e0208979.

94 J. Murphy, R. Summer, A. A. Wilson, D. N. Kotton and A. Fine, The prolonged life-span of alveolar macrophages, *Am. J. Respir. Cell Mol. Biol.*, 2008, **38**, 380–385.

95 S. Yona, K. W. Kim, Y. Wolf, A. Mildner, D. Varol, M. Breker, D. Strauss-Ayali, S. Viukov, M. Guilliams, A. Misharin, D. A. Hume, H. Perlman, B. Malissen, E. Zelzer and S. Jung, Fate mapping reveals origins and dynamics of monocytes and tissue macrophages under homeostasis, *Immunity*, 2013, **38**, 79–91.

Conclusion

Cette étude a mis en évidence les modifications de protéome suivantes : régulation du stress oxydant, métabolisme central et lipidique lors de l'exposition aiguë, avec un retour à l'homéostasie cellulaire pour la majorité des voies précédentes après la période de récupération. Cependant, les fonctions spécialisées du macrophage comme la sécrétion de cytokines ou la production d'oxyde nitrique restent supérieures au contrôle après la phase de récupération. Une persistance de certains effets de l'exposition aux nanoparticules d'argent est mise en évidence. Et cette persistance est comparable à celle rapportée *in vivo* chez le rat par exemple (Chung et al. 2017). Cette étude confirme donc la pertinence du système *in vitro*, qui reproduit les effets observés *in vivo*, à moindre coûts, plus rapidement et de manière plus éthique.

I d) Utilisation du système sur les silices amorphes de synthèse

How reversible are the effects of fumed silica on macrophages? A proteomic-informed view

Présentation du projet

Les expériences précédentes ont permis de valider et perfectionner notre système d'étude de la persistance des effets suite à une exposition à des nanomatériaux. Le système a donc ensuite été utilisé pour étudier la persistance des effets suite à une exposition aigue à un type de silice amorphe de synthèse : une silice pyrogénée. La silice pyrogénée utilisée dans cette étude possède une surface spécifique de 200m²/g, avec une taille de particule primaire de 14nm. La silice pyrogénée (fumed silica) est connue pour induire plus d'effets que les SAS produites par voie humide (silices précipitées) (Gazzano et al. 2012). Cela vient des imperfections de surface, présentes également sur les silices cristallines (H. Y. Zhang et al. 2012). Cependant, la persistance de ces effets n'est pas connue, dans la littérature les expériences de toxicité ont été menées juste après la période d'exposition. Dans cet article (Torres, Dalzon, Collin-Faure, Diemer, et al. 2020), nous avons exposé les macrophages RAW264.7 à 20µg/ml pendant 24h suivi par 72h sans SAS. Des études de protéomiques et des tests de validations ont été réalisés.

nanomaterials

MDPI

Article

How Reversible Are the Effects of Fumed Silica on Macrophages? A Proteomics-Informed View

Anaelle Torres [1], Bastien Dalzon [1], Véronique Collin-Faure [1], Hélène Diemer [2], Daphna Fenel [3], Guy Schoehn [3], Sarah Cianférani [2], Marie Carrière [4] and Thierry Rabilloud [1,*]

1 Laboratory of Chemistry and Biology of Metals, University Grenoble Alpes, CNRS, CEA, UMR 5249, CEDEX 09, 38054 Grenoble, France; anaelle.torres@cea.fr (A.T.); bastien.dalzon@cea.fr (B.D.); veronique.collin@cea.fr (V.C.-F.)

2 Laboratoire de Spectrométrie de Masse BioOrganique, Université de Strasbourg, CNRS, IPHC UMR 7178, F-67087 Strasbourg, France; hdiemer@unistra.fr (H.D.); sarah.cianferani@unistra.fr (S.C.)

3 Institute for Structural Biology, Université Grenoble Alpes, CNRS, CEA, F-38000 Grenoble, France; daphna.fenel@ibs.fr (D.F.); guy.schoehn@ibs.fr (G.S.)

4 Chimie Interface Biologie pour l'Environnement, la Santé et la Toxicologie (CIBEST), University Grenoble-Alpes, CEA, CNRS UMR 5819, IRIG-SyMMES, F-38054 Grenoble, France; marie.carriere@cea.fr

* Correspondence: thierry.rabilloud@cnrs.fr

Received: 17 August 2020; Accepted: 23 September 2020; Published: 29 September 2020

Abstract: Synthetic amorphous silica is one of the most used nanomaterials, and numerous toxicological studies have studied its effects. Most of these studies have used an acute exposure mode to investigate the effects immediately after exposure. However, this exposure modality does not allow the investigation of the persistence of the effects, which is a crucial aspect of silica toxicology, as exemplified by crystalline silica. In this paper, we extended the investigations by studying not only the responses immediately after exposure but also after a 72 h post-exposure recovery phase. We used a pyrolytic silica as the test nanomaterial, as this variant of synthetic amorphous silica has been shown to induce a more persistent inflammation in vivo than precipitated silica. To investigate macrophage responses to pyrolytic silica, we used a combination of proteomics and targeted experiments, which allowed us to show that most of the cellular functions that were altered immediately after exposure to pyrolytic silica at a subtoxic dose, such as energy metabolism and cell morphology, returned to normal at the end of the recovery period. However, some alterations, such as the inflammatory responses and some aldehyde detoxification proteins, were persistent. At the proteomic level, other alterations, such as proteins implicated in the endosomal/lysosomal pathway, were also persistent but resulted in normal function, thus suggesting cellular adaptation.

Keywords: amorphous silica; pyrolytic silica; macrophages; inflammation; persistence; proteomics

1. Introduction

Nanomaterials based on amorphous silica are widely used in the industry for various purposes, e.g., as abrasives or as mineral charges in consumer products such as tires. This, in turn, brings the question of their toxicological effects. While crystalline silica is known to be the etiological agent of silicosis through a permanent inflammation [1], amorphous silica has been shown to induce transient inflammation in vivo and in vitro [2], though this inflammation can also be pronounced [3].

This strong difference in the toxicity of amorphous vs. crystalline silica has brought many questions about the mechanisms at play, and it has been shown that crystallinity and, especially, the presence of sharp edges are critical determinants for the persistence of the toxic effects in crystalline silica [4,5]. The fact that persistent effects can be obtained with some types of amorphous silica [5]

raises the question of the relative persistence of effects for the different types of amorphous silica that are currently in use. In this framework, it is interesting to compare the effects of amorphous silicas produced by wet or pyrolytic routes, as they show different surface chemistries [6].

Pyrolytic silica has been shown to induce stronger effects on cells than amorphous silica synthetized by a wet route [6–8], and this effect has been correlated with surface defects in silica [7], a phenomenon that has also shown to be at play with vitreous [5] and crystalline [4] silicas.

However, studies about the effects of pyrolytic silica on cells have all been conducted to date in an acute exposure mode, where the biological endpoints are read immediately after exposure to the silica particles for times ranging from 6 to 48 h [7,8]. While such studies are very informative in documenting the intensity and nature of the cellular responses, they cannot be used to predict the persistence of the effects of the silica particles over time. Moreover, these studies have investigated a few parameters at a time, e.g., the secretion of nitric oxide or pro-inflammatory cytokines, which are relevant parameters in the frame of chronic inflammation but do not describe the changes occurring in cell physiology at a broader scale that may influence cellular responses in complex environments. Wider studies such as those based on omics techniques can be useful to address such questions. Transcriptomic studies of the effects of silica on cells have been published and have shown unexpected results, such as a modulation of the expression of genes implicated in the epithelial–mesenchymal transition or in cell adhesion [9]. Proteomic studies have also been applied to silica nanoparticle toxicology on several cell types such as lung epithelial cells [10] and macrophages [11]. Here again, unexpected effects have been predicted from omics studies and verified by targeted studies, e.g., a cross-toxicity between colloidal silica nanoparticles and DNA alkylating agents such as styrene oxide [11]. It thus seemed interesting to apply omics studies in a cell culture system that allowed for the investigation of the persistence of the effects of silica nanoparticles. One system consists of exposing the cells to the nanomaterial of interest and then removing the exposure medium and replacing it with a fresh culture medium in order to investigate the cellular responses during this recovery period. This type of exposure has been applied in the case of silver nanowires [12], and it has shown a persistence of the inflammatory effects induced by long nanowires, as is consistent with the effects observed in an in vivo exposure study [13].

In the present study, we thus combined the recovery in vitro system with combined proteomic and targeted studies to investigate the persistence of the effects of pyrolytic silica on macrophages.

2. Materials and Methods

Most experiments have been essentially performed as described in previous publications [11,14–16]. Details are given here for the sake of the consistency of the paper. All experiments were performed on independent biological triplicates.

2.1. Nanoparticles

The pyrolytic silica nanoparticles were purchased from Sigma (Saint Quentin Fallavier, France) (catalog number #S5505). They were suspended in water as a 50 mg/mL stock solution and dispersed by sonication in a water sonication bath (BPAC-06VG). The suspension was then sterilized by pasteurization at 80 °C overnight. Prior to use, the suspension was homogenized by vortexing and bath sonication for 15 min.

The hydrodynamic size of the particles was determined after dilution in water or in a complete culture medium by dynamic light scattering (DLS) using a Wyatt Dynapro Nanostar instrument.

The morphology of nanoparticles was observed by TEM. Samples were absorbed to the clean side of a carbon film on mica and transferred to a 400-mesh copper grid. The images were taken at the magnifications of ×11K, ×13K, ×23K, and ×30K times with defocus values between 1.2 and 2.5 µm on an FEI Tecnai 12 LaB6 electron microscope (Hillsboro, OR, USA) at 120 kV accelerating voltage using a Gatan Orius 1000 CCD Camera (Pleasanton, CA, USA).

2.2. Cell Culture

The mouse macrophage cell line RAW 264.7 was obtained from the European Cell Culture Collection (Salisbury, UK). The cells were cultured in an RPMI1640 medium and 10% fetal bovine serum (FBS). For routine culture, cells were seeded on non-adherent flasks (i.e., suspension culture flasks from Greiner) at 200,000 cells/mL and harvested 48 h later at 1,000,000 cells/mL. Cell viability was measured by a dye exclusion assay, either with eosin (1 mg/mL) under the microscope or with propidium iodide (1 µg/mL) in a flow cytometry mode.

For treatment with pyrolytic silica, cells were seeded at 500,000 cells/mL and left for 24 h at 37 °C for cell adhesion. The medium volume was adjusted to keep a constant medium height for all the culture supports used (2 mL for 6-well plates and 15 mL for 75 cm^2 flasks). The cells were grown to confluence for 48 h. The cells were then treated using the scheme described in Figure 1, as used before for silver nanoparticles [15]; in this study, however, we used 20 µg/mL pyrolytic silica.

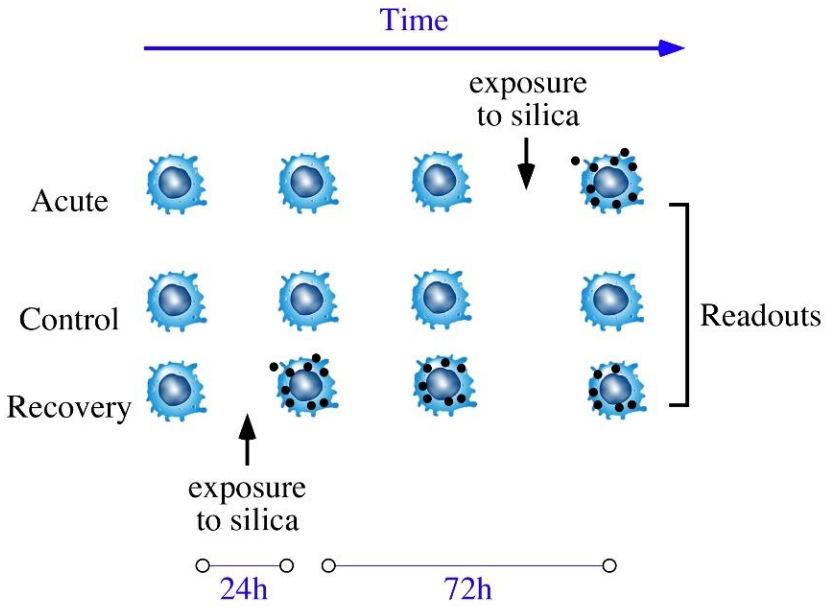

Figure 1. Schematic representation of the exposure schemes used in the study.

In the control condition (center), cells were not exposed to silica. In the acute exposure condition (top row), cells were exposed to 20 µg/mL silica at day 3 post-seeding and sampled after 24 h of exposure. In the recovery exposure condition (bottom row), cells were exposed to 20 µg/mL silica at day 1 post-seeding, and then at day 2, the exposure medium was replaced by a fresh cell culture medium and cells were sampled at day 4.

2.3. Enzyme Assays

The cell extracts for enzyme assays were prepared as described previously [15]. The dehydrogenases or dehydrogenase-coupled activities were assayed at 500 nm using the phenazine methosulfate/iodonitrotetrazolium coupled assay [15]. Biliverdin reductase was assayed at 450 nm as described previously [17]. Pyridoxal kinase was assayed directly at 388 nm [18]. Pyruvate kinase was assayed by a decrease of nicotinamide adenine dinucleotide hydrate (NADH) at 340 nm in a lactate dehydrogenase-coupled assay [19]. Phosphoglycerate kinase was assayed by a decrease of NADH at 340 nm in a glyceraldehyde phosphate dehydrogenase (GAPDH)-coupled assay [20].

2.4. Phagocytosis and Particle Internalization Assay

The phagocytic activity was measured using fluorescent latex beads (1 µm diameter, green labelled, catalog number L4655 from Sigma) with the exclusion of the dead cells from the analysis, as described previously [15].

2.5. Mitochondrial Transmembrane Potential Measurement

The mitochondrial transmembrane potential was assessed by Rhodamine 123 uptake at low concentration (80 nM) to avoid quenching as described previously [15].

2.6. Lysosomal Function Evaluation

Ratiometric acridine orange fluorescence was used to investigate the lysosomal function. Cells were seeded into 6-well plates and exposed to the indicated dose of pyrolytic silica for twenty-four hours at 37 °C followed or not by a recovery period without nanoparticles. Acridine orange (Sigma A6529) was added to the cell culture (100 ng/mL), and the culture returned to the incubator for 30 min. Then, cells were harvested and washed with phosphate buffer saline-glucose (PBSG). The pellets were suspended with 250 µL of PBSG supplemented with Sytox Red (5 nM) and analyzed by flow cytometry. Acridine orange was excited at 475 nm, and the 526 and 650 nm emissions were recorded. The ratio between the two fluorescence intensities (red/green) was then calculated and used as an index of the lysosomal function [21].

2.7. NO Production and Cytokines Production

The cells were grown to confluence in 6-well plates and treated with silica, as described in Section 2.2. Then, half of the wells were treated with 100 ng/mL lipopolysaccharide (LPS) (from *Escherichia coli*, Sigma #L2880), and arginine monohydrochloride was added to all the wells (5 mM final concentration) to give a high concentration of substrate for the nitric oxide synthase. After 18 h of incubation, the nitrite concentration in the medium was assayed with the Griess reagent, as described previously [15].

For cytokine production, a commercial kit **(**BD Cytometric Bead Array, catalog number 552364 from BD Biosciences) was used. The supernatant of cells treated with silica was recovered and analyzed as indicated in the kit protocol.

2.8. F-Actin Staining

The experiments were performed essentially as previously described [15] using Phalloidin-Atto 550 (Sigma). The cells were cultured on coverslips placed in 6-well plates and exposed as described in Section 2.2. At the end of the exposure time, cells were washed and fixed in 4% paraformaldehyde for 30 min at room temperature. The cells were then processed as described previously [15].

2.9. Proteomics

The 2D gel-based proteomic experiments were carried out as previously described [15] on three independent biological replicates.

For protein identification, the MS/MS data were interpreted using a local Mascot server with the MASCOT 2.5.1 algorithm (Matrix Science, London, UK) against UniProtKB/SwissProt (version 2018_11,558,898 sequences). The research was carried out in all species. The protein identification parameters have been described previously [15]. Pathway analysis was performed using the DAVID tool [22].

3. Results

3.1. Nanoparticles Characterization and Determination of the Effective Doses

As shown in Figure 2A, the pyrolytic silica particles appeared as non-spherical aggregates of primary particles in the 5–10 nm size range. The hydrodynamic diameter of the aggregates, determined by dynamic light scattering (DLS), was close to 250 nm (mean value of 252 nm and polydispersity index of 0.25) in water and the zeta potential was measured at −11.27 ± 0.29 mV. This value did not appreciably change with time. In the complete culture medium (containing fetal calf serum), the starting value was similar to that observed in water (278 nm), but some aggregation took place, as indicated by a highly multimodal signal. Furthermore, the size of the aggregates increased over time, with an average value of 912 nm after 24 h of incubation in the complete cell medium (Figure 2B).

The effect of the pyrolytic silica particles on cell viability was then determined. The results, shown in Figure 2C, indicated a lethal dose 20% (LD20) of around 20 μg/mL, and this concentration was used for all further experiments.

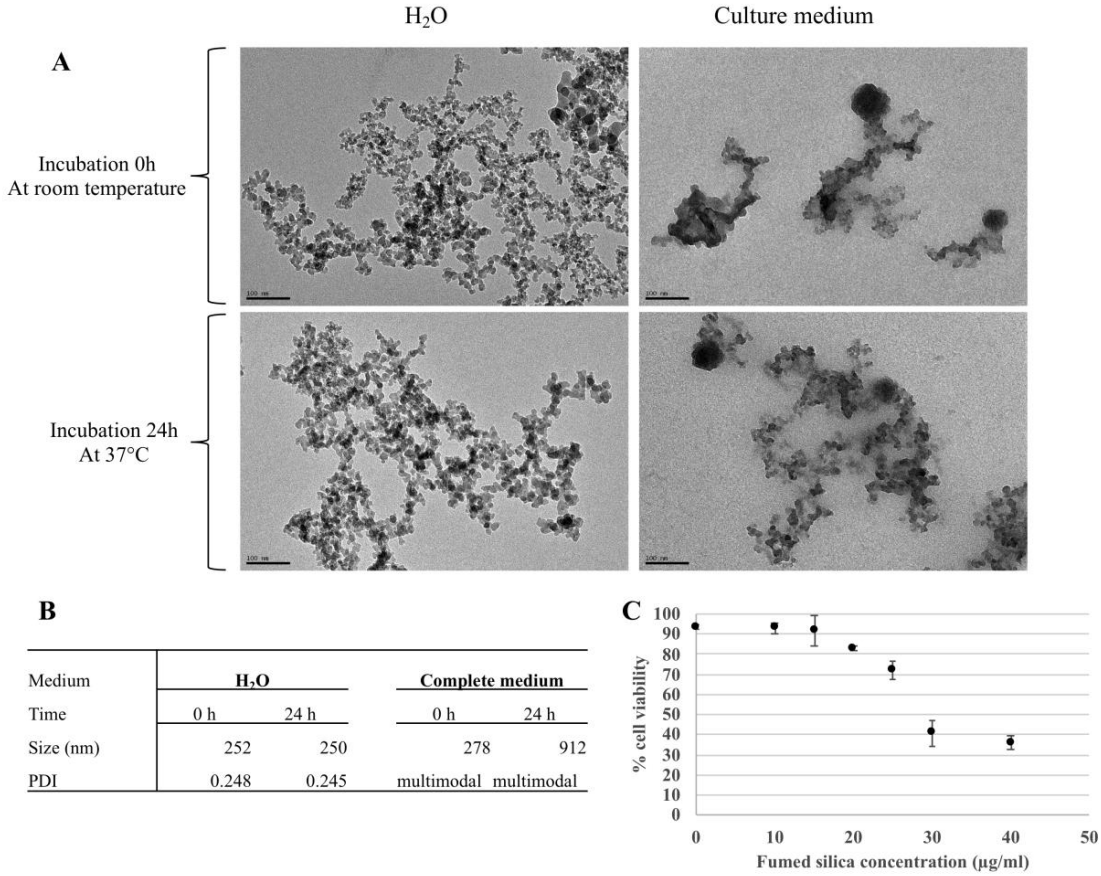

Medium	H_2O		Complete medium	
Time	0 h	24 h	0 h	24 h
Size (nm)	252	250	278	912
PDI	0.248	0.245	multimodal	multimodal

Figure 2. Pyrolytic silica characterization (by transmission electron microscope and dynamic light scattering) and cell viability with flow cytometer. (**A**) Observation by TEM. Nanoparticles were incubated in H_2O (left) or culture medium (right) for either 0 h of incubation at room temperature (top) or 24 h of incubation at 37 °C and 5% CO_2 (bottom). Scale bar = 100 nm. (**B**) Table Showing measures by DLS of the hydrodynamic diameter of nanoparticles in water and a culture medium at 0 and after 24 h of incubation. PDI: polydispersity percentage. (**C**) Cell viability of RAW264.7 exposed to fumed silica for 24 h using propidium iodide (1 μg/mL).

3.2. Proteomic Studies

In order to gain further insights into the molecular responses of cells to the pyrolytic silica nanoparticles, we performed proteomic studies using two-dimensional electrophoresis, and annotated 2D gel images are shown in Supplementary Figures S1–S3. We first used the proteomic results globally, as described previously, by selecting a subset of proteins showing a variation ($p < 0.25$) in either the acute vs. control or the recovery vs. control comparisons [15]. This dataset was then analyzed by hierarchical clustering using the PAST statistical software suite [23]. The results, shown in Figure 3, indicate that the recovery and control conditions co-clustered, except for the acute exposure condition.

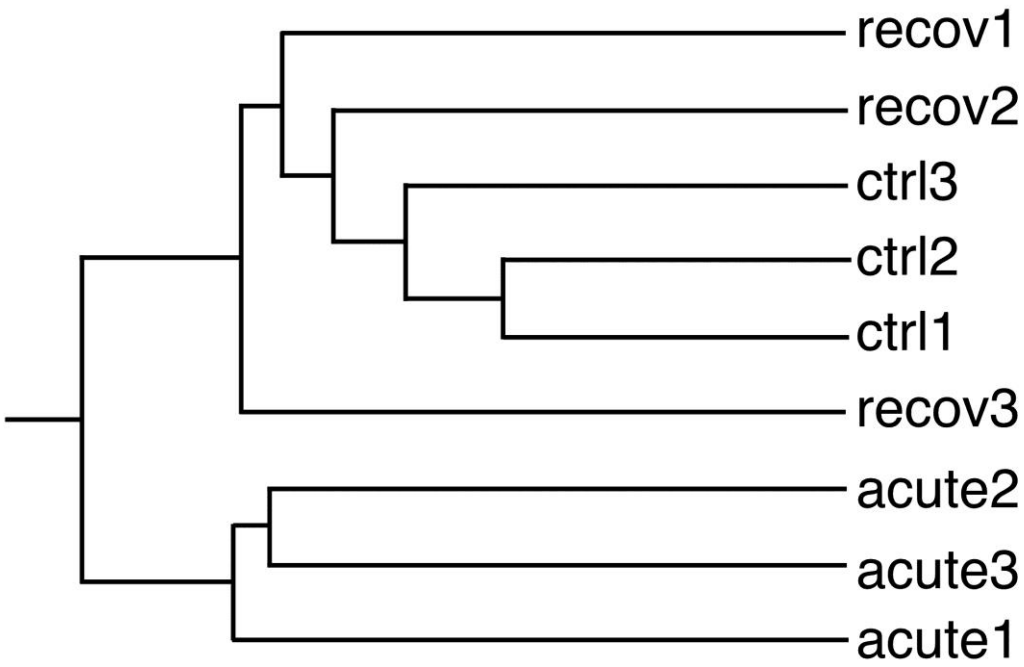

Figure 3. Global analysis of the proteomic experiment by hierarchical clustering. Quantitative proteomic data (i.e., spot intensities in 2D gel-based proteomics) were used to determine the similarities between biological samples. The PAST software package was used for calculations using the Gower similarity index and a paired group algorithm. This classification tree should be read from left to right. The earlier the bifurcation point, the more dissimilar the groups are. ctrl (1–3): unexposed cells; acute (1–3): cells exposed to pyrolytic silica for 24 h and collected just after exposure; recov (1–3): cells exposed to pyrolytic silica for 24 h and left to recover without silica for 72 h. Thus, this tree shows that proteome-wise, the cells just at the end of the exposure time were the most different from the other two conditions, while the three replicates for the acute condition were quite consistent among themselves. The three replicates for control cells were also consistent, while the replicates for the recovery condition were less consistent, indicating variability detected at the proteome scale.

For a more detailed analysis of the proteomic results, we then selected proteins with significantly varied abundances ($p \leq 0.05$) in at least one of the two comparisons (acute vs. control or recovery vs. control). The list of the selected proteins, together with their identification data, is given in Supplementary Table S1, and a selection of modulated proteins is displayed in Table 1.

Table 1. Selection of differentially-expressed proteins identified in the proteomic screen.

Code	Name	Accession	Ratio/*t*-Test Acute/Control	Ratio/*t*-Test Recov./Control
akr1a1	***Alcohol dehydrogenase [NADP(+)]***	***Q9JII6***	***1.23/0.39***	***0.75/0.07***
akr1b1	**Aldose reductase**	**P45376**	**0.91/0.34**	**0.83/0.04**
ap3m1	AP-3 complex subunit mu-1	Q9JKC8	2.23/0.01	0.79/0.64
atpb	ATP synthase subunit beta, mitochondrial	P56480	1.55/0.01	1.22/0.27
bpnt1	3′(2′),5′-bisphosphate nucleotidase 1	Q9Z0S1	2.09/0.02	1.28/0.37
bvra ac	Biliverdin reductase A	Q9CY64	0.41/0.04	1.01/0.98
cap1	Adenylyl cyclase-associated protein 1	P40124	0.69/0.03	1.01/0.96
capg	Macrophage-capping protein	P24452	0.82/0.04	0.90/0.31
casp3	**Caspase-3**	**P70677**	**0.99/0.99**	**0.68/0.04**
catS	Cathepsin S	O70370	0.71/0.02	0.91/0.33
caza2	F-actin-capping protein subunit alpha-2	P47754	1.31/0.02	0.96/0.56
chm2a	**Charged multivesicular body protein 2a**	**Q9DB34**	**0.95/0.40**	**0.65/0.01**
cof	*Cofilin-1*	*P18760*	*0.52/0.06*	*0.95/0.88*
dj1	*Protein deglycase DJ-1*	*Q99LX0*	*1.65/0.09*	*0.93/0.77*
esd	S-formylglutathione hydrolase	Q9R0P3	1.26/0.03	0.86/0.10
fkbp4	*Peptidyl-prolyl cis-trans isomerase FKBP4*	*P30416*	*1.56/0.11*	*0.91/0.72*
fpps	Farnesyl pyrophosphate synthase	Q920E5	1.40/0.04	1.25/0.35
gapdh	Glyceraldehyde-3-phosphate dehydrogenase	P16858	0.56/0.01	1.03/0.85
gmfb	Glia maturation factor beta	Q9CQI3	0.75/0.03	1.22/0.29
grp75	Stress-70 protein, mitochondrial	O35501	1.94/0.007	1.02/0.89
hook3	**Protein Hook homolog 3**	**Q8BUK6**	**1.07/0.65**	**0.45/0.005**
kpym	Pyruvate kinase PKM	P52480	0.66/0.048	0.98/0.88
ldha	L-lactate dehydrogenase A chain	P06151	0.60/0.00675	0.91/0.64
ndus3	NADH dehydrogenase [ubiquinone] iron-sulfur protein 3, mitochondria	Q9DCT2	1.76/0.01	1.06/0.71
nit1	Nitrilase homolog 1	Q8VDK1	0.53/0.01	0.82/0.10
odo2	Dihydrolipoyllysine-residue succinyltransferase component of 2-oxoglutarate dehydrogenase complex, mitochondrial	Q9D2G2	1.33/0.02	0.94/0.80
pdcd6	Programmed cell death protein 6	P12815	1.32/0.04	1.06/0.53
pddc1	**Parkinson disease 7 domain-containing protein 1**	**Q8BFQ8**	**0.70/0.20**	**0.77/0.01**
pgk1	Phosphoglycerate kinase 1	P09411	0.70/0.03	0.95/0.50
phb	Prohibitin	P67778	1.27/0.0018	0.98/0.78
prx3	Thioredoxin-dependent peroxide reductase, mitochondrial	P20108	1.83/0.02	0.82/0.37
psa1	Proteasome subunit alpha type-1	Q9R1P4	1.35/0.03	0.86/0.06
psb10	Proteasome subunit beta type-10	O35955	1.45/0.03	0.64/0.06
psb4	Proteasome subunit beta type-4	P99026	2.90/0.04	1.02/0.93
psmd2	26S proteasome non-ATPase regulatory subunit 2	Q8VDM4	1.69/0.04	1.05/0.79
psmd14	26S proteasome non-ATPase regulatory subunit 14	O35593	1.51/0.05	0.91/0.61
snx6	**Sorting nexin-6**	**Q6P8 × 1**	**0.97/0.53**	**0.88/0.007**
spb6	**Serpin B6**	**Q60854**	**0.83/0.11**	**1.23/0.02**
spre	Sepiapterin reductase	Q64105	0.76/0.03	1.21/0.39
tmem11	Transmembrane protein 11, mitochondrial	Q8BK08	1.50/0.02	1.21/0.55
twf2	Twinfilin-2	Q9Z0P5	0.68/0.03	0.92/0.65
vata	V-type proton ATPase catalytic subunit A	P50516	1.66/0.01	1.01/0.95
vps29	**Vacuolar protein sorting-associated protein 29**	**Q9QZ88**	**0.99/0.99**	**0.67/0.03**

Bold: proteins with a change greater in amplitude at the end of the recovery period compared to the change observed immediately after exposure. Italics: proteins showing a significant change by the Mann–Whitney U test but not by the Student *t* test.

Consistent with the results obtained at the global analysis stage, only a minority of proteins (highlighted in bold in Supplementary Table S1) showed an abundance change at the end of the recovery period greater than the change observed at the end of the exposure period. In order to get an integrated view of the results, a pathway analysis was performed using the DAVID tool [22]. A simplified view of the results is given in Table 2, and the detailed results are presented in Supplementary Table S2. Several pathways were altered (e.g., cell adhesion actin cytoskeleton, carbon metabolism, mitochondrion, and proteasome), which led to validation studies, as described below.

Table 2. Selection of modulated pathways highlighted by the DAVID functional annotation chart tool.

Term	Count [1]	*p*-Value [2]	FDR in % [3]
GO:0005925~focal adhesion	7	0.0049	0.068
GO:0098609~cell–cell adhesion	5	0.0086	0.96
GO:0007005~mitochondrion organization	5	3.94×10^{-4}	0.22
GO:0005739~mitochondrion	24	1.59×10^{-7}	5.775×10^{-6}
Proteasome	5	4.58×10^{-5}	0.0016
Hydrolase	18	4.97×10^{-5}	0.0016
Ubl conjugation	17	6.13×10^{-5}	0.0016
GO:0000502~proteasome complex	5	1.44×10^{-4}	0.0033
mmu01200: Carbon metabolism	7	1.64×10^{-4}	0.011
GO:0006006~glucose metabolic process	4	0.0030	0.43
GO:0005975~carbohydrate metabolic process	6	0.0018	0.39
Glycolysis	3	0.0068	0.083
GO:0006096~glycolytic process	3	0.010	0.96
NAD	6	4.77×10^{-4}	0.0089
Oxidoreductase	9	0.0018	0.029
IPR002108: Actin-binding, cofilin/tropomyosin type	3	6.57×10^{-4}	0.082
Actin-binding	6	0.0019	0.029
GO:0051016~barbed-end actin filament capping	3	0.0021	0.39
GO:0003779~actin binding	7	0.0040	0.27
GO:0031982~vesicle	5	0.0043	0.065
GO:0005765~lysosomal membrane	5	0.015	0.18

[1] Count: number of proteins in the total list of modulated proteins assigned to the selected pathway. [2] *p*-Value: probability for the selected pathway to be selected by random. [3] FDR (false discovery rate): *p*-Value corrected for multiple testing.

3.3. Validation Studies

In addition to the data obtained from the pathway analysis, we used previous knowledge obtained on other nanoparticles, such as colloidal amorphous silica [11] or silver nanoparticles [15] to select the biological parameters to be investigated in the validation studies.

3.3.1. Enzyme Activities

Carbon metabolism—especially glycolysis—was one of the pathways highlighted in the pathway analysis, with several glycolytic enzymes involved such as lactate dehydrogenase (P06151), glyceraldehyde 3-phosphate dehydrogenase (P16858), phosphoglycerate kinase (P09411), or pyruvate kinase (P52480). In order to validate the proteomic results, the activity of these enzymes was measured, and the results are displayed in Table 3. The activity measurements were consistent with those obtained through proteomics. For the glycolytic enzymes, a major decrease in activity was observed immediately after exposure to pyrolytic silica, with a restoration of normal or close to normal activities at the end of the recovery period. For the two non-glycolytic enzymes tested (biliverdin reductase and pyridoxal kinase), there was a good correlation between the proteomic and activity data at the end of the exposure period. The concordance was less pronounced at the end of the recovery period.

Table 3. Enzyme activities.

Enzyme	Control	Acute	Recov
BVR	1.86 ± 0.62	0.58 ± 0.41 *	1.08 ± 0.26
GAPDH	19.83 ± 3.33	1.50 ± 1.00 *	19.50 ± 1.73
LDH	119.50 ± 16.26	23.17 ± 14.74 *	134.17 ± 10.27
PDXK	9.33 ± 2.91	15.33 ± 3.05	16.67 ± 5.29
PGK	3547 ± 546	2242 ± 1059	2950 ± 597
PKM	4219 ± 607	983 ± 581 *	4998 ± 195

All the activities are expressed in nmole substrate converted/min/mg total protein. Statistical significance of the results in the Student *t* test: * $p < 0.05$. Abbreviations: BVR: biliverdin reductase; GAPDH: glyceraldehyde phosphate dehydrogenase; LDH: lactate dehydrogenase; PDXK: pyridoxal kinase; PGK: phosphoglycerate kinase; PKM: pyruvate kinase.

3.3.2. Cytoskeleton and Phagocytosis

Several proteins associated with the actin cytoskeleton, such as cofilin (P18760) and cap1 (P40124), emerged from the proteomic screen, as did capping or debranching proteins (P47754, P24452, and Q9CQI3). Consistent with these observations, "actin cytoskeleton" was one of the terms appearing in the pathway analysis (Supplementary Table S2). This led us to study whether the actin cytoskeleton was altered in macrophages upon treatment with silica. The results, displayed in Figure 4A–C, showed that pyrolytic silica induced a decrease in the surface of the cytoplasmic projections (lamellipodia and filipodia) observed at the surface of the macrophages, as previously observed with colloidal silica [11]. This effect was persistent at the end of the 72 h recovery period. As the actin cytoskeleton is also involved in phagocytosis, we also tested this macrophage function. The results, displayed in Figure 4D, showed no significant effect of the exposure of cells to pyrolytic silica, either immediately after exposure or at the end of the recovery period.

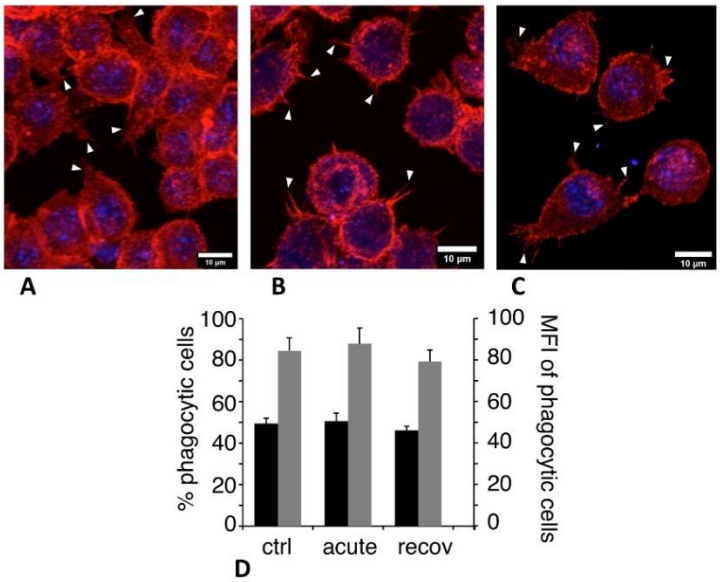

Figure 4. Actin cytoskeleton and phagocytosis. In panels (**A**–**C**), the actin cytoskeleton was visualized with fluorescent Atto 550 phalloidin (500 ng/mL) using LSM880 confocal microscopy. A Z-project reconstruction is shown for each condition. Examples of cytoplasmic projections (lamellipodia and filipodia) are indicated by white arrowheads. (**A**) Unexposed cells. (**B**) Cells exposed to pyrolytic silica for 24 h and analyzed just after exposure. (**C**) Cells exposed to pyrolytic silica for 24 h and left to recover without silica for 72 h. In panel (**D**), the phagocytic capacity was assessed by fluorescent latex beads internalization. Black bars: proportion of positive cells in the viable cell population; grey bars: mean cellular fluorescence of positive cells; ctrl: unexposed cells; acute: cells exposed to pyrolytic silica for 24 h and collected just after exposure; and recov: cells exposed to pyrolytic silica for 24 h and left to recover without silica for 72 h.

3.3.3. Mitochondrial Potential

A few mitochondrial proteins were also detected by the proteomic screen, among which a chaperone (O35501), a stress response protein (P20108), a Krebs cycle protein (Q9D2G2), prohibitin (P67778), TMEM11 (Q8BK08), a mitochondrial deamidase (Q8VDK1), a subunit of respiratory complex I (Q9DCT2), and an ATP synthase subunit (P56480). This led us to test whether the mitochondrial transmembrane potential was altered upon exposure to pyrolytic silica. The results showed no significant effect, either in the proportion of rhodamine-positive cells (>90% in all cases) or in the intensity of the rhodamine signal (range of 942–1187 fluorescence units), which is an indirect index of the mitochondrial transmembrane potential.

3.3.4. Lysosomal Integrity

A few proteins implicated in endosomal/lysosomal function, such as AP3-mu1 (Q9JKC8), cathepsin S (O70370), CHM2A (Q9DB34), hook 3 (Q8BUK6) serpin b6 (Q60854), sorting nexin 6 (Q6P8X1), VATA (P50516), and VPS29 (Q9QZ88) also emerged from the proteomic screen. This prompted us to test the lysosomal integrity via the acridine orange ratiometric method [21]. The red/green fluorescence intensity ratios were as follows:

- Control cells: 0.9884 ± 0.0116.
- Cells acutely exposed to 20 μg/mL pyrolytic silica for 24 h and analyzed just after exposure: 0.9888 ± 0.0038.
- Cells acutely exposed to 20 μg/mL pyrolytic silica for 24 h and analyzed after a 72 h recovery period: 1.0001 ± 0.0044.
- These data showed no significant perturbation in the lysosomal integrity under the conditions tested.

3.3.5. Inflammatory Responses

As silica is known to exert a proinflammatory effect on macrophages, the persistence of which differs between amorphous and crystalline silica, we tested this parameter in two different schemes. With cells unstimulated by lipopolysaccharide, we tested the intrinsic proinflammatory effects of the pyrolytic silica. The results, displayed in Figure 5A, showed no significant change in the NO production upon treatment with pyrolytic silica or during the recovery phase. Regarding cytokine secretion, the persistence of the effect differed to some extent for the two measured cytokines. Tumor necrosis factor alpha (TNF) levels showed a trend to return to basal levels, but the levels were still significantly higher at the end of the recovery period than in unexposed cells (Figure 5D, black bars). The production of interleukin 6 (IL-6) did not decrease (and even increased slightly) during the recovery period compared to acute exposure (Figure 5B). Thus, the results obtained on both TNF and IL-6 showed a persistence of the intrinsic pro-inflammatory effect of pyrolytic silica.

With cells stimulated with lipopolysaccharide, we tested the interference that exposure to silica may bring to macrophage responses to bacteria. The results, displayed in Figure 5C,D (grey bars), showed an increase in the production of IL-6 immediately after exposure, and this was lost at the end of the recovery period. No significant effects were observed on nitric oxide or on TNF production.

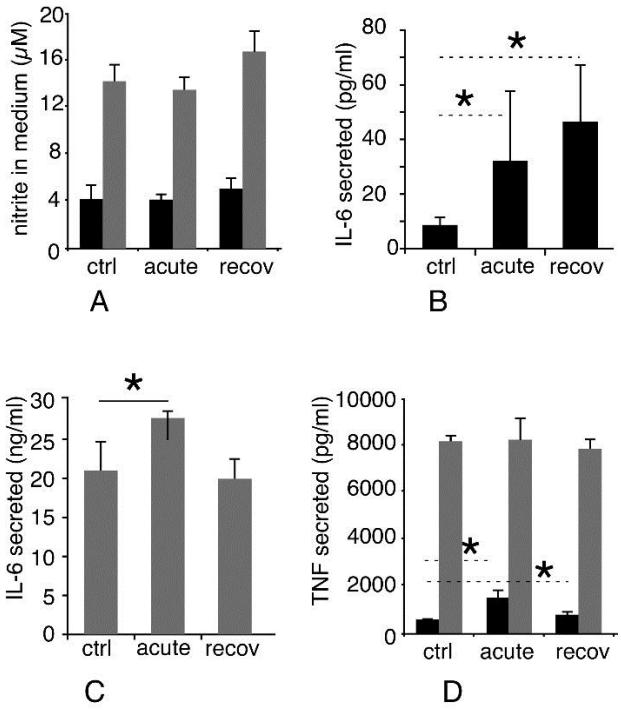

Figure 5. Inflammatory responses. The secretion of NO, interleukin-6, and TNF alpha was measured in response to pyrolytic silica, either alone or in combination with LPS. Ctrl: unexposed cells; acute: cells exposed to pyrolytic silica for 24 h and collected just after exposure; and recov: cells exposed to pyrolytic silica for 24 h and left to recover without silica for 72 h. (**A**) Production of nitric oxide. Black bars: production after treatment for 24 h with pyrolytic; grey bars: production after treatment for 24 h with pyrolytic silica and stimulation with LPS for the last 18 h of culture. (**B**) Production of interleukin-6 in the absence of LPS stimulation. (**C**) Production of interleukin-6 in the presence of LPS stimulation. (**D**) Production of TNF. Black bars: production after treatment for 24 h with pyrolytic silica; grey bars: production after treatment for 24 h with pyrolytic and stimulation with LPS for the last 18 h of culture. Symbols indicate the statistical significance (Mann–Whitney U-test): * $p < 0.05$.

4. Discussion

Though both are classified as amorphous silica and used at levels of millions of tons per year worldwide, pyrolytic silica and silica produced by a wet route seem to have different effects on cells, at least at the inflammatory level [7,8]. Using a proteomic screen and comparing the present data obtained on pyrolytic silica with the ones obtained on the same cell line but with a colloidal silica [11] allowed us to widen the comparison of the relative effects of the two silica types on macrophages. Though the modulated proteins can be different between the two types of amorphous silica (Supplementary Table S3), some pathways are clearly shared for both types of amorphous silica, as shown by the comparison of the pyrolytic (Supplementary Table S2) and colloidal (Supplementary Table S4) pathway analyses. For example, a clear induction of several proteasome subunits was shown in both cases. Different proteins involved in the control of the actin cytoskeleton were also modulated by the colloidal and pyrolytic silica, with the same outcome of the reduction of the cytoplasmic projections. This reduction was, however, not linked to particle internalization itself, as it was not observed for zirconium oxide nanoparticles (e.g., [24]), thus showing the good correlation between the results of the proteomic screen and the phenotypic result.

Going into more detail, for most of the proteins that showed a significant change in their abundance upon treatment with both types of silica, the same type of change was observed for pyrolytic (this study) and colloidal silica [11]. This consistency held true for bpnt1 (Q9Z0S1), bvra (Q9CY64), fkbp4 (P30416), fpps (Q920E5), pddc1 (Q8BFQ8), phb (P67778), spre (Q64105), ssrd (Q62186), and twf2 (Q9Z0P5),

i.e., proteins belonging to very different pathways. This documented the fact that part of the cellular response is common for both types of amorphous silica. However, the proteomic screen also revealed many differences in the cellular response to the two types of silica (see Supplementary Table S3), e.g., a major decrease in glycolytic enzymes observed for pyrolytic silica but not for colloidal silica.

Going on with cellular energetics, several abundance changes were noticed by proteomics for mitochondrial proteins at the end of the exposure period, while the mitochondrial function appeared normal. In this context, it should be noted that the abundance increased, especially for proteins involved in mitochondrial maintenance such as prohibitin [25] and TMEM11 [26], suggesting a successful adaptation of the cells to the stress induced by the uptake of pyrolytic silica.

This cellular response to stress was also documented at the proteomic level by increases in the abundance of the deglycase DJ-1 (Q99LX0), formylglutathione hydrolase esd (Q9R0P3), and protein pdcd6 (P12815), which is involved in membrane repair [27].

Phenotypically, the results described here with one type of pyrolytic silica were consistent with those described with the reference pyrolytic silica material NM203 and macrophages [8]. In particular, the inflammatory responses (the production of IL-6 and TNF) were similar in both cases, showing the consistency of the macrophages' responses toward different pyrolytic silica.

However, most results obtained in vitro on amorphous silica and present in the literature have used an acute exposure scheme where the cellular response was analyzed immediately after exposure. Such a scheme does not allow for the investigation of the persistence of the cellular effects. Because amorphous silica and especially pyrolytic silica have shown persistent effects in vivo [3,28], it was interesting to set up an in vitro system to help to investigate the effect persistence. We used a system where the exposure was followed by a recovery period, during which the persistence of the effects could be investigated. As macrophages are known to internalize various types of particulate materials, including amorphous silica (e.g., in [16]), and keep insoluble materials internalized for extended periods of time [29,30], this system investigated the longer-term responses of cells to the internalized nanomaterials.

This is why we previously used this system to investigate the persistent effects of silver nanomaterials, e.g., nanowires [12] and nanoparticles [15]. When used on pyrolytic silica, this system demonstrated a persistence of the inflammatory response (IL-6 and TNF) in line with the prolonged inflammation described in vivo [3,28]. Such a persistence was not observed with a colloidal silica [12], which was used as a control.

Going into more detail about this system, we selected macrophages as the target cell type because they are the scavenger cell type for particulate materials, are found in numerous locations in the body, and are key players in inflammatory reactions [31]. Mouse macrophage cell lines show excellent responses to many stimuli and can be used in various exposure scenarii such as chronic exposures [32]. For such long-term experiments and for medium-term experiments such as the recovery scheme used here, the cells must be cultured in a complete culture medium containing serum because they will not survive for such extended period of times in serum-free media. Because the formation of a protein corona is known to alter the toxicity of amorphous silica [33,34], the relevance of our system for toxicological evaluation purposes can be questioned. In this frame, it should be kept in mind that all biological fluids, including pulmonary surfactant [35–37], contain rather high concentrations and a large variety of proteins. Thus, it seems to us that the culture conditions used should be a reasonable model of the conditions occurring in vivo, both in terms of nanomaterial aggregation and cellular physiology. Indeed, our in vitro results (the intrinsic induction of IL-6 and TNF, low effects in the case of silica-LPS co-exposure, no effect on phagocytic capacity) paralleled-well to those obtained in vivo in a model of pneumonia [38]. This shows that our system is not plagued by gross artifacts. Moreover, it should be kept in mind that exposure to amorphous silica does not only occur by the pulmonary route, as amorphous silica is also used as a food additive in cosmetics and in toothpastes. For such non-pulmonary routes where macrophages are located below the body barriers, there is no question about the presence of high concentrations of proteins when the nanomaterials come in contact with the macrophages.

When focusing on the recovery phase, the proteomic study showed that many cellular functions had returned to normal levels at the end of the recovery period. In this respect, the recovery was much more obvious for pyrolytic silica than for silver nanoparticles [15]. It was then of interest to study the few proteins for which a stronger change of abundance was observed at the end of the recovery period rather than immediately after exposure to pyrolytic silica. Among these few proteins, an early trend emerged in proteins implicated in the endosomal/lysosomal pathway, mostly proteins implicated in vesicular traffic such as CHM2A (Q9DB34) [39], hook 3 (Q8BUK6) [40] sorting nexin 6 (Q6P8X1) [41], and VPS29 (Q9QZ88) [42]. The hook 3 protein also binds the scavenger receptor [43], which is known to be implicated in silica internalization [44,45]. In addition, Serpin B-6 (Q60854) was also increased during the recovery phase. This protein is known to inhibit lysosomal proteases [46] and may play a role against cytosolic damage induced by the liberation of lysosomal proteases, thus prompting us to investigate lysosomal integrity. While lysosomal rupture has been described in the case of crystalline silica-induced apoptosis [47], i.e., at high doses, we did not detect any massive lysosomal rupture under our conditions, which was in line with what has been previously described with amorphous silica on the same RAW264.7 cells at non-lethal concentrations [48].

Additionally noteworthy was an increase in two detoxifying proteins, aldo-keto-reductases 1a1 (Q9JII6) and 1b1 (P45376). These proteins reduce a wide range of toxic electrophiles [49,50], including acrolein [51], glyceraldehyde [52], and methylglyoxal [50,53]. Thus, the induction of these detoxifying proteins may be linked with the observed impairment of glycolysis during acute exposure. Glycolysis inhibition increases the concentration of toxic aldehydes, as exemplified by zinc oxide nanoparticles [24]. Thus, we may observe a sequential process in which the glycolysis is impaired first, thus liberating aldehydes that must be destroyed during the recovery phase.

Overall, the fact that several biological parameters (e.g., phagocytic ability, mitochondrial potential, and lysosomal integrity) were not altered during the exposure to pyrolytic silica at a non-lethal dose suggested that the changes observed through the proteomic screen were successful adaptive changes.

5. Conclusions

In conclusion, the simple exposure/recovery in vitro system described here proved to be able to replicate a part of the inflammation persistence phenomena observed during in vivo studies [3,28] and to differentiate between the inflammatory effects of colloidal silica [12] and pyrolytic silica (this study). Coupling with proteomics allowed for a broader understanding of the molecular phenomena at play in the cells during both the exposure and recovery periods.

Such features are promising in the development of simple in vitro assays that may be used as first screens to limit the use of laboratory animals following the 3R principles that are now developing in some areas of the world, e.g., in the EU (http://eur-lex.europa.eu/legal-content/EN/TXT/PDF/?uri=CELEX:32010L0063&from=EN%7CDirective2010/63/EU of the European Parliament and of the Council on the protection of animals used for scientific purposes).

Supplementary Materials: The following are available online at http://www.mdpi.com/2079-4991/10/10/1939/s1: Figure S1: annotated gel image 1; Figure S2: annotated gel image 2; Figure S3: annotated gel image 3; Table S1: proteins showing a significant change in abundance vs. control in one of the two tested conditions; Table S2: Modulated pathways highlighted by the DAVID annotation tool for pyrolytic silica; Table S3: comparison of modulated proteins for pyrolytic and colloidal silica; and Table S4: Modulated pathways highlighted by the DAVID annotation tool for colloidal silica.

Author Contributions: Conceptualization, T.R.; formal analysis, T.R.; investigation, A.T., B.D., V.C.-F., H.D., D.F.; M.C., and T.R.; writing—original draft preparation, T.R.; writing—review and editing, A.T., B.D., G.S., S.C., and M.C.; funding acquisition, T.R., M.C., G.S., and S.C. A.T. and B.D. performed the confocal microscopy, phagocytosis, and mitochondrial potential. A.T. performed the enzymology experiments and cytokine production experiments. B.D., D.F., M.C. and G.S. performed the nanosilica characterization. V.C.-F and T.R. performed the two-dimensional electrophoresis experiments, while H.D. and S.C. performed protein identification by mass spectrometry. T.R. wrote the initial draft of the manuscript, which was corrected and amended by all co-authors. All authors have read and agreed to the published version of the manuscript.

Funding: This work was funded by the French National Research Program for Environmental and Occupational Health of ANSES (PNREST 2015/032, Silimmun Grant), and the French National Research Agency (ANR-16-CE34-0011, Paipito grant). This work is a contribution to the Labex Serenade (n° ANR-11-LABX-0064) funded by the «Investissements d'Avenir» French Government program of the French National Research Agency (ANR). This work used the platforms of the Grenoble Instruct-ERIC centre (ISBG; UMS 3518 CNRS-CEA-UGA-EMBL) within the Grenoble Partnership for Structural Biology (PSB), supported by FRISBI (ANR-10-INBS-05-02) and GRAL, financed within the University Grenoble Alpes graduate school (Ecoles Universitaires de Recherche) CBH-EUR-GS (ANR-17-EURE-0003), as well as the platforms of the French Proteomic Infrastructure (ProFI) project (grant ANR-10-INBS-08-03). The electron microscope facility is supported by the Auvergne-Rhône-Alpes Region, the Fondation pour la Recherche Médicale (FRM), the fonds FEDER and the GIS-Infrastructures en Biologie Sante et Agronomie (IBISA). IBS acknowledges integration into the Interdisciplinary Research Institute of Grenoble (IRIG, CEA). We also thank the Fondation pour la Recherche Médicale for financial support of a Synapt HDMS mass spectrometer.

Acknowledgments: We thank the microscopy facility MuLife of IRIG/DBSCI, funded by CEA Nanobio and labex Gral for equipment access and use.

Conflicts of Interest: The authors declare no conflict of interests.

References

1. Hamilton, R.F., Jr.; Thakur, S.A.; Holian, A. Silica binding and toxicity in alveolar macrophages. *Free. Radic. Biol. Med.* **2008**, *44*, 1246–1258. [CrossRef] [PubMed]
2. Sayes, C.M.; Reed, K.L.; Warheit, D.B. Assessing toxicity of fine and nanoparticles: Comparing in vitro measurements to in vivo pulmonary toxicity profiles. *Toxicol. Sci.* **2007**, *97*, 163–180. [CrossRef]
3. Arts, J.H.E.; Muijser, H.; Duistermaat, E.; Junker, K.; Kuper, C.F. Five-day inhalation toxicity study of three types of synthetic amorphous silicas in Wistar rats and post-exposure evaluations for up to 3 months. *Food Chem. Toxicol.* **2007**, *45*, 1856–1867. [CrossRef]
4. Turci, F.; Pavan, C.; Leinardi, R.; Tomatis, M.; Pastero, L.; Garry, D.; Anguissola, S.; Lison, D.; Fubini, B. Revisiting the paradigm of silica pathogenicity with synthetic quartz crystals: The role of crystallinity and surface disorder. *Part. Fibre Toxicol.* **2016**, *13*, 32. [CrossRef]
5. Ghiazza, M.; Polimeni, M.; Fenoglio, I.; Gazzano, E.; Ghigo, D.; Fubini, B. Does vitreous silica contradict the toxicity of the crystalline silica paradigm? *Chem. Res. Toxicol.* **2010**, *23*, 620–629. [CrossRef]
6. Gazzano, E.; Ghiazza, M.; Polimeni, M.; Bolis, V.; Fenoglio, I.; Attanasio, A.; Mazzucco, G.; Fubini, B.; Ghigo, D. Physicochemical determinants in the cellular responses to nanostructured amorphous silicas. *Toxicol. Sci.* **2012**, *128*, 158–170. [CrossRef] [PubMed]
7. Zhang, H.Y.; Dunphy, D.R.; Jiang, X.M.; Meng, H.; Sun, B.B.; Tarn, D.; Xue, M.; Wang, X.; Lin, S.J.; Ji, Z.X.; et al. Processing Pathway Dependence of Amorphous Silica Nanoparticle Toxicity: Colloidal vs Pyrolytic. *J. Am. Chem. Soc.* **2012**, *134*, 15790–15804. [CrossRef] [PubMed]
8. Di Cristo, L.; Movia, D.; Bianchi, M.G.; Allegri, M.; Mohamed, B.M.; Bell, A.P.; Moore, C.; Pinelli, S.; Rasmussen, K.; Riego-Sintes, J.; et al. Proinflammatory Effects of Pyrogenic and Precipitated Amorphous Silica Nanoparticles in Innate Immunity Cells. *Toxicol. Sci.* **2016**, *150*, 40–53. [CrossRef] [PubMed]
9. Kodali, V.; Littke, M.H.; Tilton, S.C.; Teeguarden, J.G.; Shi, L.; Frevert, C.W.; Wang, W.; Pounds, J.G.; Thrall, B.D. Dysregulation of Macrophage Activation Profiles by Engineered Nanoparticles. *Acs Nano* **2013**, *7*, 6997–7010. [CrossRef]
10. Okoturo-Evans, O.; Dybowska, A.; Valsami-Jones, E.; Cupitt, J.; Gierula, M.; Boobis, A.R.; Edwards, R.J. Elucidation of Toxicity Pathways in Lung Epithelial Cells Induced by Silicon Dioxide Nanoparticles. *PLoS ONE* **2013**, *8*, e72363. [CrossRef]
11. Dalzon, B.; Aude-Garcia, C.; Collin-Faure, V.; Diemer, H.; Beal, D.; Dussert, F.; Fenel, D.; Schoehn, G.; Cianferani, S.; Carriere, M.; et al. Differential proteomics highlights macrophage-specific responses to amorphous silica nanoparticles. *Nanoscale* **2017**, *9*, 9641–9658. [CrossRef] [PubMed]
12. Toybou, D.; Celle, C.; Aude-Garcia, C.; Rabilloud, T.; Simonato, J.-P. A toxicology-informed, safer by design approach for the fabrication of transparent electrodes based on silver nanowires. *Environ. Sci. Nano* **2019**, *6*, 684–694. [CrossRef]
13. Silva, R.M.; Xu, J.; Saiki, C.; Anderson, D.S.; Franzi, L.M.; Vulpe, C.D.; Gilbert, B.; Van Winkle, L.S.; Pinkerton, K.E. Short versus long silver nanowires: A comparison of in vivo pulmonary effects post instillation. *Part. Fibre Toxicol.* **2014**, *11*, 52. [CrossRef] [PubMed]

14. Triboulet, S.; Aude-Garcia, C.; Armand, L.; Collin-Faure, V.; Chevallet, M.; Diemer, H.; Gerdil, A.; Proamer, F.; Strub, J.M.; Habert, A.; et al. Comparative proteomic analysis of the molecular responses of mouse macrophages to titanium dioxide and copper oxide nanoparticles unravels some toxic mechanisms for copper oxide nanoparticles in macrophages. *PLoS ONE* **2015**, *10*, e0124496. [CrossRef] [PubMed]
15. Dalzon, B.; Torres, A.; Diemer, H.; Ravanel, S.; Collin-Faure, V.; Pernet-Gallay, K.; Jouneau, P.-H.; Bourguignon, J.; Cianférani, S.; Carrière, M.; et al. How reversible are the effects of silver nanoparticles on macrophages? A proteomic-instructed view. *Environ. Sci. Nano* **2019**, *6*, 3133–3157. [CrossRef]
16. Torres, A.; Dalzon, B.; Collin-Faure, V.; Rabilloud, T. Repeated vs. Acute Exposure of RAW264.7 Mouse Macrophages to Silica Nanoparticles: A Bioaccumulation and Functional Change Study. *Nanomater. Basel* **2020**, *10*, 215. [CrossRef]
17. Huang, T.J.; Trakshel, G.M.; Maines, M.D. Detection of 10 variants of biliverdin reductase in rat liver by two-dimensional gel electrophoresis. *J. Biol. Chem.* **1989**, *264*, 7844–7849.
18. Kerry, J.A.; Rohde, M.; Kwok, F. Brain pyridoxal kinase. Purification and characterization. *Eur. J. Biochem.* **1986**, *158*, 581–585. [CrossRef]
19. Malcovati, M.; Valentini, G.; Wood, W.A. AMP- and fructose 1, 6-bisphosphate-activated pyruvate kinases from Escherichia coli. In *Methods in Enzymology*; Academic Press: Cambridge, MA, USA, 1982; Volume 90, pp. 170–179.
20. Kuntz, G.n.W.K.; Krietsch, W.K.G. Phosphoglycerate kinase from animal tissue. In *Methods in Enzymology*; Academic Press: Cambridge, MA, USA, 1982; Volume 90, pp. 103–110.
21. Thomé, M.P.; Filippi-Chiela, E.C.; Villodre, E.S.; Migliavaca, C.B.; Onzi, G.R.; Felipe, K.B.; Lenz, G. Ratiometric analysis of Acridine Orange staining in the study of acidic organelles and autophagy. *J. Cell Sci.* **2016**, *129*, 4622–4632. [CrossRef]
22. Huang, D.W.; Sherman, B.T.; Lempicki, R.A. Systematic and integrative analysis of large gene lists using DAVID bioinformatics resources. *Nat. Protoc.* **2009**, *4*, 44–57. [CrossRef]
23. Hammer, O.; Harper, D.A.T.; Ryan, P.D. Paleontological statistics software package for education and data analysis. *Palaeontol. Electron.* **2001**, *4*, 9.
24. Aude-Garcia, C.; Dalzon, B.; Ravanat, J.L.; Collin-Faure, V.; Diemer, H.; Strub, J.M.; Cianferani, S.; Van Dorsselaer, A.; Carriere, M.; Rabilloud, T. A combined proteomic and targeted analysis unravels new toxic mechanisms for zinc oxide nanoparticles in macrophages. *J. Proteom.* **2016**, *134*, 174–185. [CrossRef] [PubMed]
25. Merkwirth, C.; Langer, T. Prohibitin function within mitochondria: Essential roles for cell proliferation and cristae morphogenesis. *Mol. Cell Res.* **2009**, *1793*, 27–32. [CrossRef] [PubMed]
26. Rival, T.; Macchi, M.; Arnauné-Pelloquin, L.; Poidevin, M.; Maillet, F.; Richard, F.; Fatmi, A.; Belenguer, P.; Royet, J. Inner-membrane proteins PMI/TMEM11 regulate mitochondrial morphogenesis independently of the DRP1/MFN fission/fusion pathways. *EMBO Rep.* **2011**, *12*, 223–230. [CrossRef] [PubMed]
27. La Cour, J.M.; Winding Gojkovic, P.; Ambjorner, S.E.B.; Bagge, J.; Jensen, S.M.; Panina, S.; Berchtold, M.W. ALG-2 participates in recovery of cells after plasma membrane damage by electroporation and digitonin treatment. *PLoS ONE* **2018**, *13*, e0204520. [CrossRef] [PubMed]
28. Sun, B.B.; Wang, X.; Liao, Y.P.; Ji, Z.X.; Chang, C.H.; Pokhrel, S.; Ku, J.; Liu, X.S.; Wang, M.; Dunphy, D.R.; et al. Repetitive Dosing of Fumed Silica Leads to Profibrogenic Effects through Unique Structure-Activity Relationships and Biopersistence in the Lung. *ACS Nano* **2016**, *10*, 8054–8066. [CrossRef]
29. Sadauskas, E.; Danscher, G.; Stoltenberg, M.; Vogel, U.; Larsen, A.; Wallin, H. Protracted elimination of gold nanoparticles from mouse liver. *Nanomedicine* **2009**, *5*, 162–169. [CrossRef]
30. Aude-Garcia, C.; Villiers, F.; Collin-Faure, V.; Pernet-Gallay, K.; Jouneau, P.H.; Sorieul, S.; Mure, G.; Gerdil, A.; Herlin-Boime, N.; Carriere, M.; et al. Different in vitro exposure regimens of murine primary macrophages to silver nanoparticles induce different fates of nanoparticles and different toxicological and functional consequences. *Nanotoxicology* **2016**, *10*, 586–596. [CrossRef]
31. Mowat, A.M.; Scott, C.L.; Bain, C.C. Barrier-tissue macrophages: Functional adaptation to environmental challenges. *Nat. Med.* **2017**, *23*, 1258–1270. [CrossRef]
32. Dalzon, B.; Aude-Garcia, C.; Diemer, H.; Bons, J.; Marie-Desvergne, C.; Pérard, J.; Dubosson, M.; Collin-Faure, V.; Carapito, C.; Cianférani, S.; et al. The longer the worse: A combined proteomic and targeted study of the long-term versus short-term effects of silver nanoparticles on macrophages. *Environ. Sci. Nano* **2019**, *7*, 2032–2046. [CrossRef]

33. Mortensen, N.P.; Hurst, G.B.; Wang, W.; Foster, C.M.; Nallathamby, P.D.; Retterer, S.T. Dynamic development of the protein corona on silica nanoparticles: Composition and role in toxicity. *Nanoscale* **2013**, *5*, 6372–6380. [CrossRef] [PubMed]
34. Docter, D.; Bantz, C.; Westmeier, D.; Galla, H.J.; Wang, Q.; Kirkpatrick, J.C.; Nielsen, P.; Maskos, M.; Stauber, R.H. The protein corona protects against size- and dose-dependent toxicity of amorphous silica nanoparticles. *Beilstein J. Nanotechnol.* **2014**, *5*, 1380–1392. [CrossRef] [PubMed]
35. Wattiez, R.; Hermans, C.; Cruyt, C.; Bernard, A.; Falmagne, P. Human bronchoalveolar lavage fluid protein two-dimensional database: Study of interstitial lung diseases. *Electrophoresis* **2000**, *21*, 2703–2712. [CrossRef]
36. Garmany, T.H.; Moxley, M.A.; White, F.V.; Dean, M.; Hull, W.M.; Whitsett, J.A.; Nogee, L.M.; Hamvas, A. Surfactant composition and function in patients with ABCA3 mutations. *Pediatr. Res.* **2006**, *59*, 801–805. [CrossRef]
37. Leroy, B.; Falmagne, P.; Wattiez, R. Sample preparation of bronchoalveolar lavage fluid. *Methods Mol. Biol.* **2008**, *425*, 67–75.
38. Delaval, M.; Boland, S.; Solhonne, B.; Nicola, M.A.; Mornet, S.; Baeza-Squiban, A.; Sallenave, J.M.; Garcia-Verdugo, I. Acute exposure to silica nanoparticles enhances mortality and increases lung permeability in a mouse model of Pseudomonas aeruginosa pneumonia. *Part. Fibre Toxicol.* **2015**, *12*, 1. [CrossRef]
39. Takahashi, Y.; He, H.; Tang, Z.; Hattori, T.; Liu, Y.; Young, M.M.; Serfass, J.M.; Chen, L.; Gebru, M.; Chen, C.; et al. An autophagy assay reveals the ESCRT-III component CHMP2A as a regulator of phagophore closure. *Nat. Commun.* **2018**, *9*, 2855. [CrossRef]
40. Xu, L.; Sowa, M.E.; Chen, J.; Li, X.; Gygi, S.P.; Harper, J.W. An FTS/Hook/p107FHIP Complex Interacts with and Promotes Endosomal Clustering by the Homotypic Vacuolar Protein Sorting Complex. *Mol. Biol. Cell* **2008**, *19*, 5059–5071. [CrossRef]
41. Fuster, J.J.; Gonzàlez, J.M.; Edo, M.D.; Viana, R.; Boya, P.; Cervera, J.; Verges, M.; Rivera, J.; Andrés, V. Tumor suppressor p27Kip1 undergoes endolysosomal degradation through its interaction with sorting nexin 6. *FASEB J.* **2010**, *24*, 2998–3009. [CrossRef]
42. Damen, E.; Krieger, E.; Nielsen, J.E.; Eygensteyn, J.; van Leeuwen, J.E. The human Vps29 retromer component is a metallo-phosphoesterase for a cation-independent mannose 6-phosphate receptor substrate peptide. *Biochem. J.* **2006**, *398*, 399–409. [CrossRef]
43. Sano, H.; Ishino, M.; Kr√§mer, H.; Shimizu, T.; Mitsuzawa, H.; Nishitani, C.; Kuroki, Y. The microtubule-binding protein Hook3 interacts with a cytoplasmic domain of scavenger receptor A. *J. Biol. Chem.* **2007**, *282*, 7973–7981. [CrossRef] [PubMed]
44. Iyer, R.; Hamilton, R.F.; Li, L.; Holian, A. Silica-induced apoptosis mediated via scavenger receptor in human alveolar macrophages. *Toxicol. Appl. Pharmacol.* **1996**, *141*, 84–92. [CrossRef]
45. Orr, G.A.; Chrisler, W.B.; Cassens, K.J.; Tan, R.; Tarasevich, B.J.; Markillie, L.M.; Zangar, R.C.; Thrall, B.D. Cellular recognition and trafficking of amorphous silica nanoparticles by macrophage scavenger receptor A. *Nanotoxicology* **2011**, *5*, 296–311. [CrossRef] [PubMed]
46. Scott, F.L.; Hirst, C.E.; Sun, J.; Bird, C.H.; Bottomley, S.P.; Bird, P.I. The intracellular serpin proteinase inhibitor 6 is expressed in monocytes and granulocytes and is a potent inhibitor of the azurophilic granule protease, cathepsin G. *Blood* **1999**, *93*, 2089–2097. [CrossRef]
47. Thibodeau, M.S.; Giardina, C.; Knecht, D.A.; Helble, J.; Hubbard, A.K. Silica-Induced Apoptosis in Mouse Alveolar Macrophages Is Initiated by Lysosomal Enzyme Activity. *Toxicol. Sci.* **2004**, *80*, 34–48. [CrossRef]
48. Sohaebuddin, S.K.; Tang, L. A Simple Method to Visualize and Assess the Integrity of Lysosomal Membrane in Mammalian Cells Using a Fluorescent Dye. In *Cellular and Subcellular Nanotechnology*; Humana Press: Totowa, NJ, USA, 2013; Volume 991, pp. 25–31. [CrossRef]
49. Shen, Y.; Zhong, L.; Johnson, S.; Cao, D. Human aldo-keto reductases 1B1 and 1B10: A comparative study on their enzyme activity toward electrophilic carbonyl compounds. *Chem. Biol. Interact.* **2011**, *191*, 192–198. [CrossRef]
50. O'Connor, T.; Ireland, L.S.; Harrison, D.J.; Hayes, J.D. Major differences exist in the function and tissue-specific expression of human aflatoxin B1 aldehyde reductase and the principal human aldo-keto reductase AKR1 family members. *Biochem. J.* **1999**, *343 Pt 2*, 487–504. [CrossRef]
51. Kurahashi, T.; Kwon, M.; Homma, T.; Saito, Y.; Lee, J.; Takahashi, M.; Yamada, K.-i.; Miyata, S.; Fujii, J. Reductive detoxification of acrolein as a potential role for aldehyde reductase (AKR1A) in mammals. *Biochem. Biophys. Res. Commun.* **2014**, *452*, 136–141. [CrossRef]

52. Del Corso, A.; Costantino, L.; Rastelli, G.; Buono, F.; Mura, U. Aldose reductase does catalyse the reduction of glyceraldehyde through a stoichiometric oxidation of NADPH. *Exp. Eye Res.* **2000**, *71*, 515–521. [CrossRef]
53. Vander Jagt, D.L.; Hassebrook, R.K.; Hunsaker, L.A.; Brown, W.M.; Royer, R.E. Metabolism of the 2-oxoaldehyde methylglyoxal by aldose reductase and by glyoxalase-I: Roles for glutathione in both enzymes and implications for diabetic complications. *Chem.-Biol. Interact.* **2001**, *130–132*, 549–562. [CrossRef]

Conclusion

Cette étude met en évidence la nécessité de réaliser les tests de toxicologie pour chaque nanomatériau. En effet, les effets observés ici avec la SAS pyrogénée ne sont pas complètement comparables avec ceux obtenus pour une SAS colloïdale (Dalzon et al. 2017). Les analyses protéomique ont montré des différences dans l'expression de certaines protéines (enzyme de la glycolyse, par exemple), cependant des voies métaboliques sont également modifiées par l'exposition aux deux types de SAS (cytosquelette, mitochondrie, protéine de réparation membranaire). Les tests de validations révèlent que l'adhésion des cellules exposées est plus faible et la sécrétion de cytokines pro-inflammatoires augmente suite à l'exposition à la SAS pyrogénée. Le potentiel mitochondrial et l'équilibre oxydo-réducteur de la cellule restent stables et proches au contrôle. Après la période de récupération, l'analyse protéomique montre majoritairement un retour à la normale de l'expression des protéines, excepté les lysosomes. Les tests de validation après la période de récupération mettent en évidence un maintien de l'homéostasie et de l'intégrité des lysosomes, de même que l'activité phagocytaire, ce qui avait été observée avec la SAS colloïdale. Ces résultats, en utilisant un système *in vitro*, sont comparables au phénomène observé *in vivo* (Arts et al. 2007).

L'utilisation de ce protocole appliqué à deux matériaux différents (silice amorphe de synthèse et nanoparticules d'argent) mène à une conclusion : chaque matériau doit être testé car les effets ne sont pas prédictibles à partir des expériences à court terme (24h). Le système *in vitro* est pertinent par rapport aux expériences *in vivo*, mais chaque nanomatériau doit être évalué afin de connaître sa toxicité à long terme, et la persistance de ses effets.

La publication citée ci-dessus a en particulier mis en évidence un phénomène général de retour à la normale des paramètres biologiques des macrophages (du moins ceux étudiés) à l'issue de la phase de récupération post-exposition, à l'exception de la production d'IL-6 qui reste soutenue dans le temps. Ce phénomène de décroissance des effets biologiques avec le temps étant au cœur de la moindre toxicité des silices amorphes par rapport à la silice cristalline, il convenait de s'assurer que notre système *in vitro* ne présentait pas de biais systématique qui pourrait faire conclure à une décroissance des effets qui n'existerait pas *in vivo*, et donc de vérifier que des NMx connus pour donner des effets persistants *in vivo* donnaient aussi des effets persistants dans notre système *in vitro*.

I e) Optimisation du système

A low-serum culture system for prolonged *in vitro* toxicology experiments on macrophages

Présentation du projet

Pour ce projet, nous nous sommes concentrés sur l'optimisation du protocole de culture, et notamment pour les cultures longues. En effet, les macrophages murins sont une lignée cellulaire, et se divisent avec un temps de génération d'environ 17h d'après l'ATCC. Nous étudions les macrophages au niveau pulmonaire, et physiologiquement leur division est très lente, contrairement par exemple aux cellules épithéliales intestinales qui se renouvellent en permanence. Ce paramètre de division cellulaire est problématique dans le cas de cultures longues, car les cellules exposées le premier jour, ne sont plus les mêmes après 4 ou 10 jours de culture, comme illustré par (Bourquin et al. 2019), étant donné que la charge à laquelle elles ont été exposées initialement se divise en se répartissant entre les cellules filles à chaque génération. Afin de limiter cette croissance et de s'affranchir de cette division résiduelle, nous avons choisi de modifier le sérum du milieu de culture. En effet, le protocole de culture prévoit l'utilisation de 10% de sérum de veau fœtal (SVF). Or, celui-ci contient des facteurs de croissance (et également moins de protéines du complément ou immunoglobulines), par rapport à un sérum adulte. Nous avons donc testé un protocole de culture utilisant du sérum adulte et en plus faible concentration : 1% de sérum de cheval (HS). Nous avons réalisé des comparaisons de division cellulaire entre les deux milieux de culture ainsi qu'un test de viabilité, un test de phagocytose et un dosage de la réponse inflammatoire. Nous avons aussi validé ces protocoles de culture avec des tests de persistance suite à une exposition à des pigments, les premiers à base de silice (partiellement cristalline) et les autres de cobalt, sur des durées de cultures différentes. Ces études de cas permettant de s'assurer sur la persistance des effets est mesurable et visible dans le cas de nanomatériaux persistants.

frontiers in Toxicology

METHODS
published: 06 December 2021
doi: 10.3389/ftox.2021.780778

A Low-Serum Culture System for Prolonged *in Vitro* Toxicology Experiments on a Macrophage System

*Bastien Dalzon[1], Anaelle Torres[1], Julie Devcic[1], Daphna Fenel[2], Jacques-Aurélien Sergent[3] and Thierry Rabilloud[1]**

[1]Chemistry and Biology of Metals, Université Grenoble Alpes, CNRS UMR5249, CEA, IRIG-DIESE-LCBM-ProMIT, Grenoble, France, [2]Institut de Biologie Structurale, Université Grenoble Alpes, CEA, CNRS, Grenoble, France, [3]Toxicological and Environmental Risk Assessment Unit, Solvay SA, Neder-Over-Heembeek, Belgium

Immunotoxicology *sensu lato* comprises not only toxicity toward immune cells, but also biological reactions from immune cells exposed to toxicants, reactions that may have deleterious effects at the organismal level. Within this wide frame, a specific case of interest is represented by the response of macrophages to particulate materials, with the epitome examples of asbestos and crystalline silica. For such toxicants that are both persistent and often encountered in an occupational setting, i.e. at low but repeated doses, there is a need for *in vitro* systems that can take into account these two parameters. Currently, most *in vitro* systems are used in an acute exposure mode, i.e., with a single dose and a readout made shortly if not immediately after exposure. We describe here how adequate changes of the culture methods applied to the murine macrophage cell line J774A.1 enable longer periods of culture (several days), which represents a first opportunity to address the persistence and dose-rate issues. To respond to this, the protocol uses a reduction in the concentration of the animal serum used for cell culture, as well as a switch from fetal to adult serum, which is less rich in proliferation factors. By doing so, we have considerably reduced cell proliferation, which is a problem with cell lines when they are supposed to represent slowly-dividing cells such as resident macrophages. We also succeeded in maintaining the differentiated functions of macrophages, such as phagocytosis or inflammatory responses, over the whole culture period. Furthermore, the presence of serum, even at low concentrations, provides excellent cell viability and keeps the presence of a protein corona on particulate materials, a feature that is known to strongly modulate their effects on cells and is lost in serum-free culture. Besides data showing the impact of these conditions on macrophages cell line cultures, illustrative examples are shown on silica- and cobalt-based pigments.

Keywords: macrophages, effect persistence, silica, cobalt, pigments, immunotoxicology

OPEN ACCESS

Edited by:
François Huaux, Catholic University of Louvain, Belgium

Reviewed by:
Philipp R. Esser, Medical Center-University of Freiburg, Germany
Sonika Patial, Louisiana State University, United States

****Correspondence:***
Thierry Rabilloud
thierry.rabilloud@cnrs.fr

Specialty section:
This article was submitted to Immunotoxicology, a section of the journal Frontiers in Toxicology

Received: *21 September 2021*
Accepted: *15 November 2021*
Published: *06 December 2021*

Citation:
Dalzon B, Torres A, Devcic J, Fenel D, Sergent J-A and Rabilloud T (2021) A Low-Serum Culture System for Prolonged in Vitro *Toxicology Experiments on a Macrophage System. Front. Toxicology. 3:780778. doi: 10.3389/ftox.2021.780778*

INTRODUCTION

Macrophages are an important cell type to consider in immunotoxicology *sensu lato*, i.e., not only the situations where the functions of the immune system are decreased by a toxicant so that it does not play its full protective role any longer, but also the situations where a sustained activation of the immune system and especially the innate immune system is part of the

pathological process. The epitome of this latter situation is represented by chronic inflammatory pulmonary diseases such as asbestosis and silicosis, where a sustained inflammation is observed. In the frame of the 3R principles (Refine Reduce Replace) aiming at limiting the use of laboratory animals, it is highly desirable to have *in vitro* models that mimic as closely as possible the *in vivo* situation.

In the case of macrophages, the *in vivo* situation is quite complex because of the plasticity and heterogeneity of macrophages. Indeed, two main different macrophage populations exist, i.e., the tissue resident macrophages and the monocyte-derived macrophages. It has been shown that tissue resident macrophages derive from the fetal liver (Ginhoux and Guilliams, 2016), have a prolonged lifespan in the body (Murphy et al., 2008) and are maintained by self renewal (Hashimoto et al., 2013; Ginhoux and Jung, 2014). In the peritoneal cavity, resident macrophages and monocyte-derived macrophages are phenotypically and functionally different (Ghosn et al., 2010), so that their dynamics can be studied in different conditions. Such studies have shown that monocyte-derived macrophages are responsible for acute inflammatory responses, and disappear after the acute inflammatory phase (Cassado Ados et al., 2015). The situation is however made more complex by the fact that a small proportion of the monocyte-derived macrophages can "*trans*-differentiate" into resident macrophages and replace the embryo-derived resident macrophages over time or in situations where the original embryo-derived resident macrophage population is depleted, e.g., by a macrophage-targeting infectious agent (Bain et al., 2016).

Thus in terms of immunotoxicology, it would be highly desirable to have at hand an *in vitro* model mimicking the resident macrophages, i.e. able of a prolonged lifespan *in vitro*, with a slow proliferation rate, and keeping the essential macrophage functions such as phagocytosis, ability to produce inflammatory response, and also the ability to reach different polarization states.

Because of the high interest in macrophages, numerous models have been described in the scientific literature. The oldest ones are both differentiated macrophages isolated *ex vivo* (e.g., thioglycollate elicited peritoneal macrophages (Adams, 1979) and cell lines of murine (RAW264.7, P388D1, J774A.1, to name just a few), rat (NR8383) and human (HL-60, THP-1, U937) origin. However, the human cell lines require to be chemically differentiated *in vitro*, most often by phorbol esters (Rovera et al., 1979; Bernal and Chen, 1982; Tsuchiya et al., 1982).

More recent macrophage systems have focused on primary cells, obtained from adult precursors, mostly bone marrow for murine cells (Schleicher and Bogdan, 2009) and monocytes for human cells (Davies and Gordon, 2004). More recently, human macrophages were prepared from pluripotent stem cells (Gutbier et al., 2020).

Unfortunately, none of these systems is completely satisfactory. Monocyte and bone-marrow derived macrophages have all the characteristics of *in vivo* monocyte-derived macrophages. As such, they do not proliferate at all and can be maintained *in vitro* for very limited time, up to only a few days after full differentiation (Aude-Garcia et al., 2016). Production of macrophages from pluripotent stem cells is rather complex, and their survival capacity once fully differentiated has not been evaluated yet. Phorbol ester-differentiated cell lines also show no proliferation capacity. Moreover, they de-differentiate over time when the phorbol ester stimulus is removed (Bertram et al., 2008). However, the phorbol ester stimulus cannot be kept permanently because of its toxicity.

Rodent cell lines present the opposite problem. While they keep excellent differentiated characteristics without the need for any chemical stimulus, they also keep a high proliferation rate. This may not be a problem for short-term studies, but it is for longer term studies. As an example, a recent study on the persistence of silver nanoparticles in macrophages has concluded to a decrease of intracellular silver content over time (Dalzon et al., 2019b). However, careful examination of the data shows that the total silver content is almost constant but that the number of cells increases during the experiment, thereby explaining the effect. Consequently, some authors have preferred to switch to serum-free culture conditions, as common for the rat NR8383 model system (Wiemann et al., 2016). However, such conditions allow for a very limited cell survival over time and are thus not suitable for any longer-term studies. Moreover, serum-free conditions are not physiological, as even alveolar macrophages bathe in pulmonary surfactant that does contain serum proteins (Wattiez et al., 2000).

Thus, there is a need for an *in vitro* system that would allow studies lasting longer than the classical overnight exposure. This would be of high interest in toxicological studies where a persistent effect has to be studied. Currently, this notion of chronicity and persisting effects is typically monitored using epidemiologic studies (Dockery et al., 1993), and *in vivo* studies (Miller et al., 1999; Oszlánczi et al., 2011; Tian et al., 2015; Boudard et al., 2019). Chronic or long-term exposures have rarely been studied *in vitro* beforehand in order to determine the cellular and molecular mechanisms behind the phenomenon, mostly because of this lack of convenient *in vitro* systems.

While mineral materials represent an obvious case where such effects persistence is interesting to study, other interesting cases can be foreseen, e.g. persistent organic toxicants such as dioxins, which are known to modulate macrophages functions through their binding to the aromatic hydrocarbon receptor (Kimura et al., 2009), or polychlorobiphenyls, which chronic inflammatory effects are currently tested *in vivo* (Petriello et al., 2018), while their short-term effects can be tested *in vitro* (Wang et al., 2019).

It is for these two reasons, i.e. the lack of *in vitro* models to determine long-term toxicity and the key role played by macrophages in the evolution of inflammation [e.g., *via* the modulation of the secretion of reactive oxygen species, nitric oxide (NO) or cytokines (Fang, 2004)] as well as in tissue homeostasis (Koh and DiPietro, 2011; Landén et al., 2016), that we seeked to implement an *in vitro* model of monocyte/macrophage cell lines enabling the detection of persisting effects, in accordance with the 3 Rs (Replace, Reduce, Refine) regulation awareness, aiming at the reduction of the use of laboratory animals.

In this study, i) thanks to functional assays (Dalzon et al., 2019a, 2020b; Torres et al., 2020b), we determined the reliability of our long-term culture model after changing the composition of culture medium, in comparison with common culture medium. The classical 10% fetal bovine serum (FBS) supplement added to DMEM supplemented was decreased (1% instead of 10%) and replaced by adult horse serum. The change in concentration and type of serum permitted to limit growth factors and thus experiments, cells were cultivated prevented cell proliferation from inducing various stresses due to a high degree of confluence and cell detachment. Indeed, cell detachment can induce artifacts because it is necessary to change culture medium every 2 days. ii) then, we determined the main functional damage caused by long-term exposure of macrophages to various mineral particles such as silica and cobalt particles.

The results showed that switching from the classical DMEM supplemented with 10% FBS to DMEM +1% horse serum improves long-term culture conditions, restricts cell proliferation and detachment. Functional assays conducted on J774A.1 macrophages without particles showed that both acute exposure (24 h to DMEM +10% FBS) and long-term exposure (10 days to DMEM +1% horse serum) provided exploitable results. Indeed, the functional capacity (phagocytosis and inflammatory) of J774A.1 cells were maintained. Thus, after 10 days, it was possible to assess the modulation of the main functions of macrophages exposed to mineral particles in comparison to controls without treatment.

MATERIALS AND METHODS

Cell Culture and Viability Assessment

The J774A1 cell line (mouse macrophages) was purchased from European cell culture collection (Salisbury, UK). Cells were routinely propagated in DMEM supplemented with 10% fetal bovine serum (FBS) in non-adherent flasks (Cellstar). For short-term (24 h) experiments, cells were cultivated in 12-well non-adherent plate (CellStar, catalogue number 665102). For cell culture for medium-term (4 days) and long-term (10 days) experiments, cells were cultivated in 12-well adherent plates (Falcon, catalog number 353043). Starting from a growing culture made in classical culture medium (supplement with 10% fetal bovine serum), the cells were seeded at 700,000 cell/ml in DMEM +1% horse serum (1% HS) in 12-well adherent plates. For the establishment of the system, control cultures were seeded in DMEM+10% FBS. The medium was then changed every 2 days for up to 10 days in culture, without any further splitting of the cells.

For *in vitro* toxicological testing, after 2 days of cell adaptation to the low serum medium (DMEM+ 1% horse serum), the medium was changed and the cells exposed to the test substance. After the exposure period (usually 24 h), the medium was removed and replaced by fresh DMEM+1%HS medium, which was changed every 2 days during the recovery period (respectively 3 or 9 days). The same medium changes were applied to control (untreated) cultures. To obtain reference values of the effects of the substances tested, acute exposures, i.e., 24 h exposures with readouts made immediately after exposure, were also performed. In order to take cell ageing into account, these acute exposures in the long-term experiments (4 and 10 days) were carried out on days 3 and 9, respectively. Cell viability was measured using FACScalibur flow cytometer equipped with CellQuest software program (6.0, Becton Dickinson Biosciences, Le Pont-de-Claix, France). Cells were previously dyed with propidium iodide (480 nm excitation and 600 nm emission) at 1 μg/ml final concentration. For every test substance, LD20 was assessed in acute exposure mode in standard short-term (24 h) experiments.

Overall, the culture and exposure system is schematized in **Figure 1**.

Crystal Violet Quantification

The cell layer was rinsed with PBS and fixed *via* 1 ml of mix of ethanol 50% v/v and acetic acid 1% v/v (an acid alcohol solution) for 30 min. The cells were stained by crystal violet with a concentration of 4 μg/ml (final concentration) in PBS at room temperature for 30 min. Then, cells were rinsed with PBS before elution with 1 ml of acid alcohol solution. The released color was read at 590 nm using a Jenway 7,315 spectrophotometer. To convert the crystal violet measures into cell numbers, a calibration curve was constructed by seeding a known number of cells on adherent plates for 18 h, so that the cells could attach but did not have time to proliferate. These cell layers were then submitted to the crystal violet protocol, and the absorbance values used to build the calibration curve.

Particle Characterization

Cobalt aluminate $CoAl_2O_4$, also named Pigment Blue 28 (PB28) was purchased from Kama Pigments (Montreal, Canada). Crystalline aluminum oxide spinel (Corundum) was purchased from Sigma-Aldrich (ref#ERMFD066). These materials were received in powder form. Then, 100 μg/ml were suspended in gum arabic (previously sterilized at 80 °C for 24 h). The final particular suspension was sterilized for 24 h at 80°C. The suspension was sonicated with a sonicator equipped with a Cup Horn probe (Vibra cell VC 750, VWR, Fontenay sous Bois, France) with the following settings: time = 30 min–1 s ON, 1 s OFF—Amplitude = 60%, corresponding to 90 W/pulse. The sterile suspension was then used on cells.

Silica-based pigments (tiger eye, agate and jasper) were purchased from Kremer Pigmente (Aichstetten, Germany). Jasper is quartz containing iron oxide, giving it its brown color. Agate is a form of chalcedony, i.e. formed by quartz and moganite microcrystallites, colored by iron oxide. Both quartz and moganite are silica, crystallizing in different systems. Tiger eye is composed of fibrous assemblies of quartz and amphibole (iron and magnesium silicate) microcrystallites. These pigments are sized by sieving to a nominal size of 5 μm. Opposite to colbalt aluminate, silica-based pigments suspend well in water. Resuspension was carried out as previously described (Dalzon et al., 2019b; Torres et al., 2020b). The commercial powders were solubilized in water at 10 mg/ml, dispersed in a water sonication bath. The suspensions were then sterilized by pasteurization at 80°C

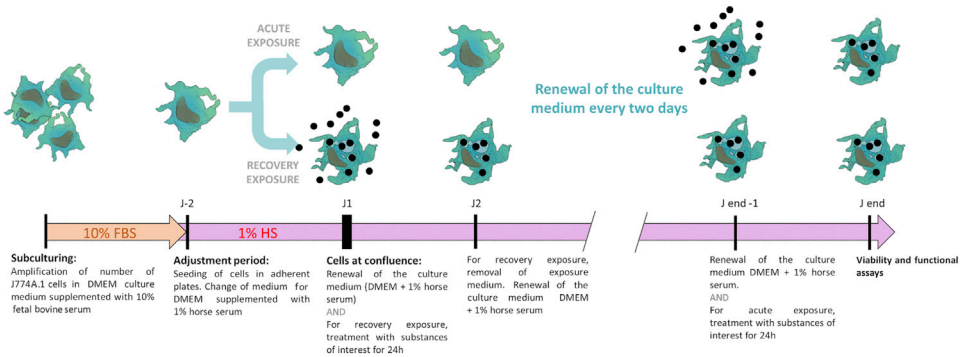

FIGURE 1 | Schematic representation of the two-phase culture system. The cells are first amplified in enriched culture medium (containing 10% fetal bovine serum), then transferred in the low-serum culture medium (containing 1% adult horse serum), to which they are first adapted. The exposure and the recovery phases are then carried out, prior to final biological endpoints readout.

overnight. They were used after a last sonication step of 10 min.

For characterization by transmission electron microscopy, samples were first diluted to 100 µg/ml. Then, 3.5 µl were added to a glow discharge grid coated with a carbon supporting film for 5 min. The excess solution was soaked off by a filter paper and the grid was air-dried. The images were taken under low dose conditions (< 10 e-/Å^2) with defocus values between 1.2 and 2.5 µm on a Tecnai 12 LaB6 electron microscope at 120 kV accelerating voltage using CCD Camera Gatan Orius 1,000.

Phagocytic Assay

Phagocytosis capacity of J774A.1 macrophages was studied by internalization of yellow/green fluorescent latex beads (Sigma-Aldrich #L4655). The percentage of phagocytic cells and their mean fluorescent intensity were measured using FACScalibur flow cytometer with CellQuest software program (6.0, Becton Dickinson Biosciences, Le Pont-de-Claix, France) as previously described in a previous publication (Torres et al., 2020b).

NO Secretion

After exposure of cells to the test substance (acute or recovery exposure), cells were activated (or not) by lipopolysaccharide (LPS) (100 ng/ml final concentration) in a medium supplemented with arginine monohydrochloride (5 mM final concentration) in order to provide unlimiting substrate for the NO synthase. When LPS activation was used, LPS was added to the cells for the last 18 h in culture. The concentration of NO released in the culture medium was measured as previously described (Torres et al., 2020b), using the Griess reagent for nitrite.

Cytokine Release

Tumor necrosis factor (TNFα) and interleukin 6 (IL-6), were measured in the supernatant from cultured cells exposed to pigments and/or activated by LPS 100 ng/ml, using the Mouse Inflammation Cytometric Bead Array kit (BD cytometric bead array, BD Biosciences, Rungis, France) according to the manufacturer's instructions. Measurements were performed on a FACScalibur flow cytometer, and the concentrations of cytokines secreted were assessed using FCAP Array Software.

RESULTS

Assessment of Culture Conditions

Comparison of Culture Conditions: Cell Proliferation and Cell Detachment

J774A.1 cells were cultivated for 1 week in DMEM +10% FBS or DMEM +1% HS and the culture media were changed every 2 days. Cells were observed *via* optical microscopy after 4 days of culture (seeding of cells = day 0). Then, cells were quantified in order to determine the number of detached and adherent cells. After 4 days of culture, the results showed (**Figure 2A**) a strong slowdown of the multiplication of J774 in DMEM supplemented with 1% HS in comparison to 10% FBS. This applies to both high (800,000 cells/ml) and low seeding concentrations (200,000 cells/ml). In DMEM +1% HS, microscopic observation revealed that cells were less round and more stretched (with filamentous extensions). In the collected culture media, the quantification of cells (**Figure 2B**) revealed much less detached cells in 1% HS (−68% with a seeding of 800,000 cells/ml and −63% with a seeding of 200,000 cells/ml, compared to the cells cultivated in DMEM +10% FBS). Moreover, the quantification of adherent cells revealed a significant decrease of 35 and 52% in comparison to 10% FBS for a seeding of 800,000 cells/ml and 200,000 cells/ml respectively (**Figure 2C**, thereby confirming a lower cell proliferation in 1% HS compared to 10% FBS.

Assessment of Cell Viability in Culture Medium DMEM +1% Horse Serum

After 24 h of culture in DMEM +1% HS, the viability of J774 cells was similar to the one in 10% FBS. Indeed, the results in **Figure 3** showed that only 11.6% of cells died (viability = 88.6%), whereas the condition with 10% FBS showed a cell death of 4.25% (Viability = 95.75%). However, this rate can be variable according to experiments. Typically, cell viability in DMEM +10% FBS, was about 90% (Torres et al., 2020a). After 4 days of culture in DMEM +1% HS, viability was 88.8%

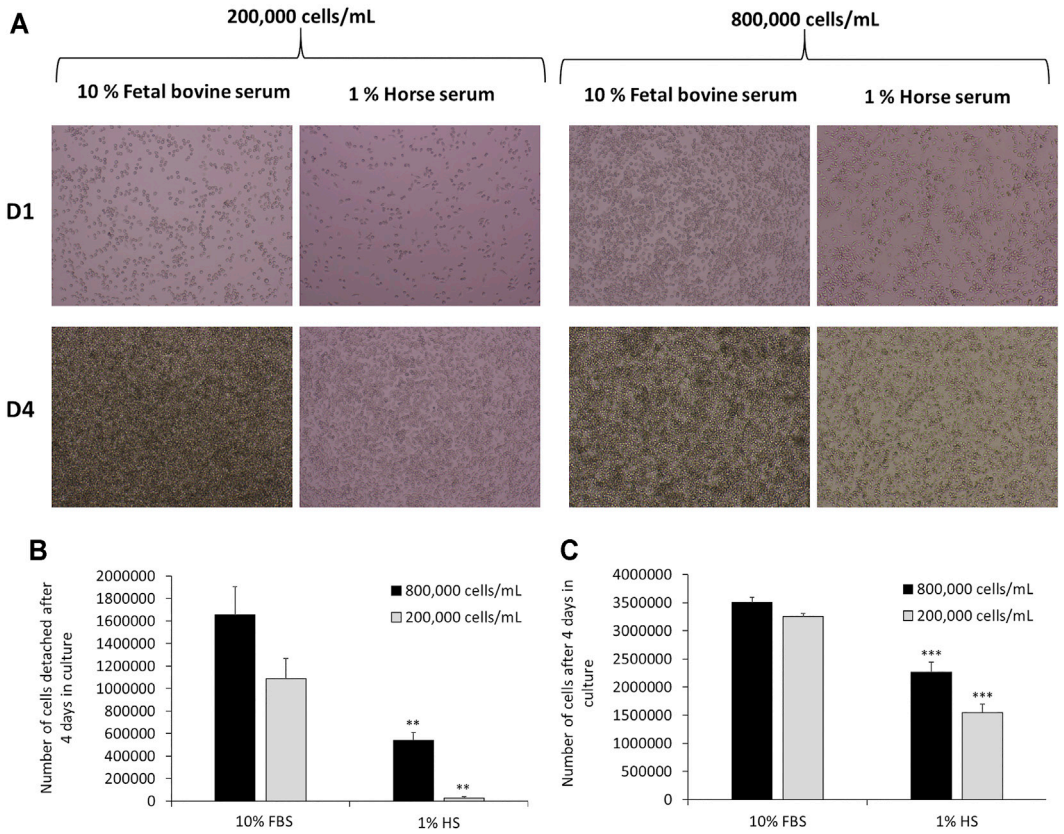

FIGURE 2 | Comparison of cell culture medium for J774 cells after 4 days in culture medium. Panel A- Microscopic observation of J774 cells after 1 day (D1) or 4 days (D4) in culture medium. Cell culture medium tested: DMEM +10% Fetal Bovine Serum (FBS) and DMEM +1% Horse Serum (HS). The seeding tested was 200,000 cells/mL or 800,000 cells/mL. Panel B- Quantification of detached cells in the supernatant *via* cell numeration. Quantification of adherent cells *via* crystal violet (N = 3). *, significant difference between the 10% fetal bovine serum and 1% horse serum conditions. Number of symbols: 2: $p < 0,01$, 3: $p < 0.001$.

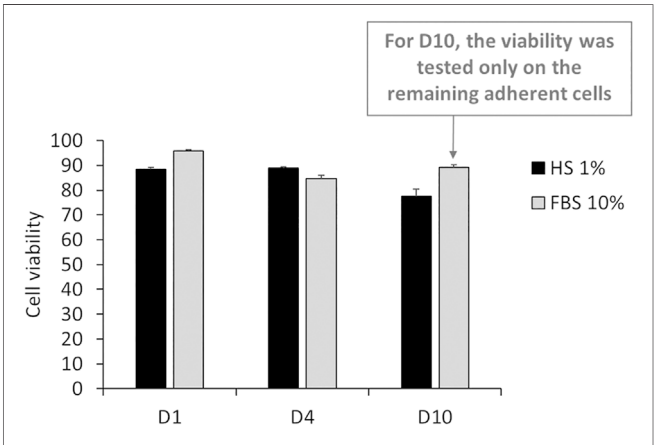

FIGURE 3 | Percentage of living cells after 24 h (D1), 4 days (D4) and 10 days (D10) of culture in DMEM +1% Horse Serum (1% HS). Black bars; culture medium supplemented with DMEM +1% Horse Serum (1% HS). Grey bars; culture medium supplemented with DMEM +10% Fetal Bovine Serum (FBS) (N = 3).

and after 10 days, viability decreased slightly to reach 77.6%. In comparison, in DMEM +10% FBS, viability was 84.68%. and increased to 89% for 10% FBS after 4 days. However, for the DMEM+10% FBS condition, many more cells were detached. Thus, many cells were eliminated of the experiment after each renewal of the culture medium. Consequently, this viability level is not relevant.

Comparison of Culture Conditions: Maintaining of the Main Functionalities of Macrophages (Phagocytic and Inflammatory Capacities)

The results in **Figure 4A** show that after 24 h of culture in DMEM +1% HS, the percentage of phagocytic cells was 79.7%. This percentage was similar after 4 days (77.6%). After 10 days of culture in DMEM +1% HS, the percentage of phagocytic cells decreased to 68%. Despite this slight reduction of the phagocytic capacity, after 10 days in culture medium, a great majority of cells were still able to maintain their phagocytic activity. While the initial phagocytosis was similar for DMEM +1% HS and DMEM +10% FBS, phagocytosis seemed to have a tendency to decrease in DMEM +10% FBS medium after 4 days in culture (only 59% of cells maintain their phagocytic capacity). For NO secretion, the results in **Figure 4B** show that in DMEM +1% HS, J774A.1 cells maintained an adequate response to LPS (100 ng/ml) stimuli for the final 18 h of culture. Indeed, the concentration of NO was 19.8 μM after 24 h of culture, 17 μM after 4 days of culture and

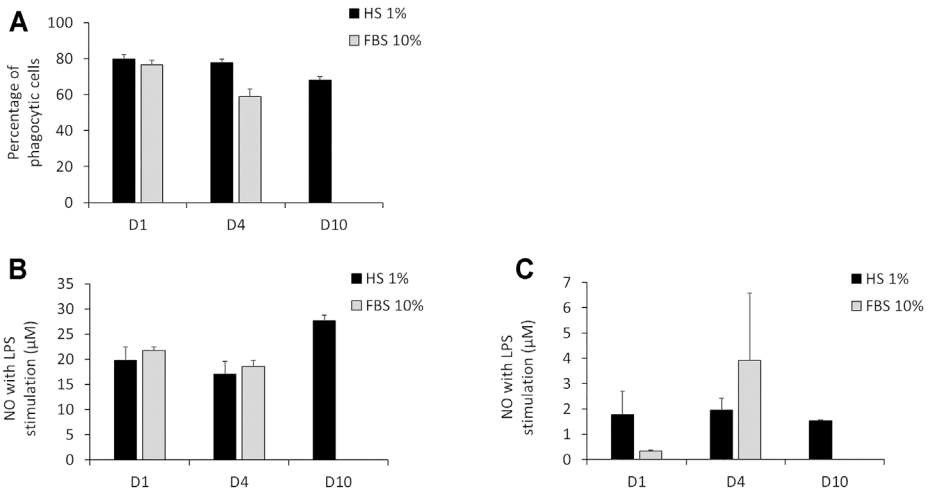

FIGURE 4 | Main functionalities measurement of macrophages. **(A)** Percentage of phagocytic cells measured *via* engulfment of Y/G fluorescent latex beads. **(B)** NO secretion with LPS stimulation for 12 h. **(C)** NO secretion without LPS stimulation. 24 h (D1), 4 days (D4) and 10 days (D10) of culture in DMEM +1% horse serum (1% HS). Black bars; culture medium supplemented with DMEM +1% Horse Serum (1% HS). Grey bars; culture medium supplemented with DMEM +10% Fetal Bovine Serum (FBS) (N = 3). No measurements were made for cells maintained in DMEM+10% FBS because of the important cell detachment occurring, as mentioned in the previous section.

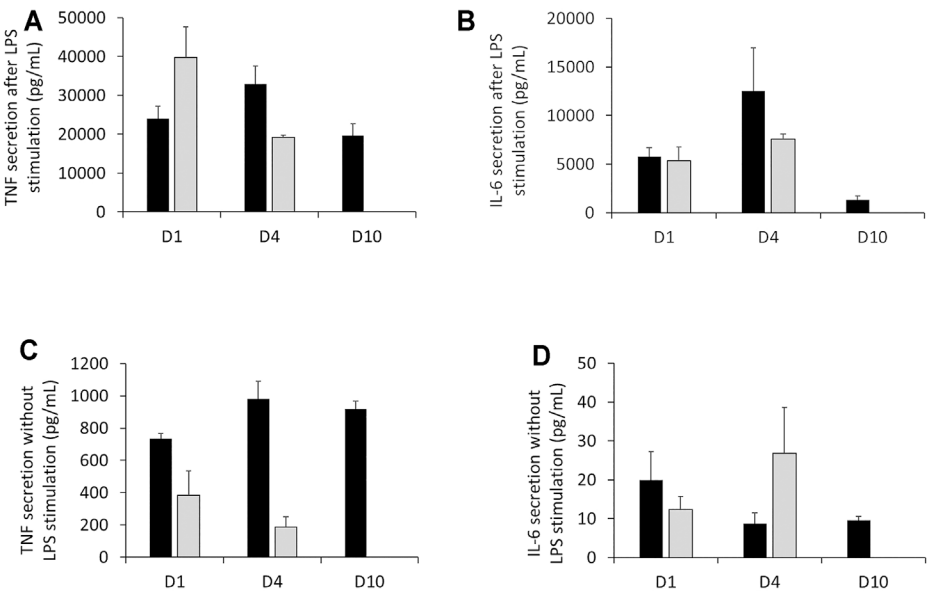

FIGURE 5 | Measurement of TNF secretion and IL-6 cytokines in the presence or absence of LPS stimulation. **(A)** Assessment of TNF released by J77A.1 cells with LPS stimulation (pg/ml). **(B)** Assessment of the IL-6 released by J774A.1 cells with LPS stimulation (pg/ml). **(C)** Assessment of TNF released by J774A.1 cells without LPS stimulation (pg/ml). **(D)** Assessment of IL-6 released by J774A.1 cells without LPS stimulation (pg/ml) (N = 3). Black bars; culture medium supplemented with DMEM +1% Horse Serum (1% HS). Grey bars; culture medium supplemented with DMEM +10% Fetal Bovine Serum (FBS). No measurements were made for cells maintained in DMEM+10% FBS at day 10, because of the important cell detachment, as mentioned in the previous section.

27.7 µM after 10 days of culture. Thus, cells appear to be more sensitive when cultured for a long time. Without LPS stimulation, NO secretion was very low: between 1.5 and 2 µM regardless of cell culture duration (**Figure 4C**), showing that culture conditions did not induce a spurious response at this level. In DMEM+10% FBS, results showed after 4 days of culture, the NO secretion seems less stable with a higher standard deviation.

We chose to extend our assessment of the inflammatory ability according to the duration of culture in DMEM supplemented with 1% HS. Regarding TNF and IL-6, the results in **Figure 5** showed that J774A.1 had a strong response to LPS (100 ng/ml)

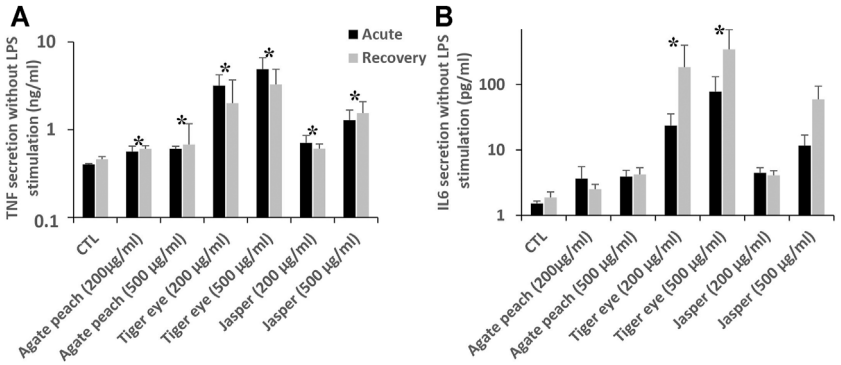

FIGURE 6 | Intrinsic cytokine secretion in J774A.1 cells after exposure to pigment containing silica, followed or not by a recovery period of 72 h. Black bars for acute exposure and grey bars for recovery protocol. Data are represented as Mean +SD **(A)** TNF secretion **(B)**. IL-6 secretion All the treated cells are significantly different from the secretion of the control (Mann-Whitney statistic test, $p < 0.05$) in both acutely exposed cells and recovery scenario (N = 4).

stimulation for short and long-term cell culture in DMEM +1% HS. Indeed, despite a variability of responses (especially for IL-6) dependent on duration of culture, for the three conditions, the secretion of TNF and IL-6 was significantly higher than in the conditions without LPS stimulation. For example, with LPS stimulation, TNF secretion was comprised between 19,604 and 32,935 pg/ml (**Figure 5A**) and IL-6 secretion was between 1,350 and 12,547 pg/ml (with high standard deviations) (**Figure 5B**). Without LPS, TNF secretion was comprised between 736 and 981 pg/ml **Figure 5C**) and IL-6 secretion was between 20 pg/ml (with large standard deviations) and 8.7 pg/ml according to duration of cell culture (**Figure 5D**). In comparison to DMEM supplemented with 10% FBS, even if the raw values were different, the results showed that the orders of magnitude of TNF and IL-6 concentrations were the same for the two culture conditions, both in the presence and absence of LPS. That is, in the presence of LPS, TNF secretion is between 39,777 and 19,175 pg/ml, and for IL-6, it is between 5,346 and 7,579 pg/ml. In the absence of LPS, TNF secretion drops to 383 and 187 pg/ml while IL-6 concentration ranges from 12.3 to 26.8 pg/ml.

As mentioned in *Assessment of cell viability in culture medium DMEM + 1% horse serum* above, strong detachment was observed for cells cultured for 10 days in DMEM+10% FBS. This meant that the cultures were no longer exploitable, so that no functional measurements were performed for this precise condition.

Validation of the DMEM +1% HS Culture Medium System for Medium-Term (4 days) Experiments: Example of the Effects of Silica-Based Pigments

The characterization of the silica-based pigments was carried out by transmission electronic microscopy and is shown in **Supplementary Figure S1**. It confirms a high variety of shapes and sizes of the tested particles with micrometric particles, as expected from the supplier specifications, but also sub-micrometric particles. Working doses of 200 and 500 µg/ml, corresponding respectively to one and 2.5 of particles (5 µm nominal diameter) per cell, were used. These concentrations proved to be non-cytotoxic during the timespan of the experiments (4 days). In these experiments, the parameter tested was cytokine release, as various forms of silica are known to induce inflammatory responses *in vivo* (Arts et al., 2007) and *in vitro* (e.g., in (Wiemann et al., 2016; Torres et al., 2020a)). The results, shown in **Figure 6**, revealed a secretion of pro-inflammatory cytokines after exposure to these silica-based pigments.

First, for tumor necrosis factor α (TNF), all the pigment-exposed cells showed a significantly higher TNF secretion. In the control cells, a basal TNF secretion of 400 pg/ml was observed. After an acute exposure to pigments, TNF secretion was increased from 560 pg/ml (agate) to 4,800 pg/ml (tiger eye 500 µg/ml). These increases were largely persistent even after the 72 h recovery period. Then, after an acute exposure there is a significant increase of IL-6 secretion, which become detectable (24 and 78 pg/ml), for cells exposed to tiger eye. After the recovery period, the cells exposed to tiger eye are still secreting IL-6 in higher doses than just after the exposure (185 and 346 pg/ml). There is therefore a persistence and a delayed effect after exposure to tiger eye. After the recovery period, there is also a significant detectable signal of IL-6 secretion (60 pg/ml) after the exposure to jasper at the higher dose (500 µg/ml). Here again, a dose dependency phenomenon could be observed.

Validation of the DMEM +1% HS Culture Medium System for Long-Term (10 days) Experiments: Example of the Effects of a Cobalt-Based Pigment

The characterization of the cobalt-based pigment PB28 (cobalt blue) was carried out by transmission electronic microscopy and is shown in **Supplementary Figure S1**. Here again, micron-sized and sub-micron sized particles were observed. Preliminary experiments led to determine that the LD 20 was reached at 500 µg/ml. Corundum was used as a negative control (Wiemann et al., 2016) at the same concentration.

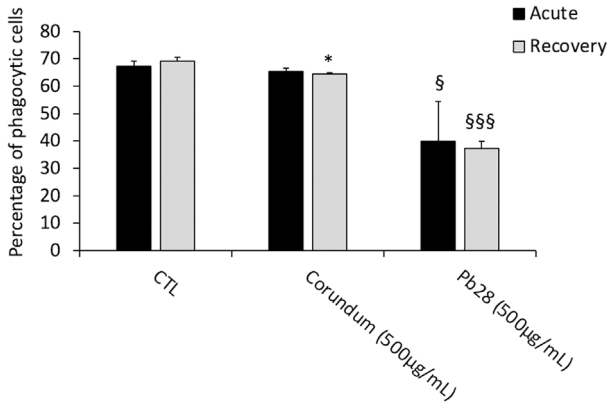

FIGURE 7 | Phagocytic capacity. Black bars; acute exposure (last day of culture = 24 h). Grey bars; recovery exposure (first day of culture = 24 h) and 9 days recovery post exposure. Percentage of cells able to phagocyte fluorescent Y/G labeled latex beads. Data are represented as Mean +SD. Significance symbols: *, significant change compared to negative control only (cells without treatment). §, significant change compared to negative control and corundum control (same concentration). Number of symbols: 1: $p < 0.05$, 2: $p < 0.01$, 3: $p < 0.001$ (Student t test, N = 3).

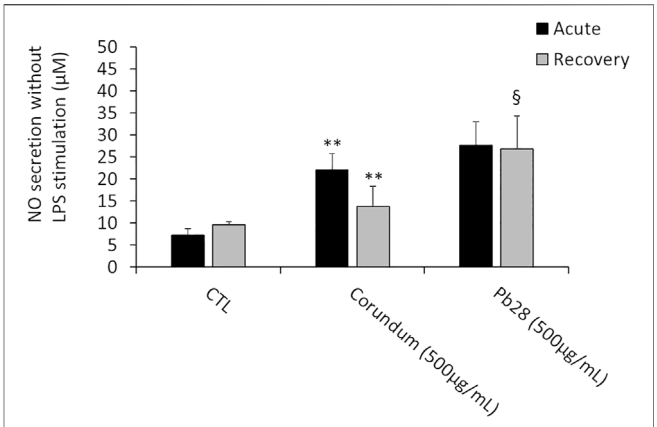

FIGURE 8 | NO secretion. Black bars; acute exposure (last day of culture = 24 h). Grey bars; recovery exposure (first day of culture = 24 h) and 9 days recovery post exposure. Data are represented as Mean +SD. Significance symbols: *, significant change compared to negative control only (cells without treatment). §, significant change compared to negative control and corundum control (same concentration). Number of symbols: 1: $p < 0.05$, 2: $p < 0.01$ (Student t test, N = 3).

Phagocytic Capacity

Results in **Figure 7** showed that for PB28 (500 µg/ml), in acute exposure mode, the percentage of phagocytic cells dropped dramatically (about 40%) when compared to controls. Interestingly enough, after the 10 days post-exposure recovery, the results showed that the proportion of phagocytic cells remained very low, as in acute exposure mode (−47% and −42% when compared to control without treatment and corundum (500 µg/ml). Regarding the corundum control, a slight decrease was observed after recovery, suggesting a slight effect due to a high concentration of particles regardless of the material used. However, we could conclude that PB28 (500 µg/ml) has a significant, long-lasting effect on the phagocytic capacity of J774A.1 macrophages.

Inflammatory Ability (Nitric Oxide and Pro-inflammatory Cytokine Secretion)

In these experiments, we assessed the intrinsic effects of particles after 10 days of culture, in acute and recovery exposure modes, after a challenge with PB28 or corundum.

NO Secretion

Without LPS stimulation and under acute exposure, the results (**Figure 8**) showed a significant increase of NO secretion for corundum-treated cells (500 µg/ml) in comparison to the negative control. For PB28-treated cells (500 µg/ml), the NO production appeared to be similar to that of corundum-treated cells. Thus, the results suggested that the internalization of a high quantity of particles had a pro-inflammatory effect for these two chemically different particles.

After 10 days post-exposure recovery (**Figure 8**), the concentration of NO released after exposure to corundum returned to values that were not significantly different from the negative controls. However, a persisting increase of NO secretion was observed for PB28-treated cells in comparison to negative controls and to corundum-treated cells.

IL-6 and TNF Secretion

In these experiments, only the intrinsic effects of corundum and cobalt blue were investigated. In the acute exposure mode, the results in **Figure 9B** showed a significant increase of IL-6 secretion for corundum (500 µg/ml) and PB28 (500 µg/ml) in comparison to control without treatment. However, despite this increase, no significant difference was observed between corundum and PB28 However, regarding TNF secretion (**Figure 9A**), even if the results also showed an increase of TNF for corundum and PB28, the TNF secretion in the presence of PB28 (3542,5 pg/ml) was significantly higher than in the presence of corundum (1878,4 pg/ml) while the basal TNF secretion in the control was 916.9 pg/ml.

In the recovery exposure mode (**Figure 9A**), the TNF secretion after 9 days of recovery was maintained at 1,308.6 and 1,677.1 pg/ml for corundum and PB28, respectively, when compared to negative control (896.4 pg/ml). Thus, regarding TNF, a persisting inflammatory effect was observed even if the values are lower than in acute exposure mode. Surprisingly enough, for IL-6 (**Figure 9B**), the concentration decreased in the presence of corundum (2.6 pg/ml) and for PB28, the concentration declined drastically (1.1 pg/ml). The results suggest persisting inflammation disorders in the presence of a high quantity of particles. This phenomenon is exacerbated in the presence of cobalt.

DISCUSSION

A critical aspect in *in vitro* toxicology is to use conditions that are as close as possible as those prevailing *in vivo*. This aspect is even more important for toxicological studies that investigate responses

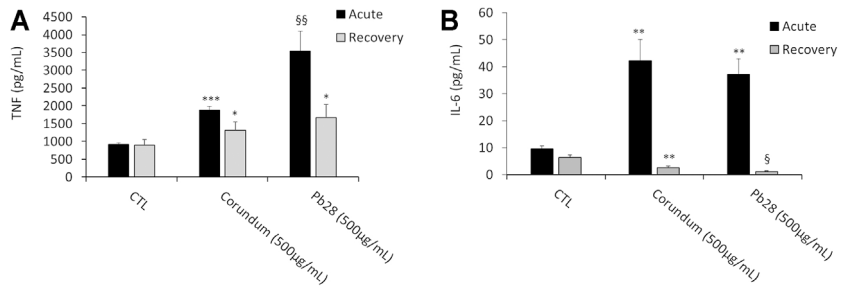

FIGURE 9 | Pro-inflammatory cytokines secretion. Black bars; acute exposure (last day of culture = 24 h). Grey bars; recovery exposure (first day of culture = 24 h) and 9 days recovery post exposure. Data are represented as Mean +SD. Panel A- TNF secretion without LPS stimulation. Panel B- IL-6 secretion without LPS stimulation. Significance symbols: *, significant change compared to negative control only (cells without treatment). §, significant change compared to negative control and corundum control (same concentration). Number of symbols: 1: $p < 0.05$, 2: $p < 0.01$, 3: $p < 0.001$ (Student t test, N = 3).

on a longer time scale than the few hours usually used in most *in vitro* toxicological studies. In this respect, the proliferation dimension is a key aspect to be taken into account in such medium/long term *in vitro* studies. Thus, for epithelial cells that proliferate at a relatively high rate *in vivo*, the proliferation must be kept in the *in vitro* systems. In the frame of toxicological studies, this has been the case for keratinocytes (Comfort et al., 2014), lung (Gliga et al., 2018; Murugadoss et al., 2021) or intestinal (Chen et al., 2016; Vila et al., 2017; Murugadoss et al., 2021) epithelial cells.

For maintaining cell proliferation fetal bovine serum is the additive of choice in cell culture. It has long been shown to be the most active serum for inducing cell proliferation in a wide variety of systems (Puck et al., 1958; Sirbasku and Kirkland, 1976; Yasin et al., 1981; Zamansky et al., 1983). Its widespread use is thus legitimate for such proliferating cells.

The situation is quite different for immune cells. In the immune system, only the immature cells proliferate, and the mature immune cells are post-mitotic. The only exceptions known are the clonal expansion of stimulated lymphocytes (Williamson et al., 1976; Lee et al., 2002), and the slow self-renewal of resident macrophages (Hashimoto et al., 2013; Ginhoux and Jung, 2014; Ginhoux and Guilliams, 2016). When using cell lines representing immune cells, the proliferation induced by fetal bovine serum becomes a problem in medium/long-term experiments.

Because of their key role in the control of the inflammatory responses, macrophages are indeed an important cell type to be tested in toxicology, and especially in the toxicology of persistent materials and chemicals. There are thus numerous publications that use *in vitro* models of macrophages to test immunotoxicity *sensu lato*, i.e., including inflammatory responses. However, most of these publications use a short-term exposure, and are thus unable to address the question of persistence. In the few papers that do address this question (Dalzon et al., 2019b; Torres et al., 2020a), or that study the effects of repeated exposures (Dalzon et al., 2020a; Torres et al., 2020b; Murugadoss et al., 2021) technical problems linked to cell proliferation were encountered. This discrepancy between the classical cell growth in culture and the negligible macrophage proliferation were addressed by working at high cell concentrations (confluency) in some cases (Dalzon et al., 2019b, 2020a; Torres et al., 2020a, 2020b) and neglected in other studies (Murugadoss et al., 2021). There is thus a need for a system that would limit cell proliferation, while keeping cell viability and functionality for an extended period.

Serum-free culture has been advocated by several authors (Wiemann et al., 2016; Leibe et al., 2019). While it does inhibit proliferation, it also exacerbates cytotoxicity and the kinetics of the cellular responses (Leibe et al., 2019). While the use of serum-free cultures may be relevant for the study of pulmonary toxicity, although this can be considered as an open question due to the presence of serum proteins in the pulmonary surfactant (Wattiez et al., 2000), serum-free cultures cannot represent the conditions prevailing in the body. Furthermore, cell viability cannot be maintained for extended time periods in serum-free culture, which precludes the use of these systems for any study on effect persistence. There is thus a need for a system that would both decrease cell proliferation and keep cell viability and functionality for extended times.

Based on this reasoning, the use of horse serum, and especially of low concentrations thereof, is an already documented, albeit rarely used, process used to decrease proliferation and increase differentiation, as described in several systems (Yaffe and Dym, 1973; Auersperg, 1978; Fedoroff and Hall, 1979; Czarnetzki and Behrendt, 1981; Brunner and Tschank, 1982; Schlüns and Drewes, 1984; Voisin et al., 1993). These systems take advantage of the different growth support properties of fetal bovine serum and of adult horse serum (Yasin et al., 1981). They use fetal bovine serum to passage and amplify the cell lines of interest. Once the adequate density required for the experiments is reached, the cells are switched to a medium containing horse serum to stop proliferation and induce differentiation (Yaffe and Dym, 1973; Auersperg, 1978; Fedoroff and Hall, 1979). The system described in the present paper works exactly on the same principle. The J774A1 cells are propagated and expanded using classical culture conditions (10% fetal bovine serum). Once the adequate density has been reached, the culture medium is changed to a medium containing only 1% horse serum.

This use of low concentrations of horse serum did decrease proliferation, favored attachment to the support, which is also a critical feature to avoid spurious cell selection by detachment from the culture support, and helped in maintaining the differentiated functions (e.g; phagocytosis or cytokine production) of macrophages cell lines over time. Moreover, in the frame of the 3R approach, the use of low concentrations of

horse serum is of higher ethical standards than the use of fetal bovine serum, as horse serum usually comes from donor herds, while fetal bovine serum comes from slaughterhouses.

The application examples showed that this culture system kept sensitivity not only to the dose but also to structure of the tested toxicants, as exemplified on the silica pigments. The culture system was able to reveal that the response did not only depend of the particle size or of the mineral, but also of its composition, form and surface. The three silica based pigments are indeed composed of silica colored by iron oxide. However, the fine structure of the three minerals differ, mostly in the fine arrangement of the quartz microcystallites in the minerals. In this comparative study, the tiger eye is the most inflammatory material. Tiger eye is composed of quartz crystals and fibers of amphibole, which is quite similar to asbestos composition (Janik and Wrona, 2017). Indeed, tiger eye is sometime considered as a variety of amosite, which is one form of asbestos. The important point of these experiments is that this simple *in vitro* system allowed demonstrating the persistence of the inflammatory effects when challenged with well-known persistent proinflammatory substances.

The second application example on the cobalt pigment showed that the positive features of the culture system could be used on a material with completely different characteristics (e.g., different chemical composition), and that the persistence of the effects could be studied on a longer time scale (at least up to 10 days) and on a variety of parameters, so that the system is not restricted to cytokine release studies.

In conclusion, the low serum culture system described here represents an easy to implement system that allows performing toxicological studies on macrophages for extended time periods, using widely-available cell lines. Such a system should increase the type and relevance of *in vitro* immunotoxicological studies.

DATA AVAILABILITY STATEMENT

The raw data supporting the conclusions of this article will be made available by the authors, without undue reservation.

AUTHOR CONTRIBUTIONS

TR and JS designed and supervised the study. AT performed the experiments on silica particles. DF performed the TEM characterization of particles. BD performed the primary validation experiments. BD and JD performed the experiments on the cobalt pigment. TR and BD drafted the initial version of the manuscript, which was completed and amended by AT DF and JS in their respective fields. All co authors approved the final version of the manuscript.

FUNDING

This work used the EM facility at the Grenoble Instruct-ERIC Center (ISBG; UMS 3518 CNRS CEA-UGA-EMBL) with support from the French Infrastructure for Integrated Structur-al Biology (FRISBI; ANR-10-INSB-05-02) and GRAL, a project of the University Grenoble Alpes graduate school (Ecoles Universitaires de Recherche) CBH-EUR-GS (ANR-17-EURE-0003). The IBS Electron Microscope facility is supported by the Auvergne Rhône-Alpes Re-gion, the Fonds Feder, the Fondation pour la Recherche Médicale and GIS-IBiSA. AT was co-financed by an Industrial PhD bursary from Solvay SA (CIFRE programme).

ACKNOWLEDGMENTS

We thank Guy Schoehn for setting up and maintaining the EM facility.

SUPPLEMENTARY MATERIAL

The Supplementary Material for this article can be found online at: https://www.frontiersin.org/articles/10.3389/ftox.2021.780778/full#supplementary-material

REFERENCES

Adams, D. O. (1979). "[43] Macrophages," in *Methods in Enzymology* (Elsevier), 494–506. doi:10.1016/S0076-6879(79)58164-6

Arts, J. H. E., Muijser, H., Duistermaat, E., Junker, K., and Kuper, C. F. (2007). Five-day Inhalation Toxicity Study of Three Types of Synthetic Amorphous Silicas in Wistar Rats and post-exposure Evaluations for up to 3months. *Food Chem. Toxicol.* 45, 1856–1867. doi:10.1016/j.fct.2007.04.001

Aude-Garcia, C., Villiers, F., Collin-Faure, V., Pernet-Gallay, K., Jouneau, P.-H., Sorieul, S., et al. (2016). Differentin Vitroexposure Regimens of Murine Primary Macrophages to Silver Nanoparticles Induce Different Fates of Nanoparticles and Different Toxicological and Functional Consequences. *Nanotoxicology* 10, 586–596. doi:10.3109/17435390.2015.1104738

Auersperg, N. (1978). Effects of Culture Conditions on the Growth and Differentiation of Transformed Rat Adrenocortical Cells. *Cancer Res.* 38, 1872–1884.

Bain, C. C., Hawley, C. A., Garner, H., Scott, C. L., Schridde, A., Steers, N. J., et al. (2016). Long-Lived Self-Renewing Bone Marrow-Derived Macrophages Displace Embryo-Derived Cells to Inhabit Adult Serous Cavities. *Nat. Commun.* 7, ncomms11852. doi:10.1038/ncomms11852

Bernal, S. D., and Chen, L. B. (1982). Induction of Cytoskeleton-Associated Proteins during Differentiation of Human Myeloid Leukemic Cell Lines. *Cancer Res.* 42, 5106–5116.

Bertram, C., von Neuhoff, N., Skawran, B., Steinemann, D., Schlegelberger, B., and Hass, R. (2008). The Differentiation/retrodifferentiation Program of Human U937 Leukemia Cells Is Accompanied by Changes of VCP/p97. *BMC Cel. Biol.* 9, 12. doi:10.1186/1471-2121-9-12

Boudard, D., Aureli, F., Laurent, B., Sturm, N., Raggi, A., Antier, E., et al. (2019). Chronic Oral Exposure to Synthetic Amorphous Silica (NM-200) Results in Renal and Liver Lesions in Mice. *Kidney Int. Rep.* 4, 1463–1471. doi:10.1016/j.ekir.2019.06.007

Brunner, G., and Tschank, G. (1982). Contracting Striated Muscle Fibres Differentiated from Primary Rat Pituitary Cultures. *Cell Tissue Res.* 224, 655–662. doi:10.1007/BF00213760

Cassado Ados, A., DImpério Lima, M. R., and Bortoluci, K. R. (2015). Revisiting Mouse Peritoneal Macrophages: Heterogeneity, Development, and Function. *Front. Immunol.* 6, 225. doi:10.3389/fimmu.2015.00225

Chen, N., Song, Z.-M., Tang, H., Xi, W.-S., Cao, A., Liu, Y., et al. (2016). Toxicological Effects of Caco-2 Cells Following Short-Term and Long-Term Exposure to Ag Nanoparticles. *Int. J. Mol. Sci.* 17, 974. doi:10.3390/ijms17060974

Comfort, K. K., Braydich-Stolle, L. K., Maurer, E. I., and Hussain, S. M. (2014). Less Is More: Long-Term *In Vitro* Exposure to Low Levels of Silver Nanoparticles Provides New Insights for Nanomaterial Evaluation. *ACS Nano* 8, 3260–3271. doi:10.1021/nn5009116

Czarnetzki, B. M., and Behrendt, H. (1981). Studies on the *In Vitro* Development of Rat Peritoneal Mast Cells. *Immunobiology* 159, 256–268. doi:10.1016/S0171-2985(81)80084-8

Dalzon, B., Bons, J., Diemer, H., Collin-Faure, V., Marie-Desvergne, C., Dubosson, M., et al. (2019a). A Proteomic View of Cellular Responses to Anticancer Quinoline-Copper Complexes. *Proteomes* 7, 26. doi:10.3390/proteomes7020026

Dalzon, B., Torres, A., Diemer, H., Ravanel, S., Collin-Faure, V., Pernet-Gallay, K., et al. (2019b). How Reversible Are the Effects of Silver Nanoparticles on Macrophages? A Proteomic-Instructed View. *Environ. Sci. Nano* 6, 3133–3157. doi:10.1039/c9en00408d

Dalzon, B., Aude-Garcia, C., Diemer, H., Bons, J., Marie-Desvergne, C., Pérard, J., et al. (2020a). The Longer the Worse: a Combined Proteomic and Targeted Study of the Long-Termversusshort-Term Effects of Silver Nanoparticles on Macrophages. *Environ. Sci. Nano* 7, 2032–2046. doi:10.1039/C9EN01329F

Dalzon, B., Torres, A., Reymond, S., Gallet, B., Saint-Antonin, F., Collin-Faure, V., et al. (2020b). Influences of Nanoparticles Characteristics on the Cellular Responses: The Example of Iron Oxide and Macrophages. *Nanomaterials* 10, 266. doi:10.3390/nano10020266

Davies, J. Q., and Gordon, S. (2004). "Isolation and Culture of Human Macrophages," in *Basic Cell Culture Protocols* (New Jersey: Humana Press), 105–116. doi:10.1385/1-59259-838-2:105

Dockery, D. W., Pope, C. A., Xu, X., Spengler, J. D., Ware, J. H., Fay, M. E., et al. (1993). An Association between Air Pollution and Mortality in Six U.S. Cities. *N. Engl. J. Med.* 329, 1753–1759. doi:10.1056/NEJM199312093292401

Fang, F. C. (2004). Antimicrobial Reactive Oxygen and Nitrogen Species: Concepts and Controversies. *Nat. Rev. Microbiol.* 2, 820–832. doi:10.1038/nrmicro1004

Fedoroff, S., and Hall, C. (1979). Effect of Horse Serum on Neural Cell Differentiation in Tissue Culture. *In Vitro* 15, 641–648. doi:10.1007/BF02623400

Ghosn, E. E. B., Cassado, A. A., Govoni, G. R., Fukuhara, T., Yang, Y., Monack, D. M., et al. (2010). Two Physically, Functionally, and Developmentally Distinct Peritoneal Macrophage Subsets. *Proc. Natl. Acad. Sci.* 107, 2568–2573. doi:10.1073/pnas.0915000107

Ginhoux, F., and Guilliams, M. (2016). Tissue-Resident Macrophage Ontogeny and Homeostasis. *Immunity* 44, 439–449. doi:10.1016/j.immuni.2016.02.024

Ginhoux, F., and Jung, S. (2014). Monocytes and Macrophages: Developmental Pathways and Tissue Homeostasis. *Nat. Rev. Immunol.* 14, 392–404. doi:10.1038/nri3671

Gliga, A. R., Di Bucchianico, S., Lindvall, J., Fadeel, B., and Karlsson, H. L. (2018). RNA-sequencing Reveals Long-Term Effects of Silver Nanoparticles on Human Lung Cells. *Sci. Rep.* 8, 6668. doi:10.1038/s41598-018-25085-5

Gutbier, S., Wanke, F., Dahm, N., Rümmelin, A., Zimmermann, S., Christensen, K., et al. (2020). Large-Scale Production of Human iPSC-Derived Macrophages for Drug Screening. *Int. J. Mol. Sci.* 21, 4808. doi:10.3390/ijms21134808

Hashimoto, D., Chow, A., Noizat, C., Teo, P., Beasley, M. B., Leboeuf, M., et al. (2013). Tissue-Resident Macrophages Self-Maintain Locally throughout Adult Life with Minimal Contribution from Circulating Monocytes. *Immunity* 38, 792–804. doi:10.1016/j.immuni.2013.04.004

Janik, H., and Wrona, M. (2017). "Asbestos ☆," in *Reference Module in Chemistry, Molecular Sciences and Chemical Engineering* (Elsevier). B9780124095472142000. doi:10.1016/B978-0-12-409547-2.14311-2

Kimura, A., Naka, T., Nakahama, T., Chinen, I., Masuda, K., Nohara, K., et al. (2009). Aryl Hydrocarbon Receptor in Combination with Stat1 Regulates LPS-Induced Inflammatory Responses. *J. Exp. Med.* 206, 2027–2035. doi:10.1084/jem.20090560

Koh, T. J., and DiPietro, L. A. (2011). Inflammation and Wound Healing: the Role of the Macrophage. *Expert Rev. Mol. Med.* 13, e23. doi:10.1017/S1462399411001943

Landén, N. X., Li, D., and Ståhle, M. (2016). Transition from Inflammation to Proliferation: a Critical Step during Wound Healing. *Cell. Mol. Life Sci.* 73, 3861–3885. doi:10.1007/s00018-016-2268-0

Lee, W. T., Pasos, G., Cecchini, L., and Mittler, J. N. (2002). Continued Antigen Stimulation Is Not Required during CD4(+) T Cell Clonal Expansion. *J. Immunol.* 168, 1682–1689. doi:10.4049/jimmunol.168.4.1682

Leibe, R., Hsiao, I.-L., Fritsch-Decker, S., Kielmeier, U., Wagbo, A. M., Voss, B., et al. (2019). The Protein corona Suppresses the Cytotoxic and Pro-inflammatory Response in Lung Epithelial Cells and Macrophages upon Exposure to Nanosilica. *Arch. Toxicol.* 93, 871–885. doi:10.1007/s00204-019-02422-9

Miller, B., Searl, A., Davis, J. M., Donaldson, K., Cullen, R. T., Bolton, R. E., et al. (1999). Influence of Fibre Length, Dissolution and Biopersistence on the Production of Mesothelioma in the Rat Peritoneal Cavity. *Ann. Occup. Hyg.* 43, 155–166. doi:10.1016/s0003-4878(99)00018-6

Murphy, J., Summer, R., Wilson, A. A., Kotton, D. N., and Fine, A. (2008). The Prolonged Life-Span of Alveolar Macrophages. *Am. J. Respir. Cel Mol. Biol.* 38, 380–385. doi:10.1165/rcmb.2007-0224RC

Murugadoss, S., Godderis, L., Ghosh, M., and Hoet, P. H. (2021). Assessing the Toxicological Relevance of Nanomaterial Agglomerates and Aggregates Using Realistic Exposure *In Vitro*. *Nanomaterials* 11, 1793. doi:10.3390/nano11071793

Oszlánczi, G., Papp, A., Szabó, A., Nagymajtényi, L., Sápi, A., Kónya, Z., et al. (2011). Nervous System Effects in Rats on Subacute Exposure by lead-Containing Nanoparticles via the Airways. *Inhalation Toxicol.* 23, 173–181. doi:10.3109/08958378.2011.553248

Petriello, M. C., Brandon, J. A., Hoffman, J., Wang, C., Tripathi, H., Abdel-Latif, A., et al. (2018). Dioxin-like PCB 126 Increases Systemic Inflammation and Accelerates Atherosclerosis in Lean LDL Receptor-Deficient Mice. *Toxicol. Sci.* 162, 548–558. doi:10.1093/toxsci/kfx275

Puck, T. T., Cieciura, S. J., and Robinson, A. (1958). Genetics of Somatic Mammalian Cells. III. Long-Term Cultivation of Euploid Cells from Human and Animal Subjects. *J. Exp. Med.* 108, 945–956. doi:10.1084/jem.108.6.945

Rovera, G., Santoli, D., and Damsky, C. (1979). Human Promyelocytic Leukemia Cells in Culture Differentiate into Macrophage-like Cells when Treated with a Phorbol Diester. *Proc. Natl. Acad. Sci.* 76, 2779–2783. doi:10.1073/pnas.76.6.2779

Schleicher, U., and Bogdan, C. (2009). "Generation, Culture and Flow-Cytometric Characterization of Primary Mouse Macrophages," in *Macrophages And Dendritic Cells Methods in Molecular Biology™*. Editor N. E. Reiner (Totowa, NJ: Humana Press), 203–224. doi:10.1007/978-1-59745-396-7_14

Schlüns, J., and Drewes, B. (1984). Isolation, Culture, and Preliminary Characterization of Ellipsoids (Sheathed Capillaries of Schweigger-Seidel) of the Pig Spleen. *Histochemistry* 81, 291–295. doi:10.1007/BF00495642

Sirbasku, D. A., and Kirkland, W. L. (1976). Control of Cell Growth. IV. Growth Properties of a New Cell Line Established from an Estrogen-dependent Kidney Tumor of the Syrian Hamster1,2. *Endocrinology* 98, 1260–1272. doi:10.1210/endo-98-5-1260

Tian, L., Lin, B., Wu, L., Li, K., Liu, H., Yan, J., et al. (2015). Neurotoxicity Induced by Zinc Oxide Nanoparticles: Age-Related Differences and Interaction. *Sci. Rep.* 5, 16117. doi:10.1038/srep16117

Torres, A., Dalzon, B., Collin-Faure, V., Diemer, H., Fenel, D., Schoehn, G., et al. (2020a). How Reversible Are the Effects of Fumed Silica on Macrophages? A Proteomics-Informed View. *Nanomaterials* 10, 1939. doi:10.3390/nano10101939

Torres, A., Dalzon, B., Collin-Faure, V., and Rabilloud, T. (2020b). Repeated vs. Acute Exposure of RAW264.7 Mouse Macrophages to Silica Nanoparticles: A Bioaccumulation and Functional Change Study. *Nanomaterials* 10, 215. doi:10.3390/nano10020215

Tsuchiya, S., Kobayashi, Y., Goto, Y., Okumura, H., Nakae, S., Konno, T., et al. (1982). Induction of Maturation in Cultured Human Monocytic Leukemia Cells by a Phorbol Diester. *Cancer Res.* 42, 1530–1536.

Vila, L., Marcos, R., and Hernández, A. (2017). Long-Term Effects of Silver Nanoparticles in Caco-2 Cells. *Nanotoxicology* 11, 771–780. doi:10.1080/17435390.2017.1355997

Voisin, P., Viratelle, O., Girault, J.-M., Morrison-Bogorad, M., and Labouesse, J. (1993). Plasticity of Astroglial Glutamate and ?-Aminobutyric Acid Uptake in Cell Cultures Derived from Postnatal Mouse Cerebellum. *J. Neurochem.* 60, 114–127. doi:10.1111/j.1471-4159.1993.tb05829.x

Wang, C., Petriello, M. C., Zhu, B., and Hennig, B. (2019). PCB 126 Induces Monocyte/macrophage Polarization and Inflammation through AhR and NF-Kb Pathways. *Toxicol. Appl. Pharmacol.* 367, 71–81. doi:10.1016/j.taap.2019.02.006

Wattiez, R., Hermans, C., Cruyt, C., Bernard, A., and Falmagne, P. (2000). Human Bronchoalveolar Lavage Fluid Protein Two-Dimensional Database: Study of Interstitial Lung Diseases. *Electrophoresis* 21, 2703–2712. doi:10.1002/1522-2683(20000701)21:13<2703:aid-elps2703>3.0.co;2-w

Wiemann, M., Vennemann, A., Sauer, U. G., Wiench, K., Ma-Hock, L., and Landsiedel, R. (2016). An *In Vitro* Alveolar Macrophage Assay for Predicting the Short-Term Inhalation Toxicity of Nanomaterials. *J. Nanobiotechnol.* 14, 16. doi:10.1186/s12951-016-0164-2

Williamson, A. R., Zitron, I. M., and McMichael, A. J. (1976). Clones of B Lymphocytes: Their Natural Selection and Expansion. *Fed. Proc.* 35, 2195–2201.

Yaffe, D., and Dym, H. (1973). Gene Expression during Differentiation of Contractile Muscle Fibers. *Cold Spring Harbor Symp. Quant. Biol.* 37, 543–547. doi:10.1101/SQB.1973.037.01.065

Yasin, R., Kundu, D., and Thompson, E. J. (1981). Growth of Adult Human Cells in Culture at Clonal Densities. *Cel Differ.* 10, 131–137. doi:10.1016/0045-6039(81)90033-6

Zamansky, G. B., Arundel, C., Nagasawa, H., and Little, J. B. (1983). Adaptation of Human Diploid Fibroblasts *In Vitro* to Serum from Different Sources. *J. Cel Sci.* 61, 289–297. doi:10.1242/jcs.61.1.289

Conflict of Interest: JS was employed by Solvay SA.

The remaining authors declare that the research was conducted in the absence of any commercial or financial relationships that could be construed as a potential conflict of interest.

Conclusion

Cette étude a mis en évidence l'importance du sérum dans la croissance cellulaire. En effet, en utilisant un sérum de cheval adulte nous avons réduit de façon importante la prolifération cellulaire, qui est un paramètre important en culture cellulaire. Nous avons également montré que les cultures de 5 et 10 jours sont possibles avec cet ajustement du milieu de culture. De plus, les cellules gardent leur fonction différenciée et répondent de manière spécifique aux matériaux d'exposition. En particulier, nous observons des réponses différentes aux pigments à base de cobalt d'une part, et aux pigments à base de silice d'autre part. Enfin et surtout, ces pigments à base de silice, cristalline ou microcristalline, voire apparentés à l'amiante (œil de tigre) ont bien montré des réponses inflammatoires persistantes sur plusieurs jours post-exposition.

I f) Etude comparative des silices amorphes de synthèse

Déterminants des effets de la silice amorphe de synthèse et dissolution

Présentation du projet

Pour approfondir le projet précédent sur la SAS pyrogénée qui a montré des effets différents de la SAS colloïdale, nous avons voulu tester s'il existait des déterminants des effets de la silice. En effet, les SAS possèdent différentes caractéristiques telles que la taille de leur particule primaire, leur surface spécifique, leur agrégation, leur procédé de fabrication, ou encore la présence de silanols à leur surface. Pour cela, nous avons utilisé 6 silices amorphes de synthèse différentes :

Tableau 2 : Matériaux utilisés pour l'étude des déterminants des effets de la silice.

Silices	**Procédé de fabrication**	**Taille de particule primaire** (nm)	**Surface spécifique** (m^2/g)	**Informations complémentaires**
SPr	Silice précipitée	13	200	
MPr	Silice précipitée	20	55	
SC	Silice colloïdale	20	220	
MC	Silice colloïdale	30	140	
SPy	Silice pyrogénée	14	200	
D	Terre de diatomée		23	1-3% Silice cristalline, naturelle
Cor	Corindon			Al_2O_3

Les silices choisies permettent d'étudier plusieurs caractéristiques une par une. En effet, en comparant par paire les effets des silices nous pouvons répondre à nos hypothèses. Concernant le mode de synthèse, il faut comparer les « Pr » *vs* les « C » *vs* la « SPy », pour la surface spécifique, la « SPr » *vs* la « MPr » ou encore la « SC » *vs* la « MC », et concernant la taille de particule primaire, il faut comparer « SPr – SC » *vs* « MPr – MC ». Enfin, la terre de diatomée permet d'étudier une silice majoritairement amorphe et naturelle, mais qui contient une part de silice cristalline (de l'ordre de 1 à 3%). Le corindon quant à lui permet de vérifier que les effets observés sont dus spécifiquement aux SAS et non à la simple internalisation d'un matériau. Afin de comprendre les différents effets observés, nous avons également dosé la quantité de silice dans les cellules, après 24h d'exposition et après 72h de récupération, par ICP-AES.

About the inflammatory effects of synthetic amorphous silica and their persistence: an in vitro study on macrophages *(article en rédaction)*

Anaëlle Torres [1,2,*], Véronique Collin-Faure [2], Daphna Fenel [3], Christine Moriscot [3,4], Guy Schoehn [3], Jacques-Aurélien Sergent [5] and Thierry Rabilloud [2*]

[1] Solvay/GBU Silica, Lyon, France, [2] Chemistry and Biology of Metals, Univ. Grenoble Alpes, CNRS UMR5249, CEA, IRIG-LCBM, F-38054 Grenoble, France, [3] Institut de Biologie Structurale, Université Grenoble Alpes, CEA, CNRS, Grenoble France, [64] Integrated Structural Biology Grenoble (ISBG) CNRS, CEA, Université Grenoble Alpes, EMBL, France, [7] Solvay SA/Toxicological and Environmental Risk Assessment unit, Brussels, Belgium

* Correspondence: anaelle.torres@cea.fr (A.T.); Thierry.Rabilloud@cnrs.fr (T.R.)

Introduction

Crystalline silica, which is widely represented in nature, is known to be the etiological agent of silicosis [1,2]. Silicosis occurs mainly from industrial activities such as mining, construction work or sandblasting, but can also occur in rare cases from residential exposure to high levels of crystalline silica dust [3]. In order to alleviate these problems but also to wide the scope of the industrial use of silica, the chemical industry has introduced the production and use of another form of silica, namely amorphous silica, which can be produced by a variety of routes, leading to products of different characteristics in terms of particle and aggregates sizes and structures. Because of the obvious parallel between the two forms of silica, extensive toxicological testing has been carried out on synthetic amorphous silica (see Napierska et al.[4] or Fruijtier-Polloth[5] for review). In particular, comparative studies between crystalline and amorphous silica have been carried out, and have concluded to a strong effect persistence for crystalline silica while the effects of amorphous silicas has been shown to be transient [6–9] for all three major types of synthetic amorphous silicas, namely colloidal, precipitated or pyrolytic.
Opposed to other nanomaterials (e.g. silver nanoparticles), which are toxic for a wide range of cell types, the effects of silica, either crystalline or amorphous, seem to be mediated mainly via their effects on macrophages, for which silica is both toxic[10,11] and pro inflammatory [12–16], while these effects are not found on other cell types [17] . Recent research has also shown that pyrolytic amorphous silica induces stronger responses than precipitate amorphous silica [18–20].

The selective toxicity of silica toward macrophages has attracted extensive research on its mechanisms [21–24], as the chemical pathways that might be at play are much less obvious than for other nanomaterials, e.g. those that can liberate toxic ions such as silver or zinc oxide. In comparison, the mechanisms by which amorphous silica induces only transient effects compared to crystalline silica has been much less studied, although it has been shown that the silicon content of lungs in rats exposed to either amorphous or crystalline silica did not change at the same rate [25]. We thus decided to investigate this phenomenon into further detail by comparing how macrophages reacted to various grades of synthetic amorphous silica after exposure, using corundum as a negative particulate control[26].

Results

Synthetic amorphous silicas characterization

The various silicas used in this study were characterized by transmission electron microscopy. The results are shown in Figure 1, and in more detail in Supplementary Figure 1.

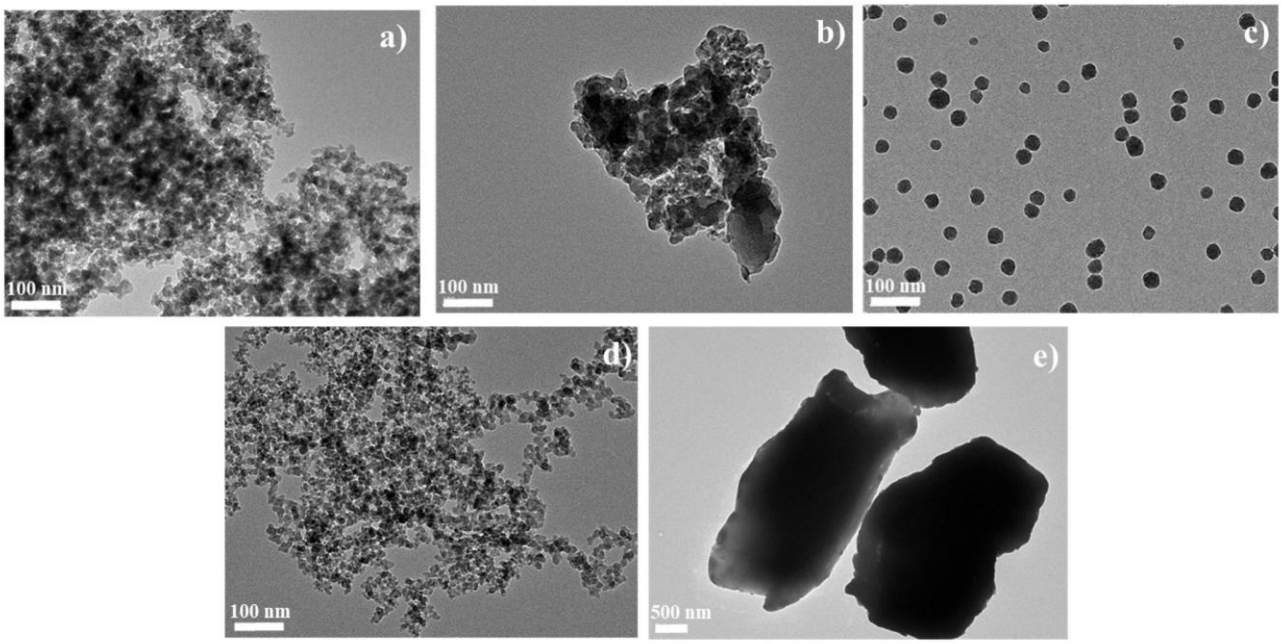

Figure 1: **SAS characterization by transmission electron microscopy**.
a) SPr: small-particle precipitated silica 220m²/g 23000x
b) MPr: medium-particle precipitated silica 55m²/g 23000x
c) MC: medium-particle colloidal silica 140m²/g 23000x
d) SPy: small-particle pyrogenic silica 200m²/g 23000x
e) Cor: Corundum ERM-FD066 Al_2O_3 2900x

As expected, the colloidal silicas consisted of well dispersed nanoparticles, and the observed sizes corresponded to the specifications. The medium-particle colloidal silica consisted of particles of a diameter close to 20 nm, while the small-particle colloidal silica consisted of particles of a diameter close to 12 nm, as previously published[27]. The precipitated silicas consisted of micrometric or submicrometric aggregates of primary particles close to 150 nm, which form in turn micrometric agglomerates. Finally, the pyrolytic silica also consisted of aggregates (micron range size) of primary particles close to 10 nm in size[27] .

Effects of silica on macrophages

Effects on phagocytosis

First, we tested the effects of SAS exposure on the phagocytic capabilities of the cells. The results, shown on Figure 2, indicated that all SAS with small primary particle sizes induced a transient decrease in the percentage of phagocytic cells. The intrinsic cell phagocytic activity, measured through the number of internalized fluorescent beads, was decreased just after exposure to small-particle colloidal silica or pyrolytic silica, but was increased after the recovery period for cells exposed to small-particle colloidal silica.

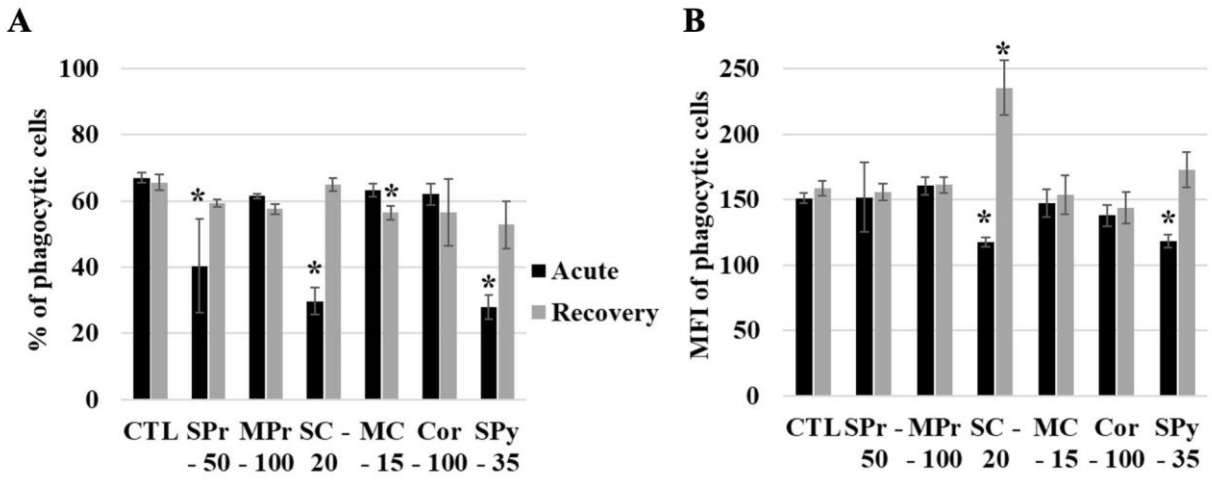

Figure 2: **Phagocytic activity of cells exposed to SiO_2** particles, by flow cytometry. The acute exposure is (or not) followed by a 72-hour recovery period.
CTL: control cells, SPr: small-particle precipitated silica 220m²/g, MPr: medium-particle precipitated silica 55 m²/g, SC: colloidal 220 m²/g, MC: colloidal 140m²/g, Cor: corundum, SPy: small-particle pyrogenic silica 200m²/g. Black bars for acutely exposed cells, grey bars for recovery protocol.
A Proportion of phagocytic cells
B Phagocytic activity of the cells

Effects on cytokine production

As silica is known to induce a pro-inflammatory reaction in macrophages, we examined the secretion of the two inflammatory cytokines TNFα and IL-6. The results, shown in Figure 3, indicated a small response for IL-6 only for cells exposed to small-particle colloidal silica. For TNF, all SAS induced an increased secretion juste after exposure. At the end of the recovery period, this TNF secretion decreased (while remaining higher than for control cells) except for the two colloidal SAS where an increase of secretion was observed at the end of the recovery period compared to immediately after exposure. When the cells were stimulated with LPS for the last 24 hours in culture, a synergistic LPS-SAS effect was observed in IL-6 secretion for all SAS but pyrolytic SAS just after exposure. This effect was not observed at the end of the recovery period except for pyrolytic SAS, where it appeared. For TNF secretion, a synergistic LPS-SAS effect was observed just after exposure for cells exposed to small-particles colloidal SAS or pyrolytic SAS. This effect disappeared at the end of the recovery period but was detected in cells exposed to medium-particle precipitated SAS.

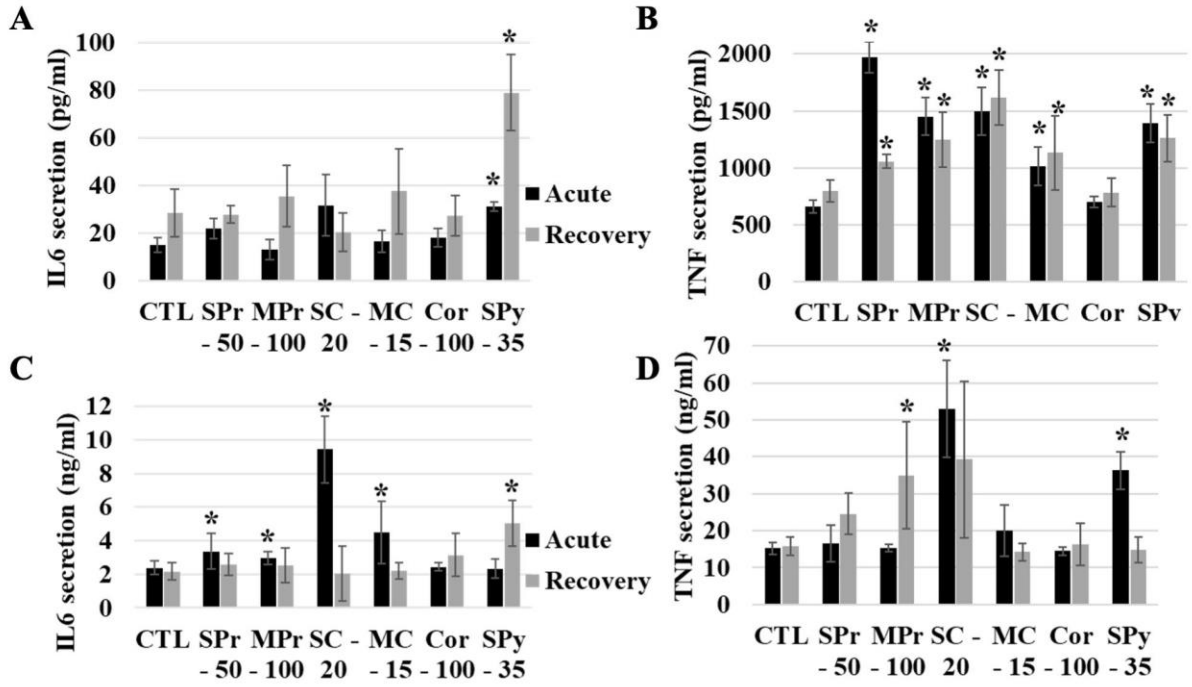

Figure 3: **Cytokine responses of cells exposed to SiO_2** particles and stimulated or not with lipopolysaccharides, by flow cytometry. The acute exposure is (or not) followed by a 72-hour recovery period. CTL: control cells, SPr: small-particle precipitated silica 220m²/g, MPr: medium-particle precipitated silica 55 m²/g, SC: colloidal 220 m²/g, MC: colloidal 140m²/g, Cor: corundum, SPy: small-particle pyrogenic silica 200m²/g. Black bars for acutely exposed cells, grey bars for recovery protocol.

A Intrinsic IL-6 secretion of cells exposed to SiO_2: Cells acutely exposed to MC have a significant increase of their IL-6 secretion
B Intrinsic TNF secretion
C IL-6 secretion after a LPS stimulation
D TNF secretion after a LPS stimulation

Silica uptake and persistence in cells

To determine the silica uptake, the cells were incubated with the silica-containing media for 24 hours. After this exposure period, the cell culture medium was removed, the cell layer was rinsed and then lysed directly in an adequate buffer. An aliquot of this cell extract suspension was then submitted to the mineralisation and silicon assay procedure to determine the amount of silica that had been taken by the cells, while another aliquot was used to determine the amount of cellular proteins in the extract, thereby affording a control related to the number of cells present in the culture well. The results are shown in Table 1A.
Because of the varied input silica concentrations, the amount of silica internalized by the cells was variable from one synthetic amorphous silica to another. Nevertheless, the proportion of silica internalized by the cells varied from ca 15% (pyrolytic silica) to 40% (medium-particle precipitated silica). When a statistical analysis (ANOVA + Tukey's pairwise test) was performed, the uptake of the pyrolytic silica was found different from the uptake of all other silica except for the small-particle precipitated silica. There was thus no correlation between the uptake and the size of the primary particle, nor with the overall size of the aggregates.

To determine the persistence of the silica itself in cells post-exposure, the cells were exposed to synthetic amorphous silicas for 24 hours. The silica-containing medium was then removed and replaced by fresh complete culture medium without silica, and the cells were let to recover in this medium for 72 hours, with one medium change at 36 hours to avoid exhaustion and keep the cells viable. The results, shown in Table 1B, showed a significant decrease in the amount of synthetic amorphous silicas still present in the cells after the 72 hours recovery period, with only one fifth to one third of the initial internalized dose still present in the cells after the recovery period.

Table 1: silica dosage in cells exposed to various SAS

A) Acute exposure

Cell lysate

Condition	mean measured amount/well (ng)	mean of corrected amount*	mean ng Si/µg proteins	fraction silica incorporated in cells
CTL	0	0.000	0.000	N/A
SC - 20	4.800	11.950	8.646	0.299
MC - 15	5.039	10.555	5.798	0.352
SPr - 100	10.816	40.767	38.857	0.204
MPr - 100	14.960	80.822	53.145	0.404
SPy - 35	3.964	10.225	5.698	0.146

B) Recovery

Cell lysate

Condition	mean measured amount/well (ng)	mean of corrected amount	mean ng Si/µg prot	fraction silica incorporated in cells	ratio D4/D1
CTL	0.000	0.000	0.000	N/A	
SC - 20	1.332	3.544	1.476	0.089	0.297
MC - 15	0.952	2.194	1.560	0.073	0.208
SPr - 100	3.895	14.169	5.893	0.071	0.348
MPr - 100	35.525	169.102	77.850	0.846	2.092
SPy - 35	1.140	3.340	1.606	0.048	0.327

*: the yield-corrected amount is calculated by dividing the measured amount by the mineralisation yield determined in Supplementary Table 1. N=3 biological replicates, 3 silicon measurements per sample

An intriguing result was however observed for the medium-particle precipitated silica, where an apparent increase of the silicon concentration was observed at the end of the recovery period compared to the condition just after exposure. As the experimental scheme does not allow this to happen, the only remaining explanation possible was that the amorphous silica became more easily mineralisable in the cells during the recovery period. In order to test this hypothesis, we suspended synthetic amorphous silicas in complete cell culture medium for 4 days at 37°C. This medium was chosen as a proxy for the cellular cytosol, as the complete culture medium and the cellular cytosol share many common characteristics such as pH, osmolarity, ionic composition and presence of high concentrations of a wide variety of proteins.

As sedimentation of the silicas may have occurred over the 4 days period and may be quite different from one synthetic amorphous silica to another, the culture medium incubated with silicas was homogeneized by repeated pipetting before collection. In order to gain further insights into the phenomena that may have occurred, a portion of the medium after the 4 days incubation and imaged by

TEM (Figure S2). Another portion was centrifuged at 15,000g for 45 minutes, in order to remove the large aggregates, and the supernatant was assayed for silicon with the same procedure.

When comparing the results, shown in Table 2, with those shown on Table S1, a significant increase in the mineralisation yield could be observed after a 4 days incubation in complete culture medium for all conditions. The increase observed in this particular medium did not fully explain, however, the increase showed in the cellular amount of mineralisable silica for the medium-particle precipitated silica.

Table 2

D4 DMEM	Mean amount measured (µg/ml)	mineralisation yield	ratio D4/D0 (yield)
DMEM	0.000		
SPr - 100	58.688	0.587	2.196
MPr - 100	32.784	0.328	1.729
SPy - 100	67.371	0.674	1.711

D4 DMEM centrifuged	Mean amount measured (µg/ml)	Non sedimentable fraction
DMEM	0.000	
SPr - 100	37.816	0.644
MPr - 100	22.368	0.682
SPy - 100	41.675	0.619

Another striking phenomenon is the fact that 2/3 of the measurable silica at 4 days appeared in the supernatant fraction, indicating a partial disaggregation of the synthetic amorphous silica under biotic conditions. In order to calibrate our centrifugation procedure, we used fluorescent polystyrene beads (spherical, d=1.05) of various sizes. This experiment (suppl Table X) showed that our centrifugation procedure was able to completely sediment all polystyrene particles with a diameter equal or greater than 200 nm, while 100 nm diameter particles were sedimented with an efficiency of ca 50%. Thus, it is highly likely that the silica present in the supernatant is at least nanoparticular or dissolved as silicate.

Synthetic amorphous silica observation after four days in cells

In order to gain insights into the two above-mentioned hypotheses, we first imaged the synthetic amorphous silicas incubated for 4 days in culture medium by transmission electron microscopy. The results, shown in Supplementary Figures X and Y, showed a strong remodeling of all amorphous silicas, with an aggregation of the colloidal silicas, but a partial disaggregation of the precipitated and a disappearance of the chain-like structure of the pyrolytic silica. In addition, we observed very small particles in the pyrolytic and precipitated silicas samples, which may explain the lesser proportion of sedimentable silica after the recovery period. In order to investigate the fate of SAS in cells, we exposed macrophages for 24 hours to SAS and let them recover without SAS. We then lysed the cells and imaged the silica by TEM. The results, shown in Figure 4, showed an aggregation of the colloidal silica, but a strong disaggregation of precipitated and pyrolytic silica.

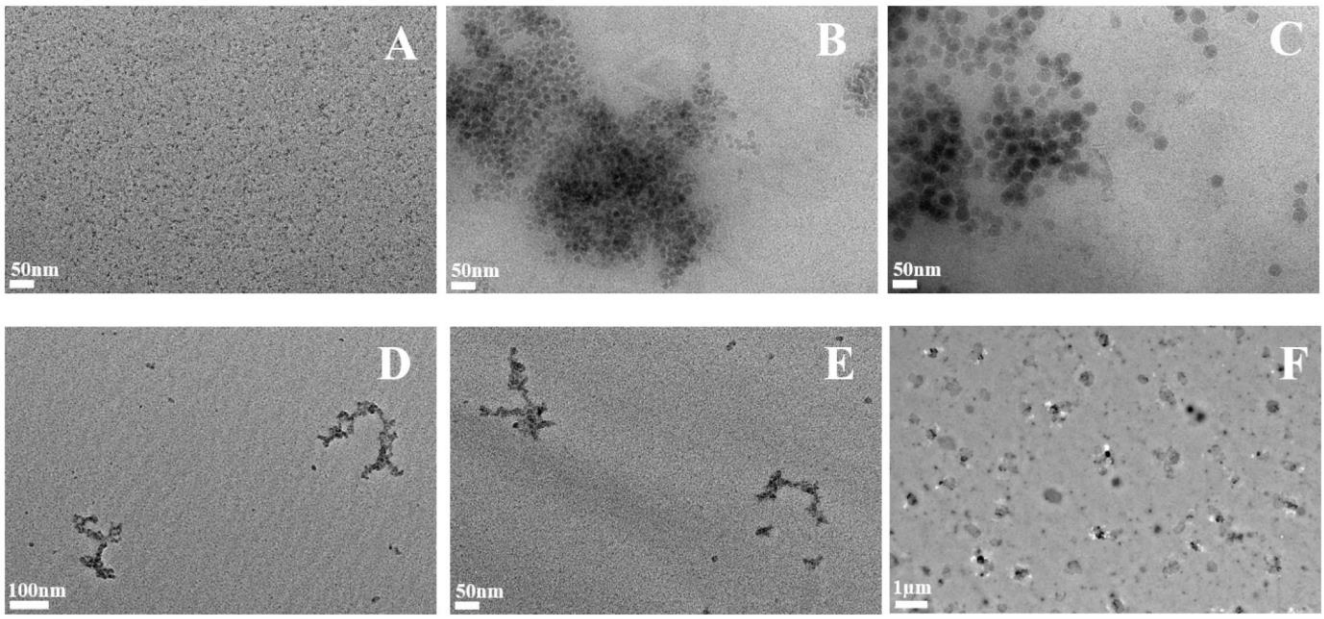

Figure 4: Examination by TEM of SAS extracted from cells
Macrophage cells were exposed to SAS for 24 hours and let to recover for 72 hours. At the end of the culture the cells were recovered, lysed and the lysate digested sequentially by a nuclease and a protease. The clarified lysate was examined by TEM to investigate the state of the internalized SAS.
A: control cells (no silica treatment) magnification 30,000x
B : SC: small-particle colloidal silica 220m²/g 30,000x
C: MC: medium-particle colloidal silica 140m²/g 30,000x
D: SPr: small-particle precipitated silica 220m²/g 23000x
E: MPr: medium-particle precipitated silica 55m²/g 23000x
F: SPy: small-particle pyrogenic silica 200m²/g 23000x

Discussion

With a yearly production (and use) in millions of tons worldwide, understanding the factors governing the adverse effects of SAS is an important topic in the field of nanosafety, especially in the general frame of silica toxicity and silicosis. Considerable efforts have been devoted to unravel the structural bases of silica toxicity [21–24] , but their application in the field of SAS are not straightforward. For colloidal silicas the influence of the particle size has been demonstrated [28,29]. For more aggregated silicas, which represent the highest part of SAS produced, a "divide and conquer" strategy has been used to demonstrate that small aggregates were more toxic than large ones [30]. This latter approach is however not devoid of issues, as the fracturation process used to disrupt the large aggregates may produce the reactive entities that cause silica adverse effects[23,24] .This is why we rather chose to compare different commercial SAS with different parameters to gain insights into the determinants of SAS adverse effects. It appears that the principal driver of toxicity is the overall particle size, with colloidal silicas being more toxic than more aggregated ones. The difference, however, was lesser than one order of magnitude, showing that all SAS exhibit a somewhat similar toxicity. When going into more details into the adverse effects of SAS on macrophages, the second important driver was the specific surface area. The SAS with the lowest specific surface area ($55m^2/g$) was both the least toxic and the one with the lowest effects, even when used at a higher concentration than the other ones. Quire remarkably, the adverse effects did not correlate well with the amount of SAS internalized. This represents a way to be explored when designing new SAS with lower biological adverse effects.

When pursuing this goal of "safe by design" SAS, the second key point is the persistence of the effects, a crucial parameter in the chronic inflammation present in silicosis. In vivo studies have shown that the pulmonary effects of SAS are transient [6–8], and this is correlated with a decrease of the amount of silica (measured through elemental Si) in the lungs [9]. However, two widely different hypotheses can explain the SAS elimination process. Once the silica has been captured by the macrophages, either the particle-laden macrophages are eliminated as a whole, as described for TiO_2 particles [31], or the silica is dissolved in the macrophages and then eliminated, e.g. as silicate. To test the second hypothesis, we measured the silicon levels in macrophages exposed to SAS immediately after exposure and after a 72 h post-exposure recovery period. Silicon elimination was observed confirming this hypothesis. Furthermore, were able to observe a disaggregation of precipitated and pyrolytic SAS in macrophages at the end of this recovery period, while colloidal silicas, which had the most persistent effects in our system, were aggregated by the macrophages, a paradoxical behavior that certainly deserves further investigation.
Overall, these results strongly argue for an intracellular dissolution process after silica uptake by the macrophages as the SAS elimination process. This further shows the variety of the particles elimination processes, which can range from particle dissolution (as shown here or for metal-based nanoparticles[32,33]) to macrophage-mediated elimination, either direct [31] or indirect[34], or translocation through the epithelia into secondary organs [35]. Although simple in vitro systems can investigate easily only mechanisms linked to one cell type, they can do it in detail, as shown here for the investigation of the short effect persistence for SAS.

Methods

SAS observation and characterization

In this work, five different synthetic amorphous silicas (SAS) were used:
i) a colloidal silica with small (12 nm) particles, purchased from Sigma-Aldrich (# 420808), thereafter designated as SC. This silica shows a specific area of 220m2/g
ii) a colloidal silica with medium (22 nm) particles, purchased from Sigma-Aldrich (# 420778), thereafter designated as MC. This silica shows a specific area of 140 m2/g
iii) a precipitated silica with small (13 nm) primary particles, from Solvay Silica thereafter designated as SPr. This silica shows a specific area of 220m2/g
iv) a precipitated silica with medium (20 nm) primary particles, from Solvay Silica thereafter designated as MPr. This silica shows a specific area of 55 m2/g
v) a pyrolytic silica with small (12 nm) primary particles, purchased from VWR (# ACRO403731500) thereafter designated as SPy. This silica shows a specific area of 200m2/g
For material characterization with TEM microscopy: samples were diluted to 100µg/ml. Negative Stain On Grid Technique (SOG): 10 µL was added to a glow discharge grid coated with a carbon supporting film for 5 minutes. The excess solution was soaked off by a filter paper and the grid was air-dried. The images were taken under low dose conditions (<10 $e^-/Å^2$) with defocus values between 1.2 and 2.5 µm on a Tecnai 12 LaB6 electron microscope at 120 kV accelerating voltage using CCD Camera Gatan Orius 1000.

Viability assay

The lethal dose 20 were determined for each SAS. The cells were seeded in 6-well culture plates at 600,000 cells/ml in DMEM FBS 10%, and left for 24 hours at 37°C and 5% CO_2 for cell adhesion. Then, cells were exposed for 24 hours to the indicated doses of SAS. The cells were harvested in phosphate buffer saline (PBS 1X), and centrifuged 5minutes at 200g. The pellets were resuspended in PBS

1X with 1µg/ml propidium iodide (excitation 533 nm, and emission 617 nm; Merck P4864). Cells were analyzed with FacsCalibur flow cytometer (Becton Dickinson) by using CellQuestPro software.

Nanoparticles

The SAS were suspended in water at 10mg/ml, they were sonicated in an ultrasonic bath for 10 minutes and then they were incubated overnight at 80°C in a preheated water bath. SAS were sonicated again for 10 minutes before to be used.

Cell culture

The murine macrophage cell line J774A1, obtained from the European Cell Culture Collection (Salisbury, UK) , was used for the cellular internalization studies. The cells were routinely grown on non adherent plastic vessels in DMEM supplemented with 10% fetal bovine serum, and transferred to adherent 6-well plates for exposure to silica, as described below.

For treatment with SAS, cells were seeded at 300,000 cells/mLin DMEM HS1% and left for 72 h at 37 °C for cell adhesion and for growth at confluence. The cells were then treated using the following scheme: the control cells were not exposed to SAS. The recovery scenario consists in an acute exposure (24 hours) followed by a 72 hours period without any SAS. The acutely exposed cells were exposed to SAS for 24 hours in the same time than the last 24 hours of recovery of the secondary scenario cells (in order to have cells with the same ageing on plates)[36]. In this study, we have used 15µg/ml for colloidal silica 140m²/g (MC), 20µg/ml for colloidal silica 220m²/g (SC), 50 µg/ml for small-particle precipitated silica (SPr), 100µg/ml for medium-particle precipitated silica (MPr) and for corundum (Cor). Except for corundum, these doses corresponded to the LD20 of the various forms of SAS, previously determined in preliminary experiments.

Phagocytic activity assay

This experiment allows evaluating the phagocytic capacity of the cells. Indeed, the fluorescent latex beads have a diameter of 1µm, which corresponds to the size of bacteria. Briefly, after the exposure (acute or recovery period), the cells were exposed for 3 hours to FITC-latex beads (previously coated in a FBS 10%—PBS 1X solution for 30 min at 37 ◦C, Sigma L4655, excitation 492nm, emission 517nm). Then cells were harvested and washed with PBS, centrifuged 5 min at 1200 rpm, the pellets were suspended with 3 mL of water for a few seconds and 1 mL of NaCl (3.5%) was added under vortex mixing to restore the osmotic pressure. The cells were centrifuged and the pellets were resuspended with 200 µL of PBS 1X—Propidium iodide 1 µg/mL, and analyzed by flow cytometry.

Nitric oxide production dosage

As previously, cells were grown into 6-well plates and exposed to the indicated dose of silica particles for twenty-four hours (followed or not by a recovery period) at 37 ◦C. The cells were also primed or not with LPS (100 ng/mL) for the last 18 h of culture. L-arginine monohydrochloride (5mM) was also added for 18 h, the supernatants are collected and centrifuged to eliminate non adherent cells. Then, 300 µL of Griess reagent were added to 300 µL of supernatants, from sample and standards (0 to 50 µM in NO2 using a Standard Nitrite solution). The mixture was incubated at room temperature for 20 min, and the absorbance read at 540 nm with a Jenway 7315 spectrophotometer.

Cytokine secretion dosages

The supernatants were obtained as described above. The experiment was carried out with the Cytometric Bead Array Mouse Inflammation Kit (BD Biosciences), and analyzed with FCAP Array software (3.0, BD Biosciences). This Flex-set kit allows measuring Interleukin-6 (IL-6) and TNF protein levels in a single sample. The mixed capture beads were added to the all assay tubes containing supernatant samples and standards (from 0 to 5000 pg/mL), the mouse inflammation phycoerythrin (PE, excitation 488 nm, emission 575 nm) detection reagent was added, and the mixture was incubated for 2 h at room temperature, protected from light. The wash buffer was added to each tube, which were then centrifuged 5 min at 200g, the pellets were resuspended with the wash buffer, and analyzed by FacsCalibur flow cytometer.

SAS quantification by ICP-AES

Sample preparation:
For SAS quantification in water or medium (DMEM HS 1%), the SAS were added in T25 flask at a final concentration of 100µg/ml. The first sample was taken at Day 0, and allowed to determine the mineralization efficiency for each SAS. The flasks were then incubated for four days at 37°C, and then, the second sample was taken.
For SAS internalization and quantification in the cells, the cells were grown on adherent 6-well plates in DMEM supplemented with 1% horse serum (DMEM HS 1%). The scheme of exposure had already been described in[36,37] . The acutely exposed cells were exposed for 24 hours, and lysed at the end of the exposure. The recovery cells were exposed for 24 hours, in parallel to the acutely ones, and this exposure was followed by a 72 hours recovery period without any SAS and with one medium change. Then, the cells were lysed as the acutely exposed cells. The lysis solution contained 5mM HEPES pH 7.5, 0.75 mM spermine tetrahydrochloride, and 0.1% SB 3-14. One milliliter of lysis solution was added in the wells, after the medium had been removed and the cell layer washed once with PBS. After quantification of proteins in each lysate with Bradford assay [38] , the lysates were aliquoted and frozen. The day before the quantification by ICP-AES, the samples were mineralized: in each sample, an equal volume of 1N potassium hydroxide was added, the samples were then incubated overnight at 80°C in a preheated water bath[39,40]

ICP-AES dosage:
The standards were first prepared, in HNO_3 10%, the standard was purchased from Sigma-Aldrich (ref 92091). At the end of the standard measurement, samples were prepared two at a time (base-mineralized silica is not stable in HNO_3): from 125µl to 500µl of mineralisate was added to *qsp* 6ml of HNO_3 10%. The samples were measured in a ICP-AES Shimadzu 9000 with ICPE solution Launcher software.

For TEM analysis of internalized SAS by macrophages, cells were exposed to SAS as described above. After the recovery scenario or the acute exposure, the cells were harvested in PBS 1X and centrifuged. The pellets were lysed in HEPES buffer 10mM, MgCl2 2mM (10 volume of lysis solution for 1 volume of cell pellet). Serratia marcescens nuclease (Benzonase ®, ref 71206-3 from Sigma) was added at the concentration of 5U/ml , and the cells were incubated at 37°C under stirring, for 6 hours. Then, a solution containing Proteinase K (ref P4850 Sigma) and CaCl2 was added (final concentrations 100µg/ml and 2mM respectively). The cells were incubated overnight. Then, the solutions were stocked at 4°C until the use in TEM, the same day. These samples were analyzed by TEM with the same parameters than described above.

ACKNOWLEDGEMENTS

This work used the EM facilities at the Grenoble Instruct-ERIC Center (ISBG; UMS 3518 CNRS CEA-UGA-EMBL) with support from the French Infrastructure for Integrated Structural Biology (FRISBI; ANR-10-INSB-05-02) and GRAL, a project of the University Grenoble Alpes graduate school (Ecoles Universitaires de Recherche) CBH-EUR-GS (ANR-17-EURE-0003) within the Grenoble Partnership for Structural Biology. The IBS Electron Microscope facility is supported by the Auvergne Rhône-Alpes Region, the Fonds Feder, the Fondation pour la Recherche Médicale and GIS-IBiSA.

This work used the ICP-AES platform from IRIG-DIESE-LCBM laboratory. We thank Dr. J. Pérard for his assistance with the ICP-AES experiments.

REFERENCES

1. Silicosis and Silicate Disease Committee. Diseases associated with exposure to silica and nonfibrous silicate minerals. *Arch Pathol Lab Med* **112**, 673–720 (1988).
2. American Thoracic Society Committee of the Scientific Assembly on Environmental and Occupational Health. Adverse effects of crystalline silica exposure. *Am J Respir Crit Care Med* **155**, 761–768 (1997).
3. Norboo, T. *et al.* Silicosis in a Himalayan village population: role of environmental dust. *Thorax* **46**, 341–343 (1991).
4. Napierska, D., Thomassen, L. C., Lison, D., Martens, J. A. & Hoet, P. H. The nanosilica hazard: another variable entity. *Part Fibre Toxicol* **7**, 39 (2010).
5. Fruijtier-Polloth, C. The toxicological mode of action and the safety of synthetic amorphous silica-A nanostructured material. *Toxicology* **294**, 61–79 (2012).
6. Warheit, D. B., McHugh, T. A. & Hartsky, M. A. Differential pulmonary responses in rats inhaling crystalline, colloidal or amorphous silica dusts. *Scand J Work Environ Health* **21 Suppl 2**, 19–21 (1995).
7. Johnston, C. J. *et al.* Pulmonary chemokine and mutagenic responses in rats after subchronic inhalation of amorphous and crystalline silica. *Toxicol Sci* **56**, 405–13 (2000).
8. Sayes, C. M., Reed, K. L. & Warheit, D. B. Assessing toxicity of fine and nanoparticles: comparing in vitro measurements to in vivo pulmonary toxicity profiles. *Toxicol Sci* **97**, 163–80 (2007).
9. Arts, J. H. E., Muijser, H., Duistermaat, E., Junker, K. & Kuper, C. F. Five-day inhalation toxicity study of three types of synthetic amorphous silicas in Wistar rats and post-exposure evaluations for up to 3 months. *Food and Chemical Toxicology* **45**, 1856–1867 (2007).
10. Costantini, L. M., Gilberti, R. M. & Knecht, D. A. The Phagocytosis and Toxicity of Amorphous Silica. *Plos One* **6**, (2011).
11. Breznan, D. *et al.* Differential cytotoxic and inflammatory potency of amorphous silicon dioxide nanoparticles of similar size in multiple cell lines. *Nanotoxicology* 1–45 (2017).

12. Park, M. *et al.* In vitro evaluation of cytotoxic and inflammatory properties of silica nanoparticles of different sizes in murine RAW 264.7 macrophages. *Journal of Nanoparticle Research* **13**, 6775–6787 (2011).
13. Panas, A. *et al.* Screening of different metal oxide nanoparticles reveals selective toxicity and inflammatory potential of silica nanoparticles in lung epithelial cells and macrophages. *Nanotoxicology* **7**, 259–273 (2013).
14. Wang, X., Sun, B. B., Liu, S. J. & Xia, T. Structure activity relationships of engineered nanomaterials in inducing NLRP3 inflammasome activation and chronic lung fibrosis. *Nanoimpact* **6**, 99–108 (2017).
15. Sandberg, W. J. *et al.* Comparison of non-crystalline silica nanoparticles in IL-1 beta release from macrophages. *Particle and Fibre Toxicology* **9**, (2012).
16. Fritsch-Decker, S., Marquardt, C., Stoeger, T., Diabaté, S. & Weiss, C. Revisiting the stress paradigm for silica nanoparticles: decoupling of the anti-oxidative defense, pro-inflammatory response and cytotoxicity. *Arch Toxicol* **92**, 2163–2174 (2018).
17. Uboldi, C. *et al.* Amorphous silica nanoparticles do not induce cytotoxicity, cell transformation or genotoxicity in Balb/3T3 mouse fibroblasts. *Mutation Research/Genetic Toxicology and Environmental Mutagenesis* **745**, 11–20 (2012).
18. Zhang, H. Y. *et al.* Processing Pathway Dependence of Amorphous Silica Nanoparticle Toxicity: Colloidal vs Pyrolytic. *Journal of the American Chemical Society* **134**, 15790–15804 (2012).
19. Di Cristo, L. *et al.* Proinflammatory Effects of Pyrogenic and Precipitated Amorphous Silica Nanoparticles in Innate Immunity Cells. *Toxicological Sciences* **150**, 40–53 (2016).
20. Sun, B. B. *et al.* Repetitive Dosing of Fumed Silica Leads to Profibrogenic Effects through Unique Structure-Activity Relationships and Biopersistence in the Lung. *ACS Nano* **10**, 8054–8066 (2016).
21. Fubini, B. *et al.* Relationship between Surface Properties and Cellular Responses to Crystalline Silica: Studies with Heat-Treated Cristobalite. *Chem. Res. Toxicol.* **12**, 737–745 (1999).
22. Ghiazza, M. *et al.* Does vitreous silica contradict the toxicity of the crystalline silica paradigm? *Chem Res Toxicol* **23**, 620–9 (2010).

23. Turci, F. *et al.* Revisiting the paradigm of silica pathogenicity with synthetic quartz crystals: the role of crystallinity and surface disorder. *Part Fibre Toxicol* **13**, 32 (2016).
24. Pavan, C. *et al.* Nearly free surface silanols are the critical molecular moieties that initiate the toxicity of silica particles. *Proc Natl Acad Sci USA* **117**, 27836–27846 (2020).
25. Reuzel, P. G., Bruijntjes, J. P., Feron, V. J. & Woutersen, R. A. Subchronic inhalation toxicity of amorphous silicas and quartz dust in rats. *Food Chem Toxicol* **29**, 341–54 (1991).
26. Wiemann, M. *et al.* An in vitro alveolar macrophage assay for predicting the short-term inhalation toxicity of nanomaterials. *J Nanobiotechnol* **14**, 16 (2016).
27. Dussert, F. *et al.* Toxicity to RAW264.7 Macrophages of Silica Nanoparticles and the E551 Food Additive, in Combination with Genotoxic Agents. *Nanomaterials (Basel)* **10**, E1418 (2020).
28. Rabolli, V. *et al.* Influence of size, surface area and microporosity on the *in vitro* cytotoxic activity of amorphous silica nanoparticles in different cell types. *Nanotoxicology* **4**, 307–318 (2010).
29. Decan, N. *et al.* Characterization of in vitro genotoxic, cytotoxic and transcriptomic responses following exposures to amorphous silica of different sizes. *Mutation Research/Genetic Toxicology and Environmental Mutagenesis* **796**, 8–22 (2016).
30. Murugadoss, S. *et al.* Is aggregated synthetic amorphous silica toxicologically relevant? *Part Fibre Toxicol* **17**, 1 (2020).
31. Kreyling, W. G. *et al.* Quantitative biokinetics over a 28 day period of freshly generated, pristine, 20 nm titanium dioxide nanoparticle aerosols in healthy adult rats after a single two-hour inhalation exposure. *Part Fibre Toxicol* **16**, 29 (2019).
32. Beck-Speier, I. *et al.* Soluble iron modulates iron oxide particle-induced inflammatory responses via prostaglandin E(2)synthesis: In vitro and in vivo studies. *Part Fibre Toxicol* **6**, 34 (2009).
33. Kreyling, W. G. *et al.* Quantitative biokinetics over a 28 day period of freshly generated, pristine, 20 nm silver nanoparticle aerosols in healthy adult rats after a single 1½-hour inhalation exposure. *Part Fibre Toxicol* **17**, 21 (2020).
34. Semmler-Behnke, M. *et al.* Efficient elimination of inhaled nanoparticles from the alveolar region: evidence for interstitial uptake and subsequent reentrainment onto airways epithelium. *Environ Health Perspect* **115**, 728–733 (2007).

35. Semmler, M. *et al.* Long-term clearance kinetics of inhaled ultrafine insoluble iridium particles from the rat lung, including transient translocation into secondary organs. *Inhal Toxicol* **16**, 453–459 (2004).
36. Dalzon, B. *et al.* A Low-Serum Culture System for Prolonged in Vitro Toxicology Experiments on a Macrophage System. *Front. Toxicol.* **3**, 780778 (2021).
37. Torres, A. *et al.* How Reversible Are the Effects of Fumed Silica on Macrophages? A Proteomics-Informed View. *Nanomaterials (Basel)* **10**, 1939 (2020).
38. Rabilloud, T. Optimization of the cydex blue assay: A one-step colorimetric protein assay using cyclodextrins and compatible with detergents and reducers. *PLoS One* **13**, e0195755 (2018).
39. Decuzzi, P. *et al.* Size and shape effects in the biodistribution of intravascularly injected particles. *J Control Release* **141**, 320–327 (2010).
40. Viveros, R. D., Liberman, A., Trogler, W. C. & Kummel, A. C. Alkaline and ultrasonic dissolution of biological materials for trace silicon determination. *Journal of Vacuum Science & Technology B, Nanotechnology and Microelectronics: Materials, Processing, Measurement, and Phenomena* **33**, 031803 (2015).

Supplementary data

Viability studies

in a first series of experiments, we determined which concentrations of the various synthetic amorphous silicas could be used on the macrophages, by performing viability assays. The results, shown in Figure 2, led us to the highest concentrations that could be used without inducing massive cell death. These concentrations ranged from 15-20µg/ml for the colloidal silicas to 100µg/ml for the precipitated silicas, the pyrolytic one being intermediate with a usable concentration of 35µg/ml.
Once these concentrations were determined, they were used in the uptake experiments

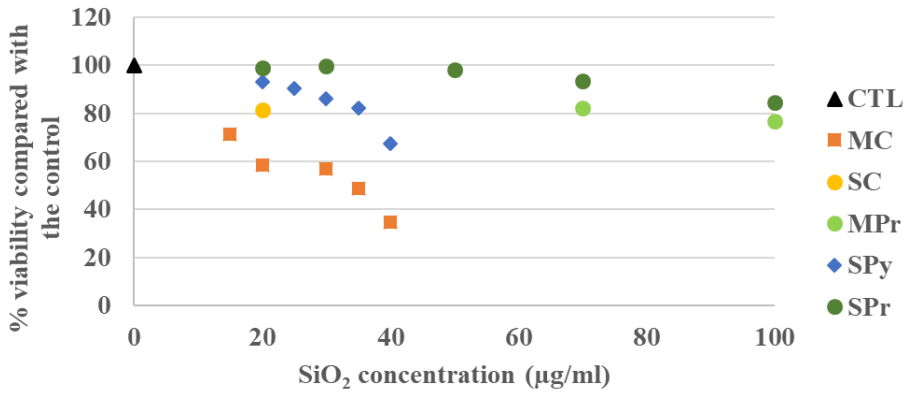

Figure S1: **viability assays of SAS exposure (24h), on J774A.1 macrophages**.
Precipitated silicas are in green, colloidal silicas in orange and the pyrolytic SAS in blue. Round dot are for small particle SAS and square dots for medium particle SAS. The lethal doses 20 were estimated to 15µg/ml for MC, 20µg/ml for SC, 100µg/ml for SPr and MPr and 35µg/ml for SPy.

Mineralisation efficiency

As the mineralisation efficiency may be different from one synthetic amorphous silica to another, we first determined this parameter in a medium close to a cellular lysate, i.e. the cell culture medium supplemented with horse serum. To this purpose, we mixed the synthetic amorphous silicas with the complete culture medium to the adequate concentrations, drew an aliquot portion that was submitted to the mineralisation and silicon assay procedure, and added the remaining of the silica-supplemented medium to the cells. The results, shown in Table S1, indicate that the overall silicon determination yield varied from 20-25% for the precipitated silicas to 40-50% for the colloidal ones, the pyrolytic silica being once again in the middle.

Table S1

Condition	Amount measured in well (µg)	mean measured amount/well (µg)	mineralisation yield	Mean mineralisation yield
CTL	1.531	0.988	N/A	N/A
	0.558		N/A	
	0.876		N/A	
SC - 20	21.760	16.213	0.544	0.405

	12.384		0.310	
	14.496		0.362	
MC - 15	14.560	14.357	0.485	0.479
	14.752		0.492	
	13.760		0.459	
SPr - 100	54.368	53.461	0.272	0.267
	50.176		0.251	
	55.840		0.279	
MPr - 100	29.152	37.920	0.146	0.190
	36.992		0.185	
	47.616		0.238	
SPy - 35	28.480	27.563	0.407	0.394
	25.280		0.361	
	28.928		0.413	

These yields were used in the subsequent experiments to correct the silicon concentration measured in the cell lysates for these various efficiencies.

In vitro dissolution studies

In these experiments, SAS was suspended in complete cell culture medium (DMEM+ 10% FBS) and incubated at 37°C for 4 days in cell culture conditions. The suspensions were then images by TEM as descriBed in the experimental section. The results, shown in Figure S2, indicated a partial breakdown of SAS aggregates, with the appearance of isolated primary particles. This suggested partial dissolution of silica under biological conditions (neutral pH, moderate temperature, and presence of proteins)

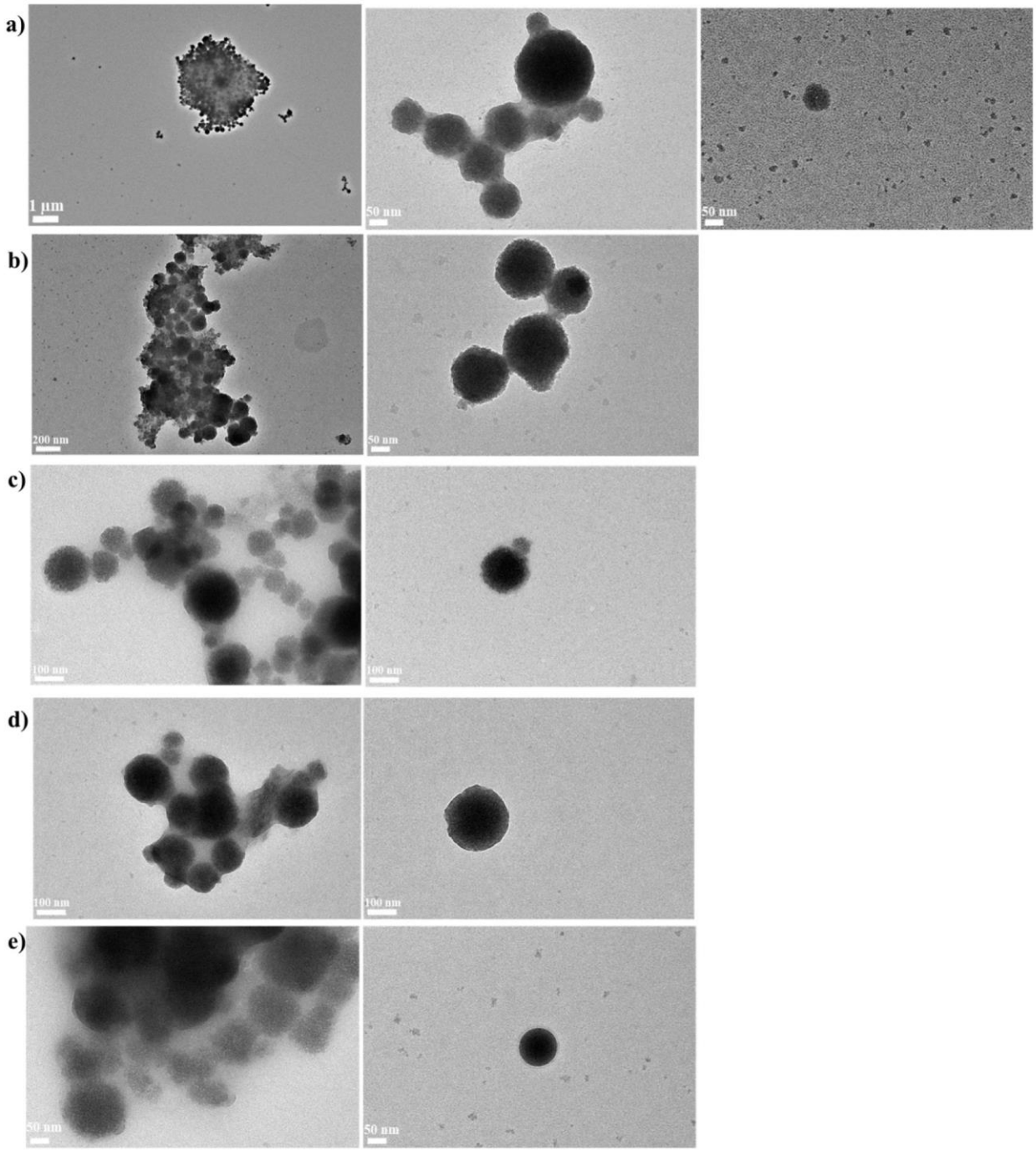

Figure S2: **TEM images of SAS after 4 days in DMEM HS1%**.
a) SPr 220m²/g 1,900 and 30,000x
b) SC 220m²/g 9,300x and 30,000x
c) MPr 55m²/g 23,000x
d) MC 140m²/g 23,000x
e) SPy 200m²/g 30,000x

Conclusion

Ce projet nous a permis de vérifier que les effets suite à l'exposition aux SAS sont majoritairement réversibles, ce qui n'est pas le cas pour les cellules exposées à la silice pyrogénée ou à la terre de diatomée pour lesquelles les effets sont persistants. Ensuite, nous pouvons conclure et répondre partiellement aux hypothèses qui ont conduit à ce travail. Le procédé de fabrication semble jouer un rôle dans la toxicité des SAS, au moins au niveau de la viabilité cellulaire. En effet, les doses létales 20 (DL20) des silices colloïdales (15 et 20µg/ml) sont plus faibles que celle de la silice pyrogénée (35 µg/ml), elle-même plus faible que celles des silices précipitées (50 et 100µg/ml). Ceci suggère fortement un rôle important de l'agrégation des SAS, les silices précipitées étant les plus agrégées (et les moins toxiques). Concernant notre hypothèse sur la surface spécifique, il semblerait que la faible surface spécifique de la MPr soit favorable par rapport à la SPr, mais le phénomène inverse est observé pour les silices colloïdales. Ensuite la taille de particule primaire pourrait intervenir dans la toxicité des SAS, puisque les SPr et SC entraînent plus d'effets que les MPr et MC, cependant MPr et SC possèdent des particules de 20nm de diamètre, ce paramètre seul ne suffit pas à expliquer la toxicité observée. Enfin, la silice pyrogénée est difficile à classer puisque sa DL20 se trouve entre les colloïdales et les précipitées, sa surface spécifique est grande, sa taille de particule primaire est faible, elle est agrégée comme les précipitées mais elle entraîne des effets proches de ceux des colloïdales. Nous avons donc pensé que la présence de silanol à la surface de silices pyrogénées pouvait être à l'origine de cette toxicité. En effet, les silices pyrogénées possèdent en moyenne 5 groupements OH par nm² dont 80% sont isolés, contre 1 à 2 groupements OH par nm² et 10% de silanols isolées pour les silices précipitées. Pour tester cette hypothèse, l'entreprise Solvay a élaboré une silice précipitée possédant autant de silanols à sa surface qu'une silice pyrogénée, et elle a été testée en exposition aiguë. Cette silice induit des effets similaires aux autres silices précipitées testées : pas de cytotoxicité à 500µg/ml, pas d'effets sur la phagocytose ou la production de NO (intrinsèque ou avec stimulation LPS. Nous pouvons conclure que la présence de silanol n'est pas responsable à elle seule de la toxicité des silices pyrogénées.
Cette étude des déterminants des effets de la silice permet d'établir des familles de réponses pour les SAS, et de prédire (par catégorie) les effets d'une SAS en fonction de sa ressemblance au niveau des caractéristiques physico-chimiques avec les SAS déjà testées.
Durant cette étude, nous nous sommes demandé pourquoi les effets des SAS étaient faiblement persistants par rapport à d'autres matériaux ou aux silices contenant des cristaux de silice (Powers et al. 2011; Toybou et al. 2019). Les dosages des surnageants et lysats cellulaires ont permis de montrer que les macrophages sont capables de dissoudre les SAS, leur persistance est donc faible et leurs effets également
Enfin, cette étude confirme que la présence d'un domaine cristallin de silice entraîne une persistance des effets, observés ici avec la terre de diatomée et également avec les pigments à base de silice (Dalzon et al. 2021).

II Système d'étude des expositions répétées

Le deuxième grand axe de mon projet de thèse a été d'étudier l'effet d'une exposition répétée aux silices amorphes de synthèse. En effet, en tenant compte du contexte historique de la silice cristalline à laquelle les travailleurs étaient exposés quotidiennement, il est important d'étudier ce paramètre de répétition. En effet, il en est de même aujourd'hui avec les silices amorphes de synthèse, les producteurs et les entreprises qui utilisent et transforment ou mélangent ces silices peuvent être exposés quotidiennement, notamment par inhalation. Les consommateurs sont également exposés quotidiennement, dans une moindre mesure, par l'intermédiaire des cosmétiques, de l'alimentation ou des dentifrices, mais aussi par inhalation des poussières d'usure des pneus par exemple.
C'est dans ce contexte que nous avons mis au point un protocole d'exposition permettant d'étudier les effets d'une exposition répétée aux silices amorphes de synthèse. Les macrophages sont exposés de

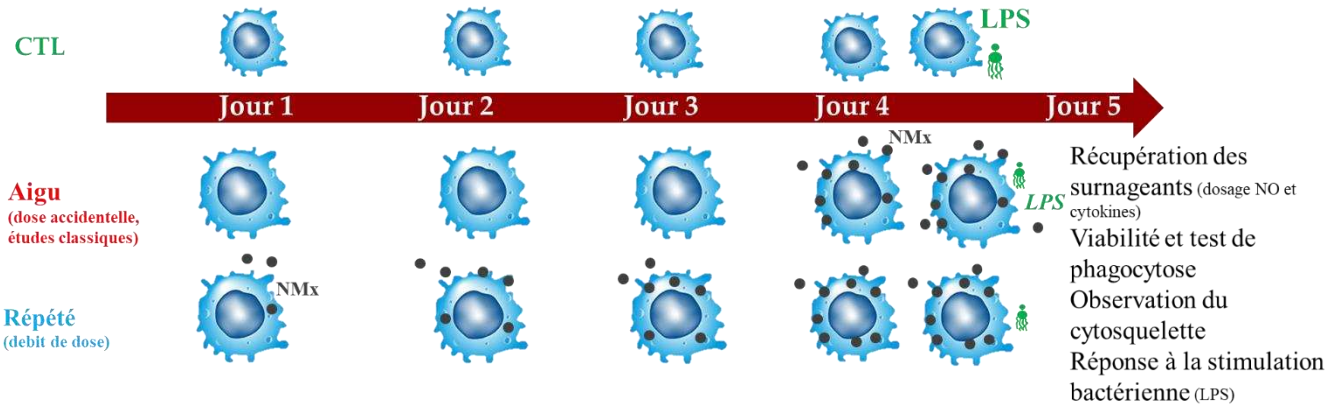

Figure 54 : Protocole d'exposition permettant d'étudier l'effet du débit de dose (ou dose fractionnée) de l'exposition aux nanomatériaux. CTL : contrôle, LPS : lipopolysaccharides, NMx : nanomatériaux, NO : oxyde nitrique

façon quotidienne à une faible dose de silice, généralement la dose létale 20 répartie sur le nombre de jours d'exposition. Suite à cette exposition, les paramètres précédemment évalués sont testés en comparaison de l'exposition aiguë.

II a) Contexte scientifique

Comme dans le cas des études sur la persistance des effets, il existe quelques publications étudiant l'effet d'exposition répétées des cellules à des NMx sur des systèmes *in vitro*. De façon remarquable, ces études se focalisent essentiellement sur les nanoparticules d'argent. L'argent et en particulier l'ion argent est connu pour être toxique, et il est d'ailleurs utilisé comme biocide. Cependant, la dissolution des nanoparticules d'argent est supposée être lente, ce qui pourrait conduire d'une part à des phénomènes de toxicité au long cours, mais aussi et d'autre part à ce que les cellules exposées de façon répétitive à de faibles doses d'argent s'avèrent capables d'une réponse adaptative permettant de contrer ces effets toxiques.
A cet égard, une des premières études publiées à ce sujet (Comfort et al. 2014), menée sur une lignée de kératinocytes humains (HaCat) utilisait à la fois des doses très faibles (exprimées en pg/ml) et des temps très longs (3 mois). Dans ces conditions, les auteurs ont mis en évidence une réponse permettant aux cellules de s'adapter à cette exposition répétée. Cependant, cette adaptation n'était pas neutre et se traduisait par une altération de la signalisation cellulaire en réponse à l'EGF. De plus, cette étude comparaissait les effets de l'exposition répétée à ceux d'une exposition unique à la dose cumulée, et montrait que les deux réponses étaient totalement différentes.

Dans une autre étude menée sur des cellules intestinales (Caco-2), exposées à des concentrations de l'ordre de 1µg/ml/jour pendant 6 semaines (Vila, Marcos, and Hernandez 2017), les auteurs ont montré que les cellules prolifèraient normalement, mais devenaient capables d'une croissance dans des conditions de non-adhérence (agar mou) qui pour la majorité des cellules est indicative de cellules cancéreuses. La lignée Caco-2 étant issue d'un cancer colorectal il est nécessaire de ne pas surinterpréter ce résultat, mais il pose question.

Enfin, une étude menée sur des cellules épithéliales bronchiques humaines non cancéreuses (BEAS2), exposées à des concentrations de l'ordre de 1µg/ml/jour pendant 6 semaines (Gliga et al. 2018) a clairement montré une réponse cellulaire marquée, en l'absence de toxicité observée, et conduisant à une transition épithélio-mésenchymateuse, qui est clairement associée au cancer.

Malheureusement ni cette étude ni celle de Vila et al ne comparaient les effets observés en réponse à une exposition répétée à ceux d'une exposition unique à la dose cumulée.

Dans ce contexte, une étude a été réalisée dans l'équipe sur 20 jours en exposant les macrophages quotidiennement à 1µg/ml de nanoparticules d'argent (donc les doses utilisées par (Vila, Marcos, and Hernandez 2017; Gliga et al. 2018)), et en comparant avec les effets d'une exposition aiguë à 20µg/ml (Dalzon et al. 2020).

Dans cette étude, les études de protéomique et les tests de validation ont montré que l'exposition chronique était plus toxique que l'exposition aiguë, notamment avec une diminution importante de la phagocytose et de la production de NO et d'IL6, mais aussi au niveau métabolique (potentiel mitochondrial et glutathion réduit). Nous n'avons observé aucun indice permettant de conclure à une transformation cancéreuse, au contraire des travaux réalisés sur les cellules épithéliales. Cependant, il est nécessaire de garder à l'esprit que les macrophages se divisent très lentement, et qu'au contraire des travaux menés sur les cellules épithéliales qui chercher à faire proliférer les cellules, nous nous étions placés dans des conditions limitant la prolifération. De plus, les macrophages sont très résistants à la transformation cancéreuse, comme le montre la rareté des histiocytomes (tumeurs des macrophages). Il n'est donc pas surprenant que nos résultats soient fondamentalement différents de ceux observés sur les cellules épithéliales.

Ceci étant, cette publication montrait des différences très importantes dans les réponses des macrophages à une exposition répétée à un nanomatériau, par rapport à une exposition unique à une dose élevée. Ce résultat nous a renforcés dans notre conviction à mener des études sur les réponses des macrophages à des doses répétées de SAS.

II b) Dose fractionnée 4jours

Repeated versus acute exposure of RAW264.7 Mouse Macrophages to Silica Nanoparticles: A Bioaccumulation and Functional Change Study

Présentation du projet

Nous avons d'abord travaillé avec une silice fluorescente afin de mieux suivre et comprendre l'internalisation de la silice par les cellules. Pour cela, nous avons choisi une silice colloïdale fluorescente à cœur afin de s'assurer de mesurer la fluorescence de la silice et non pas du fluorophore seul. Les cellules ont été exposées à 2 ou 5 µg/ml par jour (durant 4 jours) et comparées avec des cellules exposées une seule fois à 2, 5, 10 ou 20µg/ml durant 24 heures. Puis ce même protocole a été utilisé avec une silice colloïdale commerciale, la LS30. Nous avons mesuré la viabilité, l'activité phagocytaire, la réponse à la stimulation bactérienne (LPS et bactérie *Escherichia coli*).

nanomaterials

MDPI

Article

Repeated vs. Acute Exposure of RAW264.7 Mouse Macrophages to Silica Nanoparticles: A Bioaccumulation and Functional Change Study

Anaëlle Torres *, Bastien Dalzon, Véronique Collin-Faure and Thierry Rabilloud *

Laboratory of Chemistry and Biology of Metals, University Grenoble Alpes, CNRS, CEA IRIG-LCBM, 38000 Grenoble, France; bastien.dalzon@cea.fr (B.D.); veronique.collin@cea.fr (V.C.-F.)

* Correspondence: anaelle.torres@cea.fr (A.T.); Thierry.Rabilloud@cnrs.fr (T.R.)

Received: 26 December 2019; Accepted: 22 January 2020; Published: 27 January 2020

Abstract: Synthetic amorphous silica is used in various applications such as cosmetics, food, or rubber reinforcement. These broad uses increase human exposure, and thus the potential risk related to their short- and long-term toxicity for both consumers and workers. These potential risks have to be investigated, in a global context of multi-exposure, as encountered in human populations. However, most of the in vitro research on the effects of amorphous silica has been carried out in an acute exposure mode, which is not the most relevant when trying to assess the effects of occupational exposure. As a first step, the effects of repeated exposure of macrophages to silica nanomaterials have been investigated. The experiments have been conducted on in vitro macrophage cell line RAW264.7 (cell line from an Abelson murine leukemia virus-induced tumor), as this cell type is an important target cell in toxicology of particulate materials. The bioaccumulation of nanomaterials and the persistence of their effects have been studied. The experiments carried out include the viability assay and functional tests (phagocytosis, NO and reactive oxygen species dosages, and production of pro- and anti-inflammatory cytokines) using flow cytometry, microscopy and spectrophotometry. Accumulation of silica nanoparticles (SiO_2 NP) was observed in both exposure scenarii. However, differences in the biological effects between the exposure scenarii have also been observed. For phagocytosis, NO production and Tumor Necrosis Factor (TNF) release, repeated exposure tended to induce fewer effects than acute exposure. Nevertheless, repeated exposure still induces alterations in the macrophage responses and thus represents a scenario to be tested in detail.

Keywords: nanoparticles; macrophage; bioaccumulation

1. Introduction

Silica nanoparticles SiO_2NP are used in many applications such as cosmetics, food or rubber reinforcement [1,2]. According to a report of the Ministère de l'Energie et des ressources naturelles of Quebec, based on the U.S. Geological Survey data, the world production of silica was 142 million tons in 2013, making it one of the most produced nanomaterials. The precipitated silica, which is produced by a wet route in a solvent, is used as a rubber reinforcing agent and as cleaning and polishing agent in toothpastes [3]. It is also used as an anti-caking agent in food and pharmaceutical additives [4]. Finally, the food-grade silica, known as E551 food additive agent, is commercially available as amorphous silica, but is not considered as nanosilica [5]. Although its primary particle is a nanoparticle (NP) of ~20 nm in diameter, E551 occurs in clusters of micrometer size, which is similar to the fumed silica but does not contain crystalline domains, and the ingested dose is estimated to 35 mg per day [6].

The crystalline silica is well known to be toxic, and its effects are irreversible. The proinflammatory response is at the origin of the silicosis (a lung chronic inflammation disease) [7,8]. In this context, the

effects of the industrial amorphous silica have to be investigated. The silica effects are already well referenced for high doses during an short period [7,9,10]. For example, Joshi et al. have observed the specific phagocytosis phenomenon of silica particles, which results in a phagolysosomal leakage and cell death for both crystalline and amorphous silica. Following the phagocytic activity, reactive oxygen species (ROS) were produced, such as hydrogen peroxide, but in the case of silica, H_2O_2 may be converted in a more toxic radicals [11]. Regarding the ROS generation in RAW264.7 cells, an increased level of ROS was observed following an acute exposure [12]. Furthermore, after 24h of silica exposure, the secretion of proinflammatory cytokines was increased as shown by Park and Park and also Di Cristo et al. for two types of silicas (pyrogenic and precipitated) [12,13]. However, the increasing uses of silica, in many daily consumer products, raise the question of the chronic exposure of workers and more widely the general population, by various routes, e.g., inhalation and intestinal. To study the effects of amorphous silica in a context of chronic exposure, the macrophages, i.e., scavenging immune cells that ingest all sorts of particulate material, have been used. The main function of this cell type is the phagocytosis of foreign substances, such as exogenous pathogens. The other functions are the antigen presentation to T cells for the initiation of the specific immune response and the signaling to amplify the immune response with the release of cytokines and nitric oxide.

Moreover, knowing that the two most risky routes for nanosilica exposure are inhalation and intestinal absorption, the macrophages encountered in these two sites have to be studied. First, the intestines are exposed to various elements from the outside and contain a wide bacterial population: part of the gut microbiota. The silica NP could be found in food, the problem of its passage through the intestinal barrier arises. To shed light on this event in the intestinal model, studies on the translocation of particles into and across the gastrointestinal barrier have been realized, especially the transcytosis pathway via the M-cell layer (microfold cells) of the Peyer's Patches, which also contain macrophages [14,15]. This site represents an important immune sensor with a constant surveillance of pathogens and antigens of the intestinal lumen, containing the largest population of resident macrophages in the body. The second important site is represented by the lungs, which are the center of the air exchange, and makes them a privileged site for the infection originating from inhalation pathway. In the lungs, the immune cells are also present and are mainly localized at the alveolar surface. Alveolar macrophages represent 95% of the bronchoalveolar immune cells. Together with 1 to 4% lymphocytes and 1% neutrophils, they are the sentinel phagocytic cell of the innate immunity [16].

Note that the vast majority of studies on the effects of nanoparticles on cells use an acute exposure scheme in which the cells are exposed to a high but subtoxic concentration of nanoparticles and the effects are read immediately after exposure. Thus, there is a need for studies in which a repeated exposure scenario is used, which is a better mimic of consumer or occupational (and not accidental) exposures. Furthermore, biological responses can be different after acute or repeated exposures, as exemplified in the literature for silver [17], zinc oxide [18], or titanium dioxide [19,20] nanoparticles.

We thus decided to investigate the effects of the exposure modes on macrophages, using fluorescent amorphous nanosilicas. In the present study, we have exposed macrophages to low doses of silica for four days to follow the chronic effect of SiO_2NP on the cell metabolism, cytoskeleton, and immune function, and compared the results to those obtained by the classical acute exposure scheme.

2. Materials and Methods

Most experiments were performed as described in previous publications [21,22]. The details are given here for clarity and readers' convenience.

2.1. Nanoparticles Characterization with Dynamic Light Scattering (DLS)

Sicastar®-greenF (FITC) (ref 42.00.301, emission 485 nm, excitation 510 nm) was purchased from Micromod Partikeltechnologie (GmbH, Rostock, Germany). LUDOX® LS colloidal silica was purchased from Sigma-Aldrich (ref 420808) (Merck, Darmstadt, Germany) and is produced by Grace. The size of the nanoparticles was determined after dilution in water or in culture medium by means of dynamic

light scattering using a Wyatt Dynapro Nanostar instrument (Wyatt Technology, Santa Barbara, CA, USA). All these silicas are produced by a wet route starting from organosilane precursors [23]. The study has been carried out with the green fluorescent silica because it has been reported that the fluorescein is a stable and nontoxic dye [24]. This polar anionic compound passes poorly through the membrane. Consequently, it can be internalized only through NP internalization and, once internalized, cannot escape from the cytoplasm by leaching, allowing the count of NP internalization.

2.2. Bacteria Stimulation

Escherichia coli bacteria were grown in agitated liquid cultures at 37 °C in lysogeny broth (LB) medium up to an OD600 of 0.7. The bacteria were harvested by centrifugation, rinsed 3 times in warm (37 °C) phosphate buffer saline (PBS) supplemented with 1 g/L of glucose, and resuspended in 50 mL PBS-glucose containing 16 μg/mL rhodamine B isothiocyanate. The bacteria were maintained under agitation at 37 °C for 30 min in this medium. The bacteria were then collected by centrifugation and rinsed three times in 50 mL PBS. The suspension was sterilized by incubation at 70 °C for 2 h. From the initial OD value of 0.7, the suspension contained 500 million cells/ml, and was diluted in sterile PBS to the adequate concentrations prior to use to obtain a concentration of 10 or 30 bacteria per cell in the plates of macrophage culture.

2.3. Cell Culture of RAW264.7 Cells and Viability Assay

RAW264.7 murine macrophage cells were cultured in Roswell Park Memorial Institute (RPMI) (ThermoFisher, Waltham, MA, USA) 1640 medium supplemented with 10% FBS (fetal bovine serum) and 5 μg/mL Ciprofloxacin. Cells were seeded every 2 days at 250,000 cells/mL and harvested at 1 million cells/mL. For repeated exposure (4 days), the cells were seeded into 6-well treated plates at 100,000 cells/mL. After 2 days of culture to reach confluence, the silica dose was added every day and the medium was changed every 2 days.

After silica exposure for 24 h or some days, the viability of the cells was tested. The cells were harvested and flushed with PBS 1X washed with phosphate buffered saline (PBS) and centrifuged for 5 min at 1200 rpm (200 g). Pellets are resuspended in PBS1X-Sytox Blue (final concentration 2 μg/mL, excitation 444 nm, and emission 480 nm; ThermoFisher S34857). Cells were analyzed with a FacsCalibur flow cytometer equipped with the CellQuest software (6.0, Becton Dickinson Biosciences, Le Pont-de-Claix, France) or a FacsMelody flow cytometer (BD Biosciences) equipped with FacsChorus software (1.3, BD Biosciences).

2.4. Phagocytosis Activity Measurement

The fluorescent beads have a diameter of 500 nm, which is close to a bacterial size. This assay illustrates the phagocytosis of pathogen by macrophages; the red fluorescence allows quantifying the phagocytic activity of the cell and the green fluorescence corresponding to silica internalization. The cell culture was performed as described previously. Briefly, cells were seeded into 6-well plates and exposed to the indicated dose of silica for twenty-four hours at 37 °C. The red fluorescent latex beads (Sigma L3280, excitation 575 nm, emission 610 nm) were first coated in a FBS 10%—PBS 1X solution for 30 min at 37 °C. This solution was then added to cell culture, and the culture returned to the incubator for 3 h. Then cells were harvested and washed with PBS, centrifuged 5 min at 1200 rpm, the pellets were suspended with 3 mL of water for a few seconds and 1 mL of NaCl (3.5%) was added under vortex mixing to restore the osmotic pressure. The cells were centrifuged and the pellets were resuspended with 200 μL of PBS 1X—Sytox Blue 2 μg/mL, and analyzed by flow cytometry.

2.5. Nitric Oxide Production

This experiment is used to determine if there is an interference of silica with the NO production by macrophages induced by bacteria or the bacterial wall component lipopolysaccharide (LPS). LPS induces a strong proinflammatory response, resulting into a detectable NO_2 production measured as

nitrite in the culture medium. Cells grown into 6-well plates were exposed to the indicated dose of silica particles for twenty-four hours at 37 °C and also primed or not with LPS (100 ng/mL) or bacteria for 18 h. L-arginine monohydrochloride (5mM) was also added for 15 h, the supernatants are collected and centrifuged to eliminate nonadherent cells. Then, 500 µL of Griess reagent were added to 500 µL of supernatants, from sample and standards (0 to 50 µM in NO_2 using a Standard Nitrite solution). The mixture was incubated at room temperature for 20 min, and the absorbance read at 540 nm with a Jenway 7315 spectrophotometer.

2.6. Cytokine Dosage in RAW264.7

Cytokines are involved in many homeostatic processes and notably in immune response. This signaling pathway can modulate macrophage functions and cell surface marker expression; they are central actors and markers of the inflammation.

The supernatants were obtained as described above. The experiment was carried out with the Cytometric Bead Array Mouse Inflammation Kit (BD Biosciences), and analyzed with FCAP Array software (3.0, BD Biosciences). This Flex-set kit allows measuring Interleukin-6 (IL-6) and TNF protein levels in a single sample. The mixed capture beads were added to the all assay tubes containing supernatant samples and standards (from 0 to 5000 pg/mL), the mouse inflammation phycoerythrin (PE, excitation 488 nm, emission 575 nm) detection reagent was added, and the mixture was incubated for 2 h at room temperature, protected from light. The wash buffer was added to each tube, which were then centrifuged 5 min at 200 g, the pellets were resuspended with the wash buffer, and analyzed by FacsCalibur flow cytometer.

2.7. Immunofluorescence of RAW264.7 Cells in Microscopy

Cells were seeded on glass coverslips at 100,000 cells/mL and exposed to the indicated dose of silica and/or bacteria. Cells were fixed with 4% paraformaldehyde for 30 min and permeabilized with 0.1% Triton-X100 (Eurobio, GAUTTR00-01) for 5 min. Cells were stained with fluorescently labelled phalloidin, which detects polymerized actin (Sigma-Aldrich, Merck, phalloidin-Atto 550) in a final concentration of 500 nM for 20 min at room temperature, protected from light. Nuclei were stained with Vectashield mounting medium containing DAPI (Vector laboratories, Vectashield H-1200). Microscope analysis was performed on a Zeiss LSM 880 microscope (Zeiss, Marly le Roi, France) (confocal). Fluorescence pictures were taken at the same exposure and gain conditions to allow comparison of fluorescence intensity. The raw data were treated and adjusted by using the same parameters with the ImageJ software (1.52s, Wayne Rasband National Institutes of Health, USA).

2.8. Numerical Analyses

The Student *t*-test was applied to all the results. The experiments were conducted 2 or 3 times on independent biological replicates. Data are presented as means ± standard deviations; * $p \leq 0.05$, ** $p \leq 0.01$, *** $p \leq 0.001$. Note that the systematic use of propidium iodide or Sytox Blue (ThermoFisher) allows analysis of live cells only.

3. Results

3.1. Nanoparticle Characterization

Industry sells their product by communicating some characteristics, including a mean particle size in the case of nanomaterials. We had to verify the size of the SiO_2 NP by using DLS. The three commercial silica nanoparticles were characterized as shown in Table 1.

Table 1. Nano-size distribution of silica nanoparticles in water and culture media by DLS. LS30 for Ludox® LS silica from Grace, SiG for Sicastar®-greenF, RPMI for Roswell Park Memorial Institute 1640 medium, FBS for fetal bovine serum. The Z-average of particles and their proportion in the solution are reported.

Nanoparticle	Solvant	Peak 1	Peak 2	Peak 3
SiG (40 µg/mL)	H_2O	33.8 nm (100%)	0	0
	RPMI	34.4 nm (100%)	0	0
	RPMI 10% FBS	7.99 nm (22.8%)	43.5 m (74.4%)	527 nm (2.9%)
LS30 (20 µg/mL)	H_2O	24 nm (100%)	0	0
	RPMI	22.6 nm (100%)	0	0
	RPMI 10% FBS	10.3 nm (17.7%)	63.3 nm (82.3%)	0
Media	H_2O	0	0	0
	RPMI	0	0	0
	RPMI 10% FBS	39.7 nm (100%)	0	0

The dynamic light scattering (DLS) method allows obtaining the hydrodynamic diameter of the particle. The suppliers provide sizes for their particles in distilled water, which were verified. The fluorescent silicas were given for 30 nm in diameter, and in water, the green silica (SiG) showed a diameter of 34 nm. The colloidal silica (LS30) had a diameter of 22 nm. It is however known that the particles can form agglomerates in culture medium, which could modify their internalization by the cells, and consequently their effects [25]. These NPs have been characterized in the medium used (RPMI 10% FBS), and showed some aggregation. The fluorescent NPs were present in two populations 25% have a diameter of 10 nm and 75% a diameter of 50 nm. The LS30 was distributed in 10 nm (20%) and 65 nm (80%) NP diameters, the size distribution diagrams can be found in supplementary data (Table S1). Thus, the NPs tended to form agglomerates but their sizes remained nanoparticular.

3.2. Silica Accumulation in Various Exposure Modes

3.2.1. Internalization and Fluorescence Measurement in Acute Exposure

First, the effects of silica were tested on the cell lines. The viability assay was carried out with different doses and different silica, with an acute exposure scenario (24 h) to determine the lethal dose 20 (LD20), at which 20% of the cells died and the effects of the treatment were visible. Therefore, for the amorphous LS30 silica and the green fluorescent silica (SiG) this dose corresponded to 20 µg/mL for the RAW264.7 cell line (data not shown). The fluorescent dye did not impact the cell mortality compared with the non-fluorescent silica. The first scenario studied was the acute exposure, which allowed verifying the sensitivity of the flow cytometer. Different doses were tested and the results are presented on Figure 1. The fluorescence intensity increased almost linearly with the concentration of silica as long as the concentration remained lower than the toxic doses. Indeed, the silica green MFI of cells exposed to 5 µg/mL is 1700, the MFI was 3100 for 10 µg/mL exposed cells and for 20 µg/mL exposed cells the MFI was about twice more than for the 10 µg/mL SiG dose with a MFI of 8700. As the background fluorescence of unexposed cells was around 180, this means in then that flow cytometry was sensitive enough to detect the green (SiG) silica fluorescence intensity even at low, non-lethal doses. The obtained values were significantly different from each other (p-value lower than 0.05), and this was used to follow the silica NP internalization by the macrophages. The MFI value can change according to the SiG internalization by the cells, but throughout all the experiments, the MFI were always dose-dependent.

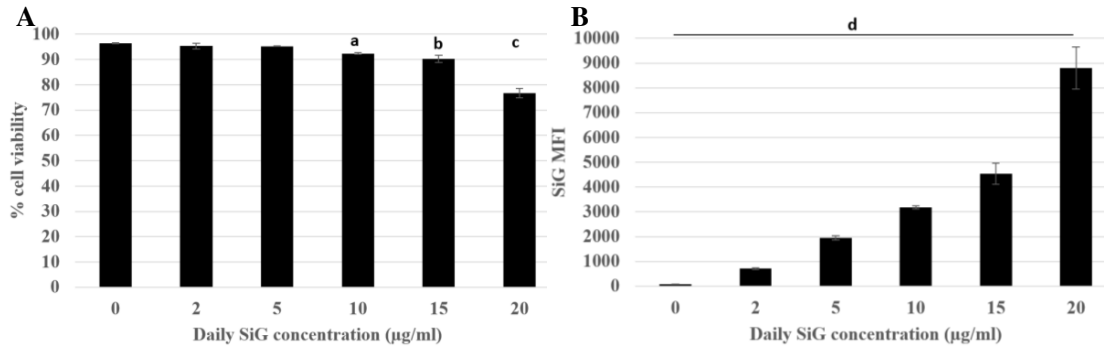

Figure 1. Green silica internalization and viability of RAW264.7 cells after an acute exposure. Green silica MFI obtained with BD Facs Melody flow cytometer. (**A**) Cell viability of exposed cells (a: Control versus acute 10 µg/mL, p value < 0.01; b: control versus acute 15 µg/mL, p-value < 0.05; c: Control versus acute 20 µg/mL, p value < 0.01). (**B**) SiG mean fluorescence intensity depending on NP concentration, (d: all the conditions are significantly different from the control p-value < 0.05). The figure represents the duplicate means of three independent experiments, $n = 6$.

3.2.2. Silica Accumulation for a 4-Day Exposure

Herein, the aim was to determine if the daily exposure to silica has a toxic effect on the immune system or not, in the frame of the well-known and irreversible effects of crystalline silica. This chronic exposure mimicked the daily exposure of the workers in industry but also the consumers who absorb food-grade silica in many powdered products. The chronic scenario was tested with a four-day exposure, as illustrated in Figure 2, for the green silica. The viability was measured for the repeatedly exposed cells and for the cells exposed for 24 h. The cells of both scenarios were seeded the same day, which allowed to obtaining the result for an acute exposure on cells with the same ageing in culture.

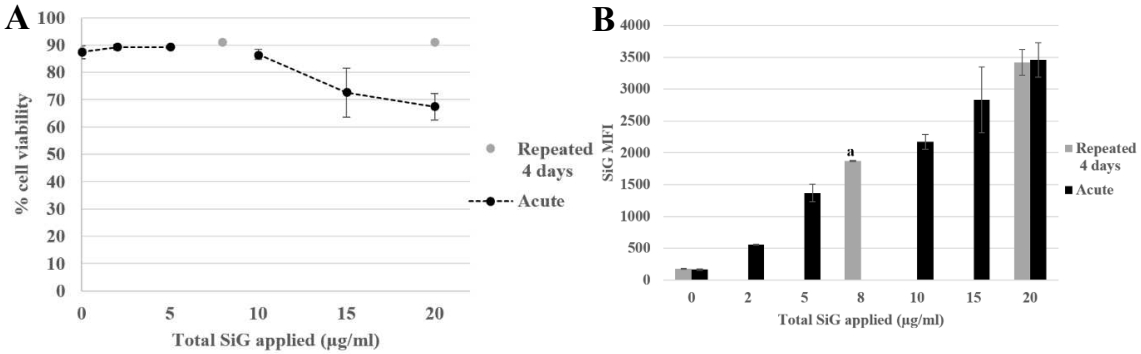

Figure 2. 4-day exposure repeated exposure of RAW264.7 cells to SiO_2 NP compared with acute exposure, by flow cytometer. (**A**) Viability assay of SiG exposed cells measured with propidium iodide. (**B**) Green silica (SiG) internalization. (a: repeated 2 µg/mL versus acute 5 and 10 µg/mL, p-value < 0.05).

It appeared that the applied silica doses did not impact cell viability, either in repeated or acute dose, except for the acute 20 µg/mL (LD20). The silica fluorescence was measured in cells. The fluorescence intensity obtained for repeatedly exposed cells (2 µg/mL as a daily dose for 4 days corresponding to 8 µg/mL a total dose) led to a MFI of 1700, i.e., higher than the one obtained for a single exposure to 2 µg/mL silica (500) in the same dose applied in one acute exposure, and corresponded to the MFI intermediate between the one obtained for cells exposed to a single 5 µg/mL dose and the one obtained for cells exposed to a single 10 µg/mL dose. The same phenomenon was observed with the repeated exposure to 5 µg/mL for 4 days compared with the acute dose of 20 µg/mL. In summary, the silica was internalized and accumulated in the cells upon repeated exposure, although the fluorescent obtained after a repeated exposure was always lower than the one observed after a single exposure to the same

cumulated dose. This observation was crucial for the study of the amorphous silica toxicity. Indeed, the regulatory agencies have defined an occupational exposure limit corresponding to 10 mg amorphous silica/m^3 of air and less than 5 mg/m^3 present in the alveolar fraction. These limitations have taken into account the accumulation of the silica in the organism. A single dose could be nontoxic but the accumulation could lead to some health problems. As a matter of fact, a dose applied at once (acute) or in a cumulative way (repeated) may not lead to the same cellular responses. In this context, the effects of a repeated exposure to amorphous silica have to be seriously investigated, due to the presence of SiO_2 NP in the industry and in many daily products, which exposes the workers and the consumers to a chronic exposure.

3.3. Biological Effect of the Silica Accumulation in Macrophages

3.3.1. Morphological Changes

The cells exposed to Sicastar® fluorescent silica NP were observed in fluorescent microscopy to check the NP internalization and to verify the cytoskeleton of the macrophages. The results are presented in Figure 3 with confocal microscopy images of fixed RAW264.7 cells exposed to green fluorescent silica for 24 h. There was heterogeneity for both parameters: the silica NP internalization and the cell cytoskeleton. First, the cell morphologies were diverse with highly adherent cells with long actin filaments and round cells with a few, short filaments. Despite this heterogeneity, there was a tendency in which the silica-exposed cells were less adherent, and it appeared that the cells exposed at the LD20 dose were less spread out than the control, unexposed cells, or cells exposed to lower doses. This phenomenon appeared to be correlated with the applied dose of silica. Regarding the silica internalization, the microscope was less sensitive than the flow cytometers and it did not allow quantifying the SiG fluorescence without specific software.

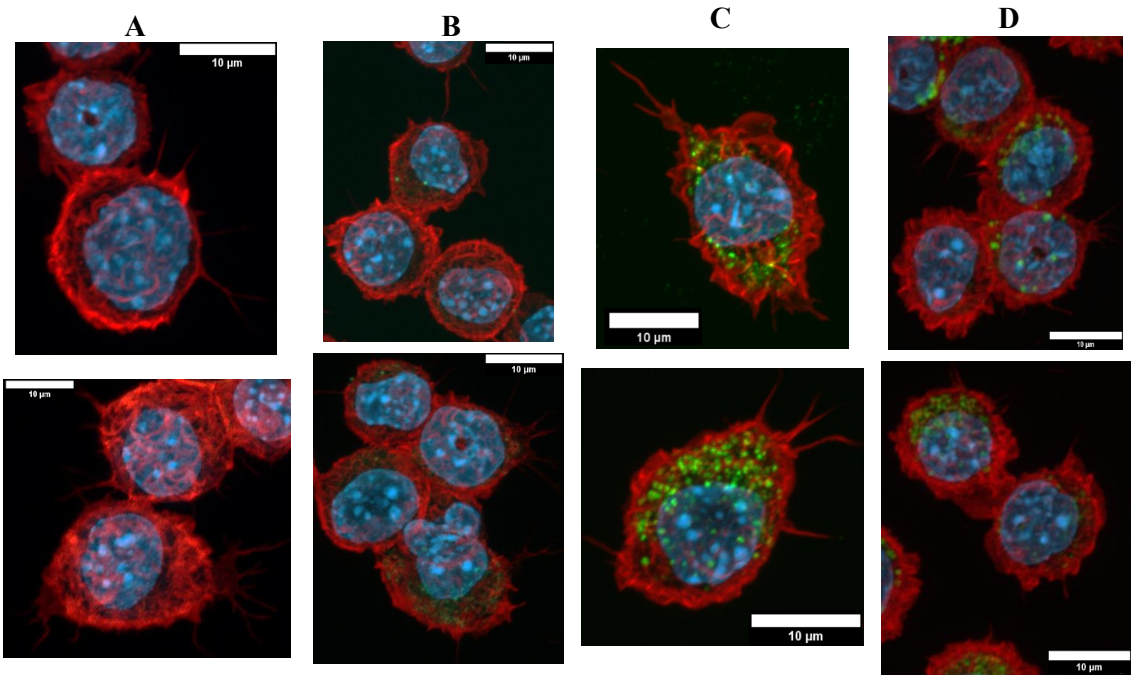

Figure 3. Green silica internalization and cytoskeleton changes of RAW264.7 cells after acute exposure. (**A**–**D**) Control and green silica internalization of cells exposed to 5 µg/mL, 20 µg/mL, and 30 µg/mL during 24 h, respectively, obtained by confocal microscopy (nucleus in blue (DAPI), actin in red (phalloidin), silica in green (FITC)), $n = 2$.

Then, as presented in Figure 4, cytoskeleton changes were observed for repeatedly exposed cells. As a reminder, the cells have been maintained for 4 days at confluence. Under these conditions the cells

were less adherent than in the previous figure, where the cells have been maintained for 24 h only. After 4 days of NP exposure, the cells were more vesicular than the acutely exposed cells. Although the silica NP were dispersed in all the cytoplasm, there were more widespread in the repeated exposure scenario.

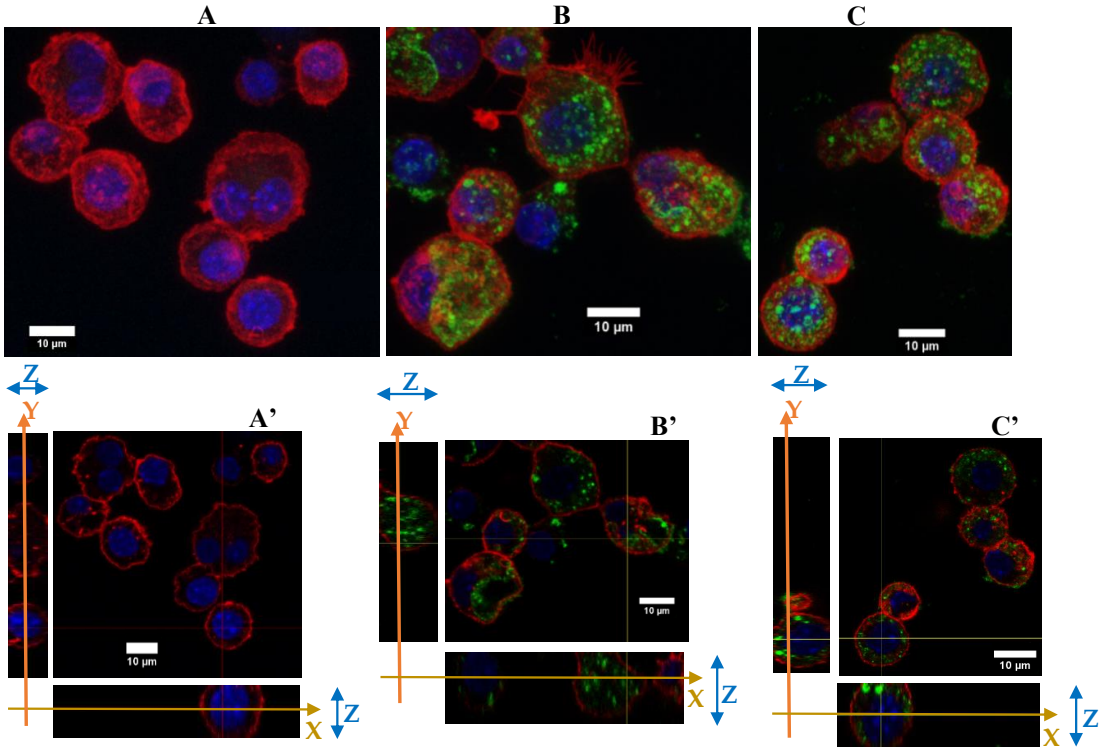

Figure 4. Green silica internalization and cytoskeleton changes of RAW264.7 cells after chronic and acute exposure. (**A**–**C**) Control and green silica internalization of cells exposed repeatedly to 5 µg/mL during 4 days, and 10 µg/mL during 24 h, respectively, obtained by confocal microscopy (nucleus in blue (DAPI), actin in red (phalloidin-atto 550), silica in green (FITC), $n = 2$. Z-project reconstitution. (**A'**–**C'**) Same conditions as previously, represented in orthogonal views. The actin cell membrane is labeled in red by phalloidin-atto550, the nucleus is labeled in blue and the silica nanoparticles are green fluorescent. The stack of the cells corresponding to a slice in the thickness of the cells is illustrated. The combination of the *XY* and *YZ* confocal plans demonstrate the internalization of the silica nanoparticles.

To conclude with the cytoskeleton, the silica seems to have induced a change in the cytoskeleton of the cells by reducing their filaments and their adherence abilities, for cells cultured for 48 h overall. The NPs were well dispersed in the cytoplasm with an important number of vesicles.

3.3.2. Functional Changes

To investigate the impact of nanosilica on macrophages, some important functions of the macrophages were tested. The results of the phagocytosis assay are presented in Figure 5.

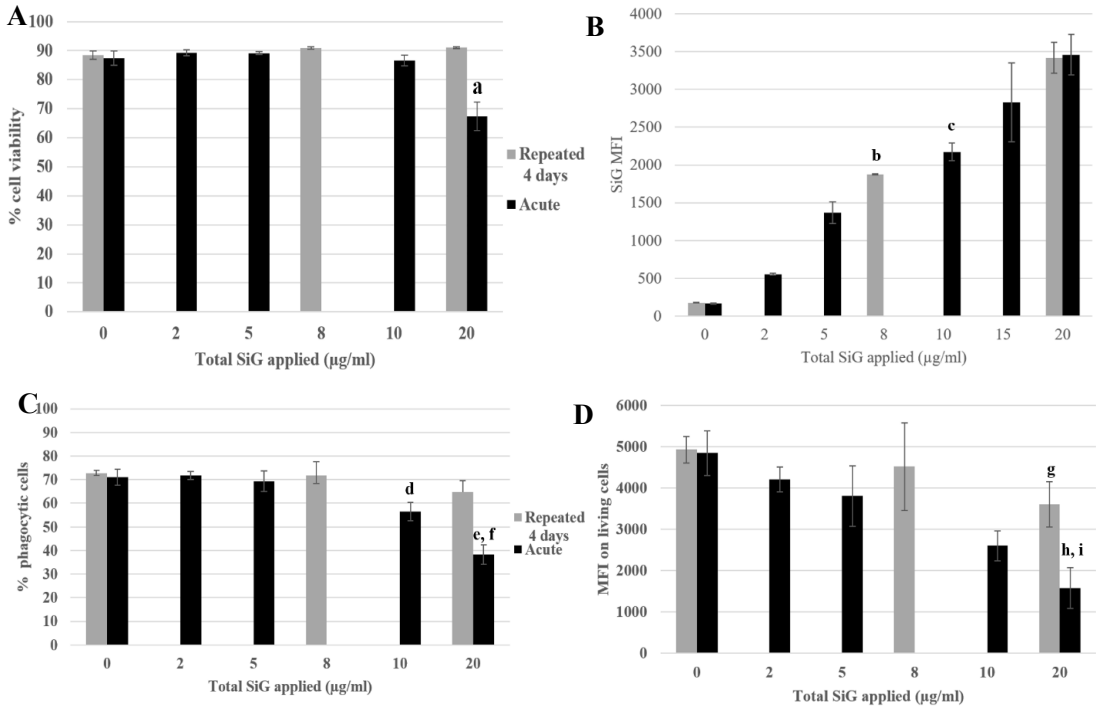

Figure 5. 4-day repeated exposure of RAW264.7 to SiG NP compared with acute exposure. (**A**) Cell viability with propidium iodide. (a: CTL versus acute 20 µg/mL, *p*-value < 0.01). (**B**) SiG internalization (b: acute 5 µg/mL versus repeated 2 µg/mL, *p*-value < 0.01; c: acute 10 µg/mL versus repeated 2 µg/mL, *p*-value < 0.05). (**C**) Proportion of phagocytic cells (d: CTL versus acute 10 µg/mL, *p*-value < 0,01; e: CTL versus acute 20 µg/mL, *p*-value < 0.01; f: repeated 5 µg/mL versus acute 20 µg/mL, *p* value < 0.01). (**D**) Phagocytosis of the cells. (g: CTL versus repeated 5 µg/mL, *p*-value < 0,05; h: CTL versus acute 20 µg/mL, *p*-value < 0.01; i: repeated 5 µg/mL versus acute 20 µg/mL, *p* value < 0.05).

The cell viability and the silica internalization are presented to confirm the cell exposure to NP (Figure 5A,B) and the red beads uptake is presented in Figure 5C,D, corresponding to the percentage of phagocytic cells and the phagocytic activity of these positive cells. The cells exposed repeatedly to 5 µg/mL (20 µg/mL in a cumulative dose) showed a similar proportion of phagocytic cells as in the control, but with a lower phagocytic activity (a 25% decrease). The cells acutely exposed to 20 µg/mL have a lesser proportion of phagocytic cells compared with the control (decrease of 50%) and also a less phagocyte activity, with a decrease of 70% (Figure 5D). The phagocyte function of acutely exposed cells was thus clearly more impacted than for the repeatedly exposed cells. This was also verified for the repeated 4 × 2 µg/mL-exposed cells compared with the 10 µg/mL acute dose. To conclude about phagocytosis, while acutely exposed cells showed a marked decrease in their phagocytic activity, the decrease was much less important for repeatedly exposed cells. Both the proportion of phagocytic cells and the intensity of phagocytosis, as determined by the MFI of the fluorescent latex beads used for the assay, were higher for repeatedly exposed cells than for acutely exposed ones, although the silica internalization was similar for the two exposure scenarios.

The signaling functions of the macrophages were tested, as shown in Figure 6, with the nitric oxide (NO) production and the cytokine release. The cells were exposed to SiG (acutely or repeatedly), and to lipopolysaccharides (LPS) for 18 h or not, to mimic bacteria encounter. As a reminder, LPS is a component of Gram-negative bacterial membrane. For cells not stimulated with LPS (Figure 6A,C), the 4 × 5 µg/mL-repeatedly exposed cells showed a slight decrease of 15% of the basal NO production compared with the control, whereas the 20 µg/mL-acutely exposed cells produced 16% more NO. Regarding the basal TNF release, the repeatedly-exposed cells produced 3 times more TNF than the control, and the acutely exposed cells 5-fold more than the control. For cells stimulated with LPS, the

NO production of the repeatedly exposed cells (4 × 5 µg/mL) was 5% lower than the control, and the acute 20 µg/mL was 30% lower. Concerning IL-6 release, there was a decrease of 80% of the repeated exposed cells (4 × 5 µg/mL) release compared to the control, and a decrease of 70% for cells exposed to a single 20 µg/mL dose. No significant changes were observed in the LPS-induced TNF release.

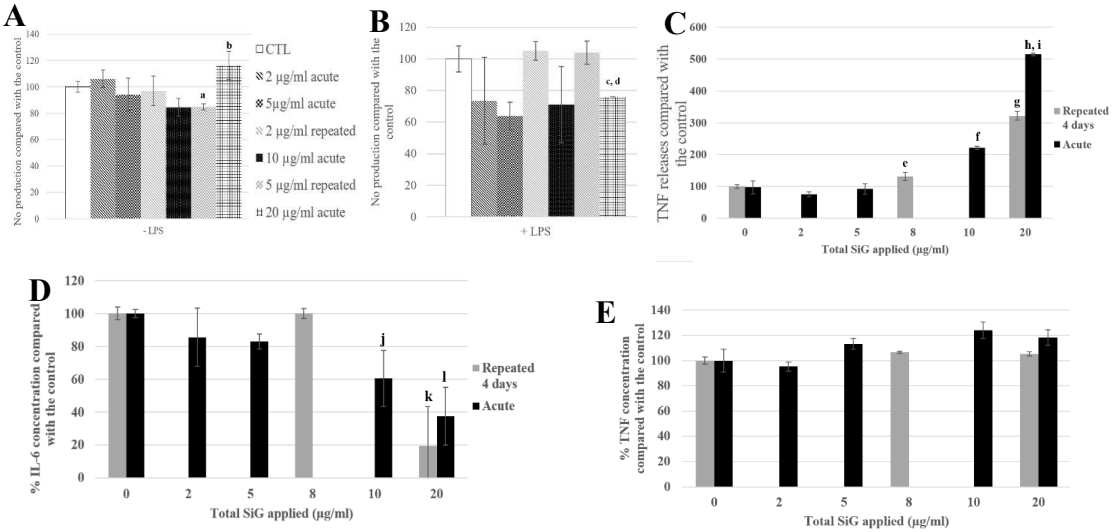

Figure 6. 4-day chronic exposure of RAW264.7 to SiG NP and 18 h to LPS compared with silica acute exposure. (**A**,**B**) NO dosage with the Griess reagent by spectrophotometry without or with LPS stimulation (a: CTL versus repeated 5 µg/mL, p-value < 0.05; b: repeated 5 µg/mL versus acute 20 µg/ml, p value < 0.01, c: CTL versus acute 20 µg/mL, p-value < 0.01; d: repeated 5 µg/mL versus acute 20 µg/mL, p-value < 0.05). (**C**) TNF releases of RAW264.7 cells exposed to SiG only, measured by flow cytometry (e: CTL versus repeated 2 µg/mL, p-value < 0.05; f: CTL versus acute 10 µg/mL, p-value < 0.001; g: CTL versus repeated 5 µg/mL, p-value < 0.001; h: CTL versus acute 20 µg/mL, p-value < 0.001; i: repeated 5 µg/mL versus acute 20 µg/mL, p-value < 0.01). (**D**,**E**) Cytokine release measurement of LPS stimulated cells by flow cytometry, respectively IL-6 and TNF. (j: CTL versus acute 10 µg/mL, p-value < 0.05; k: CTL versus repeated 5 µg/mL, p-value < 0.001; l: CTL versus acute 20 µg/mL, p-value < 0.01).

3.3.3. Physiological Situation of Co-Exposure: Industrial SiO_2 and LPS

Following these experiments of 4-day exposure with the model fluorescent silica SiG, we transposed our work on silica nanoparticles used in industry. The colloidal Stöber LS30 silica has also a diameter of 30 nm, the process of fabrication is similar to that of the SiG, i.e., a wet chemistry synthetic process [26]. As previously, the lethal dose 20 had been determined, and corresponded to approximately 20 µg/mL (Figure 7). The same experiments following the same scenario were carried out. First, the viability assay showed that the cells repeatedly exposed to 5 µg/mL have a significant decrease of their viability of 20% compared with the control. The acutely exposed cells to 20 µg/mL showed a decrease of 40% compared with the control in these experiments. These two exposure conditions were also significantly different from each other (repeated 5 µg/mL versus acute 20 µg/mL).

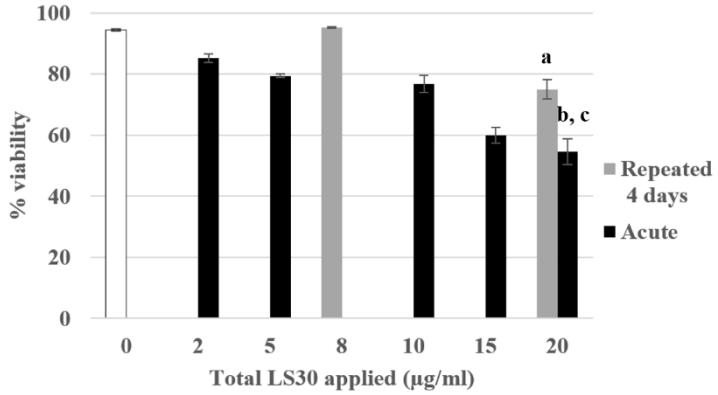

Figure 7. 4-day chronic exposure of RAW264.7 to LS30 NP compared with acute exposure. Cell viability with propidium iodide by flow cytometry (a: repeated 5 µg/mL versus CTL, p-value < 0.001; b: acute 20 µg/mL versus CTL, p-value < 0.001; c: acute 20 µg/mL versus repeated 5 µg/mL, p-value < 0.01).

The NO production tests showed that in the absence of LPS stimulation, there were no significant differences between the control, the repeatedly exposed cells and the acutely exposed ones (Figure 8A). In the presence of LPS, the repeatedly exposed cells to 4 × 5 µg/mL and the control cells showed a similar NO production, whereas the acutely exposed cells to the LD20 showed a significant decrease of 27% compared with the control.

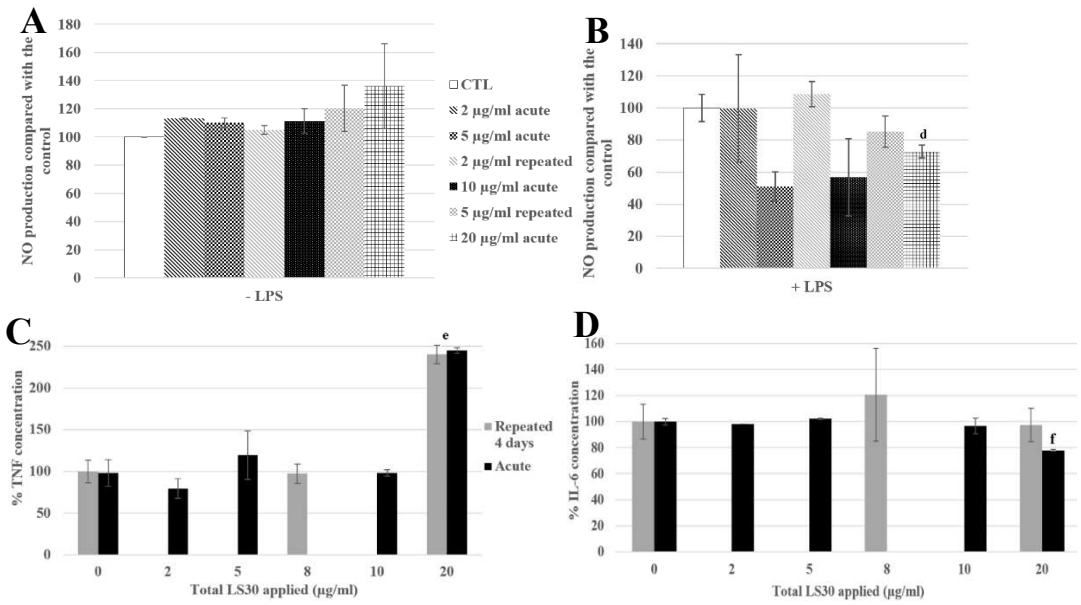

Figure 8. 4-day chronic exposure of RAW264.7 to LS30 NP and 18h to LPS compared with silica acute exposure. (**A**,**B**) NO dosage with the Griess reagent by spectrophotometry without or with LPS stimulation (d: CTL versus acute 20 µg/mL, p-value < 0.01). (**C**) TNF releases of RAW264.7 cells exposed to LS30 only, measured by flow cytometry (e: repeated 5 µg/mL and acute 20 µg/mL versus CTL, p-value < 0.01). (**D**) IL-6 release measurement of LPS stimulated cells by flow cytometry (f: CTL versus acute 20 µg/mL, p-value < 0.01).

Regarding the cytokine releases, in the absence of LPS stimulation, the TNF secretion was 2.4 fold higher for 4 × 5 µg/mL and 1 × 20 µg/mL exposures than in the control (Figure 8C). The IL-6 secretion was decreased, with LPS stimulation, by the exposure to 20 µg/mL (22% compared with the control), and significantly different from the 4 × 5 µg/mL exposed cells, which were not different from the control cells.

3.3.4. Physiological Situation of Co-Exposure: SiO_2 and *E. coli*

In all the previous experiments, the bacterial encounter that occurs in vivo was mimicked by an exposure to LPS. To further increase the relevance of our experiments, the repeated exposure to silica was combined to an exposure to killed bacteria. The cells were exposed for 4 days to the amorphous silica LS30, and for the last 18 h they were co-exposed to *E. coli* (which have been heat-killed after rhodamine B uptake) or LPS. Different doses were tested, and to be physiologically relevant with a signal measurable by flow cytometry, the bacterial concentration chosen was 30 bacteria per cell (b/c). This dose corresponded to a basal dose of bacteria in a non-sterile environment. For this co-exposure scenario, the viability and the bacteria fluorescence were measured, the phagocytosis, the nitric oxide (NO), and the cytokines were assayed. The results are presented in Figures 9 and 10.

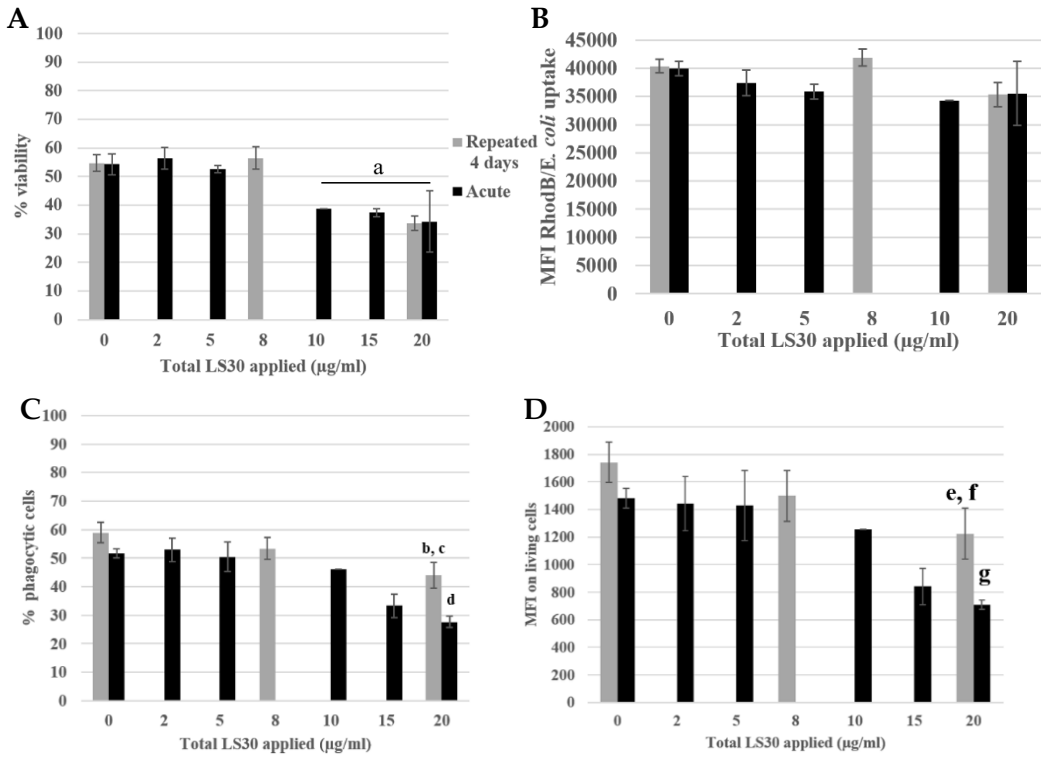

Figure 9. Phagocytosis assay of LS30 exposed cells, stimulated by Escherichia coli. (**A**) Cell viability (a: CTL versus acute 10 µg/mL, 15 µg/mL, acute 20 µg/mL and repeated 5 µg/mL, p value < 0.05). (**B**) *Escherichia coli* uptake followed by rhodamine B fluorescence. (**C**) Proportion of phagocytic cells (b: CTL versus repeated 5 µg/mL, p-value < 0.05; c: repeated 5 µg/mL versus acute 20 µg/mL, p-value < 0.01; d: CTL versus acute 20 µg/mL, p-value < 0.01). (**D**) Phagocytic activity of the cells (e: CTL versus repeated 5 µg/mL, p-value < 0.05; f: repeated 5 µg/mL versus acute 20 µg/mL, p-value < 0.01; g: CTL versus acute 20 µg/mL, p-value < 0.01.

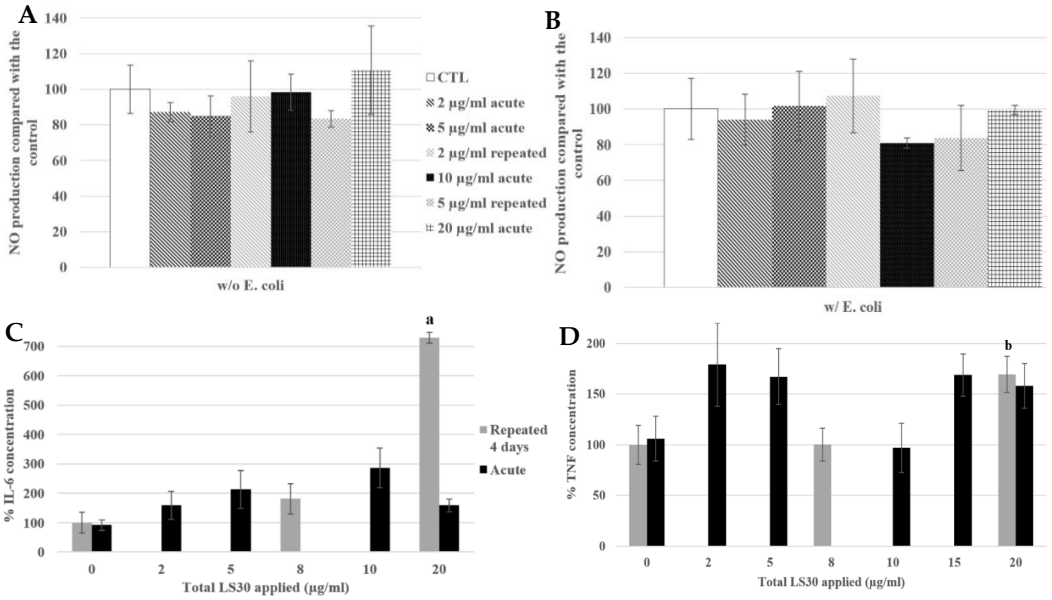

Figure 10. 4-day chronic exposure of RAW264.7 to LS30 NP and 18 h to Escherichia coli compared with silica acute exposure. (**A**,**B**) NO dosage with the Griess reagent by spectrophotometry without or with *E. coli* stimulation. (**C**,**D**) Cytokine release measurement of LS30 exposed cells, in absence of *E. coli* stimulation by flow cytometry, respectively IL-6 and TNF. (a: CTL versus repeated 5 µg/mL, p-value < 0.01; b: CTL versus repeated 5 µg/mL, p-value < 0.05).

The viability is presented in Figure 9A, the LD20 was obtained for an acute 20 µg/mL dose and repeated 4 × 5 µg/mL). The *E. coli* uptake was measured by flow cytometry following the rhodamine B fluorescence. There were no differences between the different condition and the control. The proportion of phagocytic cells was decreased for the repeated 5 µg/mL compared with the control (12% decrease) and there was a decreased of 30% for the acutely exposed cells to 20 µg/mL compared with the control. Then, the phagocytic activity of the cells was measured. The activity of the repeatedly exposed cells to 4 × 5 µg/mL was 30% lower than the control, and the 1 × 20 µg/mL acutely exposed cells were 60% less active than the control.

We still obtained no intrinsic effect of LS30 in NO production whatever the LS30 exposure scenario. In presence of *E. coli* stimulation, the NO production was doubled in all the conditions (from about 7 µM in control without stimulation to 16 µM with *E. coli* stimulation).

In absence of stimulation, Il-6 release was increased 7.3-fold by the 4 × 5 µg/mL exposure compared with the control. The TNF was also increased by the repeated 5 µg/mL exposure, 1.7-fold compared with the control. The cytokine releases of IL-6 and TNF after *E. coli* stimulation were equivalent between all the conditions, there were no differences between the control, repeatedly exposed cells and the acutely ones. This suggested that the bacterium stimulation, which induced stronger effects than LPS alone, had erased the effects of LS30 exposure.

4. Discussion

In the context of an increasing use of amorphous silica in many products, it appears important to assess the effects of silica in a repeated exposure mode, and to compare the results to those obtained for the classical single dose exposure most often used in in vitro toxicology. As a target cell type, we used a macrophage cell line, as macrophages are the scavenger cells dealing with particulate materials in our body, and are also key players in inflammatory and immune responses. Then, two different exposure scenarios were performed to address these questions: a single, acute exposure and 4-day repeated exposure. Firstly, concerning silica internalization itself, it was shown that the SiO_2 NP were internalized and accumulated in the cells, without any effect of the fluorescent dye. Furthermore, the intensities of fluorescence of the repeated doses were similar to the acute dose corresponding to the

cumulative chronic dose. A major difference, however, is that repeated exposure did not produce the same effect on cellular viability than a single exposure to the same cumulated dose. For example, the acute 20 μg/mL has a decrease of 24% of the cell viability compared with the control, whereas the repeated exposure to even 4 × 10 μg/mL (40 μg/mL in a cumulative way) led to the same viability as the control. Similar observations were made with the LS30 silica concerning the signaling functions of macrophages: for 4-day exposure, the cumulative LD20 (4 × 5 μg/mL) applied in a daily treatment has an effect different from the LD20 in acute treatment. This, combined with the adhesion changes could modify the functionalities of the cells and their responses to SiO_2 NP. One of the characteristic of the macrophages is the cell migration to the inflammation site. The acute SiO_2 NP exposure did seem to modify the cell adhesion, which have been already see with ZrO_2 NP, whereas ZnO_2 NP induced a decrease of adherence ability of macrophages [27]. In the repeated exposure scenario, the apparently reduced adhesion was observed in control and exposed cells, so that it should be attributed to the long time at confluence rather than the exposure to silica.

For the second axis of the project regarding the cross-toxicity with bacteria, it was observed that the bacteria were internalized, regardless of the pre-exposure to silica (except the LD20 cumulative or acute doses) (data not shown). We used *Escherichia coli* as a bacterium stimulation because of it contained LPS, allowing a direct comparison with the classical LPS alone model stimulation. The effect of the LPS component and of the complete bacteria is reported in this study. At the bacterial concentration chosen (30 bacteria per cell), there was no effect on the cell viability in the absence of silica or for an acute exposure to silica at doses lower than the LD20 (i.e., 20 μg/mL for this cell line). This bacteria concentration corresponded to dose that the immune cells can encounter because of the non-sterile environment of our organism. The acute exposure to a high dose of silica and bacteria may have a synergistic effect on the cell viability.

Concerning one of the important functions of this cell type, namely phagocytosis, a decrease of phagocytic cells has been observed in both acute 20 μg/mL and repeated 5 μg/mL conditions, respectively, 64% and 38% compared with the control. However, the cells were more active to phagocytose the red beads in repeatedly exposed cells. Although the phagocytosis was decreased by the silica exposure, the phagocytic function was much less impacted by the repeated exposure than the acute one.

After these observations, the signaling function of macrophages was probed with the NO production and the cytokine release assays.

With the first model (RAW264.7 and SiG, stimulated or not with LPS), the NO production was modified. For the intrinsic effect of SiG, the chronic exposure resulted in a 15% decrease of the basal NO production, compared to unexposed cells, whereas the acute exposure led to an increase of 16%. Therefore, the silica nanoparticles have a proinflammatory effect in case of one high dose exposure but the intrinsic effect of repeated exposure decreases the NO production compared to the nonexposed cells. The opposite trend was observed with the LPS-stimulated cells, with a moderate, nonsignificant increase of 5% for the 4 × 5 μg/mL-chronic dose and a decrease of 30% for the 20 μg/mL-acute dose. The effect of exposure scenarios were opposed, with or without LPS stimulation. Then, the cytokine releases were also modified with silica exposure. In absence of LPS stimulation, there was an intrinsic effect of SiG, with an increase of TNF release in repeated and acute exposure, respectively, 3- and 5-fold compared with the control. With LPS stimulation, the exposure mode to silica have no significant effect on TNF release, but the IL-6 release was decreased, 80% for the repeated 5 μg/mL and 70% for the acute 20 μg/mL. The silica exposure altered the signaling response of macrophages in case of infection, and according to the silica exposure mode, the response was also different.

With the second model (LS30 with or without LPS), we did not observe the same effect. The LS30 did not modify the NO production, there was no intrinsic effect of the LS30 (in the absence of LPS). Indeed, with the LPS stimulation a decrease of the NO production had been observed in acute exposure to LD20. The co-exposure led to a synergistic effect on the NO production.

The co-exposure of RAW264.7 to 4 × 5 µg/mL LS30 silica and *E. coli* for 18 h did not affect the NO production, compared to the control, unlike the scenario 1 × 20 µg/mL LS30 and LPS. The *E. coli* stimulation seems to have erased the slight effect of the synergistic LS30/LPS effect, perhaps because of the higher NO response with complete bacterium stimulation.

The cytokine releases followed the same tendency for the exposure to LS30, with an increase of the proinflammatory cytokine secretion (TNF-α), in absence of stimulation. Furthermore, in repeated exposure to 5 µg/mL of LS30 silica, there was an increase of IL-6 release. These up-releases of proinflammatory cytokines may lead to an abnormal response of the immune system with a hyper stimulation of the immune cells. The TNF-α is involved in inflammation and regulation of immune cells, in addition, some links have been suggested between this cytokine and the IBD and COPD diseases [28,29]. These results are again supporting the importance of the repeated exposure, by illustrating the diversity of cellular responses between the different exposure scenarios.

With LPS stimulation, a decrease of IL-6 for the acutely exposed cells to 20 µg/mL had been observed. However, the *E. coli* stimulation did not show the same observation, as there was no effect of the silica exposure on the cytokine releases. These results, as those obtained for the NO production (with LPS or *E. coli*) shed light on the specificity of the stimulation source. The macrophage responses to LPS or complete bacteria were clearly different, even though the silica NP exposure was identical (LS30).

Herein, we observed that the inflammatory response of macrophages to silica was specific to the precipitated silica type (even though the physical parameters were similar), the exposure mode (acute or repeated) and the biological stimulus (bacterial LPS component or complete bacteria). This model is clearly relevant to study the long time effects of silica NP exposure, it would be a great alternative to in vivo models on rodents, which have been already used to investigate the chronic effects of amorphous silica [30]. An in vivo study of lung mice has also reported different responses between the single and the repeated inhalation exposure to ZnO_2 NP [31], and also on silica where the absence of direct interference between nanosilica and bacterial clearance of macrophages has been observed [32]. In the context of minimization of animal experimentation, the development of in vitro systems is desirable, at least for the initial phases of the toxicological assessment of substances including nanomaterials. In this frame, advanced in vitro systems have been shown to be predictive for silver nanoparticles [33]. In addition, macrophage cell lines have brought interesting primary results, as exemplified on silver nanowires, where an advanced use of in vitro macrophage systems can recapitulate some of the events observed on in vivo mouse models [34]. In this respect, our in vitro results parallel those observed in vivo on the absence of effects of nanosilica on bacterial clearance by macrophages [32].

5. Conclusions

In conclusion, this work brought useful information about the silica NP. First, the SiO_2 NPs are accumulated by the macrophages and change the adhesion properties of the cells. They interfere with the inflammation response to bacteria and modify the immune cell signalization by increasing the TNF-α and IL-6 releases. All these results lead to conclude that the acute exposure to low doses of NPs seems to not be toxic for the macrophages and the immune system. However, the repeated exposure to the same doses affects the cell viability, the phagocytosis and their signalization in case of the encounter with pathogens. This has to be taken into account to raise awareness the industrial workers to the risks at which they are exposed. It must be kept in mind that alveolar macrophages have a lifespan of several months.

Supplementary Materials: The following are available online at http://www.mdpi.com/2079-4991/10/2/215/s1, Table S1: Nano-size distribution of silica nanoparticles in water and culture media by DLS.

Author Contributions: Methodology, B.D. and V.C.-F.; supervision and writing review, T.R.; formal analysis and writing—original draft preparation and editing, A.T. All authors read and agreed to the published version of the manuscript.

Funding: The project leading to this publication has received funding from Excellence Initiative of Aix-Marseille University—A*MIDEX, a French "Investissements d'Avenir" program, through its associated Labex SERENADE project. This work was funded by the French National Research Program for Environmental and Occupational Health of ANSES (PNREST 2015/032, Silimmun Grant) and the French National Research Agency (ANR-16-CE34-0011, Paipito grant).

Acknowledgments: We thank the microscopy facility MuLife of IRIG/DBSCI, funded by CEA Nanobio and labex Gral for equipment access and use.

Conflicts of Interest: The authors declare no conflicts of interest. The funders had no role in the design of the study; in the collection, analyses, or interpretation of data; in the writing of the manuscript; or in the decision to publish the results.

References

1. Nie, S.; Xing, Y.; Kim, G.J.; Simons, J.W. Nanotechnology Applications in Cancer. *Ann. Rev. Biomed. Eng.* **2007**, *9*, 257–288. [CrossRef]
2. Silica, amorphous [MAK Value Documentation, 1991]. *MAK-Collect. Occup. Health Saf.* **2012**, 158–179. [CrossRef]
3. Murphy, F.A.; Schinwald, A.; Poland, C.A.; Donaldson, K. The mechanism of pleural inflammation by long carbon nanotubes: Interaction of long fibres with macrophages stimulates them to amplify pro-inflammatory responses in mesothelial cells. *Part Fibre Toxicol.* **2012**, *9*, 8. [CrossRef]
4. Flörke, O.W.; Graetsch, H.; Brunk, F.; Benda, L.; Paschen, S.; Bergna, H.E.; Roberts, W.O.; Welsh, W.A.; Chapman, D.M.; Ettlinger, M.; et al. Silica. *Ullmanns Encycl. Ind. Chem.* **2000**. [CrossRef]
5. Dekkers, S.; Krystek, P.; Peters, R.J.B.; Lankveld, D.P.K.; Bokkers, B.G.H.; van Hoeven-Arentzen, P.H.; Bouwmeester, H.; Oomen, A.G. Presence and risks of nanosilica in food products. *Nanotoxicology* **2011**, *5*, 393–405. [CrossRef]
6. Powell, J.J.; Faria, N.; Thomas-McKay, E.; Pele, L.C. Origin and fate of dietary nanoparticles and microparticles in the gastrointestinal tract. *J. Autoimmun.* **2010**, *34*, J226–J233. [CrossRef]
7. Rees, D.; Murray, J. Silica, silicosis and tuberculosis [State of the Art Series. Occupational lung disease in high- and low-income countries, Edited by M. Chan-Yeung. Number 4 in the series]. *Int. J. Tuberc. Lung Dis.* **2007**, *11*, 474–484.
8. Work Safely with Silica n.d. Available online: https://www.silica-safe.org/ (accessed on 15 April 2019).
9. Johnston, C.J.; Driscoll, K.E.; Finkelstein, J.N.; Baggs, R.; O'Reilly, M.A.; Carter, J.; Gelein, R.; Oberdorster, G. Pulmonary Chemokine and Mutagenic Responses in Rats after Subchronic Inhalation of Amorphous and Crystalline Silica. *Toxicol. Sci.* **2000**, *56*, 405–413. [CrossRef]
10. Joshi, G.; Gilberti, R.; Knecht, D. Single Cell Analysis of Phagocytosis, Phagosome Maturation, Phagolysosomal Leakage, and Cell Death Following Exposure of Macrophages to Silica Particles. *Methods Mol. Biol. Clifton NJ* **2017**, *1519*, 55–77. [CrossRef]
11. Joshi, G.N.; Goetjen, A.M.; Knecht, D.A. Silica particles cause NADPH oxidase–independent ROS generation and transient phagolysosomal leakage. *Mol. Biol. Cell* **2015**, *26*, 3150–3164. [CrossRef]
12. Park, E.-J.; Park, K. Oxidative stress and pro-inflammatory responses induced by silica nanoparticles in vivo and in vitro. *Toxicol. Lett.* **2009**, *184*, 18–25. [CrossRef]
13. Di Cristo, L.; Movia, D.; Bianchi, M.G.; Allegri, M.; Mohamed, B.M.; Bell, A.P.; Moore, C.; Pinelli, S.; Rasmussen, K.; Riego-Sintes, J.; et al. Proinflammatory Effects of Pyrogenic and Precipitated Amorphous Silica Nanoparticles in Innate Immunity Cells. *Toxicol. Sci.* **2016**, *150*, 40–53. [CrossRef]
14. Geppert, M.; Sigg, L.; Schirmer, K. A novel two-compartment barrier model for investigating nanoparticle transport in fish intestinal epithelial cells. *Environ. Sci. Nano* **2016**, *3*, 388–395. [CrossRef]
15. Hodges, G.M.; Carr, E.A.; Hazzard, R.A.; Carr, K.E. Uptake and translocation of microparticles in small intestine. *Dig. Dis. Sci.* **1995**, *40*, 967–975. [CrossRef] [PubMed]
16. Martin, T.R.; Frevert, C.W. Innate Immunity in the Lungs. *Proc. Am. Thorac Soc.* **2005**, *2*, 403–411. [CrossRef] [PubMed]
17. Aude-Garcia, C.; Villiers, F.; Collin-Faure, V.; Pernet-Gallay, K.; Jouneau, P.-H.; Sorieul, S.; Mure, G.; Gerdil, A.; Herlin-Boime, N.; Carrière, M.; et al. Different in vitro exposure regimens of murine primary macrophages to silver nanoparticles induce different fates of nanoparticles and different toxicological and functional consequences. *Nanotoxicology* **2016**, *10*, 586–596. [CrossRef] [PubMed]

18. Annangi, B.; Rubio Lorente, L.; Alaraby, M.; Bach Griera, J.; Marcos, R.; Hernández, A. Acute and long-term in vitro effects of zinc oxide nanoparticles. *Arch. Toxicol.* **2015**, *90*. [CrossRef] [PubMed]
19. Armand, L.; Tarantini, A.; Beal, D.; Biola-Clier, M.; Bobyk, L.; Sorieul, S.; Pernet-Gallay, K.; Marie-Desvergne, C.; Lynch, I.; Herlin-Boime, N.; et al. Long-term exposure of A549 cells to titanium dioxide nanoparticles induces DNA damage and sensitizes cells towards genotoxic agents. *Nanotoxicology* **2016**, *10*, 913–923. [CrossRef]
20. Armand, L.; Biola-Clier, M.; Bobyk, L.; Collin-Faure, V.; Diemer, H.; Strub, J.M.; Cianferani, S.; Van Dorsselaer, A.; Herlin-Boime, N.; Rabilloud, T.; et al. Molecular responses of alveolar epithelial A549 cells to chronic exposure to titanium dioxide nanoparticles: A proteomic view. *J. Proteomics* **2016**, *134*, 163–173. [CrossRef]
21. Dalzon, B.; Aude-Garcia, C.; Collin-Faure, V.; Diemer, H.; Béal, D.; Dussert, F.; Fenel, D.; Schoehn, G.; Cianférani, S.; Carrière, M.; et al. Differential proteomics highlights macrophage-specific responses to amorphous silica nanoparticles. *Nanoscale* **2017**, *9*, 9641–9658. [CrossRef]
22. Triboulet, S. Etude des effets de deux types de nanoparticules métalliques sur des macrophages murins par une approche protéomique. Ph.D. Thesis, Université de Grenoble, Grenoble, France, 2013.
23. Teller JDRNH, Grüttner CD rer nat, Rudershausen SDRN, Westphal FD-P. Verfahren zur Herstellung gefärbter und fluoreszenter Polykieselsäure-Partikel. EP1036763A1, 2000.
24. Jones, K.H.; Senft, J.A. An improved method to determine cell viability by simultaneous staining with fluorescein diacetate-propidium iodide. *J. Histochem. Cytochem.* **1985**, *33*, 77–79. [CrossRef] [PubMed]
25. Fede, C.; Selvestrel, F.; Compagnin, C.; Mognato, M.; Mancin, F.; Reddi, E.; Celloti, L. The toxicity outcome of silica nanoparticles (Ludox®) is influenced by testing techniques and treatment modalities. *Anal. Bioanal. Chem.* **2012**, *404*, 1789–1802. [CrossRef] [PubMed]
26. Stöber, W.; Fink, A.; Bohn, E. Controlled growth of monodisperse silica spheres in the micron size range. *J. Colloid Interface Sci.* **1968**, *26*, 62–69. [CrossRef]
27. Aude-Garcia, C.; Dalzon, B.; Ravanat, J.-L.; Collin-Faure, V.; Diemer, H.; Strub, J.M.; Cianferani, S.; Van Dorsselaer, A.; Carrière, M.; Rabilloud, T. A combined proteomic and targeted analysis unravels new toxic mechanisms for zinc oxide nanoparticles in macrophages. *J. Proteomics* **2016**, *134*, 174–185. [CrossRef]
28. Athinarayanan, J.; Periasamy, V.S.; Alsaif, M.A.; Al-Warthan, A.A.; Alshatwi, A.A. Presence of nanosilica (E551) in commercial food products: TNF-mediated oxidative stress and altered cell cycle progression in human lung fibroblast cells. *Cell Biol. Toxicol.* **2014**, *30*, 89–100. [CrossRef]
29. Keely, S.; Talley, N.J.; Hansbro, P.M. Pulmonary-intestinal cross-talk in mucosal inflammatory disease. *Mucosal Immunol.* **2012**, *5*, 7–18. [CrossRef]
30. Arts, J.H.E.; Muijser, H.; Duistermaat, E.; Junker, K.; Kuper, C.F. Five-day inhalation toxicity study of three types of synthetic amorphous silicas in Wistar rats and post-exposure evaluations for up to 3months. *Food Chem. Toxicol.* **2007**, *45*, 1856–1867. [CrossRef]
31. Zhang, Y.; Nguyen, K.C.; Caldwell, D.; Fine, J.H.; Lefebvre, D.E.; Tayabali, A.F. Immune responses during single and repeated murine endotracheal exposures of zinc oxide nanoparticles. *NanoImpact* **2017**, *7*, 54–65. [CrossRef]
32. Delaval, M.; Boland, S.; Solhonne, B.; Nicola, M.-A.; Mornet, S.; Baeza-Squiban, A.; Sallenave, J.-M.; Garcia-Verdugo, I.; et al. Acute exposure to silica nanoparticles enhances mortality and increases lung permeability in a mouse model of Pseudomonas aeruginosa pneumonia. *Part Fibre Toxicol.* **2015**, 12. [CrossRef]
33. Braakhuis, H.M.; Giannakou, C.; Peijnenburg, W.J.; Vermeulen, J.; van Loveren, H.; Park, M.V. Simple in vitro models can predict pulmonary toxicity of silver nanoparticles. *Nanotoxicology* **2016**, *10*, 770–779. [CrossRef]
34. Toybou, D.; Celle, C.; Aude-Garcia, C.; Rabilloud, T.; Simonato, J.-P. A toxicology-informed, safer by design approach for the fabrication of transparent electrodes based on silver nanowires. *Environ. Sci.* **2019**, *6*, 684–694. [CrossRef]

Conclusion

Le premier résultat important est le phénomène d'accumulation observé avec la silice fluorescente : les cellules exposées à 4x5µg/ml ont une fluorescence similaire aux cellules exposées à 1x20µg/ml. D'autre part, les effets sur les macrophages de cette exposition répétée sont moins importants que ceux d'une exposition aiguë. En effet, la mortalité des cellules est plus faible : pas de mortalité pour une exposition de 4x10µg/ml et une mortalité de 24% avec une exposition à 1x20µg/ml, avec la silice fluorescente. Les mêmes tendances sont observées avec la LS30. L'adhérence des cellules est diminuée suite à une exposition aiguë à la silice, l'exposition répétée quant à elle ne modifie pas la physiologie des cellules par rapport aux cellules non exposées. La fonction principale des macrophages, la phagocytose, est altérée par l'exposition à la silice amorphe de synthèse. Le nombre de cellules phagocytaires diminue de 64% et 38% pour l'exposition aiguë et répétée respectivement, par rapport au contrôle.

II c) Dose fractionnée 10jours

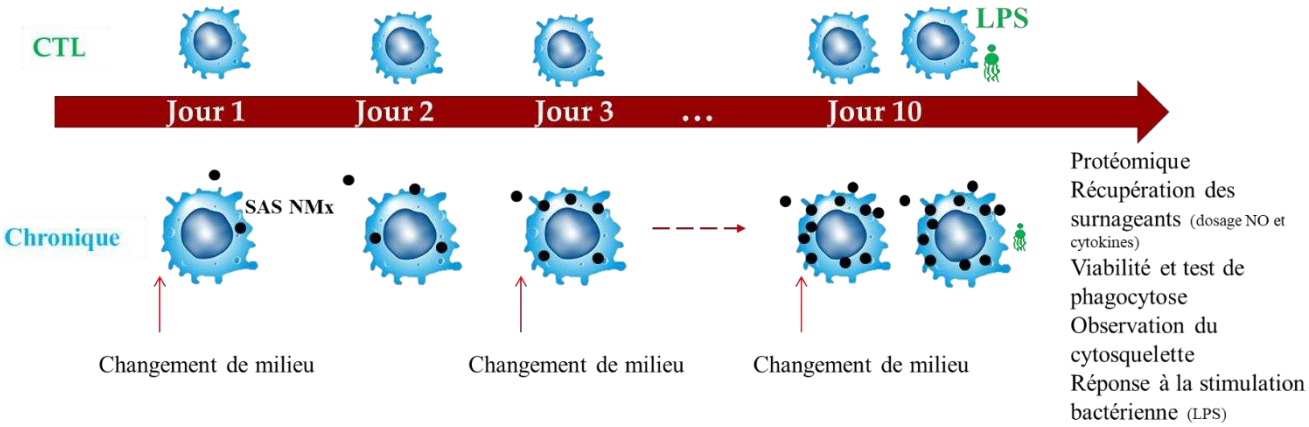

Figure 55 : Protocole d'exposition permettant d'étudier l'effet du débit de dose (ou dose fractionnée) de l'exposition aux nanomatériaux, pendant 10 jours.

Répété 10 jours silice fluorescente

Présentation du projet

Le schéma d'exposition est le même que précédemment utilisé (figure 55), les cellules sont exposées quotidiennement durant 10 jours à 1 ou 2 µg/ml de silice fluorescente (SiG), et comparées avec des cellules non exposées. Des tests de cytotoxicité et fonctionnels ont été réalisés pour évaluer les effets d'une exposition répété plus longue que dans l'étude précédente mais à la même dose cumulée finale, soit 20µg/ml.

Résultats

Les résultats sont présentés sur la figure 56. Les cellules ont été observées en microscopie confocale afin de voir l'effet d'une exposition répétée sur la morphologie des cellules. Après 10 jours de culture, les macrophages sont ronds et possèdent quelques filaments et élongations d'actine, la morphologie des cellules semble similaire entre les différentes conditions observées. Les cellules exposées ont internalisé la silice fluorescente, il n'y a pas de silice adsorbée visible. Les cellules exposées de façon répétée à 2µg/ml sont plus fluorescentes

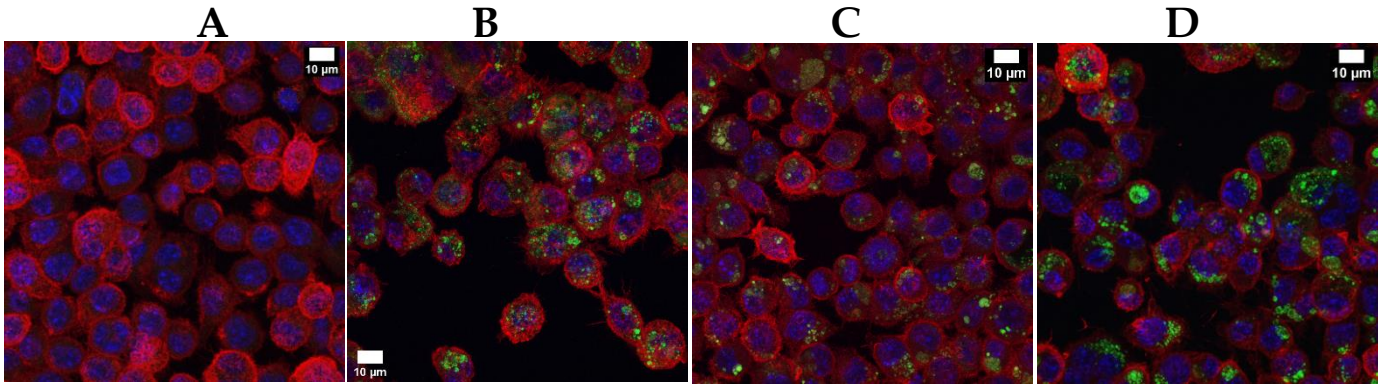

Figure 56 : Observation du cytosquelette de macrophages exposés durant 10 jours à la silice fluorescente, par microscopie confocale LSM880. A) Contrôle : cellules non traitées, B) cellules exposées 24h (aigu) à 5µg/ml, C) Cellules exposées de façon répétée à 1µg/ml/jour et D) Répété 2µg/ml/jour. Noyau coloré au DAPI, actine colorée en phalloïdine 550 et silice verte colorée à cœur en FITC Sicastar-GreenF 42-00-301.

en FITC que les cellules exposées à 1µg/ml/jour. Le marquage FITC n'est pas présent de manière diffuse dans le cytoplasme cellulaire, le signal est concentré, probablement au sein de vésicules.

Ensuite, la cytotoxicité de l'exposition répétée à la silice fluorescente a été comparée à celle d'une exposition aiguë (comparaison entre dose équivalente, cumulée ou en une seule dose) (figure 57). Les cellules exposées en une dose à 20µg/ml ont eu tendance à se décoller, ce qui a rendu certaines analyses impossibles pour cette condition. Les cellules exposées en dix fois à 20µg/ml ont une viabilité équivalente aux cellules non exposées (96%). Les cellules exposées en une simple dose à 10µg/ml ont une mortalité de 30% par rapport aux cellules contrôles. Ensuite, l'intensité de fluorescence de la silice verte (SiG) a été mesurée afin de connaître son internalisation. On observe une certaine accumulation de la silice appliquée en plusieurs fois. Cependant, contrairement à l'étude précédente ou l'accumulation était équivalente entre aigu et répété pour la même dose cumulée, ici, la fluorescence des cellules exposées à 1x20µg/ml (aigu) est supérieure à celles exposées à 10x2µg/ml (répété). De même, les cellules exposées 10 fois à 1µg/ml ne sont pas aussi fluorescentes en FITC que les cellules exposées à 10µg/ml en une dose. Concernant la phagocytose, la proportion de cellules phagocytaires diminue de 10% pour les cellules exposées durant 10 jours à 1µg/ml par rapport aux cellules contrôles, alors que cette diminution est de 25% pour les cellules exposées une fois à 10µg/ml. Ces cellules exposées sont également moins phagocytaires que les contrôles, avec une diminution de l'activité de 20% pour l'exposition répétée et de 50% pour l'exposition aiguë.

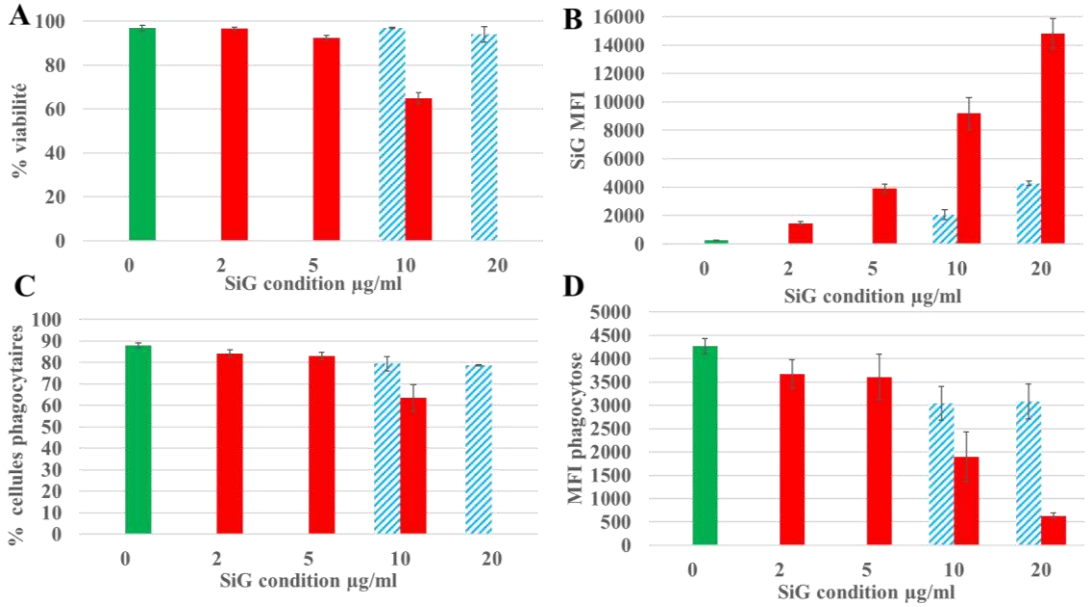

*Figure 57 : Viabilité et phagocytose des macrophages exposés 10 jours à la silice fluorescente. En vert : les cellules non exposées, en rouge : les cellules exposées à une seule dose (aigu), en hachuré bleu : les cellules exposées durant 10 jours quotidiennement. Concentration en SiG exprimée en dose totale (cumulée ou simple dose). **A**) Viabilité cellulaire, **B**) internalisation de la silice fluorescente, **C**) proportion de cellules phagocytaires parmi les cellules vivantes et **D**) activité phagocytaire.*

La production d'oxyde nitrique a ensuite été mesurée, les résultats sont présentés sur la figure 58. En absence de stimulation au LPS, il y a une augmentation de 30% de la sécrétion de NO des cellules exposées à 20µg/ml par rapport aux contrôles, les cellules exposées quotidiennement à 2µg/ml ont une sécrétion équivalente aux cellules non exposées. Avec la stimulation au LPS (dernières 18h de culture), la sécrétion de NO est diminuée de 50% chez les

cellules exposées 24h à 20µg/ml, par rapport aux contrôles, les cellules exposées de façon répétée sont équivalentes aux cellules non exposées.

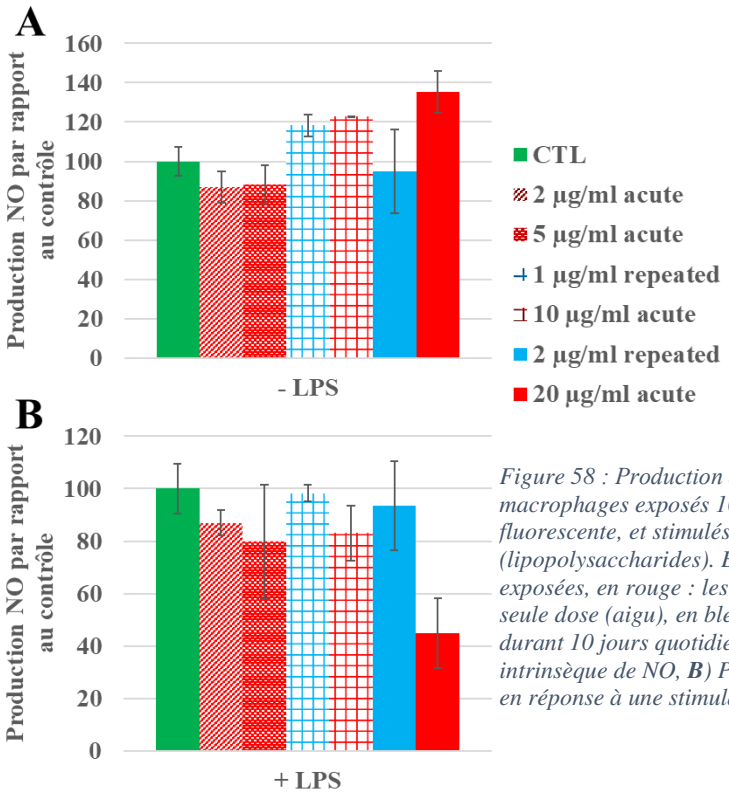

*Figure 58 : Production d'oxyde nitrique des macrophages exposés 10 jours à la silice fluorescente, et stimulés ou non au LPS (lipopolysaccharides). En vert : les cellules non exposées, en rouge : les cellules exposées à une seule dose (aigu), en bleu : les cellules exposées durant 10 jours quotidiennement. **A**) Production intrinsèque de NO, **B**) Production des macrophages en réponse à une stimulation bactérienne.*

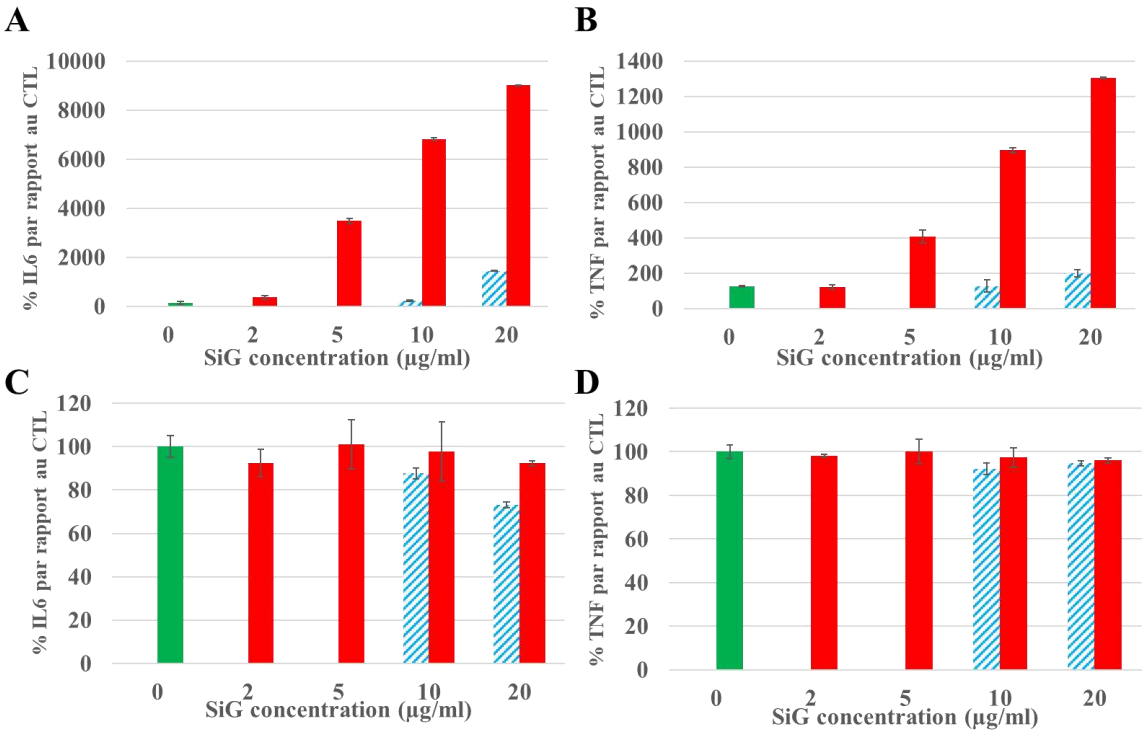

*Figure 59 : Réponse inflammatoire des macrophages exposés 10 jours à la silice fluorescente. En vert : les cellules non exposées, en rouge : les cellules exposées à une seule dose (aigu), en hachuré bleu : les cellules exposées durant 10 jours quotidiennement. Concentration en SiG exprimée en dose totale (cumulée ou simple dose). **A**) Sécrétion intrinsèque d'IL6, **B**) sécrétion intrinsèque de TNF, **C**) sécrétion d'IL6 avec stimulation au LPS et **D**) sécrétion de TNF avec stimulation au LPS.*

La sécrétion de cytokines pro-inflammatoires a ensuite été mesurée, pour l'IL6 et le TNF, les résultats sont présentés sur la figure 59. La sécrétion intrinsèque d'IL6 des cellules non traitées est inférieure au seuil de détection du kit utilisé, soit inférieure à 5pg/ml. Les cellules exposées à 10x2µg/ml sécrètent 20pg/ml, à titre de comparaison les cellules exposées à 1x20µg/ml sécrètent 125pg/ml. Concernant la sécrétion de TNF, les cellules non traitées sécrètent 0,9 ng/ml, les cellules exposées à 10x2µg/ml sécrètent 1,6 ng/ml (augmentation de 1,5 fois par rapport au contrôle) et les cellules exposées 24h à 20µg/ml, 10,4 ng/ml (augmentation de 10fois par rapport au contrôle). Avec la stimulation au LPS, les cellules non exposées à la silice sécrètent 60ng/ml d'IL6, similaire aux cellules exposées 24h à 20µg/ml (54ng/ml). Les cellules du scénario répété sécrètent 45 ng/ml d'IL6, soit une diminution de 25% par rapport au contrôle. Pour le TNF, les sécrétions sont équivalentes entre les différentes conditions, soit environ 8 ng/ml.

Conclusion

Ce projet a permis de compléter l'étude précédente menée sur 4 jours. Si certaines tendances sont maintenues entre l'exposition 4 jours et 10 jours (cytotoxicité, phagocytose), cela n'est pas le cas pour tous les paramètres. La bioaccumulation totale précédemment observée en 4 jours ne se maintient pas sur 10 jours, il existe seulement une accumulation partielle de la silice fluorescente : la MFI de la condition 10x2µg/ml est légèrement supérieure à celle de 1x5µg/ml. Cette faible accumulation peut expliquer les effets modérés d'une exposition répétée par rapport aux effets de l'exposition aiguë, notamment pour la phagocytose et la sécrétion de cytokines. Cette observation suggère qu'un phénomène a lieu entre le quatrième et le dixième jour, qui limite l'accumulation de la silice, et nous a conduit à émettre deux hypothèses concernant le devenir de la silice : celle-ci est relarguée dans le milieu ou bien le macrophage est capable de dissoudre la silice internalisée dans les vésicules. Nos travaux (Torres et al. En rédaction About the inflammatory effects of synthetic amorphous silica and their persistence: an in vitro study on macrophages) ont permis de répondre à cette question, en étudiant la persistance des effets, nous avons constaté que les macrophages sont capables de dissoudre (sous forme de silicates probablement) la silice amorphe de synthèse. Ce qui, d'une part la faible persistance des effets, mais également la toxicité plus faible pour une exposition répétée.

Ces projets confirment la nécessité de tester chacun des scénarii d'exposition en fonction de leur pertinence pour le (nano)matériau étudié, les effets d'une exposition aiguë n'étant pas transposable ou prédictifs pour une exposition répétée.

II c) Exposition chronique silice précipitée et fumée

Présentation du projet

Les études précédentes ont permis de montrer les effets d'une exposition répétée au niveau de la réponse des macrophages, et cela sur 4 jours et 10 jours pour la silice, ou 20 jours dans le cas de l'argent, précédemment publié dans l'équipe (Dalzon, Aude-Garcia, et al. 2020). Ce projet se concentre sur la comparaison de deux SAS (précipitée et fumée de surface spécifique équivalente) durant 10 jours afin de mieux mimer une exposition quotidienne telle que celle des travailleurs ou des consommateurs. Une étude protéomique a permis d'effectuer une approche large des effets provoqués par cette exposition répétée de 10 jours à 2 µg/ml/jour. Cette étude a été complétée par des expériences de validation sur la viabilité, la réponse inflammatoire, la phagocytose et les voies métaboliques mises en évidence par l'analyse protéomique.

nanomaterials

MDPI

Article

Repeated Exposure of Macrophages to Synthetic Amorphous Silica Induces Adaptive Proteome Changes and a Moderate Cell Activation

Anaelle Torres [1], Véronique Collin-Faure [1], Hélène Diemer [2,3], Christine Moriscot [4], Daphna Fenel [5], Benoît Gallet [5], Sarah Cianférani [2,3], Jacques-Aurélien Sergent [6] and Thierry Rabilloud [1,*]

1 Chemistry and Biology of Metals Laboratory, Université Grenoble Alpes, Centre National de la Recherche Scientifique, Commissariat à l'Energie Atomique, Interdisciplinary Research Institute of Grenoble, 38054 Grenoble, France; anaelle.torres@cea.fr (A.T.); veronique.colllin@cea.fr (V.C.-F.)
2 Laboratoire de Spectrométrie de Masse BioOrganique (LSMBO), Centre National de la Rech erche Scientifique, Hubert Curien Pluridisciplinary Institute UMR 7178, Strasbourg University, 67087 Strasbourg, France; hdiemer@unistra.fr (H.D.); sarah.cianferani@unistra.fr (S.C.)
3 Infrastructure Nationale de Protéomique ProFI—FR2048, 67087 Strasbourg, France
4 Integrated Structural Biology Grenoble (ISBG), European Molecular Biology Laboratory Université Grenoble Alpes, Centre National de la Recherche Scientifique, Commissariat à l'Energie Atomique, 71 Avenue des Martyrs, 38042 Grenoble, France; christine.moriscot@ibs.fr
5 Institute of Structural Biology (IBS), Université Grenoble Alpes, Centre National de la Recherche Scientifique, Commissariat à l'Energie Atomique, Interdisciplinary Research Institute of Grenoble, 38044 Grenoble, France; daphna.fenel@ibs.fr (D.F.); benoit.gallet@ibs.fr (B.G.)
6 Toxicological and Environmental Risk Assessment Unit, Solvay SA, 1120 Brussels, Belgium; jacques-aurelien.sergent@solvay.com
* Correspondence: thierry.rabilloud@cnrs.fr; Tel.: +33-43-878-3212

Abstract: Synthetic amorphous silica (SAS) is a nanomaterial used in a wide variety of applications, including the use as a food additive. Two types of SAS are commonly employed as a powder additive, precipitated silica and fumed silica. Numerous studies have investigated the effects of synthetic amorphous silica on mammalian cells. However, most of them have used an exposure scheme based on a single dose of SAS. In this study, we have used instead a repeated 10-day exposure scheme in an effort to better simulate the occupational exposure encountered in daily life by consumers and workers. As a biological model, we have used the murine macrophage cell line J774A.1, as macrophages are very important innate immune cells in the response to particulate materials. In order to obtain a better appraisal of the macrophage responses to this repeated exposure to SAS, we have used proteomics as a wide-scale approach. Furthermore, some of the biological pathways detected as modulated by the exposure to SAS by the proteomic experiments have been validated through targeted experiments. Overall, proteomics showed that precipitated SAS induced a more important macrophage response than fumed SAS at equal dose. Nevertheless, validation experiments showed that most of the responses detected by proteomics are indeed adaptive, as the cellular homeostasis appeared to be maintained at the end of the exposure. For example, the intracellular glutathione levels or the mitochondrial transmembrane potential at the end of the 10 days exposure were similar for SAS-exposed cells and for unexposed cells. Similarly, no gross lysosomal damage was observed after repeated exposure to SAS. Nevertheless, important functions of macrophages such as phagocytosis, TNFα, and interleukin-6 secretion were up-modulated after exposure, as was the expression of important membrane proteins such as the scavenger receptors, MHC-II, or the MAC-1 receptor. These results suggest that repeated exposure to low doses of SAS slightly modulates the immune functions of macrophages, which may alter the homeostasis of the immune system.

Keywords: synthetic amorphous silica; macrophages; proteomics; inflammation; repeated exposure

Citation: Torres, A.; Collin-Faure, V.; Diemer, H.; Moriscot, C.; Fenel, D.; Gallet, B.; Cianférani, S.; Sergent, J.-A.; Rabilloud, T. Repeated Exposure of Macrophages to Synthetic Amorphous Silica Induces Adaptive Proteome Changes and a Moderate Cell Activation. *Nanomaterials* **2022**, *12*, 1424. https://doi.org/10.3390/nano12091424

Academic Editors: Dumitriţa Rugină, Cristina Coman and David M. Brown

Received: 3 February 2022
Accepted: 18 April 2022
Published: 22 April 2022

1. Introduction

Synthetic amorphous silica (SAS) is one of the most produced (and used) nanomaterials, with a worldwide production in millions of tons per year [1]. Due to this high production and use, the potential adverse effects of this nanomaterial need to be investigated in detail. This investigation is made even more acutely needed by the fact that another form of silica, namely crystalline silica, is known to be the etiological agent of a severe disease, silicosis [2,3]. Silicosis is generally linked to working conditions such as mining or sandblasting, but may also occur through environmental exposure [4]. Silicosis being a chronic inflammatory disease, innate immune cells such as macrophages are at the root of the disease's etiology [5–10]. Based on this paradigm, studies of the toxicological impact of SAS have focused on the persistence of the effects on in vivo model [11–14] and on macrophage models for in vitro systems (as reviewed for example in [15,16]). These studies have shown that SAS is selectively toxic for macrophages [17,18] but not for other cell types [19], and also induces a pro-inflammatory response [20–23]. This suggests a strong parallel between the toxicology of SAS and the one of crystalline silica. However, the in vitro studies that have investigated the pro-inflammatory effects of SAS have used a classical acute exposure mode, and thus cannot investigate the persistence of the effects, which is a key dimension in the etiology of silicosis. In vivo studies have shown that the effects of SAS are transient [11–14], which has been recently transposed (and confirmed) using dedicated in vitro systems [24].

When assessing the toxicology of SAS, another point to be taken into account is that the exposures to this nanomaterial are generally chronic, i.e., repeated and at low concentrations over a long period, e.g., through the use of SAS as a food additive or in cosmetics. This is a critical dimension to consider when studying the effects of SAS on macrophages in vitro. Indeed, the few studies that have investigated the effects of repeated exposures, mostly on silver nanoparticles, have reported different effects than those observed after an exposure to a single dose [25–30]. Such studies are much less common for silica [31] and have centered more on the structural determinants of the effects of silica on cells rather than on the cellular responses. This is an active area of research [32–35], as the chemical determinants of the effects of silica on cells are much less obvious than for metallic nanoparticles, which often produce their effects through partial dissolution and liberation of toxic metal ions [36].

In complement to the studies devoted to the understanding of the chemical features that drive silica toxicity, we decided to carry out a study centered on the cellular responses of macrophages to SAS. We thus chose to investigate the effects of two different types of SAS, namely precipitated silica and fumed silica. Precipitated silica is prepared via a wet route starting from alkaline silicates in water, while fumed silica is prepared via a pyrolytic route starting from silicon halides that are burnt in a flame in the presence of oxygen. Both types of silica are produced and sold as solids and can be used in a variety of applications ranging from tires and resins reinforcement to additives in food and cosmetics. As exposures to these forms of SAS are typically occupational, we chose to investigate the effects of a repeated exposure on macrophages, using a combination of proteomics and targeted studies. Omics studies in general and proteomics in particular have been shown to be interesting tools to better decipher the cellular responses to nanomaterials [28,29,37,38], sometimes allowing us to unravel new mechanisms at play in the effects of nanomaterials [28,37,38].

2. Materials and Methods

2.1. Nanomaterials and Reagents

The precipitated SAS used in this study was provided based on a collaboration with Solvay (Solvay GBU Silica, Lyon, France), reflecting a commercial grade of SAS. The primary particle size was in the 10–20 nm range, the agglomerate size in the micron range, and the specific surface area close to 220 m^2/g. The fumed silica used in this study was purchased from Sigma (catalog #S5055, St. Louis, MI, USA). Its primary particle size was in the 20–30 nm range, the agglomerate size in the 250-nm range, and the specific surface area close to 200 m^2/g. More characterization details have been provided in previous

publications [24,39] and are also available in Supplementary Materials Figure S1. For use in cell cultures, both forms of silica were suspended in ultrapure water at the concentration of 10 mg/mL and pasteurized overnight after 10 min of sonication in an ultrasonic bath.

Unless otherwise stated, all reagents were at least 99% pure and purchased from Sigma (St. Louis, MO, USA)

2.2. Cell Culture

The mouse macrophage cell line J774A.1 was obtained from the European Cell Culture Collection (Salisbury, UK). The cells were cultured in DMEM medium +10% fetal bovine serum (FBS) under an air 5% CO_2 atmosphere. For routine culture, cells were seeded on non-adherent flasks (e.g., suspension culture flasks from Greiner) at 200,000 cells/mL and harvested 48 h later, at 1,000,000 cells/mL. Cell viability was measured by a dye exclusion assay, either with eosin (1 mg/mL) under the microscope or with propidium iodide (1 µg/mL) in a flow cytometry mode.

For treatment with SAS, cells were seeded at 500,000 cells/mL and cultured for 24 h at 37 °C for cell adhesion. The medium volume was adjusted to keep a constant medium height for all the culture supports used (2 mL for six-well plates and 15 mL for 75 cm^2 flasks). The cells were then grown to confluence for 48 h. The cells were then treated daily with 2 µg/mL silica for ten days, with a culture medium change every two days. In order to take cell detachment into account [40], the medium removed at each medium changed was centrifuged (100 g, 5 min) to collect the detached cells. The cell pellets obtained at this stage were resuspended in the fresh culture medium and added to the remaining cell layer. At the end of the exposure period, the cell culture medium was removed and the cells were collected by scraping in PBS, then rinsed twice in PBS and processed. In order to investigate cell responses to bacteria, stimulation with LPS (100 ng/mL) was carried out in some experiments for the last 24 h in culture before harvesting. When an exposure to fluorescent colloidal silica (Micromod Sicastar green ref 42.00.301) was carried out, the cells were exposed for the last 24 h in culture to a concentration of 20 µg/mL of fluorescent silica.

2.3. SAS Quantification by ICP-AES

2.3.1. Sample Preparation

For SAS internalization and quantification in the cells, the cells were grown on adherent six-well plates and exposed to silica as described above. One milliliter of lysis solution (5 mM HEPES pH 7.5, 0.75 mM spermine tetrahydrochloride, and 0.1% tetradecyldimethylammonio propane sulfonate) was added in the wells, after the medium had been removed and the cell layer washed once with PBS. The lysates were aliquoted and frozen. The day before the quantification by ICP-AES, the samples were mineralized: in each sample, an equal volume of 1 N potassium hydroxide was added; the samples were then incubated overnight at 80 °C in a preheated water bath [41].

2.3.2. ICP-AES Dosage

The multi-elemental standards for ICP were purchased from Sigma-Aldrich (ref 92091) and were first prepared in 10% HNO_3. At the end of the standard measurement, samples were prepared two at a time (base-mineralized silica is not stable in HNO_3). From 250 to 500 µL of mineralisate was added to 10% HNO_3 to reach a final volume of 6 mL. The samples were measured in an ICP-AES Shimadzu 9000 with ICPE solution Launcher software (v1.31, Shimadzu France, Noisiel, France).

2.4. Proteomics

2.4.1. Sample Preparation

The cell pellets obtained after exposure to SAS (or from mock-exposed cells cultivated under the same conditions) were lysed in were extracted with 10 pellet volumes of lysis solution (7 M urea, 2 M thiourea, 15 mM spermine base, 15 mM spermine tetrahydrochloride, 10 mM Tris (carboxyethyl) phosphine hydrochloride and 4% (*w*/*v*) CHAPS). After

extraction at room temperature for one hour, the extracts were clarified by centrifugation (15,000× *g* 15 min), the supernatants collected, and their protein concentration determined by a modified Bradford assay [42]. The protein extracts were stored frozen at −20 °C until use.

2.4.2. Sample Processing and Mass Spectrometry

For the shotgun proteomic analysis, the samples were included in polyacrylamide plugs according to Muller et al. [43], with some modifications to downscale the process [44]. To this purpose, the photopolymerization system using methylene blue, toluene sulfonate, and diphenyliodonium chloride was used [45].

First, a sample dilution solution (8 M urea in 200 mM Tris-HCl, pH 8) was prepared. Then, the dye solution (0.5 mM methylene blue in sample dilution solution) was prepared. The other initiator solutions consisted of a 1 M solution of sodium toluene sulfinate in water and in a saturated water solution of diphenyliodonium chloride. The ready-to-use polyacrylamide solution consisted of 1.2 mL of a commercial 40% acrylamide/bis solution (37.5/1) to which 100 µL of diphenyliodonium chloride solution, 100 µL of sodium toluene sulfinate solution, and 100 µL of water were added.

Protein samples (20 µg each) were first diluted to a 9 µL final volume with sample dilution solution in a 500 µL conical microtube (Eppendorf, Hamburg, Germany). To this solution, 6 µL of dye solution then 5 µL of acrylamide solution were then added and mixed by pipetting. Then, 100 µL of water-saturated butanol were layered on top of the samples, and polymerization was carried out under a 1500 lumen 2700 K LED lamp for 2 h, during which the initially blue gel solution discolored. At the end of the polymerization period, the butanol was removed, and the gel plugs were fixed for 2 × 1 h with 200 µL of 30% ethanol 2% phosphoric acid, followed by a 30-min wash in 30% ethanol. The fixed gel plugs were then stored at −20 °C until use.

Gel plug processing, digestion, peptide extraction, and nanoLC-MS/MS was performed as previously described [44], without the robotic protein handling system and using a Q-Exactive Plus mass spectrometer (Thermo Fisher Scientific, Bremen, Germany).

2.4.3. Protein Identification

For protein identification, the MS/MS data were interpreted using a local Mascot server with MASCOT 2.6.2 algorithm (Matrix Science, London, UK) against an in-house database containing all Mus musculus and Rattus norvegicus entries from UniProtKB/SwissProt (version 2019_10, 50,313 sequences) and the corresponding 50,313 reverse entries. Spectra were searched with a mass tolerance of 10 ppm for MS and 0.07 Da for MS/MS data, allowing a maximum of one trypsin missed cleavage. Trypsin was specified as an enzyme. Acetylation of protein n-termini, carbamidomethylation of cysteine residues, and oxidation of methionine residues were specified as variable modifications. Identification results were imported into Proline software version 2.1 (http://proline.profiproteomics.fr/) for validation. Peptide Spectrum Matches (PSM) with pretty rank equal to one were retained. False Discovery Rate was then optimized to be below 1% at PSM level using Mascot Adjusted E-value and below 1% at Protein Level using Mascot Mudpit score.

Mass spectrometry data are available via ProteomeXchange [46] with the identifier PXD03002, associated with the doi: 10.6019/PXD030002.

2.4.4. Label Free Quantification

Peptide Abundances were extracted using the Proline software version 2.1 (http://proline.profiproteomics.fr/) with a m/z tolerance set at 10 ppm. Alignment of the LC-MS runs was performed using Loess smoothing. Cross Assignment was performed within groups only. Protein Abundances were computed by sum of peptide abundances (normalized using the median).

2.4.5. Data Analysis

For the global analysis of the protein abundances data, we first excluded all proteins identified by only one peptide. The protein abundances data were normalized to the sum of all protein abundances, converted to ppb (part per billion), and missing data were imputated with a low, non-null value. The relative abundances data were used directly for global analysis using the PAST software suite [47] without any transformation. Principal correspondence analysis and non-metric multidimensional scaling were used to assess the global differences between samples. In order to minimize the quantitative bias due to the widely different protein abundances within each sample, the Gower distance (i.e., a normalized distance) was used to perform the principal correspondence analysis.

Proteins were considered as significantly different if their U value in the Mann–Whitney U test was $\leq$2 in the control vs. SAS-treated comparison. As the proteomics experiments were performed on five independent biological replicates, this corresponded to $p < 0.05$. No quantitative change threshold value was applied. However, a false discovery rate was calculated for each selected protein, using the sequential Fisher test approach [48]. The selected proteins were then submitted to pathway analysis using the DAVID tool [49], with a FDR cutoff value set at 0.1.

2.5. Phagocytosis and Particle Internalization Assay

The phagocytic activity was measured using fluorescent latex beads (1 µm diameter, green labelled, catalog number L4655 from Sigma), with exclusion of the dead cells from the analysis, as described previously [50].

2.6. Mitochondrial Transmembrane Potential Measurement

The mitochondrial transmembrane potential was assessed by Rhodamine 123 uptake at low concentration (80 nM) to avoid quenching [51], as described previously [52].

2.7. Reduced Glutathione Measurement

The reduced glutathione was assessed by using monochlorobimane at 70 µM final concentration, with exclusion of the dead cells from the analysis, as described previously [53]. This experiment was carried out with a FacsMelody flow cytometer and the FacsChorus software (v1.3.3. BD Biosciences, Le Pont de Claix, France) for data analysis.

2.8. Lysosomal Function Evaluation

The ratiometric acridine orange fluorescence was used to investigate the lysosomal function. Cells were seeded into six-well plates and exposed to silica, as described above. Acridine orange (Sigma A6529) was added to the cell culture (100 ng/mL), and the culture returned to the incubator for 30 min. Then, cells were harvested and washed with PBS-glucose (PBSG). The pellets were suspended with 250 µL of PBSG supplemented with Sytox Red (5 nM), and analyzed by flow cytometry. Acridine orange was excited at 475 nm, and the 526 nm and 650 nm emissions were recorded. The ratio between the two fluorescence intensities (Red/Green) was then calculated and used as an index of the lysosomal function [54].

2.9. Surface Markers

The cell surface labelling was used as a marker of cellular status. Cells were seeded into six-well plates and exposed to SAS for 10 days, as described above. Cells were harvested, washed with PBS, and fixed for 30 min with paraformaldehyde 4% at room temperature. Cells were washed again and stored at 4 °C until the cell surface labelling. The fixed cells were collected and dispersed in a 96-well plate with 300,000 cells per well. After a step of washing and centrifugation (1 min at 800× *g*), the cells were incubated 10 min at room temperature with PBS-fluo (PBS 1X containing 0.16% sodium azide and 3% of FBS) and Fc-block (purchased from eBiosciences, dilution 1/50). The cells were centrifuged and then incubated 20 min protected from light with PBS-fluo containing antibody of interest (CD14-

APC: BD ref 560634 dilution 1/200, CD38-FITC: BD ref 558813 dilution 1/200, CD86-APC: BD ref 558703 dilution 1/200, MARCO-FITC: R&Dsystems ref FAB2956F dilution 1/25, CD11b-FITC: eBiosciences ref dilution 1/100, CD204-PE: Invitrogen ref 12-2046-82 dilution 1/100, CD18-APC: BD Pharmingen ref 562828 dilution 1/50). Then, cells were washed twice with PBS-fluo, and finally, the cell pellets were suspended in 200 µL of PBS fluo for FACS analysis.

(FITC: excitation 488 nm emission 525 nm, APC: excitation 633 nm emission 760 nm, PE: excitation 488 nm, emission 575 nm.)

2.10. Cytokines and Nitric Oxide Production

Cells were grown into six-well plates and exposed to the indicated dose of SAS for 10 days at 37 °C. The cells were also primed or not with LPS (100 ng/mL) for the last 24 h of culture. For nitric oxide production, 5 mM arginine monohydrochloride were added for the last 24 h of culture, in order to provide unlimiting substrate for the NO synthase. The supernatants are collected and centrifuged to eliminate non-adherent cells. For nitric oxide, the nitrite concentration of the supernatants was measured with the Griess reagent at 540 nm. For cytokines, the experiments were carried out with the Cytometric Bead Array Mouse Inflammation Kit (BD Biosciences) and analyzed with FCAP Array software (3.0, BD Biosciences, Le Pont de Claix, France). This Flex-set kit allows measuring Interleukin-6 (IL-6) and TNFα protein levels in a single sample. The mixed capture beads were added to all assay tubes containing supernatant samples and standards (from 0 to 2500 pg/mL), the mouse inflammation phycoerythrin (PE, excitation 488 nm, emission 575 nm) detection reagent was added, and the mixture was incubated for 2 h at room temperature, protected from light. The wash buffer was added to each tube, which were then centrifuged 5 min at 200× *g*, and the pellets were resuspended with the wash buffer and analyzed by FacsCalibur flow cytometer.

3. Results

3.1. Toxic Effects of Repeated Exposure to Synthetic Amorphous Silica

First, we checked that the repeated treatment with either form of SAS was not toxic to the cells. Indeed, the dose was determined from a previous work with fumed silica [24], in which an acute LD20 dose was determined to be 20 µg/mL for 24 h. Thus, we fractionated the dose in 10 subdoses of 2 µg/mL each. As shown in Figure 1, this treatment had no visible toxicity on macrophages.

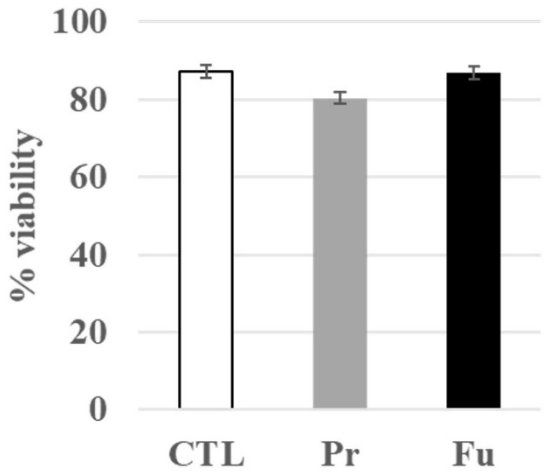

Figure 1. Viability of J774A.1 cells after a 10-day exposure to silica (2 µg/mL/day). CTL: control, cells without nanomaterials, Pr: precipitated silica 220 m^2/g, Fu: fumed silica 200 m^2/g.

3.2. Silica Uptake

Silica uptake was measured after the 10 days exposure period and also after a 24 h exposure to the same cumulative dose (1 × 20 µg/mL vs. 10 × 2 µg/mL/day). The results, shown in Table 1, indicate a significant uptake of silica in exposed macrophages. Interestingly, the uptake was more pronounced for precipitated silica than for fumed silica in the case of the 10 days exposure. This may be linked to the different aggregate sizes observed for the two forms of SAS after being in contact with proteins, as is the case for complete culture medium (Figure S1).

Table 1. SiO_2 internalization of J774A.1 cells after a 10-days exposure to silica by ICP-AES dosage, compared with acute exposure.

Si Amount µg/Well (Acute Exposure)	Si Amount µg/Well (Repeated Exposure)	Condition
1.06 ± 0.2	1.6 ± 0.2	Control
36.3 ± 4.4	10.9 ± 4.1	Precipitated silica
27.2 ± 1.1	5.8 ± 0.4	Fumed silica

Moreover, the uptake was much lower in the case of the 10 days exposure than in the 24 h exposure. This phenomenon has also been described for silver nanoparticles [29], but not in the case of a short-term (4 days) repeated exposure to colloidal silica [50].

Regarding silica uptake, we also checked by confocal and electron microscopy that, even after 24 h of exposure, silica was present mostly inside the cells and not only at their surface, which could have biased the uptake measurements (Figures S2 and S3).

3.3. Global Analysis of the Proteomic Results

When the raw proteomic data were filtered for proteins identified and quantified by at least two independent peptides, 2322 proteins were selected. As a first step in the exploitation of the proteomic data, a global analysis was performed. The purpose of such an analysis is to use all the protein abundance data (Supplementary Table S1) to determine the intensity of the global effects of the repeated exposures to precipitated and fumed silica.

The results, shown in Figure 2, indicated that precipitated silica had an overall greater effect on macrophages than fumed silica. The first two axes accounted for 35 and 10% of the variance, respectively.

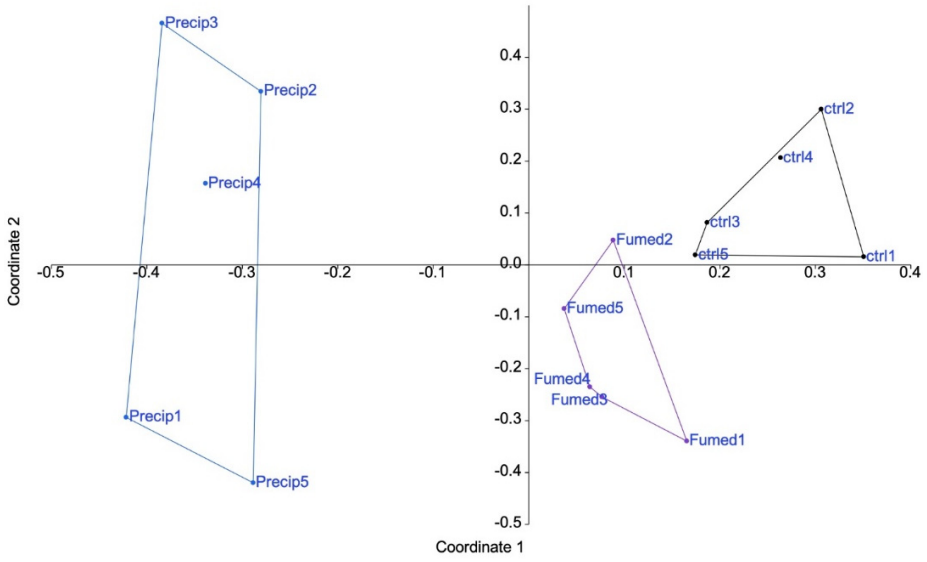

Figure 2. Proteomic results of J774A.1 cells after a 10-days exposure to silica. CTL: control, cells without nanomaterials, Pr: precipitated silica 220 m^2/g, Fu: fumed silica 200 m^2/g.

In order to take all the information into account, non-metric multidimensional scaling was used. The results, shown in Figure S4, confirmed the results of the principal correspondence analysis, and thus that precipitate silica induced more proteome changes than fumed silica.

In a second step, the protein showing significant expression changes ($p < 0.05$, i.e., $U \leq 2$ in the Mann–Whitney U test) between the exposed and control cells was selected, resulting in two separate lists for the proteins modulated by the treatment with precipitated silica (Supplementary Table S2) and the proteins modulated by the treatment with fumed silica (Supplementary Table S3). Regarding numbers, 287 proteins were modulated in response to fumed silica, while 814 proteins were modulated in response to precipitated silica. Of all these proteins, 209 were modulated by both treatments, leaving 78 proteins modulated only in response to fumed silica and 605 modulated only in response to precipitated silica.

Both lists were used to perform pathways analyses by the DAVID software (update 2021, Frederick National Laboratory for Cancer Research, Frederick, MD USA). The results of the pathway analyses are detailed in Tables S4 and S5, respectively. Some highlighted pathways indicated a global stress response (e.g., carbon metabolism, splicing, translation), which is expected for any cellular stress, while other pathways (e.g., lysosome, mitochondrion, phagosome, antigen presentation, immunity) were more specific. The main pathways highlighted by the DAVID software are summarized in Figure 3.

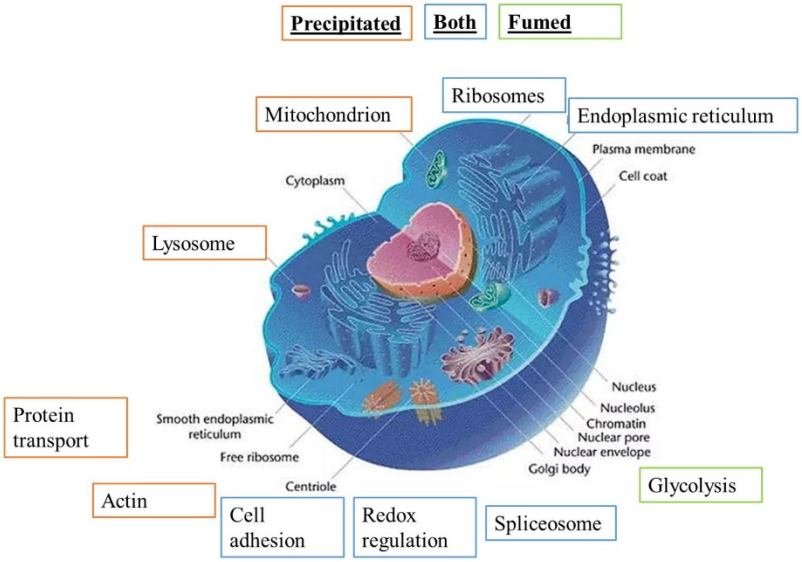

Figure 3. Modified pathways observed with proteomic study (DAVID analysis), adapted from Common Wikimedia Orange: pathway highlighted for precipitated SAS, green: pathway highlighted for fumed SAS, and blue: pathway highlighted for both SAS.

Precipitated synthetic amorphous silica is responsible for more protein changes in cell metabolism, function and binding than fumed SAS. Both these specific pathways and the proteins highlighted in them by the software were selected for detailed analysis.

3.4. Detailed Analysis of the Proteomic Results and Validation Experiments

In addition to the results of the pathway analysis, a manual analysis of the modulated protein lists was performed. This allowed for the selection of interesting proteins that escaped the pathway analysis because of either their poor annotation or the fact that they did not belong in an enriched-enough pathway to be selected by the software. Based on these data, we focused our detailed analyses on a few subsets of proteins

3.4.1. Mitochondrial Proteins

Seventy-six mitochondrial proteins were found to be modulated by the pathway analysis software (Table S6). Of these, 32 were decreased upon treatment with precipitated silica while 44 were increased, with a median fold change (in both directions) of ±21%. Furthermore, 14 of these proteins were also modulated in response to exposure to fumed silica. These numbers indicated rather minor, adaptive changes. For example, the 27 kDa subunit of the MICOS complex (accession number Q78IK4), implied in mitochondrial architecture, was decreased by 10% upon treatment with both forms of SAS. However, the 13, 19, 25, and 60 kDa subunits were also detected in the proteomic screen and did not show any significant change in response to either treatment. This further suggested small amplitude and adaptive changes. To test this hypothesis, we measured the mitochondrial transmembrane potential. The results, shown in Figure 4A,B, indicated an absence of alteration of the transmembrane potential, supporting the hypothesis of adaptive changes in the mitochondrial proteins.

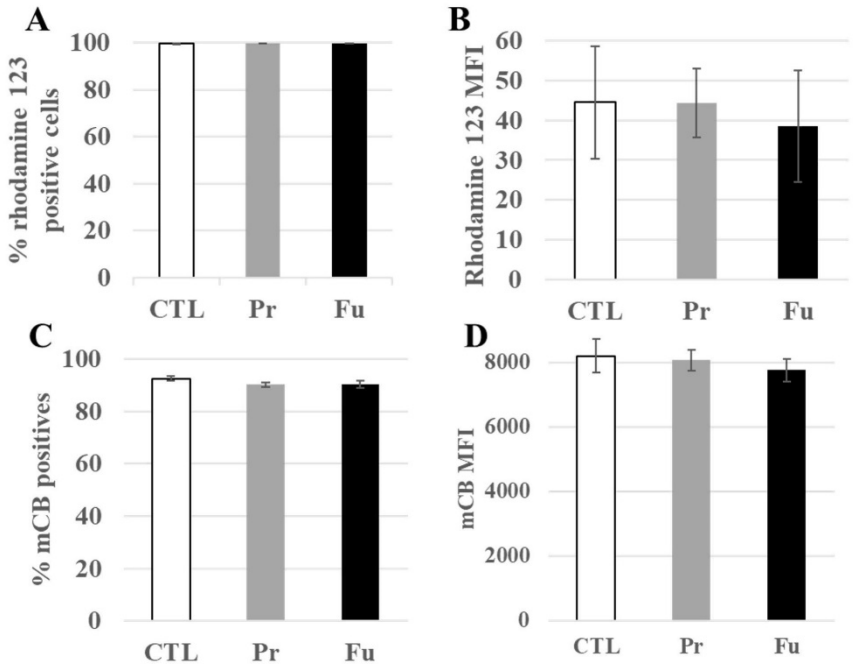

Figure 4. Mitochondrial transmembrane potential and redox potential of J774A.1 cells after a 10-day exposure to silica. (**A**) Proportion of rhodamine 123 positive cells, (**B**) MFI of rhodamine 123 positive cells, (**C**) Proportion of positive cells to monochlorobimane (mCB), (**D**) MFI of mCB+ cells. CTL: control, cells without nanomaterials, Pr: precipitated silica 220 m^2/g, Fu: fumed silica 200 m^2/g.

3.4.2. Glutathione Levels

"Cell redox homeostasis" was among the functional clusters highlighted by the pathway analysis, with 17 proteins modulated (Table S7). Of these, five were also modulated in response to exposure to fumed silica, and one (glutathione reductase) was modulated in response to exposure to fumed silica, but not precipitated silica.

The modulated proteins included five of the six peroxiredoxins, i.e., proteins involved in the destruction of peroxides, but also two proteins involved in glutathione metabolism, namely glutathione synthase and glutathione reductase. To check whether the repeated exposure to synthetic amorphous silica may induce perturbations in the redox balance, we measured the level of intracellular reduced glutathione. The results, shown in Figure 4C,D, indicated no change in the intracellular glutathione level.

3.4.3. Lysosomes and Phagocytosis

Forty-four lysosome-associated proteins were found modulated by the treatment with precipitated silica (Table S8). Of these, 12 were also modulated in response to exposure to

fumed silica. Interestingly, the luminal lysosomal proteins (e.g., cathepsins B, D, S and Z, alpha and beta mannosidases, arylsulfatases A and B) showed decreased abundances upon treatment, with a moderate median change of −30%, while the few lysosomal membranes detected (Q9CQW9, P52875, Q9Z0M5, P24668) were increased. This prompted us to test the lysosomal integrity by the acridine orange ratiometric method [54]. The results, shown in Figure 5A, indicated no change in the 650 nm/526 nm fluorescence, thereby indicating no gross alteration of the lysosomes upon treatment with either form of SAS.

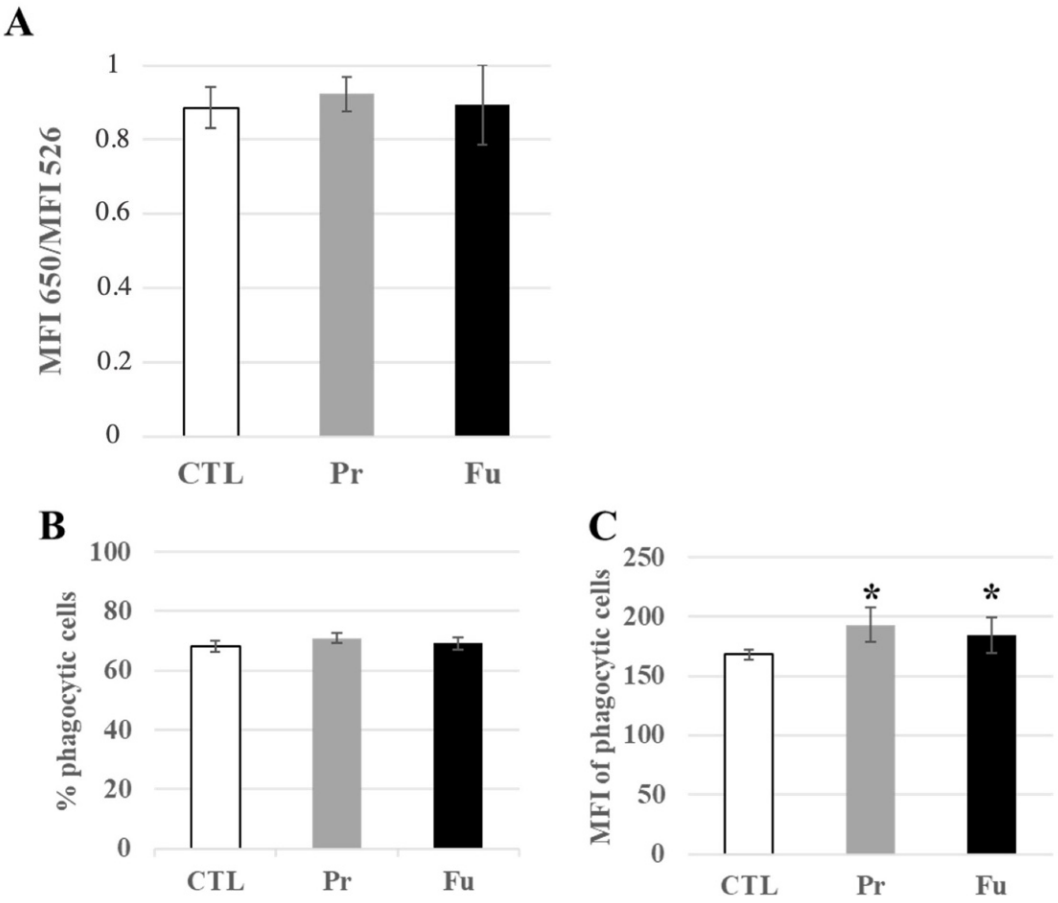

Figure 5. Lysosomal and phagocytic activity of J774A.1 cells after a 10-days exposure to silica. (**A**) Lysosomal ratio using acridine orange (entire/altered lysosomes), (**B**) Proportion of phagocytic cells, (**C**) Activity of phagocytic cells, MFI: mean fluorescent intensity. CTL: control, cells without nanomaterials, Pr: precipitated silica 220 m^2/g, Fu: fumed silica 200 m^2/g. Statistical significance in a Student *t*-test: * $p < 0.05$.

In macrophages, lysosomes are also associated with the phagocytic function, and this link was highlighted in the pathway analysis by functional clusters such as "actin cytoskeleton", but also by the modulation of subunits of the proton ATPase (P50408, P50518, P51863, P63081, Q9CR51), of granulins (P28798), and of activators of the NADPH oxidase (O70145, Q09014). We therefore probed the phagocytic function by flow cytometry. The results, shown in Figure 5B,C, indicated that the proportion of phagocytic cells in the culture remained constant, even after the treatment with either form of synthetic amorphous silica. However, detailed analysis of the fluorescence pattern showed a slight but significant increase in the phagocytic capacity of silica-treated cells over untreated cells.

3.4.4. Immunity-Associated Proteins

Thirty proteins associated with the keyword "immunity" were found to be modulated by the treatment with precipitated silica. (Table S9). In addition to these, other immunity-associated proteins, and especially surface markers such as CD11b, CD18, CD86, or CD204,

were also found significantly modified in their abundances upon treatment with precipitated silica, as well as fumed silica for CD11b and CD18. While CD11b and CD 18 showed a moderate decrease in their abundances upon treatment with precipitated silica (−11% and −15%, respectively), CD14 showed a moderate increase in abundance (+11%), while CD 86 and CD204 showed a higher increase in their abundances (+20% and +40%, respectively). In order to validate these proteomics results, a flow cytometry analysis of the surface expression of these markers was carried out. In addition to the markers detected by proteomics (CD11b, CD14, CD18, CD74 = MHC Class II, CD86, and CD204), we also tested a marker of M1 polarization (CD38) [55,56] and another form of scavenger receptor (MARCO) [57,58], and the results are shown in Figure 6. They indicated a slight but significant increase in the surface expression of CD11b and CD18 and an important increase in the proportion of CD14-positive cells after treatment with both forms of synthetic amorphous silica. An important increase in the proportion of positive cells was also observed in response to exposure to both forms of synthetic amorphous silica for CD38, MARCO, and CD74 (MHC class II). For CD86, the proportion of positive cells was slightly but significantly decreased in response to fumed silica but not to precipitated silica. However, the signal of the positive cells was significantly lower in cells exposed to both forms of silica than in control cells.

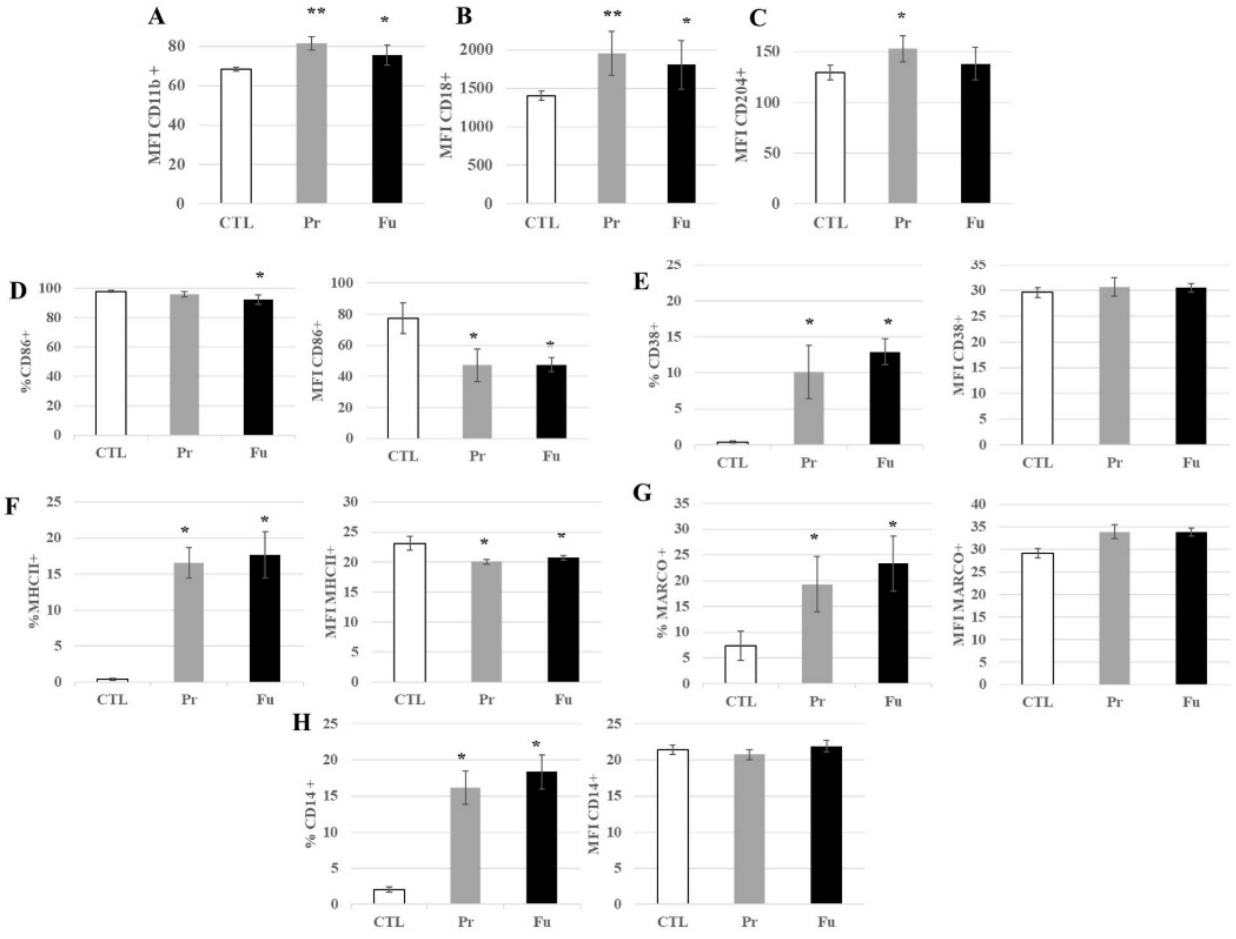

Figure 6. Expression of surface markers of J774A.1 cells after a 10-days exposure to silica. (**A**) CD11b marker (monocyte-macrophage, integrin α), (**B**) CD18 marker (integrin β), (**C**) CD204 marker (scavenger receptor), (**D**) CD86 marker (B7 family), (**E**) CD38 marker (inflammation, induced by IFNγ and LPS), (**F**) MHC class II (inflammation, signalization with CD4 T lymphocytes), (**G**) MARCO marker (scavenger receptor), (**H**) CD14 marker (LPS receptor), (**A**–**C**) All the conditions expressed these markers; only the amount of marker detected at the cell surface is different for cells exposed to SiO_2. CTL: control, cells without nanomaterials, Pr: precipitated silica 220 m^2/g, Fu: fumed silica 200 m^2/g. Statistical significance in a Student *t*-test: * $p < 0.05$; ** $p < 0.01$.

Regarding CD204, a slight but significant increase in its surface expression was observed after exposure to precipitated silica but not to fumed silica.

As scavenger receptors are known to be the receptors of silica [59–61], we checked whether this slight overexpression could be linked to a saturation of the silica internalization process after 10 days of continuous exposure. To this purpose, we treated macrophages for nine days with the SAS of interest, and exposed them to fluorescent colloidal amorphous silica for the last day. The results, shown in Figure 7, indicated that silica-treated cells internalized more fluorescent colloidal silica than untreated cells, which correlated with the increased expression of CD204 and MARCO.

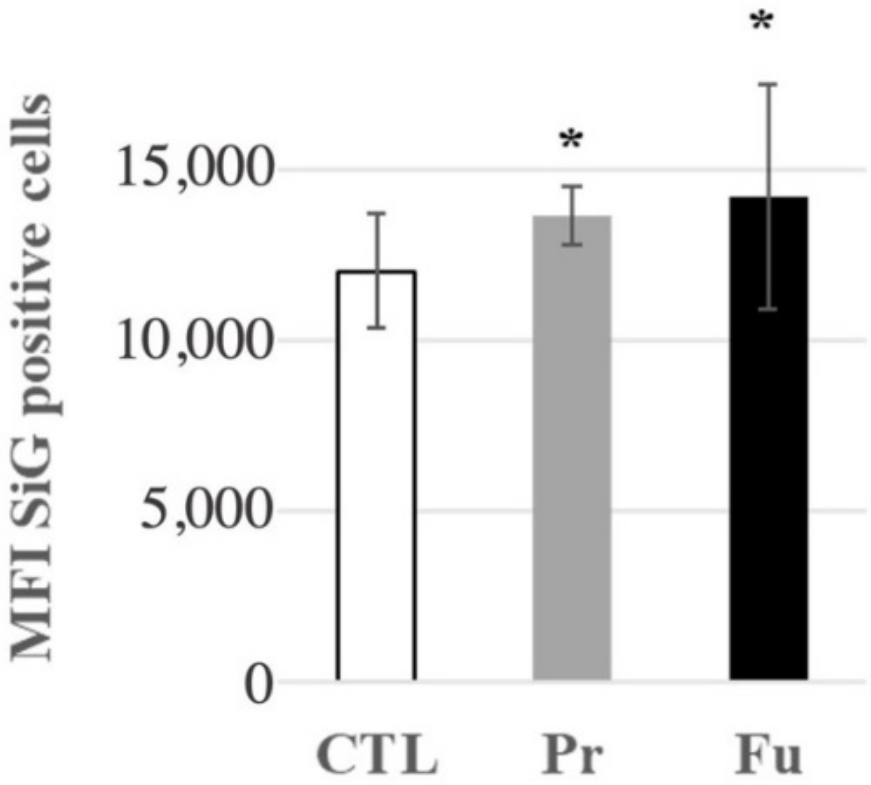

Figure 7. Fluorescent green silica (SiG) internalization of J774A.1 cells after a 10-day exposure to silica. Cells were exposed for 24 h to SiG (days 9 to 10). CTL: control, cells without nanomaterials, Pr: precipitated silica 220 m^2/g, Fu: fumed silica 200 m^2/g. Statistical significance in a Student *t*-test: * $p < 0.05$.

As proteomics cannot easily test secreted proteins because of their high efflux and low steady state levels in cells, we decided to test some pro-inflammatory cytokines. We thus tested the secretion of NO, TNFα, and IL-6 in response to the repeated exposure to synthetic amorphous silica, with and without terminal LPS stimulation. The results, shown in Figure 8, indicated a slight but significant increase in NO and TNFα production after treatment with SAS. In the case of TNFα, a more pronounced increase was observed after treatment with fumed silica compared to precipitated silica. This increase was also observed after LPS stimulation and was just transposed in range from the high pg/mL range (without LPS) to the medium ng/mL range with LPS. Regarding IL-6, its secretion remained undetectable (i.e., below 5 pg/mL) without LPS stimulation. With LPS stimulation, an increase in LPS secretion was observed after repeated exposure to fumed silica, but not to precipitated silica.

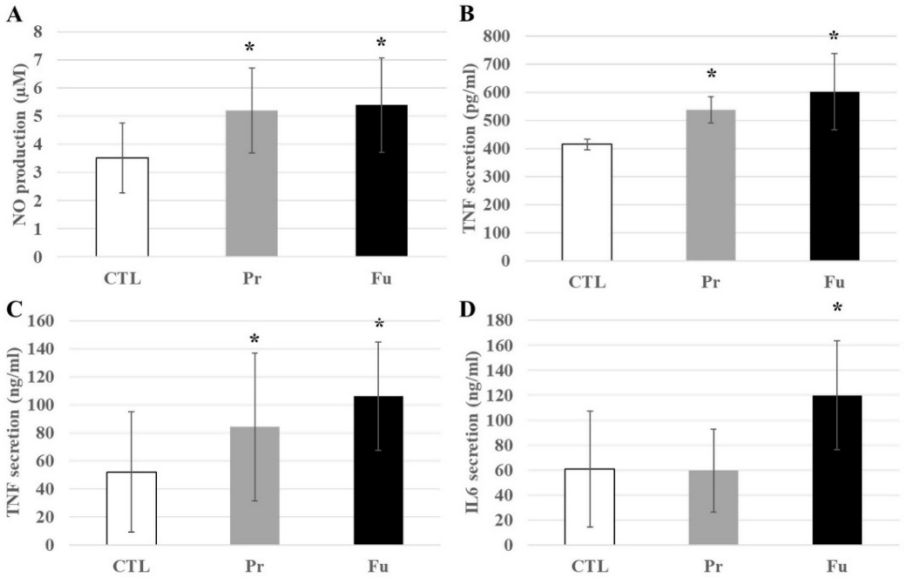

Figure 8. Inflammatory responses of J774A.1 cells after a 10-day exposure to silica, stimulated or not with LPS. (**A**) NO production without LPS, (**B**) TNFα secretion without LPS, (**C**) TNFα secretion with LPS, (**D**) IL-6 secretion with LPS. CTL: control, cells without nanomaterials, Pr: precipitated silica 220 m^2/g, Fu: fumed silica 200 m^2/g. Statistical significance in a Student *t*-test: * $p < 0.05$.

4. Discussion

Synthetic amorphous silica is used in a wide variety of applications and comes in three main forms, i.e., colloidal silica, precipitated silica, and fumed silica. Opposed to colloidal silica, which is by definition a suspension of silica nanoparticles in water, precipitated and fumed silica are produced as powders. Consequently, exposure to their dusts may occur in workers and in the general public, depending on their modalities of use. Such exposures are, by definition, repeated exposures, and it was thus necessary to use a repeated exposure scheme to reproduce the in vivo reality as closely as possible in our in vitro experiments. Indeed, it has been shown in the literature that repeated exposures produce a different biological outcome than single dose exposures, as described on silver nanoparticles [25,28,29] and on colloidal silica [50].

The dose that we have applied (2 µg/mL daily) has also been used in the literature [31] and considered as a realistic dose, in line with the typical exposure at the workplace or by consumers. Contrasting with this publication, we focused on the amorphous silica "as present and marketed", i.e., without forced disaggregation, compared two types of commercial SAS (precipitated and fumed) with similar descriptors, and used proteomics to get a wider description of the macrophages responses to silica.

Although the basic parameters of the two SAS compared in this study were very similar (specific surface area of ca. 200 m^2/g, primary particle size of ca. 20 nm, aggregate size in the 200–500 nm range), the biological responses, as revealed by proteomics, were significantly different. The precipitated silica induced a much stronger response, as indicated by the number of proteins showing a significant change in their amounts (938 for precipitated silica, 342 for fumed silica). Of those, 238 were significantly changed by both types of silica. The differences in numbers and thus in the extent of the cellular response may be correlated with the differences observed in silica uptake, which was higher for precipitated silica than for fumed silica, a phenomenon that was also found in the case of a single exposure for 24 h. This different uptake may be due either to a different intrinsic uptake due to structural differences between both types of silica or to a slightly different sedimentation behavior, leading to different amounts reaching the cell surface in culture.

Regarding silica uptake, the fact that the uptake was significantly lower in the case of repeated exposure compared to a single exposure to the same cumulative dose was worth investigating. It may be due to a culture artifact linked to cell proliferation and

thus dilution via cell division. However, previous data obtained on the J774A.1 cell line suggested that a cell density plateau is reached after four days in culture [40], so that this hypothesis cannot explain the difference between acutely and repeatedly-exposed cells. It may be caused by a lesser internalization capacity induced by the repeated exposure or by an elimination mechanism. As the former hypothesis would go against the increased surface expression of the scavenger receptors CD204 and MARCO, we specifically tested silica uptake at the end of the repeated exposure with a fluorescently-labelled colloidal silica and found an increased uptake compared to control cells, i.e., in line with the surface receptors. This suggests that repeatedly-exposed cells are able to eliminate some of the internalized silica, maybe by dissolution or by vomocytosis [62]. However, we could not detect silicon release in the cell culture medium after exposure to SAS (Figure S5), which may be simply linked to a lack of sensitivity of the technique compared to the low amounts of silicon to be detected.

Pathway analysis of the proteomic-detected changes revealed that very different pathways were altered. Some were ubiquitous, in the sense that they are part of the homeostasis of many different cell types. Pathways such as "endoplasmic reticulum", "mitochondria"," cell redox homeostasis", or "lysosome" belong to this class. As this may indicate a major dysfunction of the cells after this repeated exposure to silica, validation experiments were carried out. They indicated no major cellular dysfunction, which was in line with the low toxicity of amorphous silica upon repeated exposure [31,50]. Thus, the responses observed by proteomics can be described as successful adaptive changes of the proteome, resulting in cell adaptation to the repeated exposure to silica.

In this frame, it was relevant to dissect in greater detail the changes highlighted by the proteomic analysis. A good example is represented by the lysosome, which was highlighted as modified when the cells were treated with precipitated silica. Indeed, most of the luminal lysosomal proteins were decreased upon the treatment with silica by a factor varying from 1.2 to 2 (mean 1.47), while the membrane lysosomal proteins were increased by a factor varying from 1.1 to 1.7 (mean 1.35). One explanation to this phenomenon may be an adsorption of the luminal proteins to the silica present in the lysosomes (where silica is known to be located [63]), thereby decreasing their extractability for the proteomic analyses.

The situation was very different for the mitochondrial proteins. For this protein subset, on the 87 proteins for which the abundance changed upon treatment with precipitated silica, 39 showed a decreased abundance (mean fold change 1.4) and 48 showed an increased abundance (mean fold change 1.25). Interestingly, the ATP synthase and ADP/ATP translocase were increased, as well as mitofusin, i.e., a protein that controls mitochondrial fusion [64]. Conversely, the protein import machinery proteins were decreased, as well as the master regulator Myg1 [65], by factors of 1.2–1.25. As the cell viability and the mitochondrial transmembrane potential were not different from those of the control cells, these changes point to a fine tuning of the proteome to keep the mitochondrial function homeostatic.

The toxicology of amorphous silica has been described as involving oxidative stress [20,66,67]. In this frame, it was logical that the cluster "redox cell homeostasis" appeared in the pathway analysis. A major protein family appearing in this cluster was that of peroxiredoxins and their indirect partner thioredoxin reductase, which is implicated in their activity [68] and is increased in response to precipitated silica. Of the six peroxiredoxins known to date, only Prdx2 was not modulated in response to the treatment with silica. Peroxiredoxins 5 and 6 were found to be reduced. In the case of peroxiredoxin 6, this may be linked with its lysosomal localization [69], as discussed above. For peroxiredoxin 5, which has a complex intracellular localization [70], the situation is less clear. The other three peroxiredoxins, namely Prdx 1, 3, and 4, were increased in response with precipitated silica (Prdx3) or both forms of silica (Prdx 1 and 4). Prdx3 being a mitochondrial protein, its induction, although moderate, suggests an increased oxidative stress at the mitochondrial level. The induction of Prdx4 is worth discussing. In the endoplasmic reticulum, Prdx4 plays a role in protein oxidative folding [71]. Thus, its induction suggests a mechanism by which cells maintain

their redox balance in the endoplasmic reticulum, which is critical for the production of membrane and secreted proteins. Moreover, Prdx4 is known not to be fully retained in the reticulum, so that part of it is secreted. Thus, the increase that we observed through proteomics, i.e., the increase in the intracellular fraction, may also indicate an increase in the secreted fraction. As secreted Prdx4 has been implicated in the control of inflammation [72], this may represent one mechanism by which macrophages control their inflammatory response following exposure to silica.

Apart from changes in the peroxiredoxin system, we also detected changes in the amounts of proteins implicated in glutathione metabolism, namely glutathione synthase and glutathione reductase. As decreases in reduced glutathione levels have been reported in macrophages acutely treated with silica [20,67], we investigated the levels of reduced glutathione in cells repeatedly treated with synthetic amorphous silica and found no decrease, indicating that the changes observed in the proteins controlling the cellular redox status can be viewed as successful adaptive changes.

Regarding the surface markers, the first, technical point that needs to be discussed is the discrepancy that can sometimes occur between the proteomic results and the flow cytometry ones. For example, proteomics detected a decrease in the amount of CD11b and CD18 in response to cell exposure to silica, while flow cytometry detected an increase. The converse was true for CD86. In our opinion, this can be simply explained by the fact that both approaches do not measure the same parameter. Proteomics measures the global expression within the whole cell, without distinguishing the various forms of the protein (e.g., precursor vs. mature forms), while flow cytometry in the format used measures the surface expression of the protein. Thus, either intracellular turnover phenomena or masking/unmasking of the protein at the cell surface may explain this discrepant result. This also further demonstrates, if needed, the requirement for validation of proteomic data by functional assays.

This stated, the surface expression data suggested that repeated exposure to synthetic amorphous silica induced an increased surface expression of scavenger receptors, so that the macrophages become prepared to ingest more silica. This is also consistent with the increased phagocytic capacity that was observed after the repeated exposure to silica.

Secondly, the data pointed to a M1 polarization, as exemplified by the increased expression of CD38 [56] and the increased production of NO and pro-inflammatory cytokines (e.g., TNFα), and also suggested some form of macrophage activation. The data are, however, not univocal: CD74 (MHC-II) is increased, as well as the expression of CD11b, which has been reported to be pro-inflammatory [73], although an anti-inflammatory role of CD11b has also been reported [74]. In addition, the co-stimulatory molecule CD86 is decreased. Nevertheless, this response is similar to the silica-driven activation that has been described for dendritic cells [75–77], i.e., a closely-related immune cell type.

Regarding the cytokinic inflammatory responses, comparing the responses after an acute exposure or a repeated exposure could be interesting. To this purpose, we used our previous results obtained with the same fumed silica nanomaterial, but on the RAW264.7 model [24] instead of the J774A.1 model used in the present study. While this difference in cell line means that a direct and complete comparison cannot be made, the fact that both cell lines are established murine macrophage models suggests that such a comparison can be relevant.

Within this frame, the increase in TNFα production upon exposure to fumed silica was lower after repeated exposure (1.5-fold) than after acute exposure (2.5-fold). Such a lower increase after a time fractioned dose has also been observed for colloidal silica [50]. The stronger difference was, however, observed for IL-6, which remained undetectable after repeated exposure to both forms of synthetic amorphous silica (this study) while it was clearly detectable (and induced) after an acute exposure to fumed silica [24].

Besides this intrinsic response of the cells to SAS, we also investigated whether the treatment with SAS would modulate the physiological response of macrophages to a bacterial challenge, mimicked by an exposure to LPS. To this purpose, the cells were

first exposed repeatedly to SAS and finally to LPS. Our results showed an increased pro-inflammatory response in cells exposed to SAS, suggesting a hyper-reactive state and an exacerbated response. This phenomenon was more pronounced for fumed silica than for precipitated silica.

5. Conclusions

In conclusion, proteomics revealed that, although classified both as synthetic amorphous silica, precipitated silica and fumed silica did not induce identical cellular responses after a repeated exposure at non-toxic doses, a phenomenon already described using acute exposure and either precipitated or colloidal silica in comparison with fumed silica [78,79]. Most of the changes detected through proteomics did not reflect functionally as deleterious cellular responses, showing that these changes were adaptive and probably linked to the maintenance of cellular homeostasis. However, macrophage activation and polarization were detected, in line with the well-known pro-inflammatory effects of silica on this cellular type [16,20,22,61,80–82], but in acute exposure schemes. It shall be underlined that the pro-inflammatory effects that we detected under these repeated exposure conditions were of lower magnitude than those described after an acute exposure, which further demonstrates, if needed, the importance of the dose rate, even in in vitro toxicology. Indeed, the few repeated exposure experiments that have been carried out in in vitro toxicology [25,27–29,31,83] have generally demonstrated different responses when compared to acute exposures. However, the relative effects of both types of exposure cannot be predicted. In the case of silver nanoparticles, short repetition results in smaller effects than acute exposure [26,30], while long repetitions induce stronger effects [28,29,83]. In the case of silica, both short [50] and long (this study), [31] repetitions induce smaller effects than acute exposures. Of note, although the effects detected by proteomics were significantly higher for precipitated silica than for fumed silica, the functional effects, e.g., the effects on surface markers and cytokine production, were similar for both types of silica. This phenomenon may be linked to the common responses detected by proteomics for both types of SAS.

Supplementary Materials: The following supporting information can be downloaded at: https://www.mdpi.com/article/10.3390/nano12091424/s1, Figure S1: TEM characterization in water and stability of SAS in culture medium containing 10%FBS, incubation time 2 h 30 at 37 °C; Figure S2: Cellular internalization observed by confocal microscopy; Figure S3: Cellular SAS internalization observed by TEM; Figure S4: Analysis of the proteomic results obtained on J774A.1 cells after a 10-day exposure to silica by the non-metric multidimensional scaling approach; Figure S5: Synthetic amorphous silica exposure and quantification, by ICP-AES dosage; Table S1: List of identified and quantified proteins, with abundances normalized in part per billion; Table S2: List of proteins modulated in response to treatment with precipitated silica; Table S3: List of proteins modulated in response to treatment with fumed silica; Table S4: Results of the pathway analysis by the DAVID tool using proteins modulated by precipitated silica; Table S5: Results of the pathway analysis by the DAVID tool using proteins modulated by fumed silica; Table S6: Proteins linked to mitochondria; Table S7: Proteins linked to cell redox homeostasis; Table S8: Proteins linked to lysosomes; Table S9: Proteins linked to immunity.

Author Contributions: Conceptualization, J.-A.S. and T.R.; validation, A.T., V.C.-F. and H.D.; formal analysis, A.T., V.C.-F., H.D. and T.R.; investigation, A.T., V.C.-F., H.D., C.M., D.F. and B.G.; data curation, H.D.; writing—original draft preparation, T.R.; writing—review and editing, A.T., V.C.-F., H.D., B.G., S.C. and J.-A.S.; visualization, A.T., C.M., D.F., B.G. and T.R.; supervision, J.-A.S. and T.R.; project administration, J.-A.S. and T.R.; funding acquisition, S.C., J.-A.S. and T.R. All authors have read and agreed to the published version of the manuscript.

Funding: This work was funded by grants from the Agence Nationale de Sécurité Environnementale et Sanitaire (ANSES, SILIMMUN grant PNREST-2015-32) and from the Agence Nationale de la Recherche (ANR, Paipito grant ANR-16-CE34-0011). This work used the flow cytometry facility supported by GRAL, a project of the University Grenoble Alpes graduate school (Ecoles Universitaires de Recherche) CBH-EUR-GS (ANR-17-EURE-0003), as well as the platforms of the French Proteomic

Infrastructure (ProFI) project (grant ANR-10-INBS-08-03) and the EM facilities at the Grenoble Instruct-ERIC Center (ISBG; UMS 3518 CNRS CEAUGA-EMBL) with support from the French Infrastructure for Integrated Structural Biology (FRISBI; ANR-10-INSB-05-02) and GRAL, a project of the University Grenoble Alpes graduate school (Ecoles Universitaires de Recherche) CBH-EUR-GS (ANR-17-EURE-0003) within the Grenoble Partnership for Structural Biology. The electron Microscope facility is headed by Guy Schoehn and supported by the Auvergne Rhône-Alpes Region, the Fonds Feder, the Fondation pour la Recherche Médicale, and GIS-IBiSA. AT was co-financed by an Industrial PhD bursary from Solvay SA (CIFRE programme).

Informed Consent Statement: Not applicable.

Data Availability Statement: Mass spectrometry data are available via ProteomeXchange with the identifier PXD03002 with the doi:10.6019/PXD030002.

Acknowledgments: The authors thank the microscopy facility MuLife of IRIG/DBSCI, funded by CEA Nanobio and labex Gral, for equipment access and use. The authors also thank Guy Schoehn for the direction of the Electron Microscopy facility and Julien Pérard for the maintenance of the ICP-AES instrument and his assistance for the ICP-AES experiments.

Conflicts of Interest: The authors declare no conflict of interest.

References

1. Flörke, O.W.; Graetsch, H.A.; Brunk, F.; Benda, L.; Paschen, S.; Bergna, H.E.; Roberts, W.O.; Welsh, W.A.; Libanati, C.; Ettlinger, M.; et al. Silica. In *Ullmann's Encyclopedia of Industrial Chemistry*; Wiley Verlag & Co.: Weinheim, Germany, 2008; p. 23. ISBN 978-3-527-30673-2.
2. American Thoracic Society Committee of the Scientific Assembly on Environmental and Occupational Health Adverse Effects of Crystalline Silica Exposure. *Am. J. Respir. Crit. Care Med.* **1997**, *155*, 761–768. [CrossRef] [PubMed]
3. Silicosis and Silicate Disease Committee. Diseases Associated with Exposure to Silica and Nonfibrous Silicate Minerals. *Arch. Pathol. Lab. Med.* **1988**, *112*, 673–720.
4. Norboo, T.; Angchuk, P.T.; Yahya, M.; Kamat, S.R.; Pooley, F.D.; Corrin, B.; Kerr, I.H.; Bruce, N.; Ball, K.P. Silicosis in a Himalayan Village Population: Role of Environmental Dust. *Thorax* **1991**, *46*, 341–343. [CrossRef] [PubMed]
5. Lapp, N.L.; Castranova, V. How Silicosis and Coal Workers' Pneumoconiosis Develop—A Cellular Assessment. *Occup. Med.* **1993**, *8*, 35–56. [PubMed]
6. Misson, P.; van den Brûle, S.; Barbarin, V.; Lison, D.; Huaux, F. Markers of Macrophage Differentiation in Experimental Silicosis. *J. Leukoc. Biol.* **2004**, *76*, 926–932. [CrossRef] [PubMed]
7. Huaux, F. New Developments in the Understanding of Immunology in Silicosis. *Curr. Opin. Allergy Clin. Immunol.* **2007**, *7*, 168–173. [CrossRef]
8. Hornung, V.; Bauernfeind, F.; Halle, A.; Samstad, E.O.; Kono, H.; Rock, K.L.; Fitzgerald, K.A.; Latz, E. Silica Crystals and Aluminum Salts Activate the NALP3 Inflammasome through Phagosomal Destabilization. *Nat. Immunol.* **2008**, *9*, 847–856. [CrossRef]
9. Pollard, K.M. Silica, Silicosis, and Autoimmunity. *Front. Immunol.* **2016**, *7*, 97. [CrossRef]
10. Adamcakova, J.; Mokra, D. New Insights into Pathomechanisms and Treatment Possibilities for Lung Silicosis. *Int. J. Mol. Sci.* **2021**, *22*, 4162. [CrossRef]
11. Warheit, D.B.; McHugh, T.A.; Hartsky, M.A. Differential Pulmonary Responses in Rats Inhaling Crystalline, Colloidal or Amorphous Silica Dusts. *Scand. J. Work Environ. Health* **1995**, *21*, 19–21.
12. Johnston, C.J.; Driscoll, K.E.; Finkelstein, J.N.; Baggs, R.; O'Reilly, M.A.; Carter, J.; Gelein, R.; Oberdorster, G. Pulmonary Chemokine and Mutagenic Responses in Rats after Subchronic Inhalation of Amorphous and Crystalline Silica. *Toxicol. Sci.* **2000**, *56*, 405–413. [CrossRef] [PubMed]
13. Arts, J.H.E.; Muijser, H.; Duistermaat, E.; Junker, K.; Kuper, C.F. Five-Day Inhalation Toxicity Study of Three Types of Synthetic Amorphous Silicas in Wistar Rats and Post-Exposure Evaluations for up to 3 Months. *Food Chem. Toxicol.* **2007**, *45*, 1856–1867. [CrossRef] [PubMed]
14. Sayes, C.M.; Reed, K.L.; Warheit, D.B. Assessing Toxicity of Fine and Nanoparticles: Comparing in Vitro Measurements to in Vivo Pulmonary Toxicity Profiles. *Toxicol. Sci.* **2007**, *97*, 163–180. [CrossRef] [PubMed]
15. Napierska, D.; Thomassen, L.C.; Lison, D.; Martens, J.A.; Hoet, P.H. The Nanosilica Hazard: Another Variable Entity. *Part. Fibre Toxicol.* **2010**, *7*, 39. [CrossRef]
16. Fruijtier-Polloth, C. The Toxicological Mode of Action and the Safety of Synthetic Amorphous Silica-A Nanostructured Material. *Toxicology* **2012**, *294*, 61–79. [CrossRef]
17. Costantini, L.M.; Gilberti, R.M.; Knecht, D.A. The Phagocytosis and Toxicity of Amorphous Silica. *PLoS ONE* **2011**, *6*, e14647. [CrossRef]

18. Breznan, D.; Das, D.D.; O'Brien, J.S.; MacKinnon-Roy, C.; Nimesh, S.; Vuong, N.Q.; Bernatchez, S.; DeSilva, N.; Hill, M.; Kumarathasan, P.; et al. Differential Cytotoxic and Inflammatory Potency of Amorphous Silicon Dioxide Nanoparticles of Similar Size in Multiple Cell Lines. *Nanotoxicology* **2017**, *11*, 223–235. [CrossRef]
19. Uboldi, C.; Giudetti, G.; Broggi, F.; Gilliland, D.; Ponti, J.; Rossi, F. Amorphous Silica Nanoparticles Do Not Induce Cytotoxicity, Cell Transformation or Genotoxicity in Balb/3T3 Mouse Fibroblasts. *Mutat. Res. Genet. Toxicol. Environ. Mutagenesis* **2012**, *745*, 11–20. [CrossRef]
20. Park, E.J.; Park, K. Oxidative Stress and Pro-Inflammatory Responses Induced by Silica Nanoparticles in Vivo and in Vitro. *Toxicol. Lett.* **2009**, *184*, 18–25. [CrossRef]
21. Sandberg, W.J.; Lag, M.; Holme, J.A.; Friede, B.; Gualtieri, M.; Kruszewski, M.; Schwarze, P.E.; Skuland, T.; Refsnes, M. Comparison of Non-Crystalline Silica Nanoparticles in IL-1 Beta Release from Macrophages. *Part. Fibre Toxicol.* **2012**, *9*, 32. [CrossRef]
22. Panas, A.; Marquardt, C.; Nalcaci, O.; Bockhorn, H.; Baumann, W.; Paur, H.-R.; Mülhopt, S.; Diabaté, S.; Weiss, C. Screening of Different Metal Oxide Nanoparticles Reveals Selective Toxicity and Inflammatory Potential of Silica Nanoparticles in Lung Epithelial Cells and Macrophages. *Nanotoxicology* **2013**, *7*, 259–273. [CrossRef] [PubMed]
23. Fritsch-Decker, S.; Marquardt, C.; Stoeger, T.; Diabaté, S.; Weiss, C. Revisiting the Stress Paradigm for Silica Nanoparticles: Decoupling of the Anti-Oxidative Defense, pro-Inflammatory Response and Cytotoxicity. *Arch. Toxicol.* **2018**, *92*, 2163–2174. [CrossRef] [PubMed]
24. Torres, A.; Dalzon, B.; Collin-Faure, V.; Diemer, H.; Fenel, D.; Schoehn, G.; Cianférani, S.; Carrière, M.; Rabilloud, T. How Reversible Are the Effects of Fumed Silica on Macrophages? A Proteomics-Informed View. *Nanomaterials* **2020**, *10*, 1939. [CrossRef] [PubMed]
25. Comfort, K.K.; Braydich-Stolle, L.K.; Maurer, E.I.; Hussain, S.M. Less Is More: Long-Term in Vitro Exposure to Low Levels of Silver Nanoparticles Provides New Insights for Nanomaterial Evaluation. *ACS Nano* **2014**, *8*, 3260–3271. [CrossRef] [PubMed]
26. Aude-Garcia, C.; Villiers, F.; Collin-Faure, V.; Pernet-Gallay, K.; Jouneau, P.-H.; Sorieul, S.; Mure, G.; Gerdil, A.; Herlin-Boime, N.; Carrière, M.; et al. Different in Vitro Exposure Regimens of Murine Primary Macrophages to Silver Nanoparticles Induce Different Fates of Nanoparticles and Different Toxicological and Functional Consequences. *Nanotoxicology* **2016**, *10*, 586–596. [CrossRef]
27. Chen, N.; Song, Z.-M.; Tang, H.; Xi, W.-S.; Cao, A.; Liu, Y.; Wang, H. Toxicological Effects of Caco-2 Cells Following Short-Term and Long-Term Exposure to Ag Nanoparticles. *Int. J. Mol. Sci.* **2016**, *17*, 974. [CrossRef]
28. Gliga, A.R.; Di Bucchianico, S.; Lindvall, J.; Fadeel, B.; Karlsson, H.L. RNA-Sequencing Reveals Long-Term Effects of Silver Nanoparticles on Human Lung Cells. *Sci. Rep.* **2018**, *8*, 6668. [CrossRef]
29. Dalzon, B.; Aude-Garcia, C.; Diemer, H.; Bons, J.; Marie-Desvergne, C.; Pérard, J.; Dubosson, M.; Collin-Faure, V.; Carapito, C.; Cianférani, S.; et al. The Longer the Worse: A Combined Proteomic and Targeted Study of the Long-Term *versus* Short-Term Effects of Silver Nanoparticles on Macrophages. *Environ. Sci. Nano* **2020**, *7*, 2032–2046. [CrossRef]
30. Bobyk, L.; Tarantini, A.; Beal, D.; Veronesi, G.; Kieffer, I.; Motellier, S.; Valsami-Jones, E.; Lynch, I.; Jouneau, P.-H.; Pernet-Gallay, K.; et al. Toxicity and Chemical Transformation of Silver Nanoparticles in A549 Lung Cells: Dose-Rate-Dependent Genotoxic Impact. *Environ. Sci. Nano* **2021**, *8*, 806–821. [CrossRef]
31. Murugadoss, S.; Godderis, L.; Ghosh, M.; Hoet, P.H. Assessing the Toxicological Relevance of Nanomaterial Agglomerates and Aggregates Using Realistic Exposure In Vitro. *Nanomaterials* **2021**, *11*, 1793. [CrossRef]
32. Fubini, B.; Zanetti, G.; Altilia, S.; Tiozzo, R.; Lison, D.; Saffiotti, U. Relationship between Surface Properties and Cellular Responses to Crystalline Silica: Studies with Heat-Treated Cristobalite. *Chem. Res. Toxicol.* **1999**, *12*, 737–745. [CrossRef] [PubMed]
33. Ghiazza, M.; Polimeni, M.; Fenoglio, I.; Gazzano, E.; Ghigo, D.; Fubini, B. Does Vitreous Silica Contradict the Toxicity of the Crystalline Silica Paradigm? *Chem. Res. Toxicol.* **2010**, *23*, 620–629. [CrossRef] [PubMed]
34. Turci, F.; Pavan, C.; Leinardi, R.; Tomatis, M.; Pastero, L.; Garry, D.; Anguissola, S.; Lison, D.; Fubini, B. Revisiting the Paradigm of Silica Pathogenicity with Synthetic Quartz Crystals: The Role of Crystallinity and Surface Disorder. *Part. Fibre Toxicol.* **2016**, *13*, 32. [CrossRef] [PubMed]
35. Pavan, C.; Santalucia, R.; Leinardi, R.; Fabbiani, M.; Yakoub, Y.; Uwambayinema, F.; Ugliengo, P.; Tomatis, M.; Martra, G.; Turci, F.; et al. Nearly Free Surface Silanols Are the Critical Molecular Moieties That Initiate the Toxicity of Silica Particles. *Proc. Natl. Acad. Sci. USA* **2020**, *117*, 27836–27846. [CrossRef] [PubMed]
36. Le Ouay, B.; Stellacci, F. Antibacterial Activity of Silver Nanoparticles: A Surface Science Insight. *Nano. Today* **2015**, *10*, 339–354. [CrossRef]
37. Triboulet, S.; Aude-Garcia, C.; Armand, L.; Collin-Faure, V.; Chevallet, M.; Diemer, H.; Gerdil, A.; Proamer, F.; Strub, J.M.; Habert, A.; et al. Comparative Proteomic Analysis of the Molecular Responses of Mouse Macrophages to Titanium Dioxide and Copper Oxide Nanoparticles Unravels Some Toxic Mechanisms for Copper Oxide Nanoparticles in Macrophages. *PLoS ONE* **2015**, *10*, e0124496. [CrossRef]
38. Aude-Garcia, C.; Dalzon, B.; Ravanat, J.L.; Collin-Faure, V.; Diemer, H.; Strub, J.M.; Cianferani, S.; Van Dorsselaer, A.; Carriere, M.; Rabilloud, T. A Combined Proteomic and Targeted Analysis Unravels New Toxic Mechanisms for Zinc Oxide Nanoparticles in Macrophages. *J. Proteom.* **2016**, *134*, 174–185. [CrossRef]
39. Dussert, F.; Arthaud, P.-A.; Arnal, M.-E.; Dalzon, B.; Torres, A.; Douki, T.; Herlin, N.; Rabilloud, T.; Carriere, M. Toxicity to RAW264.7 Macrophages of Silica Nanoparticles and the E551 Food Additive, in Combination with Genotoxic Agents. *Nanomaterials* **2020**, *10*, 1418. [CrossRef]

40. Dalzon, B.; Torres, A.; Devcic, J.; Fenel, D.; Sergent, J.-A.; Rabilloud, T. A Low-Serum Culture System for Prolonged in Vitro Toxicology Experiments on a Macrophage System. *Front. Toxicol.* **2021**, *3*, 780778. [CrossRef]
41. Viveros, R.D.; Liberman, A.; Trogler, W.C.; Kummel, A.C. Alkaline and Ultrasonic Dissolution of Biological Materials for Trace Silicon Determination. *J. Vac. Sci. Technol. B* **2015**, *33*, 031803. [CrossRef]
42. Rabilloud, T. Optimization of the Cydex Blue Assay: A One-Step Colorimetric Protein Assay Using Cyclodextrins and Compatible with Detergents and Reducers. *PLoS ONE* **2018**, *13*, e0195755. [CrossRef] [PubMed]
43. Muller, L.; Fornecker, L.; Chion, M.; Van Dorsselaer, A.; Cianférani, S.; Rabilloud, T.; Carapito, C. Extended Investigation of Tube-Gel Sample Preparation: A Versatile and Simple Choice for High Throughput Quantitative Proteomics. *Sci. Rep.* **2018**, *8*, 8260. [CrossRef] [PubMed]
44. Cavazza, C.; Collin-Faure, V.; Pérard, J.; Diemer, H.; Cianférani, S.; Rabilloud, T.; Darrouzet, E. Proteomic Analysis of Rhodospirillum Rubrum after Carbon Monoxide Exposure Reveals an Important Effect on Metallic Cofactor Biosynthesis. *J. Proteom.* **2022**, *250*, 104389. [CrossRef] [PubMed]
45. Lyubimova, T.; Caglio, S.; Gelfi, C.; Righetti, P.G.; Rabilloud, T. Photopolymerization of Polyacrylamide Gels with Methylene Blue. *Electrophoresis* **1993**, *14*, 40–50. [CrossRef] [PubMed]
46. Vizcaino, J.A.; Deutsch, E.W.; Wang, R.; Csordas, A.; Reisinger, F.; Rios, D.; Dianes, J.A.; Sun, Z.; Farrah, T.; Bandeira, N.; et al. ProteomeXchange Provides Globally Coordinated Proteomics Data Submission and Dissemination. *Nat. Biotechnol.* **2014**, *32*, 223–226. [CrossRef] [PubMed]
47. Hammer, O.; Harper, D.A.T.; Ryan, P.D. Paleontological Statistics Software Package for Education and Data Analysis. *Palaeontol. Electron.* **2001**, *4*, 9.
48. Diz, A.P.; Carvajal-Rodriguez, A.; Skibinski, D.O. Multiple Hypothesis Testing in Proteomics: A Strategy for Experimental Work. *Mol. Cell. Proteom.* **2011**, *10*, M110.004374. [CrossRef]
49. Huang, D.W.; Sherman, B.T.; Lempicki, R.A. Bioinformatics Enrichment Tools: Paths toward the Comprehensive Functional Analysis of Large Gene Lists. *Nucleic Acids Res.* **2009**, *37*, 1–13. [CrossRef]
50. Torres, A.; Dalzon, B.; Collin-Faure, V.; Rabilloud, T. Repeated vs. Acute Exposure of RAW264.7 Mouse Macrophages to Silica Nanoparticles: A Bioaccumulation and Functional Change Study. *Nanomaterials* **2020**, *10*, 215. [CrossRef]
51. Perry, S.W.; Norman, J.P.; Barbieri, J.; Brown, E.B.; Gelbard, H.A. Mitochondrial Membrane Potential Probes and the Proton Gradient: A Practical Usage Guide. *Biotechniques* **2011**, *50*, 98–115. [CrossRef]
52. Dalzon, B.; Torres, A.; Diemer, H.; Ravanel, S.; Collin-Faure, V.; Pernet-Gallay, K.; Jouneau, P.-H.; Bourguignon, J.; Cianférani, S.; Carrière, M.; et al. How Reversible Are the Effects of Silver Nanoparticles on Macrophages? A Proteomic-Instructed View. *Environ. Sci. Nano* **2019**, *6*, 3133–3157. [CrossRef]
53. Dalzon, B.; Torres, A.; Reymond, S.; Gallet, B.; Saint-Antonin, F.; Collin-Faure, V.; Moriscot, C.; Fenel, D.; Schoehn, G.; Aude-Garcia, C.; et al. Influences of Nanoparticles Characteristics on the Cellular Responses: The Example of Iron Oxide and Macrophages. *Nanomaterials* **2020**, *10*, 266. [CrossRef] [PubMed]
54. Thomé, M.P.; Filippi-Chiela, E.C.; Villodre, E.S.; Migliavaca, C.B.; Onzi, G.R.; Felipe, K.B.; Lenz, G. Ratiometric Analysis of Acridine Orange Staining in the Study of Acidic Organelles and Autophagy. *J. Cell. Sci.* **2016**, *129*, 4622–4632. [CrossRef] [PubMed]
55. Lund, F.E. Signaling Properties of CD38 in the Mouse Immune System: Enzyme-Dependent and -Independent Roles in Immunity. *Mol. Med.* **2006**, *12*, 328–333. [CrossRef] [PubMed]
56. Jablonski, K.A.; Amici, S.A.; Webb, L.M.; Ruiz-Rosado, J.d.D.; Popovich, P.G.; Partida-Sanchez, S.; Guerau-de-Arellano, M. Novel Markers to Delineate Murine M1 and M2 Macrophages. *PLoS ONE* **2015**, *10*, e0145342. [CrossRef]
57. Arredouani, M.S. Is the Scavenger Receptor MARCO a New Immune Checkpoint? *OncoImmunology* **2014**, *3*, e955709. [CrossRef]
58. Hamilton, R.F.; Thakur, S.A.; Mayfair, J.K.; Holian, A. MARCO Mediates Silica Uptake and Toxicity in Alveolar Macrophages from C57BL/6 Mice. *J. Biol. Chem.* **2006**, *281*, 34218–34226. [CrossRef]
59. Orr, G.A.; Chrisler, W.B.; Cassens, K.J.; Tan, R.; Tarasevich, B.J.; Markillie, L.M.; Zangar, R.C.; Thrall, B.D. Cellular Recognition and Trafficking of Amorphous Silica Nanoparticles by Macrophage Scavenger Receptor A. *Nanotoxicology* **2011**, *5*, 296–311. [CrossRef]
60. Kelley, J.L.; Ozment, T.R.; Li, C.; Schweitzer, J.B.; Williams, D.L. Scavenger Receptor-A (CD204): A Two-Edged Sword in Health and Disease. *Crit. Rev. Immunol.* **2014**, *34*, 241–261. [CrossRef] [PubMed]
61. Gallud, A.; Bondarenko, O.; Feliu, N.; Kupferschmidt, N.; Atluri, R.; Garcia-Bennett, A.; Fadeel, B. Macrophage Activation Status Determines the Internalization of Mesoporous Silica Particles of Different Sizes: Exploring the Role of Different Pattern Recognition Receptors. *Biomaterials* **2017**, *121*, 28–40. [CrossRef]
62. Seoane, P.I.; May, R.C. Vomocytosis: What We Know so Far. *Cell Microbiol.* **2020**, *22*, e13145. [CrossRef] [PubMed]
63. Mendoza, A.; Torres-Hernandez, J.A.; Ault, J.G.; Pedersen-Lane, J.H.; Gao, D.; Lawrence, D.A. Silica Nanoparticles Induce Oxidative Stress and Inflammation of Human Peripheral Blood Mononuclear Cells. *Cell Stress Chaperones* **2014**, *19*, 777–790. [CrossRef] [PubMed]
64. Chen, H.; Detmer, S.A.; Ewald, A.J.; Griffin, E.E.; Fraser, S.E.; Chan, D.C. Mitofusins Mfn1 and Mfn2 Coordinately Regulate Mitochondrial Fusion and Are Essential for Embryonic Development. *J. Cell Biol.* **2003**, *160*, 189–200. [CrossRef] [PubMed]
65. Grover, R.; Burse, S.A.; Shankrit, S.; Aggarwal, A.; Kirty, K.; Narta, K.; Srivastav, R.; Ray, A.K.; Malik, G.; Vats, A.; et al. Myg1 Exonuclease Couples the Nuclear and Mitochondrial Translational Programs through RNA Processing. *Nucleic Acids Res.* **2019**, *47*, 5852–5866. [CrossRef]

66. Eom, H.-J.; Choi, J. Oxidative Stress of Silica Nanoparticles in Human Bronchial Epithelial Cell, Beas-2B. *Toxicol. In Vitro* **2009**, *23*, 1326–1332. [CrossRef]
67. Napierska, D.; Rabolli, V.; Thomassen, L.C.J.; Dinsdale, D.; Princen, C.; Gonzalez, L.; Poels, K.L.C.; Kirsch-Volders, M.; Lison, D.; Martens, J.A.; et al. Oxidative Stress Induced by Pure and Iron-Doped Amorphous Silica Nanoparticles in Subtoxic Conditions. *Chem. Res. Toxicol.* **2012**, *25*, 828–837. [CrossRef]
68. Lu, J.; Holmgren, A. The Thioredoxin Antioxidant System. *Free Radic. Biol. Med.* **2014**, *66*, 75–87. [CrossRef]
69. Sorokina, E.M.; Feinstein, S.I.; Milovanova, T.N.; Fisher, A.B. Identification of the Amino Acid Sequence That Targets Peroxiredoxin 6 to Lysosome-like Structures of Lung Epithelial Cells. *Am. J. Physiol. Lung Cell. Mol. Physiol.* **2009**, *297*, L871–L880. [CrossRef]
70. Knoops, B.; Goemaere, J.; Van der Eecken, V.; Declercq, J.-P. Peroxiredoxin 5: Structure, Mechanism, and Function of the Mammalian Atypical 2-Cys Peroxiredoxin. *Antioxid. Redox Signal.* **2011**, *15*, 817–829. [CrossRef]
71. Zhu, L.; Yang, K.; Wang, X.; Wang, X.; Wang, C. A Novel Reaction of Peroxiredoxin 4 towards Substrates in Oxidative Protein Folding. *PLoS ONE* **2014**, *9*, e105529. [CrossRef]
72. Yamada, S.; Guo, X. Peroxiredoxin 4 (PRDX4): Its Critical in Vivo Roles in Animal Models of Metabolic Syndrome Ranging from Atherosclerosis to Nonalcoholic Fatty Liver Disease. *Pathol. Int.* **2018**, *68*, 91–101. [CrossRef] [PubMed]
73. Schmid, M.C.; Khan, S.Q.; Kaneda, M.M.; Pathria, P.; Shepard, R.; Louis, T.L.; Anand, S.; Woo, G.; Leem, C.; Faridi, M.H.; et al. Integrin CD11b Activation Drives Anti-Tumor Innate Immunity. *Nat. Commun.* **2018**, *9*, 5379. [CrossRef] [PubMed]
74. Zhang, Q.; Lee, W.-B.; Kang, J.-S.; Kim, L.K.; Kim, Y.-J. Integrin CD11b Negatively Regulates Mincle-Induced Signaling via the Lyn-SIRPα-SHP1 Complex. *Exp. Mol. Med.* **2018**, *50*, e439. [CrossRef] [PubMed]
75. Liu, S.; Hao, C.; Bao, L.; Zhao, D.; Zhang, H.; Hou, J.; Wang, D.; Chen, H.; Feng, F.; Yao, W. Silica Particles Mediate Phenotypic and Functional Alteration of Dendritic Cells and Induce Th2 Cell Polarization. *Front. Immunol.* **2019**, *10*, 787. [CrossRef] [PubMed]
76. Winkler, H.C.; Kornprobst, J.; Wick, P.; von Moos, L.M.; Trantakis, I.; Schraner, E.M.; Bathke, B.; Hochrein, H.; Suter, M.; Naegeli, H. MyD88-Dependent pro-Interleukin-1β Induction in Dendritic Cells Exposed to Food-Grade Synthetic Amorphous Silica. *Part. Fibre Toxicol.* **2017**, *14*, 21. [CrossRef]
77. Feray, A.; Guillet, E.; Szely, N.; Hullo, M.; Legrand, F.-X.; Brun, E.; Rabilloud, T.; Pallardy, M.; Biola-Vidamment, A. Synthetic Amorphous Silica Nanoparticles Promote Human Dendritic Cell Maturation and CD4 + T-Lymphocyte Activation. *Toxicol. Sci.* **2021**, *185*, kfab120. [CrossRef]
78. Di Cristo, L.; Movia, D.; Bianchi, M.G.; Allegri, M.; Mohamed, B.M.; Bell, A.P.; Moore, C.; Pinelli, S.; Rasmussen, K.; Riego-Sintes, J.; et al. Proinflammatory Effects of Pyrogenic and Precipitated Amorphous Silica Nanoparticles in Innate Immunity Cells. *Toxicol. Sci.* **2016**, *150*, 40–53. [CrossRef]
79. Zhang, H.Y.; Dunphy, D.R.; Jiang, X.M.; Meng, H.; Sun, B.B.; Tarn, D.; Xue, M.; Wang, X.; Lin, S.J.; Ji, Z.X.; et al. Processing Pathway Dependence of Amorphous Silica Nanoparticle Toxicity: Colloidal vs Pyrolytic. *J. Am. Chem. Soc.* **2012**, *134*, 15790–15804. [CrossRef]
80. Park, M.; Lynch, I.; Ramirez-Garcia, S.; Dawson, K.A.; de la Fonteyne, L.; Gremmer, E.; Slob, W.; Briede, J.J.; Elsaesser, A.; Howard, C.V.; et al. In Vitro Evaluation of Cytotoxic and Inflammatory Properties of Silica Nanoparticles of Different Sizes in Murine RAW 264.7 Macrophages. *J. Nanopart. Res.* **2011**, *13*, 6775–6787. [CrossRef]
81. Napierska, D.; Thomassen, L.C.J.; Vanaudenaerde, B.; Luyts, K.; Lison, D.; Martens, J.A.; Nemery, B.; Hoet, P.H.M. Cytokine Production by Co-Cultures Exposed to Monodisperse Amorphous Silica Nanoparticles: The Role of Size and Surface Area. *Toxicol. Lett.* **2012**, *211*, 98–104. [CrossRef]
82. Murugadoss, S.; Lison, D.; Godderis, L.; Van Den Brule, S.; Mast, J.; Brassinne, F.; Sebaihi, N.; Hoet, P.H. Toxicology of Silica Nanoparticles: An Update. *Arch. Toxicol.* **2017**, *91*, 2967–3010. [CrossRef] [PubMed]
83. Vila, L.; Marcos, R.; Hernández, A. Long-Term Effects of Silver Nanoparticles in Caco-2 Cells. *Nanotoxicology* **2017**, *11*, 771–780. [CrossRef] [PubMed]

Figure S1: TEM characterization in water and stability of SAS in culture medium containing 10%FBS, incubation time 2h30 at 37°C.

Methods:
Synthetic amorphous silicas were incubated at 20µg/ml in water or culture medium for 2h30 at 37°C. The SAS incubated in culture medium were then centrifuged 25 minutes at 10,000g and resuspended in water (to avoid culture medium-derived salt crystallization on grid for microscope observation).
Negative Stain On Grid Technique (SOG): 10 µL was added to a glow discharge grid coated with a carbon supporting film for 5 minutes. The excess solution was soaked off by a filter paper and the grid was air-dried. The images were taken under low dose conditions (<10 $e^-/Å^2$) with defocus values between 1.2 and 2.5 µm on a Tecnai 12 LaB6 electron microscope at 120 kV accelerating voltage using CCD Camera Gatan Orius 1000.

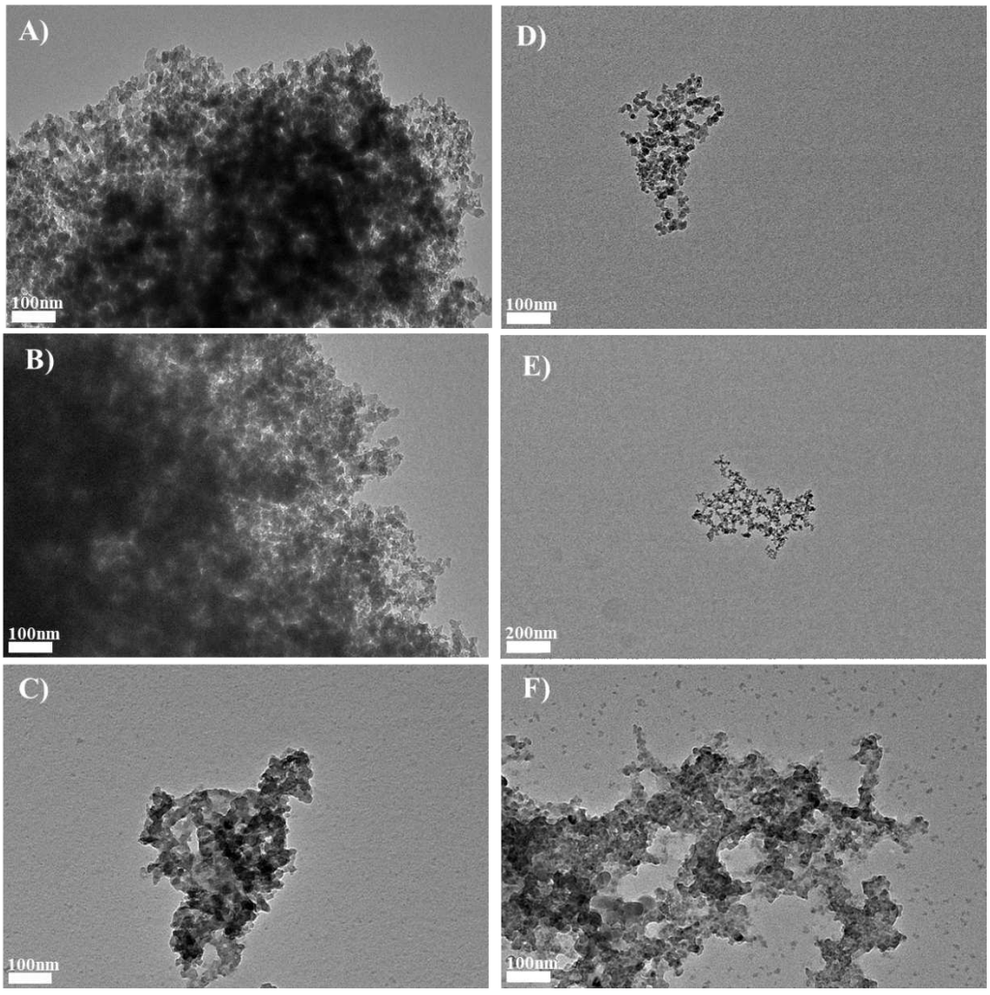

SAS characterization in water: **A-B)** Precipitated silica magnification 23,000× and **D-E)** Fumed silica in water, magnification 23,000× and 9,300×
SAS stability in culture medium DMEM 10% FBS: **C)** Precipitated and **F)** Fumed silica, magnification 23,000×

Results:
The precipitated silica in water is composed of aggregates around 3-5 µm, with a primary particle size of 20 nm. The fumed silica is slightly aggregated, with a primary particle size of 15 nm. The precipitated silica seems to be less aggregated in culture medium, with a size of 300 nm, while the fumed silica seems more aggregated with a size of 3-5 µm.

Supplementary figure 2: SAS internalization observed by confocal microscopy.

Methods:
The precipitated and fumed silica were labelled with rhodamine B as described in Huang X. *et al* (2020) https://doi.org/10.1007/s11051-019-4720-1. The conjugation used aminopropyl triethoxysilane dans rhodamine B isothiocyanate, instead of fluorescein isothiocyanate in the original publication.
The labelled nanoparticles were collected by centrifugation, and then washed three times with ethanol. The particles were resuspended in sterilized water with care to avoid exposure to light.

The cells were cultured as described for acute exposure. The cells were seeded on glass slide at 500,000 cells/slide, and then exposed for 24 hours to 20µg/ml of rhodamineB-fluorescent silica (rhodB-silica). The cells were fixed with 4% paraformaldehyde for 30min after a wash with PBS 1X. The cells were washed with PBS1X before permeabilization with 0.1% Triton-X100 (Eurobio, GAUTTR00-01) for 5 min. Cells were stained with fluorescently labelled phalloidin, which detects polymerized actin (Sigma-Aldrich, Merck, phalloidin-Atto 390) in a final concentration of 500 nM for 20 min at room temperature, protected from light. Nuclei were stained with SytoxRed probe at 10nM in PBS for 5min. A Vectashield mounting medium was used (Vector laboratories, Vectashield H-1000). Microscope analysis was performed on a Zeiss LSM 880 confocal microscope (Zeiss, Marly le Roi, France). Fluorescence pictures were taken at the same exposure and gain conditions to allow comparison of fluorescence intensity. The raw data were treated and adjusted by using the same parameters with the ImageJ software (1.52s, Wayne Rasband National Institutes of Health, USA).

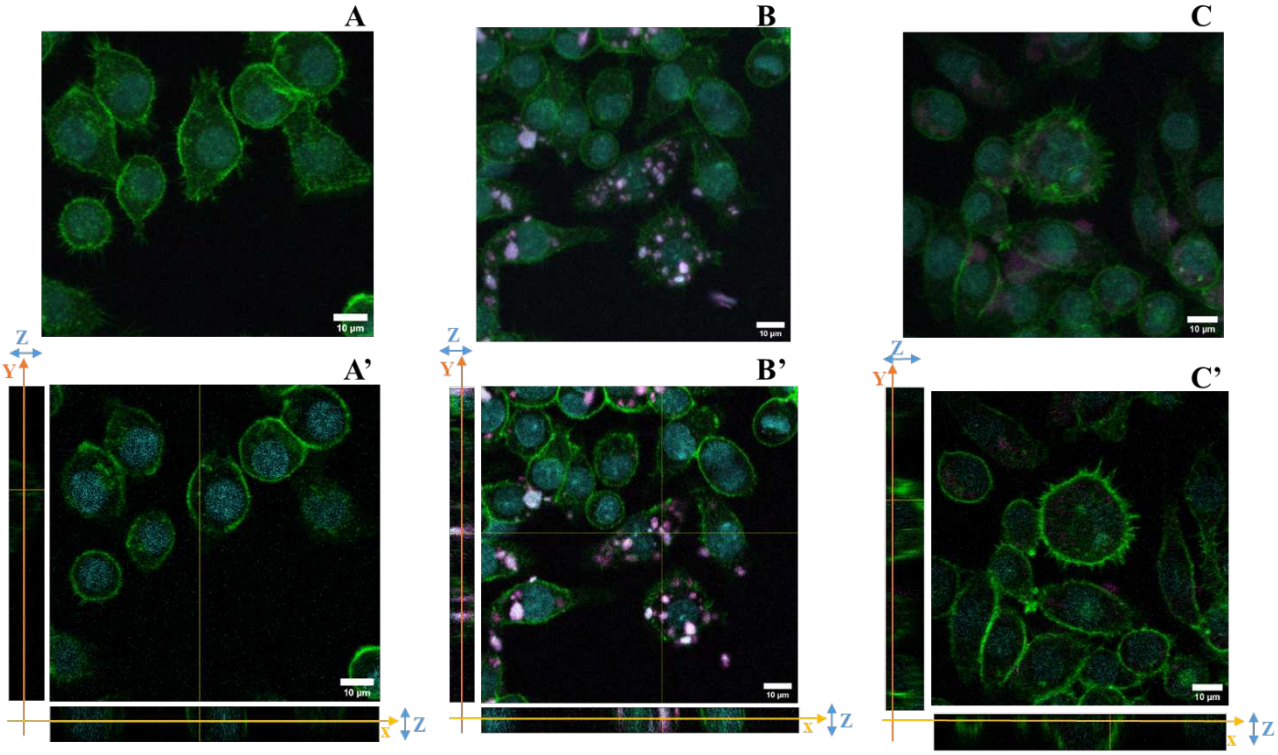

(**A-C**) Control and rhodB-silica internalization of cells exposed to 20 µg/mL during 24 h, obtained by confocal microscopy (artificial colors: nucleus in blue (SytoxRed), actin in green (phalloidin-atto 390), silica in magenta (rhodB)), $n = 2$. Z-project reconstitution, **B** precipitated and **C** fumed SAS. (**A'**–**C'**) Same conditions as previously, represented in orthogonal views. The stack of the cells corresponding to a slice in the thickness of the cells is illustrated. The combination of the *XY* and *YZ* confocal plans demonstrate the internalization of the silica nanoparticles.

Results:
The rhodamine B labelling of SAS was efficient for precipitated silica, but not for fumed silica. The SAS particles were mainly visible inside the cells, in the cytoplasm.

Figure S3: cellular SAS internalization observed by TEM inclusion.

Methods:
For imaging cells *via* transmission electron microscopy (TEM), cells were seeded on Labtek chamber slides at 170,000 cells/500 µl in DMEM 10% FBS. They were then exposed or not to 20 µg/ml of precipitated or fumed silica, for 24 hours. The medium was removed and a solution of DMEM (without serum) and fixative solution (4% paraformaldehyde, 0.4% glutaraldehyde, 0.2 M PHEM) v/v was added for 30 minutes at room temperature. They were then fixed for another 30 minutes at room temperature in 2% paraformaldehyde, 0.2% glutaraldehyde in 0.1 M PHEM (30 mM PIPES, 12.5 mM HEPES, 5 mM $MgCl_2$, 1 mM EGTA, pH 7). Cells were rinsed three times in 0.1 M PHEM and post-fixed in 1% osmium tetroxide (OsO_4), 1.5% potassium ferrocyanide in 0.1 M PHEM buffer for 1h at room temperature. After 3 washes in water, they were post-stained using 0.5% uranyl acetate in 30% ethanol for 30 min at room temperature, in the dark. Cells were then dehydrated in graded ethanol series (50 to 100%), and embedded in Epon resin. After polymerization during 48 hours at 65 °C, the blocs were cut on a Leica UC7 ultra-microtome. Ultrathin sections (70 nm) were collected on Formvar carbon coated copper grids and post-stained. Images were recorded on a Tecnai G2 Spirit BioTwin (FEI) transmission electron microscope (TEM), operating at 120 kV, using an ORIUS SC1000 CCD camera (Gatan).

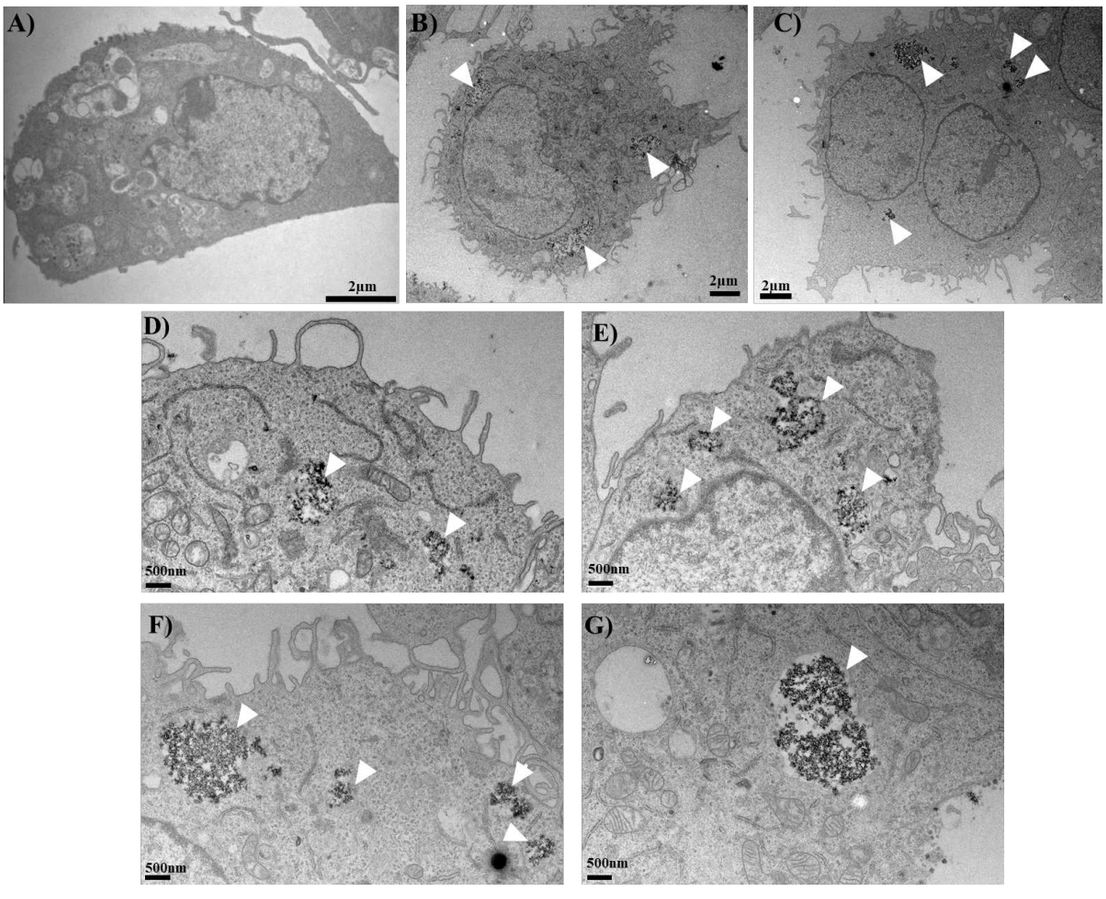

A) control cells (untreated)
B) cells exposed to precipitated SAS, magnification 690×
C) cells exposed to fumed SAS, magnification 890×
D) and **E)** Precipitated silica magnification 2900×
F) and **G)** Fumed silica magnification 2900×
The arrows indicate internalized silica in the cells.

Results:
The cells were adherent with actin filaments. The macrophages exposed to precipitated or fumed silica have internalized the SAS inside vesicles, with no visible SAS around the cells or at the cell surface.

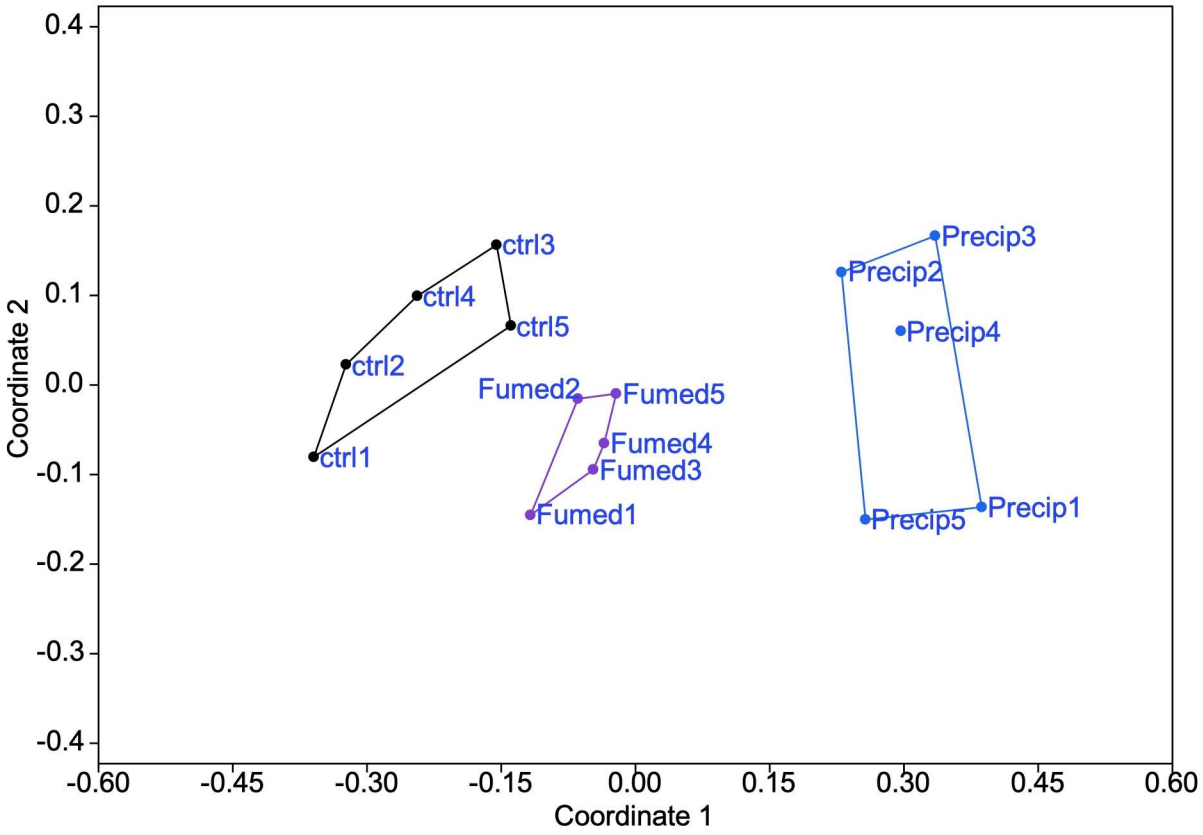

Figure S4: Analysis of the proteomic results obtained on J774A.1 cells after a 10 days exposure to silica by the non-metric multidimensional scaling approach.
CTL: control, cells without nanomaterials, Pr: precipitated silica 220 m^2/g, Fu: fumed silica 200 m^2/g
The results show that 1) the groups are consistent (no interpenetration of the groups) and 2) that precipitated silica induced more changes of the proteome than fumed silica

Supplementary figure 5: Synthetic amorphous silica exposure and quantification, by ICP-AES dosage.

Methods:
For SAS quantification in the supernatants, the cells were grown on adherent 6-well plates in DMEM supplemented with 10% fetal bovine serum (DMEM FBS 10%). The medium, containing or not 20 µg/ml of SAS (precipitated or fumed) was applied on cells for 24 hours (T0). At the end of exposure, the medium was removed (T24h) and replaced by a fresh DMEM 10%FBS, without any SAS. The medium was changed again after 36 hours, and finally, the medium was collected for dosage (T72h).
The collected media were centrifuged to remove any non-adherent cell, for 5 minutes at 200g. Then, the supernatants were centrifuged or not 30 minutes at 10,000g, in order to collect the supernatant with small size particles only (<200nm). The day before the quantification by ICP-AES, the samples were mineralized: in each sample, an equal volume of 1N potassium hydroxide was added, and the samples were then incubated overnight at 80°C in a preheated water bath.
The standards were first prepared, in HNO_3 10%, the multi-elemental standard was purchased from Sigma-Aldrich (ref 92091). At the end of the standard measurement, samples were prepared two at a time (base-mineralized silica is not stable in HNO_3): from 250 µl to 500 µl of mineralisate were added to HNO_3 10% to reach a final volume of 6 ml. The samples were measured in an ICP-AES Shimadzu 9000 with ICPE solution Launcher software.

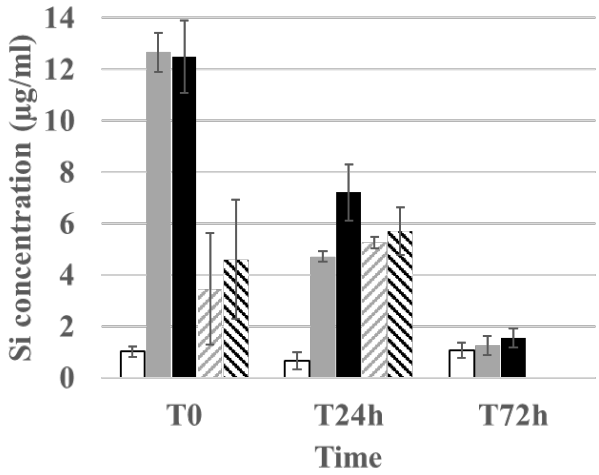

Supernatant of control cells, untreated (white bars), supernatant of cells exposed to precipitated SAS (grey bars, plain or hatched), and supernatant of cells exposed to fumed SAS (black bars, plain or hatched). Hatched bars are for centrifuged supernatants.

Results:
The mineralization yield of both silica is around 60%, determined in T0 supernatants (grey and black plain bars). A proportion of 25% is measured in the supernatant after high-speed centrifugation, and correspond to SAS smaller than 200 nm, that means nanoparticular or silicates. After 24 hours of exposure, 30% of initial amount remained in the medium, and seems to correspond to the smallest SAS particles, and can be explained by the sedimentation speed. After 72 hours of culture without any SAS, there was no detectable release of SAS by the macrophages.

Table S6: proteins linked to mitochondria

accession number	gene_name	description	ratio Pr/ctrl	ratio Fu/ctrl	T test Pr vs ctrl	T test Py vs ctrl
O35129	Phb2	Prohibitin-2	1.129835927	1.034913261	0.002533893	0.193535478
O35658	C1qbp	Complement component 1 Q subcomponent-binding protein, mitochondrial	1.246582495	1.009048216	0.005126001	0.886624753
P00405	Mtco2	Cytochrome c oxidase subunit 2	0.735392594	0.998870793	0.015434415	0.986849666
P09671	Sod2	Superoxide dismutase [Mn], mitochondrial	1.332345703	0.993033623	0.00222107	0.87326313
P11928	Oas1a	2'-5'-oligoadenylate synthase 1A	1.285445563	1.096041935	0.027726763	0.193590535
P16332	Mut	Methylmalonyl-CoA mutase, mitochondrial	1.17406184	1.017172881	0.005280587	0.665421768
P19783	Cox4i1	Cytochrome c oxidase subunit 4 isoform 1, mitochondrial	1.107095629	1.065006288	0.002540912	0.015186435
P20108	Prdx3	Thioredoxin-dependent peroxide reductase, mitochondrial Prx3	1.157475522	1.069655803	0.002485883	0.069271673
P28352	Apex1	DNA-(apurinic or apyrimidinic site) lyase	0.819428042	0.879554978	0.030341022	0.054971364
P29758	Oat	Ornithine aminotransferase, mitochondrial	1.267633192	1.042378612	3.99937E-05	0.042302865
P32020	Scp2	Non-specific lipid-transfer protein	0.719113476	0.788356734	0.007574101	0.004745788
P36552	Cpox	Oxygen-dependent coproporphyrinogen-III oxidase, mitochondrial	0.676224731	0.968451308	0.006153699	0.742848346
P38060	Hmgcl	Hydroxymethylglutaryl-CoA lyase, mitochondrial	0.819813757	0.959369323	0.004561241	0.410133949
P38647	Hspa9	Stress-70 protein, mitochondrial	1.263736865	1.073657338	0.004889481	0.302685727
P41216	Acsl1	Long-chain-fatty-acid--CoA ligase 1	1.197712734	1.013246654	0.006746039	0.725914863
P48962	Slc25a4	ADP/ATP translocase 1	1.176749339	1.034227196	0.000999067	0.317209232
P51174	Acadl	Long-chain specific acyl-CoA dehydrogenase, mitochondrial	1.116231094	1.050999123	0.004417197	0.175955813
P51881	Slc25a5	ADP/ATP translocase 2	1.218654174	1.026985015	0.000157509	0.425442585
P56135	Atp5mf	ATP synthase subunit f, mitochondrial	1.221393033	1.109296296	0.000560756	0.01847533
P56480	Atp5f1b	ATP synthase subunit beta, mitochondrial	1.104016508	1.05561257	0.02764585	0.076372893
P59017	Bcl2l13	Bcl-2-like protein 13	0.339690983	0.884244902	0.019963606	0.616853809
P62908	Rps3	40S ribosomal protein S3	1.123328077	1.008923814	0.00255899	0.747024505
P63038	Hspd1	60 kDa heat shock protein, mitochondrial	1.125244274	1.038345336	0.000320689	0.044564605
P63087	Ppp1cc	Serine/threonine-protein phosphatase PP1-gamma catalytic subunit	0.840743359	0.914840159	0.005791729	0.057155038
P67778	Phb	Prohibitin	1.123958779	1.002925161	0.010113763	0.926671094

P99029	Prdx5	Peroxiredoxin-5, mitochondrial	0.758889457	0.857463329	0.003933749	0.060601088
Q03265	Atp5f1a	ATP synthase subunit alpha, mitochondrial	1.101111398	1.032742313	0.003000464	0.060770771
Q05921	Rnasel	2-5A-dependent ribonuclease	0.683721407	0.750508144	0.011798925	0.066830648
Q14C51	Ptcd3	Pentatricopeptide repeat domain-containing protein 3, mitochondrial	1.354000989	1.095789987	0.034473285	0.127217175
Q3TL44	Nlrx1	NLR family member X1	0.841418495	0.953612312	0.085814762	0.289174857
Q60597	Ogdh	2-oxoglutarate dehydrogenase, mitochondrial	1.140917251	1.060496406	0.000120067	0.038505047
Q60931	Vdac3	Voltage-dependent anion-selective channel protein 3	1.152675268	1.018637496	0.001376895	0.563536334
Q62465	Vat1	Synaptic vesicle membrane protein VAT-1 homolog	0.732685002	0.989629175	0.001912047	0.842823689
Q6P3A8	Bckdhb	2-oxoisovalerate dehydrogenase subunit beta, mitochondrial	0.563177632	0.815164552	0.006279063	0.148122198
Q6PB66	Lrpprc	Leucine-rich PPR motif-containing protein, mitochondrial	1.184423355	1.076639133	0.00353685	0.118913828
Q78IK2	Atp5md	Up-regulated during skeletal muscle growth protein 5	1.144676857	0.94535141	0.003949396	0.226226199
Q78IK4	Apool	MICOS complex subunit Mic27	0.918855935	0.938495996	0.021896988	0.063203722
Q811U4	Mfn1	Mitofusin-1	1.758044799	1.095676459	0.004433715	0.692082075
Q8BGH2	Samm50	Sorting and assembly machinery component 50 homolog	1.172946106	1.029190215	0.003570799	0.663343489
Q8BH86	Dglucy	D-glutamate cyclase, mitochondrial	0.635894178	0.818974968	0.001061496	0.02270373
Q8BH95	Echs1	Enoyl-CoA hydratase, mitochondrial	0.81513449	0.87439013	0.004987222	0.023936642
Q8BMF4	Dlat	Dihydrolipoyllysine-residue acetyltransferase component of pyruvate dehydrogenase complex, mitochondrial	1.119977864	1.060972461	0.01512153	0.054667904
Q8BMS1	Hadha	Trifunctional enzyme subunit alpha, mitochondrial	0.884115547	0.956841894	0.002220491	0.1297981
Q8BP40	Acp6	Lysophosphatidic acid phosphatase type 6	0.744733387	0.88203816	0.007667602	0.326682704
Q8CGK3	Lonp1	Lon protease homolog, mitochondrial	1.153231196	1.102458889	0.007621942	0.028061524
Q8JZR0	Acsl5	Long-chain-fatty-acid--CoA ligase 5	1.110855155	1.00971884	0.009702883	0.773577546
Q8QZT1	Acat1	Acetyl-CoA acetyltransferase, mitochondrial	0.85669917	0.909236673	0.002081238	0.020956994
Q8R1I1	Uqcr10	Cytochrome b-c1 complex subunit 9	1.222113776	1.048813555	0.004470015	0.358517296

Q8VDK1	Nit1	Deaminated glutathione amidase	0.600417003	0.814885405	0.005428763	0.119433048
Q8WTY4	Ciapin1	Anamorsin	0.419992511	0.701233726	1.28693E-05	0.04810254
Q99LX0	Park7	Protein/nucleic acid deglycase DJ-1	0.683484548	0.897481046	0.00475433	0.160566324
Q9CPQ1	Cox6c	Cytochrome c oxidase subunit 6C	1.213058624	1.049462551	0.000347832	0.153293215
Q9CPQ3	Tomm22	Mitochondrial import receptor subunit TOM22 homolog	0.849591285	1.072415204	0.036739609	0.261491408
Q9CPV4	Glod4	Glyoxalase domain-containing protein 4	0.810717354	0.972547966	0.000578651	0.30961383
Q9CQN1	Trap1	Heat shock protein 75 kDa, mitochondrial	1.440789908	1.278062455	0.000830321	0.066341924
Q9CQN6	Tmem14c	Transmembrane protein 14C	1.270038298	1.036161387	0.008086005	0.649579907
Q9CR62	Slc25a11	Mitochondrial 2-oxoglutarate/malate carrier protein	1.135506908	1.120601088	0.012552281	0.023143678
Q9CXT8	Pmpcb	Mitochondrial-processing peptidase subunit beta	1.206171867	0.864809902	0.001528758	0.557885593
Q9CYG7	Tomm34	Mitochondrial import receptor subunit TOM34	0.830737984	0.889982954	0.021865182	0.136182571
Q9CZD3	Gars	Glycine--tRNA ligase	1.161207289	1.060155091	0.017496975	0.083260838
Q9CZU6	Cs	Citrate synthase, mitochondrial	1.165369721	1.057230626	0.000758099	0.005533219
Q9D172	Gatd3a	Glutamine amidotransferase-like class 1 domain-containing protein 3A, mitochondrial	0.813822625	0.865534683	0.004131675	0.063834172
Q9D6K5	Synj2bp	Synaptojanin-2-binding protein	1.270926418	1.07243633	0.012714228	0.247341673
Q9D6U8	Fam162a	Protein FAM162A	1.347411615	1.135720045	0.002408274	0.072679044
Q9D880	Timm50	Mitochondrial import inner membrane translocase subunit TIM50	0.938113622	0.970462852	0.028275219	0.174855024
Q9D964	Gatm	Glycine amidinotransferase, mitochondrial	0.813274821	0.869573	0.000980394	0.03719697
Q9DCN2	Cyb5r3	NADH-cytochrome b5 reductase 3	1.21038842	1.077371373	0.003638862	0.038532839
Q9EPB4	Pycard	Apoptosis-associated speck-like protein containing a CARD	0.883879676	0.841254737	0.001444539	0.021412344
Q9JIK9	Mrps34	28S ribosomal protein S34, mitochondrial	1.137472101	0.988529205	0.015233536	0.787494993
Q9JK81	Myg1	UPF0160 protein MYG1, mitochondrial	0.80861539	0.946486505	0.000172796	0.072743279
Q9JM90	Stap1	Signal-transducing adaptor protein 1	1.375519337	1.069388073	0.012401315	0.340023646
Q9QYR9	Acot2	Acyl-coenzyme A thioesterase 2, mitochondrial	0.829231863	0.913943398	0.024604635	0.169339435

Q9R0X4	Acot9	Acyl-coenzyme A thioesterase 9, mitochondrial	1.236014962	1.255790773	0.012366826	0.009974659
Q9WTP6	Ak2	Adenylate kinase 2, mitochondrial	0.877418771	0.904475564	0.022543927	0.05362444
Q9WUM5	Suclg1	Succinate--CoA ligase [ADP/GDP-forming] subunit alpha, mitochondrial	0.888785741	0.861061759	0.001077851	0.002579821
Q9Z110	Aldh18a1	Delta-1-pyrroline-5-carboxylate synthase	1.265385246	1.048428033	0.000150112	0.340822589

Table S7: proteins linked to cell redox homeostasis

accession number	gene_name	description	ratio rPr/ctrl	ratio Fu/ctrl	T test Pr vs. ctrl	T test Fu vs ctrl
P28352	Apex1	DNA-(apurinic or apyrimidinic site) lyase	0.819428	0.879555	0.030341	0.0549714
Q8R180	Ero1a	ERO1-like protein alpha	1.4267517	1.0507847	0.0005103	0.4003907
Q8BZW8	Nhlrc2	NHL repeat-containing protein 2	1.5002926	1.4896671	0.0317271	0.0348889
P09103	P4hb	Protein disulfide-isomerase	1.3321121	1.0523063	0.0002386	0.0305743
P27773	Pdia3	Protein disulfide-isomerase A3	1.0986432	1.0465273	0.0002576	0.0101618
P08003	Pdia4	Protein disulfide-isomerase A4	1.1827833	1.0572835	0.000747	0.1560396
Q922R8	Pdia6	Protein disulfide-isomerase A6	1.1337347	0.9820241	0.0008646	0.3990531
P35700	Prdx1	Peroxiredoxin-1	1.1591502	1.1129194	1.406E-05	0.0036429
P20108	Prdx3	Thioredoxin-dependent peroxide reductase, mitochondrial Prx3	1.1574755	1.0696558	0.0024859	0.0692717
O08807	Prdx4	Peroxiredoxin-4	1.2954477	1.1735089	0.0002375	0.0046681
P99029	Prdx5	Peroxiredoxin-5, mitochondrial	0.7588895	0.8574633	0.0039337	0.0606011
O08709	Prdx6	Peroxiredoxin-6	0.8286838	0.9322557	0.0016014	0.0868954
Q91VW3	Sh3bgrl3	SH3 domain-binding glutamic acid-rich-like protein 3	0.7380794	1.4321918	0.0332647	0.4175075
Q8VBT0	Tmx1	Thioredoxin-related transmembrane protein 1	1.1900357	0.9962529	0.0004372	0.9396225
Q9JMH6	Txnrd1	Thioredoxin reductase 1, cytoplasmic	1.3005555	1.0432999	0.0074358	0.5895408
P46413	Gss	Glutathione synthetase	0.7014626	0.8743287	0.0240252	0.1522542
P47791	Gsr	Glutathione reductase, mitochondrial	0.9701236	0.9343079	0.2482618	0.0039174

Conclusion

Le premier résultat important de cette étude est la différence des profils protéomiques entre la silice amorphe précipitée et la fumée : la première induit davantage de modifications du protéome par rapport aux cellules non-exposées. Cependant, ces modifications au niveau protéique sont le résultat d'adaptation des macrophages pour maintenir une réponse cellulaire équivalente, et assurer l'homéostasie cellulaire. Par exemple, les voies énergétique et antioxydante sont modifiées par l'exposition à la SAS précipitée, les expériences de validation sur le potentiel mitochondrial et le glutathion ont montré une réponse équivalente à celle des cellules contrôles. Ce phénomène de compensation n'est pas observé pour les fonctions principales du macrophage : la phagocytose et la sécrétion de TNF et IL-6 sont augmentées par l'exposition répétée aux SAS, de même que certains marqueurs de surface comme le récepteur scavenger de la silice (CD208) ou MARCO. Ces résultats montrent que l'exposition répétée à de faibles doses de SAS modifie le protéome des macrophages mais également leurs fonctions immunitaires, de façon bien moins intense que lors d'une exposition aiguë à une dose équivalente de silice. Cette expérience montre également que chaque matériau est toléré de manière différente par les cellules selon sa nature et le temps d'exposition. Par exemple, les nanoparticules d'argent produisent moins d'effets en exposition répétée courte (Aude-Garcia, Villiers, et al. 2016; Bobyk et al. 2021) ce qui n'est pas le cas lors d'expositions répétées plus longues (Dalzon, Aude-Garcia, et al. 2020; Comfort et al. 2014). Ce phénomène d'effets plus intenses lors d'expositions répétées longues se retrouve avec des nanoparticules de dioxyde de titane (Armand et al. 2016).

Cette partie sur l'étude de deux scenarii d'exposition différents a permis d'évaluer la persistance des effets et l'influence d'une exposition répétée aux nanomatériaux. Il a été mis en évidence que chaque nanomatériau induit une réponse spécifique qui dépend du mode d'exposition, de la dose, de la nature du matériau, et de ses caractéristiques physico-chimiques.

Dans les études précédentes, il s'agit principalement d'une évaluation des effets intrinsèques d'une exposition à une unique substance, une SAS, suivie dans certains cas d'une co-stimulation à un composé bactérien, le LPS. Cela permet de mesurer la réponse inflammatoire des macrophages en cas d'infection bactérienne qui surviendrait après l'exposition à la silice. Cependant, dans l'environnement industrialisé et urbain dans lequel nous vivons, les bactéries ne sont pas les seuls pathogènes ou substances exogènes, il existe des substances chimiques polluantes présentes dans l'air comme par exemple les particules diesel, les cendres volcaniques, le monoxyde de carbone, les sous-produits d'usinage ou d'usure (soudure, freinage, gomme pneumatique…), les fumées (gaz échappement, tabac, feu)… Certaines études montrent que l'exposition aux particules de pollution atmosphérique ont des effets à court et long terme sur la santé (irritation oculaire, difficultés respiratoires (asthme ou pathologie pulmonaire), arrêt cardiaque, réduction de l'espérance de vie…) comme cela a été répertorié par le Gouvernement australien, le National Institute of Environmental Health Science ou dans la bibliographie (Müller, Seifart, and Barth 1998).

Les effets d'une exposition multiple sont faiblement étudiés, notamment car les systèmes d'étude de toxicité croisée sont complexes variés. Les recherches commencent se porter sur ces expositions plus complètes et représentatives de l'environnement urbain.

II d) Comparaison exposition répétée et aiguë

Toxicity to RAW264.7 Macrophages of Silica Nanoparticles and the E551 Food Additive, in Combination with Genotoxic Agents

Présentation du projet

Ce projet a pour but d'étudier la co-exposition à la silice et à un agent contaminant environnemental génotoxique, tel que le benzo[a]pyrène (B[a]P) et le méthane méthylsulfonate (MMS). Le B[a]P est un hydrocarbure aromatique polycyclique présent dans l'atmosphère en raison de la combustion incomplète de matière organique, de charbon et du pétrole. Le MMS est un agent alkylant qui introduit des mutations de l'ADN (méthylation) et induit des lésions. Trois types de silices amorphes de synthèse sont utilisées (colloïdale, précipitée alimentaire et pyrogénée) ainsi que 3 types cellulaires différents : RAW264.7, et une co-culture de Caco-2 et HT29MTX (modèle d'épithélium intestinal). Les cellules sont exposées suivant deux protocoles : aigu (10, 20, 50 ou 100µg/ml durant 24h) ou répété (3x1 ou 2µg/ml pendant 3 semaines). Des tests de cytotoxicité et génotoxicité et d'expression génique ont été réalisés pour évaluer l'impact de l'exposition aux trois types de silice et la co-stimulation ou non avec des agents génotoxiques.

nanomaterials

MDPI

Article

Toxicity to RAW264.7 Macrophages of Silica Nanoparticles and the E551 Food Additive, in Combination with Genotoxic Agents

Fanny Dussert [1], Pierre-Adrien Arthaud [1], Marie-Edith Arnal [1], Bastien Dalzon [2], Anaëlle Torres [2], Thierry Douki [1], Nathalie Herlin [3], Thierry Rabilloud [2] and Marie Carriere [1,*]

1 Université Grenoble-Alpes, CEA, CNRS, IRIG-DIESE, SyMMES, Chemistry Interface Biology for the Environment, Health and Toxicology (CIBEST), F-38000 Grenoble, France; fanny.dussert@cea.fr (F.D.); piarthaud@laposte.net (P.-A.A.); marie-edith.arnal@wanadoo.fr (M.-E.A.); thierry.douki@cea.fr (T.D.)

2 Chemistry and Biology of Metals, Université Grenoble Alpes, CNRS UMR5249, CEA, IRIG-DIESE-LCBM-ProMD, F-38054 Grenoble, France; bastien.dalzon@cea.fr (B.D.); Anaelle.torres@cea.fr (A.T.); thierry.rabilloud@cnrs.fr (T.R.)

3 Université Paris Saclay, CEA Saclay, IRAMIS NIMBE UMR 3685, 91191 Gif/Yvette CEDEX, France; nathalie.herlin@cea.fr

* Correspondence: marie.carriere@cea.fr; Tel.: +33-4-3878-0328

Received: 29 June 2020; Accepted: 16 July 2020; Published: 21 July 2020

Abstract: Synthetic amorphous silica (SAS) is used in a plethora of applications and included in many daily products to which humans are exposed via inhalation, ingestion, or skin contact. This poses the question of their potential toxicity, particularly towards macrophages, which show specific sensitivity to this material. SAS represents an ideal candidate for the adsorption of environmental contaminants due to its large surface area and could consequently modulate their toxicity. In this study, we assessed the toxicity towards macrophages and intestinal epithelial cells of three SAS particles, either isolated SiO_2 nanoparticles (LS30) or SiO_2 particles composed of agglomerated-aggregates of fused primary particles, either food-grade (E551) or non-food-grade (Fumed silica). These particles were applied to cells either alone or in combination with genotoxic co-contaminants, i.e., benzo[a]pyrene (B[a]P) and methane methylsulfonate (MMS). We show that macrophages are much more sensitive to these toxic agents than a non-differenciated co-culture of Caco-2 and HT29-MTX cells, used here as a model of intestinal epithelium. Co-exposure to SiO_2 and MMS causes DNA damage in a synergistic way, which is not explained by the modulation of DNA repair protein mRNA expression. Together, this suggests that SiO_2 particles could adsorb genotoxic agents on their surface and, consequently, increase their DNA damaging potential.

Keywords: silica; SiO_2; nanoparticle; E551; toxicity; genotoxicity; macrophage; intestine; co-exposure

1. Introduction

Synthetic amorphous silica (SAS) is an authorized food additive, known as E551 in the European Union. It is used for its anti-caking property in powdered food, including creamers, lyophilized soups, salt, and sugar [1]. It consists in particles with a primary diameter in the nano-range, i.e., lower than 100 nm, which aggregate to form large clusters with diverse morphologies [2]. This wide use has raised the concern of its safety and potential toxicity, in particular for the gastro-intestinal system. In the lung, inhalation exposure to SiO_2 has been reported to induce inflammation [3,4]. Moreover, risk assessment conducted with this substance and focused on the liver estimates a potential liver accumulation at the same level in humans and rodents in which adverse effects were found, suggesting

that it could also be detrimental to human liver [5]. A recent review summarizing the literature relative to its safety assessment concludes in the absence of any relevant toxicity both at the systemic and local level after oral exposure [6]. The re-evaluation of this food additive by the EFSA Panel on Food Additives and Nutrient Sources added to Food (ANS), published in 2017, also concludes in the absence of toxic effects of E551 at the currently used levels, although silica was found to be absorbed through the gastro-intestinal tract and to accumulate in internal organs and the immune system. Synthetic amorphous silica are "generally recognized as safe" (GRAS) according to the US EPA. In particular, they were shown to induce only minor damage to DNA, which was considered to be within the normal physiological range [6]. Two recent reviews report that the literature relative to SiO_2-NP genotoxicity show inconsistent results, with some studies showing significant genotoxicity while others report the opposite [7,8].

Despite this apparent biocompatibility, combined effect of silica with other pollutants have been reported. The group of Zhiwei Sun described the impact of co-exposure of lung epithelial cells and zebrafish embryos to SiO_2-NPs with methylmercury or lead, as well as co-exposure to SiO_2-NPs and benzo[a]pyrene (B[a]P) on BEAS-2B bronchial epithelial cells, HUVEC endothelial cells, and zebrafish embryos [9–12]. These studies highlight increased cytotoxicity, apoptosis, oxidative stress, and inflammation in co-exposed cells, with both additive or synergistic effects of SiO_2 and the co-pollutant. The cardiovascular system is shown to be the main target organ where effects of these co-pollutants are observed. Synergistic interaction has also been reported between SiO_2-NPs and lead acetate in A549 alveolar epithelial cells, causing mitochondria-dependent apoptosis [13]. Moreover, cytotoxicity, oxidative stress, and apoptosis were reported for arsenic when co-exposed with SiO_2-NPs in HepG2 liver cells and fibroblasts [14]. Recently, Cao et al. reported increased cytotoxicity, oxidative stress, and translocation of the fungicide boscalid upon co-exposure of in vitro intestinal epithelial models to the E551 food additive (SiO_2), previously submitted to an in vitro simulated digestion [15]. All of these studies aiming at elucidating the impact of co-exposure of SiO_2 and environmental pollutants have been conducted on epithelial cells, endothelial cells, or fibroblasts. They show both additive or synergistic effect of SiO_2 and the co-contaminant, suggesting either SiO_2 particles acting as a cargo for the co-contaminant and facilitating its accumulation in cells, or a possible sensitization of cells towards the co-contaminant by SiO_2 particles.

Macrophages are major targets of SiO_2 in the organism, because they play a significant role in immunity and show particular sensitivity towards SiO_2-NPs [16,17]. However, systematic studies on the impact of co-exposure to SiO_2 and other pollutants, as well as studies on the genotoxicity of SiO_2 on this cell type are lacking, although we recently hypothesized that SiO_2-NPs could sensitize RAW264.7 macrophages towards DNA alkylating agents [17]. In this context, the aim of the present study was to compare the toxicity of SiO_2-NPs and the food additive E551 towards RAW264.7 macrophages and epithelial intestinal cells, with special focus on their genotoxicity and the impact of co-exposure with genotoxic pollutants. We chose two well-known genotoxic agents that cause DNA damage via different mechanisms, i.e., benzo[a]pyrene (B[a]P) and methane methylsulfonate (MMS). The rationale for these choices was that SiO_2-NPs are present in indoor air of some workplaces [18,19] while polycyclic aromatic hydrocarbon (PAHs) and among them B[a]P is an ubiquitous environmental pollutant, present in the atmospheric particulate matter as a consequence of incomplete combustion of organic matter as well as coal or petroleum distillation [20]. PAH are also present in the urban polluted atmosphere, sometimes in combination with inorganic NPs, like SiO_2, leading to co-exposure of the populations by inhalation. Last, PAHs are produced during cooking and SiO_2 is largely used as food additive [1]; therefore, co-exposure of the populations would also occur via ingestion. Exposure to B[a]P results in DNA strand breaks and adducts formed by benzo[a]pyrene-7,8-dihydrodiol-9,10-epoxide (BPDE), its most reactive metabolite. These two type of DNA damage, which can be detected with the comet assay and by HPLC-M/MS, respectively, are produced in the 1:10 ratio [21]. MMS is a typical model of N-alkylating agent that produces methylated bases in DNA, which are alkali-labile lesions that can be detected via the comet assay [22]. This model genotoxic agent was chosen because

of our previously-published observation that SiO_2-NPs sensitized macrophages towards alkylating agents [17], with the aim of addressing the hypothesis that the E551 food additive would cause the same effect.

2. Materials and Methods

2.1. Chemicals and Reagents

Unless otherwise indicated, chemicals and reagents were >98% pure and were from Sigma–Aldrich. Silica particles were obtained from Sigma–Aldrich (Saint-Quentin Fallavier, France) (Ludox LS30, produced by Grace, and Fumed silica) or from an industrial collaborator producing food-grade precipitated silica (E551). Ludox LS30 was provided as a suspension, it was diluted in ultrapure water to reach the concentration of 1 mg/mL. Fumed silica and E551 were provided as powders, they were suspended in ultrapure water at the concentration of 1 mg/mL. They were not sonicated, because it would potentially degrade the structure of the food additive, which is primary particles aggregated as chaplets and then further agglomerated. These three particles were sterilized by heating at 80 °C overnight.

2.2. Cell Culture and Exposure

RAW 264.7 mouse macrophages and Caco-2 colorectal adenocarcinoma cells were obtained from the European Cell Culture Collection (ECACC, Salisbury, UK). RAW 264.7 were maintained at 37 °C, in a 5% CO_2 and 100% humidity incubator and grown in suspension, in non-adherent flasks, in RPMI 1640-Glutamax to which was added 50 U/mL of penicillin, 50 µg/mL streptomycin and 10% (*v*/*v*) fetal bovine serum (FBS). The cells were sub-cultured three times per week and then seeded at 200,000 cells per mL of growth medium. Caco-2 were maintained in DMEM Glutamax to which was added 1% nonessential amino-acids, 50 U/mL of penicillin, 50 µg/mL streptomycin, and 10% (*v*/*v*) FBS. HT29-MTX were kindly provided by Dr. T. Lesuffleur (INSERM) [23] and grown in the same medium as Caco-2 cells. Caco-2 and HT29-MTX cells were co-cultured at 75% Caco-2 and 25% HT29-MTX, as previously [24]. For acute exposure to particles, the cells were seeded in adherent plates, either 96-well (WST-1, trypan blue and LDH assay), 12-well (comet assay), or six-well (8-oxo-7,8-dihydro-2'-deoxyguanosine, 8-oxo-dGuo, measurement). In the acute exposure scheme, the cells were seeded at 500,000 cells per mL the day before exposure. They were exposed for 24 h to 10, 20, 50, or 100 µg/mL SiO_2 (WST1 and LDH assays), 10, 20, or 50 µg/mL SiO_2 (trypan blue cytotoxicity assay), or 10 µg/mL SiO_2 (comet assay and 8-oxo-dGuo measurement). In the repeated exposure scheme, the cells were seeded at 500,000 cells per mL and, then exposed 24 h later to 1 or 2 µg/mL SiO_2. Every second day during three weeks, the exposure medium was replaced with fresh medium containing 1 or 2 µg/mL SiO_2. This corresponds to nine successive exposures to SiO_2. At the end of this repeated exposure period, the cells were harvested with trypsin and seeded in clean plates, either 96-well (WST-1 assay), 12-well (comet assay), or six-well (Reverse transcription-quantitative polymerase chain reaction (RT-qPCR)). They were exposed 24 h later to 2, 5, 10, 25, or 50 µg/mL of fumed silica (WST1) or 10 µg/mL of fumed silica (comet assay, RT-qPCR).

2.3. Cytotoxicity Assays

Cytotoxicity was evaluated via the WST-1 assay (Roche, Mannheim, Germany), measuring cell metabolic activity and via staining with trypan blue (Sigma–Aldrich, Saint-Quentin Fallavier, France) and counting both viable cells (non-colored) and cells having impaired plasma membrane integrity (blue-colored cells). In the WST-1 assay, after the exposure period, the exposure medium was discarded and replaced by 100 µL of WST-1 diluted to the tenth, as indicated by the supplier. After 1.5 h of incubation at 37 °C, the quantification of metabolic activity was calculated from absorbance measurement at 450 nm, to which was subtracted background absorbance measured at 650 nm. The interference of SiO_2 particles with this assay was checked by centrifuging the plates, sampling

50 µL of each well and transferring it to a clean plate. Absorbance was then measured at 540 and 650 nm, and the obtained values were compared with those that were obtained before the centrifugation. The values were similar, we therefore considered that SiO_2 particles did not interfere with the WST1 assay. In the trypan blue assay, after the exposure period, the cells were harvested with trypsin-EDTA and trypan blue was applied to the cell suspension. Non-colored and blue cells were counted while using an automated cell counter (Countess, ThermoFisher Scientific, Illkirch, France). The absence of interference with the trypan blue assay was visually checked, by manually counting some samples and comparing the data with those that were obtained with the automatic counter. No significant difference was observed in cells that were exposed to 10–50 µg/mL SiO_2; however, at higher concentrations significant difference was observed, which were probably due to impaired detection of blue color or no color in cells having accumulated large quantities of NPs. For this reason, the results presented here were obtained at exposure concentrations that did not exceed 50 µg/mL. Cell membrane integrity was assessed using the Lactate dehydrogenase assay (Sigma–Aldrich, Saint-Quentin Fallavier, France), following the manufacturer's instructions, i.e., one volume of supernatant of exposed cells was sampled after the incubation period and mixed with two volumes of assay mix composed of equal proportions of assay substrate, cofactor, and dye. After incubation for 30 min at room temperature and in the dark, the reaction was stopped by adding 1/10 volume of 1N HCl and absorbance at 490 nm was measured. Triton X-100 (1%) was used as positive control. The absence of interference of SiO_2 particles with the assay was checked by centrifuging the supernatant of exposed cells, then measuring the absorbance at 490 nm and comparing it to the values obtained in samples that had not been centrifuged. We did not detect any significant difference, therefore we considered that SiO_2 particles did not interfere with the assay.

2.4. Genotoxicity Assays

DNA strand breaks and alkali-labile sites were assessed via the alkaline version of the Comet assay. At the end of the exposure period, cells were collected and stored at ~80 °C in sucrose (85.5 g/L), DMSO (50 mL/L) prepared in citrate buffer (11.8 g/L), pH 7.6. Ten thousand cells were mixed with 0.6% low melting point agarose (LMPA) and deposited on a slide that was previously coated with 1% agarose (n = 3). The cell/LMPA mix was allowed to solidify on ice for 10 min, then immersed in cold lysis buffer (2.5 M NaCl, 100 mM EDTA, 10 mM Tris, 10% DMSO, 1% Triton X-100, pH10) and incubated for 1 h at room temperature. The slides were then rinsed three times for 5 min in 0.4 M Tris pH 7.4. Subsequently, DNA was allowed to unwind for 30 min in the electrophoresis buffer (300 mM NaOH, 1 mM EDTA, pH > 13) and an electric field of 0.7 V/cm and 300 mA for 30 min was applied. Slides were neutralized in 0.4 M Tris pH 7.4 and stained with 50 µL of GelRed (Thermo Fisher Scientific, Illkirch, France). As positive control for the alkaline comet assay, 250 µM H_2O_2 was deposited onto the agarose layer containing the cells, and then incubated for 5 min on ice. Fifty comets per slide were analyzed while using Comet IV software (Perceptive Instruments, Suffolk, UK). The potential interference of SiO_2 nanoparticles with the comet assay have been assessed previously (for instance, see [25,26]). No significant interference was detected by Magdolenova et al. [26], while a slight overestimation of DNA damage is reported by Ferraro et al. In HeLa cells that were exposed for 48 h to 500 µg/mL SiO_2-NPs, but not to 50 or 200 µg/mL SiO_2-NPs [25]. In the present study, the cells were exposed to much lower concentrations of SiO_2 particles, and for shorter periods of time, we therefore considered that interference of SiO_2 particles with the comet assay is unlikely to be significant in our experimental conditions.

For quantification of modified DNA bases (HPLC-MS/MS), DNA was extracted as follows: the samples were extracted using DNeasy Blood and Tissue Kit (Qiagen, Les Ullis, France). They were homogenized in AL buffer from the kit, then proteinase K was added and the samples were incubated for 10 min at 56 °C. They were treated with RNase A for 2 min at room temperature and then loaded onto DNeasy Mini spin columns. After centrifugation, the samples loaded onto the columns were washed with AW1 buffer then with AW2 buffer. In the last step, DNA was eluted in 0.1 M deferoxamine

to avoid spurious DNA oxidation. At this stage, the SiO_2 particles that were accumulated in cell cytoplasm are eliminated, because they are not eluted from the column. The samples were then digested for 2 h at 37 °C and pH 5.5 with a cocktail of enzymes (all purchased from Sigma–Aldrich, Saint-Quentin Fallavier, France) composed of phosphodiesterase II, DNase II, nuclease P1, and then for another 2 h at 37 °C, pH 8, with alkaline phosphatase and phosphodiesterase I. These samples were neutralized with HCl 0.1 N, filtered on 0.22 µm filter units to eliminate any remaining SiO_2 particles and injected onto the high performance liquid chromatography-tandem mass spectrometry system (HPLC/MS-MS). An API 3000 mass spectrometer (SCIEX, Villebon-sur-Yvette, France) was used in the multiple reaction monitoring mode with positive electrospray ionization. We monitored the *m*/*z* 284 $[M + H]^+ \rightarrow$ *m*/*z* 168 $[M + h\ -116]^+$ transition for the quantification of for 8-oxodGuo [27] and *m*/*z* 570 → 257 and *m*/*z* 570 → 454 for BPDE-N^2-dGuo [21]. A C18 reversed phase Uptisphere ODB column (Interchim, Montluçon, France) was used for chromatographic separations in an Agilent HPLC system (Agilent, Massy, France). The flow rate was 0.2 mL/min. The HPLC eluent was also analyzed using a UV detector set at 270 nm for the quantification of unmodified nucleosides. For the detection of 8-oxodGuo, elution was performed with a gradient of methanol in 2 mM ammonium formate, leading to a retention time of around 29 min. For the quantification of BPDE-N^2-dGuo, the HPLC mobile phase was a gradient of 6 to 80% of acetonitrile in 2 mM ammonium formate (pH 6). The retention time of the BPDE-N^2-dGuo adduct was 24.5 min. For both 8-oxodGuo and BPDE-N^2-dGuo measurements, results were expressed in the number of adducts per million normal bases. Because no SiO_2 particle was injected in the columns, we consider that SiO_2 particles could not interfere with the measurements.

2.5. RT-qPCR

RNA from exposed cells was extracted using the GenElute™ mammalian total RNA miniprep kit (Sigma–Aldrich, Saint-Quentin Fallavier, France) with the optional DNAse treatment step and reverse-transcribed to complementary DNA (cDNA) while using the SuperScript III Reverse Transcriptase kit (Thermo Fisher Scientific, Illkirch, France), according to the manufacturers' protocols. The first step in this assay consists in the elimination of any cell debris and material via filtration on a column. We consider that SiO_2 particles must be retained on this column and, therefore, are unlikely to interfere with the following stages of mRNA extraction, RT, and qPCR. RNA concentration and purity were assessed by measuring A260/A280 and A260/A230 absorbance ratios using a Nanodrop ND-1000 (Thermo Fisher Scientific, Illkirch, France). For the qPCR, cDNA from each of the three biological replicates of each exposure condition was loaded in duplicate on a 96-well qPCR plate. qPCR was performed on a CFX96 thermocycler (Biorad, Marne-la-coquette, France) using the following thermal cycling steps: 95 °C for 5 min, then 95 °C for 15 s, 55 °C for 20 s and 72 °C for 40 s 40 times, and finally 95 °C for 1 min, 55 °C for 30 s and 95 °C for 30 s for the dissociation curve. Cq was determined by the CFX96 Manager (Biorad, Marne-la-coquette, France) used with default settings. Glyceraldehyde-3-phosphate dehydrogenase (GAPDH) and 18S ribosomal 1 (S18) were chosen as reference genes for normalization, and validated while using the BestKeeper tool, version 1 [28]. mRNA expression analysis, normalization, and statistical analysis were performed with REST 2009 software [29], which uses the ΔΔCq method and a pair-wise fixed reallocation randomization test. The PCR efficiencies were experimentally checked for compliance using a mix of all samples, with a quality criterion of 2 ± 0.3.

2.6. Statistical Analysis

Each experiment was repeated at least three times independently. The statistical tests were performed using the Statistica software (version 7.1, Statsoft, Chicago, IL, USA). As normality assumptions for valid parametric analyses were not satisfied, a non-parametric test was used, i.e., Kruskal–Wallis one-way analysis of variance. When significance was demonstrated, paired comparisons were performed using Mann–Whitney tests. The results were considered to be statistically significant (*) when the p value was <0.05.

3. Results

3.1. Physico-Chemical Characterization of SiO_2 Particles

The three SiO_2 particles were prepared as suspensions in water and sterilized by pasteurization. Their size distribution analysis showed the agglomeration of E551, which formed agglomerates of particles with diameter >2 µm. Conversely, Fumed silica and LS30 formed stable suspensions with mean hydrodynamic diameters of 270 and 24 nm, respectively (Figure 1a). Polydispersity indexes were 0.28, 0.21, and 0.24 for E551, Fumed SiO_2, and LS30, respectively. Their zeta potential was slightly negative, with values between ~10 and ~30 mV (Figure 1b), which suggested a tendency towards agglomeration. In RAW 264.7 exposure medium, all three particles agglomerated. Fumed silica and LS30 still formed stable suspensions, with hydrodynamic diameters of 1203 and 381 nm, respectively, while E551 formed very large agglomerates with diameter >5 µm. The values were similar in Caco-2/HT29-MTX exposure medium (not shown). As expected, the TEM images showed that E551 (Figure 1c) and Fumed SiO_2 (Figure 1d) were composed of aggregates of fused nanoparticles with primary diameter of 15–20 nm, while LS30 was composed of SiO_2 nanoparticles with average primary diameter 14.3 ± 2.2 nm, as measured from 100 particles on TEM images (Figure 1e).

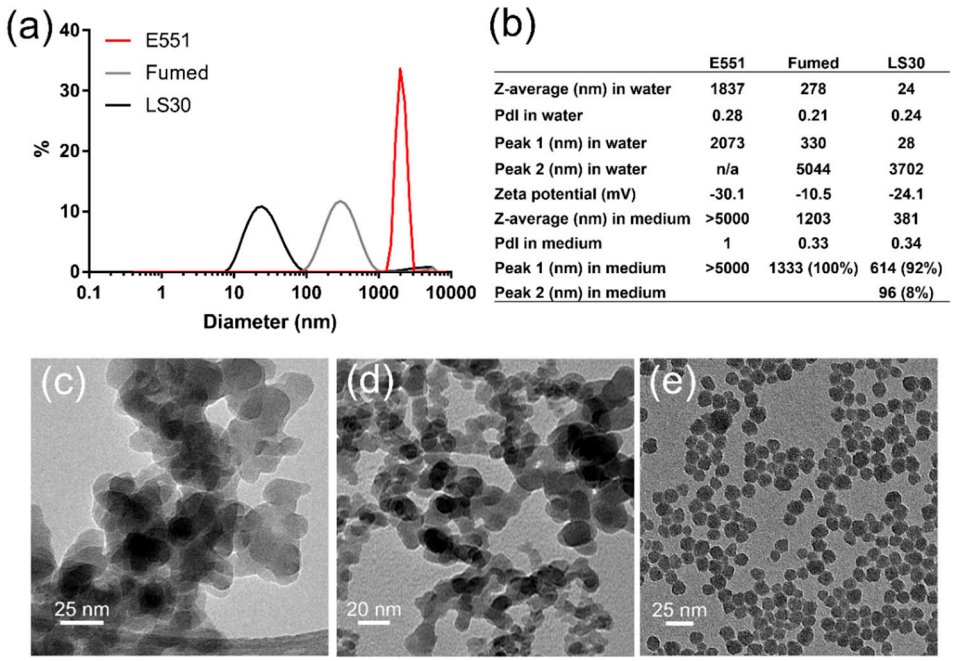

	E551	Fumed	LS30
Z-average (nm) in water	1837	278	24
PdI in water	0.28	0.21	0.24
Peak 1 (nm) in water	2073	330	28
Peak 2 (nm) in water	n/a	5044	3702
Zeta potential (mV)	-30.1	-10.5	-24.1
Z-average (nm) in medium	>5000	1203	381
PdI in medium	1	0.33	0.34
Peak 1 (nm) in medium	>5000	1333 (100%)	614 (92%)
Peak 2 (nm) in medium			96 (8%)

Figure 1. Physico-chemical characterization of SiO_2 particles. (**a**) Size distribution of SiO_2 particles in water; (**b**) hydrodynamic diameter, polydispersity index and zeta potential for SiO_2 particles dispersed in water; (**c**) TEM image of E551; (**d**) TEM image of Fumed silica; and, (**e**) TEM image of LS30.

3.2. Acute Cytotoxicity and Genotoxicity of SiO_2 Particles

First, cell viability was assessed on RAW264.7 macrophages and Caco-2/HT29-MTX exposed to the three SiO_2 particles. All three SiO_2 particles altered RAW 264.7 cell viability after acute exposure for 24 h (Figure 2). In the WST1 assay, Fumed silica altered more intensely cell metabolic activity than E551, which itself altered more intensely cell metabolic activity than LS30 (Figure 2a). Using the trypan blue assay, the three particles showed similar cytotoxicity, which was lower than cell metabolic activity alteration (Figure 2b). Conversely, in Caco-2/HT29-MTX cells, no significant reduction of cell metabolic activity (WST1 assay) and cell membrane integrity (LDH assay) were detected (Figure 2c,d, respectively).

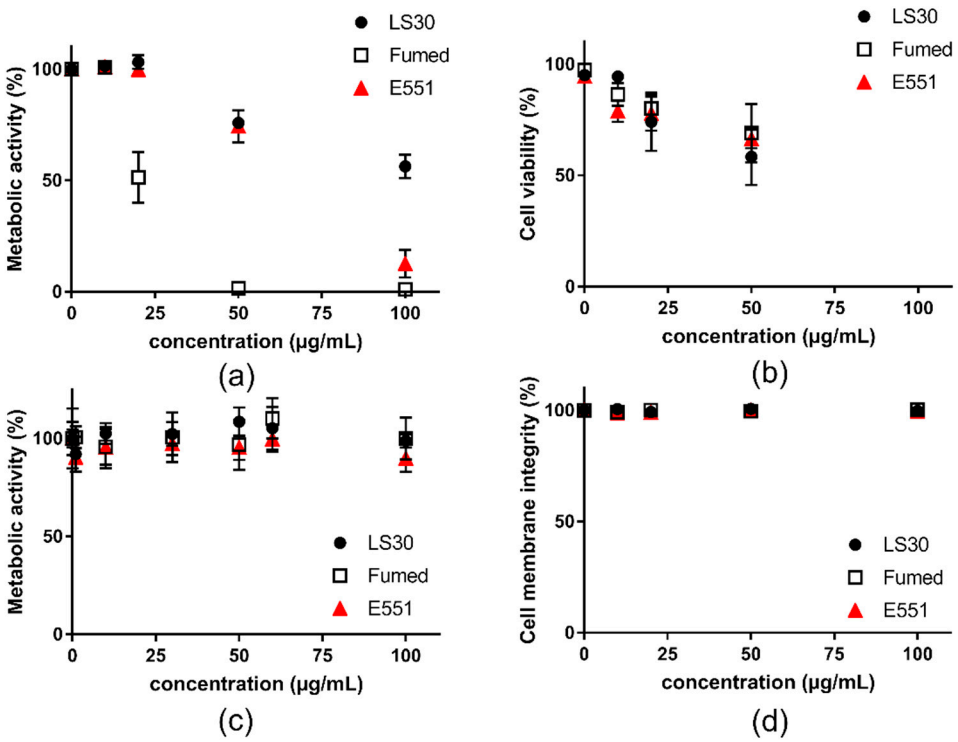

Figure 2. Cytotoxicity of SiO_2 particles, acute exposure for 24 h to SiO_2 particles. (**a**) metabolic activity of RAW264.7 cells assessed via the WST-1 assay; (**b**) cytotoxicity assessed in RAW264.7 cells via trypan blue staining; (**c**) metabolic activity of Caco-2/HT29-MTX cells assessed via the WST-1 assay; and, (**d**) membrane integrity of Caco-2/HT29-MTX cells assessed via the LDH assay. Mean ± standard deviation of five replicates (n = 5).

This experiment allowed the determination of the dose to be applied in genotoxicity assays, particularly in the comet assay, which should be a concentration leading to less than 20–30% of cell death. With respect to these results, the genotoxicity assays were performed on RAW264.7 cells that were exposed to 10 µg/mL SiO_2, because it was the highest tested concentration causing no significant cell death in both WST-1 and trypan blue assays. For Caco-2HT29-MTX, since no cytotoxicity of SiO_2 particles was observed, even at the highest concentrations tested, we chose to expose cells to 5, 15, and 30 µg/mL SiO_2 particles, as suggested to avoid any interference with the assays [30].

At these sub-lethal concentrations, the three SiO_2 particles significantly increased the number of strand breaks and/or alkali-labile sites in RAW264.7 cells, in the alkaline comet assay (Figure 3a), which probes their capacity to induce oxidative damage to DNA. The level of DNA damage was similar in cells that were exposed to Fumed silica and E551; it was significantly higher than the level of DNA damage that was caused by LS30. Conversely, none of these SiO_2 particles increased the level of 8-oxo-dGuo in the DNA of exposed cells (Figure 3b). In Caco-2/HT29-MTX cells, none of the particles induced any increase of DNA damage in exposed cells, neither in the comet assay nor via direct measurement of 8-oxo-dGuo by HPLC-MS/MS (Figure 3c,d, respectively).

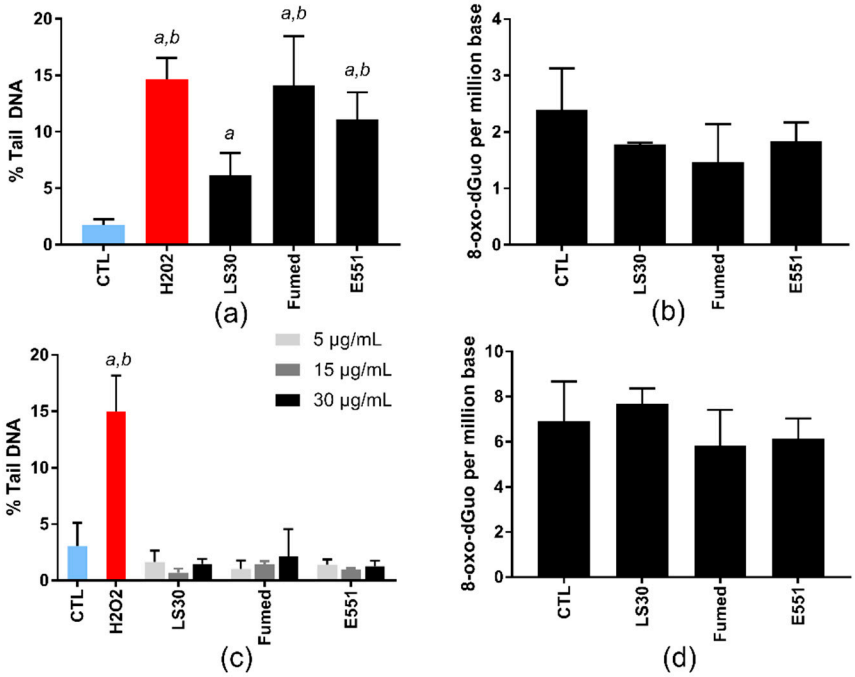

Figure 3. Genotoxicity of SiO_2 particles, acute exposure. (**a**,**c**) DNA strand breaks and/or alkali-labile sites, assessed via the alkaline comet assay, in RAW264.7 cells exposed to 10 µg/mL SiO_2 (**a**) and in Caco-2/HT29-MTX cells exposed to 5, 15, or 30 µg/mL SiO_2 (**c**). H_2O_2 (250 µM) was used as positive control. Mean ± standard deviation of five independent experiments (n = 5); (**b**,**d**) quantification of 8-oxo-dGuo by high performance liquid chromatography-tandem mass spectrometry system (HPLC-MS/MS), in RAW264.7 cells exposed to 10 µg/mL SiO_2 (**b**) and Caco-2/HT29-MTX cells exposed to 50 µg/mL SiO_2 (**d**). Mean ± standard deviation of three independent replicates from the same experiment (n = 3). Statistical significance, ^{a} $p < 0.05$, exposed vs. CTL (untreated cells), ^{b} $p < 0.05$, exposed vs. LS30.

3.3. Cytotoxicity and Genotoxicity of LS30, Fumed Silica or E551 after Repeated Exposure

Because SiO_2 particles only showed toxic outcomes in RAW264.7, we then focused on this cell line in the following experiments. The cells were repeatedly exposed to 1 or 2 µg/mL of these SiO_2 particles in order to assess the hypothesis of progressive accumulation of SiO_2 particles in RAW264.7 leading to additive level of DNA damage. This protocol mimics long term exposure to SiO_2 particles via ingestion. Cells were seeded in adherent plates and exposed nine times to these concentrations of SiO_2 particles at the frequency of one exposure every two days. This corresponds to three weeks of exposure and the cumulative dose was 9 and 18 µg/mL, respectively. This repeated exposure did not cause any overt alteration of cell metabolic activity (Figure 4a). For comparison, acute exposure to 10 µg/mL or 20 µg/mL SiO_2 particles also did not decrease cell viability, except in RAW 264.7 cells that were exposed to 20 µg/mL Fumed SiO_2, which led to ~50% decrease of cell metabolism (see Section 3.2). Conversely, this repeated exposure induced DNA strand breaks and/or alkali-labile sites, which increased with exposure concentration (Figure 4b). At each exposure concentration, all three SiO_2 particles produced the same level of DNA damage in RAW 264.7 cells. The level of DNA damage in cells repeatedly exposed to 1 µg/mL SiO_2 particles (cumulative concentration: 9 µg/mL SiO_2) was slightly less intense than in cells that were acutely exposed to 10 µg/mL SiO_2 (see Section 3.2). Conversely, in cells repeatedly exposed to 2 µg/mL SiO_2 particles (cumulative concentration: 18 µg/mL SiO_2), the level of DNA damage was much higher, i.e., close to 50% Tail DNA; with high variability.

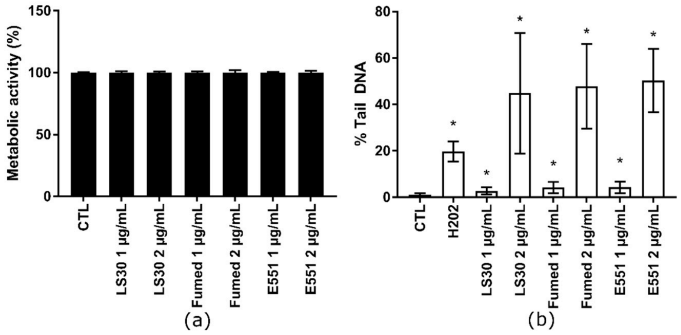

Figure 4. Cytotoxicity of SiO_2 particles, repeated exposure. RAW 264.7 were exposed repeatedly to 1 or 2 µg/mL SiO_2 particles, three times per week for 3 weeks. (**a**) Metabolic activity of RAW264.7 cells measured using the WST-1 assay and (**b**) genotoxicity of SiO_2 particles assessed via alkaline comet assay. Mean ± standard deviation of five replicates (WST-1) and three comet experiments performed independently, with three slides per experiment. Statistical significance: * $p < 0.05$, CTL vs. exposed.

We then investigated the potential of each of these SiO_2-NP to modify the effects of the most genotoxic NP studied here, namely Fumed silica (see Section 3.2). This mimics a situation where SiO_2 is chronically ingested every day, and then one day of intense pollution a significant amount of SiO_2 is inhaled, then ingested acutely due to mucociliary clearance. Cells were repeatedly exposed to 1 µg/mL of SiO_2-NPs three times per week for 3 weeks and then subsequently acutely exposed to 10 µg/mL of Fumed silica. In the cytotoxicity assay, the preliminary repeated exposure to SiO_2 did not significantly change the overall response to subsequent acute exposure to Fumed silica (Figure 5a). In contrast, in the genotoxicity assay, the level of DNA damage caused by the acute exposure to Fumed silica was significantly increased in cells that had been previously exposed to 1 µg/mL SiO_2, as compared to cells not previously exposed to SiO_2 (Figure 5b, white bars). When adding the level of damage caused by the repeated exposure to SiO_2 particles to that caused by a single acute exposure to 10 µg/mL of Fumed SiO_2 (without pre-exposure), the obtained value was similar to that observed in cells that were repeatedly exposed to SiO_2 and then acutely to Fumed SiO_2 (Figure 5b, grey bars). This suggest progressive, cumulative accumulation of SiO_2 in repeatedly- and then acutely-exposed cells, resulting in additive levels of DNA damage.

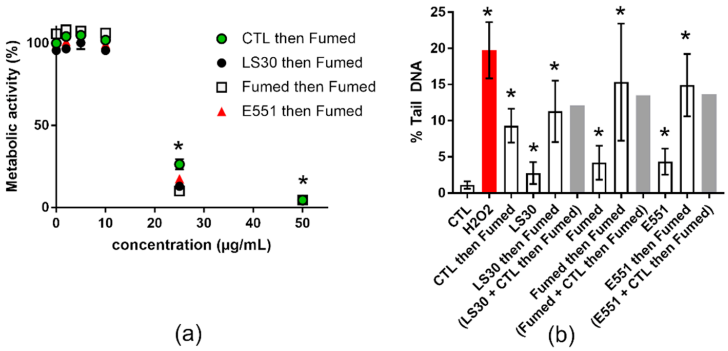

Figure 5. Cyto- and genotoxicity of SiO_2 particles, repeated exposure followed by acute exposure to Fumed SiO_2. (**a**) Cell metabolic activity impairment after repeated exposure to 1 µg/mL SiO_2 particles (CTL or LS30 or Fumed SiO_2), followed by 24 h exposure to 2, 5, 10, 25, or 50 µg/mL of Fumed silica. (**b**) Genotoxicity assessed via alkaline comet assay, on RAW 264.7 cells exposed repeatedly to 1 µg/mL SiO_2 particles, three times per week for three weeks, followed by a single acute exposure to 10 µg/mL Fumed SiO_2 for 24 h. Mean ± standard deviation of five replicates (WST-1) and three comet experiments performed independently, with three slides per experiment. Statistical significance: * $p < 0.05$, CTL vs. exposed.

3.4. Cytotoxicity and Genotoxicity after Co-Exposure to SiO_2 and B[a]P or MMS

We then tested the hypothesis of sensitization of RAW264.7 macrophages towards genotoxic agents by SiO_2-NPs. RAW264.7 were acutely co-exposed to SiO_2 particles and known genotoxic agents. First, they were exposed to 0.2–2 µM B[a]P or a mixture of 0.2–2 µM of B[a]P and 10 µg/mL SiO_2 particles. In these conditions, no significant modulation of cell viability was detected (Figure 6a) up to 2 µM of B[a]P, which is very high as compared to environmentally-relevant concentrations. Indeed, the values measured in the bloodstream of contaminated people are in the range of some nm, and they can reach 1 µM in some industrial sectors. The main damage to DNA caused by B[a]P are DNA-BPDE adducts and DNA strand breaks, the former being much more frequent than the latter [31]. Analysis of the DNA extracted from cells exposed to either 0.2–2 µM B[a]P or a mixture of 0.2–2 µM of B[a]P and 10 µg/mL SiO_2 particles revealed the absence of BPDE adducts. Figure 6b show the retention time of BPDE-N^2-dGuo in HPLC-MS/MS (Figure 6b, blue chromatogram), the spectrum obtained from RAW264.7 cells exposed to 2 µM B[a]P (Figure 6b, red chromatogram) or to 2 µM B[a]P and 10 µg/mL Fumed SiO_2 for 24 h (Figure 6b, green chromatogram), showing no evidence of a BPDE-N^2-dGuo peak. The spectra obtained from cells co-exposed to 0.2–2 µM of B[a]P and 10 µg/mL LS30, Fumed SiO_2 or E551 were similar.

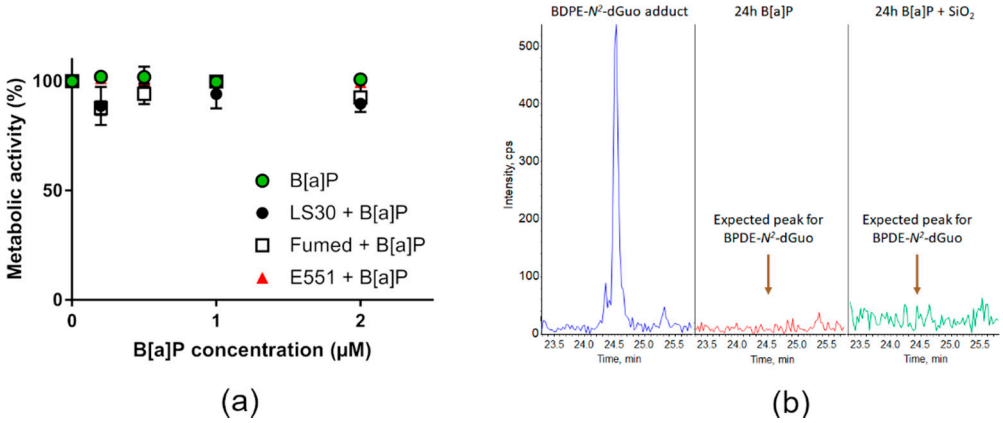

Figure 6. Cyto- and genotoxicity of B[a]P or SiO_2 co-exposed with B[a]P towards RAW264.7 cells. (**a**) Cell metabolic activity, assessed via the WST1 assay; (**b**) HPLC-MS/MS chromatograms obtained upon quantification of BPDE adduct to DNA showing the expected position of the BPDE adduct peak (BPDE-N^2-dGuo) (blue, left), of DNA extracted from cells exposed to 2 µM B[a]P (red, middle) and of DNA extracted from cells exposed to 2 µM B[a]P and 10 µg/mL Fumed SiO_2 (green, right).

The cells were directly exposed to BPDE then their DNA was extracted and the presence of BPDE-N^2-dGuo adducts was monitored by HPLC-MS/MS in order to verify that this absence of BPDE adducts reported in Figure 6 did not result from the incapacity of RAW264.7 cells to metabolize B[a]P to BPDE. Again, no BPDE-N^2-dGuo adduct was detected (not shown), confirming that the absence of BPDE adducts in cells B[a]P-exposed was not due to a lack of metabolization of B[a]P.

The cells were then exposed to MMS or a mixture of MMS and 10 µg/mL SiO_2. The cytotoxicity of all three SiO_2 particles, when cells were co-exposed to 10 µg/mL SiO_2 particle and 100–500 µM MMS, did not differ from cytotoxicity of the corresponding concentration of MMS (Figure 7a). As expected, MMS induced a dose-dependent elevation of DNA strand breaks and/or alkali-labile sites in RAW264.7 cells in the alkaline comet assay (Figure 7b). When considering cells that were exposed to a mixture of 10 µg/mL SiO_2 particle and 100 µM MMS, the level of DNA damage was greater, as compared to cells exposed to 100 µM MMS (Figure 7b). We then added the level of damage observed in cells exposed to 10 µg/mL SiO_2 to that observed in cells that were exposed to 100 µM MMS, while assuming that the effect of these two toxic agents could be purely additive. When comparing these calculated values with the experimental values that were obtained upon co-exposure to SiO_2

and MMS, the experimental values were greater than the calculated values (Figure 7c), suggesting a synergistic interaction between SiO_2 particles and MMS.

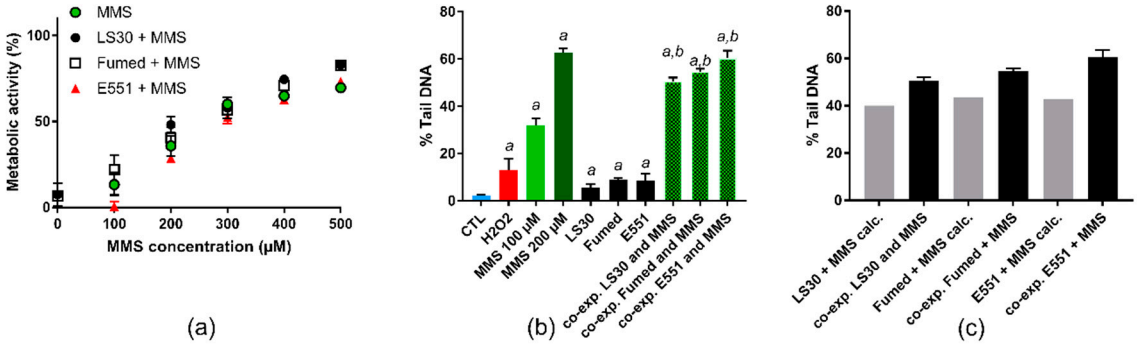

Figure 7. Cyto- and genotoxicity on RAW264.7 cells of MMS or co-exposure to MMS and SiO_2. (**a**) Cell metabolic activity, assessed via the WST1 assay; (**b**) DNA strand breaks and/or alkali-labile sites assessed via the alkaline comet assay in RAW264.7 cells exposed to 10 µg/mL SiO_2. Positive control: H_2O_2 (250 µM); (**c**) comparison of experimental results (level of DNA damage in cells co-exposed to MMS and SiO_2) and calculated values (level of DNA damage in cells exposed to MMS + level of DNA damage in cells exposed to SiO_2) WST1: mean ± standard deviation of five independent experiments (n = 5); comet assay: mean ± standard deviation of two independent experiments with three slides per experiment (n = 2). Statistical significance, *a*: $p < 0.05$, exposed vs. CTL (untreated cells), *b*, $p < 0.05$, co-exposed to SiO_2 particle and MMS vs. exposed to the respective SiO_2 particle.

A hypothesis for explaining this synergistic interaction between SiO_2 particles and MMS would be that SiO_2 particles would impair DNA repair activities in exposed cells. To test this hypothesis, the mRNA expression of genes encoding DNA repair proteins were analyzed in cells that were exposed to LS30, Fumed SiO_2, and E551. MMS is an alkylating agent, which mainly methylates N7-deoxyguanosine and N3-deoxyadenosine. These methylated bases are unstable and are rapidly hydrolyzed into an abasic site. Damage that is caused by MMS is repaired via the base-excision repair (BER) pathway and DNA methyltransferases [32,33]. We measured the mRNA expression of DNA repair enzymes involved in the BER pathway, namely the endonuclease APE1, XRCC1, and PARP1 that coordinate the resynthesis and polymerization steps of BER (for more detail on this DNA repair pathway, see [33]). No significant modulation of mRNA expression of these three proteins was observed (Figure 8), which suggested that this DNA repair pathway was not affected by exposure to SiO_2 particles.

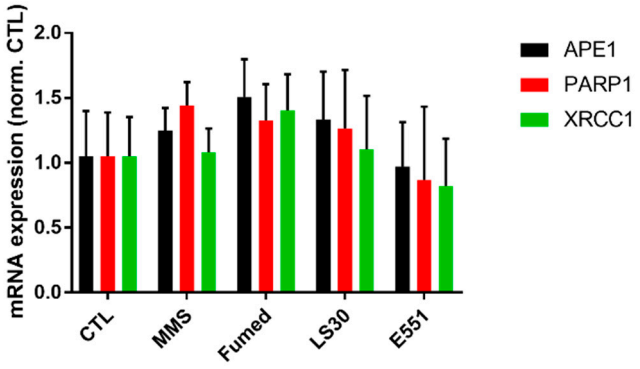

Figure 8. mRNA expression of three proteins involved in DNA repair via the base-excision pathway. Mean ± standard deviation of two independent experiments with three slides per experiment (n = 2). Statistical significance, none of the conditions induced statistically significant changes ($p > 0.05$, exposed vs. CTL).

4. Discussion

In this study, we compared the toxicity of synthetic amorphous silica in RAW264.7 macrophages and in Caco-2/HT29-MTX epithelial intestinal cells, and showed that RAW264.7 are more sensitive to SiO_2 than these epithelial cells, with greater impact on cell viability, as assessed via the WST1 assay and a higher level of DNA damage in the comet assay. This greater sensitivity of macrophages has already been described in several reports, e.g., in [17]. It is certainly related to their capacity to accumulate larger quantities of particles as compared to epithelial cells. This is explained by their physiological function, which is the scavenging of exogenous matter in the body, especially large-sized material, such as bacteria and viruses. The size of SiO_2 agglomerates to which RAW264.7 cells have been exposed in the present study, particularly Fumed SiO_2 and E551, falls within the optimal size range of material that is efficiently phagocytosed by macrophages, i.e., 2–3 µm [34]. This suggests that intracellular accumulation of SiO_2 in RAW 264.7 cells would be intense, while accumulation in intestinal epithelial cells, which are not phagocytosis-competent, would be less efficient, as it mainly derives from endocytosis [35]. Moreover, we used here a Caco-2/HT29-MTX co-culture, in which HT29-MTX cells produce some protective mucus [23,36] and this could also explain their resistance to SiO_2 particles, also owing to lower intracellular accumulation due to the entrapment of particles in mucus.

The three SiO_2 particles used here vary in their physico-chemical properties. LS30 is composed of isolated nanoparticles, while Fumed SiO_2 and E551 are composed of constituent nanoparticles fused together to form large chaplets of particles. Moreover, Fumed SiO_2 is a pyrogenic silica, while LS30 and the E551 used in this study are both produced by a wet process (i.e., precipitated SiO_2). We observed that Fumed SiO_2 shows greater toxicity than E551 and LS30, which is in line with the literature [37,38]. The greater toxicity of pyrogenic silica has been related to their higher surface reactivity [37], which could be explained by the presence of strained three-membered rings, to higher hydroxyl content and chainlike agglomeration [38]. Here, the cytotoxicity data obtained with the three SiO_2 confirm these hypotheses, with LS30 non-aggregated colloidal SiO_2 being the least toxic, followed by E551 aggregated SiO_2 (and synthesized as precipitated SAS), and then finally Fumed SiO_2, which is aggregated and pyrogenic. Regarding their genotoxicity, E551 and Fumed SiO_2 do not show a significant difference, but LS30 is less prone to damaging DNA. This could be the basis of future recommendation on the physico-chemistry of SiO_2 that are authorized as food additive, with possibly the suggestion of reducing, as much as possible, the structural defects in pyrogenic SiO_2 in order to reduce their toxicity.

Our initial objective was to evaluate whether co-exposure to SiO_2 and genotoxic agents could modulate the DNA damaging potential of genotoxic agents. Indeed, SiO_2 could adsorb metals or environmental pollutants on their surface and facilitate their accumulation in cells or organisms. This would increase their toxicity. In contrast, the adsorption of some pollutants on the surface of SiO_2 particles could inactivate these co-contaminants by modifying their configuration [39] or could reduce their availability, therefore reducing their toxicity. Moreover, we previously reported that RAW264.7 macrophages were more sensitive to the alkylating agent styrene oxide when previously exposed to SiO_2 nanoparticles [17]. We observe increased genotoxicity of MMS when co-exposed to RAW264.7 macrophages with the three SiO_2 particles, and the interaction between MMS and SiO_2 was synergistic rather than simply additive. We attempted similar experiments with B[a]P, but could not detect any genotoxic potential of this substance in RAW 264.7 cells. The synergistic interaction of SiO_2 particles with co-contaminants has been reported in various studies, particularly with metals, such as cadmium, methylmercury, arsenic, and lead [13,14,40–44], or with B[a]P [10–12]. Increased genotoxic potential has been highlighted for SiO_2 and B[a]P in epithelial cells [10,11,44]. The authors used the comet assay to assess DNA damage that is caused by B[a]P and, therefore, only detected strand breaks, which have been shown to be produced in lower amount as compared to the BPDE-DNA adducts in hepatocytes and lung cells [21,31]. Moreover, the sensitivity of BPDE-DNA adducts is largely higher than the sensitivity of the comet assay. Some BPDE-DNA adducts can be detected and quantified in

cells exposed to some tens of femtomolars of B[a]P, while the exposure concentration should be higher than 1 μM to be able to detect some DNA damage in the comet assay [31]. A hypothesis to explain that we did not detect any DNA-BPDE adducts in RAW 264.7 macrophages would be that these cells do not have the capacity to metabolize B[a]P to BPDE. However, the RAW 264.7 cell line has been shown to express active P450 cytochromes, which are responsible for this metabolization [45]. Moreover, we did not observe any BPDE-DNA adduct, even when RAW 264.7 cells were directly exposed to BPDE. One possible reason to explain the absence of DNA-BPDE adducts would be that BPDE is quickly expulsed out of RAW264.7 cells before being able to reach the cell nucleus and to damage DNA. Another explanation could be a much more active phase II detoxification pathways leading a complete conversion of BPDE into excreted metabolites. The situation may be different in epithelial and endothelial cells, which have very different metabolisms as compared to macrophages. Macrophages, whose physiological function is to clean the organism from toxic substances and materials, certainly shows a greater ability to discard such metabolites. The genotoxic impact of B[a]P and SiO_2 was shown to be synergistic in HUVEC cells in the study by Otieno-Asweto et al. [10] and additive in BEAS-2B cells the study by Wu et al. [11]. The major differences between these two studies are i) the cell line on which the assays were conducted and ii) the applied concentrations. BEAS-2B had been exposed to 5 μg/mL SiO_2-NPs and 5 μM B[a]P, while HUVECs had been exposed to 10 μg/mL SiO_2 and 1 μM B[a]P. Both of the cell lines were exposed in the same medium. The use of different exposure concentrations does not allow for direct comparison of the results; still, HUVECs cells respond more intensely to these toxic agents than BEAS-2B cells, which suggests that they are more sensitive. In both studies, the rate of apoptosis in cells co-exposed to SiO_2 and B[a]P was significant, i.e., 50% of apoptosis rate in co-exposed cells compared to 25% in control HUVECs cells (approximately 20% of cell death in the CCK-8 assay) [10] and approximately 25% in co-exposed cells as compared to 15% in control BEAS-2B cells (<10% of cell death in the CCK-8 assay) [11]. Because the authors do not measure BPDE-DNA adducts, but rather use the comet assay to assess the genotoxicity of B[a]P, one can hypothesize that the DNA damage detected in these studies could be rather an indirect measurement of DNA fragmentation occurring when cells undergo apoptosis, than a direct impact of SiO_2 and B[a]P on DNA. It could also derive from the oxidative stress that results from HAP metabolization. The authors do not propose any hypothesis that could explain the either synergistic of additive interaction of SiO_2 and B[a]P in the genotoxicity experiments. One explanation could be that SiO_2 particles impair DNA repair processes. This hypothesis is not supported by our mRNA expression experiments. However, DNA repair processes function on the basis of already existing DNA repair proteins, so mRNA expression measurement is perhaps not a reliable method for assessing DNA repair activity in these cells. Importantly, we previously detected a decrease in the level of proteins related to the nucleotide excision repair pathway (NER) in RAW 264.7 cells that were exposed to a colloidal silica NPs with similar characteristics as LS30 [17]. We could hypothesize that a similar mechanism could be at play here, with the BER pathway. Unfortunately, such low amplitude changes, although putatively biologically significant, are technically difficult to detect. One could also hypothesize that SiO_2 particles adsorb large amounts of MMS on their surface and act as a vector to transport it inside cells, thereby increasing the overall level of cell exposure to this genotoxic agent. In this model, silica behaves as an adsorptive material, such as when it is used in chemistry as a chromatographic support. In this frame, the medium hydrophilicity of MMS (LogKow = ~0.87) makes it a good candidate for an adsorption–release mechanism on silica, where the much more hydrophobic B[a]P (LogKow = 6.1) will not adsorb appreciably on silica in a complex environment, where more hydrophobic macromolecules (e.g., proteins) are present.

When considering the experiment where cells were subjected to repeated exposure to SiO_2 particles followed by acute exposure to Fumed SiO_2, the level of DNA damage measured in cells is exactly the cumulative level calculated by adding the level of damage after repeated exposure to the level of damage after acute exposure. This suggests that the genotoxicity of SiO_2 particles towards RAW264.7 cells is cumulative, certainly deriving from progressive accumulation of SiO_2 particles

that is not compensated by any exocytosis of the particles out of cells. This confirms the previously observed trend of progressive accumulation of fluorescent SiO_2-NPs in this cell line [46].

SiO_2 particles are generally considered to be non-toxic, especially non-genotoxic, although several recent studies show their potency to cause DNA damage, as assessed via the comet assay, micronucleus assay, and gene mutation assay (for instance, see [47–50]). Here, we show significant damage to DNA caused by the three SiO_2 particles on macrophages. The rationale for testing nanoparticle genotoxicity on macrophages can be questioned, because genotoxicity is classically assessed as a preliminary event leading to gene mutation, which may then lead to cancer. However, cancers that are linked to macrophages, i.e., histiocytomas, are very rare. However macrophages are interesting tools to study particle toxicity because they heavily accumulate particles. Therefore, they could serve as model cells to predict the hazard dimension of particle genotoxicity.

5. Conclusions

In this article we show that SiO_2 particles cause genotoxic damage in the RAW 264.7 cell line, but not in a co-culture of Caco-2 and HT29-MTX intestinal epithelial cells, which confirms the particular sensitivity of macrophages towards SiO_2 that has already been observed elsewhere. The genotoxic damage is significant whatever the SiO_2 physico-chemical properties and purity, i.e., either with isolated nanoparticles or with agglomerated-aggregates of fused primary particles and either with food-grade SiO_2 or with non-food-grade SiO_2. The level of DNA damage increases linearly upon repeated exposure, which suggests progressive accumulation of particles into cells causing progressive elevation of the level of DNA lesions, and no release of particles from cells. While B[a]P do not induce any DNA damage in RAW 264.7 cells, SiO_2 particles and MMS synergistically induce the elevation of DNA damage in exposed cells. This synergistic effect is not correlated with any significant modulation of DNA repair in exposed cells. Taken together, these data suggest that SiO_2 particles could serve as cargo for genotoxic agents, therefore increasing their DNA damaging potential.

Author Contributions: Data curation, M.C.; Formal analysis, M.C.; Funding acquisition, T.R. and M.C.; Investigation, F.D., P.-A.A., M.-E.A., B.D., A.T., T.D., N.H. and M.C.; Methodology, T.R. and M.C.; Project administration, T.R. and M.C.; Resources, T.R. and M.C.; Supervision, T.R. and M.C.; Writing—original draft, M.C.; Writing—review & editing, M.-E.A., T.D. and T.R. All authors have read and agreed to the published version of the manuscript.

Funding: This research was funded by Excellence Initiative of Aix-Marseille University—A*MIDEX, a French "Investissements d'Avenir" program (grant number ANR-11-IDEX-0001-02), through its associated Labex SERENADE project (grant number ANR-11-LABX-0064). This work was funded by the French National Research Program for Environmental and Occupational Health of ANSES (PNREST 2015/032, Silimmun Grant) and the French National Research Agency (ANR-16-CE34-0011, PAIPITO grant).

Acknowledgments: This work used the platforms of the Grenoble Instruct centre (ISBG; UMS 3518 CNRS-CEA-UJF-EMBL) with support from FRISBI (ANR-10-INSB-05-02) and GRAL (ANR-10-LABX-49-01) within the Grenoble Partnership for Structural Biology (PSB). The IBS electron microscope facility is supported by the Rhône-Alpes Region, the Fondation Recherche Medicale (FRM), the fonds FEDER, the Centre National de la Recherche Scientifique (CNRS), the CEA, the University of Grenoble, EMBL, and the GIS-Infrastrutures en Biologie Sante et Agronomie (IBISA). The authors particularly thank Daphna Fenel and Guy Schoehn for providing access to this infrastructure. We also thank Olivier Renard for providing access to DLS equipment at the CEA/LVME laboratory.

Conflicts of Interest: The authors declare no conflict of interest.

References

1. Dekkers, S.; Krystek, P.; Peters, R.J.; Lankveld, D.P.; Bokkers, B.G.; van Hoeven-Arentzen, P.H.; Bouwmeester, H.; Oomen, A.G. Presence and risks of nanosilica in food products. *Nanotoxicology* **2011**, *5*, 393–405. [CrossRef] [PubMed]
2. De Temmerman, P.J.; Van Doren, E.; Verleysen, E.; Van der Stede, Y.; Francisco, M.A.; Mast, J. Quantitative characterization of agglomerates and aggregates of pyrogenic and precipitated amorphous silica nanomaterials by transmission electron microscopy. *J. Nanobiotechnol.* **2012**, *10*, 24. [CrossRef] [PubMed]

3. Arts, J.H.; Muijser, H.; Duistermaat, E.; Junker, K.; Kuper, C.F. Five-day inhalation toxicity study of three types of synthetic amorphous silicas in Wistar rats and post-exposure evaluations for up to 3 months. *Food Chem. Toxicol.* **2007**, *45*, 1856–1867. [CrossRef] [PubMed]
4. Sun, B.; Wang, X.; Liao, Y.P.; Ji, Z.; Chang, C.H.; Pokhrel, S.; Ku, J.; Liu, X.; Wang, M.; Dunphy, D.R.; et al. Repetitive Dosing of Fumed Silica Leads to Profibrogenic Effects through Unique Structure-Activity Relationships and Biopersistence in the Lung. *ACS Nano* **2016**, *10*, 8054–8066. [CrossRef] [PubMed]
5. van Kesteren, P.C.; Cubadda, F.; Bouwmeester, H.; van Eijkeren, J.C.; Dekkers, S.; de Jong, W.H.; Oomen, A.G. Novel insights into the risk assessment of the nanomaterial synthetic amorphous silica, additive E551, in food. *Nanotoxicology* **2015**, *9*, 442–452. [CrossRef] [PubMed]
6. Fruijtier-Polloth, C. The safety of nanostructured synthetic amorphous silica (SAS) as a food additive (E 551). *Arch. Toxicol.* **2016**, *90*, 2885–2916. [CrossRef] [PubMed]
7. Murugadoss, S.; Lison, D.; Godderis, L.; Van Den Brule, S.; Mast, J.; Brassinne, F.; Sebaihi, N.; Hoet, P.H. Toxicology of silica nanoparticles: An update. *Arch. Toxicol.* **2017**, *91*, 2967–3010. [CrossRef]
8. Yazdimamaghani, M.; Moos, P.J.; Dobrovolskaia, M.A.; Ghandehari, H. Genotoxicity of amorphous silica nanoparticles: Status and prospects. *Nanomedicine Nanotechnol. Boil. Med.* **2019**, *16*, 106–125. [CrossRef]
9. Asweto, C.O.; Hu, H.; Liang, S.; Wang, L.; Liu, M.; Yang, H.; Duan, J.; Sun, Z. Gene profiles to characterize the combined toxicity induced by low level co-exposure of silica nanoparticles and benzo[a]pyrene using whole genome microarrays in zebrafish embryos. *Ecotoxicol. Environ. Saf.* **2018**, *163*, 47–55. [CrossRef]
10. Asweto, C.O.; Wu, J.; Hu, H.; Feng, L.; Yang, X.; Duan, J.; Sun, Z. Combined Effect of Silica Nanoparticles and Benzo[a]pyrene on Cell Cycle Arrest Induction and Apoptosis in Human Umbilical Vein Endothelial Cells. *Int. J. Environ. Res. Public Health* **2017**, *14*, 289. [CrossRef]
11. Wu, J.; Shi, Y.; Asweto, C.O.; Feng, L.; Yang, X.; Zhang, Y.; Hu, H.; Duan, J.; Sun, Z. Co-exposure to amorphous silica nanoparticles and benzo[a]pyrene at low level in human bronchial epithelial BEAS-2B cells. *Environ. Sci. Pollut. Res. Int.* **2016**, *23*, 23134–23144. [CrossRef] [PubMed]
12. Wu, J.; Zhang, J.; Nie, J.; Duan, J.; Shi, Y.; Feng, L.; Yang, X.; An, Y.; Sun, Z. The chronic effect of amorphous silica nanoparticles and benzo[a]pyrene co-exposure at low dose in human bronchial epithelial BEAS-2B cells. *Toxicol. Res.* **2019**, *8*, 731–740. [CrossRef] [PubMed]
13. Lu, C.F.; Li, L.Z.; Zhou, W.; Zhao, J.; Wang, Y.M.; Peng, S.Q. Silica nanoparticles and lead acetate co-exposure triggered synergistic cytotoxicity in A549 cells through potentiation of mitochondria-dependent apoptosis induction. *Environ. Toxicol. Pharmacol.* **2017**, *52*, 114–120. [CrossRef] [PubMed]
14. Ahamed, M.; Akhtar, M.J.; Alhadlaq, H.A. Co-Exposure to SiO_2 Nanoparticles and Arsenic Induced Augmentation of Oxidative Stress and Mitochondria-Dependent Apoptosis in Human Cells. *Int. J. Environ. Res. Public Health* **2019**, *16*, 3199. [CrossRef] [PubMed]
15. Cao, X.Q.; DeLoid, G.M.; Bitounis, D.; De La Torre-Roche, R.; White, J.C.; Zhang, Z.Y.; Ho, C.G.; Ng, K.W.; Eitzer, B.D.; Demokritou, P. Co-exposure to the food additives SiO_2 (E551) or TiO_2 (E171) and the pesticide boscalid increases cytotoxicity and bioavailability of the pesticide in a tri-culture small intestinal epithelium model: Potential health implications. *Environ. Sci.-Nano* **2019**, *6*, 2786–2800. [CrossRef]
16. Costantini, L.M.; Gilberti, R.M.; Knecht, D.A. The phagocytosis and toxicity of amorphous silica. *PLoS ONE* **2011**, *6*, e14647. [CrossRef]
17. Dalzon, B.; Aude-Garcia, C.; Collin-Faure, V.; Diemer, H.; Béal, D.; Dussert, F.; Fenel, D.; Schoehn, G.; Cianférani, S.; Carrière, M.; et al. Differential proteomics highlights macrophage-specific responses to amorphous silica nanoparticles. *Nanoscale* **2017**, *9*, 9641–9658. [CrossRef]
18. Kim, B.; Kim, H.; Yu, I.J. Assessment of nanoparticle exposure in nanosilica handling process: Including characteristics of nanoparticles leaking from a vacuum cleaner. *Ind. Health* **2014**, *52*, 152–162. [CrossRef]
19. Oh, S.; Kim, B.; Kim, H. Comparison of nanoparticle exposures between fumed and sol-gel nano-silica manufacturing facilities. *Ind. Health* **2014**, *52*, 190–198. [CrossRef]
20. Tarantini, A.; Douki, T.; Personnaz, M.B.; Besombes, J.L.; Jafrezzo, J.L.; Maitre, A. Effect of the chemical composition of organic extracts from environmental and industrial atmospheric samples on the genotoxicity of polycyclic aromatic hydrocarbons mixtures. *Toxicol. Environ. Chem.* **2011**, *93*, 941–954. [CrossRef]
21. Tarantini, A.; Maitre, A.; Lefebvre, E.; Marques, M.; Marie, C.; Ravanat, J.L.; Douki, T. Relative contribution of DNA strand breaks and DNA adducts to the genotoxicity of benzo[a]pyrene as a pure compound and in complex mixtures. *Mutat. Res.* **2009**, *671*, 67–75. [CrossRef] [PubMed]

22. Nikolova, T.; Marini, F.; Kaina, B. Genotoxicity testing: Comparison of the γH2AX focus assay with the alkaline and neutral comet assays. *Mutat. Res.* **2017**, *822*, 10–18. [CrossRef] [PubMed]
23. Lesuffleur, T.; Porchet, N.; Aubert, J.P.; Swallow, D.; Gum, J.R.; Kim, Y.S.; Real, F.X.; Zweibaum, A. Differential expression of the human mucin genes MUC1 to MUC5 in relation to growth and differentiation of different mucus-secreting HT-29 cell subpopulations. *J. Cell Sci.* **1993**, *106*, 771–783. [PubMed]
24. Dorier, M.; Tisseyre, C.; Dussert, F.; Béal, D.; Arnal, M.E.; Douki, T.; Valdiglesias, V.; Laffon, B.; Fraga, S.; Brandão, F.; et al. Toxicological impact of acute exposure to E171 food additive and TiO_2 nanoparticles on a co-culture of Caco-2 and HT29-MTX intestinal cells. *Mutat. Res.* **2019**, *845*, 402980. [CrossRef] [PubMed]
25. Ferraro, D.; Anselmi-Tamburini, U.; Tredici, I.G.; Ricci, V.; Sommi, P. Overestimation of nanoparticles-induced DNA damage determined by the comet assay. *Nanotoxicology* **2016**, *10*, 861–870. [CrossRef]
26. Magdolenova, Z.; Lorenzo, Y.; Collins, A.; Dusinska, M. Can standard genotoxicity tests be applied to nanoparticles? *J. Toxicol. Environ. Health Part A* **2012**, *75*, 800–806. [CrossRef] [PubMed]
27. Ravanat, J.L.; Duretz, B.; Guiller, A.; Douki, T.; Cadet, J. Isotope dilution high-performance liquid chromatography-electrospray tandem mass spectrometry assay for the measurement of 8-oxo-7,8-dihydro-2′-deoxyguanosine in biological samples. *J. Chromatogr. B Biomed. Sci. Appl.* **1998**, *715*, 349–356. [CrossRef]
28. Pfaffl, M.W.; Tichopad, A.; Prgomet, C.; Neuvians, T.P. Determination of stable housekeeping genes, differentially regulated target genes and sample integrity: BestKeeper—Excel-based tool using pair-wise correlations. *Biotechnol. Lett.* **2004**, *26*, 509–515. [CrossRef]
29. Pfaffl, M.W. A new mathematical model for relative quantification in real-time RT-PCR. *Nucleic Acids Res.* **2001**, *29*, e45. [CrossRef]
30. Drasler, B.; Sayre, P.; Steinhauser, K.G.; Petri-Fink, A.; Rothen-Rutishauser, B. In vitro approaches to assess the hazard of nanomaterials (vol 8, pg 99, 2017). *Nanoimpact* **2018**, *9*, 51. [CrossRef]
31. Genies, C.; Maître, A.; Lefèbvre, E.; Jullien, A.; Chopard-Lallier, M.; Douki, T. The extreme variety of genotoxic response to benzo[a]pyrene in three different human cell lines from three different organs. *PLoS ONE* **2013**, *8*, e78356. [CrossRef] [PubMed]
32. Lindahl, T.; Wood, R.D. Quality control by DNA repair. *Science* **1999**, *286*, 1897–1905. [CrossRef] [PubMed]
33. Wyatt, M.D.; Pittman, D.L. Methylating agents and DNA repair responses: Methylated bases and sources of strand breaks. *Chem. Res. Toxicol.* **2006**, *19*, 1580–1594. [CrossRef] [PubMed]
34. Champion, J.A.; Walker, A.; Mitragotri, S. Role of particle size in phagocytosis of polymeric microspheres. *Pharm. Res.* **2008**, *25*, 1815–1821. [CrossRef] [PubMed]
35. Oh, N.; Park, J.H. Endocytosis and exocytosis of nanoparticles in mammalian cells. *Int. J. Nanomed.* **2014**, *9* (Suppl. S1), 51–63. [CrossRef]
36. Dorier, M.; Beal, D.; Tisseyre, C.; Marie-Desvergne, C.; Dubosson, M.; Barreau, F.; Houdeau, E.; Herlin-Boime, N.; Rabilloud, T.; Carriere, M. The food additive E171 and titanium dioxide nanoparticles indirectly alter the homeostasis of human intestinal epithelial cells in vitro. *Environ. Sci.-Nano* **2019**, *6*, 1549–1561. [CrossRef]
37. Di Cristo, L.; Movia, D.; Bianchi, M.G.; Allegri, M.; Mohamed, B.M.; Bell, A.P.; Moore, C.; Pinelli, S.; Rasmussen, K.; Riego-Sintes, J.; et al. Proinflammatory Effects of Pyrogenic and Precipitated Amorphous Silica Nanoparticles in Innate Immunity Cells. *Toxicol. Sci.* **2016**, *150*, 40–53. [CrossRef]
38. Zhang, H.; Dunphy, D.R.; Jiang, X.; Meng, H.; Sun, B.; Tarn, D.; Xue, M.; Wang, X.; Lin, S.; Ji, Z.; et al. Processing pathway dependence of amorphous silica nanoparticle toxicity: Colloidal vs pyrolytic. *J. Am. Chem. Soc.* **2012**, *134*, 15790–15804. [CrossRef]
39. Klein, G.; Devineau, S.; Aude, J.C.; Boulard, Y.; Pasquier, H.; Labarre, J.; Pin, S.; Renault, J.P. Interferences of Silica Nanoparticles in Green Fluorescent Protein Folding Processes. *Langmuir* **2016**, *32*, 195–202. [CrossRef]
40. Feng, L.; Yang, X.; Shi, Y.; Liang, S.; Zhao, T.; Duan, J.; Sun, Z. Co-exposure subacute toxicity of silica nanoparticles and lead acetate on cardiovascular system. *Int. J. Nanomed.* **2018**, *13*, 7819–7834. [CrossRef]
41. Guo, M.; Xu, X.; Yan, X.; Wang, S.; Gao, S.; Zhu, S. In vivo biodistribution and synergistic toxicity of silica nanoparticles and cadmium chloride in mice. *J. Hazard. Mater.* **2013**, *260*, 780–788. [CrossRef] [PubMed]
42. Hu, H.; Shi, Y.; Zhang, Y.; Wu, J.; Asweto, C.O.; Feng, L.; Yang, X.; Duan, J.; Sun, Z. Comprehensive gene and microRNA expression profiling on cardiovascular system in zebrafish co-exposured of SiNPs and MeHg. *Sci. Total Environ.* **2017**, *607*, 795–805. [CrossRef] [PubMed]

43. Yang, X.; Feng, L.; Zhang, Y.; Hu, H.; Shi, Y.; Liang, S.; Zhao, T.; Cao, L.; Duan, J.; Sun, Z. Co-exposure of silica nanoparticles and methylmercury induced cardiac toxicity in vitro and in vivo. *Sci. Total Environ.* **2018**, *631*, 811–821. [CrossRef] [PubMed]
44. Yu, Y.; Duan, J.; Li, Y.; Yu, Y.; Jin, M.; Li, C.; Wang, Y.; Sun, Z. Combined toxicity of amorphous silica nanoparticles and methylmercury to human lung epithelial cells. *Ecotoxicol. Environ. Saf.* **2015**, *112*, 144–152. [CrossRef] [PubMed]
45. Nakamura, M.; Imaoka, S.; Amano, F.; Funae, Y. P450 isoforms in a murine macrophage cell line, RAW264.7, and changes in the levels of P450 isoforms by treatment of cells with lipopolysaccharide and interferon-gamma. *Biochim. Biophys. Acta* **1998**, *1385*, 101–106. [CrossRef]
46. Torres, A.; Dalzon, B.; Collin-Faure, V.; Rabilloud, T. Repeated vs. Acute Exposure of RAW264.7 Mouse Macrophages to Silica Nanoparticles: A Bioaccumulation and Functional Change Study. *Nanomaterials* **2020**, *10*, 215. [CrossRef]
47. Demir, E.; Castranova, V. Genotoxic effects of synthetic amorphous silica nanoparticles in the mouse lymphoma assay. *Toxicol. Rep.* **2016**, *3*, 807–815. [CrossRef]
48. Haase, A.; Dommershausen, N.; Schulz, M.; Landsiedel, R.; Reichardt, P.; Krause, B.C.; Tentschert, J.; Luch, A. Genotoxicity testing of different surface-functionalized SiO_2, ZrO_2 and silver nanomaterials in 3D human bronchial models. *Arch. Toxicol.* **2017**, *91*, 3991–4007. [CrossRef]
49. Maser, E.; Schulz, M.; Sauer, U.G.; Wiemann, M.; Ma-Hock, L.; Wohlleben, W.; Hartwig, A.; Landsiedel, R. In vitro and in vivo genotoxicity investigations of differently sized amorphous SiO_2 nanomaterials. *Mutat. Res. Genet. Toxicol. Environ. Mutagen.* **2015**, *794*, 57–74. [CrossRef]
50. Wills, J.W.; Hondow, N.; Thomas, A.D.; Chapman, K.E.; Fish, D.; Maffeis, T.G.; Penny, M.W.; Brown, R.A.; Jenkins, G.J.; Brown, A.P.; et al. Genetic toxicity assessment of engineered nanoparticles using a 3D in vitro skin model (EpiDerm™). *Part. Fibre Toxicol.* **2016**, *13*, 50. [CrossRef]

Conclusion

Cette étude nous a permis de mettre en évidence la sensibilité spécifique de chaque type cellulaire. En effet, les macrophages murins RAW264.7 sont plus sensibles (cytotoxicité et dommage de l'ADN) que les cellules de l'épithélium intestinal. Cette différence provient essentiellement de leur rôle de cellules phagocytaires, elles accumulent davantage de silice que les cellules épithéliales, ces dernières produisant du mucus qui limite l'internalisation de la silice. De plus, cette étude montre que la silice colloïdale est celle induisant le moins d'effets, suivie par la silice précipitée puis la pyrogénée, cela provient de la taille des SAS et également du procédé de fabrication. Les effets génotoxiques observés augmentent avec la répétition d'exposition aux SAS, cet effet est encore augmenté par la stimulation au MMS, la silice jouerait un rôle de transporteur.

Ce projet soulève les problèmes de contaminations croisées possibles entre la silice (alimentaire ou autre) et les substances présentes, notamment dans un environnement urbain (poussières ou aérosols). Les études de toxicologie classique (exposition aiguë) ne permettent pas de tenir compte des expositions à répétition et des co-expositions possibles, il est nécessaire de développer des systèmes *in vitro* permettant ces études.

Autres projets

Nanomatériaux de fer

Présentation du projet

Ce premier projet parallèle a permis d'utiliser notre système en évaluant les effets de nanomatériaux de fer sur les macrophages, et ainsi tester un autre type de matériaux. Cette étude compare deux tailles de matériaux (20 et 100nm), correspondant aux différentes poussières d'usure produites dans un milieu urbain (rails de métro ou train). L'exposition aiguë a été étudiée dans le but de comprendre comment les nanoparticules de plus grande taille impactent davantage les macrophages, nous avons réalisé des tests fonctionnels, et physiologiques.

nanomaterials

MDPI

Article

Influences of Nanoparticles Characteristics on the Cellular Responses: The Example of Iron Oxide and Macrophages

Bastien Dalzon [1,*], Anaëlle Torres [1], Solveig Reymond [2], Benoit Gallet [3], François Saint-Antonin [4], Véronique Collin-Faure [1], Christine Moriscot [5], Daphna Fenel [3], Guy Schoehn [3], Catherine Aude-Garcia [1,†] and Thierry Rabilloud [1,*]

1 Grenoble Alpes University, CNRS, CEA, Laboratory of Chemistry and Biology of Metals, BIG-LCBM, 38000 Grenoble, France; Anaelle.torres@cea.fr (A.T.); veronique.collin@cea.fr (V.C.-F.); catherine.aude-garcia@cea.fr (C.A.-G.)
2 Grenoble Alpes University, CNRS, CEA, INAC, SyMMES, RSRM, 38000 Grenoble, France; solveig.reymond@gmail.com
3 Institut de Biologie Structurale (IBS), University Grenoble Alpes, CEA, CNRS, 38044 Grenoble, France; benoit.gallet@ibs.fr (B.G.); daphna.fenel@ibs.fr (D.F.); guy.schoehn@ibs.fr (G.S.)
4 Grenoble Alpes University, CEA-Grenoble, LITEN, DTNM, L2N, 17 rue des Martyrs, CEDEX 09, 38054 Grenoble, France; francois.saint-antonin@cea.fr
5 Integrated Structural Biology Grenoble (ISBG) CNRS, CEA, Université Grenoble Alpes, EMBL, 71 Avenue des Martyrs, 38042 Grenoble, France; christine.moriscot@ibs.fr
* Correspondence: bastien.dalzon@cea.fr (B.D.); thierry.rabilloud@cea.fr (T.R.); Tel.: +33-4-3878-4574 (B.D.); +33-4-3878-3212 (T.R.)
† Deceased person (21 November 2018).

Received: 30 December 2019; Accepted: 1 February 2020; Published: 5 February 2020

Abstract: Iron oxide nanoparticles/microparticles are widely present in a variety of environments, e.g., as a byproduct of steel and iron degradation, as, for example, in railway brakes (e.g., metro station) or in welding fumes. As all particulate material, these metallic nanoparticles are taken up by macrophages, a cell type playing a key role in the innate immune response, including pathogen removal phagocytosis, secretion of free radical species such as nitric oxide or by controlling inflammation via cytokine release. In this paper, we evaluated how macrophages functions were altered by two iron based particles of different size (100 nm and 20 nm). We showed that at high, but subtoxic concentrations (1 mg/mL, large nanoparticles induced stronger perturbations in macrophages functions such as phagocytic capacity (tested with fluorescent latex microspheres) and the ability to respond to bacterial endotoxin lipopolysaccharide stimulus (LPS) in secreting nitric oxide and pro-cytokines (e.g., Interleukin-6 (IL-6) and Tumor Necrosis Factor (TNF)). These stronger effects may correlate with an observed stronger uptake of iron for the larger nanoparticles.

Keywords: macrophage; iron oxide; nanoparticle

1. Introduction

Determining the toxicity of nanoparticles (NP) is very complex due to the multitude of types of materials, the various mixes of materials, the shape and size polymorphisms [1] and the various coatings which compose NP, etc. However, comparing only the effects that various materials have on cells (e.g., Au-NP vs. Ag-NP or other materials) is not sufficient [2] because the toxicity of particles depends on numerous parameters, such as their aggregation or dissolution, the corona, influenced itself by the particles size [3,4], the shape of particles which influence their kinetic of internalization, their surface

charge that may cause bilayer lipidic disorders of cells (positive charge induce high risks of membrane disruption contrary to negative charge) [5], etc. Hence, it is important to go deeper into the field of nanotoxicology and take these parameters into account, but it is almost impossible to evaluate such a variety of parameters in a single series of experiments. In this direction, we sought to assess the possible effects that NP size may have on cell functions for a given nanomaterial, as previously suggested [6]. In this article, we thus assessed the effect of two maghemite/hematite iron oxide nanoparticles (Fe_2O_3-NP) of different sizes. Such NPs are commonly found in the urban landscape, for example, in train or metro stations (subway) where particles comprising predominantly Fe_2O_3-NP are emitted/released in large amounts due to wheel-rail contact, in particular, during braking [7,8]. Therefore, drivers and railroad workers inhale a large amount of maghemite NP. Train or metro users are impacted, although to a lesser extent. Other occupational exposures to Fe_2O_3-NP include welding with the inhalation of welding fumes during the soldering process. These forms of air pollution raise public health questions. As an example, mild steel welding fumes induce inflammation and increase adhesion and infection of bacteria such as Streptococcus pneumonia via the increase of platelet-activating factor (PAFR) in lungs, leading to an increase in pulmonary infections [9].

In order to pursue studies perform on pulmonary cells [10], assessing the effect of NP on macrophages is not meaningless as various nanomaterials are known to be responsible for respiratory illnesses (such as asbestosis or silicosis) and many toxicological studies have found that nanoparticles are able to induce pro-inflammatory responses [11–15] and/or immunological effects [16,17]. In this context, macrophages are of paramount importance in toxicology as (i) they are present in all the tissues of the human body [18,19], (ii) their scavenger function may increase their sensitivity to the effects of NP [20] and (iii) they play a key role in the management of inflammation [21,22]. An impairment of the functionalities of macrophages could cause damage to tissues and induce other immunological diseases (autoimmunity or immune deficiency) [23–26].

Very different particle sizes can be found in airborne NP present in train stations [27]. Therefore, we decided to investigate the effects of iron oxides nanoparticles of two different sizes (20 and 100 nm) on macrophages at a single and subtoxic exposure concentration of 1 mg/mL. As iron oxide nanoparticles show a strong tendency to aggregate strongly in aqueous solutions, we had to use an organic and biocompatible coating to limit this aggregation. We therefore used a commercially available ferric carboxymaltose nanoparticle (FERINJECT®, Vifor Pharma, Bern, Switzerland) for the 20 nm size. FERINJECT® is composed of Fe(III)-oxyhydroxide core obtained through a thermal annealing process described in the original patent [28] and similar to [29] and stabilized/surrounded by a carbohydrate (carboxymaltose) shell which is derived from maltodextrin [30]. We also used a plain 100 nm Fe_2O_3-NP purchased from Sigma-Aldrich that we then coated with carboxymaltose. Experiments on the J774A.1 macrophage cell line carried in this manuscript show a significant difference between the way macrophages respond to these two types (and sizes) of iron-based nanoparticles. We show that at the same subtoxic exposure concentration, the larger-sized Fe_2O_3-NP produced more effects on macrophages than the smaller-sized ones. In this article, we sought to understand the causes of this difference.

2. Material and Methods

Most experiments have been carried out as described in the publications [31–33] but details are given in this article to assist in the understanding of this paper. Biological experiments were driven on three independent biological replicates. For cytometry measurement, dead cells were systematically excluded of the assessment with propidium iodide at 1 µg/mL or SytoxRed (Fisher Scientific, Illkirch, France) at 5 nM.

2.1. Nanoparticles

Twenty-nanometer ferric carboxymaltose nanoparticles (FERINJECT®, 50 mg/mL) were purchased from Vifor Pharma (Bern, Switzerland). One hundred-nanometer maghemite nanoparticles were purchased from Sigma-Aldrich (catalog number: 720704, Sigma-Aldrich, Saint Quentin Fallavier,

France), directly as a concentrated suspension at 20% in H2O. We added carboxymaltose in accordance with the patent on FERINJECT® [28] in order (i) to limit aggregation of the particles in the culture medium and (ii) to assess and compare exclusively the effect of size on cells without interferences brought by possible effects of the coating.

2.2. Nanoparticle Characterization

The hydrodynamic diameter and particle size distribution were characterized using dynamic light scattering (DLS) after dilution in H_2O or culture medium DMEM after 0 h or 24 h of incubation at 37 °C, 5% CO_2. Nanoparticles were diluted at final concentration at 10 µg/mL for measurement. The size and distribution of the particles were assessed after dilution in water or in culture medium by DLS using a Wyatt Dynapro Nanostar machine (Wyatt Technology, Santa Barbara, CA, USA). The morphology of nanoparticles was observed using Transmission Electron Microscopy (TEM) (Thermo Fisher Scientific, Eindhoven, The Netherlands), as previously described [34].

2.3. Cell Culture

The mouse macrophage cell line J774A1 was obtained from the European Cell Culture Collection (Salisbury, UK). The cells were cultured in DMEM medium supplemented with 10% fetal bovine serum (FBS). Cells were seeded at 200,000 cells/mL in suspension culture flasks (Greiner Bio-One, Reference 658195, Dutscher, Brumath, France) and harvested at 1,000,000 cells/mL. For treatment with nanoparticles, cells were seeded at 500,000 cells/mL. They were treated with nanoparticles on the following day and analyzed after a further 24 h in culture. In some control experiments, cells were treated with an iron citrate complex (1:2 molarity) prepared for iron (III) sulfate and trisodium citrate, so that an iron concentration in the medium equivalent to the one obtained with 1 mg/mL Fe_2O_3 was obtained (i.e., 12.5mM iron). The viability of cells was measured via Facscalibur flow cytometer (BD Biosciences, Le Pont-de-Claix, France) using dye exclusion (propidium iodide at 1 µg/mL or sytoxRed at 5 nM).

Primary macrophages were obtained as described by Dalzon et al. [34].

2.4. Particle Internalization Measurement

Qualitative (Perls staining), and quantitative measurement (bathophenantroline and ICP-MS assays) of iron uptake were performed as already described in Dalzon et al. [34].

For TEM- and EDX-microscopy, exposed cells or control cells where fixed for 1 h at room temperature in a fixative solution composed of paraformaldehyde 2% and glutaraldehyde 0.2% in PHEM 0.1 M. Post-fixation was performed during 1 h under shaking in an osmium solution composed of 1% osmium and 1.5% potassium hexaferrocyanate in 0.1 M PHEM buffer. Then, samples were washed with water and stained 30 min under shaking with uranyl acetate 0.5% (in 30% ethanol). Before substitution then impregnation in Embed 812 resin (EPON substitute, EMS), samples were dehydrated in graded series of ethanol (50 to 100%). After polymerisation during 48 h at 65 °C, the blocs were ready to be cut via an Ultramicrotome UC7 (Leica, Rueil-Malmaison, France) in order to produce 80-nm sections. Sections were then collected on formvar-carbon coated copper grids and observed via an FEI Tecnai G2 Spirit BioTwin transmission electron microscope operating at 120 kV with an Orius SC1000B CCD camera (Thermo Fisher Scientific, Eindhoven, The Netherlands) [35,36]. Scanning Transmission Electron Microscopy (STEM) and Energy Dispersive X-rays Spectrum (EDX) (Bruker, Berlin, Germany) for elemental mapping, were achieved via a TECNAI OSIRIS electron microscope (Thermo Fisher Scientific, Eindhoven, The Netherlands) operated at 200 kV and equipped with a 4K GATAN camera (GATAN, Portland, Oregon, USA). The EDX maps were treated with the "ESPRIT" software (version 1.9, Bruker, Berlin, Germany) to minimize the noise.

2.5. Phagocytosis Assays

Phagocytosis was assayed by internalization of fluorescent latex beads using flow cytometry as previously described [31,37].

2.6. NO and Cytokines Production

In the supernatant culture of cells exposed to NP and activated by LPS, the concentration of NO and cytokines such as interleukin 6 (IL-6), interleukin 10 (IL-10), monocyte chemoattractant protein-1 (MCP-1) and tumor necrosis factor (TNFa) were measured as prevously described [34,38].

2.7. F-Actin Staining

Visualization of F-Actin cytoskeleton was assayed by phalloidin staining according to previously published protocols [38–40]

2.8. Glutathione Assays

Intracellular glutathione levels were assessed using the monochlorobimane technique, with some modifications [33]. Briefly, the cells were harvested, centrifuged during 5 min, and labeled with 75 µM monochlorobimane (diluated in warm PBS) for 5 min at 37 °C. The reaction was stopped via an incubation in ice for 5 min in the dark. The cells were washed twice with cold PBS and finally, the they were analyzed via BD FACSMelodyTM flow cytometer (BD Biosciences, Le Pont-de-Claix, France) using a laser excitation at 405 nm and an emission at 448 ± 45 nm.

2.9. Mitochondrial Transmembrane Potential Measurement

The mitochondrial transmembrane potential was assessed using the rhodamine 123 uptake assay, as previously described [40].

2.10. Quantitative Bathophenanthroline Assay

The assays were conducted as described in [41] but with some changes. After incubation for 0 h or 24 h at 37 °C, 5% CO_2 in H_2O or culture medium, to check the quantity of iron in the two iron-based nanoparticle conditions i.e., FERINJECT® and NP-Fe_2O_3 (Sigma, Saint Quentin Fallavier, France), 1 volume of particles (theoretical concentration = 1 mg/mL) or standard solution (Mohr's salt 17.9 mmol/L) was dissolved with 4 volumes of aqua regia (3:1 volume of 37% hydrocholoric acid and 70% nitric acid). This step required several agitations with vortex mix and a period of incubation of at least 1 h. After dissolution, the samples and standard solution were diluted with water at 1/100. They were then mixed *v/v* with a protein precipitant solution (composed of ascorbic acid 2.5 g/L and trichloracetic acid 100 g/L). Then, they were centrifuged at 1500× *g* for 30 min. Finally, an equivalent volume of chromogen solution (composed of bathophenanthroline 0.25 g/L and Na-acetate 123 g/L) was added to the samples. After 10 min of incubation, the absorbance was measured at 535 nm.

For supernatant measurement, 1 mL of iron-based particle suspension was ultracentrifuged at 279,000× *g* for 45 min at 4 °C. The recovered supernatant or standard solution (Mohr's salt 35.78 µmol/L) was processed as described above from the protein precipitation step to the absorbance measurement step.

For calculating the iron concentration:

$$\frac{\text{Abs sample unknown} - \text{Abs blank}}{\text{Abs iron standard} - \text{Abs blank}} \times 35.78 = \text{concentration of iron } \mu\text{mol/L}$$

3. Results

3.1. Nanoparticle Behavior

NPs were characterized using DLS and TEM microscopy. Overall, the commercial 20 nm ferric carboxymaltose named FERINJECT® was considered monodisperse (percentage of dispersity < 15%) and had a hydrodynamic diameter comprised between 23 and 25 nm in H_2O or DMEM. After 24 h of incubation at 37 °C, 5% CO_2, FERINJECT® was still considered monodisperse and the hydrodynamic diameter is similar to 0 h of incubation (but maybe with a very slightly decreased diameter (1 to 2 nm) in DMEM). The 100 nm Fe_2O_3-NP (with carboxymaltose coating) from Sigma-Aldrich had a higher hydrodynamic

diameter in H_2O (both at t0 and after 24 h of incubation) and contrarily to FERINJECT®, these NP were strongly agglomerated in the culture medium, with the size of agglomerates > 1 µm of diameter even with the carboxymaltose coating. (Table 1) Examination via Transmission Electron Microscopy (TEM) revealed that FERINJECT® have an irregular shape whereas NP-Sigma are rod-shaped. NP-Sigma have different sizes and we confirmed that they were agglomerated in culture medium (Figure 1).

Table 1. Characterization of FERINJECT® and Fe_2O_3-NP Sigma by DLS. Nanoparticles were incubated in H_2O or DMEM (with carboxymaltose coating for Fe_2O_3-NP Sigma) after 24 h of incubation at 37 °C, 5% CO_2.

	FERINJECT®				**Fe_2O_3-NP (Sigma)**			
Medium	H_2O		DMEM		H_2O		DMEM	
Incubation time	0 h	24 h	0 h	24 h	0 h	24 h	0 h	24 h
Size (nm)	23.4	22.4	24.3	21.9	73.4	79.6	1258	1120
Dispersity (%)	8.8	11.7	8.5	12.2	22.4	22.6	Multimodal	Multimodal

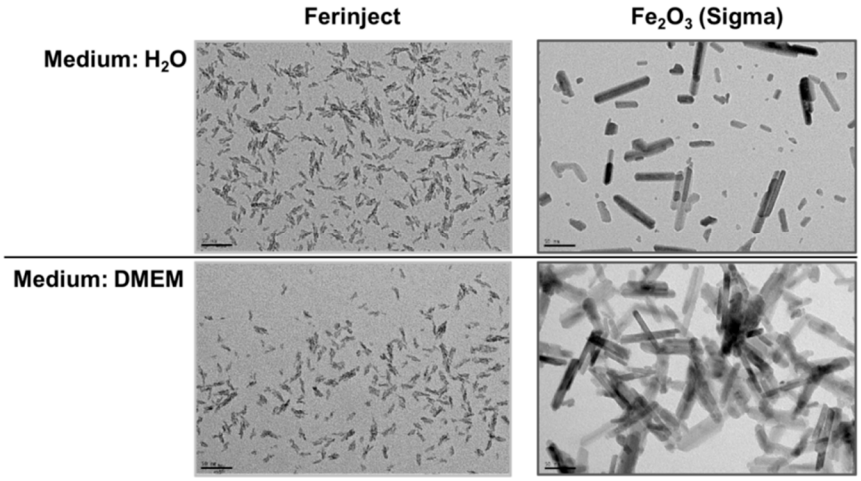

Figure 1. Characteristics of FERINJECT® and Fe_2O_3-NP by TEM. Nanoparticles were incubated in H_2O or DMEM (with carboxymaltose coating for Fe_2O_3-NP) after 24 h of incubation at 37 °C, 5% CO_2. Scale bar 50 nm.

3.2. Fe_2O_3-NPs and Iron Uptake by J774A.1

The effect of the two types of Fe_2O_3-NP nanoparticles on cell viability was analyzed and the results are shown in Figure 2. For all the subsequent experiments, a concentration of 1 mg/mL^{-1} was selected, as it is the highest exposure concentration before observing noticeable mortality. We chose this concentration because it corresponds to LD20 (lethal dose 20%) on primary macrophages and allows the testing of functional effects on cells without appreciable cellular mortality. For us, defining an experimental dose similar to environmental exposure is not feasible due to the extreme variability of dose exposure. Taking just the example of a metro station, it depends on the city, the traffic frequency, the age of the metro system and the speed reached, the localization of people: on board or on the subway platform, the type of ventilation, etc. [8,42–44] In other words, the chosen a concentration for J774A.1 cells line offered a good compromise between very small cell mortality (J774A.1 were not more affected by Fe_2O_3-NP and ferric citrate control, the mortality being below or close to 10%) and the highest probability of observing biological effects.

As a first test, we checked the presence of NPs and iron in cells by microscopy (Perls staining, TEM and EDX microscopy) and a quantitative method (bathophenanthroline assay). Perls staining was used here to reveal the presence of ferric elements inside the cells, as revealed by a prussian blue deposit in J774A.1 cells when cells are incubated with the two types of Fe_2O_3-NP (Figure 3A). TEM experiments

then showed that NP were present in the vesicles (Figure 3B). TEM also revealed some differences between FERINJECT® and NP-Sigma regarding their uptake. FERINJECT® is present in many vesicles whereas NP-Sigma are always gathered in a single large phagolysosome. EDX microscopy confirmed that iron is associated with both types of Fe_2O_3-NP (Figure 3C). Iron loading in the cells was more accurately quantified by the bathophenanthroline assay, which shows that there is an important amount of iron in the cells exposed to Fe_2O_3-NP. Our results show a large quantitative difference between FERINJECT® (7.4 pg/cell) and NP-Sigma (73.46 pg/cell) (Figure 3D). The quantification was compared with advanced-technologies such as ICP-MS (Figure S1) which showed results similar to those of the bathophenanthroline assay.

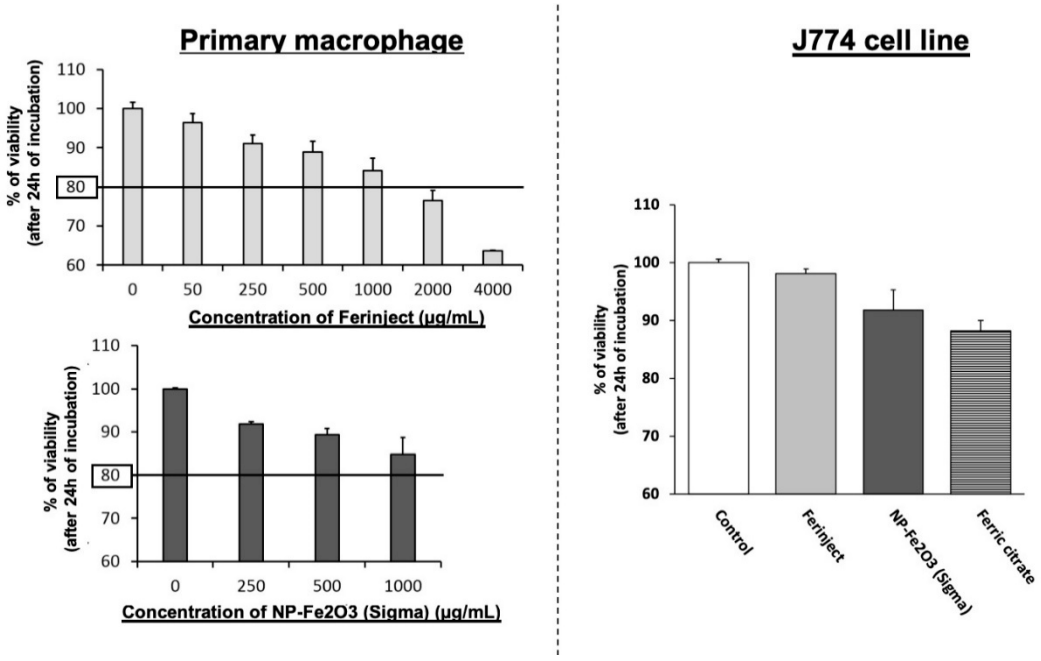

Figure 2. Viability of macrophages. Left graphic: primary mouse macrophages were exposed for 24 h to increasing exposure concentration of FERINJECT® or Fe_2O_3-NP Sigma in order to determining LD20. Right graphic: J774A.1 cells lines were incubated with 1 mg/mL of these nanoparticles or equivalent Ferric citrate. Viability was measured using propidium iodide (1 µg/mL).

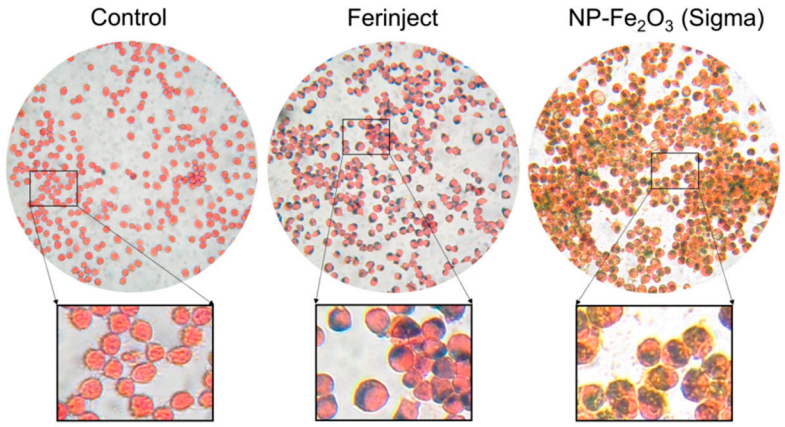

(**A**)

Figure 3. *Cont.*

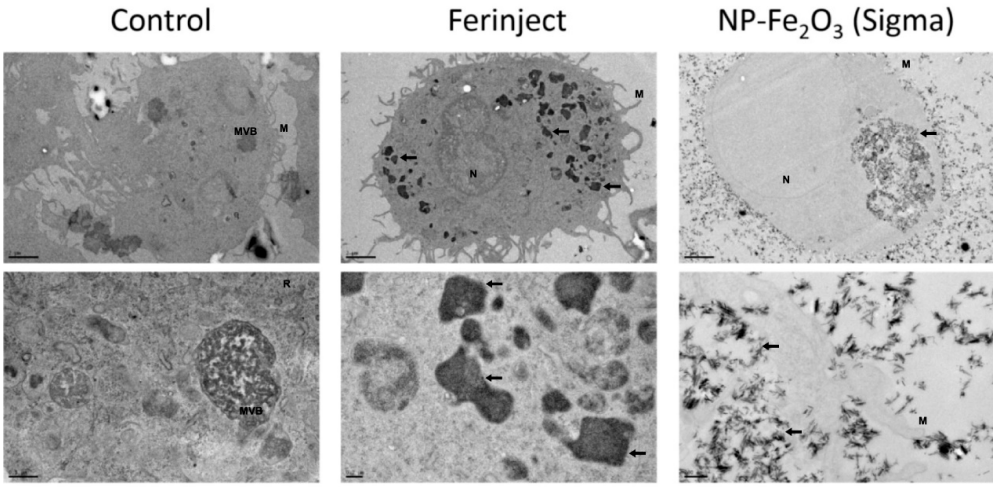

(**B**)

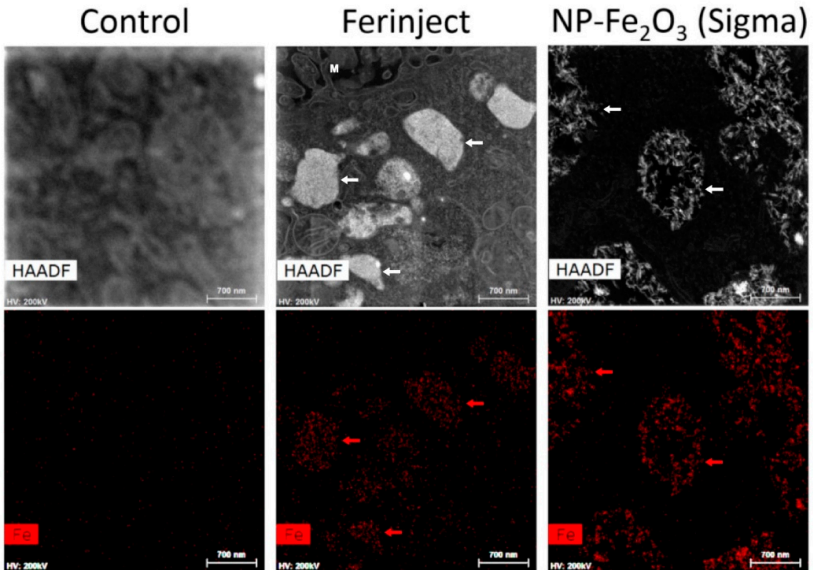

(**C**)

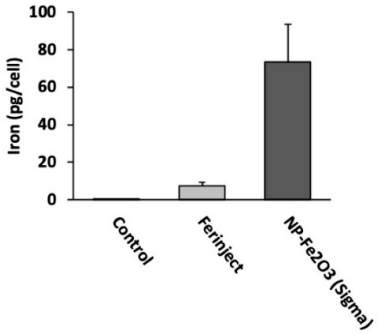

(**D**)

Figure 3. The presence of iron and nanoparticles in J774A.1 cell line incubated 24 h with or without FERINJECT® or Fe_2O_3-NP Sigma. Panel (**A**): Perls staining. Blue staining: complex KFe [Fe(CN)6] named Prussian blue. Red staining: Safranin cytosolic staining; Panel (**B**): TEM microscopy. Scale bar, top line = 2 µm; below line = 0.5 µm (Control) or 0.2 µm (FERINJECT® and Fe_2O_3-NP Sigma). Panel (**C**): Top line: HAADF (High-Angle Annular Dark Field microscopy) with, in white high-density zone. Below line: EDX (Energy Dispersive X-ray Analysis) with, in red iron elements. N = Nucleus; M = Microvillosity; R = Reticulum; MVB = Multivesicular bodies; arrow = vesicle with iron particles. Panel (**D**): Quantitative assessment of the iron engulfed by macrophages using the bathophenanthroline method.

We then studied the ability of macrophages to engulf FERINJECT® and NP-Sigma on a kinetic basis. TEM microscopy and EDX microscopy revealed that contrarily to FERINJECT®, NP-Sigma are more rapidly internalized by J774A.1 macrophages after a short period of exposure to NP such as 1 h 30 (Figure 4A). In the case of FERINJECT®, we only noticed a small (if any) quantity of FERINJECT® in cells while a large quantity of NP-Sigma was already present in the vesicles. We confirmed these results using the quantitative bathophenanthroline assay. After short incubation periods (1 h, 3 h, 6 h), the uptake of NP-Sigma was much higher than that of FERINJECT®. Furthermore, the problem of cell detachment observed after 24 h was not encountered after shorter periods of time so that the quantitative determination of iron was more precise in this case. The bathophenanthroline assay (Figure 4B) confirmed what had been observed using TEM microscopy and revealed that NP-Sigma were internalized much faster than FERINJECT® (e.g., internalization of FERINJECT® after 1 h 00 = 0.83 pg/cell, whereas internalization of NP-Sigma = 17.9 pg/cell).

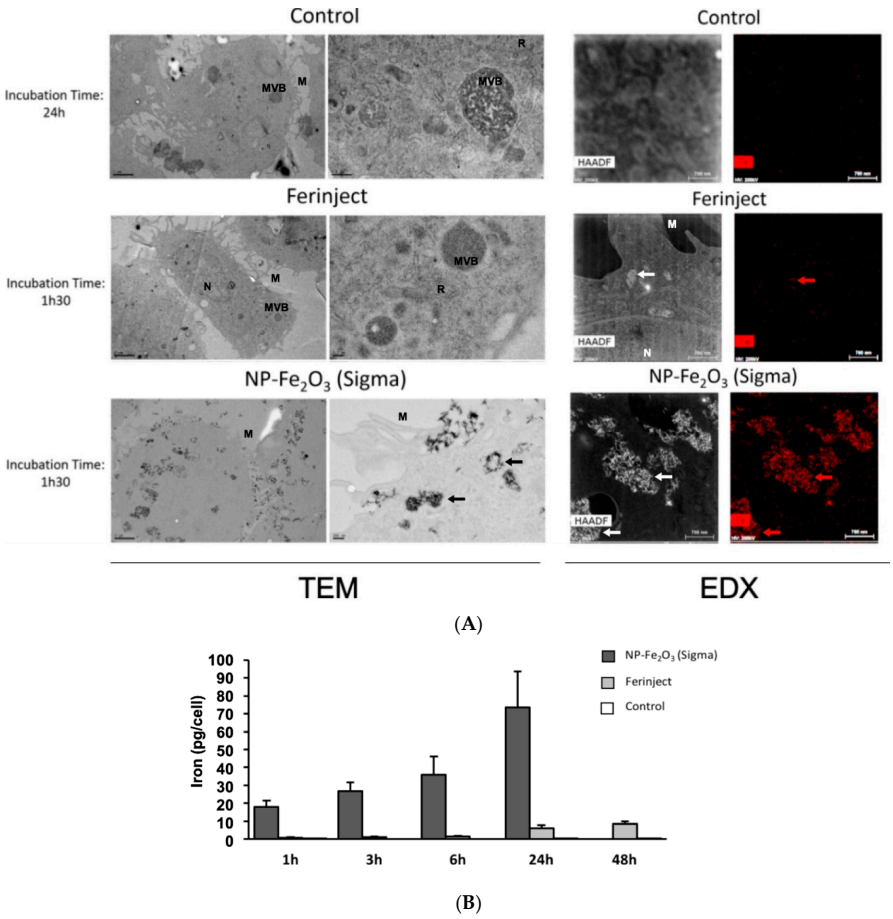

Figure 4. Assessment of Kinetic of iron uptake in J774A.1 cells incubated for various times of incubation with or without FERINJECT® or Fe_2O_3-NP. Pannel (**A**): TEM and HAADF-EDX microscopy. J774A.1 were incubated 1h30 with FERINJECT® or Fe_2O_3-NP (compared with Figure 3B) TEM scale bar, Left column = 2 µm; Right column = 0.2 µm. HAADF and EDX microscopy scales bar = 0.7µm. N = Nucleus; M = Microvillosity; R = Reticulum; MVB = Multivesicular bodies; arrow = vesicle with iron particles. Pannel (**B**): Quantitative assessment of the Kinetic of iron engulfed by macrophages (1 h to 24 h of incubation with FERINJECT® or Fe_2O_3-NP) using the bathophenanthroline method.

3.3. Functional Studies of J774A.1

Functional studies were set up to determine if macrophages in contact with iron particles retained their main biological functions. Phagocytic ability consists in cleaning, for example, apoptotic cells and microorganisms in order to maintain tissue homeostasis. Macrophages should be able to maintain

their phagocytic activity even in the presence of Fe_2O_3-NP in order to protect the organism against pathogens. On the contrary, the secretion of inflammatory mediators should not be exacerbated by Fe_2O_3-NP to avoid damaging healthy tissues (e.g., inflammatory disease). This is why we tested the impact of iron oxide NP on the classical functions of macrophages such as the phagocytic ability, and the modulation of the LPS-induced production of cytokines and NO.

3.3.1. Phagocytic Activity

Regarding phagocytosis, flow cytometry allows the investigation of two parameters, i.e., the proportion of cells that remain phagocytic after being exposed to NP and the intensity of the phagocytic activity for phagocytosis-positive cells. The results displayed in Figure 5A show that when J774A.1 macrophages were incubated with FERINJECT® for 24 h, their phagocytic capacity was not altered. Contrarily to FERINJECT®, NP-Sigma and ferric citrate significantly altered the functionality of J774A.1 macrophages because the phagocytic capacity dropped drastically. Only 37% of cells (NP-Sigma) and 13% (ferric citrate) were able to phagocytize fluorescent beads; furthermore, their phagocytosis ability dropped by 40% to 45% in comparison with the control without NP.

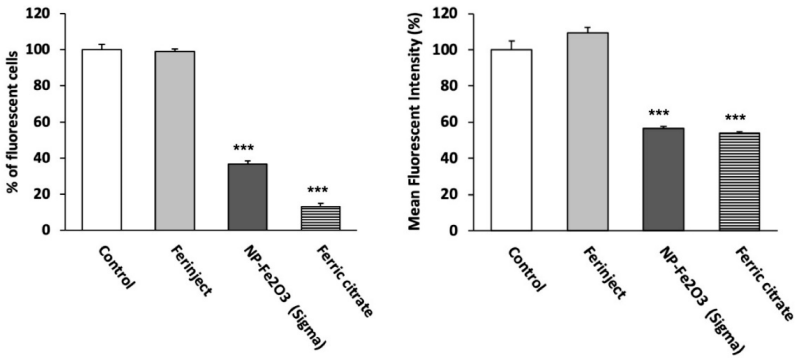

(**A**)

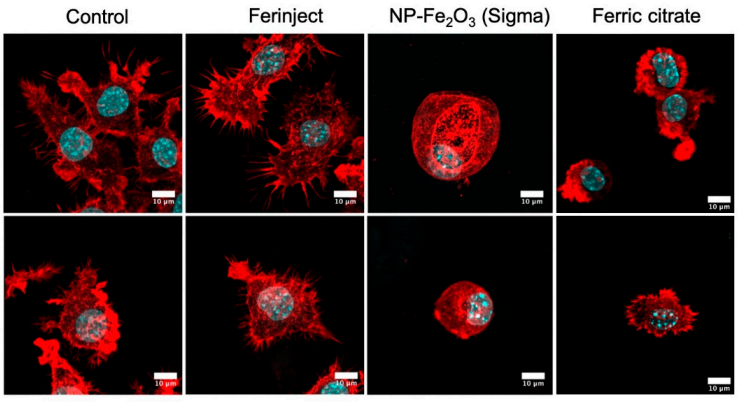

(**B**)

Figure 5. Pannel (**A**): Phagocytic ability. Left graphic: percentage of cells able to phagocyte fluorescent FITC-labeled latex beads (positive cells). Right graphic: phagocytic ability of positive cells. Pannel (**B**): Confocal microscopy (Z-stacks combined): Observation of actin filaments with phalloidin labeled in red (Atto 560). The cell nucleus is colored blue by Dapi. Upper section = apical microscopy view; middle section = center of cell; lower section = basal microscopy view. Statistical confidence (student *t*-test) is indicated as follows *** $p \leq 0.001$.

3.3.2. Actin Cytoskeleton

In order to complement the phagocytosis results, we visualized the integrity of the conformation state of the F.actin cytoskeleton (Figure 5B). Indeed, a number of studies using cytochalasin D (which

dismantles the actin cytoskeleton) have shown that the conformation of the actin cytoskeleton has a critical role in the phagocytosis process [45–47]. When incubated with NP-Sigma, cells were less adherent and showed fewer cytoplasmic elongations than the control without NP (basal view). Moreover, cells were more spherical than the control and showed large vacuoles (middle view). In contrast, we did not observe any differences between the cells incubated with FERINJECT® and control without NP. Ferric citrate cells were generally smaller, less adherent and with fewer cytoplasmic elongations than the control. These results confirm that NP-Sigma and ferric citrate induced damages to the F.actin cytoskeleton, which may explain, at least in part, the results of the phagocytosis assay. Furthermore, in the case of NP-Sigma, we observed a strong vesicularization of the cells that may be linked with an autophagic process [48] (Figure S2).

3.3.3. Secretion of Inflammatory Mediators

Figure 6A shows that after stimulation with LPS, the secretion of NO was slightly altered in the presence of FERINJECT® as it decreases by only 10%. Conversely, NO secretion drastically decreased (by 69%) for cells exposed to NP-Sigma and was not detectable for cells exposed to ferric citrate because of a strong interference between iron citrate and the Griess reagent. It can be noticed that without stimulation with LPS, NO secretion is significantly lower whatever the NP used. This last result was expected because J774A.1 macrophages were not previously stimulated and therefore, could not mature to inflammatory M1 macrophages. It also showed that iron particles themselves did not induce spontaneous inflammatory signals in J774A.1 cells. A flow cytometric analysis revealed that in the presence of LPS, FERINJECT® did not affect the production of pro-inflammatory cytokines (Figure 6B). The rates of IL-6, MCP-1 and TNF were similar to those of control without NP. However, when cells were incubated with NP-Sigma, the production of pro-inflammatory cytokines was defective for two of the three measured (−65% for IL-6 and −27% for TNF). The secretion of MCP-1 remained unchanged (Figure 6B). The production of all measured cytokines was significantly decreased with ferric citrate.

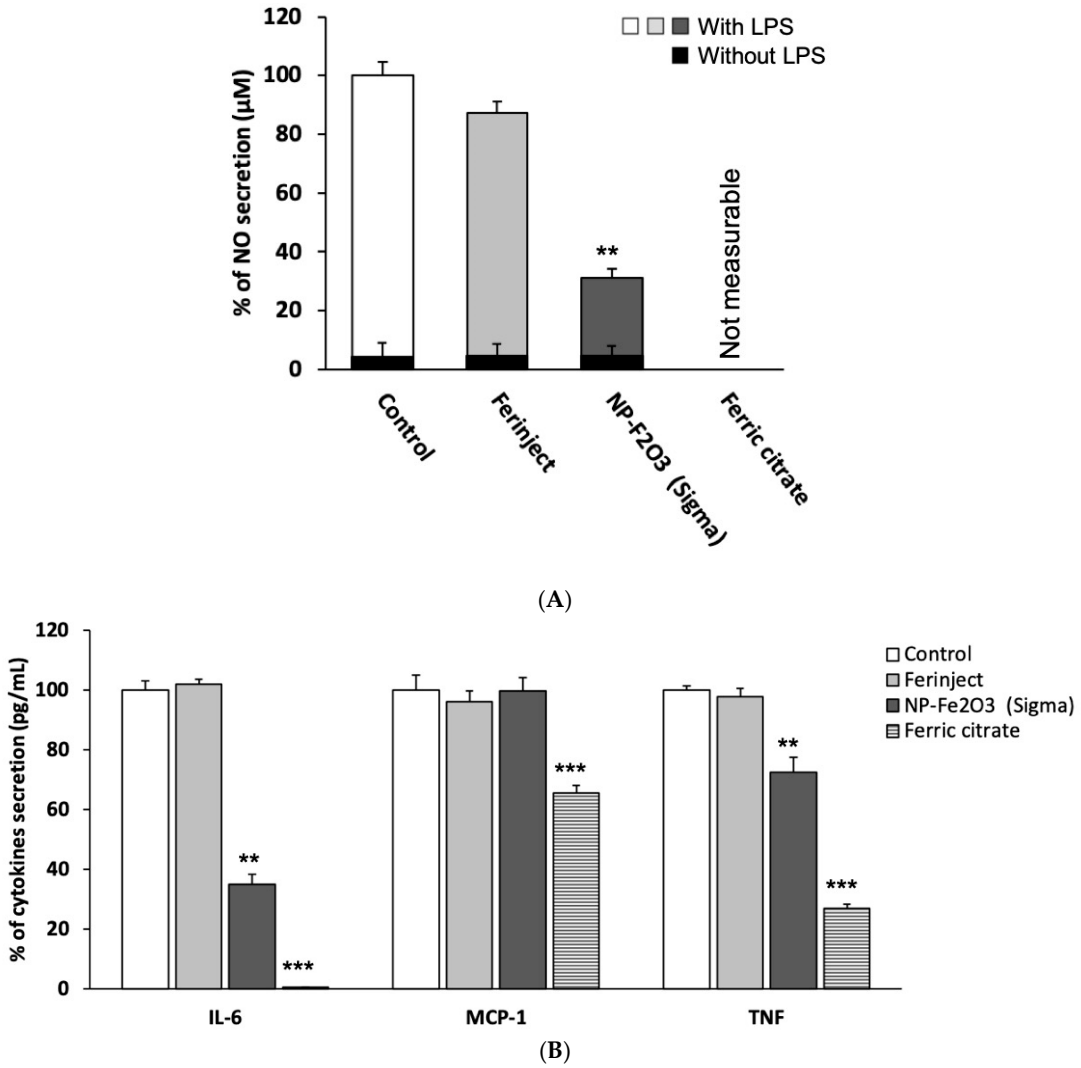

Figure 6. Inflammation ability. Panel (**A**): NO secretion with or without LPS stimulation. Panel (**B**): Secretion of inflammatory cytokines after LPS stimulation. Statistical confidence (student *t*-test) is indicated as follows ** $p \leq 0.01$; *** $p \leq 0.001$.

3.3.4. Cell Physiology Studies: Mitochondrial Potential and Glutathione Level

The various functional studies showed that contrarily to FERINJECT®, NP-Sigma had a significant effects on the functionality of macrophages. We tried to obtain further insight into the physiology of macrophages to better understand the differences between the two iron oxide particles. Regarding the mitochondrial membrane potential, our results show that when J774A.1 macrophages were incubated with FERINJECT®, their transmembrane mitochondrial potential was not different from that of control, non-exposed cells (Figure 7A), whereas NP-Sigma and ferric citrate caused severe damage to the respiratory ability of J774A.1 macrophages: after exposure to NP-Sigma or ferric citrate, the mitochondrial potential of the cells decreased by 40%. As a consequence, the results suggest that NP-Sigma may induce a decrease in the available energy in the cells. Regarding glutathione, FERINJECT® induced a slight decrease in the rate of free glutathione reduced (GSH) in cells (89% of the control value), whereas with NP-Sigma, it decreased to 43% of the control value (first population) with a second population where the GSH dropped to 19% (Figure 7B). Here again, the test did not work for iron citrate-treated cells, for unknown reasons. The decreased free glutathione content may be due to depletion by metal chelation, as observed for silver [49] and copper [33] nanoparticles. These results suggested that NP-Sigma may alter free glutathione-dependent cellular processes.

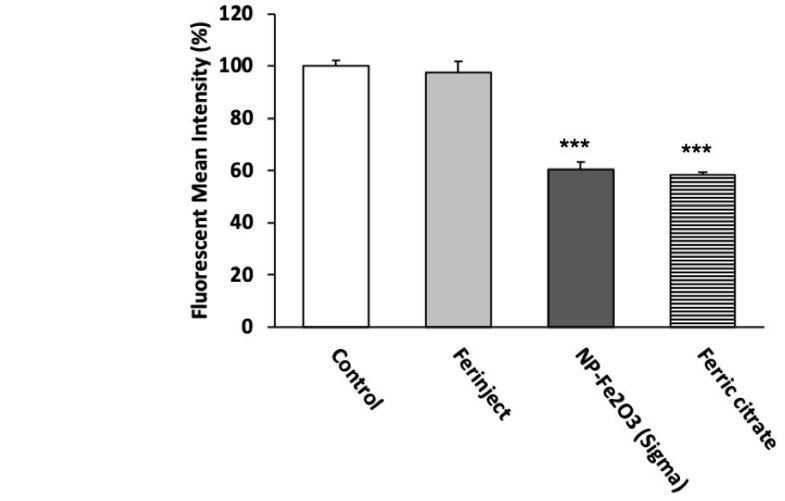

(**A**)

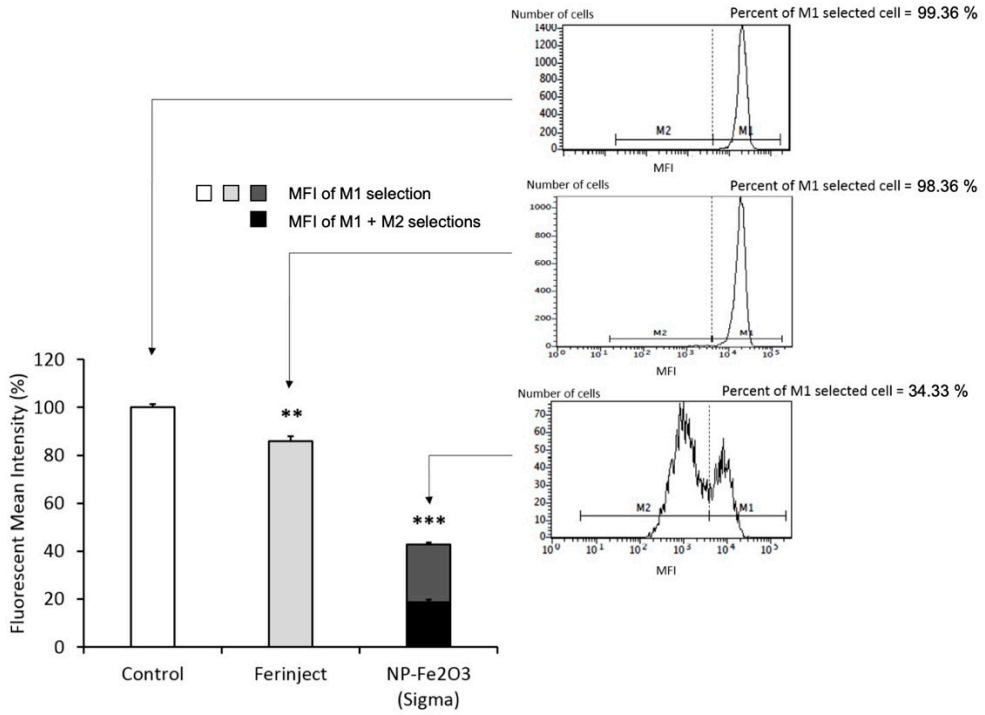

(**B**)

Figure 7. Cell physiology studies of J774A.1 cells incubated 24 h at 37 °C, 5% CO_2 with or without FERINJECT® or Fe_2O_3-NP. Pannel (**A**). Mitochondrial cell assay is measuring fluorescence of Rhodamine 123 accumulated in cells. Analyses with Facscalibur cytometer. Pannel (**B**). Analysis of the glutathione-based antioxidant system. Variations of the intracellular levels of reduced glutathione (GSH). GSH conjugate with monochlorobimane (MCB) form a fluorescent signal which is analysed by Cytometer. Statistical confidence (student's *t*-test) is indicated as follows ** $p \leq 0.01$; *** $p \leq 0.001$.

4. Discussion

Our results point to alterations of the macrophage physiology upon exposure to iron and must first be put into context. Many occupational lung diseases due to the inhalation of particles have been mentioned in the scientific literature (e.g., silicosis and asbestosis caused by crystalline silica or asbestos fibers) [50]. These pathologies enlist macrophages and impair their main functionalities, causing inflammatory and mitochondrial disorders, apoptosis, etc. [25,50,51]. Iron oxide particles are

now widespread (e.g., present in metro stations or welding fumes). However, contrarily to silica or asbestos, they can be managed by macrophages [52], but they may be dissolved via acidic phagosomes and may disturb iron homeostasis locally. Indeed, macrophages, in addition to their key role in the initiation and sustainability of the inflammatory response, have a central role in the management of iron homeostasis. This link between inflammatory response, pathogen defense and iron homeostasis control has already been documented [53–57].

In several diseases, due to iron overload, such as hereditary hemochromatosis, an impairment of the main functions of macrophages has been observed, especially in the phagocytic activity (a decrease of 62.5% compared with healthy donors) [58] and in the bactericidal activity via, for example, a deficiency of the secretion of TNF (it is in between 1.9 and 7.0 times lower than the healthy control depending on the period of incubation with LPS) [59]. Concerning pulmonary diseases such as idiopathic pulmonary fibrosis (IPF), an impairment of the functionalities of macrophages, with an alteration of iron homeostasis in pulmonary fibrosis was observed. In this disease, alveolar macrophages are characterized by a deficient transferrin uptake, a reduced phagocytosis of *S. aureus* and an increase of NO production for unstimulated cells [60]. In such diseases, the functional effects observed on macrophages are linked to an overload in soluble iron. In our experiments, we also observed important effect on macrophages functionalities when cells were treated with a high concentration of soluble iron. Interestingly, most of these effects were also observed for macrophages treated with NP-Sigma, but not for cells treated with smaller nanoparticles (FERINJECT®). Moreover, these effects were not due to a spontaneous strong dissolution of particles in the culture medium which would release a high quantity of ionic iron. Very little or no iron was measured in the supernatant for all the conditions tested (Table S1). While we did not observe an intrinsic effect of NP-Sigma on NO, as observed in lung fibrosis, we also observed a decrease in phagocytosis for macrophages exposed to these large nanoparticles. Thus, although macrophages are known to manage iron and thus are less sensitive to iron overload and resist to it (low mortality) [61,62], inhaling a high quantity of large iron particles may (i) alter the first line of defense mechanisms of the lungs against pathogens, (ii) promote lung fibrosis, because even if we show that Fe2O3-NP are not toxic at a high concentration (such as 1 mg/mL, LD20 not reached), the functionalities of macrophages can be strongly impacted, and iii) increase bacterial infections which use the excess of iron to develop quicker.

Overall, the uptake kinetics experiments that we performed strongly suggest that the higher effects induced by large particles may be due to the fact that at the end of the 24 h exposure period, cells exposed to larger particles have been exposed to a higher concentration of intracellular iron for a longer time. This observation is in line with sedimentation models to explain the effects of nanoparticles [63]. However, sedimentation is not the only phenomenon that explains the variations in the internalization of particles/nanoparticles. Indeed, in our experiments presented in Figure S3, we assessed the internalization of fluorescent latex beads of 30 nm and 1 µm (corresponding to the size of aggregates of NP-Fe_2O_3) and we compared this uptake with phagocytic (J774A.1) and non-phagocytic (MPC11) myeloid cells. This experiment showed that the uptake ratio between J774A.1 and MPC11 changed when we compared the two latex beads sizes. For the 30 nm latex beads, the uptake was similar for J774A.1 and MPC11, while for 1 µm diameter latex beads, the uptake was 20 times more efficient in J774A.1 cells than in MPC11 cells. If the internalization of particle depended solely of the sedimentation phenomenon, the uptake ratios of distinct particles should not be different between the two cell lines. Thus, the final uptake depends not only on sedimentation, which brings the nanoparticles in contact with cells, but also on the internalization ability of the cells, i.e., of the uptake pathways used and their efficiency. In this line, Hslao I-L et al. compared the uptake of 50 nm and 600 nm particles and discussed the differences in their uptake processes. Small particles are preferentially internalized by pinocytosis if not passive diffusion pathways (low energy consumption), while large particle are engulfed by active internalization (high energy consumption) [64].

Nevertheless, although important cell parameters such as the mitochondrial transmembrane potential and the intracellular glutathione content are deeply affected by the large particles, the cells are still alive, and retain some level of functionality. However, the strong effects of large Fe_2O_3-NP

observed on glutathione and mitochondria resemble ferroptosis, in which the observed effects are linked to the quantity of iron into cells [65].

The present article highlights that contrarily to the received opinion and some articles, nanoparticles are not systematically more noxious (or more toxic) than larger particles such as microparticles. Of course, not all materials react in a similar manner and a lot of parameters influence the toxicity of nanoparticles [66]. Given that the toxicity of NPs depends on a multitude of parameters, the nanotoxicology discipline is extremely complex [67] and the analysis of one peculiar group cannot be generalized to all nanoparticles. Regarding our in vitro study, even if the larger Fe_2O_3 microparticles induce more effects than nanoparticles, they are not necessarily more toxic in vivo. In fact, nanoparticles, because of their small size, can enter the respiratory system more deeply (e.g., pulmonary alveoli) [68,69] and seem to cross biological barriers (mucus, surfactant, etc.) more easily [70] and are thus more likely to enter the bloodstream via the respiratory tract. Furthermore, particles with a large size are more easily removed by exhalation [63] whereas small particles are eliminated by phagocytosis via the macrophages or accumulate in the alveolae [71]. Therefore, it is more difficult to eliminate them from the body and they are more likely to persist in the lungs. According to a study by TSI Incorporated, when 20 nm nanoparticles are inhaled, 40% to 60% are found in the alveolae.

It must, however, be mentioned that according to the same study (measuring nanoparticle exposure application note of Thermo-System Inc. via the Nanoparticle Surface Area Monitor (Application Note NSAM-001), 10% to 20% of inhaled large particles (≥100 nm) are deposited in the alveoli. [72]. Thus, even if large particles are less present in alveolar regions, their quantity is not negligible, particularly when a high quantity is released into the air (which is the case of metro stations during braking). Moreover, the previously mentioned figures are numbers of particles. As large particles imply a considerably higher mass of material than smaller ones at equal numbers, it is therefore highly relevant to investigate the toxicity of large particles.

Even if we cannot actually conclude which of the two particles is more toxic in real life due to lack of in vivo data, it remains interesting to note that at a same concentration, two iron based particles with different sizes and aggregate forms do not induce the same effects on macrophages. Moreover we show that even without inducing important cell death, particles can have a drastic impact on the functionalities of macrophages and thus, may facilitate the occurrence of pathologies, as observed for welding fumes [9], e.g., by decreasing the overall efficiency of the immune system. Finally, in real-life conditions, nanoparticles are not isolated but on the contrary, exist alongside a variety of other elements mix (particulate, nanoparticulate or other chemical species). Therefore, in order to build on our results, we plan to pursue with cross-toxicity studies which, like existing experiments on other nanoparticles by [20,31], better reflect real-life conditions. We also aim at investigating the potential cross-toxicity between exposure to nanoparticles and certain aspects of lifestyle (e.g., cigarette smoke, etc.). [73,74]

Supplementary Materials: The following are available online at http://www.mdpi.com/2079-4991/10/2/266/s1, Figure S1: Quantitative assessment of the iron, Figure S2: Confocal microscopy and, Figure S3: Internalization of FITC-labeled latex beads by MPC11 or RAW for 24 h at 37 °C, 5% CO2. Figure S4: Internalization of FITC-labeled latex beads by MPC11 or RAW for 24h at 37 °C, 5%CO2. Table S1: Quantitative bathophenanthroline assay.

Author Contributions: B.D. and C.A.-G. performed the DLS, phagocytosis, NO, cytokines, Glutathione, mitochondrial and mitochondrial potential experiments. In addition, B.D. performed perls staining, bathophenanthroline assays and F-Actin. A.T. performed the assays concerning the beads latex uptake by MPC-11 and J774A.1. S.R. performed ICP-MS. D.F., C.M., B.G. and G.S. performed TEM microscopy visualization. F.S.-A. performed EDX microscopy visualization. V.C.-F. helped to adjust flow cytometer settings. The manuscript was written by B.D. and T.R. All authors have read and agreed to the published version of the manuscript.

Funding: This work used the EM facilities at the Grenoble Instruct-ERIC Center (ISBG; UMS 3518 CNRS CEA-UGA-EMBL) with support from the French Infrastructure for Integrated Structural Biology (FRISBI; ANR-10-INSB-05-02) and GRAL, a project of the University Grenoble Alpes graduate school (Ecoles Universitaires de Recherche) CBH-EUR-GS (ANR-17-EURE-0003) within the Grenoble Partnership for Structural Biology. The IBS Electron Microscope facility is supported by the Auvergne Rhône-Alpes Region, the Fonds Feder, the Fondation pour la Recherche Médicale and GIS-IBiSA. This work is a contribution to the Labex Serenade (n° ANR-11-LABX-0064) funded by the «Investissements d'Avenir» French Government program of the French National Research Agency (ANR) through the A*MIDEX project (n° ANR-11-IDEX-0001-02). Figure 3C and

4A were obtained with the TEM OSIRIS, Plateform Nano-Safety, CEA-Grenoble. This work was supported by by the French Agence National Research Agency (ANR), program 'Investissements d'Avenir'. Contract reference ANR-10-EQPX-39.

Acknowledgments: This paper is dedicated to the memory of Catherine Aude-Garcia, deceased 21 November 2018. BD thanks the CNRS for disability PhD funding.

Conflicts of Interest: There are no conflict of interest to declare.

References

1. Dorier, M.; Brun, E.; Veronesi, G.; Barreau, F.; Pernet-Gallay, K.; Desvergne, C.; Rabilloud, T.; Carapito, C.; Herlin-Boime, N.; Carrière, M. Impact of anatase and rutile titanium dioxide nanoparticles on uptake carriers and efflux pumps in Caco-2 gut epithelial cells. *Nanoscale* **2015**, *7*, 7352–7360. [CrossRef]
2. Bahadar, H.; Maqbool, F.; Niaz, K.; Abdollahi, M. Toxicity of Nanoparticles and an Overview of Current Experimental Models. *Iran. Biomed. J.* **2016**, *20*, 1–11.
3. Satzer, P.; Svec, F.; Sekot, G.; Jungbauer, A. Protein adsorption onto nanoparticles induces conformational changes: Particle size dependency, kinetics, and mechanisms. *Eng. Life Sci.* **2016**, *16*, 238–246. [CrossRef]
4. Lundqvist, M.; Stigler, J.; Elia, G.; Lynch, I.; Cedervall, T.; Dawson, K.A. Nanoparticle size and surface properties determine the protein corona with possible implications for biological impacts. *Proc. Natl. Acad. Sci. USA* **2008**, *105*, 14265–14270. [CrossRef]
5. Lin, J.; Zhang, H.; Chen, Z.; Zheng, Y. Penetration of Lipid Membranes by Gold Nanoparticles: Insights into Cellular Uptake, Cytotoxicity, and Their Relationship. *ACS Nano* **2010**, *4*, 5421–5429. [CrossRef]
6. Jiang, W.; Kim, B.Y.S.; Rutka, J.T.; Chan, W.C.W. Nanoparticle-mediated cellular response is size-dependent. *Nat. Nanotechnol.* **2008**, *3*, 145–150. [CrossRef]
7. ANSES Rapport D'expertise Collective. Pollution Chimique de l'air des Enceintes de Transports Ferroviaires Souterrains et Risques Sanitaires Associés Chez les Travailleurs. 2015. Available online: https://www.anses.fr/fr/content/pollution-de-l%E2%80%99air-dans-les-enceintes-ferroviaires-souterraines-et-risques-pour-la-sant%C3%A9-des (accessed on 4 September 2019).
8. Eom, H.-J.; Jung, H.-J.; Sobanska, S.; Chung, S.-G.; Son, Y.-S.; Kim, J.-C.; Sunwoo, Y.; Ro, C.-U. Iron Speciation of Airborne Subway Particles by the Combined Use of Energy Dispersive Electron Probe X-ray Microanalysis and Raman Microspectrometry. *Anal. Chem.* **2013**, *85*, 10424–10431. [CrossRef]
9. Suri, R.; Periselneris, J.; Lanone, S.; Zeidler-Erdely, P.C.; Melton, G.; Palmer, K.T.; Andujar, P.; Antonini, J.M.; Cohignac, V.; Erdely, A.; et al. Exposure to welding fumes and lower airway infection with Streptococcus pneumoniae. *J. Allergy Clin. Immunol.* **2016**, *137*, 527–534.e7. [CrossRef]
10. Karlsson, H.L.; Nilsson, L.; Möller, L. Subway Particles Are More Genotoxic than Street Particles and Induce Oxidative Stress in Cultured Human Lung Cells. *Chem. Res. Toxicol.* **2005**, *18*, 19–23. [CrossRef]
11. Ebabe Elle, R.; Gaillet, S.; Vidé, J.; Romain, C.; Lauret, C.; Rugani, N.; Cristol, J.P.; Rouanet, J.M. Dietary exposure to silver nanoparticles in Sprague–Dawley rats: Effects on oxidative stress and inflammation. *Food Chem. Toxicol.* **2013**, *60*, 297–301. [CrossRef]
12. Martínez-Gutierrez, F.; Thi, E.P.; Silverman, J.M.; de Oliveira, C.C.; Svensson, S.L.; Hoek, A.V.; Sánchez, E.M.; Reiner, N.E.; Gaynor, E.C.; Pryzdial, E.L.G.; et al. Antibacterial activity, inflammatory response, coagulation and cytotoxicity effects of silver nanoparticles. *Nanomed. Nanotechnol. Biol. Med.* **2012**, *8*, 328–336. [CrossRef]
13. Falagan-Lotsch, P.; Grzincic, E.M.; Murphy, C.J. One low-dose exposure of gold nanoparticles induces long-term changes in human cells. *Proc. Natl. Acad. Sci. USA* **2016**, *113*, 13318–13323. [CrossRef]
14. Khanna, P.; Ong, C.; Bay, B.; Baeg, G. Nanotoxicity: An Interplay of Oxidative Stress, Inflammation and Cell Death. *Nanomaterials* **2015**, *5*, 1163–1180. [CrossRef]
15. Manke, A.; Wang, L.; Rojanasakul, Y. Mechanisms of Nanoparticle-Induced Oxidative Stress and Toxicity. *BioMed Res. Int.* **2013**, *2013*, 1–15. [CrossRef]
16. Pandey, R.K.; Prajapati, V.K. Molecular and immunological toxic effects of nanoparticles. *Int. J. Biol. Macromol.* **2018**, *107*, 1278–1293. [CrossRef] [PubMed]
17. Pratsinis, A.; Hervella, P.; Leroux, J.-C.; Pratsinis, S.E.; Sotiriou, G.A. Toxicity of Silver Nanoparticles in Macrophages. *Small* **2013**, *9*, 2576–2584. [CrossRef] [PubMed]
18. Murray, P.J.; Wynn, T.A. Protective and pathogenic functions of macrophage subsets. *Nat. Rev. Immunol.* **2011**, *11*, 723–737. [CrossRef] [PubMed]

19. Mowat, A.M.; Scott, C.L.; Bain, C.C. Barrier-tissue macrophages: Functional adaptation to environmental challenges. *Nat. Med.* **2017**, *23*, 1258–1270. [CrossRef]
20. Dalzon, B.; Aude-Garcia, C.; Collin-Faure, V.; Diemer, H.; Béal, D.; Dussert, F.; Fenel, D.; Schoehn, G.; Cianférani, S.; Carrière, M.; et al. Differential proteomics highlights macrophage-specific responses to amorphous silica nanoparticles. *Nanoscale* **2017**, *9*, 9641–9658. [CrossRef]
21. Koh, T.J.; DiPietro, L.A. Inflammation and wound healing: The role of the macrophage. *Expert Rev. Mol. Med.* **2011**, *13*, e23. [CrossRef]
22. Landén, N.X.; Li, D.; Ståhle, M. Transition from inflammation to proliferation: A critical step during wound healing. *Cell. Mol. Life Sci.* **2016**, *73*, 3861–3885. [CrossRef] [PubMed]
23. Navegantes, K.C.; de Souza Gomes, R.; Pereira, P.A.T.; Czaikoski, P.G.; Azevedo, C.H.M.; Monteiro, M.C. Immune modulation of some autoimmune diseases: The critical role of macrophages and neutrophils in the innate and adaptive immunity. *J. Transl. Med.* **2017**, *15*, 36. [CrossRef]
24. Chen, G.Y.; Nuñez, G. Sterile inflammation: Sensing and reacting to damage. *Nat. Rev. Immunol.* **2010**, *10*, 826–837. [CrossRef] [PubMed]
25. Hamilton, R.F.; Thakur, S.A.; Holian, A. Silica binding and toxicity in alveolar macrophages. *Free Radic. Biol. Med.* **2008**, *44*, 1246–1258. [CrossRef] [PubMed]
26. Chanmee, T.; Ontong, P.; Konno, K.; Itano, N. Tumor-Associated Macrophages as Major Players in the Tumor Microenvironment. *Cancers* **2014**, *6*, 1670–1690. [CrossRef]
27. Lee, Y.; Choi, K.; Jung, W.; Versoza, M.E.; Barabad, M.L.M.; Kim, T.; Park, D. Generation Characteristics of Nanoparticles Emitted from Subways in Operation. *Aerosol Air Qual. Res.* **2018**, *18*, 2230–2239. [CrossRef]
28. Geisser, P.; Philipp, E.; Richle, W. Aqueous Iron Carbohydrate Complexes, Their Production and Medicaments Containing Them. US Patent US20100099647A1, 22 April 2010.
29. Wen, B.; Li, J.; Lin, Y.; Liu, X.; Fu, J.; Miao, H.; Zhang, Q. A novel preparation method for γ-Fe2O3 nanoparticles and their characterization. *Mater. Chem. Phys.* **2011**, *128*, 35–38. [CrossRef]
30. Neiser, S.; Rentsch, D.; Dippon, U.; Kappler, A.; Weidler, P.G.; Göttlicher, J.; Steininger, R.; Wilhelm, M.; Braitsch, M.; Funk, F.; et al. Physico-chemical properties of the new generation IV iron preparations ferumoxytol, iron isomaltoside 1000 and ferric carboxymaltose. *Biometals* **2015**, *28*, 615–635. [CrossRef]
31. Triboulet, S.; Aude-Garcia, C.; Carrière, M.; Diemer, H.; Proamer, F.; Habert, A.; Chevallet, M.; Collin-Faure, V.; Strub, J.-M.; Hanau, D.; et al. Molecular Responses of Mouse Macrophages to Copper and Copper Oxide Nanoparticles Inferred from Proteomic Analyses. *Mol. Cell. Proteom.* **2013**, *12*, 3108–3122. [CrossRef]
32. Triboulet, S.; Aude-Garcia, C.; Armand, L.; Gerdil, A.; Diemer, H.; Proamer, F.; Collin-Faure, V.; Habert, A.; Strub, J.-M.; Hanau, D.; et al. Analysis of cellular responses of macrophages to zinc ions and zinc oxide nanoparticles: A combined targeted and proteomic approach. *Nanoscale* **2014**, *6*, 6102–6114. [CrossRef]
33. Triboulet, S.; Aude-Garcia, C.; Armand, L.; Collin-Faure, V.; Chevallet, M.; Diemer, H.; Gerdil, A.; Proamer, F.; Strub, J.-M.; Habert, A.; et al. Comparative Proteomic Analysis of the Molecular Responses of Mouse Macrophages to Titanium Dioxide and Copper Oxide Nanoparticles Unravels Some Toxic Mechanisms for Copper Oxide Nanoparticles in Macrophages. *PLoS ONE* **2015**, *10*, e0124496. [CrossRef] [PubMed]
34. Dalzon, B.; Guidetti, M.; Testemale, D.; Reymond, S.; Proux, O.; Vollaire, J.; Collin-Faure, V.; Testard, I.; Fenel, D.; Schoehn, G.; et al. Utility of macrophages in an antitumor strategy based on the vectorization of iron oxide nanoparticles. *Nanoscale* **2019**, *11*, 9341–9352. [CrossRef] [PubMed]
35. Tarantini, A.; Wegner, K.D.; Dussert, F.; Sarret, G.; Beal, D.; Mattera, L.; Lincheneau, C.; Proux, O.; Truffier-Boutry, D.; Moriscot, C.; et al. Physicochemical alterations and toxicity of InP alloyed quantum dots aged in environmental conditions: A safer by design evaluation. *NanoImpact* **2019**, *14*, 100168. [CrossRef]
36. Bouillot, S.; Munro, P.; Gallet, B.; Reboud, E.; Cretin, F.; Golovkine, G.; Schoehn, G.; Attrée, I.; Lemichez, E.; Huber, P. Pseudomonas aeruginosa Exolysin promotes bacterial growth in lungs, alveolar damage and bacterial dissemination. *Sci. Rep.* **2017**, *7*, 2120. [CrossRef] [PubMed]
37. Abel, G.; Szöllösi, J.; Fachet, J. Phagocytosis of fluorescent latex microbeads by peritoneal macrophages in different strains of mice: A flow cytometric study. *Eur. J. Immunogenet.* **1991**, *18*, 239–245. [CrossRef] [PubMed]
38. Dalzon, B.; Torres, A.; Diemer, H.; Ravanel, S.; Collin-Faure, V.; Pernet-Gallay, K.; Jouneau, P.-H.; Bourguignon, J.; Cianférani, S.; Carrière, M.; et al. How reversible are the effects of silver nanoparticles on macrophages? A proteomic-instructed view. *Environ. Sci. Nano* **2019**, *6*, 3133–3157. [CrossRef]

39. Aude-Garcia, C.; Dalzon, B.; Ravanat, J.-L.; Collin-Faure, V.; Diemer, H.; Strub, J.M.; Cianferani, S.; Van Dorsselaer, A.; Carrière, M.; Rabilloud, T. A combined proteomic and targeted analysis unravels new toxic mechanisms for zinc oxide nanoparticles in macrophages. *J. Proteom.* **2016**, *134*, 174–185. [CrossRef]
40. Dalzon, B.; Bons, J.; Diemer, H.; Collin-Faure, V.; Marie-Desvergne, C.; Dubosson, M.; Cianferani, S.; Carapito, C.; Rabilloud, T. A Proteomic View of Cellular Responses to Anticancer Quinoline-Copper Complexes. *Proteomes* **2019**, *7*, 26. [CrossRef]
41. Derman, D.P.; Green, A.; Bothwell, T.H.; Graham, B.; McNamara, L.; MacPhail, A.P.; Baynes, R.D. A Systematic Evaluation of Bathophenanthroline, Ferrozine and Ferene in an ICSH-Based Method for the Measurement of Serum Iron. *Ann. Clin. Biochem.* **1989**, *26*, 144–147. [CrossRef]
42. Grass, D.S.; Ross, J.M.; Family, F.; Barbour, J.; James Simpson, H.; Coulibaly, D.; Hernandez, J.; Chen, Y.; Slavkovich, V.; Li, Y.; et al. Airborne particulate metals in the New York City subway: A pilot study to assess the potential for health impacts. *Environ. Res.* **2010**, *110*, 1–11. [CrossRef]
43. Martins, V.; Moreno, T.; Mendes, L.; Eleftheriadis, K.; Diapouli, E.; Alves, C.A.; Duarte, M.; de Miguel, E.; Capdevila, M.; Querol, X.; et al. Factors controlling air quality in different European subway systems. *Environ. Res.* **2016**, *146*, 35–46. [CrossRef] [PubMed]
44. Cartledge, B.T.; Majestic, B.J. Metal concentrations and soluble iron speciation in fine particulate matter from light rail activity in the Denver-Metropolitan area. *Atmos. Pollut. Res.* **2015**, *6*, 495–502. [CrossRef]
45. Ribes, S.; Ebert, S.; Regen, T.; Agarwal, A.; Tauber, S.C.; Czesnik, D.; Spreer, A.; Bunkowski, S.; Eiffert, H.; Hanisch, U.-K.; et al. Toll-Like Receptor Stimulation Enhances Phagocytosis and Intracellular Killing of Nonencapsulated and Encapsulated Streptococcus pneumoniae by Murine Microglia. *Infect. Immun.* **2010**, *78*, 865–871. [CrossRef] [PubMed]
46. MacLean-Fletcher, S. Mechanism of action of cytochalasin B on actin. *Cell* **1980**, *20*, 329–341. [CrossRef]
47. Axline, S.G. INHIBITION OF PHAGOCYTOSIS AND PLASMA MEMBRANE MOBILITY OF THE CULTIVATED MACROPHAGE BY CYTOCHALASIN B: Role of Subplasmalemmal Microfilaments. *J. Cell Biol.* **1974**, *62*, 647–659. [CrossRef]
48. Mei, Y.; Thompson, M.D.; Cohen, R.A.; Tong, X. Autophagy and oxidative stress in cardiovascular diseases. *Biochim. Et Biophys. Acta Mol. Basis Dis.* **2015**, *1852*, 243–251. [CrossRef]
49. Veronesi, G.; Aude-Garcia, C.; Kieffer, I.; Gallon, T.; Delangle, P.; Herlin-Boime, N.; Rabilloud, T.; Carrière, M. Exposure-dependent Ag^+ release from silver nanoparticles and its complexation in AgS_2 sites in primary murine macrophages. *Nanoscale* **2015**, *7*, 7323–7330. [CrossRef]
50. Davis, G.S. The Pathogenesis of Silicosis. *Chest* **1986**, *89*, 166S–169S. [CrossRef]
51. Thibodeau, M.S.; Giardina, C.; Knecht, D.A.; Helble, J.; Hubbard, A.K. Silica-Induced Apoptosis in Mouse Alveolar Macrophages Is Initiated by Lysosomal Enzyme Activity. *Toxicol. Sci.* **2004**, *80*, 34–48. [CrossRef]
52. Rojas, J.M.; Gavilán, H.; del Dedo, V.; Lorente-Sorolla, E.; Sanz-Ortega, L.; da Silva, G.B.; Costo, R.; Perez-Yagüe, S.; Talelli, M.; Marciello, M.; et al. Time-course assessment of the aggregation and metabolization of magnetic nanoparticles. *Acta Biomater.* **2017**, *58*, 181–195. [CrossRef]
53. Nairz, M.; Haschka, D.; Demetz, E.; Weiss, G. Iron at the interface of immunity and infection. *Front. Pharmacol.* **2014**, *5*, 152. [CrossRef] [PubMed]
54. Jung, M.; Mertens, C.; Brüne, B. Macrophage iron homeostasis and polarization in the context of cancer. *Immunobiology* **2015**, *220*, 295–304. [CrossRef] [PubMed]
55. Canton, J.; Neculai, D.; Grinstein, S. Scavenger receptors in homeostasis and immunity. *Nat. Rev. Immunol.* **2013**, *13*, 621–634. [CrossRef] [PubMed]
56. Kobayashi, E.H.; Suzuki, T.; Funayama, R.; Nagashima, T.; Hayashi, M.; Sekine, H.; Tanaka, N.; Moriguchi, T.; Motohashi, H.; Nakayama, K.; et al. Nrf2 suppresses macrophage inflammatory response by blocking proinflammatory cytokine transcription. *Nat. Commun.* **2016**, *7*, 11624. [CrossRef]
57. Lim, P.J.; Duarte, T.L.; Arezes, J.; Garcia-Santos, D.; Hamdi, A.; Pasricha, S.-R.; Armitage, A.E.; Mehta, H.; Wideman, S.; Santos, A.G.; et al. Nrf2 controls iron homoeostasis in haemochromatosis and thalassaemia via Bmp6 and hepcidin. *Nat. Metab.* **2019**, *1*, 519–531. [CrossRef]
58. van Asbeck, B.S.; Marx, J.J.M.; Struyvenberg, A.; Verhoef, J. Functional defects in phagocytic cells from patients with iron overload. *J. Infect.* **1984**, *8*, 232–240. [CrossRef]
59. Gordeuk, V.R.; Ballou, S.; Lozanski, G.; Brittenham, G.M. Decreased concentrations of tumor necrosis factor-alpha in supernatants of monocytes from homozygotes for hereditary hemochromatosis. *Blood* **1992**, *79*, 1855–1860. [CrossRef]

60. Allden, S.J.; Ogger, P.P.; Ghai, P.; McErlean, P.; Hewitt, R.; Toshner, R.; Walker, S.A.; Saunders, P.; Kingston, S.; Molyneaux, P.L.; et al. The Transferrin Receptor CD71 Delineates Functionally Distinct Airway Macrophage Subsets during Idiopathic Pulmonary Fibrosis. *Am. J. Respir. Crit. Care Med.* **2019**, *200*, 209–219. [CrossRef]
61. Toblli, J.; Angerosa, M. Optimizing iron delivery in the management of anemia: Patient considerations and the role of ferric carboxymaltose. *DDDT* **2014**, *8*, 2475. [CrossRef]
62. Sukhbaatar, N.; Weichhart, T. Iron Regulation: Macrophages in Control. *Pharmaceuticals* **2018**, *11*, 137. [CrossRef]
63. Cohen, J.M.; Teeguarden, J.G.; Demokritou, P. An integrated approach for the in vitro dosimetry of engineered nanomaterials. *Part. Fibre Toxicol.* **2014**, *11*, 20. [CrossRef] [PubMed]
64. Annika Mareike Gramatke, I.-L.H. Size and Cell Type Dependent Uptake of Silica Nanoparticles. *J. Nanomed. Nanotechnol.* **2014**, 5. [CrossRef]
65. Lei, P.; Bai, T.; Sun, Y. Mechanisms of Ferroptosis and Relations with Regulated Cell Death: A Review. *Front. Physiol.* **2019**, *10*, 139. [CrossRef] [PubMed]
66. Karlsson, H.L.; Gustafsson, J.; Cronholm, P.; Möller, L. Size-dependent toxicity of metal oxide particles—A comparison between nano- and micrometer size. *Toxicol. Lett.* **2009**, *188*, 112–118. [CrossRef]
67. Kong, B.; Seog, J.H.; Graham, L.M.; Lee, S.B. Experimental considerations on the cytotoxicity of nanoparticles. *Nanomedicine* **2011**, *6*, 929–941. [CrossRef]
68. Carvalho, T.C.; Peters, J.I.; Williams III, R.O. Influence of particle size on regional lung deposition—What evidence is there? *Int. J. Pharm.* **2011**, *406*, 1–10. [CrossRef]
69. INRS. Santé Sécurité au travail. Risques. Nanomatériaux, nanoparticules. Effets sur la santé. 2018. Available online: http://www.inrs.fr/risques/nanomateriaux/effets-sante.html (accessed on 4 September 2019).
70. Lamprecht, A.; Schäfer, U.; Lehr, C. Size-Dependent Bioadhesion of Micro- and Nanoparticulate Carriers to the Inflamed Colonic Mucosa. *Pharm. Res.* **2001**, *18*, 788–793. [CrossRef]
71. van Rijt, S.H.; Bein, T.; Meiners, S. Medical nanoparticles for next generation drug delivery to the lungs. *Eur. Respir. J.* **2014**, *44*, 765–774. [CrossRef]
72. Application Note NSAM-001. Measuring Nanoparticle Exposure. 2012. Available online: https://www.kenelec.com.au/wp-content/uploads/2018/04/TSI-NSAM-001-Measuring-Nanoparticle-Exposure-AppNote.pdf (accessed on 22 October 2019).
73. Lai, H.; Liu, Y.; Zhou, M.; Shi, T.; Zhou, Y.; Weng, S.; Chen, W. Combined effect of silica dust exposure and cigarette smoking on total and cause-specific mortality in iron miners: A cohort study. *Environ. Health* **2018**, *17*, 46. [CrossRef]
74. Tse, L.A.; Yu, I.T.S.; Qiu, H.; Leung, C.C. Joint Effects of Smoking and Silicosis on Diseases to the Lungs. *PLoS ONE* **2014**, *9*, e104494. [CrossRef]

Conclusion

L'exposition aux particules de fer et leur surcharge dans l'organisme peuvent être à l'origine de maladies. Dans cette étude, la caractérisation des nanomatériaux a montré que le phénomène d'agrégation, en milieu contenant des protéines, était plus important pour le fer commercial de Sigma, de 100nm. La cytotoxicité des nanomatériaux de fer est similaire pour les deux tailles de nanomatériaux, avec environ 15% de mortalité pour 1mg/ml après 24h d'exposition pour les macrophages primaires. Ce taux de mortalité descend à 5-10% pour la lignée cellulaire J774A.1. La proportion de cellules phagocytaires et leur activité sont réduites par l'exposition aux nanoparticules longues de fer et au citrate de fer. Les cellules traitées par ces formes de particules de fer entrainent également une perte d'adhérence avec une diminution des filaments et des élongations d'actine. Les réponses inflammatoires sont également réduites en cas de co-stimulation au LPS, pour les cellules exposées aux nanoparticules longues et au citrate de fer. Cette étude montre une fois de plus, non seulement l'importance du type de nanomatériaux, mais aussi de leurs caractéristiques physico-chimiques. L'effet cytotoxique n'est pas très important, mais cette dose est suffisante pour diminuer les réponses et fonctions du macrophage. Ce qui soulève, tout d'abord, la question de la toxicité croisée et de la vulnérabilité du système immunitaire en cas de co-exposition au fer et à une autre substance toxique, et valide la démarche précédente d'exposition à la silice et à un agent génotoxique environnemental. D'autre part, la cytotoxicité seule n'est donc pas un paramètre suffisamment informatif sur les effets d'une substance, puisque la substance elle-même peut avoir un rôle sur le maintien de la viabilité cellulaire. Il se trouve que le fer joue un rôle antiapoptotique sur les cellules, et inhibe également la diminution du glutathion (Lovera-Leroux et al. 2015).

Polyacrylate et cuivre

Présentation du projet

Pour ce dernier projet, nous avons étudié le mécanisme d'internalisation du cuivre, dont 2 transporteurs sont connus (CTR1 et CTR2). Le cuivre est largement utilisé et il devient toxique lorsque sa concentration devient importante. Pour cela, deux matériaux différents ont été utilisés : des ions cuivre et un complexe de polyacrylate et cuivre. Des études de protéomiques complétées d'expériences de validations sur les J774A.1 ont permis de différencier les mécanismes d'internalisation des ces deux formes de cuivre.

Journal of Proteomics 239 (2021) 104178

Contents lists available at ScienceDirect

Journal of Proteomics

journal homepage: www.elsevier.com/locate/jprot

A proteomic view of cellular responses of macrophages to copper when added as ion or as copper-polyacrylate complex

Bastien Dalzon [a], Julie Devcic [a], Joanna Bons [b], Anaelle Torres [a], Hélène Diemer [b], Stéphane Ravanel [c], Véronique Collin-Faure [a], Sarah Cianférani [b], Christine Carapito [b], Thierry Rabilloud [a,*]

[a] Chemistry and Biology of Metals, Univ. Grenoble Alpes, CNRS UMR5249, CEA, IRIG-LCBM, F-38054 Grenoble, France
[b] Laboratoire de Spectrométrie de Masse BioOrganique (LSMBO), Université de Strasbourg, CNRS, IPHC UMR 7178, 67000 Strasbourg, France
[c] Univ. Grenoble Alpes, INRAE, CNRS UMR5168, CEA-IRIG, LPCV, Grenoble, F-38000, France

A B S T R A C T

Copper is an essential metal for life, but is toxic at high concentrations. In mammalian cells, two copper transporters are known, CTR1 and CTR2. In order to gain insights on the possible influence of the import pathway on cellular responses to copper, two copper challenges were compared: one with copper ion, which is likely to use preferentially CTR1, and one with a copper-polyacrylate complex, which will be internalized via the endosomal pathway and is likely to use preferentially CTR2. A model system consisting in the J774A1 mouse macrophage system, with a strong endosomal/lysosomal pathway, was used. In order to gain wide insights into the cellular responses to copper, a proteomic approach was used. The proteomic results were validated by targeted experiments, and showed differential effects of the import mode on cellular physiology parameters.

While the mitochondrial transmembrane potential was kept constant, a depletion in the free glutahione content was observed with copper (ion and polylacrylate complex). Both copper-polyacrylate and polyacrylate induced perturbations in the cytoskeleton and in phagocytosis. Inflammatory responses were also differently altered by copper ion and copper-polyacrylate. Copper-polyacrylate also perturbed several metabolic enzymes. Lastly, enzymes were used as a test set to assess the predictive value of proteomics.

Significance: Proteomic profiling provides an in depth analysis of the alterations induced on cells by copper under two different exposure modes to this metal, namely as the free ion or as a complex with polyacrylate. The cellular responses were substantially different between the two exposure modes, although some cellular effects are shared, such as the depletion in free glutathione. Targeted experiments were used to confirm the proteomic results. Some metabolic enzymes showed altered activities after exposure to the copper-polyacrylate complex. The basal inflammatory responses were different for copper ion and for the copper-polyacrylate complex, while the two forms of copper inhibited lipopolysaccharide-induced inflammatory responses.

1. Introduction

As for several metallic elements such as zinc or iron, copper is essential for life but becomes toxic at high concentrations. For example, a defect in copper excretion is the cause of the hereditary Wilson and Menkes diseases [1] .The toxic properties of copper led to its widespread usage as a biocide, e.g. in agriculture as a fungicide (see [2] for a review), with consequences on human health among workers (e.g. in [3]). More recently and in a more subtle way, copper has been promoted for anticancer strategies, e.g. in [4–6] . The latter strategies rely on copper ionophores to increase the intracellular copper concentrations to reach cytotoxicity in target cells at copper concentrations that are not systemically toxic. Using ionophores is indeed a way to circumvent the deactivation of the copper membrane transporter CTR1 by endocytosis upon copper excess conditions [7].

Several mechanisms have been proposed to explain the toxicity of the copper complexes, including proteasome inhibition [4,8] or oxidative stress [9,10]. The two mechanisms may be linked, as copper induces oxidative alteration of the proteasome and thus its inhibition [11].

It is clear that the therapeutic effect is due to an increase in the intracellular copper concentration [12]. However, it seems that a higher sensitivity of cancer cells to proteasome inhibition [13] or oxidative stress compared to normal cells [14,15] is more likely to explain this effect than a differential increase in copper concentration between normal and cancer cells [16].

This leads to a potential way of improving the contrast in toxicity between normal and cancer cells, or toward suppressor myeloid cells that are interesting targets in anticancer approaches [17,18]. As a first

* Corresponding author.
E-mail address: thierry.rabilloud@cea.fr (T. Rabilloud).

https://doi.org/10.1016/j.jprot.2021.104178
Received 14 November 2020; Received in revised form 1 February 2021; Accepted 22 February 2021
Available online 1 March 2021

approach in this direction, we decided to test two different entry routes for copper ion in cells, either classically through the plasma membrane as free ion, or through the endocytic pathway via a complex of copper ion with an anionic polymer, in our case polyacrylate, as polymeric polyanions are well known to be unable to cross the plasma membrane. This route was intended to use the lysosomal pathway for copper entry [19], and may rely upon the alternate copper transporter CTR2 [20], which is localized in endosomes and lysosomes [21].

In order to get a better appraisal of the cellular responses to these treatments, we decided to use a proteomic approach, which gives a substantially wider view of the cellular reactions to toxicants than targeted approaches (see for example [22–24] for reviews), and validated the most striking results of the proteomic screen by targeted experiments.

2. Materials and methods

Unless specified otherwise, the chemicals used in this work were purchased from Sigma-Millipore and were at least 99% pure. As a copper source for the copper complexes, we used a titrated copper sulfate solution (4% catalog number C2284). Sodium polyacrylate (average molecular mass 15,000, #416037) was purchased directly as a water solution and sterilized by pasteurization at 80 °C overnight.

2.1. Cell culture

The mouse monocyte/macrophage cell line J774A1 was purchased from the European Cell Culture Collection (Salisbury, UK). The cells were cultured in DMEM +10% fetal bovine serum. Cells were seeded every two days at 200,000 cells/ml and harvested at 1,000,000 cells per ml. For treatment with chemicals, the following scheme was used: cells were first seeded at 500,000 cells/ml in T175 flasks (50 ml per flask). They were exposed to copper ion (150 μM), polyacrylate (0.25 mg/ml final concentration) or a combination of both on the following day and harvested after a further 4 h or 24 h in culture. Cell viability was measured by the neutral red uptake assay [25]. All experiments were carried out at least in triplicate on independent cultures.

2.2. Subcellular fractionation and ion quantification by ICP-MS

For measuring copper uptake in cells and its repartition, the cells were harvested after exposure to copper ion, polyacrylate or polyacrylate + copper ion by scraping in buffer A (Hepes 10 mM pH 7.5, sucrose 200 mM, magnesium chloride 2 mM), and collected by centrifugation (500 *g*, 5 min).

In some experiments the cell pellet (ca 50 μl in volume) was resuspended in 500 μl of buffer A to which 0.15% (*w/v*) tetradecyldimethylammonio propane sulfonate (SB 3–14) was added. After lysis for 20 min on ice, the protein concentration was determined by a modified dye-binding assay [26] and the lysate was stored frozen at −20 °C until mineralization.

In other experiments, the cell pellet was resuspended in 500 μl of buffer A on ice, and the cells were lysed in a Dounce homogeneizer by ten strokes of the tight pestle. The homogenate was first centrifuged at 1000 *g* for 5 min at +4 °C to remove unbroken cells and nuclei. The supernatant was collected and centrifuged at 15000 *g* for 20 min at +4 °C. The supernatant was collected and saved, and the pellet (particulate fraction) was resuspended in 500 μl of buffer A. The protein concentration of both extracts (particulate and supernatant) was determined by a modified dye-binding assay [26].

The extracts were then mineralized by the addition of one volume of suprapure 65% HNO_3 per volume of extract and incubation on a rotating wheel at room temperature for 18 h.

Mineralized samples were diluted in distilled water and analyzed using an iCAP RQ quadrupole mass instrument (Thermo Fisher Scientific GmbH, Germany) equipped with an ASX-560 auto-sampler (Teledyne CETAC Technologies, Omaha, USA). The instrument was used with a MicroMist U-Series glass concentric nebulizer, a quartz spray chamber cooled at 3 °C, a Qnova quartz torch, a nickel sample cone, and a nickel skimmer cone equipped with a high-sensitivity insert. Elements were analyzed using kinetic energy discrimination mode with helium as the collision cell gas (for ^{63}Cu and ^{65}Cu). Concentrations were determined using standard curves and corrected using an internal standard solution of 103Rh added online. Data integration was done using the Qtegra software (version 2.8.2944.115). The background equivalent concentration (BEC) on pure standards was 0.02 ng/ml for ^{63}Cu and ^{65}Cu.

2.3. Proteomics

For this study, 2D gel-based proteomics was used. After cell treatment with copper ion, polyacrylate, or their combination for 24 h, as described above, the culture medium was removed and the cells collected by scraping in Hepes saline (Hepes 10 mM pH 7.5, NaCl 150 mM and MgCl2 2 mM). After two rinses in the same solution, the cell pellet was lysed by the addition of ten cell pellet volumes of lysing solution (urea 7 M, thiourea 2 M, CHAPS 4%, TCEP-HCl 5 mM, spermine base 15 mM, spermine tetrahydrochloride 15 mM). After 30 min at room temperature to complete cell lysis, the lysate was centrifuged (16,000 *g*, 30 min, room temperature) to pellet the nucleic acids. The protein-containing supernatant was collected and the protein concentration determined by a modified dye binding assay [26]. Carrier ampholytes (0.4% final concentration) were then added and the lysates were stored frozen at −20 °C until use.

2D gel-based proteomics was carried out as previously described [27], using linear pH 4–8 gradients in the focusing dimension, 10% polyacrylamide gels in the second dimension and silver staining. The gels were scanned after silver staining on a flatbed scanner (Epson perfection V750), using a 16 bits grayscale image acquisition. The gel images were then analyzed using the Delta 2D software (v 4.7). Spot identification was carried out by nanoLC-MS/MS analysis on a nanoACQUITY Ultra-Performance-LC (Waters Corporation, Milford, MA, USA) coupled to a TripleTOF 5600 instrument run in Data Dependent Acquisition mode (Sciex,Framingham, MS, USA) as previously described [27]. The mass spectrometry data are deposited in PRIDE [28] under the accession number PXD021252.

For statistical analyses, the difference between two groups was determined by a Student *t*-test or a Mann Whitney *U* test. For the global analysis of the spot abundances data, we used directly the spot abundances data as provided by the gel analysis software. The software directly normalizes each spot abundance by the sum of all spot abundances detected on the gel. These relative abundances data were used directly for global analysis using the PAST software suite [29] without any transformation. Hierarchical clustering was selected as the analysis method for its insensitivity to missing or null values. In order to minimize the quantitative bias due to different protein abundances, the Gower distance (i.e. a normalized distance) was used to perform the clustering analysis.

2.4. Enzyme assays

The enzymes were assayed according to published procedures (see below).

The cell extracts for enzyme assays were prepared by lysing the cells for 20 min at 0 °C in Hepes 20 mM pH 7.5, $MgCl_2$ 2 mM, KCl 50 mM, EGTA 1 mM, tetradecyldimethylammonio propane sulfonate (SB 3–14) 0.15% (*w/v*), followed by centrifugation at 15,000 *g* for 15 min to clear the extract. The protein concentration was determined by a dye-binding assay [26].

The dehydrogenases or dehydrogenases-coupled activities were assayed at 500 nm using the phenazine methosulfate/iodonitrotetrazolium coupled assay [30]. The enzyme assay buffer contained Hepes NaOH 25 mM pH 7.5, magnesium acetate 5 mM, potassium nitrate 100

mM and Triton X-100 (1% *w/v*). It also contained 30 μM phenazine methosulfate, 200 μM iodonitrotetrazolium chloride, 250 μM of the adequate cofactor (NAD or NADP) and 1-5 mM of the organic substrate, which was used to start the reaction. For phosphate-dependent enzymes such as glyceraldehyde dehydrogenase (GAPDH) and purine phosphorylase (PNPH), 50 mM potassium phosphate pH 7.5 was added to the enzyme assay buffer. Transaldolase was assayed by a GAPDH coupled assay [31].

Purine phosphorylase (PNPH) was assayed by a xanthine oxidase–coupled assay [32]. Enolase was assayed at 340 nm by a pyruvate kinase-lactate dehydrogenase-coupled assay [33]. Aspartate aminotransferase was assayed by a glutamate dehydrogenase-coupled assay [34]. Lactoylglutathione lyase activity was assayed at 240 nm as previously described [35].

2.5. In gel detection of malate dehydrogenase activity

The enzyme was detected by a phenazine methosulfate/nitrobuetetrazolium assay after in-gel renaturation [36]. Briefly, 0.5 mg of protein extract was loaded on a 2D gel and separated as described previously. Immediately after electrophoresis, an 8 × 5 cm gel piece was cut in the region containing malate dehydrogenase, as determined from previous proteomic experiments providing x-y coordinates for the malate dehydrogenase spots on the 2D gels. The excised zone was chosen to leave room for eventual modified or cleaved malate dehydrogenase forms.

The proteins were renatured by immersing the gel piece for 2 × 20 minutes in a solution containing TrisHCl buffer pH 7.5 50 mM, NaCl 200 mM, Glycerol 10% (v/v) Triton X-100 2% (*w/v*) and DTT 1 mM, under reciprocal shaking. The gel piece was then further renatured by a 2 × 20 minutes treatment by the same solution without DTT. Finally, the activity was detected by immersing the gel piece in a solution containing Tris buffer pH 7.5 80 mM, NaCl 10 mM, MgCl2 5 mM, disodium malate 50 mM, phenazine methosulfate 2.5 μg/ml, NAD 1 mg/ml and nitro tetrazolium blue 2.5 mg/ml. The activity was detected by blue spots on a transparent background. Finally, the gel piece, was rinsed several times with water, scanned to produce a digital image, and counterstained with colloidal Coomassie blue. Major spots detected by Coomassie Blue in the excised region were used as anchor spots to carry the excised zone on the general 2D spot pattern.

2.6. Phagocytosis assay

The phagocytic activity was measured using fluorescent latex beads (1 μm diameter, green labelled, catalog number L4655 from Sigma), as described previously [37,38]. After a 2 h30 treatment with the fluorescent beads in culture medium at 37 °C, the cells were harvested in PBS). Phagocytic activity was measured by flow cytometry on a FacsCalibur instrument (Beckton Dickinson).

2.7. F-actin staining

The experiments were performed essentially as previously described [39]. The cells were cultured on coverslips placed in 6-well plates, and exposed to copper ion, polyacrylate or both, as described above. At the end of the exposure time, cells were washed twice for 5 min at 4 °C in PBS, fixed in 4% paraformaldehyde for 30 min at room temperature. After two washes (5 min/4 °C in PBS), they were permeabilized in Triton X100 (0.1% *w/v*) for 5 min at room temperature. After two more washes in PBS, Phalloidin-Atto 550 (Sigma) (500 nM) was added to the cells and let for 20 min at room temperature in the dark. Coverslips-attached cells were washed, placed on microscope slides (Thermo Scientific) using a Vectashield mounting medium containing DAPI (Eurobio) and imaged using a Zeiss LSM 800 confocal microscope. The images were processed using the ImageJ software.

2.8. Mitochondrial transmembrane potential measurement

The mitochondrial transmembrane potential was assessed by Rhodamine 123 uptake [40], using a low Rhodamine concentration (80 nM) to avoid intramitochondrial fluorescence quenching that would result in a poor estimation of the mitochondrial potential [41]. The samples were analyzed by flow cytometry on a FacsCalibur instrument (Beckton Dickinson). Both the proportion of rhodamine positive cells and the mean fluorescence of this population were recorded in the analysis.

2.9. Glutathione assay

Cellular reduced glutathione was assayed by an in vivo conjugation assay [27] based on the conjugation of glutathione to chlorodinitrobenzene by the cellular glutathione S-transferases [42].

2.10. NO and cytokines production

The cells were grown to confluence in a 6 well plate and pre-treated with copper ion, polyacrylate or both, as described above. For the final 18 h of culture, half of the wells were treated with 100 ng/ml LPS (from salmonella, purchased from Sigma), and arginine monohydrochloride was added to all the wells (5 mM final concentration) to secure a high concentration of substrate for the nitric oxide synthase. After 18 h of incubation, the cell culture medium was recovered, centrifuged at 10,000 *g* for 10 min to remove cells and debris. The supernatants were used for nitrite determination by the Griess reagent [27] and for cytokine measurements using a cytokine bead assay (BD Cytometric Bead Array, catalog number 552364 from BD Biosciences).

3. Results and discussion

3.1. Cellular copper uptake and content

Previous experiments have shown that copper ion in the 100–200 μM range was sufficient to induce functional effects on macrophages after a 24 h exposure [38]. We thus started by fixing a 150 μM concentration for the copper ion concentration. We then determined the polyacrylate concentration that, in combination with 150 μM copper ion, induced a cellular mortality of less than 20% after a 24 h exposure, leading to the 0.25 mg/ml value used. This concentration was added as polyacrylate alone as a further control condition. The rationale for using polyacrylate as a copper carrier was that polyacrylate is known to bind to the scavenger receptor [43], and is thus targeted to the endosomal/lysosomal pathway, where the CTR2 copper transporter is located [20,21]. Conversely, free copper ion is supposed to be transported by the plasma membrane transporter CTR1 [44], although the divalent metal transporter DMT1 can also play a role [45].

We first checked if this exposure led to an increase in the intracellular copper concentration, and to which extent. Thus in a first series of experiments, the copper concentration of the total cell lysate was determined by ICP-MS after a 24 h exposure to copper ion, polyacrylate and copper-polyacrylate. The background value was 16 ± 15 ng/mg cellular protein (untreated cells) while cells treated with polyacrylate alone showed a copper content of 6 ± 1 ng/mg cellular protein (not significantly different, $p = 0.43$). Cells treated with 150 μM copper ion showed a copper content of 8370 ± 1750 ng/mg cellular protein, while cells treated with copper ion and polyacrylate showed a copper content of 6900 ± 1780 ng/mg cellular protein. The two latter values were not significantly different ($p = 0.36$) while the two values obtained for copper treated cells were significantly different from those obtained for cells untreated with copper ($p < 0.025$). The fact that the copper ion and copper-polyacrylate treatments induced a similar total intracellular copper content suggests that possible differential effects should not be linked to the total intracellular copper concentration by itself, but rather

Table 1
Copper ion concentration in cellular fractions.

Condition	Cu particulate (P)	Cu supernatant (S)	Cu (P + S)
Control	42.5 ± 10.8	23.6 ± 11	27.8 ± 10.6
polyacrylate	41.5 ± 3.9	15.1 ± 2.5	19.9 ± 2.3
Cu ion	465.7 ± 73.1*	2657 ± 312*	2355 ± 283*
Cu-polyacrylate	759 ± 76.7*,†	2376 ± 219*	2156 ± 204*

Copper concentrations are expressed in ng copper/mg cellular proteins.
Protein concentrations in the particulate fractions were 0.35 ± 0.1 mg/ml, and 1.87 ± 0.28 in the supernatant fraction, and were not significantly different between the copper-treated and non-treated samples (see Supplementary Table 1 for details).
* Significantly different from control ($p < 0.01$).
† Significantly different from copper ion ($p < 0.01$).

to the differences in the entry pathways and thus in the subcellular distribution of copper.

In order to gain further insight in the difference of copper uptake pathway, which was expected in our experimental scheme, the cellular copper content was determined after 4 h of exposure both in the particulate fraction, containing the mitochondria, the endosomes and the peroxisomes, and in the supernatant fraction. This time frame was selected to be short enough to avoid complete intracellular equilibration, which could take place in a 24 h exposure, but long enough to allow sufficient and measurable copper accumulation. The results, displayed in Table 1 (with the original data in Suppl. Table 1), showed that in unexposed conditions, the majority of the cellular copper was found in the particulate fraction. However, when cells were exposed to excess copper, the majority of the cellular copper was found in the supernatant fraction. This may be due to metallothionein induction by copper, although the selected copper concentration may be borderline to induce metallothioneins [46], but also to the fact that many cellular proteins are able to bind copper when present in excess [47,48].

Moreover, while there was no significant difference in the total copper concentration between the samples treated with copper ion and those treated with the copper-polyacrylate complex, the particulate fraction of the copper-polyacrylate complex-treated samples contained significantly more copper than the particulate fraction of the copper ion-treated samples ($p < 0.01$). No significant difference could be observed between the control and polyacrylate-treated samples. These results on short exposure experiments support our initial hypothesis that copper ion and copper-polyacrylate complex do not use the same pathways to enter the cells.

3.2. Global analysis of the proteomic results

Representative 2D gel images are shown on Fig. 1, and all the raw images used for this project are available in Suppl Figs. 1–4. 2442 spots were detected and quantified on the gels (Suppl. Table 2), of which 164 were significantly altered ($p < 0.05$) by at least one of the treatments and unambiguously identified by mass spectrometry (Suppl. Table 3). The identification parameters are given in Suppl. Table 4. As another statistics-based selection, a Mann Whitney *U* test was performed and the proteins showing a U value of 0 (i.e. unidirectional p-Value of 0.05) were selected (Suppl. Table 5). These selection criteria meant in turn that for a protein appearing as multiple spots, a significant change for one spot was considered as significant for the protein, as a modified form may have a strongly modified activity (increased or decreased) compared to the main spot owing to classical post-translational modifications such as phosphorylation (e.g.in [49]) or acylation [50] or to oxidation through an oxidative stress mechanism (e.g. in [51]).

As the treatments used (i.e. copper ion, polyacrylate or their combination) are not independent, but linked together, we used the proteomic data to perform a hierarchical clustering analysis, in order to determine how the effects of the different treatments applied on cells ranked compared to the control situation. Hierarchical clustering has the advantage to be insensitive to null or missing values, thereby requiring no data imputation, and is generally easy to interpret. These features explain why it has been one of the first methods used to globally analyze proteomic results [52–54], and is still used to sort the relative impact of various conditions in a multi conditions experimental scheme (e.g. in [27,55–57].

The results are shown on Fig. 2. The biological replicates for each condition were grouped together, and the clustering pattern indicated that the two treatments containing polyacrylate (i.e. polyacrylate alone and copper + polyacrylate) were more different from the control than the treatment with copper ion alone. Although counterintuitive in the frame of effects mainly driven by copper, this result represents the overall outcome of the proteomic experiments. When interpreting this result, it should be kept in mind that this analysis takes into account all the 2442 spots. Thus, coordinated changes, which appear as not significant when taken individually, are very likely to impact the clustering. Thus, this method may prove sensitive to weak but coordinated changes that escape the classical, statistics-based, protein selection used in most of the proteomic experiments.

Biologically speaking, this result suggests that polyacrylate alone has a significant impact on macrophages. In this respect, the situation is clearly different from the one observed with the hydroxyquinoline-copper complex, where hydroxyquinoline alone showed a weak impact on the proteome [27].

3.3. The ubiquitine proteasome pathway is altered by copper treatment

As a first screen of the proteomic results, pathway analyses were carried out for each treatment using the DAVID tool [58] (Suppl Tables 6–8). In the case of copper ion, pathway analysis highlighted the proteasome (Suppl Table 6). This pathway was also detected for the copper-polyacrylate complex treatment (Suppl Table 8), which was biologically consistent.

3.4. Central metabolism enzyme activities are altered by copper and/or polyacrylate treatments

One other major pathway that was altered is “carbon metabolism”, which appeared in all conditions (Suppl Tables 6–8). Enzymes belonging to the major classes of the central metabolism were found modulated such as enzymes of the pentose phosphate pathway, glycolysis, and amino acid metabolism. This prompted us to further test some of these enzymes in targeted experiments, and the results are displayed in Table 2.

One activity (enolase) was changed by all treatments. Copper ion modulated a second activity (purine phosphorylase). In addition to enolase, polyacrylate modulated another three enzyme activities (lactoylglutathione lyase, malate dehydrogenase and transaldolase). Besides enolase, copper-polyacrylate modulated another five activities, of which two ((lactoylglutathione lyase and malate dehydrogenase) were also modulated by polyacrylate. Three additional activities (aspartate aminotransferase, glyceraldehyde phosphate dehydrogenase and lactate dehydrogenase) were modulated only by the copper-polyacrylate complex. Thus overall, copper-polyacrylate was the treatment with the most important impact on metabolic enzymes.

3.5. Use of enzyme activities to back-probe proteomic results

Proteomics and transcriptomics share the fact that they highlight differences based on amounts only. However, biology inference is made from amounts to function in most of the omics publications, either directly or indirectly through pathway analyses. This direct inference has been pointed as a potential issue [59], especially when confronted with the multiple layers of cellular regulations, as recently reviewed [60]. In this global frame, enzymes are one of the very few examples where the relevant biological outcome (i.e. the activity) can be relatively

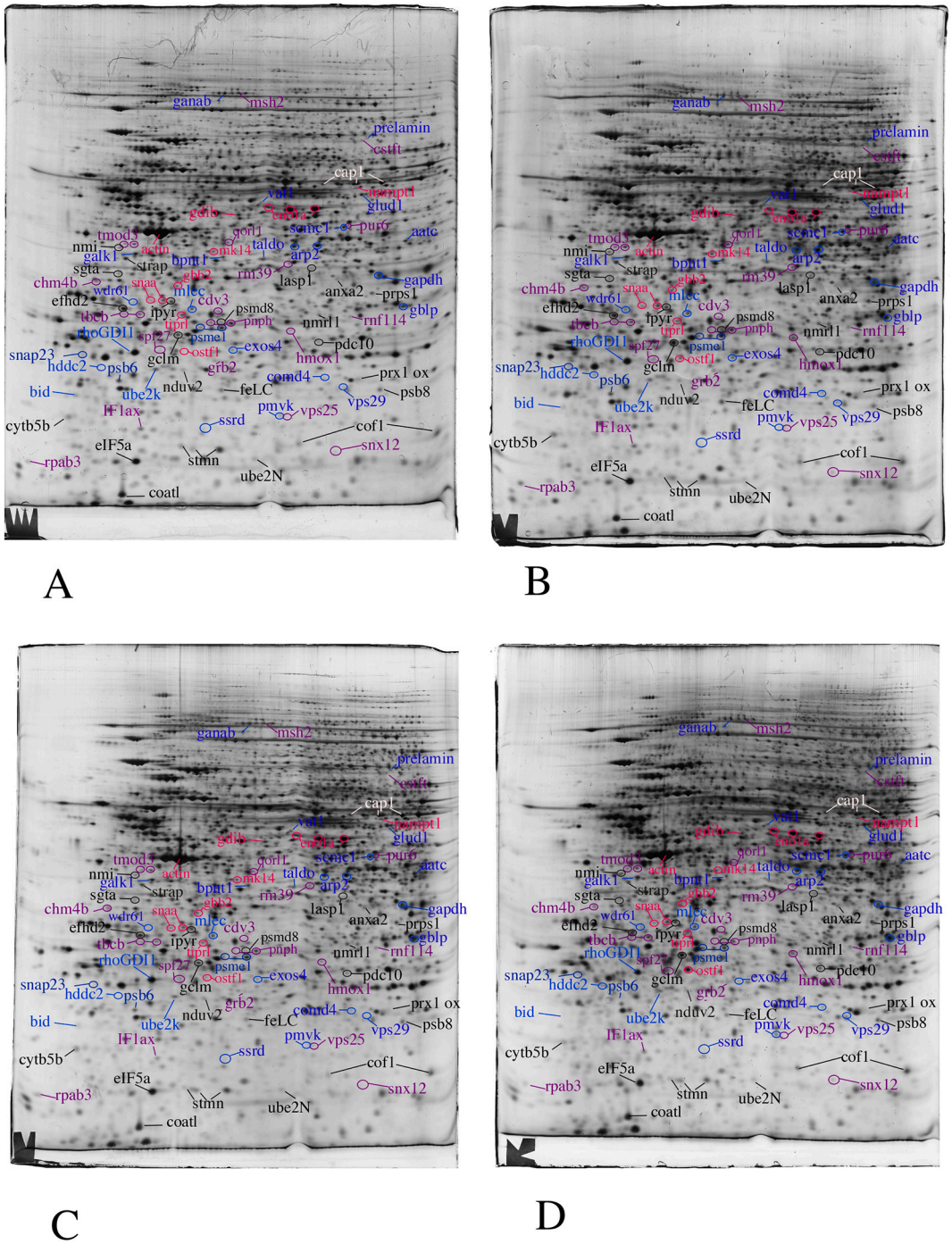

Fig. 1. Proteomic analysis of total cell extracts by 2D electrophoresis.
Total cell extracts of RAW274.7 cells were separated by two-dimensional gel electrophoresis. The first dimensions covered a 4–8 pH range and the second dimension a 15–200 kDa range. Total cellular proteins (150 μg) were loaded on the first dimension gel.
A,E: gel obtained from unexposed cells.
B,F: gel obtained from cells exposed to 150 μM copper sulfate.
C,G: gel obtained from cells exposed to 0.25 mg/ml polyacrylate.
D,H: gel obtained from cells exposed to 0.25 mg/ml polyacrylate + 150 μM copper sulfate.
The colors in the web version of the figure have been chosen only for legibility purposes.

easily measured, allowing in turn to assess important features for the proteomic analyses, such as the positive predictive value (i.e. number of true positives /(number of true positives+number of false positives), or the sensitivity (number of true positives detected by proteomics/ total number of true positives). We thus compiled the statistical values for the proteomic experiments and the enzyme activity measurements in Suppl Table 9. Taking the assumption that a true positive is an enzyme activity change at $p \leq 0.05$, then the positive predictive value (PPV) of 2D gel proteomics at the $p \leq 0.05$ threshold is 50% (7/14), with a sensitivity of 77% (7/9). Although this PPV value is very close to the 40% PPV value

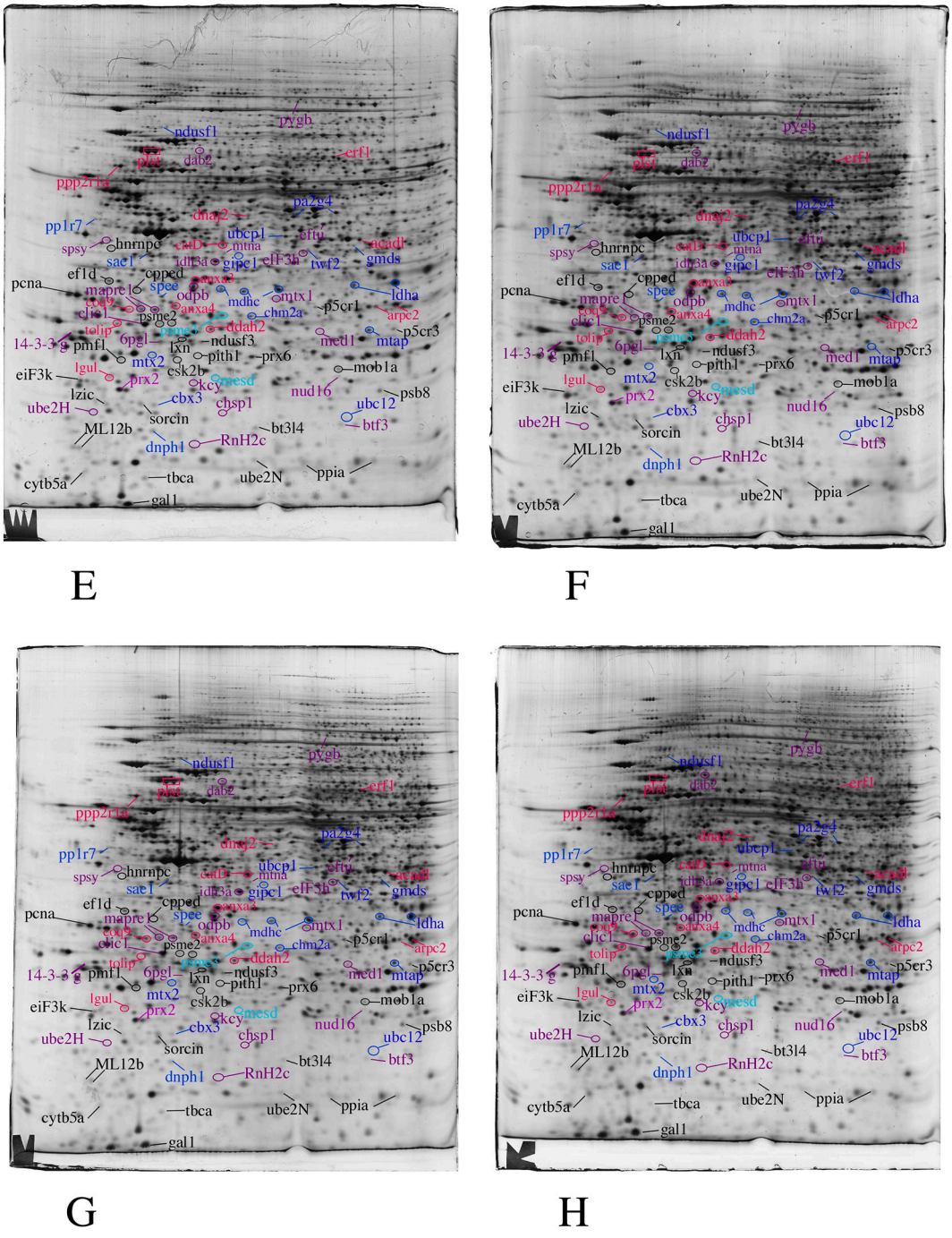

Fig. 1. (*continued*).

that can be calculated from a shotgun proteomic experiment on mitochondria [61], these values should be not taken as generic, and may vary greatly from one proteomic experiment to another.

It may be argued that enzymes may be regulated differently from other cellular proteins. However, the scope of proteins identified in phosphoproteome [62] or acetylome [63] studies extends far beyond enzymes, so that assuming that enzymes are not regulated by different mechanisms than other proteins appears reasonable. This suggests that the statistical values obtained when comparing proteomic to activity results for enzymes may be extended globally to the complete proteomic experiment.

This question is further complicated in the case of 2D proteomics because many proteins, including enzymes, appear as multiple spots, and it is thus difficult to correlate a priori the biological activity with a subset of spots or the sum of all spots corresponding to the same protein. Beyond simple correlative approaches (e.g. in [40]) we were able to address this question for malate dehydrogenase, for which 2D zymography was successful. The results, shown in Fig. 3, assigned the activity to the two most-basic spots identified on the 2D gels.

3.6. *Mitochondrial function is maintained at non-toxic copper concentrations*

The keyword « mitochondrion » also appeared in the pathway analysis (Suppl Tables 6–8). This is not surprising, as mitochondria are known to be an important actor in intracellular copper storage and

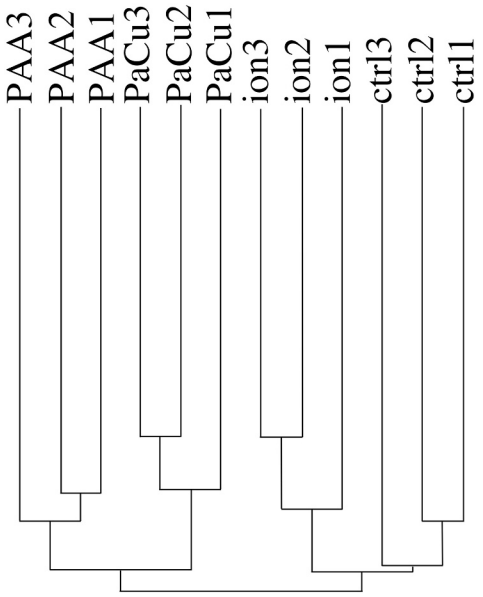

Fig. 2. Global analysis of the proteomic experiment by hierarchical clustering. Quantitative proteomic data (i.e. spots intensities in 2D gel-based proteomics) were used to determine the similarities between biological samples. The PAST software package was used for the calculations, using the Gower similarity index and a Paired group algorithm. This tree indicates the similarity between the various experimental groups (the higher the distance of the branching point between groups, the more dissimilar they are).
Ctrl(1–3): unexposed cells.
ion(1–3): cells exposed to 150 μM copper sulfate.
PAA(1–3): cells exposed to 0.25 mg/ml polyacrylate.
PaCu (1–3): cells exposed to 0.25 mg/ml polyacrylate + 150 μM copper sulfate.

Table 2
Enzyme activities.

Enzyme†	control	Copper ion	Polyacrylate	Polyacrylate + Cu
AATC	3.92 ± 0.58	4.08 ± 0.95	4.33 ± 0.63	5.33 ± 0.63*,§
enolase	281 ± 13	257 ± 5§	213 ± 21*,§	131 ± 7**,§
GAPDH	94 0.2 ± 7.1	94.5 ± 8.2	88.9 ± 4.3	78.2 ± 3.5*,§
LDH	108 ± 1	110 ± 9	104 ± 8	97 ± 11§
LGUL	27.9 ± 1.7	30.3 ± 1.1	35.9 ± 2.7*,§	31.7 ± 1.8§
MDH	41.8 ± 2.8	37.7 ± 1.6	37.3 ± 0.8§	31.7 ± 2.0*,§
PNPH	15.8 ± 2.2	23.4 ± 2*,§	12.5 ± 2	13.7 ± 4.5
TALDO	20.4 ± 0.5	21.1 ± 0.6	23.1 ± 1.1*,§	20.1 ± 1.1

All activities are expressed in nmole substrate converted/min/mg total protein.
† Enzymes full names: aatc: aspartate aminotransferase; GAPDH: glyceraldehyde phosphate dehydrogenase; LDH: lactate dehydrogenase; LGUL: lactoylglutathione lyase; MDH: malate dehydrogenase; PNPH: purine nucleotide phosphorylase; TALDO: transaldolase.
* $p < 0.05$ in the treated vs control comparison (Student *t*-test).
** $p < 0.01$ in the treated vs control comparison (Student *t*-test).
§ $p < 0.05$ in the treated vs control comparison (Mann Whitney U test).

homeostasis [64]. In this frame, the observed increase of the copper concentration in the particulate fraction (containing mitochondria) after a 4 h exposure to copper ion (Table 1) strongly suggests an increase in intramitochondrial copper concentration, with potential deleterious effects. We thus investigated the global functioning of mitochondria by probing the transmembrane mitochondrial potential. The results, shown on Fig. 4, indicated a small but significant ($p < 0.01$) reduction in the proportion of rhodamine-positive cells upon treatment with copper-polyacrylate complex, suggesting a decreased viability induced by this treatment. This was in line with the known slight mortality induced by the copper-polyacrylate treatment.

In addition, it should be noted that most of the significant changes in

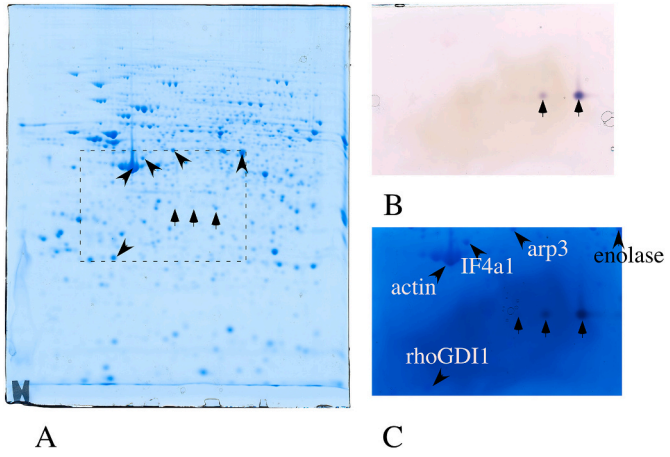

Fig. 3. Assignment of active protein forms for malate dehydrogenase activity. 500 μg of total cellular extract from control cells were loaded on two 2D gels run in parallel. One gel was directly stained by colloidal Coomassie blue (A). On the unstained second gel, a gel piece was cut according to the dashed rectangle drawn on the stained gel. The gel piece was then submitted to in gel renaturation and then detection of the malate dehydrogenase activity (B), and finally to counterstaining by colloidal Coomassie blue (C).
Vertical arrows: position of the malate dehydrogenase spots arroweads: landmark proteins.

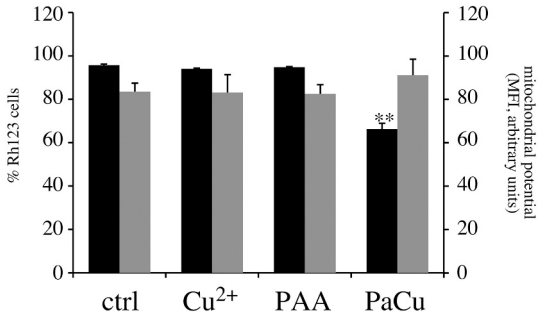

Fig. 4. Analysis of the mitochondrial transmembrane potential.
The mitochondrial potential was analyzed by the rhodamine 123 accumulation method.
black bars: proportion of positive cells in the viable cell population.
grey bars: mean cellular fluorescence.
Ctrl: unexposed cells.
Cu^{2+}: cells exposed to 150 μM copper sulfate.
PAA: cells exposed to 0.25 mg/ml polyacrylate.
PaCu: cells exposed to 0.25 mg/ml polyacrylate + 150 μM copper sulfate.
Symbols indicate the statistical significance (Student *t*-test): *: $p < 0.05$; **:$p < 0.01$; ***: $p < 0.001$.

the amounts of mitochondrial proteins induced by the various treatments are increases. This strongly suggests that these increases are a compensatory mechanism set in place by the cells to maintain mitochondrial function in spite of the increased copper content, explaining the constant transmembrane mitochondrial potential that we observed. Interestingly, the type of effects (reduction in proportion of rhodamine-positive cells, no effect on the value of the transmembrane mitochondrial potential) were also observed with the hydroxyquinoline-copper complex [27].

3.7. The reduced glutathione level is decreased by copper

One of the proteins that was strongly induced after treatment with copper ion or copper-polacrylate complex was GCLM, i.e. the regulatory subunit of the enzyme involved in the first step of glutathione

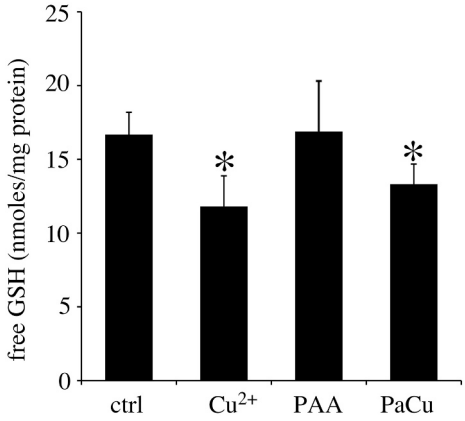

Fig. 5. Glutathione levels.
The glutathione level was measured by the CDNB conjugation method, and normalized to the protein content of the cells.
Ctrl: unexposed cells.
Cu^{2+}: cells exposed to 150 μM copper sulfate.
PAA; cells exposed to 0.25 mg/ml polyacrylate.
PaCu: cells exposed to 0.25 mg/ml polyacrylate +150 μM copper sulfate.
Symbols indicate the statistical significance (Student *t*-test): *: $p < 0.05$; **:$p < 0.01$; ***: $p < 0.001$.

biosynthesis, which is the limiting step of the pathway [65]. We thus investigated the levels of free glutathione, as previous studies have shown a reduction in the levels of free glutathione upon treatment of macrophages with copper-quinoline complexes [27] or copper oxide nanoparticles [38]. The results, shown on Fig. 5, indicated a significant reduction upon treatment with copper or copper complex, but not with polyacrylate alone, following the trend indicated by GCLM expression. Thus copper in all its forms i.e. ionic, as a polyacrylate complex (this study), as a hydroxyquinoline complex [27] or as nanoparticles [38], induces a decrease in the cellular content of free glutathione.

3.8. The actin cytoskeleton and phagocytic activity are altered by treatment with polyacrylate and copper-polyacrylate

The proteomic screen (Table 2) and the pathway analysis pointed to actin cytoskeleton as one of the major modulated function upon copper treatment, for example through proteins involved in cell shape, adhesion and motility (Suppl Tables 6 & 8). As a change in COATL detected by proteomics correlated with changes in the actin cytoskeleton [66], this prompted us to test how actin cytoskeleton responded to the treatments used in this study. The results, shown on Fig. 6 A–D, indicated a minimal effect of copper ion on the actin cytoskeleton and especially on the membrane spikes, which were more decreased upon treatment with polyacrylate and even more upon treatment with the copper-polyacrylate complex.

Phagocytosis is one of the major functions of macrophages, and depends on the actomyosin system. We thus tested this function, as changes in lysosomes-associated proteins were also observed. The results, on Fig. 6E, indicated no effect of copper ion but an important and similar effect of polyacrylate and copper-polyacrylate complex, both in the proportion of phagocytic cells and in the phagocytic capacity of the phagocytic cells.

Combined with previous results obtained on copper ion and nanoparticles [38], these results clearly show that copper ion at subtoxic concentrations has no impact on phagocytosis. An impact is obtained only when the endosomal/lysosomal pathway is at play, either by a polymer binding to the scavenger receptor (polyacrylate here) or by nanoparticles [38]. These nanoparticles do not need to contain copper, as silica nanoparticles or carbon nanotubes also induce a decrease in the phagocytic activity [40,67,68]. The only case in which an effect of copper on phagocytosis without being macromolecular or particular is as a hydroxyquinoline complex [27]. In this case however, we do not know whether the hydroxyquinoline ionophore brings copper only in the cytosol or is also able to bring copper into the endosomes.

In the frame of this study, it is also worth noting that a fair proportion of the proteins that are selectively and significantly modulated by the

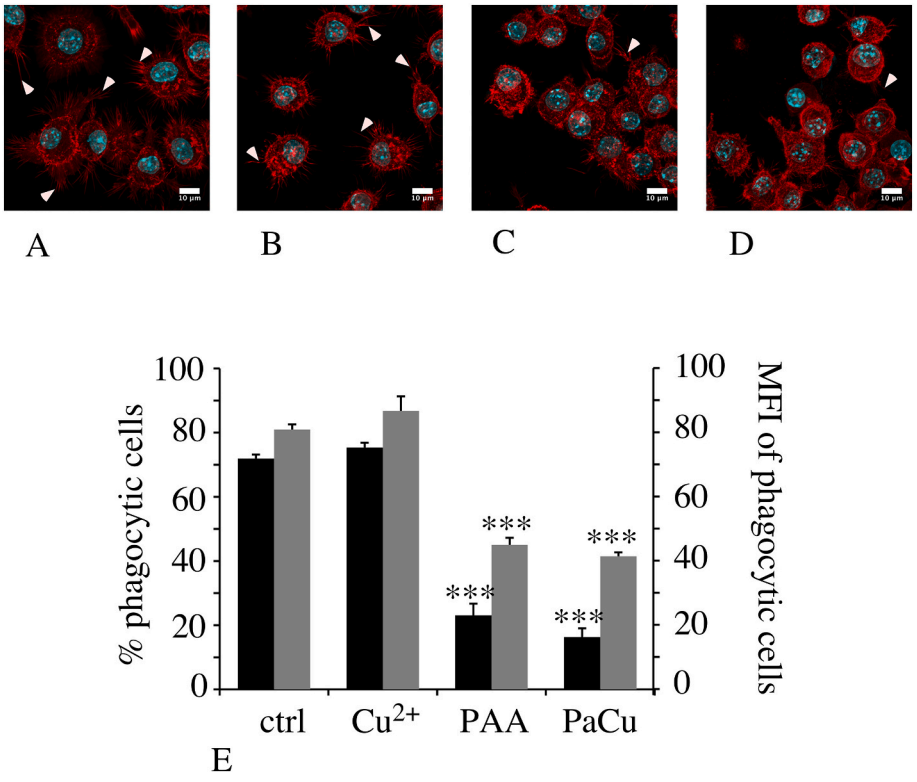

Fig. 6. : Actin cytoskeleton and phagocytosis.
In panels A–D, the actin cytoskeleton was visualized with fluorescent phalloidin and confocal microscopy. Only one confocal plane inside the cells is shown (going through the cell nucleus) Examples of membrane spikes are indicated by white arrowheads.
A: unexposed cells.
B: cells exposed to 150 μM copper sulfate.
C; cells exposed to 0.25 mg/ml polyacrylate.
D: cells exposed to 0.25 mg/ml polyacrylate +150 μM copper sulfate.
In panel E, the phagocytic capacity was assessed by fluorescent latex beads internalization.
Black bars: proportion of positive cells in the viable cell population.
Grey bars: mean cellular fluorescence.
Ctrl: unexposed cells.
Cu^{2+}: cells exposed to 150 μM copper sulfate.
PAA; cells exposed to 0.25 mg/ml polyacrylate.
PaCu: cells exposed to 0.25 mg/ml polyacrylate +150 μM copper sulfate.
Symbols indicate the statistical significance (Student t-test): *: $p < 0.05$; **:$p < 0.01$; ***: $p < 0.001$.

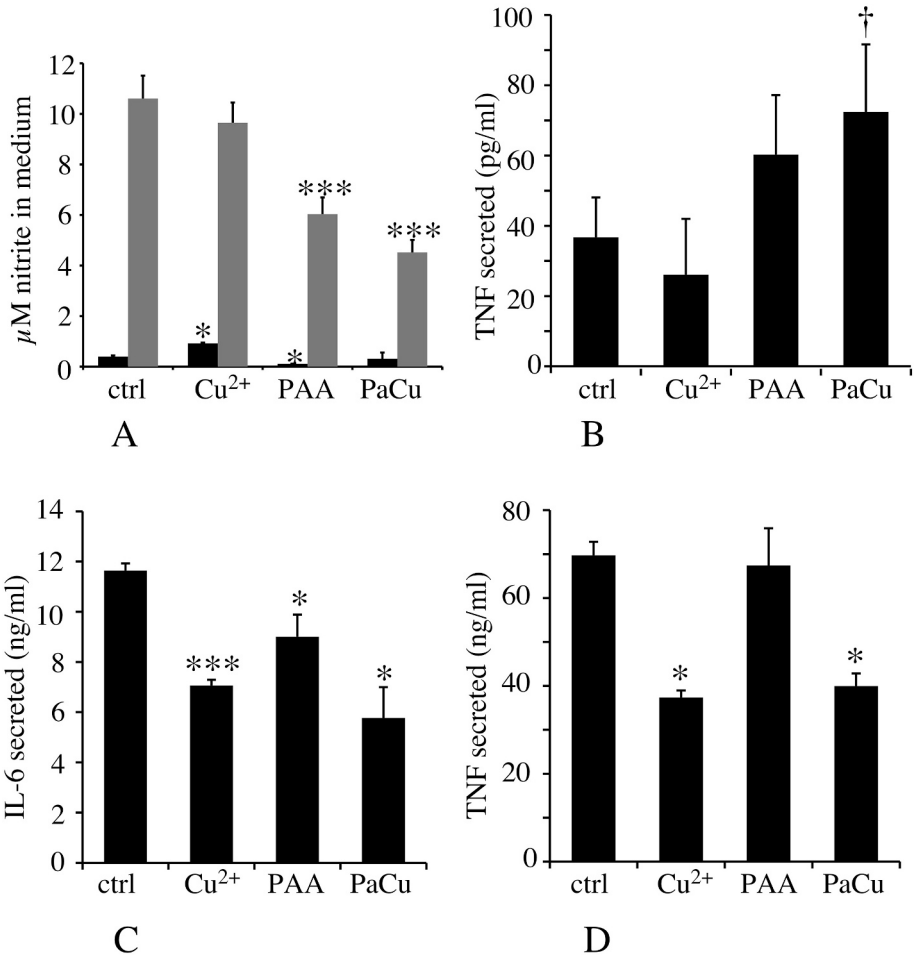

Fig. 7. Inflammatory responses.
The secretion of NO, Interleukin-6 and TNF alpha was measured in response to either copper alone, or to both copper and LPS.
Ctrl: unexposed cells.
Cu^{2+}: cells exposed to 150 µM copper sulfate.
PAA; cells exposed to 0.25 mg/ml polyacrylate.
PaCu: cells exposed to 0.25 mg/ml polyacrylate +150 µM copper sulfate.
A: Production of nitric oxide.
Black bars: production after treatment for 24 h with copper and/or polyacrylate.
grey bars: production after treatment for 24 h with copper and/or polyacrylate and stimulation with LPS for the last 18 h of culture.
B: production of TNF in absence of LPS stimulation.
C: production of interleukin-6 in the presence of LPS stimulation.
(no interleukin-6 secretion was detected in the absence of LPS stimulation)
D: production of TNF in the presence of LPS stimulation.
Symbols indicate the statistical significance (Student t-test): *: $p < 0.05$; **:$p < 0.01$; ***: $p < 0.001$. † $p < 0.05$ in the Mann-Whitney *U* test.

copper-polyacrylate treatment (Suppl. Table 5) are cytoskeletal proteins, which correlates well with the massive alteration of the cytoskeleton observed upon treatment with the copper complex.

Taken at a higher level, cell shape and cytoskeleton involve a large number of proteins. This suggests that important changes in cell shape such as those observed in response to polyacrylate and copper-polyacrylate involve a large number of changes at the protein level or at the proteoform level, as many proteins involved in the cytoskeleton are controlled by phosphorylation (e.g. cofilin [69], Rho GDIs [70], arpc5 [71], gelsolin [72] or Arp2 [73]). Consequently, many coordinated changes of maybe weak amplitude can be expected when cell shape changes. This may explain why such changes are strongly detected in the global proteomic data screening (i.e. hierarchical clustering) but not as easily by individual protein detection.

3.9. The inflammatory responses are altered in a complex way by copper and by polyacrylate

Although inflammatory responses did not appear in the pathway analysis, analysis of the proteomic data showed modulations of several proteins pointing at potential changes in the inflammatory responses upon exposure to copper and/or polyacrylate. For example, 2D gel-based proteomics highlighted modulations of nmrl1 (Q8K2T1), tollip (Q9QZ06), vps29 (Q9QZ88) and latexin (P70202). This prompted us to investigate the inflammatory responses with and without an additional stimulation by LPS. Responses without LPS stimulation point at the intrinsic effects of the treatments with copper and/or polyacrylate, while responses with LPS stimulation point at the interference of the treatments with the responses of macrophages to bacteria. The results, shown on Fig. 7, indicate no effect of polyacrylate (except for LPS-induced NO and IL-6 production), but effects of copper. Rather surprisingly, basal production of NO and TNF followed opposite trends. NO production was induced upon treatment with copper ion and reduced upon treatment with polyacrylate±copper (Fig. 7A, black bars), while the opposite was observed for TNF (Fig. 7B). An increase in NO production was also observed upon treatment with the hydroxyquinoline-copper complex and with hydroxyquinoline alone [27] . This exemplifies another case in which the ancillary molecule used to modulate copper entry had an intrinsic effect, just as polyacrylate alone for phagocytosis. These results also showed that copper polyacrylate did not behave as other forms of copper for NO production.

In the case of LPS-induced secretions, pre-treatment with copper ion or copper complex always induced a decrease in the production of pro-inflammatory mediators, whether NO (Fig. 7A, grey bars) or interleukin 6 (Fig. 7C) or TNF (Fig. 7D). This decrease of NO production after LPS stimulation has been already observed on another macrophage cell line with copper ion, copper oxide nanoparticles [38] and hydroxyquinoline-copper complex [27]. Of note, polyacrylate alone also induced a decrease in the response to LPS, both for NO (Fig. 7A, grey bars) and for interleukin 6 (Fig. 7C), but not for TNF (Fig. 7D). Such decoupled responses for NO, interleukin 6 and TNF after LPS stimulation has been observed for silver and silica nanoparticles [56,57], which both enter macrophages using scavenger receptor [74,75], as polyacrylate [43].

4. Concluding remarks

Together with previous work carried out under slightly different

conditions on the hydroxyquinoline-copper complex [27] or on copper nanoparticles [38], this work allows comparing the effects of copper ion under three different entry modes, i.e. as ion alone, hydroxyquinoline-copper complex and copper-polyacrylate complex. Some basic responses are shared by all entry modes, such as the decrease in the free glutathione concentration or the maintaining of the mitochondrial transmembrane potential, at least under sub-toxic conditions. Some differentiated responses of the macrophages are also shared by all forms of copper ion, such as the reduction in the LPS-induced NO production.

Conversely, different responses can be observed with different forms of copper. For example, a reduction in the phagocytic capacity is observed with both copper complexes but not with copper ion. Even more specifically, central metabolic enzyme activities (except enolase) are altered by the copper-polyacrylate complex but not with copper ion. These differential responses cannot be simply attributed to intracellular copper levels, as these are not significantly different between copper ion and copper-polyacrylate complex. Thus, subtle differences in the entry mode of copper or synergies with the polyacrylate carrier may explain these differences, although the molecular details underlying these differences are still unclear.

Supplementary data to this article can be found online at https://doi.org/10.1016/j.jprot.2021.104178.

Credit author statement

JD, AT and SR performed the copper assay experiments. BD performed the phagocytosis, inflammatory response, confocal microscopy and mitochondrial potential experiments. VCF and TR performed the 2D gel experiments. TR performed the glutathione assay experiments. JB, HD, CC and SC performed and reviewed the mass spectrometry experiments. TR prepared the initial draft of the manuscript, which was reviewed and amended by all co-authors.

Acknowledgments

This work was funded by the CNRS and the University Grenoble-Alpes. This work used the platforms of the French Proteomic Infrastructure (ProFI) project (grant ANR-10-INBS-08-03) and of GRAL, a programme from the Chemistry Biology Health (CBH) Graduate School of University Grenoble Alpes (ANR-17-EURE-0003).On a more scientific level, the authors would like to thank the curators of the Swissprot database for the quality of their functional annotations, which made the exploitation of the proteomic data much more fruitful and straightforward.

Declaration of competing interest

The authors declare no conflict of interest.

Data availability

Data are available in supplementary material

References

[1] P.C. Bull, D.W. Cox, Wilson disease and Menkes disease: new handles on heavy-metal transport, Trends Genet. 10 (1994) 246–252.
[2] B. Dixon, Pushing Bordeaux mixture, Lancet Infect. Dis. 4 (2004) 594.
[3] J.C. Pimentel, A.P. Menezes, Liver granulomas containing copper in vineyard sprayer's lung. A new etiology of hepatic granulomatosis, Am. Rev. Respir. Dis. 111 (1975) 189–195.
[4] K.G. Daniel, P. Gupta, R.H. Harbach, W.C. Guida, Q.P. Dou, Organic copper complexes as a new class of proteasome inhibitors and apoptosis inducers in human cancer cells, Biochem. Pharmacol. 67 (2004) 1139–1151.
[5] K.G. Daniel, D. Chen, S. Orlu, Q.C. Cui, F.R. Miller, Q.P. Dou, Clioquinol and pyrrolidine dithiocarbamate complex with copper to form proteasome inhibitors and apoptosis inducers in human breast cancer cells, Breast Cancer Res. 7 (2005) R897–R908.
[6] D. Chen, Q.P. Dou, New uses for old copper-binding drugs: converting the pro-angiogenic copper to a specific cancer cell death inducer, Expert Opin. Ther. Targets 12 (2008) 739–748.
[7] M.J. Petris, K. Smith, J. Lee, D.J. Thiele, Copper-stimulated endocytosis and degradation of the human copper transporter, hCtr1, J. Biol. Chem. 278 (2003) 9639–9646.
[8] V. Oliveri, V. Lanza, D. Milardi, M. Viale, I. Maric, C. Sgarlata, G. Vecchio, Amino- and chloro-8-hydroxyquinolines and their copper complexes as proteasome inhibitors and antiproliferative agents, Metallomics 9 (2017) 1439–1446.
[9] U. Jungwirth, C.R. Kowol, B.K. Keppler, C.G. Hartinger, W. Berger, P. Heffeter, Anticancer activity of metal complexes: involvement of redox processes, Antioxid. Redox Signal. 15 (2011) 1085–1127.
[10] J.L. Allensworth, M.K. Evans, F. Bertucci, A.J. Aldrich, R.A. Festa, P. Finetti, N. T. Ueno, R. Safi, D.P. McDonnell, D.J. Thiele, S. Van Laere, G.R. Devi, Disulfiram (DSF) acts as a copper ionophore to induce copper-dependent oxidative stress and mediate anti-tumor efficacy in inflammatory breast cancer, Mol. Oncol. 9 (2015) 1155–1168.
[11] M. Amici, K. Forti, C. Nobili, G. Lupidi, M. Angeletti, E. Fioretti, A.M. Eleuteri, Effect of neurotoxic metal ions on the proteolytic activities of the 20S proteasome from bovine brain, J. Biol. Inorg. Chem. 7 (2002) 750–756.
[12] M.A. Cater, H.B. Pearson, K. Wolyniec, P. Klaver, M. Bilandzic, B.M. Paterson, A. I. Bush, P.O. Humbert, S. La Fontaine, P.S. Donnelly, Y. Haupt, Increasing intracellular bioavailable copper selectively targets prostate cancer cells, ACS Chem. Biol. 8 (2013) 1621–1631.
[13] E.E. Manasanch, R.Z. Orlowski, Proteasome inhibitors in cancer therapy, Nat. Rev. Clin. Oncol. 14 (2017) 417–433.
[14] F.N. Akladios, S.D. Andrew, C.J. Parkinson, Selective induction of oxidative stress in cancer cells via synergistic combinations of agents targeting redox homeostasis, Bioorg. Med. Chem. 23 (2015) 3097–3104.
[15] S. Chatterjee, P. Chakraborty, K. Banerjee, A. Sinha, A. Adhikary, T. Das, S. K. Choudhuri, Selective induction of apoptosis in various cancer cells irrespective of drug sensitivity through a copper chelate, copper N-(2 hydroxy acetophenone) glycinate: crucial involvement of glutathione, Biometals. 26 (2013) 517–534.
[16] D. Denoyer, H.B. Pearson, S.A. Clatworthy, Z.M. Smith, P.S. Francis, R.M. Llanos, I. Volitakis, W.A. Phillips, P.M. Meggyesy, S. Masaldan, M.A. Cater, Copper as a target for prostate cancer therapeutics: copper-ionophore pharmacology and altering systemic copper distribution, Oncotarget 7 (2016) 37064–37080.
[17] W. Zou, Immunosuppressive networks in the tumour environment and their therapeutic relevance, Nat. Rev. Cancer 5 (2005) 263–274.
[18] S.L. Shiao, A.P. Ganesan, H.S. Rugo, L.M. Coussens, Immune microenvironments in solid tumors: new targets for therapy, Genes Dev. 25 (2011) 2559–2572.
[19] E.V. Polishchuk, R.S. Polishchuk, The emerging role of lysosomes in copper homeostasis, Metallomics 8 (2016) 853–862.
[20] H. Ohrvik, B. Logeman, G. Noguchi, I. Eriksson, L. Kjellen, D.J. Thiele, G. Pejler, Ctr2 regulates mast cell maturation by affecting the storage and expression of tryptase and proteoglycans, J. Immunol. 195 (2015) 3654–3664.
[21] P.V. van den Berghe, D.E. Folmer, H.E. Malingre, E. van Beurden, A.E. Klomp, B. van de Sluis, M. Merkx, R. Berger, L.W. Klomp, Human copper transporter 2 is localized in late endosomes and lysosomes and facilitates cellular copper uptake, Biochem. J. 407 (2007) 49–59.
[22] J. George, R. Singh, Z. Mahmood, Y. Shukla, Toxicoproteomics: new paradigms in toxicology research, Toxicol. Mech. Methods 20 (2010) 415–423.
[23] T. Rabilloud, P. Lescuyer, Proteomics in mechanistic toxicology: history, concepts, achievements, caveats, and potential, Proteomics. 15 (2015) 1051–1074.
[24] S. Suman, S. Mishra, Y. Shukla, Toxicoproteomics in human health and disease: an update, Expert Rev. Proteomics 13 (2016) 1073–1089.
[25] G. Repetto, A. del Peso, J.L. Zurita, Neutral red uptake assay for the estimation of cell viability/cytotoxicity, Nat. Protoc. 3 (2008) 1125–1131.
[26] T. Rabilloud, Optimization of the cydex blue assay: a one-step colorimetric protein assay using cyclodextrins and compatible with detergents and reducers, PLoS One 13 (2018), e0195755.
[27] B. Dalzon, J. Bons, H. Diemer, V. Collin-Faure, C. Marie-Desvergne, M. Dubosson, S. Cianferani, C. Carapito, T. Rabilloud, A proteomic view of cellular responses to anticancer quinoline-copper complexes, Proteomes. 7 (2019) 26.
[28] J.A. Vizcaino, A. Csordas, N. Del-Toro, J.A. Dianes, J. Griss, I. Lavidas, G. Mayer, Y. Perez-Riverol, F. Reisinger, T. Ternent, Q.W. Xu, R. Wang, H. Hermjakob, 2016 update of the PRIDE database and its related tools, Nucleic Acids Res. 44 (2016) 11033.
[29] O. Hammer, D.A.T. Harper, P.D. Ryan, Paleontological statistics software package for education and data analysis, Palaeontol. Electron. 4 (2001) (9 pp.).
[30] K.M. Mayer, F.H. Arnold, A colorimetric assay to quantify dehydrogenase activity in crude cell lysates, J. Biomol. Screen. 7 (2002) 135–140.
[31] P.D. Simcox, E.E. Reid, D.T. Canvin, D.T. Dennis, Enzymes of the glycolytic and pentose phosphate pathways in proplastids from the developing endosperm of *Ricinus communis* L, Plant Physiol. 59 (1977) 1128–1132.
[32] P. Fossati, Phosphate determination by enzymatic colorimetric assay, Anal. Biochem. 149 (1985) 62–65.
[33] V.E. Anderson, P.M. Weiss, W.W. Cleland, Reaction intermediate analogues for enolase, Biochemistry 23 (1984) 2779–2786.
[34] C. Salerno, J. Ovádi, T. Keleti, P. Fasella, Kinetics of coupled reactions catalyzed by aspartate aminotransferase and glutamate dehydrogenase, Eur. J. Biochem. 121 (1982) 511–517.
[35] B. Mannervik, B. Gorna-Hall, T. Bartfai, The steady-state kinetics of glyoxalase I from porcine erythrocytes. Evidence for a random-pathway mechanism involving one- and two-substrate branches, Eur. J. Biochem. 37 (1973) 270–281.

[36] R.E. Manrow, R.P. Dottin, Demonstration, by renaturation in O'Farrell gels, of heterogeneity in Dictyostelium uridine diphosphoglucose pyrophosphorylase, Anal. Biochem. 120 (1982) 181–188.
[37] G. Abel, J. Szollosi, J. Fachet, Phagocytosis of fluorescent latex microbeads by peritoneal macrophages in different strains of mice: a flow cytometric study, Eur. J. Immunogenet. 18 (1991) 239–245.
[38] S. Triboulet, C. Aude-Garcia, M. Carriere, H. Diemer, F. Proamer, A. Habert, M. Chevallet, V. Collin-Faure, J.M. Strub, D. Hanau, A. Van Dorsselaer, N. Herlin-Boime, T. Rabilloud, Molecular responses of mouse macrophages to copper and copper oxide nanoparticles inferred from proteomic analyses, Mol. Cell. Proteomics 12 (2013) 3108–3122.
[39] C. Aude-Garcia, B. Dalzon, J.L. Ravanat, V. Collin-Faure, H. Diemer, J.M. Strub, S. Cianferani, A. Van Dorsselaer, M. Carriere, T. Rabilloud, A combined proteomic and targeted analysis unravels new toxic mechanisms for zinc oxide nanoparticles in macrophages, J. Proteome 134 (2016) 174–185.
[40] B. Dalzon, C. Aude-Garcia, V. Collin-Faure, H. Diemer, D. Béal, F. Dussert, D. Fenel, G. Schoehn, S. Cianférani, M. Carrière, T. Rabilloud, Differential proteomics highlights macrophage-specific responses to amorphous silica nanoparticles, Nanoscale 9 (2017) 9641–9658.
[41] S.W. Perry, J.P. Norman, J. Barbieri, E.B. Brown, H.A. Gelbard, Mitochondrial membrane potential probes and the proton gradient: a practical usage guide, Biotechniques 50 (2011) 98–115.
[42] M. Warholm, C. Guthenberg, C. von Bahr, B. Mannervik, Glutathione transferases from human liver, Methods Enzymol. 113 (1985) 499–504.
[43] M. Fujiwara, J.D. Baldeschwieler, R.H. Grubbs, Receptor-mediated endocytosis of poly(acrylic acid)-conjugated liposomes by macrophages, Biochim. Biophys. Acta 1278 (1996) 59–67.
[44] J.H. Kaplan, E.B. Maryon, How mammalian cells acquire copper: an essential but potentially toxic metal, Biophys. J. 110 (2016) 7–13.
[45] A. Espinoza, S. Le Blanc, M. Olivares, F. Pizarro, M. Ruz, M. Arredondo, Iron, copper, and zinc transport: inhibition of divalent metal transporter 1 (DMT1) and human copper transporter 1 (hCTR1) by shRNA, Biol. Trace Elem. Res. 146 (2012) 281–286.
[46] T. Sone, K. Yamaoka, Y. Minami, H. Tsunoo, Induction of metallothionein synthesis in Menkes' and normal lymphoblastoid cells is controlled by the level of intracellular copper, J. Biol. Chem. 262 (1987) 5878–5885.
[47] S.D. Smith, Y.M. She, E.A. Roberts, B. Sarkar, Using immobilized metal affinity chromatography, two-dimensional electrophoresis and mass spectrometry to identify hepatocellular proteins with copper-binding ability, J. Proteome Res. 3 (2004) 834–840.
[48] C. Chen, Y. Song, K. Zhuang, L. Li, Y. Xia, Z. Shen, Proteomic analysis of copper-binding proteins in excess copper-stressed roots of two rice (*Oryza sativa* L.) varieties with different Cu tolerances, PLoS One 10 (2015) e0125367.
[49] M. Salim, B.A. Brown-Kipphut, M.D. Maines, Human biliverdin reductase is autophosphorylated, and phosphorylation is required for bilirubin formation, J. Biol. Chem. 276 (2001) 10929–10934.
[50] Y. Xiong, K.L. Guan, Mechanistic insights into the regulation of metabolic enzymes by acetylation, J. Cell Biol. 198 (2012) 155–164.
[51] H. Weber, S. Engelmann, D. Becher, M. Hecker, Oxidative stress triggers thiol oxidation in the glyceraldehyde-3-phosphate dehydrogenase of *Staphylococcus aureus*, Mol. Microbiol. 52 (2004) 133–140.
[52] P. Tarroux, Analysis of protein-patterns during differentiation using 2-D electrophoresis and computer multidimensional classification, Electrophoresis 4 (1983) 63–70.
[53] P. Tarroux, P. Vincens, T. Rabilloud, Hermes - a 2nd generation approach to the automatic-analysis of two-dimensional electrophoresis gels.5. Data-analysis, Electrophoresis. 8 (1987) 187–199.
[54] T. Pun, D.F. Hochstrasser, R.D. Appel, M. Funk, V. Villars-Augsburger, C. Pellegrini, Computerized classification of two-dimensional gel electrophoretograms by correspondence analysis and ascendant hierarchical clustering, Appl. Theor. Electrophor. 1 (1988) 3–9.
[55] B. Dalzon, A. Torres, H. Diemer, S. Ravanel, V. Collin-Faure, K. Pernet-Gallay, P.-H. Jouneau, J. Bourguignon, Sarah Sanglier-Cianférani, M. Carriere, C. Aude-Garcia, T. Rabilloud, How reversible are the effects of silver nanoparticles on macrophages? A proteomic-instructed view, Environ. Sci. Nano 6 (2019) 3133–3157.
[56] B. Dalzon, C. Aude-Garcia, H. Diemer, J. Bons, C. Marie-Desvergne, J. Pérard, M. Dubosson, V. Collin-Faure, C. Carapito, S. Cianférani, M. Carrière, T. Rabilloud, The longer the worse: a combined proteomic and targeted study of the long-term *versus* short-term effects of silver nanoparticles on macrophages, Environ. Sci. Nano 7 (2020) 2032–2046.
[57] A. Torres, B. Dalzon, V. Collin-Faure, H. Diemer, D. Fenel, G. Schoehn, S. Cianférani, M. Carrière, T. Rabilloud, How reversible are the effects of fumed silica on macrophages? A proteomics-informed view, Nanomaterials (Basel) 10 (2020) 1939.
[58] D.W. Huang, B.T. Sherman, R.A. Lempicki, Bioinformatics enrichment tools: paths toward the comprehensive functional analysis of large gene lists, Nucleic Acids Res. 37 (2009) 1–13.
[59] T. Rabilloud, P. Lescuyer, The proteomic to biology inference, a frequently overlooked concern in the interpretation of proteomic data: a plea for functional validation, Proteomics 14 (2014) 157–161.
[60] K. Marcus, T. Rabilloud, How do the different proteomic strategies cope with the complexity of biological regulations in a multi-omic world? Critical appraisal and suggestions for improvements, Proteomes 8 (2020) 23.
[61] J. Bons, C. Macron, C. Aude-Garcia, S.A. Vaca-Jacome, M. Rompais, S. Cianferani, C. Carapito, T. Rabilloud, A combined N-terminomics and shotgun proteomics approach to investigate the responses of human cells to rapamycin and zinc at the mitochondrial level, Mol. Cell. Proteomics 18 (2019) 1085–1095.
[62] J.V. Olsen, M. Vermeulen, A. Santamaria, C. Kumar, M.L. Miller, L.J. Jensen, F. Gnad, J. Cox, T.S. Jensen, E.A. Nigg, S. Brunak, M. Mann, Quantitative phosphoproteomics reveals widespread full phosphorylation site occupancy during mitosis, Sci. Signal. 3 (2010) ra3.
[63] J. Fang, S. Qiao, K. Wang, R. Li, L. Wang, H. Li, G. Zhang, Quantitative proteomic analysis of global protein acetylation in PRRSV-infected pulmonary alveolar macrophages, Proteomics (2020) e2000019.
[64] Z.N. Baker, P.A. Cobine, S.C. Leary, The mitochondrion: a central architect of copper homeostasis, Metallomics 9 (2017) 1501–1512.
[65] Y. Chen, H.G. Shertzer, S.N. Schneider, D.W. Nebert, T.P. Dalton, Glutamate cysteine ligase catalysis: dependence on ATP and modifier subunit for regulation of tissue glutathione levels, J. Biol. Chem. 280 (2005) 33766–33774.
[66] C. D'Anna, D. Cigna, C. Di Sano, S. Di Vincenzo, P. Dino, M. Ferraro, L. Bini, L. Bianchi, F. Di Gaudio, M. Gjomarkaj, E. Pace, Exposure to cigarette smoke extract and lipopolysaccharide modifies cytoskeleton organization in bronchial epithelial cells, Exp. Lung Res. 43 (2017) 347–358.
[67] R. Wang, M. Lee, K. Kinghorn, T. Hughes, I. Chuckaree, R. Lohray, E. Chow, P. Pantano, R. Draper, Quantitation of cell-associated carbon nanotubes: selective binding and accumulation of carboxylated carbon nanotubes by macrophages, Nanotoxicology 12 (2018) 677–698.
[68] A. Torres, B. Dalzon, V. Collin-Faure, T. Rabilloud, Repeated vs. acute exposure of RAW264.7 mouse macrophages to silica nanoparticles: a bioaccumulation and functional change study, Nanomaterials 10 (2020) 215.
[69] N. Yang, O. Higuchi, K. Ohashi, K. Nagata, A. Wada, K. Kangawa, E. Nishida, K. Mizuno, Cofilin phosphorylation by LIM-kinase 1 and its role in Rac-mediated actin reorganization, Nature. 393 (1998) 809–812.
[70] C. DerMardirossian, G. Rocklin, J.-Y. Seo, G.M. Bokoch, Phosphorylation of RhoGDI by Src regulates Rho GTPase binding and cytosol-membrane cycling, Mol. Biol. Cell 17 (2006) 4760–4768.
[71] R. Silverman-Gavrila, L. Silverman-Gavrila, G. Hou, M. Zhang, M. Charlton, M. P. Bendeck, Rear polarization of the microtubule-organizing center in neointimal smooth muscle cells depends on PKCα, ARPC5, and RHAMM, Am. J. Pathol. 178 (2011) 895–910.
[72] P. Singaravelu, W.L. Lee, S. Wee, U. Ghoshdastider, K. Ding, J. Gunaratne, J. M. Grimes, K. Swaminathan, R.C. Robinson, Yersinia effector protein (YopO)-mediated phosphorylation of host gelsolin causes calcium-independent activation leading to disruption of actin dynamics, J. Biol. Chem. 292 (2017) 8092–8100.
[73] L.L. LeClaire, M. Baumgartner, J.H. Iwasa, R.D. Mullins, D.L. Barber, Phosphorylation of the Arp2/3 complex is necessary to nucleate actin filaments, J. Cell Biol. 182 (2008) 647–654.
[74] J.H. Shannahan, R. Podila, A.A. Aldossari, H. Emerson, B.A. Powell, P.C. Ke, A. M. Rao, J.M. Brown, Formation of a protein corona on silver nanoparticles mediates cellular toxicity via scavenger receptors, Toxicol. Sci. 143 (2015) 136–146.
[75] G.A. Orr, W.B. Chrisler, K.J. Cassens, R. Tan, B.J. Tarasevich, L.M. Markillie, R. C. Zangar, B.D. Thrall, Cellular recognition and trafficking of amorphous silica nanoparticles by macrophage scavenger receptor A, Nanotoxicology 5 (2011) 296–311.

Conclusion

Cette étude a permis de mettre en évidence les réponses de la cellule en fonction du type de cuivre utilisé. En effet, certains effets sont communs aux ions et au complexe de polyacrylate. Tout d'abord, l'internalisation du cuivre libre ou complexé est équivalente après 24h d'exposition, et la quantité de cuivre dosée dans les cellules est similaire, donc les effets observés ne sont pas dus à une quantité différente de cuivre intracellulaire. Les études de protéomique ont montré que le protéasome, le métabolisme du carbone et les mitochondries sont modifiés par l'exposition au cuivre (ion et complexe). L'activité de l'énolase est diminuée par l'exposition au cuivre et au polyacrylate. L'ion cuivre modifie également l'activité de la purine phosphorylase et le complexe de cuivre altère l'aspartate aminotransférase, le glycéraldéhyde dehydrogenase et la lactate déshydrogénase. La quantité de glutathion libre est réduite par l'exposition au cuivre (complexe et ion). Le polyacrylate (seul ou complexé) modifie également le cytosquelette (moins de filaments) et la phagocytose (cellulaires phagocytaires et activité) des cellules traitées. Les réponses inflammatoires intrinsèques sont également modifiées par l'exposition au cuivre (NO : ion, TNF : complexe). La présence de cuivre diminue également la réponse pro-inflammatoire en cas de stimulation au LPS (NO, TNF et IL-6). Cette étude montre également l'importance de tester chaque matériau, car même si les fonctions altérées par l'exposition sont souvent les mêmes (phagocytose, réponse inflammatoire, glutathion réduit) les modifications des réponses sont différentes d'un matériau à l'autre.

Discussion

Cette collaboration entre l'entreprise Solvay et le laboratoire de recherche de Chimie et Biologie des Métaux a permis de réaliser ce travail et le développement de nouveaux systèmes *in vitro*. L'utilisation des macrophages murins était déjà courante, mais elle a été d'autant plus évidente pour l'étude des silices amorphes de synthèse. Les expériences réalisées ont apporté un éclairage sur les éventuels problèmes de santé posés par l'utilisation croissante des nanoparticules de silice. Pour rappel, deux modèles ont été utilisés, (lignées cellulaires J774A.1 et RAW264.7) et 5 types de silices différentes ont également été utilisées (colloïdale, précipitées, silice fluorescente verte et la silice fumée). Ensuite, quatre scénarii d'exposition différents ont été réalisés pour répondre à plusieurs questions : exposition aiguë, exposition de 4 jours, de 10 jours et protocole de récupération.

Nous avons ainsi perfectionné le système existant, en modifiant le type de sérum (fœtal à adulte) et en diminuant sa concentration (10% à 1%) pour les cultures longues (études de persistance et de débit de dose) (Dalzon et al. 2021). L'amélioration de notre système nous a permis de reproduire des expériences menées *in vivo*, et avons obtenus des résultats similaires à ceux de ces études *in vivo*, notamment avec les pigments à base de silice cristalline et les nanofils d'argent. Nous avons également montré que le support de culture utilisé n'influait pas sur la réponse des cellules, ce qui permet d'utiliser librement les lamelles pour la microscopie, les plaques adhérentes pour les cultures longues et les plaques non traitées pour les études d'exposition aiguë (Rios et al. 2021). Le système mis au point a permis d'étudier la persistance d'une exposition à la silice amorphe de synthèse pyrogénée (Torres, Dalzon, Collin-Faure, Diemer, et al. 2020) ainsi qu'aux nanoparticules de fer (Dalzon et al. 2019). Le protocole d'exposition à de faibles doses de SAS durant quatre jours (Torres, Dalzon, Collin-Faure, and Rabilloud 2020) ou dix jours (Torres et al. 2022) a montré les effets du débit de dose et mime l'exposition répétée aux nanomatériaux. Ce dernier scénario a montré qu'il existait une accumulation partielle des SAS dans les cellules grâce à l'utilisation de silice fluorescente mais également aux dosages par ICP-AES. Les différents travaux ont permis de montrer qu'il n'existait pas de déterminants aux effets de la silice. En effet, il est impossible de prédire les effets d'un SAS en fonction de ses caractéristiques physico-chimiques de base : le procédé de fabrication ou la taille des particules primaires, des agrégats ou des agglomérats n'expliquent pas la toxicité, de même que la surface spécifique. Enfin, les doses létales 20 ne sont pas révélatrices de la toxicité des SAS (la DL20 des colloïdales est inférieure à celle des pyrogénées, mais la persistance est moins importante). Pour chacun des scénarii d'exposition testés, le cytosquelette, le métabolisme des cellules (stress oxydant, potentiel mitochondrial, activité lysosomale), et les fonctions cellulaires (phagocytose, sécrétion de cytokine ou d'oxyde nitrique, marqueurs de surface) ont été examinés afin d'évaluer les effets de l'exposition aux SAS sur les macrophages. Dans le cas de la silice, il semble que l'exposition aiguë soit la plus toxique, cependant les effets sont majoritairement réversibles. En effet, les macrophages sont également capables d'éliminer les SAS, probablement par dissolution sous forme de silicates. Ce phénomène explique également la faible sensibilité des macrophages aux expositions répétés aux SAS, et l'accumulation seulement partielle de la silice amorphe. Cependant, l'exposition chronique aux doses modérées de SAS affecte la viabilité des cellules et leur signalisation en cas de rencontre avec des pathogènes. Ceci doit être pris en compte pour sensibiliser les travailleurs industriels aux risques auxquels ils sont exposés. Il faut garder à l'esprit que les macrophages alvéolaires ont une durée de vie de plusieurs mois, et que la dose journalière admissible (DJA) est estimée à 5 mg/m3 dans la fraction alvéolaire, ce qui correspond à 50 mg de silice par jour pour un travailleur. Notre système d'exposition répété prend tout son sens, lorsque l'on constate les effets observés.

Il convient cependant de comparer nos données et notre système à ceux récemment développés dans la littérature scientifique pour étudier les effets suite à une exposition répétée aux NMx.
Ces études sont peu nombreuses, et les systèmes utilisés sont très variés.

Par exemple, l' étude de (Safi et al. 2011) utilise des fibroblastes murins pour étudier les effets de nanofils magnétiques (diamètre de 200nm et longueur de 1 à 40µm). Après 24h d'exposition, ils observent une internalisation des nanofils dans le cytosol ou dans les vésicules, celles-ci sont identifiées comme étant des endosomes grâce à la protéine membranaire Lamp1. Les tests d'activité mitochondriale, de prolifération et de production de ROS ne montrent aucune toxicité des nanofils magnétiques dans les 100h qui suivent l'exposition. De plus, les cellules parviennent à dégrader les nanofils en agrégats plus petits, car les nanofils sont constitués de nanoparticules liées de façon non covalente. Ces résultats apportent de nouvelles perspectives pour la conception des nanomatériaux, mais également pour les tests de toxicologie. En effet, la formation de nanofils à partir de nanoparticules permet une dégradation par les macrophages, sans déclencher de réponse inflammatoire aiguë ou persistante.

Ce système est finalement assez similaire à celui utilisé durant ma thèse, puisqu'il consiste en une exposition de 24h suivie d'une période de récupération sans NMx (dans cette étude 100h, dans notre système 72h). Les tests effectués ensuite permettent d'observer la morphologie des cellules par microscopie, de mesurer la réponse inflammatoire (cytokine ou stress oxydant) et d'observer le devenir des NMx.

Cette autre étude s'intéresse aux nanotubes de carbone (CNTs) auxquelles les cellules épithéliales bronchiques humaines (BEAS-2B) sont exposées une fois par semaine durant 6 semaines (Barthel et al. 2021). Les concentrations choisies varient de 0,125 à 1 µg/cm², les CNTs possèdent des diamètres et longueurs différentes (12nm de diamètre et 400nm de long ou 74 nm et 5,7µm de long). Les deux CNTs induisent des mitoses anormales, la cytotoxicité des longs CNTs est plus rapides que celle des CNTs courts. De plus, après 4 à 6 semaines de traitement, les cellules épithéliales évoluent vers un phénotype de fibroblastes avec une augmentation des marqueurs mésenchymateux N-cadhérine, vimentine et fibronectine. Après 4 semaines de récupération sans CNTs, cette transition est réversible, et cela est plus rapide pour les cellules exposées aux CNTs courts à de faibles concentrations. La principale voie d'exposition est l'inhalation durant la production des CNTs ou bien leur utilisation, elle concerne donc les travailleurs. Or ceux-ci sont amenés à travailler quotidiennement dans un environnement dans lequel des CNTs sont respirables. Le protocole d'exposition utilisé ici ne permet pas d'étudier une exposition quotidienne puisque les cellules sont exposées une fois par semaine (le lundi) et le milieu est rincé ensuite (le vendredi). Cela ne représente pas une exposition réelle aux CNTs, dans le cas des travailleurs.

Un nouveau mouvement des études de toxicologie *in vitro* a pour objectif de développer des systèmes de culture 3D, dans le but de mieux mimer les organes cibles (poumon ou intestin par exemple). Un premier exemple est celui du groupe d'Armelle Baez-Squiban qui utilise des cellules épithéliales humaines bronchiques (NHBE) pour étudier les effets à long terme d'une exposition répétée, en utilisant une interface air-liquide (Boublil et al. 2013). Les cinq semaines suivant l'exposition, les réponses inflammatoires et la différentiation de l'épithélium sont

évaluées. Les nanoparticules persistent dans l'épithélium et induisent une réponse pro-inflammatoire (IL-6 et GM-CSF). Cette exposition chronique nécessite d'être mieux évaluée. Une autre étude utilise ce même système avec deux types d'épithélium alvéolaire, afin de représenter la barrière épithéliale, celle-ci peut être maintenue durant 30 jours, ce qui permettrait d'étudier des effets d'une exposition chronique mais également la persistance de ces effets (Brookes et al. 2021).

Il existe de nombreux autres modèles du système pulmonaire, l'un d'entre eux a été développé par (Radiom, He, et al. 2020). Il s'agit de nanofibres de gélatine sur lesquelles sont cultivées des cellules A549, ce système peut évoluer grâce à une structure flexible qui permet d'espacer ou de rapprocher cette couche de nanofibres de gélatine pour mimer les mouvements pulmonaires. Les cellules épithéliales s'adaptent et modifient leur cytosquelette, ce qui permet d'obtenir un tissu relativement proche de la physiologie alvéolaire. Ce système pourrait être utilisé pour étudier l'effet de substances inhalées, et réaliser des tests toxicologiques. Un autre exemple d'exposition aiguë de l'utilisation d'une interface air-liquide est cette étude qui compare la culture classique de cellules épithéliales A549 et de macrophages THP-1 et l'interface air-liquide (Dekali et al. 2014; Diabaté et al. 2021). Ces derniers auteurs observent une sensibilité plus importante des cellules exposées *via* l'interface air-liquide, les NPs de titane induisent une cytotoxicité et une modification des gènes impliqués dans l'inflammation. Un exemple d'exposition chronique est celui de (Kabadi et al. 2019a) qui utilise un système de culture 3D pour étudier la toxicité de nanotubes de carbone (CNTs). Des fibroblastes, des cellules épithéliales humaines et des macrophages sont cultivés pour former un tissu pulmonaire 3D, exposé durant 4 ou 7 jours aux CNTs ou aux fibres d'amiante. Les résultats montrent une augmentation de l'expression de gènes marqueurs d'une inflammation aiguë (TNF, et IL4 pour l'exposition 4 jours, IL10 après 7 jours), ainsi que de gènes impliqués dans le remodelage de la matrice extracellulaire. Ces résultats sont cohérents avec ceux obtenus *in vivo*, et n'avaient jusque-là jamais été obtenus *in vitro*. Il faut cependant souligner que ces auteurs ont utilisé des macrophages pré-activés par du LPS dans leur système, ce qui peut conduire à un biais dans les réponses inflammatoires.

Enfin, un dernier exemple cité ici, l'étude de (Herzog et al. 2014) utilise un système à l'interface air-liquide de co-culture contenant 3 types cellulaires (A549, monocytes humains différenciés cellules dendritiques et monocytes humains différenciés en macrophages mimant la barrière alvéolaire pulmonaire. Les cellules sont exposées à des nanoparticules d'argent par nébulisation ou en solution dans le puits supérieur (transwell). Les cellules sont exposées 4 ou 24h, les doses appliquées correspondent à une exposition aiguë (4h) ou à une dose cumulée d'exposition chronique (24h). Ils observent une agrégation des NPs en interface air-liquide, sans modification de la morphologie cellulaire, cytotoxicité, stress oxydant ou sécrétion de cytokines pro-inflammatoires. La culture en exposition liquide montre des résultats plus marqués avec une augmentation de la cytotoxicité et une réponse pro-inflammatoire (TNF et IL8). Ces deux méthodes de culture montrent des résultats très différents, avec d'une part une absence totale d'effet (interface air/liquide, durant 4 ou 24h) et d'autre part des effets cytotoxiques et pro-inflammatoires lors d'une exposition en solution et durant 24h. En tenant compte de la durée de vie d'un macrophage alvéolaire, qui est de plusieurs mois, la durée d'exposition utilisée dans cette étude semble adaptée à une exposition aiguë, accidentelle, et non à une exposition

chronique. De plus, les NPs d'argent, enrobées de polyvinylpyrrolidone (PVP), sont utilisées pour leur activité anti-microbienne, ces NPs sont principalement trouvées dans les vêtements, les produits ménagers, les médicaments… Elles sont donc peu inhalées, l'exposition réelle semble d'avantage cutanée ou orale. Les NPs seraient probablement présentes entourés d'autres substances, tels que les produits chimiques ou des molécules actives, et non enrobés d'un polymère solubilisant.

Cette étude est proche de notre protocole d'exposition aiguë qui nous permet d'étudier les effets toxiques et la réponse inflammatoire aiguë lorsque les NMx sont appliqués en solution. Et comme démontré plus haut, nous obtenons des résultats cohérents avec les effets connus et répertoriés dans la littérature.

Toutefois, ces systèmes d'exposition à l'interface air-liquide ne reproduisent pas les effets d'enrobage des nanoparticules par le surfactant pulmonaire, alors qu'il a été démontré que ce surfactant diminue considérablement les effets de la silice sur les cellules épithéliales pulmonaires (Radiom, Sarkis, et al. 2020). La prise en compte des effets du surfactant pulmonaire est possible (Leroux et al. 2022) mais nécessite des adaptations techniques subtiles qui rendent la technique délicate.

Un autre aspect concernant ce surfactant est sa présence, ou non, dans les systèmes de culture 3D. En effet, il y a d'une part la substance mais également les cellules elles-mêmes qui sont impactées par ce surfactant pulmonaire. Dans ces systèmes 3D, les macrophages sont souvent posés sur la couche épithéliale. Or, la composition du fluide broncho-alvéolaire (BALF) est connue, et notamment grâce à des études protéomiques (Wattiez and Falmagne 2005). Le BALF est le reflet de la composition protéique des voies respiratoires pulmonaires. Cette revue réunit les connaissances du protéome du BALF, qui a permis d'améliorer les connaissances sur le système pulmonaire. L'analyse du protéome permet de détecter des marqueurs : pathologie, inflammation, stress oxydant, asthme… Toutes les protéines ou les médiateurs de l'inflammation détectées dans le BALF influencent le microenvironnement, et donc les cellules voisines, ce qui entraînent une activation ou *a minima* une modification de la physiologie ou activité des cellules voisines. Ces études protéomiques montrent que le surfactant est un exsudat plasmatique enrichi en lipides tensioactifs et en protéines du surfactant (SP A à D) par les pneumocytes de type II. Les macrophages présents au niveau des alvéoles pulmonaires se nourrissent donc principalement de ce surfactant. Les études de toxicologie n'utilisant pas de surfactant ou de sérum semblent donc assez éloignées de la physiologie réelle du site pulmonaire. Par exemple, cette étude montre que la corona (enrobage protéique) inhibe la cytotoxicité de la silice colloïdale et de la silice pyrogénée ainsi que la réponse inflammatoire des RAW264.7 (Leibe et al. 2019). Ces cultures sans sérum induisent un stress supplémentaire aux macrophages en plus de les exposer aux silices « pures », ce type d'exposition étant peu probable dans la vie quotidienne. Les macrophages sont donc directement exposés aux silices, ce qui induit une réponse très forte (TNF et cytotoxicité). De même, dans cette étude les macrophages NR8383, cultivés sans sérum, sont exposés à 18 NMx inorganiques durant 16h (Wiemann et al. 2016). Les auteurs mesurent une production importante d'espèces réactives de l'oxygène, de TNF et de la cytotoxicité. Ici aussi, les NMx sont appliqués dans le milieu ne contenant que peu de protéines, il n'y a donc pas d'enrobage. Enfin, certaines études utilisent les cellules épithéliales A549 afin de reproduire l'épithélium pulmonaire et cet environnement contenant du surfactant. Les cellules A549 exposées au composé bactérien (LPS) sont moins

sensibles en présence d'une quantité importante de sérum. Cependant, ces cellules parviennent à produire du surfactant seulement lorsqu'elles sont cultivées sur une longue période et ressemblent ainsi davantage à des pneumocytes de type II, pour un temps de culture jusqu'à 25 jours dans le cas de la deuxième étude (Nova et al. 2020; Cooper et al. 2016). Enfin, un autre système permettant d'évaluer la toxicologie d'une substance au niveau pulmonaire est l'utilisation des cellules BEAS-2B (cellules bronchiques). Ces cellules ne produisent normalement pas de surfactant, et les études réalisées sans sérum ou surfactant montrent que les BEAS-2B sont moins sensibles, à l'arsenic (Zhao and Klimecki 2015) ou aux particules diesel (Rossner et al. 2019). Ces quelques exemples, soulignent l'importance de la présence de surfactant ou au moins de sérum pour réaliser des études de toxicologie.

Un autre système, mimant un autre organe barrière, est celui utilisé par (Lehner et al. 2020) qui utilise une culture 3D (Caco-2, HT29-MTX-E12 et des monocytes dérivés en macrophages ou cellules dendritiques) pour reproduire la barrière intestinale. Ils exposent cette co-culture à des microplastiques (50 à 500µm) et après 6, 24 ou 48h d'exposition, ils évaluent la cytotoxicité et la réponse inflammatoire (IL-8, TNF, IL1β) ainsi que l'intégrité de la barrière formée par la co-culture. L'exposition aux microplastiques choisis dans cette étude ne montre pas d'effets sur les paramètres testés. Ce système complexe de barrière intestinale est physiologiquement assez proche du système intestinal, avec la présence d'épithélium et de cellules immunitaires. Les microplastiques sont nébulisés sur les cellules, cette exposition est peu probable dans la vie quotidienne, les microplastiques étant présents dans les boissons ou l'alimentation.

Notre système d'exposition de SAS appliquées dans le milieu de culture est assez proche d'une exposition par l'alimentation par exemple, car les SAS sont enrobées de nutriments ou de protéines. Les cellules ne sont donc pas exposées à la substance pure, mais enrobée d'aliments dans le cas d'une exposition intestinale.

Un dernier exemple de système *in vitro* est celui utilisé pour étudier les effets d'une substance au niveau du foie, ces revues rassemblent un grand nombre de données sur les différentes études existantes (Soldatow et al. 2013; Lauschke et al. 2019). Pour ne citer qu'un seul exemple, l'étude, de culture sphéroïde ou 2D d'hépatocyte HepG2, du groupe d'Elje compare la toxicité des nanoparticules de dioxyde de titane, de dioxyde de zinc et d'argent (Elje et al. 2020). Après 24h d'exposition, les NPs d'argent induisent une plus grande mortalité dans la culture 2D que dans le système sphéroïde (dose 10 fois inférieure), les NPs de dioxyde de zinc sont majoritairement dissoutes dans les milieux, et induisent une cytotoxicité similaire dans les deux modèles, ainsi qu'une légère génotoxicité non significative. Enfin, les NPs de dioxyde de titane n'induisent aucune toxicité aux doses testées. Ce modèle sphéroïde, physiologiquement plus exact, est un modèle prometteur. Cependant il est moins sensible aux effets dépendants de la dose, la variabilité entre les sphéroïdes étant relativement importante cela atténue les effets significatifs.

Pour certaines applications, la toxicologie du XXIème siècle nécessite des systèmes rapides afin d'obtenir des résultats sur la toxicologie éventuelle d'un nanomatériau en parallèle des tests de performance. Les systèmes *in vitro* permettent ce criblage et l'obtention de réponses sur les effets d'une exposition aux nanomatériaux. Par exemple, cette étude utilise les

macrophages murins J774A.1 pour comparer les effets de nanoparticules d'or (AuNPs) (Mottas et al. 2017). Les cellules sont cultivées en plaques 96 puits pour l'expérimentation. Certaines AuNPs sont rendues fluorescentes grâce au fluorophore présent sur le polymère (alcool polyvinylique ou copolymère vinylalcool vinylamine). Les AuNPs sont appliquées durant 24h sur les cellules avant que les tests de cytotoxicité, de production de cytokine et de mesure d'internalisation des NPs soient réalisés. Une proportion de 80% des macrophages exposés aux AuNPs fluorescentes est positive, les NPs sont donc majoritairement internalisés, à 4°C, seulement 40% des macrophages ont internalisé des AuNPs, ce qui suggère une internalisation partiellement active. Le dosage de cytokine (IL-6 et TNF) ne permet pas de conclure quant à la réponse inflammatoire d'une exposition aux AuNPs. Les résultats obtenus dans cette étude sont similaires à ceux obtenus avec les mêmes AuNPs sur des cellules primaires humaines (Fytianos et al. 2016).

Le système décrit ci-dessus, est assez similaire à notre protocole d'exposition aiguë, et utilise la même lignée cellulaire. Cependant, le fluorophore et l'enrobage avec le polymère peuvent modifier la réponse de la cellule aux AuNPs elles-mêmes (comme illustré par l'augmentation de la proportion de cellule en nécrose), un dosage de l'or par ICP-AES aurait été plus pertinent, tout en permettant de ne pas modifier les NPs testées. De plus, seuls trois paramètres sont testés ici (internalisation partiellement active, cytotoxicité et sécrétion de cytokines), la phagocytose, et le métabolisme (réponse au stress oxydant, ou potentiel mitochondrial par exemple) des cellules sont d'autres paramètres primordiaux pour évaluer la toxicologie d'une substance. Enfin, les tests sont réalisés sur un faible nombre de cellules, qui de plus, sont cultivées en plaques 96 puits, ce qui peut modifier l'adhésion des macrophages, la surface disponible à leur disposition étant très faible.

Afin de réaliser des tests de toxicologie, il serait possible d'utiliser des cellules humaines provenant de donneurs, par exemple. Cependant, il faut tenir compte de l'aspect invasif de certains prélèvements mais également de la grande variabilité inter-individus. De plus, l'utilisation de cellules humaines peuvent impliquer certaines restrictions (utilisation d'un laboratoire de sécurité L2 dans le cas de sang, par exemple).Ces difficultés sur la variabilité des donneurs ont été reportés dans des études utilisant des cellules souches progénitrices dans le cas de thérapies ciblées et dans le cas d'organoïdes intestinaux sphéroïdes ou encore de cellules souches embryonnaires (Ketterl et al. 2015; Mohammadi et al. 2021; Ortmann and Vallier 2017). Les recherches sur les cellules provenant de donneurs humains ne permettent pas de réaliser des études de toxicologie rapides, fiables et reproductibles.

Ceci est une des raisons pour laquelle les systèmes de culture plus complexes présentés ci-dessus (organoïdes, sphéroïdes ou culture 3D) utilisent des lignées cellulaires et non des cellules provenant de donneurs humains (Elje et al. 2020; Boublil et al. 2013; Diabaté et al. 2021).

Parmi les systèmes modèles, la souris avec sa lignée génétiquement pure représente un système nettement moins sujet à ces phénomènes de variabilité. Le génome humain et celui de la souris partagent environ 80% de gènes codants, ce qui explique que la souris fait partie des

animaux les plus utilisés en laboratoire. Cependant, une étude *in vivo* est longue, complexe et coûteuse, comme expliqué précédemment. Il existe également des variabilités entre les souris, en fonction de l'âge ou du sexe, pour s'affranchir de ces paramètres, des souris du même sexe et âgées d'environ 8 semaines sont souvent utilisées. Les études *in vivo* ne permettent pas un criblage (« screening ») étendu, seuls quelques paramètres peuvent être mesurés et souvent l'effet d'une ou deux substances par étude. En plus de la complexité de réaliser davantage de tests en parallèle, de l'aspect financier, et de l'effet sur l'organisme entier, ou à l'échelle d'un tissu, il serait éthiquement difficile de justifier l'utilisation d'autant d'animaux, dans le contexte de la stratégie 3R.

L'utilisation de lignées cellulaires présente donc bien des avantages. Certains systèmes, comme ceux présentés ci-dessus, utilisent des co-cultures complexes de cellules épithéliales, de macrophages et de cellules dendritiques. Certes, cela est physiologiquement proche du site pulmonaire ou intestinal, mais leur mise en place est délicate, et le nombre de substances testées ou de paramètres évalués sont limités. De plus, les effets mesurés sont le résultat de l'ensemble des cellules exposées et certaines données peuvent être masquées par la complexité du système. Les tests effectués sont donc plus génériques, et ne permettent pas une grande sensibilité comme souligné dans l'étude de sphéroïde HepG2 (Elje et al. 2020). Par exemple, dans ces systèmes complexes, il est plus difficile d'évaluer les fonctions d'une population particulière, par exemple la population des macrophages. Si des études mécanistiques doivent être réalisées afin de mieux cibler une réponse ou un effet, il est plus difficile de la faire sur une co-culture, car les réponses des différents types cellulaires peuvent diluer ou atténuer le signal spécifique à une population, et donc rendre ces effets non statistiquement significatifs. Les méthodes omiques sont, en effet, basées sur les changements d'abondance des protéines, cette modification d'abondance pour une population donnée pourrait être masquée par l'abondance des autres populations. Si nous prenons un exemple fictif de co-culture de fibroblastes, de cellules épithéliales et de macrophages dans un rapport 1 :1 :1 , s'il existe des modifications de la quantité d'une protéine d'un facteur 2 chez le macrophage (suite à l'exposition à une substance), et que cette protéine est également abondante et inchangée dans les autres populations, le rapport observé dans le système total est de 4/3, ce qui risque fort de ne plus être significatif. On perd donc l'étude mécanistique qui est un point important des études de toxicologie dans l'optique d'aborder les phénomènes de toxicologie croisée. Pour pallier à ce problème, il est certes possible de décoller les cellules par trypsinisation puis par identification des marqueurs de surface en cytométrie en flux (Clift et al. 2017). Cependant, cette méthode de décollement n'est pas celle utilisée habituellement pour les macrophages et les cellules dendritiques, ce qui pourrait entraîner une modification de la physiologie des cellules et donc de la réponse détectée si les cellules sont fragilisése. C'est en partie pour cette raison que certains système air-liquide utilisent un type cellulaire unique, afin de pouvoir réaliser des études « omiques », comme par exemple (Leroux et al. 2022) avec les macrophages alvéolaire de rat NR8383.

Un autre aspect important dans les études toxicologie est le mode d'exposition, par exemple les effets d'une exposition chronique ou bien l'évaluation de la persistance. Ces systèmes complexes sont principalement utilisés pour étudier les effets à court-terme, et les études menées à plus long terme sont relativement rares. C'est le cas de certains exemple cité ci-dessus, ou bien de cette étude qui étudie les effets d'une exposition répété sur 3 jours seulement (Mueller et al. 2014). En plus des études présentées précédemment (Boublil et al. 2013; Kabadi et al. 2019b), il existe par exemple, cette étude toxicologique d'un candidat-

médicament sur des sphéroïdes du foie cultivés durant 14 jours (Vorrink et al. 2018) ou encore celle-ci dans laquelle les sphéroïdes sont cultivées durant 5 semaines (Bell et al. 2016).

Outre cet aspect de durée de culture, qui devient complexe en co-culture ou culture 3D, il se pose également le problème de la proportion de chaque type cellulaire dans ces systèmes. En effet comme expliqué plus haut, il est connu que les macrophages représentent 10% des globules blancs de l'organisme humain. Cependant, la proportion de chaque type cellulaire dans un tissu donné est peu ou mal connue, et la co-culture ne permet pas de maîtriser la répartition des différents types cellulaires, ni d'être réellement physiologique par manque de connaissances.

Notre système de culture utilise donc la lignée cellulaire murine J774A.1 qui est référencée par l'ATCC depuis 1968. Tout d'abord, les macrophages représentent 10% des globules blancs, et sont largement distribués dans l'organisme. Ils sont localisés dans la majorité des tissus (la rate, la cavité péritonéale, l'intestin, les tissus adipeux, le foie, le système nerveux central, les poumons…) (Gordon et al. 1986; Perry, Hume, and Gordon 1985). Ils ont un rôle de sentinelle, mais sont capables de phagocyter le pathogène ou l'élément étranger, et peuvent être recrutés au niveau du site de l'inflammation, si nécessaire (Cinti et al. 2005). Si la proportion de macrophages dans chacun des tissus est mal connue, il s'agit tout de même d'une cellule clé et exposée à tous types de substances (inhalée, ingérée, cutanée).

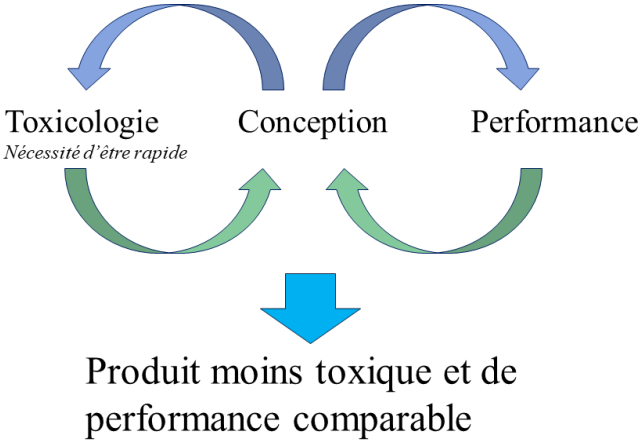

Figure 60 : Un outil "safe-by-design" : le système in vitro de macrophages murins.

L'utilisation d'une lignée cellulaire permet d'obtenir un grand nombre de résultats et rapidement. En effet, la culture est illimitée, tout en ayant une stabilité (génotypique et phénotypique) et une reproductibilité importante : la division cellulaire résulte en clones des cellules mères. Cela permet de mesurer un nombre important de paramètres en utilisant un matériel biologique simple et stable. Ce criblage est rapide et peut être mécanistique (utilisation de la protéomique) ou utiliser des tests de routine (phagocytose, potentiel mitochondrial, sécrétion de cytokine, production d'oxyde nitrique, observation des marqueurs de surface…). Ce système permet également d'étudier plusieurs protocoles d'exposition (aiguë, répétée ou récupération) et donc les effets d'une exposition accidentelle à une forte dose de NMx, l'influence du débit de dose ainsi que la persistance des effets. Ce système a donc permis de travailler en collaboration avec les services de recherches et développement de Solvay et de

leur donner une réponse rapide sur les effets des différentes silices testées comme illustré sur la figure 60. Nous avons donc développé un système *in vitro* rapide, performant et pertinent pour étudier les effets de l'exposition aux nanomatériaux, silices amorphes de synthèse, silice cristalline, pigments à base de silice ou terre de diatomée, mais pouvant être utilisé pour tester la toxicité d'autres substances.

Conclusion générale

Durant ces trois années de thèse, mes recherches ont permis de développer et mettre au point un système *in vitro* de toxicologie des nanomatériaux. Dans le but de diminuer l'utilisation de l'expérimentation animale, il est opportun de trouver des méthodes alternatives. Les nanotechnologies étant en plein essor ces dernières décennies, la nécessité de réaliser des tests est primordiale, il ne faut certes pas considérer que les NMx sont tous toxiques et doivent être bannis, mais il est important de tenir compte de l'existence potentielle de dangers liés à la production ou à l'utilisation de nanomatériaux. C'est dans cette optique que le développement de système d'évaluation des effets d'une exposition aux NMx s'intègre, en tenant compte de la nature de la substance, de la dose, de la fréquence d'exposition, des caractéristiques physico-chimiques et des secteurs d'exposition (professionnels ou consommateurs - alimentation, cosmétique, produit ménager…). Ces tests doivent permettre d'obtenir des résultats rapides, sur des modèles pertinents et performants. Les données générées permettront ainsi d'adapter les consignes et les précautions d'exposition, et également de faire de la prévention des risques.

Matériel et méthodes

Voir les articles

Références

'Abundances of the Elements in Earth's Crust, - Biosphere - BNID 110362'. n.d. Accessed 17 September 2021. https://bionumbers.hms.harvard.edu/bionumber.aspx?s=n&v=1&id=110362.

Ahamed, Maqusood, Ryan Posgai, Timothy J. Gorey, Mark Nielsen, Saber M. Hussain, and John J. Rowe. 2010. 'Silver Nanoparticles Induced Heat Shock Protein 70, Oxidative Stress and Apoptosis in Drosophila Melanogaster'. *Toxicology and Applied Pharmacology* 242 (3): 263–69. https://doi.org/10.1016/j.taap.2009.10.016.

Alberts, Bruce, Alexander Johnson, Julian Lewis, Martin Raff, Keith Roberts, and Peter Walter. 2002. 'B Cells and Antibodies'. *Molecular Biology of the Cell. 4th Edition*. https://www.ncbi.nlm.nih.gov/books/NBK26884/.

Ali, Attarad, Hira Zafar, Muhammad Zia, Ihsan ul Haq, Abdul Rehman Phull, Joham Sarfraz Ali, and Altaf Hussain. 2016. 'Synthesis, Characterization, Applications, and Challenges of Iron Oxide Nanoparticles'. *Nanotechnology, Science and Applications* 9 (August): 49–67. https://doi.org/10.2147/NSA.S99986.

Ali, Sazan, Gérard Steinmetz, Guillaume Montillet, Marie-Hélène Perrard, Anderson Loundou, Philippe Durand, Marie-Roberte Guichaoua, and Odette Prat. 2014. 'Exposure to Low-Dose Bisphenol A Impairs Meiosis in the Rat Seminiferous Tubule Culture Model: A Physiotoxicogenomic Approach'. *PLOS ONE* 9 (9): e106245. https://doi.org/10.1371/journal.pone.0106245.

American Thoracic Society Committee of the Scientific Assembly on Environmental and Occupational Health. 1997. 'Adverse Effects of Crystalline Silica Exposure.' *American Journal of Respiratory and Critical Care Medicine* 155 (2): 761–68. https://doi.org/10.1164/ajrccm.155.2.9032226.

Anagnostou, Katerina, Minas Stylianakis, Sotiris Michaleas, and Athanasios Skouras. 2020. 'Chapter Five - Biodegradable Nanomaterials'. In *Nanomaterials for Clinical Applications*, edited by Natassa Pippa and Costas Demetzos, 123–57. Micro and Nano Technologies. Elsevier. https://doi.org/10.1016/B978-0-12-816705-2.00005-9.

Anderson, Donald S., Esther S. Patchin, Rona M. Silva, Dale L. Uyeminami, Arjun Sharmah, Ting Guo, Gautom K. Das, et al. 2015. 'Influence of Particle Size on Persistence and Clearance of Aerosolized Silver Nanoparticles in the Rat Lung'. *Toxicological Sciences* 144 (2): 366–81. https://doi.org/10.1093/toxsci/kfv005.

Armand, Lucie, Mathilde BIOLA-CLIER, Laure Bobyk, Véronique Collin-Faure, Hélène Diemer, Jean Marc Strub, Sarah Cianférani, et al. 2016. 'Molecular Responses of Alveolar Epithelial A549 Cells to Chronic Exposure to Titanium Dioxide Nanoparticles: A Proteomic View.' *Journal of Proteomics*, Towards deciphering proteomes via the proteoform, protein speciation, moonlighting and protein code concepts, 134: 163–73. https://doi.org/10.1016/j.jprot.2015.08.006.

Arts, Josje H. E., Hans Muijser, Evert Duistermaat, Karin Junker, and C. Frieke Kuper. 2007. 'Five-Day Inhalation Toxicity Study of Three Types of Synthetic Amorphous Silicas in Wistar Rats and Post-Exposure Evaluations for up to 3months'. *Food and Chemical Toxicology* 45 (10): 1856–67. https://doi.org/10.1016/j.fct.2007.04.001.

Aslam, Bilal, Madiha Basit, Muhammad Atif Nisar, Mohsin Khurshid, and Muhammad Hidayat Rasool. 2017. 'Proteomics: Technologies and Their Applications'. *Journal of Chromatographic Science* 55 (2): 182–96. https://doi.org/10.1093/chromsci/bmw167.

Aude-Garcia, Catherine, Bastien Dalzon, Jean-Luc Ravanat, Véronique Collin-Faure, Hélène Diemer, Jean Marc Strub, Sarah Cianférani, et al. 2016. 'A Combined Proteomic and Targeted Analysis Unravels New Toxic Mechanisms for Zinc Oxide Nanoparticles in Macrophages'. *Journal of Proteomics* 134 (February): 174–85. https://doi.org/10.1016/j.jprot.2015.12.013.

Aude-Garcia, Catherine, Florent Villiers, Véronique Collin-Faure, Karin Pernet-Gallay, Pierre-Henri Jouneau, Stéphanie Sorieul, Geoffrey Mure, et al. 2016. 'Different in Vitro Exposure Regimens of Murine Primary Macrophages to Silver Nanoparticles Induce Different Fates of Nanoparticles and Different Toxicological and Functional Consequences.' *Nanotoxicology* 10 (5): 586–96. https://doi.org/10.3109/17435390.2015.1104738.

Ball, Philip. 2015. 'Les nanostructures pour créer de la couleur, un art inspiré par la nature'. *Photoniques*, January, 42–47. https://doi.org/10.1051/photon/20150142.

Baptista, Trino, Nairy Rangel, Virginia Fernández, Edgardo Carrizo, Yamily El Fakih, Euderruh Uzcátegui, Tatiana Galeazzi, et al. 2007. 'Metformin as an Adjunctive Treatment to Control Body Weight and Metabolic Dysfunction during Olanzapine Administration: A Multicentric, Double-Blind, Placebo-Controlled Trial'. *Schizophrenia Research* 93 (1–3): 99–108. https://doi.org/10.1016/j.schres.2007.03.029.

Baroli, Biancamaria. 2010. 'Penetration of Nanoparticles and Nanomaterials in the Skin: Fiction or Reality?' *JOURNAL OF PHARMACEUTICAL SCIENCES* 99 (1): 30.

Barquet, Nicolau. 1997. 'Smallpox: The Triumph over the Most Terrible of the Ministers of Death'. *Annals of Internal Medicine* 127 (8_Part_1): 635. https://doi.org/10.7326/0003-4819-127-8_Part_1-199710150-00010.

Barthel, Hélène, Christian Darne, Laurent Gaté, Athanase Visvikis, and Carole Seidel. 2021. 'Continuous Long-Term Exposure to Low Concentrations of MWCNTs Induces an Epithelial-Mesenchymal Transition in BEAS-2B Cells'. *Nanomaterials (Basel, Switzerland)* 11 (7): 1742. https://doi.org/10.3390/nano11071742.

Bayda, Samer, Muhammad Adeel, Tiziano Tuccinardi, Marco Cordani, and Flavio Rizzolio. 2019. 'The History of Nanoscience and Nanotechnology: From Chemical–Physical Applications to Nanomedicine'. *Molecules* 25 (1): 112. https://doi.org/10.3390/molecules25010112.

Beck-Speier, Ingrid, Wolfgang G. Kreyling, Konrad L. Maier, Niru Dayal, Mette C. Schladweiler, Paula Mayer, Manuela Semmler-Behnke, and Urmila P. Kodavanti. 2009. 'Soluble Iron Modulates Iron Oxide Particle-Induced Inflammatory Responses via Prostaglandin E(2)Synthesis: In Vitro and in Vivo Studies'. *Particle and Fibre Toxicology* 6 (December): 34. https://doi.org/10.1186/1743-8977-6-34.

Bell, Catherine C., Delilah F. G. Hendriks, Sabrina M. L. Moro, Ewa Ellis, Joanne Walsh, Anna Renblom, Lisa Fredriksson Puigvert, et al. 2016. 'Characterization of Primary Human Hepatocyte Spheroids as a Model System for Drug-Induced Liver Injury, Liver Function and Disease'. *Scientific Reports* 6 (May): 25187. https://doi.org/10.1038/srep25187.

Bobyk, Laure, Adeline Tarantini, David Beal, Giulia Veronesi, Isabelle Kieffer, Sylvie Motellier, Eugenia Valsami-Jones, et al. 2021. 'Toxicity and Chemical Transformation of Silver Nanoparticles in A549 Lung Cells: Dose-Rate-Dependent Genotoxic Impact'. *Environmental Science: Nano* 8 (3): 806–21. https://doi.org/10.1039/D0EN00533A.

Boublil, Laura, Emeline Assémat, Marie-Caroline Borot, Sonja Boland, Laurent Martinon, Jean Sciare, and Armelle Baeza-Squiban. 2013. 'Development of a Repeated Exposure Protocol of Human Bronchial Epithelium in Vitro to Study the Long-Term Effects of Atmospheric Particles'. *Toxicology in Vitro* 27 (2): 533–42. https://doi.org/10.1016/j.tiv.2012.11.008.

Bourquin, Joël, Dedy Septiadi, Dimitri Vanhecke, Sandor Balog, Lukas Steinmetz, Miguel Spuch-Calvar, Patricia Taladriz-Blanco, Alke Petri-Fink, and Barbara Rothen-Rutishauser. 2019. 'Reduction of Nanoparticle Load in Cells by Mitosis but Not Exocytosis'. *ACS Nano* 13 (7): 7759–70. https://doi.org/10.1021/acsnano.9b01604.

Boyles, Matthew S. P., David Brown, Jilly Knox, Michael Horobin, Mark R. Miller, Helinor J. Johnston, and Vicki Stone. 2018. 'Assessing the Bioactivity of Crystalline Silica in Heated High-Temperature Insulation Wools'. *Inhalation Toxicology* 30 (7–8): 255–72. https://doi.org/10.1080/08958378.2018.1513610.

Brookes, Oliver, Sonja Boland, René Lai Kuen, Dorian Miremont, Jamileh Movassat, and Armelle Baeza-Squiban. 2021. 'Co-Culture of Type I and Type II Pneumocytes as a Model of Alveolar Epithelium'. *PLOS ONE* 16 (9): e0248798. https://doi.org/10.1371/journal.pone.0248798.

Bull, P. C., and D. W. Cox. 1994. 'Wilson Disease and Menkes Disease: New Handles on Heavy-Metal Transport'. *Trends Genet* 10 (7): 246–52.

Calderón-Jiménez, Bryan, Monique E. Johnson, Antonio R. Montoro Bustos, Karen E. Murphy, Michael R. Winchester, and José R. Vega Baudrit. 2017. 'Silver Nanoparticles: Technological Advances, Societal Impacts, and Metrological Challenges'. *Frontiers in Chemistry* 5. https://www.frontiersin.org/article/10.3389/fchem.2017.00006.

Carrizo, Edgardo, Virginia Fernández, Lisette Connell, Ignacio Sandia, Dexy Prieto, Johana Mogollón, Dennys Valbuena, Iliana Fernández, Enma Araujo de Baptista, and Trino Baptista. 2009. 'Extended Release Metformin for Metabolic Control Assistance during Prolonged Clozapine Administration: A 14 Week, Double-Blind, Parallel Group, Placebo-Controlled Study'. *Schizophrenia Research* 113 (1): 19–26. https://doi.org/10.1016/j.schres.2009.05.007.

Castranova, V., and V. Vallyathan. 2000. 'Silicosis and Coal Workers' Pneumoconiosis'. *Environmental Health Perspectives* 108 Suppl 4 (August): 675–84. https://doi.org/10.1289/ehp.00108s4675.

Charitidis, Costas A., Pantelitsa Georgiou, Malamatenia A. Koklioti, Aikaterini-Flora Trompeta, and Vasileios Markakis. 2014. 'Manufacturing Nanomaterials: From Research to Industry'. *Manufacturing Review* 1: 11. https://doi.org/10.1051/mfreview/2014009.

Chaves, S. B., L. P. Silva, Z. G. M. Lacava, P. C. Morais, and R. B. Azevedo. 2005. 'Interleukin-1 and Interleukin-6 Production in Mice's Lungs Induced by 2, 3 Meso-Dimercaptosuccinic-Coated Magnetic Nanoparticles'. *Journal of Applied Physics* 97 (10): 10Q915. https://doi.org/10.1063/1.1854531.

Chernousova, S., and M. Epple. 2013. 'Silver as Antibacterial Agent: Ion, Nanoparticle, and Metal'. *Angew Chem Int Ed Engl* 52 (6): 1636–53.

Chevallet, Mireille, Catherine Aude-Garcia, Cécile Lelong, Serge Candéias, Sylvie Luche, Véronique Collin-Faure, Sarah Triboulet, et al. 2011. 'Effects of Nanoparticles on Murine Macrophages'. *Journal of Physics Conference Series* 304 (July). https://doi.org/10.1088/1742-6596/304/1/012034.

Chung, Kian Fan, Joanna Seiffert, Shu Chen, Ioannis G. Theodorou, Angela Erin Goode, Bey Fen Leo, Catriona M. McGilvery, et al. 2017. 'Inactivation, Clearance, and Functional Effects of Lung-Instilled Short and Long Silver Nanowires in Rats'. *ACS Nano* 11 (3): 2652–64. https://doi.org/10.1021/acsnano.6b07313.

Cinti, Saverio, Grant Mitchell, Giorgio Barbatelli, Incoronata Murano, Enzo Ceresi, Emanuela Faloia, Shupei Wang, Melanie Fortier, Andrew S. Greenberg, and Martin S. Obin. 2005. 'Adipocyte Death Defines Macrophage Localization and Function in Adipose Tissue of Obese Mice and Humans'. *Journal of Lipid Research* 46 (11): 2347–55. https://doi.org/10.1194/jlr.M500294-JLR200.

Clift, Martin J. D., Kleanthis Fytianos, Dimitri Vanhecke, Sandra Hočevar, Alke Petri-Fink, and Barbara Rothen-Rutishauser. 2017. 'A Novel Technique to Determine the Cell Type Specific Response within an in Vitro Co-Culture Model via Multi-Colour Flow Cytometry'. *Scientific Reports* 7 (1): 434. https://doi.org/10.1038/s41598-017-00369-4.

Coates, Margaret, Sarah Blanchard, and Amanda S. MacLeod. 2018. 'Innate Antimicrobial Immunity in the Skin: A Protective Barrier against Bacteria, Viruses, and Fungi'. *PLOS Pathogens* 14 (12): e1007353. https://doi.org/10.1371/journal.ppat.1007353.

Combadière, Béhazine, Christophe Combadière, and Philippe Deterre. 2007. 'Les chimiokines : un réseau sophistiqué de guidage cellulaire'. *médecine/sciences* 23 (2): 173–79. https://doi.org/10.1051/medsci/2007232173.

Comfort, K. K., L. K. Braydich-Stolle, E. I. Maurer, and S. M. Hussain. 2014. 'Less Is More: Long-Term in Vitro Exposure to Low Levels of Silver Nanoparticles Provides New Insights for Nanomaterial Evaluation'. *Acs Nano* 8 (4): 3260–71.

Committee, EFSA Scientific, Simon More, Vasileios Bampidis, Diane Benford, Claude Bragard, Thorhallur Halldorsson, Antonio Hernández-Jerez, et al. 2021. 'Guidance on Risk Assessment

of Nanomaterials to Be Applied in the Food and Feed Chain: Human and Animal Health'. *EFSA Journal* 19 (8): e06768. https://doi.org/10.2903/j.efsa.2021.6768.

Cooper, James Ross, Muhammad Bilal Abdullatif, Edward C. Burnett, Karen E. Kempsell, Franco Conforti, Howard Tolley, Jane E. Collins, and Donna E. Davies. 2016. 'Long Term Culture of the A549 Cancer Cell Line Promotes Multilamellar Body Formation and Differentiation towards an Alveolar Type II Pneumocyte Phenotype'. *PLoS ONE* 11 (10): e0164438. https://doi.org/10.1371/journal.pone.0164438.

Cornick, Steve, Adelaide Tawiah, and Kris Chadee. 2015. 'Roles and Regulation of the Mucus Barrier in the Gut'. *Tissue Barriers* 3 (1–2). https://doi.org/10.4161/21688370.2014.982426.

Council, National Research. 2007. *Toxicity Testing in the 21st Century: A Vision and a Strategy*. https://doi.org/10.17226/11970.

Dale, H. H., and A. N. Richards. 1918. 'The Vasodilator Action of Histamine and of Some Other Substances'. *The Journal of Physiology* 52 (2–3): 110–65.

Dalzon, Bastien, Catherine Aude-Garcia, Véronique Collin-Faure, Hélène Diemer, David Béal, Fanny Dussert, Daphna Fenel, et al. 2017. 'Differential Proteomics Highlights Macrophage-Specific Responses to Amorphous Silica Nanoparticles'. *Nanoscale* 9 (27): 9641–58. https://doi.org/10.1039/C7NR02140B.

Dalzon, Bastien, Catherine Aude-Garcia, Hélène Diemer, Joanna Bons, Caroline Marie-Desvergne, Julien Pérard, Muriel Dubosson, et al. 2020. 'The Longer the Worse: A Combined Proteomic and Targeted Study of the Long-Term versus Short-Term Effects of Silver Nanoparticles on Macrophages'. *Environmental Science: Nano* 7 (7): 2032–46. https://doi.org/10.1039/C9EN01329F.

Dalzon, Bastien, Hélène Diemer, Véronique Collin-Faure, Sarah Sanglier-Cianférani, Thierry Rabilloud, and Catherine Aude-Garcia. 2016. 'Culture Medium-Associated Changes in the Core Proteome of Macrophages and in Their Responses to Copper Oxide Nanoparticles'. *Proteomics* 16 (October). https://doi.org/10.1002/pmic.201600052.

Dalzon, Bastien, Anaëlle Torres, Julie Devcic, Daphna Fenel, Jacques-Aurélien Sergent, and Thierry Rabilloud. 2021. 'A Low-Serum Culture System for Prolonged in Vitro Toxicology Experiments on a Macrophage System'. *Frontiers in Toxicology* 3: 780778. https://doi.org/10.3389/ftox.2021.780778.

Dalzon, Bastien, Anaelle Torres, Hélène Diemer, Stéphane Ravanel, Véronique Collin-Faure, Karin Pernet-Gallay, Pierre-Henri Jouneau, et al. 2019. 'How Reversible Are the Effects of Silver Nanoparticles on Macrophages? A Proteomic-Instructed View'. *Environmental Science: Nano*, 10.1039.C9EN00408D. https://doi.org/10.1039/C9EN00408D.

Dalzon, Bastien, Anaëlle Torres, Solveig Reymond, Benoit Gallet, François Saint-Antonin, Véronique Collin-Faure, Christine Moriscot, et al. 2020. 'Influences of Nanoparticles Characteristics on the Cellular Responses: The Example of Iron Oxide and Macrophages'. *Nanomaterials* 10 (2): 266. https://doi.org/10.3390/nano10020266.

Décret N° 2012-232 Du 17 Février 2012 Relatif à La Déclaration Annuelle Des Substances à l'état Nanoparticulaire Pris En Application de l'article L. 523-4 Du Code de l'environnement. 2012. *2012-232*.

Dekali, Samir, Christelle Gamez, Thierry Kortulewski, Kelly Blazy, Patrice Rat, and Ghislaine Lacroix. 2014. 'Assessment of an in Vitro Model of Pulmonary Barrier to Study the Translocation of Nanoparticles'. *Toxicology Reports* 1: 157–71. https://doi.org/10.1016/j.toxrep.2014.03.003.

Dekkers, Susan, Petra Krystek, Ruud J. B. Peters, Daniëlle P. K. Lankveld, Bas G. H. Bokkers, Paula H. van Hoeven-Arentzen, Hans Bouwmeester, and Agnes G. Oomen. 2011. 'Presence and Risks of Nanosilica in Food Products'. *Nanotoxicology* 5 (3): 393–405. https://doi.org/10.3109/17435390.2010.519836.

Delaval, Mathilde, Sonja Boland, Brigitte Solhonne, Marie-Anne Nicola, Stéphane Mornet, Armelle Baeza-Squiban, Jean-Michel Sallenave, and Ignacio Garcia-Verdugo. 2015. 'Acute Exposure to Silica Nanoparticles Enhances Mortality and Increases Lung Permeability in a Mouse Model of Pseudomonas Aeruginosa Pneumonia'. *Particle and Fibre Toxicology* 12 (1). https://doi.org/10.1186/s12989-014-0078-9.

‘Dendritic Cells | British Society for Immunology’. n.d. Accessed 25 January 2022. https://www.immunology.org/public-information/bitesized-immunology/cells/dendritic-cells.

Diabaté, Silvia, Lucie Armand, Sivakumar Murugadoss, Marco Dilger, Susanne Fritsch-Decker, Christoph Schlager, David Béal, et al. 2021. ‘Air–Liquid Interface Exposure of Lung Epithelial Cells to Low Doses of Nanoparticles to Assess Pulmonary Adverse Effects’. *Nanomaterials* 11 (1): 65. https://doi.org/10.3390/nano11010065.

Dixon, B. 2004. ‘Pushing Bordeaux Mixture’. *Lancet Infect Dis* 4 (9): 594.

Duval, Caroline, Fatima Teixeira-Clerc, Alix F. Leblanc, Sothea Touch, Claude Emond, Michèle Guerre-Millo, Sophie Lotersztajn, Robert Barouki, Martine Aggerbeck, and Xavier Coumoul. 2017. ‘Chronic Exposure to Low Doses of Dioxin Promotes Liver Fibrosis Development in the C57BL/6J Diet-Induced Obesity Mouse Model’. *Environmental Health Perspectives* 125 (3): 428–36. https://doi.org/10.1289/EHP316.

Elje, Elisabeth, Espen Mariussen, Oscar H. Moriones, Neus G. Bastús, Victor Puntes, Yvonne Kohl, Maria Dusinska, and Elise Rundén-Pran. 2020. ‘Hepato(Geno)Toxicity Assessment of Nanoparticles in a HepG2 Liver Spheroid Model’. *Nanomaterials (Basel, Switzerland)* 10 (3): E545. https://doi.org/10.3390/nano10030545.

Fenner, Frank, Donald A. Henderson, Isao Arita, Zdenek Jezek, Ivan Danilovich Ladnyi, and World Health Organization. 1988. *Smallpox and Its Eradication*. World Health Organization. https://apps.who.int/iris/handle/10665/39485.

Flörke, Otto W., Heribert A. Graetsch, Fred Brunk, Leopold Benda, Siegfried Paschen, Horacio E. Bergna, William O. Roberts, et al. 2008. ‘Silica’. In *Ullmann’s Encyclopedia of Industrial Chemistry*. John Wiley & Sons, Ltd. https://doi.org/10.1002/14356007.a23_583.pub3.

Flörke, Otto W., Heribert Graetsch, Fred Brunk, Leopold Benda, Siegfried Paschen, Horacio E. Bergna, William O. Roberts, et al. 2000. ‘Silica’. In *Ullmann’s Encyclopedia of Industrial Chemistry*. American Cancer Society. https://doi.org/10.1002/14356007.a23_583.

Frank, Arthur L., and T. K. Joshi. 2014. ‘The Global Spread of Asbestos’. *Annals of Global Health* 80 (4): 257–62. https://doi.org/10.1016/j.aogh.2014.09.016.

Franke, Christian, Gabriele Studinger, Georgia Berger, Stella Böhling, Ursula Bruckmann, Dieter Cohors-Fresenborg, and Ulrich Jöhncke. 1994. ‘The Assessment of Bioaccumulation’. *Chemosphere* 29 (7): 1501–14. https://doi.org/10.1016/0045-6535(94)90281-X.

Fruijtier-Polloth, C. 2012. ‘The Toxicological Mode of Action and the Safety of Synthetic Amorphous Silica-A Nanostructured Material’. *Toxicology* 294 (2–3): 61–79.

Fubini, Bice, Giovanna Zanetti, Serena Altilia, Roberta Tiozzo, Dominique Lison, and Umberto Saffiotti. 1999. ‘Relationship between Surface Properties and Cellular Responses to Crystalline Silica: Studies with Heat-Treated Cristobalite’. *Chemical Research in Toxicology* 12 (8): 737–45. https://doi.org/10.1021/tx980261a.

Fytianos, Kleanthis, Savvina Chortarea, Laura Rodriguez-Lorenzo, Fabian Blank, Christophe von Garnier, Alke Petri-Fink, and Barbara Rothen-Rutishauser. 2016. ‘Aerosol Delivery of Functionalized Gold Nanoparticles Target and Activate Dendritic Cells in a 3D Lung Cellular Model’. Research-article. ACS Publications. 19 December 2016. https://doi.org/10.1021/acsnano.6b06061.

Garlanda, Cecilia, Charles A. Dinarello, and Alberto Mantovani. 2013. ‘THE INTERLEUKIN-1 FAMILY: BACK TO THE FUTURE’. *Immunity* 39 (6): 1003–18. https://doi.org/10.1016/j.immuni.2013.11.010.

Gazzano, E., M. Ghiazza, M. Polimeni, V. Bolis, I. Fenoglio, A. Attanasio, G. Mazzucco, B. Fubini, and D. Ghigo. 2012. ‘Physicochemical Determinants in the Cellular Responses to Nanostructured Amorphous Silicas’. *Toxicological Sciences* 128 (1): 158–70.

Ghiazza, M., M. Polimeni, I. Fenoglio, E. Gazzano, D. Ghigo, and B. Fubini. 2010. ‘Does Vitreous Silica Contradict the Toxicity of the Crystalline Silica Paradigm?’ *Chem Res Toxicol* 23 (3): 620–29.

Gliga, A. R., S. Di Bucchianico, J. Lindvall, B. Fadeel, and H. L. Karlsson. 2018. ‘RNA-Sequencing Reveals Long-Term Effects of Silver Nanoparticles on Human Lung Cells’. *Sci Rep* 8 (1): 6668.

Gordon, S., P. R. Crocker, L. Morris, S. H. Lee, V. H. Perry, and D. A. Hume. 1986. 'Localization and Function of Tissue Macrophages'. *Ciba Foundation Symposium* 118: 54–67. https://doi.org/10.1002/9780470720998.ch5.

Greenberg, Michael I., and David Vearrier. 2015. 'Metal Fume Fever and Polymer Fume Fever'. *Clinical Toxicology (Philadelphia, Pa.)* 53 (4): 195–203. https://doi.org/10.3109/15563650.2015.1013548.

Griffin, Sharoon, Muhammad Irfan Masood, Muhammad Jawad Nasim, Muhammad Sarfraz, Azubuike Peter Ebokaiwe, Karl-Herbert Schäfer, Cornelia M. Keck, and Claus Jacob. 2018. 'Natural Nanoparticles: A Particular Matter Inspired by Nature'. *Antioxidants* 7 (1): 3. https://doi.org/10.3390/antiox7010003.

Guglielmotti, María B., Mariela G. Domingo, Tammy Steimetz, Emilio Ramos, María L. Paparella, and Daniel G. Olmedo. 2015. 'Migration of Titanium Dioxide Microparticles and Nanoparticles through the Body and Deposition in the Gingiva: An Experimental Study in Rats'. *European Journal of Oral Sciences* 123 (4): 242–48. https://doi.org/10.1111/eos.12190.

Hajar, Rachel. 2011. 'Animal Testing and Medicine'. *Heart Views : The Official Journal of the Gulf Heart Association* 12 (1): 42. https://doi.org/10.4103/1995-705X.81548.

Hempt, Claudia, Cordula Hirsch, Yvette Hannig, Alexandra Rippl, Peter Wick, and Tina Buerki-Thurnherr. 2021. 'Investigating the Effects of Differently Produced Synthetic Amorphous Silica (E 551) on the Integrity and Functionality of the Human Intestinal Barrier Using an Advanced in Vitro Co-Culture Model'. *Archives of Toxicology* 95 (3): 837–52. https://doi.org/10.1007/s00204-020-02957-2.

Hempt, Claudia, Jean-Pierre Kaiser, Olivier Scholder, Tina Buerki-Thurnherr, Heinrich Hofmann, Alexandra Rippl, Tobias B. Schuster, Peter Wick, and Cordula Hirsch. 2020. 'The Impact of Synthetic Amorphous Silica (E 551) on Differentiated Caco-2 Cells, a Model for the Human Intestinal Epithelium'. *Toxicology in Vitro* 67 (September): 104903. https://doi.org/10.1016/j.tiv.2020.104903.

Herzog, F., K. Loza, S. Balog, M. J. D. Clift, M. Epple, P. Gehr, A. Petri-Fink, and B. Rothen-Rutishauser. 2014. 'Mimicking Exposures to Acute and Lifetime Concentrations of Inhaled Silver Nanoparticles by Two Different in Vitro Approaches'. *Beilstein Journal of Nanotechnology* 5 (August): 1357–70.

Huang, Sui, and Donald E. Ingber. 1999. 'The Structural and Mechanical Complexity of Cell-Growth Control'. *Nature Cell Biology* 1 (5): E131–38. https://doi.org/10.1038/13043.

Inshakova, Elena, and Oleg Inshakov. 2017. 'World Market for Nanomaterials: Structure and Trends'. Edited by S. Bratan, S. Gorbatyuk, S. Leonov, and S. Roshchupkin. *MATEC Web of Conferences* 129: 02013. https://doi.org/10.1051/matecconf/201712902013.

Iwakoshi, Ayako, Taizo Nanke, and Toshikatsu Kobayashi. 2005. 'Coating Materials Containing Gold Nanoparticles'. *Gold Bulletin* 38 (3): 107–12. https://doi.org/10.1007/BF03215244.

Jamett, A., M. Santander, L. Peña, N. Gras, and L. Muñoz. 1991. 'Trace Elements in the Hair of Workers of a Copper Mine and of Children Living in the Vicinity'. *Journal of Radioanalytical and Nuclear Chemistry Letters* 155 (6): 383–89. https://doi.org/10.1007/BF02163632.

Janeway, Charles A., Paul Travers, Mark Walport, and Mark J. Shlomchik. 2001. *Immunobiology*. 5th ed. Garland Science.

Joffin, Nolwenn, Philippe Noirez, Jean-Philippe Antignac, Min-ji Kim, Philippe Marchand, Marion Falabregue, Bruno Le Bizec, et al. 2018. 'Release and Toxicity of Adipose Tissue-Stored TCDD: Direct Evidence from a Xenografted Fat Model'. *Environment International* 121 (December): 1113–20. https://doi.org/10.1016/j.envint.2018.10.027.

Johnston, Carl J., Kevin E. Driscoll, Jacob N. Finkelstein, R. Baggs, Michael A. O'Reilly, Janet Carter, Robert Gelein, and Günter Oberdörster. 2000. 'Pulmonary Chemokine and Mutagenic Responses in Rats after Subchronic Inhalation of Amorphous and Crystalline Silica'. *Toxicological Sciences* 56 (2): 405–13. https://doi.org/10.1093/toxsci/56.2.405.

Joshi, Gaurav, Renée Gilberti, and David Knecht. 2017. 'Single Cell Analysis of Phagocytosis, Phagosome Maturation, Phagolysosomal Leakage, and Cell Death Following Exposure of Macrophages to Silica Particles'. In *Methods in Molecular Biology (Clifton, N.J.)*, 1519:55–77. https://doi.org/10.1007/978-1-4939-6581-6_5.

Kabadi, Pranita K., April L. Rodd, Alysha E. Simmons, Norma J. Messier, Robert H. Hurt, and Agnes B. Kane. 2019a. 'A Novel Human 3D Lung Microtissue Model for Nanoparticle-Induced Cell-Matrix Alterations'. *Particle and Fibre Toxicology* 16 (1): 15. https://doi.org/10.1186/s12989-019-0298-0.

———. 2019b. 'A Novel Human 3D Lung Microtissue Model for Nanoparticle-Induced Cell-Matrix Alterations'. *Particle and Fibre Toxicology* 16 (1): 15. https://doi.org/10.1186/s12989-019-0298-0.

Ketterl, Nina, Gabriele Brachtl, Cornelia Schuh, Karen Bieback, Katharina Schallmoser, Andreas Reinisch, and Dirk Strunk. 2015. 'A Robust Potency Assay Highlights Significant Donor Variation of Human Mesenchymal Stem/Progenitor Cell Immune Modulatory Capacity and Extended Radio-Resistance'. *Stem Cell Research & Therapy* 6 (1): 236. https://doi.org/10.1186/s13287-015-0233-8.

Kishimoto, T, S Akira, M Narazaki, and T Taga. 1995. 'Interleukin-6 Family of Cytokines and Gp130'. *Blood* 86 (4): 1243–54. https://doi.org/10.1182/blood.V86.4.1243.bloodjournal8641243.

Korani, Mitra, Seyed Mahdi Rezayat, and Sepideh Arbabi Bidgoli. 2013. 'Sub-Chronic Dermal Toxicity of Silver Nanoparticles in Guinea Pig: Special Emphasis to Heart, Bone and Kidney Toxicities'. *Iranian Journal of Pharmaceutical Research : IJPR* 12 (3): 511–19.

Kreyling, Wolfgang G., Uwe Holzwarth, Stephanie Hirn, Carsten Schleh, Alexander Wenk, Martin Schäffler, Nadine Haberl, and Neil Gibson. 2020. 'Quantitative Biokinetics over a 28 Day Period of Freshly Generated, Pristine, 20 Nm Silver Nanoparticle Aerosols in Healthy Adult Rats after a Single 1½-Hour Inhalation Exposure'. *Particle and Fibre Toxicology* 17 (1): 21. https://doi.org/10.1186/s12989-020-00347-1.

Kreyling, Wolfgang G., Winfried Möller, Uwe Holzwarth, Stephanie Hirn, Alexander Wenk, Carsten Schleh, Martin Schäffler, Nadine Haberl, Neil Gibson, and Johannes C. Schittny. 2018. 'Age-Dependent Rat Lung Deposition Patterns of Inhaled 20 Nanometer Gold Nanoparticles and Their Quantitative Biokinetics in Adult Rats'. *ACS Nano* 12 (8): 7771–90. https://doi.org/10.1021/acsnano.8b01826.

Krishna, Sheila, and Lloyd S. Miller. 2012. 'Innate and Adaptive Immune Responses against Staphylococcus Aureus Skin Infections'. *Seminars in Immunopathology* 34 (2): 261–80. https://doi.org/10.1007/s00281-011-0292-6.

Kuppusamy, Palaniselvam, Mashitah M. Yusoff, Gaanty Pragas Maniam, and Natanamurugaraj Govindan. 2016. 'Biosynthesis of Metallic Nanoparticles Using Plant Derivatives and Their New Avenues in Pharmacological Applications – An Updated Report'. *Saudi Pharmaceutical Journal* 24 (4): 473–84. https://doi.org/10.1016/j.jsps.2014.11.013.

Lafait, Jacques, Serge Berthier, Christine Andraud, Vincent Reillon, and Julie Boulenguez. 2009. 'Physical Colors in Cultural Heritage: Surface Plasmons in Glass'. *Comptes Rendus Physique*, Physics and heritage, 10 (7): 649–59. https://doi.org/10.1016/j.crhy.2009.08.004.

'LAGEOS: LAser GEOdynamic Satellite'. n.d. Accessed 11 April 2022. https://lageos.gsfc.nasa.gov/.

Lansdown, Alan B. G. 2010. 'A Pharmacological and Toxicological Profile of Silver as an Antimicrobial Agent in Medical Devices'. *Advances in Pharmacological Sciences* 2010 (August): e910686. https://doi.org/10.1155/2010/910686.

Lauschke, Volker M., Reza Z. Shafagh, Delilah F. G. Hendriks, and Magnus Ingelman-Sundberg. 2019. '3D Primary Hepatocyte Culture Systems for Analyses of Liver Diseases, Drug Metabolism, and Toxicity: Emerging Culture Paradigms and Applications'. *Biotechnology Journal* 14 (7): 1800347. https://doi.org/10.1002/biot.201800347.

Lee, Aaron, Dedy Septiadi, Patricia Taladriz-Blanco, Mauro Almeida, Laetitia Haeni, Miguel Spuch-Calvar, Wildan Abdussalam, Barbara Rothen-Rutishauser, and Alke Petri-Fink. 2021. 'Particle Stiffness and Surface Topography Determine Macrophage-Mediated Removal of Surface Adsorbed Particles'. *Advanced Healthcare Materials* 10 (6): 2001667. https://doi.org/10.1002/adhm.202001667.

Lehner, Roman, Wendel Wohlleben, Dedy Septiadi, Robert Landsiedel, Alke Petri-Fink, and Barbara Rothen-Rutishauser. 2020. 'A Novel 3D Intestine Barrier Model to Study the Immune Response upon Exposure to Microplastics'. *Archives of Toxicology* 94 (7): 2463–79. https://doi.org/10.1007/s00204-020-02750-1.

Leibe, Regina, I-Lun Hsiao, Susanne Fritsch-Decker, Ulrike Kielmeier, Ane Marit Wagbo, Benjamin Voss, Annemarie Schmidt, et al. 2019. 'The Protein Corona Suppresses the Cytotoxic and Pro-Inflammatory Response in Lung Epithelial Cells and Macrophages upon Exposure to Nanosilica'. *Archives of Toxicology* 93 (4): 871–85. https://doi.org/10.1007/s00204-019-02422-9.

Leroux, Mélanie M., Romain Hocquel, Kevin Bourge, Boštjan Kokot, Hana Kokot, Tilen Koklič, Janez Štrancar, et al. 2022. 'Aerosol–Cell Exposure System Applied to Semi-Adherent Cells for Aerosolization of Lung Surfactant and Nanoparticles Followed by High Quality RNA Extraction'. *Nanomaterials* 12 (8): 1362. https://doi.org/10.3390/nano12081362.

'Les Nanomatériaux. Définitions, Risques Toxicologiques, Caractérisation de l'exposition Professionnelle et Mesures de Prévention - Brochure - INRS'. n.d. Accessed 21 April 2020. http://www.inrs.fr/media.html?refINRS=ED%206050.

'Lignes directrices de l'OMS pour la protection des travailleurs contre les risques potentiels des nanomatériaux manufacturés'. n.d., 96.

Littman, Robert J. 2009. 'The Plague of Athens: Epidemiology and Paleopathology'. *Mount Sinai Journal of Medicine: A Journal of Translational and Personalized Medicine* 76 (5): 456–67. https://doi.org/10.1002/msj.20137.

Lovera-Leroux, Melanie, Belinda Crobeddu, Nadim Kassis, Patrice X. Petit, Nathalie Janel, Armelle Baeza-Squiban, and Karine Andreau. 2015. 'The Iron Component of Particulate Matter Is Antiapoptotic: A Clue to the Development of Lung Cancer after Exposure to Atmospheric Pollutants?' *Biochimie* 118 (November): 195–206. https://doi.org/10.1016/j.biochi.2015.09.030.

MacLeod, Amanda S., and Jonathan N. Mansbridge. 2016. 'The Innate Immune System in Acute and Chronic Wounds'. *Advances in Wound Care* 5 (2): 65–78. https://doi.org/10.1089/wound.2014.0608.

'Manufacturing at the Nanoscale | National Nanotechnology Initiative'. n.d. Accessed 14 February 2022. https://www.nano.gov/nanotech-101/what/manufacturing.

Marambio-Jones, Catalina, and Eric M. V. Hoek. 2010. 'A Review of the Antibacterial Effects of Silver Nanomaterials and Potential Implications for Human Health and the Environment'. *Journal of Nanoparticle Research* 12 (5): 1531–51. https://doi.org/10.1007/s11051-010-9900-y.

Marcus, Katrin, and Thierry Rabilloud. 2020. 'How Do the Different Proteomic Strategies Cope with the Complexity of Biological Regulations in a Multi-Omic World? Critical Appraisal and Suggestions for Improvements'. *Proteomes* 8 (3): 23. https://doi.org/10.3390/proteomes8030023.

Martins-de-Souza, Daniel, Giuseppina Maccarrone, Thomas Wobrock, Inga Zerr, Philipp Gormanns, Stefan Reckow, Peter Falkai, Andrea Schmitt, and Christoph W. Turck. 2010. 'Proteome Analysis of the Thalamus and Cerebrospinal Fluid Reveals Glycolysis Dysfunction and Potential Biomarkers Candidates for Schizophrenia'. *Journal of Psychiatric Research* 44 (16): 1176–89. https://doi.org/10.1016/j.jpsychires.2010.04.014.

Matsuzaki, Hidenori, Megumi Maeda, Suni Lee, Yasumitsu Nishimura, Naoko Kumagai-Takei, Hiroaki Hayashi, Shoko Yamamoto, et al. 2012. 'Asbestos-Induced Cellular and Molecular Alteration of Immunocompetent Cells and Their Relationship with Chronic Inflammation and Carcinogenesis'. *Journal of Biomedicine & Biotechnology* 2012: 492608. https://doi.org/10.1155/2012/492608.

Mazzarello, Paolo. 1999. 'A Unifying Concept: The History of Cell Theory'. *Nature Cell Biology* 1 (1): E13–15. https://doi.org/10.1038/8964.

Milliat, Fabien, and Agnès François. 2018. 'Les mastocytes, stakhanovistes de l'immunité - Un rôle énigmatique dans les lésions radiques…'. *médecine/sciences* 34 (2): 145–54. https://doi.org/10.1051/medsci/20183402012.

Mitra, Korani, Rezayat Seyed Mehdi, and Ghamami Seyedeh Giti. 2013. 'Silver Nanoparticle Induced Muscle Abnormalities: A Sub-Chronic Dermal Assessment In Guinea Pig' 1 (3): 143–51.

Mohammadi, Sina, Carolina Morell-Perez, Charles W. Wright, Thomas P. Wyche, Cory H. White, Theodore R. Sana, and Linda A. Lieberman. 2021. 'Assessing Donor-to-Donor Variability in

Human Intestinal Organoid Cultures'. *Stem Cell Reports* 16 (9): 2364–78. https://doi.org/10.1016/j.stemcr.2021.07.016.
Mottas, Inès, Ana Milosevic, Alke Petri-Fink, Barbara Rothen-Rutishauser, and Carole Bourquin. 2017. 'A Rapid Screening Method to Evaluate the Impact of Nanoparticles on Macrophages'. *Nanoscale* 9 (7): 2492–2504. https://doi.org/10.1039/C6NR08194K.
Mueller, Daniel, Lisa Krämer, Esther Hoffmann, Sebastian Klein, and Fozia Noor. 2014. '3D Organotypic HepaRG Cultures as in Vitro Model for Acute and Repeated Dose Toxicity Studies'. *Toxicology in Vitro*, ESTIV 2012: Proceedings of the 17th International Congress on In Vitro Toxicology, 28 (1): 104–12. https://doi.org/10.1016/j.tiv.2013.06.024.
Müller, B, C Seifart, and P J Barth. 1998. 'Effect of Air Pollutants on the Pulmonary Surfactant System'. *European Journal of Clinical Investigation* 28 (9): 762–77. https://doi.org/10.1046/j.1365-2362.1998.00342.x.
Murphy, Fiona A, Anja Schinwald, Craig A Poland, and Ken Donaldson. 2012. 'The Mechanism of Pleural Inflammation by Long Carbon Nanotubes: Interaction of Long Fibres with Macrophages Stimulates Them to Amplify pro-Inflammatory Responses in Mesothelial Cells'. *Particle and Fibre Toxicology* 9 (April): 8. https://doi.org/10.1186/1743-8977-9-8.
Murugadoss, Sivakumar, Sybille van den Brule, Frederic Brassinne, Noham Sebaihi, Jorge Mejia, Stéphane Lucas, Jasmine Petry, et al. 2020. 'Is Aggregated Synthetic Amorphous Silica Toxicologically Relevant?' *Particle and Fibre Toxicology* 17 (1): 1. https://doi.org/10.1186/s12989-019-0331-3.
Murugadoss, Sivakumar, Dominique Lison, Lode Godderis, Sybille Van Den Brule, Jan Mast, Frederic Brassinne, Noham Sebaihi, and Peter H. Hoet. 2017. 'Toxicology of Silica Nanoparticles: An Update'. *Archives of Toxicology* 91 (9): 2967–3010. https://doi.org/10.1007/s00204-017-1993-y.
Nattrass, C., C. J. Horwell, D. E. Damby, A. Kermanizadeh, D. M. Brown, and V. Stone. 2015. 'The Global Variability of Diatomaceous Earth Toxicity: A Physicochemical and in Vitro Investigation'. *Journal of Occupational Medicine and Toxicology (London, England)* 10 (July): 23. https://doi.org/10.1186/s12995-015-0064-7.
Noever, D. A., H. C. Matsos, R. J. Cronise, L. L. Looger, R. A. Relwani, and J. U. Johnson. 1994. 'Computerized in Vitro Test for Chemical Toxicity Based on Tetrahymena Swimming Patterns'. *Chemosphere* 29 (6): 1373–84. https://doi.org/10.1016/0045-6535(94)90269-0.
Nova, Zuzana, Henrieta Skovierova, Jan Strnadel, Erika Halasova, and Andrea Calkovska. 2020. 'Short-Term versus Long-Term Culture of A549 Cells for Evaluating the Effects of Lipopolysaccharide on Oxidative Stress, Surfactant Proteins and Cathelicidin LL-37'. *International Journal of Molecular Sciences* 21 (3): 1148. https://doi.org/10.3390/ijms21031148.
OECD. 2008. *Test No. 407: Repeated Dose 28-day Oral Toxicity Study in Rodents*. Paris: Organisation for Economic Co-operation and Development. https://www.oecd-ilibrary.org/environment/test-no-407-repeated-dose-28-day-oral-toxicity-study-in-rodents_9789264070684-en.
Ortmann, Daniel, and Ludovic Vallier. 2017. 'Variability of Human Pluripotent Stem Cell Lines'. *Current Opinion in Genetics & Development* 46 (October): 179–85. https://doi.org/10.1016/j.gde.2017.07.004.
'OSHA's Respirable Crystalline Silica Standard for General Industry and Maritime'. n.d., 2.
Parihar, Arti, Timothy D. Eubank, and Andrea I. Doseff. 2010. 'Monocytes and Macrophages Regulate Immunity through Dynamic Networks of Survival and Cell Death'. *Journal of Innate Immunity* 2 (3): 204–15. https://doi.org/10.1159/000296507.
Parks, C. G., K. Conrad, and G. S. Cooper. 1999. 'Occupational Exposure to Crystalline Silica and Autoimmune Disease.' *Environmental Health Perspectives* 107 (suppl 5): 793–802. https://doi.org/10.1289/ehp.99107s5793.
Pattanayak,DK, Muduli, J, Sahu, SS, and Gouda, S. 2021. 'Production and Characterization of Amorphous Silica Nanoparticles from Coconut Shell and Coir'. *Letters in Applied NanoBioScience* 11 (4): 4040–49. https://doi.org/10.33263/LIANBS114.40404049.
Pavan, Cristina, Rosangela Santalucia, Riccardo Leinardi, Marco Fabbiani, Yousof Yakoub, Francine Uwambayinema, Piero Ugliengo, et al. 2020. 'Nearly Free Surface Silanols Are the Critical

Molecular Moieties That Initiate the Toxicity of Silica Particles'. *Proceedings of the National Academy of Sciences* 117 (45): 27836–46. https://doi.org/10.1073/pnas.2008006117.

Perry, V. H., D. A. Hume, and S. Gordon. 1985. 'Immunohistochemical Localization of Macrophages and Microglia in the Adult and Developing Mouse Brain'. *Neuroscience* 15 (2): 313–26. https://doi.org/10.1016/0306-4522(85)90215-5.

Pimentel, J. C., and A. P. Menezes. 1975. 'Liver Granulomas Containing Copper in Vineyard Sprayer's Lung. A New Etiology of Hepatic Granulomatosis'. *Am Rev Respir Dis* 111 (2): 189–95.

Pollard, Kenneth Michael. 2016. 'Frontiers | Silica, Silicosis, and Autoimmunity | Immunology'. 2016. https://www.frontiersin.org/articles/10.3389/fimmu.2016.00097/full.

Porcherie, Adeline, Patricia Cunha, Angelina Trotereau, Perrine Roussel, Florence B Gilbert, Pascal Rainard, and Pierre Germon. 2012. 'Repertoire of Escherichia Coli Agonists Sensed by Innate Immunity Receptors of the Bovine Udder and Mammary Epithelial Cells'. *Veterinary Research* 43 (1): 14. https://doi.org/10.1186/1297-9716-43-14.

Powell, Jonathan J., Nuno Faria, Emma Thomas-McKay, and Laetitia C. Pele. 2010. 'Origin and Fate of Dietary Nanoparticles and Microparticles in the Gastrointestinal Tract'. *Journal of Autoimmunity*, The Environment, Geoepidemiology and Autoimmune Disease, 34 (3): J226–33. https://doi.org/10.1016/j.jaut.2009.11.006.

Powers, Christina M., Edward D. Levin, Frederic J. Seidler, and Theodore A. Slotkin. 2011. 'Silver Exposure in Developing Zebrafish Produces Persistent Synaptic and Behavioral Changes'. *Neurotoxicology and Teratology* 33 (2): 329–32. https://doi.org/10.1016/j.ntt.2010.10.006.

Price, Elliott J., Chiara M. Vitale, Gary W. Miller, Arthur David, Robert Barouki, Karine Audouze, Douglas I. Walker, et al. 2022. 'Merging the Exposome into an Integrated Framework for "Omics" Sciences'. *IScience* 25 (3): 103976. https://doi.org/10.1016/j.isci.2022.103976.

'Principles and Methods to Assess the Risk of Immunotoxicity Associated with Exposure to Nanomaterials'. n.d. Accessed 21 April 2020. https://www.who.int/publications-detail/principles-and-methods-to-assess-the-risk-of-immunotoxicity-associated-with-exposure-to-nanomaterials.

Quadros, Marina E., Raymond Pierson, Nicolle S. Tulve, Robert Willis, Kim Rogers, Treye A. Thomas, and Linsey C. Marr. 2013. 'Release of Silver from Nanotechnology-Based Consumer Products for Children'. *Environmental Science & Technology* 47 (15): 8894–8901. https://doi.org/10.1021/es4015844.

Rabilloud, Thierry, and Pierre Lescuyer. 2015. 'Proteomics in Mechanistic Toxicology: History, Concepts, Achievements, Caveats, and Potential'. *Proteomics* 15 (5–6): 1051–74. https://doi.org/10.1002/pmic.201400288.

Rabolli, Virginie, Leen C. J. Thomassen, Catherine Princen, Dorota Napierska, Laetitia Gonzalez, Micheline Kirsch-Volders, Peter H. Hoet, et al. 2010. 'Influence of Size, Surface Area and Microporosity on the in Vitro Cytotoxic Activity of Amorphous Silica Nanoparticles in Different Cell Types'. *Nanotoxicology* 4 (3): 307–18. https://doi.org/10.3109/17435390.2010.482749.

Radiom, M, Yong He, Juan Peng, Armelle Baeza-Squiban, Jean-François Berret, and Yong Chen. 2020. 'Alveolar Mimics with Periodic Strain and Its Effect on the Cell Layer Formation', 25.

Radiom, M, M. Sarkis, O. Brookes, E. K. Oikonomou, A. Baeza-Squiban, and J.-F. Berret. 2020. 'Pulmonary Surfactant Inhibition of Nanoparticle Uptake by Alveolar Epithelial Cells'. *Scientific Reports* 10 (1): 19436. https://doi.org/10.1038/s41598-020-76332-7.

Rai, Ayushi, Saba Noor, Syed Ishraque Ahmad, Mohamed F. Alajmi, Afzal Hussain, Hashim Abbas, and Gulam Mustafa Hasan. 2021. 'Recent Advances and Implication of Bioengineered Nanomaterials in Cancer Theranostics'. *Medicina* 57 (2): 91. https://doi.org/10.3390/medicina57020091.

Rees, David, and J Murray. 2007. 'Silica, Silicosis and Tuberculosis [State of the Art Series. Occupational Lung Disease in High- and Low-Income Countries, Edited by M. Chan-Yeung. Number 4 in the Series]'. *The International Journal of Tuberculosis and Lung Disease* 11 (May): 474–84.

Règlement (UE) 2015/2283 du Parlement européen et du Conseil du 25 novembre 2015 relatif aux nouveaux aliments, modifiant le règlement (UE) n° 1169/2011 du Parlement européen et du

Conseil et abrogeant le règlement (CE) n° 258/97 du Parlement européen et du Conseil et le règlement (CE) n° 1852/2001 de la Commission (Texte présentant de l'intérêt pour l'EEE). 2015. *OJ L*. Vol. 327. http://data.europa.eu/eli/reg/2015/2283/oj/fra.

'Règlement (UE) no 1169/2011 du Parlement européen et du Conseil du 25 octobre 2011 concernant l'information des consommateurs sur les denrées alimentaires, modifiant les règlements (CE) no 1924/2006 et (CE) no 1925/2006 du Parlement européen et du Conseil et abrogeant la directive 87/250/CEE de la Commission, la directive 90/496/CEE du Conseil, la directive 1999/10/CE de la Commission, la directive 2000/13/CE du Parlement européen et du Conseil, les directives 2002/67/CE et 2008/5/CE de la Commission et le règlement (CE) no 608/2004 de la CommissionTexte présentant de l'intérêt pour l'EEE'. n.d., 46.

'Rhazes de Variolis et Morbillis : Arabice et Latine ; Cum Aliis Nonnullis Eiusdem Argumenti / Cura et Impensis Iohannis Channing, Natu et Civitate Londinensis. - Yale University Library'. n.d. Accessed 16 April 2020. http://findit.library.yale.edu/catalog/digcoll:25720.

Riedel, Stefan. 2005. 'Edward Jenner and the History of Smallpox and Vaccination'. *Proceedings (Baylor University. Medical Center)* 18 (1): 21–25.

Rios, Sacnite Ramirez, Anaelle Torres, Hélène Diemer, Véronique Collin-Faure, Sarah Cianférani, Laurence Lafanechère, and Thierry Rabilloud. 2021. 'A Proteomic-Informed View of the Changes Induced by Loss of Cellular Adherence: The Example of Mouse Macrophages'. *PLOS ONE* 16 (5): e0252450. https://doi.org/10.1371/journal.pone.0252450.

'Risques biologiques en animalerie de recherche - Article de revue - INRS'. n.d. Accessed 20 April 2022. https://www.inrs.fr/media.html?refINRS=TC%20157.

Rossner, Pavel, Tereza Cervena, Michal Vojtisek-Lom, Kristyna Vrbova, Antonin Ambroz, Zuzana Novakova, Fatima Elzeinova, et al. 2019. 'The Biological Effects of Complete Gasoline Engine Emissions Exposure in a 3D Human Airway Model (MucilAirTM) and in Human Bronchial Epithelial Cells (BEAS-2B)'. *International Journal of Molecular Sciences* 20 (22): E5710. https://doi.org/10.3390/ijms20225710.

Rubio, Laura, Pyrgiotakis, Georgios, Zhang, Yipei, and Beltran-Huarac, Juan. 2019. 'Safer-by-Design Flame-Sprayed Silicon Dioxide Nanoparticles: The Role of Silanol Content on ROS Generation, Surface Activity and Cytotoxicity'. *Particle and Fibre Toxicology*, 15. https://doi.org/10.1186/s12989-019-0325-1.

Safi, Malak, Minhao Yan, Marie-Alice Guedeau-Boudeville, Hélène Conjeaud, Virginie Garnier-Thibaud, Nicole Boggetto, Armelle Baeza-Squiban, Florence Niedergang, Dietrich Averbeck, and Jean-François Berret. 2011. 'Interactions between Magnetic Nanowires and Living Cells: Uptake, Toxicity, and Degradation'. *ACS Nano* 5 (7): 5354–64. https://doi.org/10.1021/nn201121e.

Sanderson, Katharine. 2006. 'Sharpest Cut from Nanotube Sword'. *Nature*, November, news061113-11. https://doi.org/10.1038/news061113-11.

Šantić, Žarko, Zlatko Puvačić, Svjetlana Radović, and Sandra Puvačić. 2005. 'Higher Mortality Risk of Lungs Carcinoma in Vineyard Sprayers'. *Bosnian Journal of Basic Medical Sciences* 5 (2): 65–69. https://doi.org/10.17305/bjbms.2005.3287.

Sayes, Christie M., Kenneth L. Reed, and David B. Warheit. 2007. 'Assessing Toxicity of Fine and Nanoparticles: Comparing In Vitro Measurements to In Vivo Pulmonary Toxicity Profiles'. *Toxicological Sciences* 97 (1): 163–80. https://doi.org/10.1093/toxsci/kfm018.

says, Sioe See Volaric. 2013. 'Dynamic Light Scattering (DLS) - Understanding the Basics'. AZoNano.Com. 17 October 2013. https://www.azonano.com/article.aspx?ArticleID=3662.

Scheller, Jürgen, Athena Chalaris, Dirk Schmidt-Arras, and Stefan Rose-John. 2011. 'The Pro- and Anti-Inflammatory Properties of the Cytokine Interleukin-6'. *Biochimica et Biophysica Acta (BBA) - Molecular Cell Research*, Including the Special Section: 11th European Symposium on Calcium, 1813 (5): 878–88. https://doi.org/10.1016/j.bbamcr.2011.01.034.

Schinwald, Anja, Tanya Chernova, and Ken Donaldson. 2012. 'Use of Silver Nanowires to Determine Thresholds for Fibre Length-Dependent Pulmonary Inflammation and Inhibition of Macrophage Migration in Vitro'. *Particle and Fibre Toxicology* 9 (1): 47. https://doi.org/10.1186/1743-8977-9-47.

‘Sécurité Des Nanomatériaux Manufacturés - OCDE’. n.d. Accessed 21 February 2022. https://www.oecd.org/fr/securitechimique/nanosecurite/.

Semmler, M., J. Seitz, F. Erbe, P. Mayer, J. Heyder, G. Oberdörster, and W. G. Kreyling. 2004. ‘Long-Term Clearance Kinetics of Inhaled Ultrafine Insoluble Iridium Particles from the Rat Lung, Including Transient Translocation into Secondary Organs’. *Inhalation Toxicology* 16 (6–7): 453–59. https://doi.org/10.1080/08958370490439650.

Sharma, Virender K., Jan Filip, Radek Zboril, and Rajender S. Varma. 2015. ‘Natural Inorganic Nanoparticles – Formation, Fate, and Toxicity in the Environment’. *Chemical Society Reviews* 44 (23): 8410–23. https://doi.org/10.1039/C5CS00236B.

Slezak, B. P., G. E. Hatch, M. J. DeVito, J. J. Diliberto, R. Slade, K. Crissman, E. Hassoun, and L. S. Birnbaum. 2000. ‘Oxidative Stress in Female B6C3F1 Mice Following Acute and Subchronic Exposure to 2,3,7,8-Tetrachlorodibenzo-p-Dioxin (TCDD)’. *Toxicological Sciences: An Official Journal of the Society of Toxicology* 54 (2): 390–98. https://doi.org/10.1093/toxsci/54.2.390.

Soldatow, Valerie Y., Edward L. LeCluyse, Linda G. Griffith, and Ivan Rusyn. 2013. ‘In Vitro Models for Liver Toxicity Testing’. *Toxicology Research* 2 (1): 23–39. https://doi.org/10.1039/C2TX20051A.

Sridharan, Rukmani, Brenton Cavanagh, Andrew R. Cameron, Daniel J. Kelly, and Fergal J. O’Brien. 2019. ‘Material Stiffness Influences the Polarization State, Function and Migration Mode of Macrophages’. *Acta Biomaterialia* 89 (April): 47–59. https://doi.org/10.1016/j.actbio.2019.02.048.

Störmer, A., J. Bott, D. Kemmer, and R. Franz. 2017. ‘Critical Review of the Migration Potential of Nanoparticles in Food Contact Plastics’. *Trends in Food Science & Technology* 63 (May): 39–50. https://doi.org/10.1016/j.tifs.2017.01.011.

Sun, B., S. Pokhrel, D. R. Dunphy, H. Zhang, Z. Ji, X. Wang, M. Wang, et al. 2015. ‘Reduction of Acute Inflammatory Effects of Fumed Silica Nanoparticles in the Lung by Adjusting Silanol Display through Calcination and Metal Doping’. *ACS Nano* 9 (9): 9357–72.

TANIGUCHI, N. 1974. ‘On the Basic Concept of Nanotechnology’. *Proceeding of the ICPE*. https://ci.nii.ac.jp/naid/10008480916.

Thakur, Sheetal A., Celine A. Beamer, Christopher T. Migliaccio, and Andrij Holian. 2009. ‘Critical Role of MARCO in Crystalline Silica–Induced Pulmonary Inflammation’. *Toxicological Sciences* 108 (2): 462–71. https://doi.org/10.1093/toxsci/kfp011.

‘The History of the Peloponnesian War, by Thucydides 431 BC’. n.d. Accessed 16 April 2020. https://www.gutenberg.org/files/7142/7142-h/7142-h.htm.

Torres, Anaelle, Véronique Collin-Faure, Hélène Diemer, Christine Moriscot, Daphna Fenel, Benoît Gallet, Sarah Cianférani, Jacques-Aurélien Sergent, and Thierry Rabilloud. 2022. ‘Repeated Exposure of Macrophages to Synthetic Amorphous Silica Induces Adaptive Proteome Changes and a Moderate Cell Activation’. *Nanomaterials* 12 (9): 1424. https://doi.org/10.3390/nano12091424.

Torres, Bastien Dalzon, Véronique Collin-Faure, Hélène Diemer, Daphna Fenel, Guy Schoehn, Sarah Cianférani, Marie Carrière, and Thierry Rabilloud. 2020. ‘How Reversible Are the Effects of Fumed Silica on Macrophages? A Proteomics-Informed View’. *Nanomaterials* 10 (10): 1939. https://doi.org/10.3390/nano10101939.

Torres, Bastien Dalzon, Véronique Collin-Faure, and Thierry Rabilloud. 2020. ‘Repeated vs. Acute Exposure of RAW264.7 Mouse Macrophages to Silica Nanoparticles: A Bioaccumulation and Functional Change Study’. *Nanomaterials* 10 (2): 215. https://doi.org/10.3390/nano10020215.

Toybou, Djadidi, Caroline Celle, Catherine Aude-Garcia, Thierry Rabilloud, and Jean-Pierre Simonato. 2019. ‘A Toxicology-Informed, Safer by Design Approach for the Fabrication of Transparent Electrodes Based on Silver Nanowires’. *Environmental Science.Nano* 6 (2): 684–94. https://doi.org/10.1039/c8en00890f.

‘Transmission Electron Microscope (TEM) - Uses, Advantages and Disadvantages’. n.d. MicroscopeMaster. Accessed 14 February 2022. https://www.microscopemaster.com/transmission-electron-microscope.html.

Traoré, T., C. Béchaux, V. Sirot, and A. Crépet. 2016. 'To Which Chemical Mixtures Is the French Population Exposed? Mixture Identification from the Second French Total Diet Study'. *Food and Chemical Toxicology* 98 (December): 179–88. https://doi.org/10.1016/j.fct.2016.10.028.

Traoré, T., A. Forhan, V. Sirot, M. Kadawathagedara, B. Heude, M. Hulin, B. de Lauzon-Guillain, J. Botton, M. A. Charles, and A. Crépet. 2018. 'To Which Mixtures Are French Pregnant Women Mainly Exposed? A Combination of the Second French Total Diet Study with the EDEN and ELFE Cohort Studies'. *Food and Chemical Toxicology* 111 (January): 310–28. https://doi.org/10.1016/j.fct.2017.11.016.

Triboulet, S., C. Aude-Garcia, L. Armand, V. Collin-Faure, M. Chevallet, H. Diemer, A. Gerdil, et al. 2015. 'Comparative Proteomic Analysis of the Molecular Responses of Mouse Macrophages to Titanium Dioxide and Copper Oxide Nanoparticles Unravels Some Toxic Mechanisms for Copper Oxide Nanoparticles in Macrophages'. *Plos One* 10 (4): e0124496.

Triboulet, S., C. Aude-Garcia, L. Armand, A. Gerdil, H. Diemer, F. Proamer, V. Collin-Faure, et al. 2014. 'Analysis of Cellular Responses of Macrophages to Zinc Ions and Zinc Oxide Nanoparticles: A Combined Targeted and Proteomic Approach'. *Nanoscale* 6 (11): 6102–14.

Triboulet, Sarah, Catherine Aude-Garcia, Marie Carrière, Hélène Diemer, Fabienne Proamer, Aurélie Habert, Mireille Chevallet, et al. 2013. 'Molecular Responses of Mouse Macrophages to Copper and Copper Oxide Nanoparticles Inferred from Proteomic Analyses'. *Molecular & Cellular Proteomics* 12 (11): 3108–22. https://doi.org/10.1074/mcp.M113.030742.

Turci, Francesco, Cristina Pavan, Riccardo Leinardi, Maura Tomatis, Linda Pastero, David Garry, Sergio Anguissola, Dominique Lison, and Bice Fubini. 2016. 'Revisiting the Paradigm of Silica Pathogenicity with Synthetic Quartz Crystals: The Role of Crystallinity and Surface Disorder'. *Particle and Fibre Toxicology* 13 (June). https://doi.org/10.1186/s12989-016-0136-6.

Vance, Marina E., Todd Kuiken, Eric P. Vejerano, Sean P. McGinnis, Michael F. Hochella Jr, David Rejeski, and Matthew S. Hull. 2015. 'Nanotechnology in the Real World: Redeveloping the Nanomaterial Consumer Products Inventory'. *Beilstein Journal of Nanotechnology* 6 (1): 1769–80. https://doi.org/10.3762/bjnano.6.181.

Verbanck, Marie, Mickaël Canouil, Audrey Leloire, Véronique Dhennin, Xavier Coumoul, Loïc Yengo, Philippe Froguel, and Odile Poulain-Godefroy. 2017. 'Low-Dose Exposure to Bisphenols A, F and S of Human Primary Adipocyte Impacts Coding and Non-Coding RNA Profiles'. *PLoS ONE* 12 (6): e0179583. https://doi.org/10.1371/journal.pone.0179583.

Veronesi, G., C. Aude-Garcia, I. Kieffer, T. Gallon, P. Delangle, N. Herlin-Boime, T. Rabilloud, and M. Carriere. 2015. 'Exposure-Dependent Ag+ Release from Silver Nanoparticles and Its Complexation in AgS2 Sites in Primary Murine Macrophages'. *Nanoscale* 7 (16): 7323–30.

Vila, L., R. Marcos, and A. Hernandez. 2017. 'Long-Term Effects of Silver Nanoparticles in Caco-2 Cells'. *Nanotoxicology* 11 (6): 771–80.

Villeneuve, Daniel L., Natàlia Garcia-Reyero, B. Lynn Escalon, Kathleen M. Jensen, Jenna E. Cavallin, Elizabeth A. Makynen, Elizabeth J. Durhan, et al. 2012. 'Ecotoxicogenomics to Support Ecological Risk Assessment: A Case Study with Bisphenol A in Fish'. *Environmental Science & Technology* 46 (1): 51–59. https://doi.org/10.1021/es201150a.

Vorrink, Sabine U, Yitian Zhou, Magnus Ingelman-Sundberg, and Volker M Lauschke. 2018. 'Prediction of Drug-Induced Hepatotoxicity Using Long-Term Stable Primary Hepatic 3D Spheroid Cultures in Chemically Defined Conditions'. *Toxicological Sciences* 163 (2): 655–65. https://doi.org/10.1093/toxsci/kfy058.

Wasinger, V. C., S. J. Cordwell, A. Cerpa-Poljak, J. X. Yan, A. A. Gooley, M. R. Wilkins, M. W. Duncan, R. Harris, K. L. Williams, and I. Humphery-Smith. 1995. 'Progress with Gene-Product Mapping of the Mollicutes: Mycoplasma Genitalium'. *Electrophoresis* 16 (7): 1090–94. https://doi.org/10.1002/elps.11501601185.

Wattiez, R., and P. Falmagne. 2005. 'Proteomics of Bronchoalveolar Lavage Fluid'. *Journal of Chromatography B*, Proteomic Databases Part III, 815 (1): 169–78. https://doi.org/10.1016/j.jchromb.2004.10.029.

'What Nanomaterials Exist in Nature?' 2018. AZoNano.Com. 20 April 2018. https://www.azonano.com/article.aspx?ArticleID=4837.

Wiemann, Martin, Antje Vennemann, Ursula G. Sauer, Karin Wiench, Lan Ma-Hock, and Robert Landsiedel. 2016. 'An in Vitro Alveolar Macrophage Assay for Predicting the Short-Term Inhalation Toxicity of Nanomaterials'. *Journal of Nanobiotechnology* 14 (1): 16. https://doi.org/10.1186/s12951-016-0164-2.

Winkler, Hans Christian, Julian Kornprobst, Peter Wick, Lea Maria von Moos, Ioannis Trantakis, Elisabeth Maria Schraner, Barbara Bathke, Hubertus Hochrein, Mark Suter, and Hanspeter Naegeli. 2017. 'MyD88-Dependent pro-Interleukin-1β Induction in Dendritic Cells Exposed to Food-Grade Synthetic Amorphous Silica'. *Particle and Fibre Toxicology* 14 (1): 21. https://doi.org/10.1186/s12989-017-0202-8.

Yeo, Min-Kyeong, and Jae-Won Yoon. 2009. 'Comparison of the Effects of Nano-Silver Antibacterial Coatings and Silver Ions on Zebrafish Embryogenesis'. *Molecular & Cellular Toxicology* 5 (1): 23–31.

Younes, Maged, Peter Aggett, Fernando Aguilar, Riccardo Crebelli, Birgit Dusemund, Metka Filipič, Maria Jose Frutos, et al. 2018. 'Re-Evaluation of Silicon Dioxide (E 551) as a Food Additive'. *EFSA Journal* 16 (1): e05088. https://doi.org/10.2903/j.efsa.2018.5088.

Zhang, H. Y., D. R. Dunphy, X. M. Jiang, H. Meng, B. B. Sun, D. Tarn, M. Xue, et al. 2012. 'Processing Pathway Dependence of Amorphous Silica Nanoparticle Toxicity: Colloidal vs Pyrolytic'. *Journal of the American Chemical Society* 134 (38): 15790–804.

Zhang, Xi-Feng, Zhi-Guo Liu, Wei Shen, and Sangiliyandi Gurunathan. 2016. 'Silver Nanoparticles: Synthesis, Characterization, Properties, Applications, and Therapeutic Approaches'. *International Journal of Molecular Sciences* 17 (9): 1534. https://doi.org/10.3390/ijms17091534.

Zhao, Fei, and Walter T. Klimecki. 2015. 'CULTURE CONDITIONS PROFOUNDLY IMPACT PHENOTYPE IN BEAS-2B, A HUMAN PULMONARY EPITHELIAL MODEL'. *Journal of Applied Toxicology : JAT* 35 (8): 945–51. https://doi.org/10.1002/jat.3094.

Annexes

Communications :

Présentation NanoSafe 2020

Présentation NanoTox 2021

Poster NanoTox 2021

Poster JRC summer school 2021

Présentation Journée éco-conception AXELERA 2021

Présentation Congrès Jeunes chercheurs AURA 2021

Résumé graphique JAD ED CSV 2021

Poster EuroTox 2021

Présentation STCM 2022

Towards a better trial of occupational exposures: *In vitro* macrophage systems for repeated nanomaterial exposure study

Anaëlle TORRES, Bastien DALZON and Thierry RABILLOUD

- Synthetic amorphous silica
  - Professional and consumer exposure
  - Classical toxicological studies: acute exposure but not representative
- System: macrophages
  - Scavenger and ubiquitous
  - Cultured/conducted during a week
- Results
  - Bioaccumulation
  - Decreased effects but still present

Solvay
Silica GBU

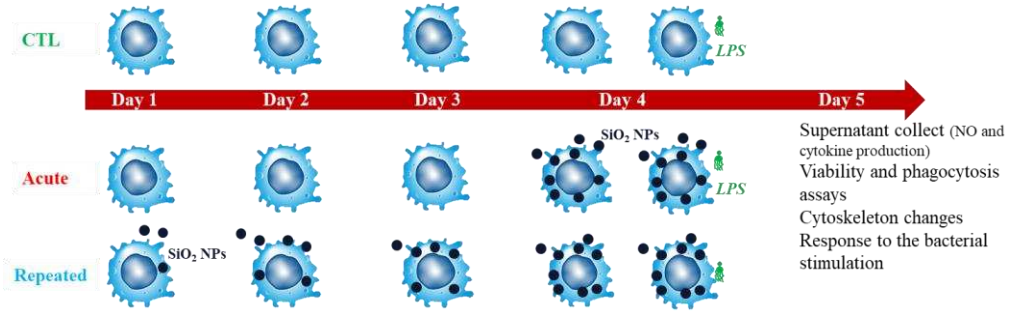

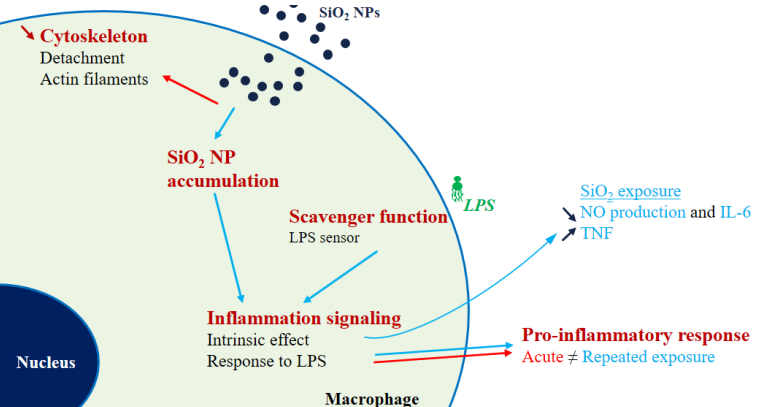

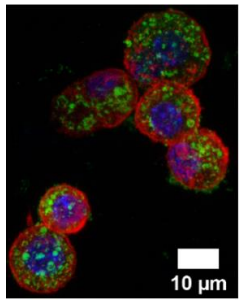

10_A µg/ml

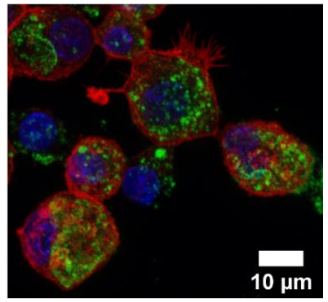

4x5_R µg/ml

nanomaterials

MDPI

Article

Repeated vs. Acute Exposure of RAW264.7 Mouse Macrophages to Silica Nanoparticles: A Bioaccumulation and Functional Change Study

Anaëlle Torres *, Bastien Dalzon, Véronique Collin-Faure and Thierry Rabilloud *

Torres A *et al.*, 2020, Nanomaterials, doi:10.3390/nano10020215

Towards a better appraisal of occupational exposures: *In vitro* macrophage systems for repeated nanomaterial exposure study

Thesis supervisor: Thierry RABILLOUD
Co-supervisor: Jacques-Aurélien SERGENT

Anaëlle Torres, Bastien Dalzon, Véronique Collin-Faure, Thierry Rabilloud. *Repeated vs. Acute Exposure of RAW264.7 Mouse Macrophages to Silica Nanoparticles: A Bioaccumulation and Functional Change Study*. *Nanomaterials, MDPI, 2020, 10 (2), pp.215. DOI:10.3390/nano10020215*

Introduction: silica

- crystalline silica (chronic inflammatory disease) *vs* synthetic amorphous silica (SAS)
- REACH regulation
- Various end-markets

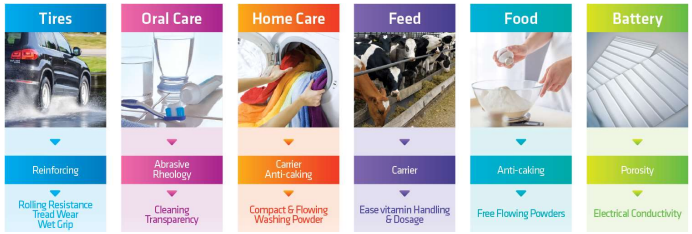

From Solvay, GBU Silica

Nanotoxicology studies on macrophages

Our working horses: macrophages ([redacted]= big & [redacted]= eat)

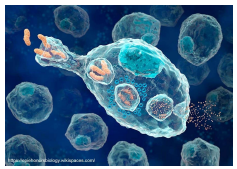

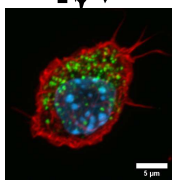

Surveillance and scavenger cells present in many body localizations (e.g. skin, lungs, digestive tract)

The tetralogy of macrophages
- tasting (*via* proteinaceous receptors located at cell membrane)
- ingesting (phagocytosis)
- digesting (phagolysosomes)
- communicating (key players in inflammation)

→ mediators (NO, prostaglandins, cytokines)

Exposure scenarii

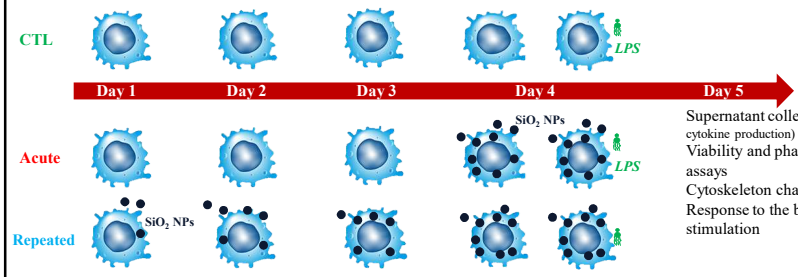

Supernatant collect (NO and cytokine production)
Viability and phagocytosis assays
Cytoskeleton changes
Response to the bacterial stimulation

- Different conditions:
  - With and without **LPS stimulation** (18 hours)
  - **Silica**
    - Acute exposure 5, 10 and 20 µg/ml
    - Repeated exposure 2 and 5 µg/ml/day

$1x20_A$ µg/ml ⇔ $4x5_R$ µg/ml/day

SiG MFI with FacsMelody and confocal microscopy

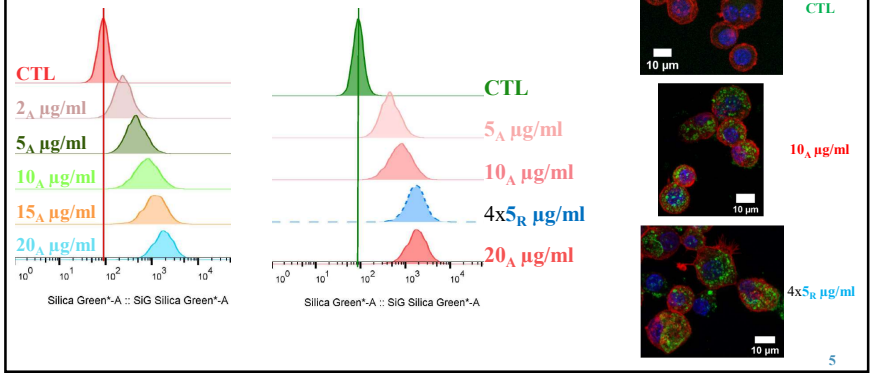

Results: LS30 repeated 4 days + LPS

Viability

- 4x5_R decrease of 15% compared with CTL
- 20_A decrease of 45% compared with CTL

→ Decrease of viability (4x5_R and 20_A) **less important** in repeated exposure

Phagocytosis

- 4x5_R decrease of 50% for phagocytic cells, 60% less active than CTL
- 20_A 60% less phagocytic than CTL and 60% less active

→ Decrease of phagocytosis (4x5_R and 20_A)

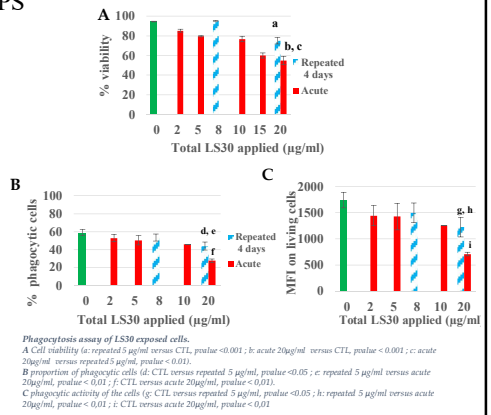

Phagocytosis assay of LS30 exposed cells.
A Cell viability (a: repeated 5 µg/ml versus CTL, pvalue <0.001 ; b: acute 20µg/ml versus CTL, pvalue < 0.001 ; c: acute 20µg/ml versus repeated 5 µg/ml, pvalue < 0.01).
B proportion of phagocytic cells (d: CTL versus repeated 5 µg/ml, pvalue <0.05 ; e: repeated 5 µg/ml versus acute 20µg/ml, pvalue < 0,01 ; f: CTL versus acute 20µg/ml, pvalue < 0,01).
C phagocytic activity of the cells (g: CTL versus repeated 5 µg/ml, pvalue <0.05 ; h: repeated 5 µg/ml versus acute 20µg/ml, pvalue < 0,01 ; i: CTL versus acute 20µg/ml, pvalue < 0,01

Results : LS30 repeated 4 days + LPS

NO production

- without LPS:
  - 4x5_R ⇔ CTL ⇔ 20_A
- with LPS:
  - 4x5_R decrease of 10% compared with CTL
  - 20_A decrease of 30%

→ No intrinsic effect of silica
→ Effect of co-exposure LPS/silica 20_A

Cytokine secretion

- without LPS:
  - TNF
    - 4x5_R ◆ 20_A 2 fold CTL

→ Intrinsic effect of silica in repeated exposure and 20_A

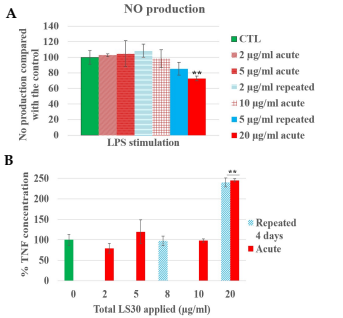

4-days chronic exposure of RAW264.7 to LS30 NP and 18h to LPS compared with silica acute exposure.
A NO dosage with the Griess reagent by spectrophotometry with LPS stimulation
B TNF cytokine release, in absence of LPS of LS30 exposed cells by flow cytometry.

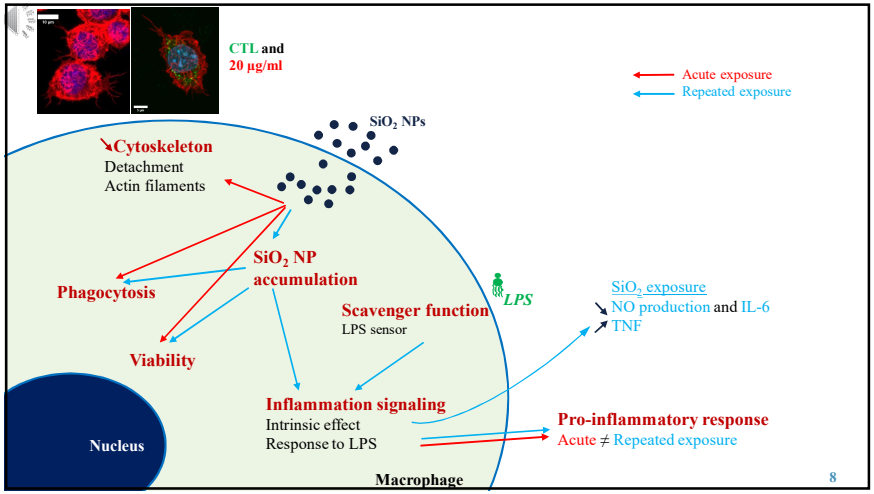

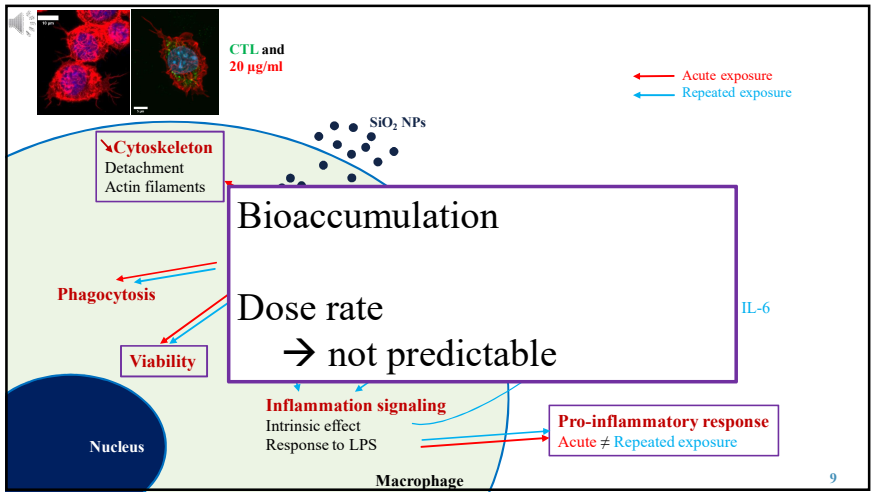

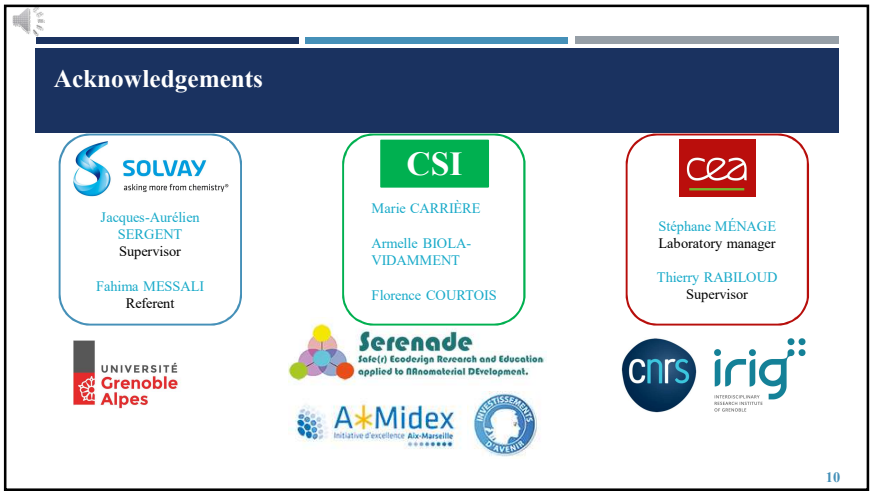

THANKS FOR YOUR ATTENTION!

In vitro macrophage systems for nanomaterial exposure study and persistence of the effects: towards a better assessment of occupational exposure

in conference

Torres A [1,5], Dalzon, B. [1], Collin-Faure, V. [1], Diemer, H. [2], Fenel, D. [3], Schoehn, G. [3], Cianférani, S. [2], Carrière, M. [4], Rabilloud, T [1]. (2020) *How reversible are the effects of fumed silica on macrophages? A proteomics-informed view. Nanomaterials* **2020**, 10, 1939; DOI:10.3390/nano10101939
Thesis supervisors: Sergent J.-A. [6] and Rabilloud T [1].

[1]Laboratory of Chemistry and Biology of Metals, University Grenoble Alpes, CNRS, CEA, UMR 5249, CEDEX 09, 38054 Grenoble, France
[2]Laboratoire de Spectrométrie de Masse BioOrganique, Université de Strasbourg, CNRS, IPHC UMR 7178, F-67087 Strasbourg, France
[3]Institute for Structural Biology, Université Grenoble Alpes, CNRS, CEA, F-38000 Grenoble, France
[4]Chimie Interface Biologie pour l'Environnement, la Santé et la Toxicologie (CIBEST), University Grenoble-Alpes, CEA, CNRS UMR 5819, IRIG-SyMMES, F-38054 Grenoble, France
[5]Solvay GBU Silica, EPA Lyon, France
[6]Solvay, Toxicological environmental risk assessment, Brussels, Belgium

Context and objective

To develop in vitro system to study reversibility of the effect to nanomaterial exposure

Synthetic Amorphous Silica (SAS) is one of the most used nanomaterials (NM), with various applications such as food additive, cosmetics ingredient or in tires to reduce rolling resistance. Considering these uses encountered in daily life, a single high-dose exposure mode, is not the most relevant mode to assess the relevant biological effects of NM exposure. Therefore, we have developed an *in vitro* system of nanomaterial exposure to evaluate the persistence of effects via a recovery period.

Model and method

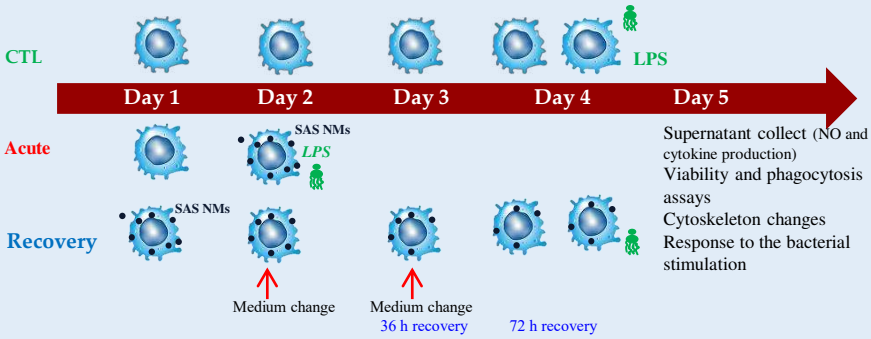

Murine macrophage cell line RAW264.7 exposed to pyrogenic SAS (CAS number 112945-52-5)

Results

SAS characterization:

- TEM (24h incubation at 37°C)

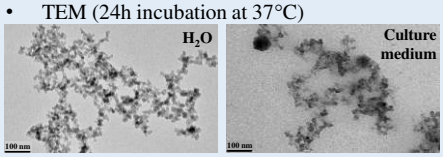

- DLS (24h incubation at 37°C): hydrodynamic diameter of the aggregates in water was 278nm *versus* 912nm in culture medium

Validation experiments based on proteomic study results

Cytoskeleton damage:
Confocal microscopy
Pyrolytic SAS induced a decrease in the surface of the cytoplasmic projections (lamellipodia and filipodia).
This effect was persistent at the end of the 72h recovery period.

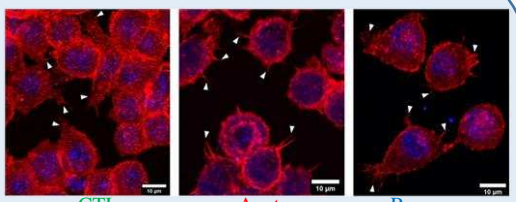

Macrophage functions:

Cell viability

The effect of pyrogenic SAS on cell viability was investigated, and had indicated a lethal dose 20% (LD20) at 20µg/ml. This concentration was used for all the further experiments.

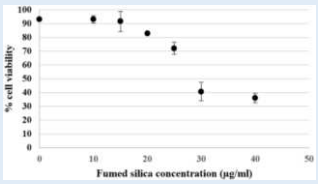

Phagocytosis

The effect of pyrogenic SAS on the key function of macrophages was investigated, and showed no significant change either immediately after exposure or after recovery period.

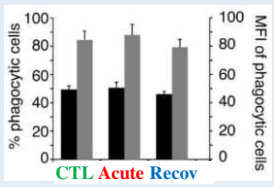

Inflammatory responses

The effects of pyrogenic SAS exposure were assayed because of the known involvement of crystalline silica in the development of the chronic inflammatory disease. We tested two different schemes: without (intrinsic proinflammatory effect of SAS) or with stimulation by lipopolysaccharides (interference of SAS to macrophage responses to bacteria).

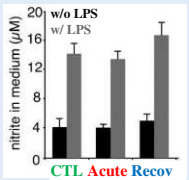

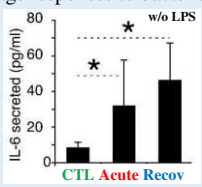

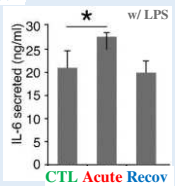

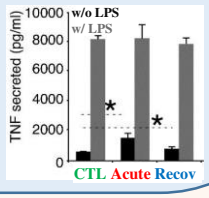

Conclusion

The recovery study reported a significant persistence of effects after pyrogenic SAS exposure as illustrated by an increase of the pro-inflammatory response (TNF and IL-6) and changes in protein abundances (cell adhesion, carbon metabolism or mitochondrion) even after a 72h recovery period.

28 days ⇔ 5 days
200 k€ 3-4 k€

Perspectives

Our systems allow testing important determinants of toxicity by investigating the general cell functions and specialized functions of the macrophages following exposure to nanomaterials. Furthermore, our *in vitro* protocols yield results consistent with those from *in vivo* mouse models.

Interesting tool toward safe by design approach

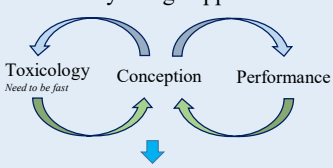

Towards a better appraisal of occupational exposures: *In vitro* macrophage systems for repeated nanomaterial exposure study

NanoTox2021

Thesis supervisor: Thierry RABILLOUD
Co-supervisor: Jacques-Aurélien SERGENT

Anaëlle Torres, Bastien Dalzon, Véronique Collin-Faure, Thierry Rabilloud. *Repeated vs. Acute Exposure of RAW264.7 Mouse Macrophages to Silica Nanoparticles: A Bioaccumulation and Functional Change Study*. *Nanomaterials, MDPI, 2020, 10 (2), pp.215. DOI:10.3390/nano10020215*

Introduction: silica

- crystalline silica (chronic inflammatory disease) *vs* synthetic amorphous silica (SAS)
- Various end-markets (industrial: tires, personal: cosmetics and food)

Introduction: macrophages

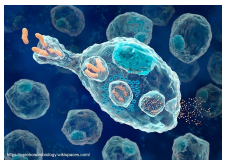

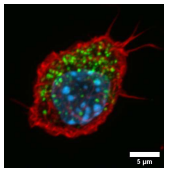

Surveillance and scavenger cells present in many body localizations (e.g. skin, lungs, digestive tract)

Management of any particulate in the body, including silica

Exposure protocols

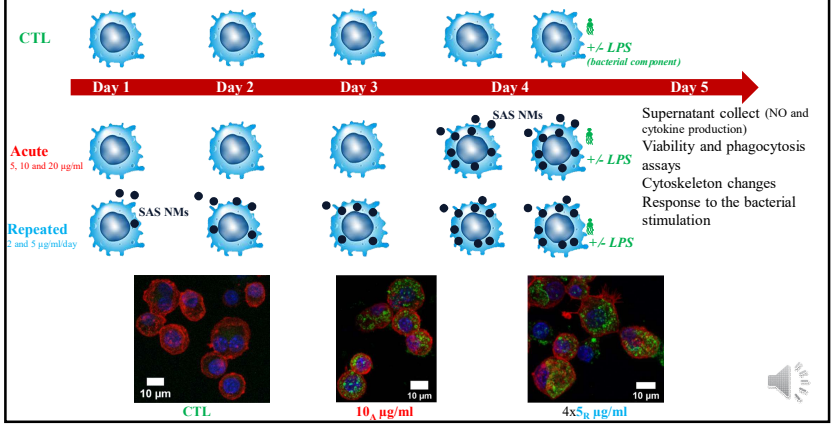

CTL | 10_A µg/ml | $4x5_R$ µg/ml

Repeated exposure
↓
Accumulation

Acute exposure

Same dose applied
(single or split doses)

15% decrease in viability
10% decrease in NO production (LPS)

45% decrease in viability
30% decrease in NO production (LPS)
Cytoskeleton changes

Decrease of phagocytosis (50%)
2 fold increase in signaling (TNF w/o LPS)

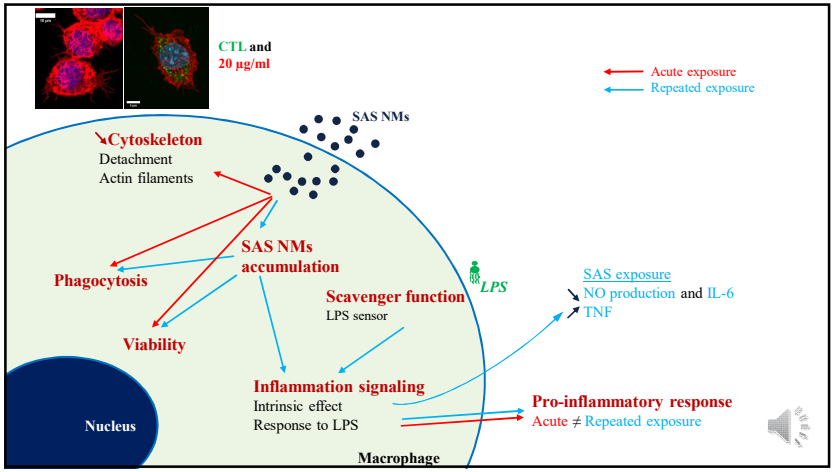

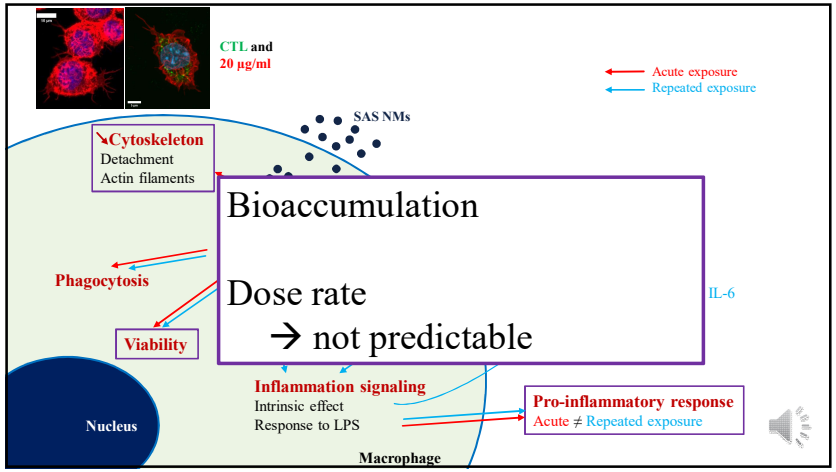

Acknowledgements

SOLVAY
asking more from chemistry®

Jacques-Aurélien SERGENT
Supervisor

Fahima MESSALI
Referent

CSI

Marie CARRIÈRE

Armelle BIOLA-VIDAMMENT

Florence COURTOIS

cea

Vincent ARTERO
Laboratory manager

Thierry RABILOUD
Supervisor

UNIVERSITÉ Grenoble Alpes

Serenade
Safe(r) Ecodesign Research and Education applied to nAnomaterial DEvelopment.

A*Midex
Initiative d'excellence Aix-Marseille

cnrs

irig

lcbm

THANKS FOR YOUR ATTENTION!

Towards a better trial of occupational exposure: *In vitro* macrophage systems for nanomaterial exposure study

Anaëlle Torres[1,2,3,4], **Bastien Dalzon**[4], **Véronique Collin-Faure**[2], **Jacques-Aurélien Sergent**[5] **and Thierry Rabilloud**[4]

[1] Solvay/GBU Silica, Lyon, France; [2] IRIG/LCBM CEA, Grenoble, France; [3] Université Grenoble Alpes, France; [4] IRIG/LCBM CNRS UMR5249 Grenoble, France; [5] Solvay SA/Toxicological and Environmental Risk Assessment unit, Brussels, Belgium

Thesis supervisors: Sergent J.-A. [6] and Rabilloud T [1].

Context

To develop in vitro system to study reversibility of the effect to nanomaterial exposure and the importance of the dose rate

Nanomaterials are defined as objects containing nanoparticles, with at least one dimension smaller than 100nm, and with peculiar physico-chemical properties. Synthetic Amorphous Silica (SAS) is one of the most used nanomaterials (NM), with various applications such as food additive, cosmetics ingredient or in tires to reduce rolling resistance. Considering these uses encountered in daily life, a single high-dose exposure mode, is not always the most relevant mode to assess the relevant biological effects of NM exposure. Therefore, we have developed *in vitro* systems of nanomaterial exposure to evaluate the persistence of effects via a recovery period and the importance of the dose rate via a repeated exposure protocol..

Model and method

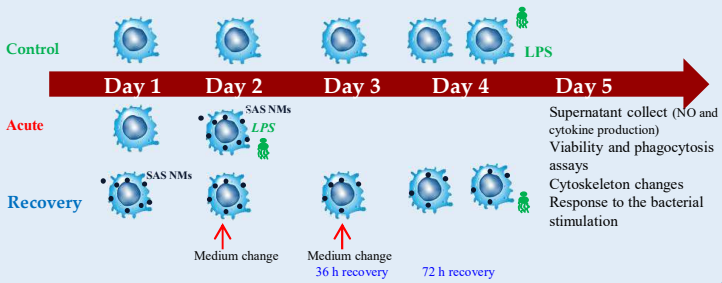

Murine macrophage cell line RAW264.7 exposed to pyrogenic SAS (CAS number 112945-52-5)

Model and method

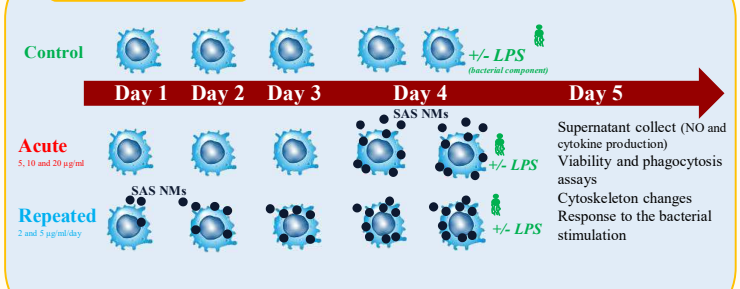

Murine macrophage cell line RAW264.7 exposed to colloidal SAS (CAS number 7631-86-9)

Results

Validation experiments based on proteomic study results

Phagocytosis

The effect of pyrogenic SAS on the key function of macrophages was investigated, and showed no significant change either immediately after exposure or after recovery period.

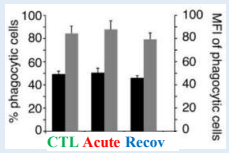

Cytoskeleton damage:

Confocal microscopy

Pyrogeniic SAS induced a decrease in the surface of the cytoplasmic projections (lamellipodia and filipodia). This effect was persistent at the end of the 72h recovery period.

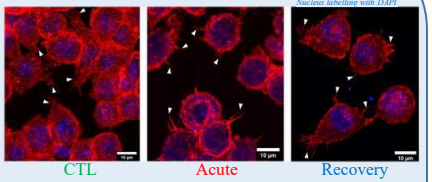

Inflammatory responses

The effects of pyrogenic SAS exposure were assayed because of the known involvement of crystalline silica in the development of the chronic inflammatory disease. We tested two different schemes: without (intrinsic proinflammatory effect of SAS) or with stimulation by lipopolysaccharides (interference of SAS to macrophage responses to bacteria).

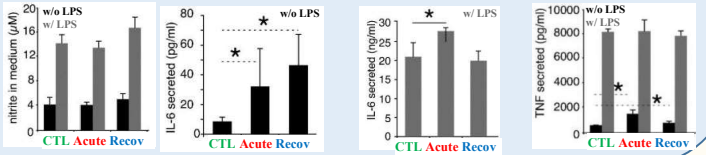

Results

Phagocytosis and viability

The LD20 was determined and the lethality is only observed in a single dose mode.

The effect of colloidal SAS dose rate on the key function of macrophages was investigated, and showed no significant change when cells are exposed to split doses of SAS contrary to single dose exposure.

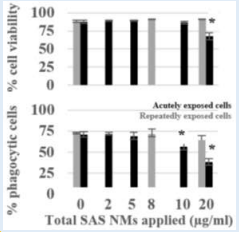

Cytoskeleton damage:

Confocal microscopy

Green fluorescent silica was internalized and accumulated in the cells. The Mean Fluorescent Intensity (MFI) of the acutely exposed cells to 20µg/ml was equivalent to the repeatedly exposed cells to 4x5µg/ml measured by flow cytometry.

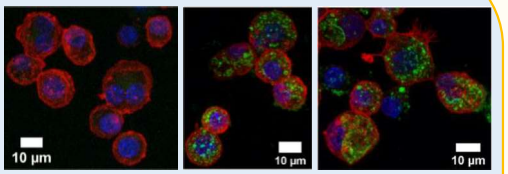

Inflammatory responses

The effects of colloidal SAS exposure were assayed because of this new protocol (mimicking daily exposure) and to compare with the literature (acute exposure studies). We tested two different schemes: without (intrinsic proinflammatory effect of SAS) or with stimulation by lipopolysaccharides (interference of SAS to macrophage responses to bacteria).

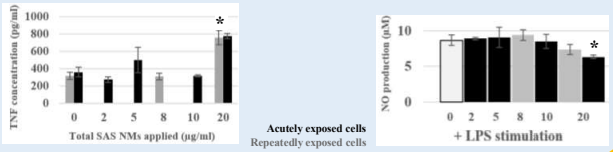

Conclusion

The recovery study reported a significant persistence of effects after pyrogenic SAS exposure as illustrated by an increase of the pro-inflammatory response (TNF and IL-6) and changes in protein abundances (cell adhesion, carbon metabolism or mitochondrion) even after a 72h recovery period.

Conclusion

The repeated exposure study highlighted light on an important key message: the effect of a repeated exposure are not predictable on the basis of acute exposure studies. The dose rate had some effects on the different parameters under investigation, and this have to be kept in mind in nanotoxicology.

Perspectives

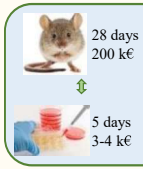

Our systems allow testing important determinants of toxicity by investigating the general cell functions and specialized functions of the macrophages following exposure to nanomaterials. Furthermore, our *in vitro* protocols yield results consistent with those from *in vivo* mouse models.

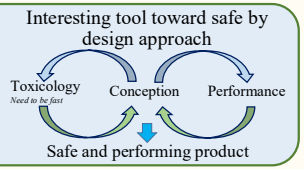

How reversible are the effects of fumed silica on macrophages? A proteomics-informed view. Nanomaterials **2020**, 10, 1939; DOI:10.3390/nano10101939

Repeated vs. Acute Exposure of RAW264.7 Mouse Macrophages to Silica Nanoparticles: A Bioaccumulation and Functional Change Study. Nanomaterials **2020**, 10, 215. DOI:10.3390/nano10020215

Système *in vitro* d'évaluation des risques liés à l'exposition à des substances chimiques (nanomatériaux)

Anaëlle TORRES
Étudiante en thèse au CEA Grenoble
anaelle.torres@cea.fr

Directeur de thèse : Thierry RABILLOUD
Co-directeur : Jacques-Aurélien SERGENT
Laboratoire principal : LCBM CEA, Grenoble
Laboratoire secondaire : Solvay, Bruxelles

27 mai 2021 – Journée AXELERA

Un outil intéressant pour une approche "safe-by-design"

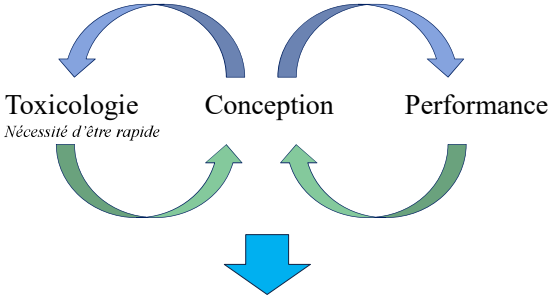

Produit moins toxique et de performance comparable

Solvay

- Nombreux domaines : automobile, aéronautique, agriculture, agroalimentaire, bien de consommation, santé, électronique, environnement, bâtiment, applications industrielles…

– GBU Silica

- Silice amorphe de synthèse, 435 000t / an

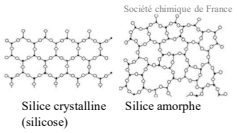

Organisation des cellules : bactérie

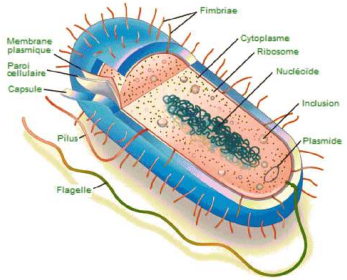

Organisation d'une cellule animale

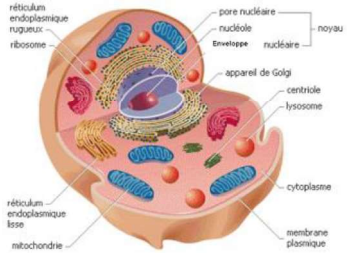

Cellule structurée

Interactions des nanomatériaux avec les organismes vivants :

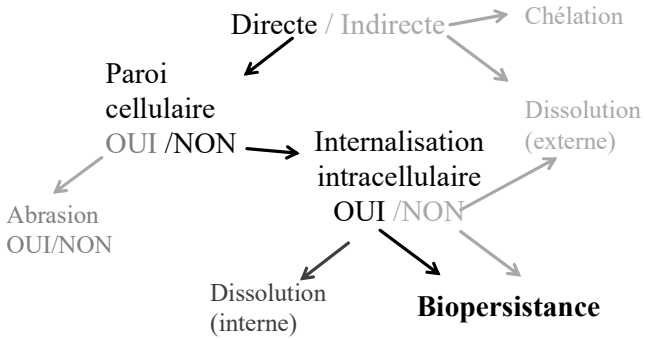

Divers effets biologiques

Métabolisme cellulaire et énergétique — Stress oxydant — Organisation cellulaire — Dommage tissulaire (direct/inflammation)

Études toxicologiques sur les macrophages

Notre cheval de bataille : macrophage (μακρος= gros & φαγειν = mangeur)

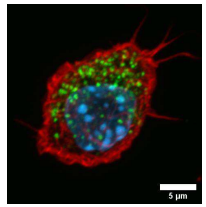

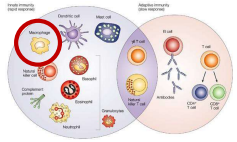

Cellules sentinelles et "éboueurs" présentes dans de nombreux sites du corps humain (peau, poumon, système digestif)

Les rôles du macrophage :

- Goûter (*via* récepteurs protéiques membranaires)
- Ingérer (phagocytose)
- Digérer (phagolysosomes)
- Communiquer (acteur clé dans l'inflammation)

→ médiateurs (NO, prostaglandines, cytokines)

Études toxicologiques :

Études *in vivo* :

✚ Persistance
Débit de dose
Pertinent au niveau physiologique
Modèle classique (règlementation REACH)

▬ Utilisation d'animaux
Coût
Recherches longues
Réponse partielle
Co-expositions difficiles
Peu de paramètres étudiés par expérience

28 jours
200 k€

⇔

Études *in vitro* :

✚ Coût modéré
Toxicité croisée (co-exposition possible)
Expériences multi-paramétriques
Stratégie des 3R

▬ Réponse des cellules (non de l'organisme entier)

5 jours
3-4 k€

Protocole d'expositions :

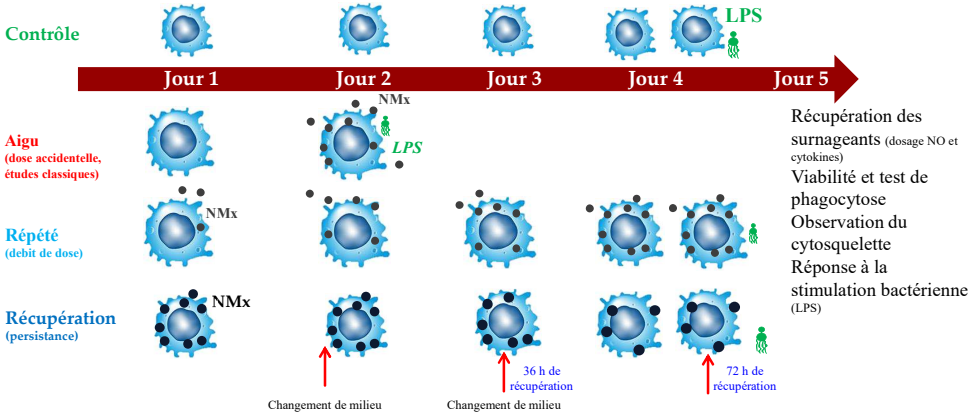

Récupération des surnageants (dosage NO et cytokines)
Viabilité et test de phagocytose
Observation du cytosquelette
Réponse à la stimulation bactérienne (LPS)

SAS colloidale 220m²/g – 20µg/ml

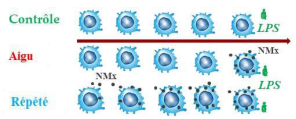

Exposition répétée

Accumulation

Dose équivalente appliquée
(dose unique ou fractionnée)

- 15% en viabilité

- 45% en viabilité
Modification du cytosquelette

Diminution de la phagocytose (50%)
Augmentation en signalisation (TNF)

Torres *et al.* (2020) *Nanomaterials* DOI : 10.3390/nano10020215

SAS précipitée 220m²/g et ***nanofils d'argent D40L20*** *- 50µg/ml*

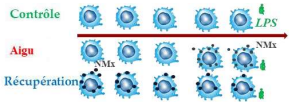

Exposition aigüe

Dose équivalente appliquée
Suivie (ou non) de 72h de
récupération sans NMx

- 20% de viabilité
- 40% phagocytose
+ 3 et **1,5 fois** signalisation (TNF)

- 10% phagocytose
+ 1,3 et **2 fois** signalisation (TNF)

Récupération

Modification du cytosquelette
(cellule géante/granulome)

Torres *et al.* (2020) *Nanomaterials* DOI : 10.3390/nano10101939
Toybou *et al.* (2020) *Environmental Science nano* DOI : 10.1039/c8en00890f

Exposition répétée

Accumulation

Dose équivalente appliquée
(dose unique ou fractionnée)

- 15% en viabilité

- 45% en viabilité
Modification du cytosquelette

Diminution de la phagocytose (50%)
Augmentation en signalisation (TNF)

Exposition aigüe

Dose équivalente appliquée
Suivie (ou non) de 72h de
récupération sans NMx

- 20% de viabilité
- 40% phagocytose
+ 3 et **1,5 fois** signalisation (TNF)

- 10% phagocytose
+ 1,3 et **2 fois** signalisation (TNF)

Récupération

Modification du cytosquelette
(cellule géante/granulome)

Bioaccumulation

Influence du débit de dose
→ Effets non prédictibles

Persistance partielle

Influence du type de NMx
→ Effets non prédictibles

Conclusion

- Résumé
  - Importance du mode d'exposition
  - Effets variés (viabilité, fonction cellulaire, structure…)

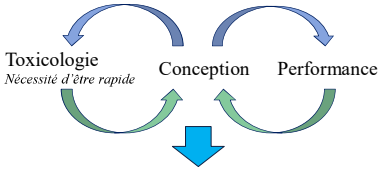

Produit moins toxique et de performance comparable

- Systèmes *in vitro*

Que nous apportent réellement les études in vitro ?

- Influence du débit de dose
- Persistance des effets
- Etudes comparatives (nanomatériaux, substances chimiques…)

28 days
200 k€

⇔

5 days
3-4 k€

Remerciements

SOLVAY
asking more from chemistry®

Jacques-Aurélien SERGENT
(Co-encadrant)

Fahima MESSALI
(Référente)

Équipe R&D
Caroline FAYOLLE
Pascaline LAURIOL-GARBEY

GBU Silica

Comité de thèse

Marie CARRIÈRE

Armelle BIOLA-VIDAMMENT

Florence COURTOIS

cea

Vincent ARTERO
Directeur du laboratoire

Équipe ProMIT
Thierry RABILLOUD
(directeur de thèse)
Bastien DALZON
Julie DEVCIC
Véronique COLLIN-FAURE

Université Grenoble Alpes
cnrs irig

pôle éco-conception
Performance du cycle de vie

ADEME
Agence de l'Environnement et de la Maîtrise de l'Energie

axelera
ENSEMBLE, CATALYSONS LES RÉUSSITES

Serenade
Safe(r) Ecodesign Research and Education applied to Nanomaterial DEvelopment.

A*Midex
Initiative d'excellence Aix-Marseille

MERCI POUR VOTRE ATTENTION !

Towards a better assessment of occupational exposures: *In vitro* macrophage systems for nanomaterial exposure study

PhD supervisor: Thierry RABILLOUD
Co-supervisor: Jacques-Aurélien SERGENT

Anaëlle TORRES, PhD student - anaelle.torres@cea.fr

Context

- Crystalline silica vs synthetic amorphous silica (SAS)
- Various applications (automobile, food, feed, cosmetics…)

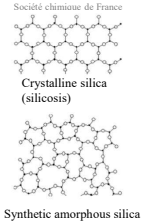

From Solvay, Silica GBU

Nanotoxicology studies on macrophages

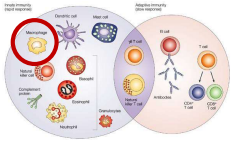

Our working horses: macrophages (μακρος= big & φαγειν = eat)

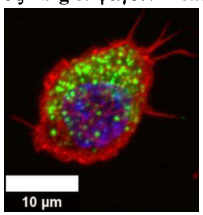

Surveillance and scavenger cells present in many body localizations (e.g. skin, lungs, digestive tract)

The tetralogy of macrophages
-ingesting (phagocytosis)
-tasting (via proteinaceous receptors located at cell membrane)
-digesting (phagolysosomes)
-communicating (key players in inflammation)
=> mediators (NO, prostaglandins, cytokines)

Phagocytosis: large, digestible (or not)

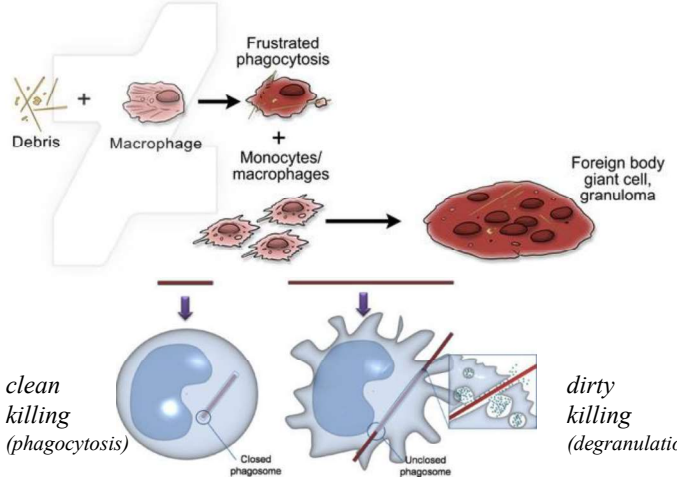

Persistence
Continuous response to the object

clean killing (phagocytosis)

dirty killing (degranulation)

Protocols

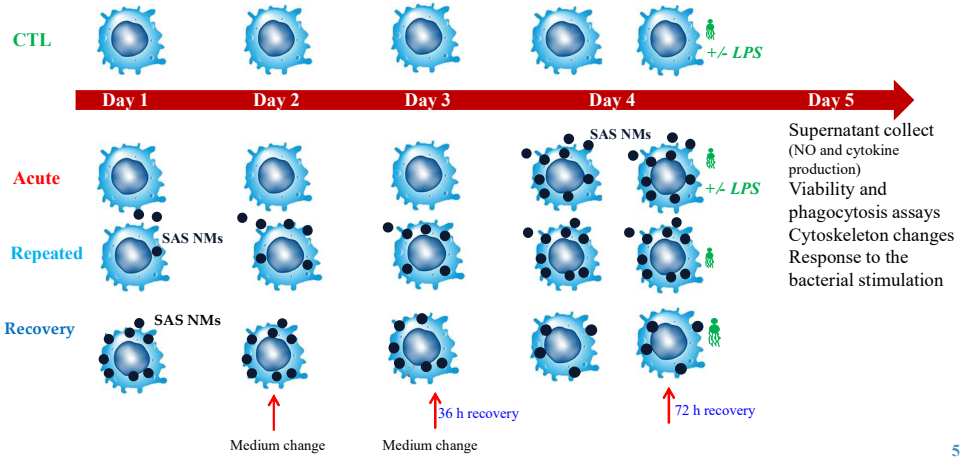

Supernatant collect
(NO and cytokine production)
Viability and phagocytosis assays
Cytoskeleton changes
Response to the bacterial stimulation

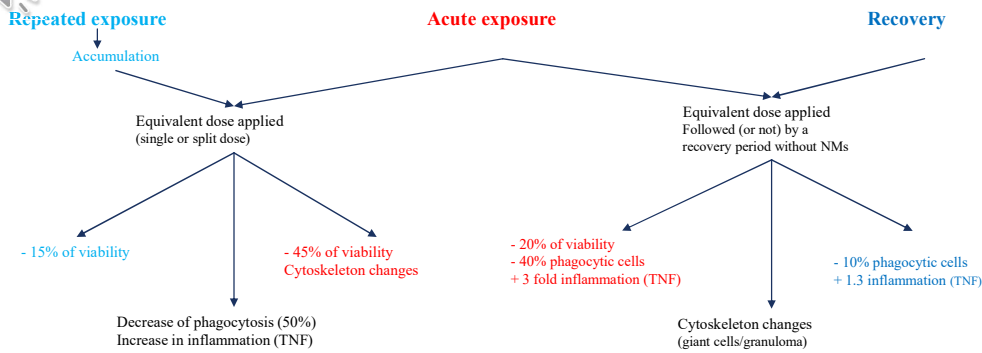

Bioaccumulation

Importance of the dose rate
→ Effects not predictable

Partial persistence

Influence of the nanomaterial
→ Effects not predictable

Conclusion

- Summary
  - Importance of exposure mode
  - Different effects (viability, cell functions, cell structure…)

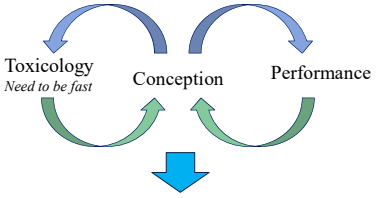

- *In vitro* systems
  - What can *in vitro* studies really deliver?
    - Influence of dose rate
    - Effect persistence
    - Comparative studies (effect determinants)

Acknowledgements

SOLVAY
asking more from chemistry®

Jacques-Aurélien SERGENT
(Supervisor)

Fahima MESSALI
(Referent)

R&D team
Caroline FAYOLLE
Pascaline LAURIOL-GARBEY

GBU Silica

Thesis committee

Marie CARRIÈRE

Armelle BIOLA-VIDAMMENT

Florence COURTOIS

cea

Vincent ARTERO
Laboratory manager

ProMD team
Thierry RABILLOUD
(Supervisor)
Bastien DALZON
Julie DEVCIC
Véronique COLLIN-FAURE

cnrs irig
UNIVERSITÉ Grenoble Alpes

Young Researchers in Biology of AURA Region Congress
Regional congress - 17 June 2021 - Videoconference NextTech AR

Serenade
Safe(r) Ecodesign Research and Education applied to Nanomaterial DEvelopment.

A*Midex

THANKS FOR YOUR ATTENTION!

In vitro macrophage systems for nanomaterial exposure study and persistence of the effects: Towards a better assessment of occupational exposure

Graphical abstract

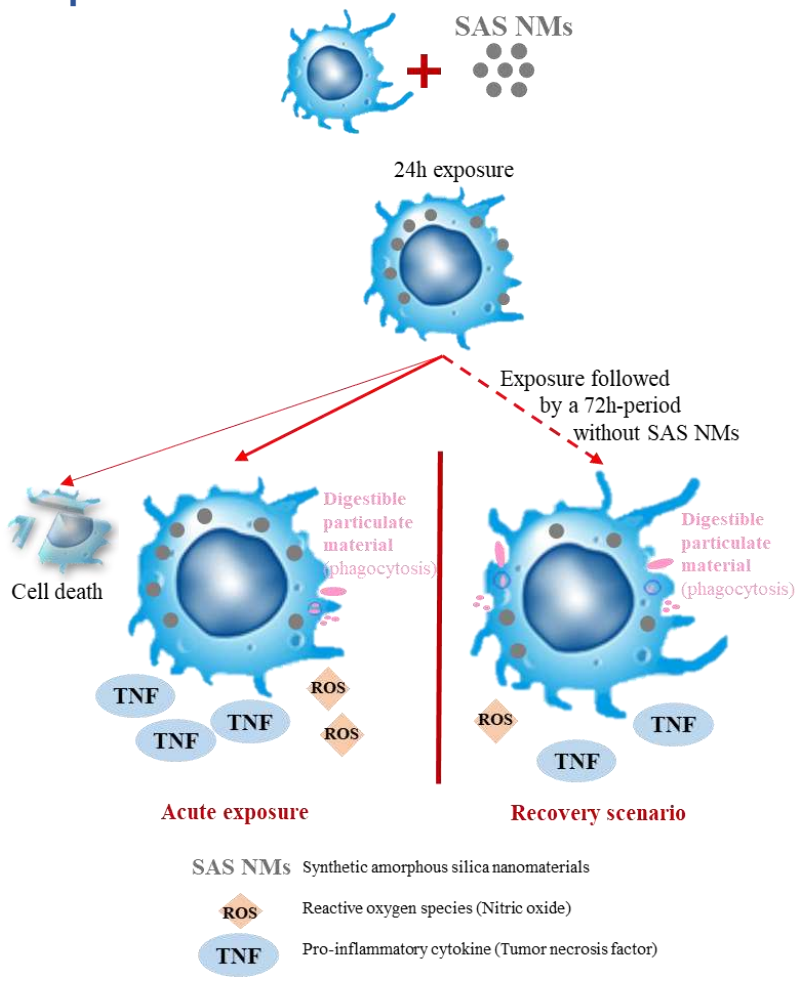

Authors

TORRES, Anaëlle
DALZON, Bastien
COLLIN-FAURE, Véronique
SERGENT, Jacques-Aurélien
RABILLOUD, Thierry

Correspondence

anaelle.torres@cea.fr
jacques-aurelien.sergent@solvay.com
thierry.rabilloud@cnrs.fr

Keywords

- **Macrophage**
- **Nanomaterials**
- **Effect persistence**
- **Recovery scenario**
- **Safer-by-design tool**

In Brief

Synthetic amorphous silicas (SAS) are largely used in industry for automobile (tires), cosmetics (toothpaste, powders…) and food (additives). In line with the recent evolution of the European regulation (REACH), we have developed safer-by-design approach, including the investigation of the persistence of the effects of SAS exposure in early stage of SAS innovation.

Université Grenoble Alpes

ÉCOLE DOCTORALE Chimie & Sciences du Vivant

EUROTOX 2021 VIRTUAL CONGRESS
27 SEPTEMBER — 1 OCTOBER 2021

Towards a better investigation of occupational exposures: *In vitro* macrophage systems for nanomaterial exposure studies

Anaëlle Torres[1,2,3,4], **Bastien Dalzon**[4], **Véronique Collin-Faure**[2], **Jacques-Aurélien Sergent**[5] **and Thierry Rabilloud**[4]

[1]Solvay/GBU Silica, Lyon, France,[2] IRIG/LCBM CEA, Grenoble, France,[3] Université Grenoble Alpes, France, [4] IRIG/LCBM CNRS UMR5249 Grenoble, France, [5] Solvay SA/Toxicological and Environmental Risk Assessment unit, Brussels, Belgium

Thesis supervisors: Sergent J.-A. [5] and Rabilloud T [4].

54th CONGRESS OF THE EUROPEAN SOCIETIES OF TOXICOLOGY
TOXICOLOGY OF THE NEXT GENERATION
WWW.EUROTOX2021.COM

Context

To develop in vitro system to study reversibility of the effect to nanomaterial exposure and the importance of the dose rate

Nanomaterials (NM) are defined as objects containing particles (in an unbound state or as an aggregate or agglomerate),where for 50 % or more of the particles in the number size distribution, one or more external dimensions is in the size range 1nm-100nm (from European commission). Synthetic Amorphous Silica (SAS) is one of the most used NM, with various applications such as food additive, cosmetics ingredient or in tires to reduce rolling resistance. Considering these uses encountered in daily life, a single high-dose exposure mode, is not always the most relevant mode to assess the relevant biological effects of NM exposure. Therefore, we have developed *in vitro* systems of nanomaterial exposure to evaluate the persistence of effects *via* a recovery period and the importance of the dose rate *via* a repeated exposure protocol.

Model and method: *persistence*

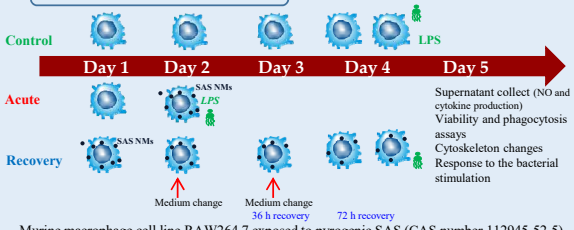

Murine macrophage cell line RAW264.7 exposed to pyrogenic SAS (CAS number 112945-52-5) or precipitated silica (CAS number 112926-00-8)

Model and method: *dose rate*

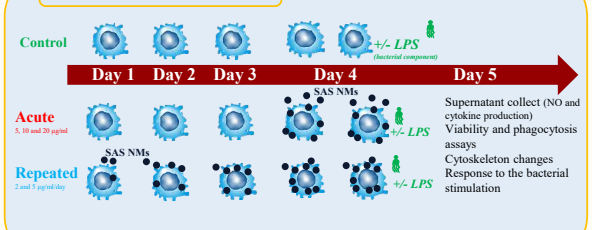

Murine macrophage cell line RAW264.7 exposed to colloidal SAS (CAS number 7631-86-9)

Results

Validation experiments based on proteomic study results

Phagocytosis

The effect of different SAS on the key function of macrophages was investigated, and showed no significant change either immediately after exposure or after recovery period.

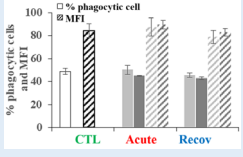

Cytoskeleton damage:

Confocal microscopy

Pyrogenic and precipitated SAS induced a decrease in the surface of the cytoplasmic projections (lamellipodia and filipodia). This effect was persistent at the end of the 72h recovery period, only for the pyrogenic SAS.

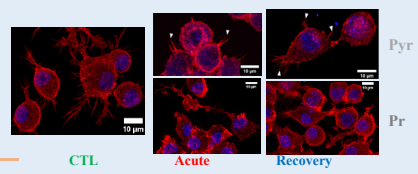

Inflammatory responses

The effects of SAS exposure were assayed because of the known involvement of crystalline silica in the development of the chronic inflammatory disease. We tested two different schemes: without (intrinsic proinflammatory effect of SAS) or with stimulation by lipopolysaccharides (interference of SAS to macrophage responses to bacteria). The results of the intrinsic effect are presented here: the pyrogenic silica induces an higher response (IL-6 and TNF) than precipitated silica (TNF only).

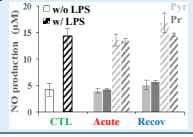

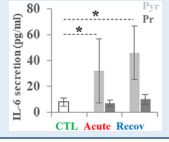

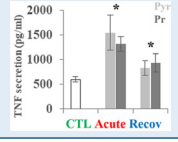

Conclusion

The recovery study reported a significant persistence of effects after SAS exposure, more pronounced for pyrogenic SAS as illustrated by an increase of the pro-inflammatory response (TNF and IL-6) and changes in protein abundances (cell adhesion, carbon metabolism or mitochondrion) even after a 72h recovery period.

Results

Phagocytosis and viability

The LD20 was determined and the lethality is only observed in a single dose mode.

The effect of colloidal SAS dose rate on the key function of macrophages was investigated, and showed no significant change when cells are exposed to split doses of SAS contrary to single dose exposure.

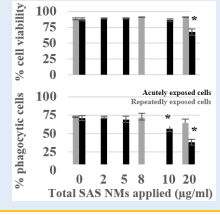

Cytoskeleton damage:

Confocal microscopy

Green fluorescent silica was internalized and accumulated in the cells. The Mean Fluorescent Intensity (MFI) of the acutely exposed cells to 20µg/ml was equivalent to the repeatedly exposed cells to 4x5µg/ml measured by flow cytometry.

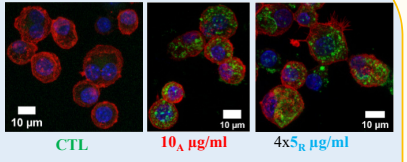

Inflammatory responses

The effects of colloidal SAS exposure were assessed because of this new protocol (mimicking daily exposure) and it was consistent with the literature (acute exposure studies). We tested two different schemes: without (intrinsic proinflammatory effect of SAS) or with stimulation by lipopolysaccharides (interference of SAS to macrophage responses to bacteria).

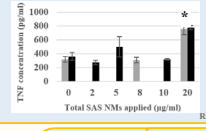

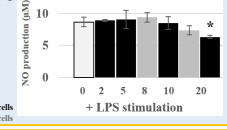

Conclusion

The repeated exposure study highlighted an important key message: the effect of a repeated exposure are not predictable on the basis of acute exposure studies. The dose rate had some effects on the different parameters under investigation, and this have to be kept in mind in nanotoxicology.

Perspectives

Our systems allow testing important determinants of toxicity by investigating the general cell functions and specialized functions of the macrophages following exposure to nanomaterials. Furthermore, our *in vitro* protocols yield results consistent with those from *in vivo* mouse models.

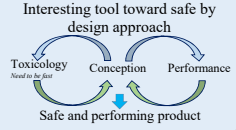

How reversible are the effects of fumed silica on macrophages? A proteomics-informed view. Nanomaterials **2020**, 10, 1939; DOI:10.3390/nano10101939

Repeated vs. Acute Exposure of RAW264.7 Mouse Macrophages to Silica Nanoparticles: A Bioaccumulation and Functional Change Study. Nanomaterials **2020**, 10, 215. DOI:10.3390/nano10020215

Système *in vitro* d'évaluation des risques liés à l'exposition à des substances chimiques (nanomatériaux)

Anaëlle TORRES
Étudiante en thèse au CEA Grenoble
anaelle.torres@cea.fr

Directeur de thèse : Thierry RABILLOUD
Co-directeur : Jacques-Aurélien SERGENT
Laboratoire principal : LCBM CEA, Grenoble
Laboratoire secondaire : Solvay, Bruxelles

Un outil intéressant pour une approche "safe-by-design"

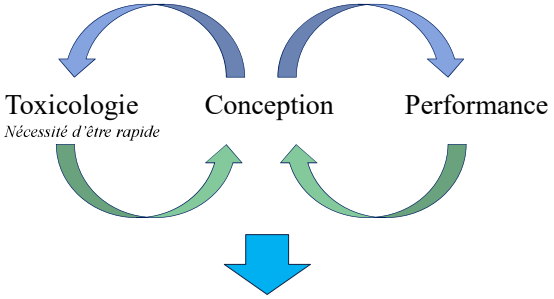

Produit moins toxique et de performance comparable

Solvay

- Nombreux domaines : automobile, aéronautique, agriculture, agroalimentaire, bien de consommation, santé, électronique, environnement, bâtiment, applications industrielles…

– GBU Silica

- Silice amorphe de synthèse, 435 000t / an

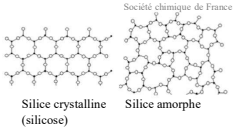

Interactions des nanomatériaux avec les organismes vivants :

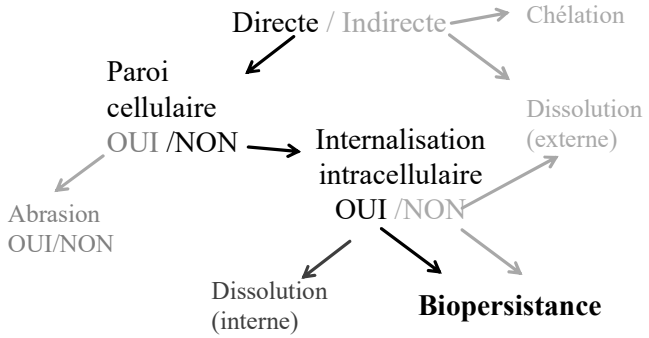

Divers effets biologiques

Métabolisme cellulaire et énergétique — Stress oxydant — Organisation cellulaire — Dommage tissulaire (direct/inflammation)

Études toxicologiques sur les macrophages

Notre cheval de bataille : macrophage (μακρος= gros & φαγειν = mangeur)

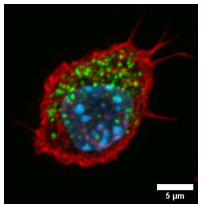

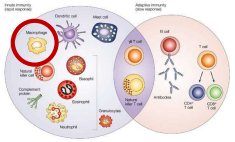

Cellules sentinelles et "éboueurs" présentes dans de nombreux sites du corps humain (peau, poumon, système digestif)

Les rôles du macrophage :

- Goûter (*via* récepteurs protéiques membranaires)
- Ingérer (phagocytose)
- Digérer (phagolysosomes)
- Communiquer (acteur clé dans l'inflammation)

→ médiateurs (NO, prostaglandines, cytokines)

Études toxicologiques :

Études *in vivo* :

✚
- Persistance
- Débit de dose
- Pertinent au niveau physiologique
- Modèle classique (règlementation REACH)

▬
- Utilisation d'animaux
- Coût
- Recherches longues
- Réponse partielle
- Co-expositions difficiles
- Peu de paramètres étudiés par expérience

Études *in vitro* :

✚
- Coût modéré
- Toxicité croisée (co-exposition possible)
- Expériences multi-paramétriques
- Stratégie des 3R

▬
- Réponse des cellules (non de l'organisme entier)

28 jours
200 k€

⇔

5 jours
3-4 k€

Protocole d'expositions :

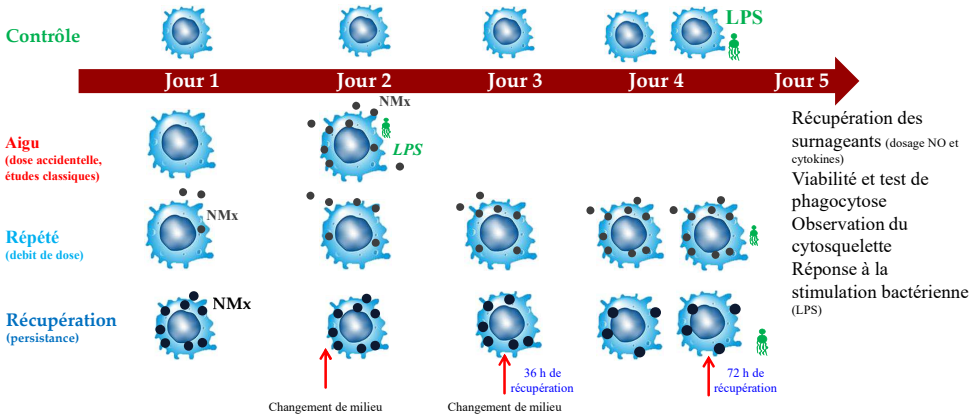

Récupération des surnageants (dosage NO et cytokines)
Viabilité et test de phagocytose
Observation du cytosquelette
Réponse à la stimulation bactérienne (LPS)

Persistance des effets et validation du système :

Silice cristalline

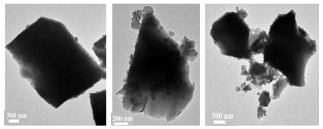

Agate pêche | Œil de tigre | Jaspe

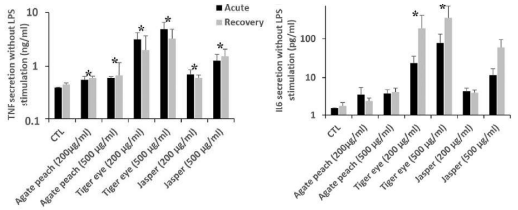

Silice amorphe de synthèse

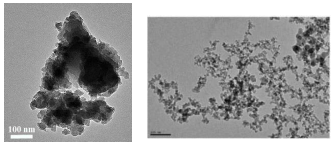

Précipitée | Fumée/pyrogénée

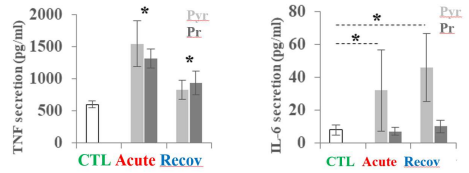

Exposition de type professionnel (chronique) :

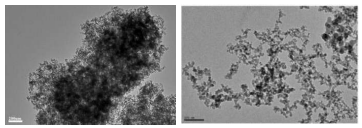

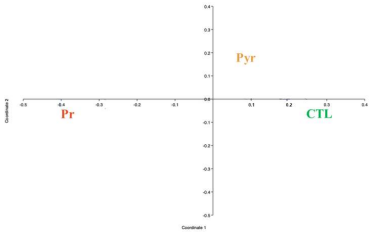

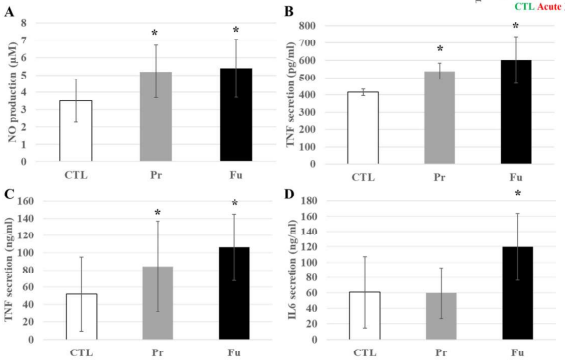

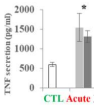

9

SAS précipitée et pyrogénée 220m²/g – 20µg/ml

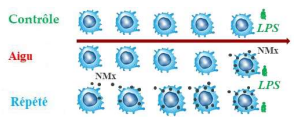

*SAS précipitée 220m²/g et **nanofils d'argent D40L20** - 50µg/ml*

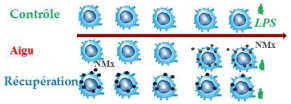

Exposition répétée

Accumulation

Dose équivalente appliquée
(dose unique ou fractionnée)

Bioaccumulation partielle

Influence du débit de dose
→ Effets non prédictibles

Torres *et al.* (2022) *Nanomaterials* en révision
Torres *et al.* (2020) *Nanomaterials* DOI:10.3390/nano10020215

Exposition aigüe

Récupération

Dose équivalente appliquée
Suivie (ou non) de 72h de
récupération sans NMx

Persistance partielle

Influence du type de NMx
→ Effets non prédictibles

Torres *et al.* (2020) *Nanomaterials* DOI : 10.3390/nano10101939
Toybou *et al.* (2020) *Environmental Science nano* DOI : 10.1039/c8en00890f

10

Conclusion

- Résumé
  - Importance du mode d'exposition
  - Effets variés (viabilité, fonction cellulaire, structure…)

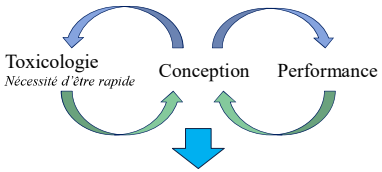

Produit moins toxique et de performance comparable

- Systèmes *in vitro*

Que nous apportent réellement les études in vitro ?

- Influence du débit de dose
- Persistance des effets
- Etudes comparatives (nanomatériaux, substances chimiques…)

11

Remerciements

SOLVAY
asking more from chemistry®

Jacques-Aurélien SERGENT
(Co-encadrant)

Fahima MESSALI
(Référente)

Équipe R&D
Caroline FAYOLLE
Pascaline LAURIOL-GARBEY

GBU Silica

Comité de thèse

Marie CARRIÈRE

Armelle BIOLA-VIDAMMENT

Florence COURTOIS

cea

Vincent ARTERO
Directeur du laboratoire

Équipe ProMIT
Thierry RABILLOUD
(directeur de thèse)
Bastien DALZON
Julie DEVCIC
Véronique COLLIN-FAURE

Université Grenoble Alpes
cnrs irig

STCM

Serenade
Safe(r) Ecodesign Research and Education applied to Nanomaterial DEvelopment.

A*Midex

12

MERCI POUR VOTRE ATTENTION !

Formations suivies Total : 409.5 heures / 35 modules

Catégorie : Activité du chercheur et pratique du métier (total 19,5h)

☛ DME-19-1 : Se développer dans son métier d'enseignant (23 septembre 2019 - 24 septembre 2019) DU - Bâtiment PLURIEL - 701 rue de la piscine - 38400 St Martin d'Hères 14 heures

☛ JEUDIS DE LA SECURITE : Le risque biologique - Français/Anglais (13 février 2020) Stendhal - amphi 4 nord - 1180, avenue Centrale - Domaine universitaire 3.5 heures

☛ JEUDIS DE LA SECURITE : Le risque chimique (06 février 2020) Stendhal - amphi 4 nord - 1180, avenue Centrale - Domaine universitaire 2 heures

Catégorie : Communication scientifique (total 15h)

☛ AFSTAL - ComPrim2021 - Raffinement des procédures et actualités (01 avril 2021 - 1 avril 2021) Alpha Visa Congrès - Montpellier enregistré par : Chimie et Sciences du Vivant.

☛ AFSTAL - ComTech2021 - Bien faire pour le Bien-être animal (19 mars 2021) Alpha VISA Congrès - Montpellier enregistré par : Chimie et Sciences du Vivant. La formation participe à l'objectif suivant : préparer le devenir professionnel des doctorants dans le secteur public comme dans le secteur privé

Catégorie : Ethique de la recherche-Sciences et société

☛ MOOC Intégrité scientifique dans les métiers de la recherche 15 heures enregistrées par : Chimie et Sciences du Vivant.

Catégorie : Formations scientifiques (total 146h)

☛ Expérimentation animale Niveau I (Concepteur) (29 juin 2020 - 25 septembre 2020) UGA 30 heures enregistrées par : Chimie et Sciences du Vivant.

☛ GAG2020 - Reproductibilité des résultats : un challenge pour vos recherches (24 novembre 2020) Groupement des animaleries de Grenoble - Grenoble 7 heures enregistrées par : Chimie et Sciences du Vivant. La formation participe à l'objectif suivant : préparer le devenir professionnel des doctorants dans le secteur public comme dans le secteur privé

☛ GAG2021 - Modèles animaux en virologie (03 juin 2021) Groupement des animaleries de Grenoble - Grenoble 7 heures enregistrées par : Chimie et Sciences du Vivant. La formation participe à l'objectif suivant : préparer le devenir professionnel des doctorants dans le secteur public comme dans le secteur privé

☛ HIV Science 15 heures enregistrées par : Chimie et Sciences du Vivant.

☛ JRC summer school on Non-Animal Approaches in Science - The Three R...evolution (17 mai 2021) European Commission - Ispra 25 heures enregistrées par : Chimie et Sciences du Vivant. La formation participe à l'objectif suivant : préparer le devenir professionnel des doctorants dans le secteur public comme dans le secteur privé

☛ Les bases de l'immunologie (18 novembre 2021) Biosciences&co, Lyon 14 heures enregistrées par : Chimie et Sciences du Vivant. La formation participe à l'objectif suivant : être directement utile pour la rédaction de la thèse ou pour l'exposition écrite ou orale des travaux de recherche

☛ MOOC - Stratégies de diagnostiques des cancers (06 septembre 2021) Université de Paris 18 heures enregistrées par : Chimie et Sciences du Vivant. La formation participe à l'objectif suivant : conforter la culture scientifique des doctorants dans leur champ disciplinaire ou en interdisciplinaire

☛ MOOC Comprendre les Nanosciences 16 heures enregistrées par : Chimie et Sciences du Vivant.

☛ Prise en main et utilisation d'un microscope électronique basse tension (11 février 2020) CEA/IRIG/LCBM - Grenoble 14 heures enregistrées par : Chimie et Sciences du Vivant.

Catégorie : Formations transversales (total 143h)

☛ Formation expérimentation Animale 10 heures enregistrées par : Chimie et Sciences du Vivant.

☛ MOOC - CNAM_Records management et dématérialisation 10 heures enregistrées par : Chimie et Sciences du Vivant.

☛ MOOC - L'anglais pour tous - Spice up your english (03 janvier 2022) FUN MOOC - Université Libre de Bruxelles 72 heures enregistrées par : Chimie et Sciences du Vivant. La formation participe à l'objectif suivant : favoriser l'ouverture internationale

☛ MOOC - renforcer ses compétences orthographiques (08 novembre 2021) UniCaen 12 heures enregistrées par : Chimie et Sciences du Vivant. La formation participe à l'objectif suivant : être directement utile pour la rédaction de la thèse ou pour l'exposition écrite ou orale des travaux de recherche

☛ MOOC- Recherche reproductible : principes méthodologiques pour une science transparente 25 heures enregistrées par : Chimie et Sciences du Vivant.

☛ Sensibilisation à l'utilisation de produits chimiques (29 avril 2021) SOCOTEC-CEA Grenoble 7 heures enregistrées par : Chimie et Sciences du Vivant. La formation participe à l'objectif suivant : conforter la culture scientifique des doctorants dans leur champ disciplinaire ou en interdisciplinaire

☛ UGA - Conduite et exploitation d'un Autoclave INITIALE (08 février 2022) UGA - Grenoble 7 heures enregistrées par : Chimie et Sciences du Vivant. La formation participe à l'objectif suivant : être directement utile pour la réalisation des travaux personnels de recherche

Catégorie : Insertion professionnelle (total 40h)

☛ Code d'intégrité des affaires (19 janvier 2021 - 19 janvier 2021) Solvay - en ligne 1 Chimie et Sciences du Vivant.

☛ Confidentiality Training (13 avril 2021) Solvay -en ligne 1 Chimie et Sciences du Vivant. La formation participe à l'objectif suivant : préparer le devenir professionnel des doctorants dans le secteur public comme dans le secteur privé

☛ MOOC 'Se former pour enseigner dans le supérieur' cours en ligne 15 heures

☛ Les bases pour bien manager les personnes (06 aout 2021) Solvay - en ligne 1 Chimie et Sciences du Vivant. La formation participe à l'objectif suivant : préparer le devenir professionnel des doctorants dans le secteur public comme dans le secteur privé

☛ Mon Portfolio de compétences, étape incontournable de mon parcours de thèse (15 avril 2022) En visioconférence 4 heures

☛ Se former pour enseigner dans le supérieur 15 heures enregistrées par : Chimie et Sciences du Vivant.

☛ Solvay - Code of Business Integrity (22 novembre 2021) Solvay 1 Chimie et Sciences du Vivant. La formation participe à l'objectif suivant : préparer le devenir professionnel des doctorants dans le secteur public comme dans le secteur privé

☛ Well-being at work (06 aout 2021) Solvay - en ligne 1 Chimie et Sciences du Vivant. La formation participe à l'objectif suivant : préparer le devenir professionnel des doctorants dans le secteur public comme dans le secteur privé

☛ Work as a team - In the battlefield you are not alone (07 septembre 2021) Solvay - en ligne 1 Chimie et Sciences du Vivant. La formation participe à l'objectif suivant : préparer le devenir professionnel des doctorants dans le secteur public comme dans le secteur privé

Catégorie : Formations du Label RES (total 20h)

☛ AUTRANS-19 : Introduction au métier d'enseignant-chercheur (11 décembre 2019 - 13 décembre 2019) Centre l'Escandille 20 heures

Catégorie : Langues (Anglais - Français langues étrangères F.L.E.) (total 15h)

☛ MOOC - Unlock your english 15 heures enregistrées par : Chimie et Sciences du Vivant.

Catégorie : Pratiques de l'enseignement (total 11h)

☛ EA-19-1 : Evaluer les apprentissages des étudiants (21 janvier 2020 - 21 janvier 2020) Bâtiment PLURIEL - 701 rue de la piscine - Domaine Universitaire 4 heures

☛ EVAL ENS-19 : Evaluation des enseignements (20 février 2020) ENSIMAG Bâtiment C salles C012-C013 7 heures